蒙古高原

Vegetation Changes and Associated Climate Variations in the Mongolian Plateau during the Past 40 000 Years

过去四万年来的植被与气候变化

主　编：冯兆东

副主编：马玉贞

甘肃科学技术出版社

责任编辑：杨丽丽
封面设计：陈妮娜

ISBN 978-7-5424-2206-4
9 787542 422064 >
定价：90.00元

蒙古高原

过去四万年来的植被与气候变化

Vegetation Changes and Associated Climate Variations in the Mongolian Plateau during the Past 40 000 Years

主　编：冯兆东
副主编：马玉贞

甘肃科学技术出版社

图书在版编目（CIP）数据

蒙古高原过去四万年来的植被与气候变化 / 冯兆东主编. -- 兰州 ： 甘肃科学技术出版社，2015.6
ISBN 978-7-5424-2206-4

Ⅰ. ①蒙… Ⅱ ①冯… Ⅲ. ①蒙古高原–植被–研究 ②蒙古高原–气候变化–研究 Ⅳ ①Q948.531 ②P468.31

中国版本图书馆CIP数据核字（2015）第117908号

出 版 人 吉西平
责任编辑 杨丽丽(0931-8773274)
封面设计 陈妮娜
出版发行 甘肃科学技术出版社(兰州市读者大道568号 0931-8773237)
印　　刷 甘肃澳翔印业有限公司
开　　本 787mm×1092mm　1/16
印　　张 23.25
字　　数 509千
版　　次 2015年6月第1版　　2015年6月第1次印刷
印　　数 1~1500
书　　号 ISBN 978-7-5424-2206-4
定　　价 90.00元

作者简介

冯兆东，男，1955年出生，甘肃定西人。1978年兰州大学地理系本科毕业，1982获兰州大学地理学硕士学位，1987年获美国华盛顿大学地质学硕士学位，1992年获美国堪萨斯大学地理学博士学位，1992~1994年在美国哥伦比亚大学Lamont-Doherty地质研究中心从事博士后研究。1994~1996年任美国犹它大学助理教授，1996~2008任美国蒙特可莱大学助理教授、副教授、教授，2000年起被聘任为教育部“长江学者奖励计划”特聘教授（兰州大学），现任中国科学院新疆生态与地理研究所特聘研究员。

马玉贞，女，1957年出生，河南太康县人。1982年获兰州大学地质学学士学位，1993年获兰州大学地质学硕士学位，2004年获兰州大学地理学博士学位。1982~2007年任兰州大学助教、讲师、、副教授、教授，1995年、1997年、2000年和2006年先后赴德国哥廷根大学孢粉研究所、柏林自由大学和美国路易斯安那州立大学进修学习和合作研究，2007年起任北京师范大学教授、环境演变与自然灾害教育部重点实验室副主任。

王维，男，1972年出生，甘肃榆中人。1994年获兰州大学材料科学学士学位，2003~2005年在兰州大学地理系攻读硕士学位，2009年获兰州大学第四纪地质学博士学位，2009年起任内蒙古大学环境与资源学院讲师、副教授。

王丽霞，女，1976年出生，山东德州人。2002年获烟台师范学院地理学学士学位，2005年获兰州大学地理学硕士学位，2005年7月至2011年5月就职于辽宁省环境监测实验中心，2011年5月至2014年3月就职于中国环境科学研究院，目前就职于环境保护部南京环境科学研究所。

孙爱芝，女，1979年出生，山东章丘人。2002年获聊城大学地理学学士学位，2007年获兰州大学第四纪地质学博士学位，2007~2011年任西南大学副教授，2011~2013年在中国科学院地质与地球物理研究所从事博士后研究，2013年起任中国科学院大学地球科学学院教师。

郭兰兰，女，1980年出生，山西晋中人。2005年获兰州大学地理学硕士学位，2008年获北京师范大学地理学博士学位，2008年起任北京师范大学减灾与应急管理研究院讲师。

冉敏，男，1983年出生，湖北京山人。2007年获兰州大学地质学学士学位，2012年获兰州大学地理学博士学位，2012~2014在新疆大学地理学博士后流动站从事博士后研究，2014年起任西南大学地理科学学院讲师。

前　言

一、与蒙古高原无关的一些事

我常常告诉我的同行朋友："如果不是偶然的机会捡起了蒙古高原，我这辈子可能就无事业可言了"。从硕士学习阶段至在兰州大学任讲师阶段（1978~1985），我一直在学习和研究冰川地貌。我后来去美国华盛顿大学继续学习和研究冰川地貌（1985~1987）。在华盛顿大学完成了第二个硕士学位后，转磨到了美国中部的堪萨斯大学攻读博士学位（1987~1991）。当时正是中国黄土研究"暴热"的时候，我的导师 William Johnson 教授希望我将停顿了近三十年的美国中西部的黄土研究再捡起来，再加上我在出国之前就涉猎过中国黄土高原的环境重建研究，我就毫不犹豫地"背叛"了冰川而"投靠"了黄土。

完成了博士论文之后（1991），我很容易地获得美国哥伦比亚大学的博士后奖学金（Postdoctoral Fellowship），跟着 George Kukla 教授继续研究美国中西部的黄土。我是兴致勃勃地走进了著名的 Lamont-Doherty Earth Observatory，但两年之后从那儿出来时我却是灰头灰脸的。我写的四个基金申请无一获准，两年博士后结束时也没有找到工作。无奈之下，哥伦比亚大学"半价地"延续了我的博士后身份半年，实际上是给了我找工作的时间缓冲。接下来的事更加烦人。我的地质学背景似乎不足以引起美国大学的地质系对我感兴趣，我的黄土和冰川背景似乎又不太适合美国大学的地理系。好在我在堪萨斯大学接受了完整的地理信息系统和遥感方面的训练。于是我用我的地理信息系统背景和我在堪萨斯地质局做过地理信息系统助手的经历说服了犹他大学地理系，他们给我提供给了一个"非终身系列"的助理教授位子（1994~1996）。我想补充：虽然我在哥伦比亚大学"一事无成"，但在那儿两年多的奋斗过程和日常见闻让我彻底理解了：做科学研究既需要一丝不苟的严谨态度，也需要"宗教狂般"的追求精神。我想感谢：犹他大学给我提供的"上讲台经历"让我在之后的"终身系列（Tenure Track）"教职寻求中十分顺利。

二、与蒙古高原有关的一些事

大概是 1995 年 3 月吧，犹他大学的一位同事告诉我，美国基金委的国际合作局正在 EOS 杂志上广告寻找对蒙古国有地学研究背景和兴趣的学者，参加他们主办的美—蒙合作启动会并撰写研究纲要。我发送了我的简历，他们说，他们对我 1993 年发表在 The

Holocene 上的关于中国全新世气候变化的评述文章很感兴趣，因为其中有关于中国内蒙古的内容。同年 10 月我参加了在南卡(South Carolina)召开的启动会，并在研究大纲中贡献了一章(Late Cenozoic Environmental Change in the Mongolian Plateau)。1996 年 9 月我又参加了一个由六名学者组成的美国基金委(US NSF)代表团，与蒙古科学院签订了合作协议，并进行了为期 20 天的野外考察。

接下来便是漫长的“基金获得过程”。1996 年我开始了我在新泽西 Montclair 州立大学长达 13 年的教书生涯。1997 年我向美国基金委递交了一个蒙古高原北部风尘历史研究的项目，返回的评语很不好。1998 年我在基金委申请到了一笔“小钱”，为我的“大项目”的申请做了一些预研究。结果呢，1999 年的项目还是被毙了。2001 年，我在美国国家地理协会(National Geographic Society)又申请到了一笔“小钱”，2002 年用那笔“小钱”获得了不少预研究资料，2003 年的基金申请以非常高的排名和比较高的支持强度获准（项目批准号：USA-NSF-ESH-04-02509；题目：Holocene Climatic Changes in the Mongolian Plateau)。与此同时，我也获得了中国国家基金委的重点项目（项目批准号：NSFC-40331012；题目：蒙古高原全新世气候环境变化时空规律的高分辨率重建)。至此，我们的“蒙古高原学术战役”算是全面展开了，这也为我们日后的“中亚学术战役”拉开了序幕。实际上，这本书的第四章、第八章、第九章是“中亚学术战役”的成果(项目批准号：NSFC-40930102；题目：西风带主导区核心地带过去一万年以来生物气候的变化)。

三、一些主要成果

上述两个项目为 6 名学生创造了博士论文研究机会，为 8 名学生创造了硕士论文研究机会，共发表 SCI 论文 24 篇，其他论文 16 篇。前后有 20 多位兰州大学的老师和学生参加了野外考察，还有 10 多位蒙古国科学院的科学家参加了野外工作。虽然我们对“蒙古高原北部过去五万年来的风尘历史和植被变化的重建”还比较满意，我们对“沿蒙古高原南—北段面做的表土有机质碳同位素和表土孢粉调查”也还满意，但我们最满意的则是我们对 “蒙古高原及周边地区全新世湿度变化的重建和比较”(见：Wang, W. and Feng, Z.-D., 2013. Holocene moisture evolution across the Mongolian Plateau and its surrounding areas: A synthesis of climatic records. Earth-Science Reviews, 122: 38~57)。

我们的重建和比较表明，受赤道太平洋海面温度的抑制和控制，蒙古高原南缘(即内蒙古南缘)和中国黄土高原全新世的湿度变化是一致的，二者均是对夏季太阳辐射的延迟响应，最湿润期发生在全新世中期。干旱和超干旱的蒙古高原大部的湿度在全新世中期是最低的，我们认为这个最低的湿度与全新世中期的温度最高有关，即高温加剧了蒸发。西伯利亚南缘(包括贝加尔湖盆地和阿尔泰山脉)的全新世湿度曲线和俄罗斯平原的全新世湿度曲线很相像：6000~9500 年前为最高，然后逐渐下降，且二者均与重建的北大西洋暖季温度曲线一致。新疆北部全新世湿度的变化与重建的挪威冬季降水变化很相

像：自8000年前以来一致上升，直到大约500年才有所下降，且二者均与重建北大西洋冷季温度变化一致。

本书的出版经费来自新疆生态与地理研究所提供的所长基金（时任所长是陈曦博士）。

冯兆东

2014年8月29日于新疆生态与地理研究所

目　录

第一章　蒙古高原现代花粉—植被—气候的关系
…… 马玉贞　王维　孙爱芝(001)
第二章　蒙古高原表土有机质碳同位素与气候的关系
…… 王丽霞　郭兰兰　冯兆东(033)
第三章　蒙古国北部夏马尔(Shaamar)风积剖面记录的过去近 40 000 年来植被与气候的变化 …… 马玉贞　王维(049)
第四章　蒙古国西部阿奇特湖(Achit Nuur)湖芯记录的过去 20 000 多年来植被与气候的变化 …… 孙爱芝　冉敏(068)
第五章　蒙古国北部岗湖（Gun Nuur）湖芯记录的过去 10 000 年植被与气候的变化
…… 冯兆东　马玉贞(082)
第六章　蒙古国中部优贵湖(Ugii Nuur)湖芯记录的过去近 9000 年来植被和气候的变化
…… 王维　马玉贞(100)
第七章　中国内蒙古中部柒盖淖尔(Qigai Nuur)湖芯记录的过去 10 000 年以来植被与气候的变化 …… 孙爱芝　冯兆东(117)
第八章　中国新疆北部湖芯记录的过去 8000 年气候与水文的变化
…… 冉敏　冯兆东(136)
第九章　哈萨克斯坦东部巴尔喀什湖(Balkhash Lake)湖芯记录的过去 2500 年气候与水文的变化 …… 冯兆东　冉敏(153)
第十章　蒙古高原及其周边地区全新世湿度演化及其机制研究
…… 王维　冯兆东(166)
后　序　蒙古高原与地中海全新世气候的可能联系 …… 冯兆东(209)

附录一 Feng, Z.-D. And Khosbayar, P., 2004. Paleosubarctic Eolian environments along the southern margin of the North American Icesheet and the southern margin of Siberia during the Last Glacial Maximum. ***Paleogeography Paleoclimatology Paleoecology***, 212: 265-275. …… (213)

附录二 Feng, Z.-D., Ma, Y.Z., Zhang, H.C., Narantsetsega, Ts. and Zhang, X.S., 2013. Holocene climate variations retrieved from Gun Nuur lake-sediment core in the northern Mongolian Plateau. ***The Holocene***, 23(12):1721-1730. …… (224)

附录三 Feng, Z.-D., Wang, L.X., Ji, Y.H., Guo, L.L., Lee, X.Q. and Dworkin, S.I., 2008. Climatic dependency of soil organic carbon isotopic composition along the S-N Transect from 34°N to 52°N in central-east Asia. ***Paleogeography Paleoclimatology Paleoecology***, 257: 335-343. …… (234)

附录四 Feng, Z.-D., Zhai, X.W., Ma, Y.Z., Huang, C.Q., Wang, W.G., Zhang, H.C., Khosbayar, P., Narantsetsega, Ts., Liu, K.-B. and Rutter, N.W., 2007. Eolian environmental changes in the Northern Mongolian Plateau during the past ~35,000 yr. ***Paleogeography Paleoclimatology Paleoecology***, 245: 505-517. …… (243)

附录五 Feng, Z.-D., Wu, H.N., Zhang, C.J., Ran, M., and Sun, A.Z., 2013. Bioclimatic change of the past 2500 years within the Balkhash Basin, eastern Kazakhstan, Central Asia. ***Quaternary International***, 311: 63-70. …… (256)

附录六 Ma, Y.Z., Liu, K.-B., Feng, Z.-D., Meng, H.W., Sang, Y.L., Wang, W. and Zhang, H.C., 2013. Vegetation changes and associated climate variations during the past 38,000 years reconstructed from the Shaamar eolian-paleosol section, northern Mongolia. ***Quaternary International***, 311: 25-35. …… (264)

附录七 Ma, Y.Z., Liu, K.-B., Feng, Z.-D., Sang, Y.L., Wang, W. and Sun, A.Z., 2008. A survey of modern pollen and vegetation along a south-north transect in Mongolia. ***Journal of Biogeography***, 35: 1512-1532. …… (275)

附录八 Ran, M., Zhang, C.J. and Feng, Z.-D., 2014. Climatic and hydrological variations during the past 8000 years in northern Xinjiang of China and the associated mechanisms. ***Quaternary International*, *Quaternary International***, 358: 21-34. …… (296)

附录九 Sun, A.Z. and Feng, Z.-D., 2013. Holocene climatic reconstructions from the fossil pollen record at Qigai Nuur in the southern Mongolian Plateau. ***The Holocene***. 23 (10): 1391-1402. …… (310)

附录十 Sun, A.Z., Feng, Z.-D., Ran, M. and Zhang, C.J., 2013. Pollen-recorded bioclimatic variations of the last 22,600 years retrieved from Achit Nuur core in the western Mongolian Plateau. ***Quaternary International***. 311: 36-43.
…… (322)

附录十一 Wang, W., Ma Y.Z., Feng Z.-D., Ts Narantsetseg., Liu K.-B. and Zhai X.W., 2011. A prolonged dry mid-Holocene climate revealed by pollen and diatom records from Lake Ugii Nuur in central Mongolia. ***Quaternary International***, 229: 74-83.
…… (330)

附录十二 Wang, W. and Feng, Z.-D., 2013. Holocene moisture evolution across the Mongolian Plateau and its surrounding areas: A synthesis of climatic records. ***Earth-Science Reviews***. 122: 38-57. …… (340)

第一章

蒙古高原现代花粉—植被—气候的关系

马玉贞[①] 王 维[②] 孙爱芝[③]

①北京师范大学 环境演变与自然灾害教育部重点实验室
②内蒙古大学 环境与资源学院
③中国科学院大学 地球科学学院

为了研究蒙古国现代花粉与植被的地理空间和气候关系，并探索这一关系重建古气候的潜力，我们在蒙古国中东部，沿跨越5个植被带的南北断面系统采集了104个表土花粉样品。本章首先运用判别分析(DA)判别现代花粉谱与植被带的关系并建立了判别函数；再使用聚类分析(HCA)和非度量多维测度法(NMS)对主要花粉类型进行自然分类并判断主要类群对环境梯度的响应。通过综合分析与5个植被带相对应的花粉谱、DA、HCA和NMS结果，发现沿着南北断面的每个植被带都有着独特的现代花粉组合特征，具体如下：1 荒漠：藜科—蒿藜科—白刺属—禾本科花粉组合；2 荒漠草原：禾本科—藜科花粉组合；3 草原：蒿属—紫菀型—禾本科—单束松型花粉组合；4 森林草原：单束松型—云杉属—蒿属—桦木属，山地非禾本草本植物/灌木花粉—蕨类孢子组合；5 山地泰加林：单束松型—云杉属—禾本科—莎草科，山地非禾本草本植物/灌木花粉—蕨类孢子组合。并根据主要花粉类型组及亚组间的比值，建议了两个能反映降水和温度条件的花粉—气候指数。进一步地检验分析显示，湿度指数(M)和温度指数(T)计算出的蒙古国南北断面温度和湿度的变化趋势很好地反映了研究区现代降水和温度的变化梯度，表明花粉—气候指数可用于该区基于化石花粉数据的古气候重建。另外，本章还讨论了10种重要花粉类型的传播模式和代表性。

关键词：聚类分析；判别分析；现代花粉谱；蒙古国；花粉—气候指数；植被

1. 引言

为了通过化石花粉数据准确地重建过去的环境，孢粉学家认为首先要了解研究区内现代花粉谱与相应植被的关系(Webb，1987；Webb等，1993)。在蒙古国，几乎没有现代花粉与植被关系的综合性研究成果发表。除少数工作外(Tarasov 等，2000a)，蒙古国全新世

花粉记录也十分少见(Dorofeyuk和Tarasov,1998; Gunin等,1999),且在这些工作中几乎没有对现代花粉组合特征的分析研究。

根据花粉和植物大化石资料,Tarasov 等(1998,1999a)重建了苏联和蒙古国现代和中全新世的生物群区。基于对欧亚大陆北部和北美洲西部的1245个表层花粉谱(其中644个来自苏联和蒙古国,但是属于后者的很少)计算得到的植物功能型(Plant functional types, PFTS)得分,重建了该地区中全新世(6 kyr BP;kyr BP = 千年前)和末次冰期极盛期(Last Glacial Maximum;大约18 kyr BP)的气候特征(Tarasov 等,1999a,b;2000b)。与此同时,据蒙古国102个现代花粉谱的研究推论出现代花粉数据可反映相对应的植被类型;但落叶松属(*Larix*)较低的花粉生产力和花粉传播能力导致其花粉的低代表性(Guninet等,1999)。Tarasov等(2000a)据这一结论和花粉—生物群区定量重建法解释了蒙古国西北部浩特湖(Hoton-Nur)盆地的花粉记录。然而,尽管上述工作都用到了来自欧亚大陆北部(包括蒙古国)的现代花粉数据,但仍未见到专门研究蒙古国现代花粉谱的文献,因而我们对这一地区花粉与植被或气候的具体关系(定量和定性)了解甚少。在蒙古国南部的荒漠和荒漠草原地区,这种知识的缺乏更为严重,在现有数据网络中,那里的表土花粉样品数据是完全缺失的(Tarasov等,1999b;2000b)。

为了建立现代花粉和植被地理空间上和统计学上的关系,我们在2002年7月和8月沿着蒙古国中东部南北断面收集了104个现代花粉样品,并对这一断面的现代花粉谱进行系统的分析。这些资料将拓展我们对该区现代花粉和植被关系的理解,并填补蒙古国现代孢粉数据网络的空缺。

2. 研究区

104个表土花粉样品采自从42°45′55″N到51°35′08″N,从99°45′55″E到51°35′08″E的广大区域,包括蒙古国中东部的东戈壁(East Gobi)和中央(Tov)省部分地区、杭爱(Hangay)—肯特山地区(Hentiy)、色楞格(Selenge)和鄂尔浑河(Orhon)流域以及库苏古尔湖(Hovsgol nuur)区。该研究区位于中亚北部,远离海洋(图1-1),气候为典型的大陆性气候(Tuvdendorzh和Myagmarzhav,1985;Orshikh等,1990)(图1-2)。年降水量自西北向东南逐渐递减。年降水量最高的地区位于库苏古尔湖区的山地,超过600mm;年降水量最低的是东戈壁省地区,约为50mm。

冬季(12~3月)很冷,最低温纪录出现在1月,月平均气温低于-16℃,最低超过-24℃。冬季也很干,其降水量只占全年的5%~10%,在北部地区和山区多有降雪。夏季(6~8月)是最湿润的季节,降水量占到了全年的70%左右。通常,7月降水量最大,也是最热的月份,从北部地区和山区到东戈壁地区,月平均气温为12℃~24℃。自西北向东南,气候逐渐变暖变干。春季(4月、5月)以强风、较低的空气湿度和较少的降水量为特征。午后经常伴有扬尘和沙尘暴(Tuvdendorzh和Myagmarzhav,1985;Orshikh等,1990)。

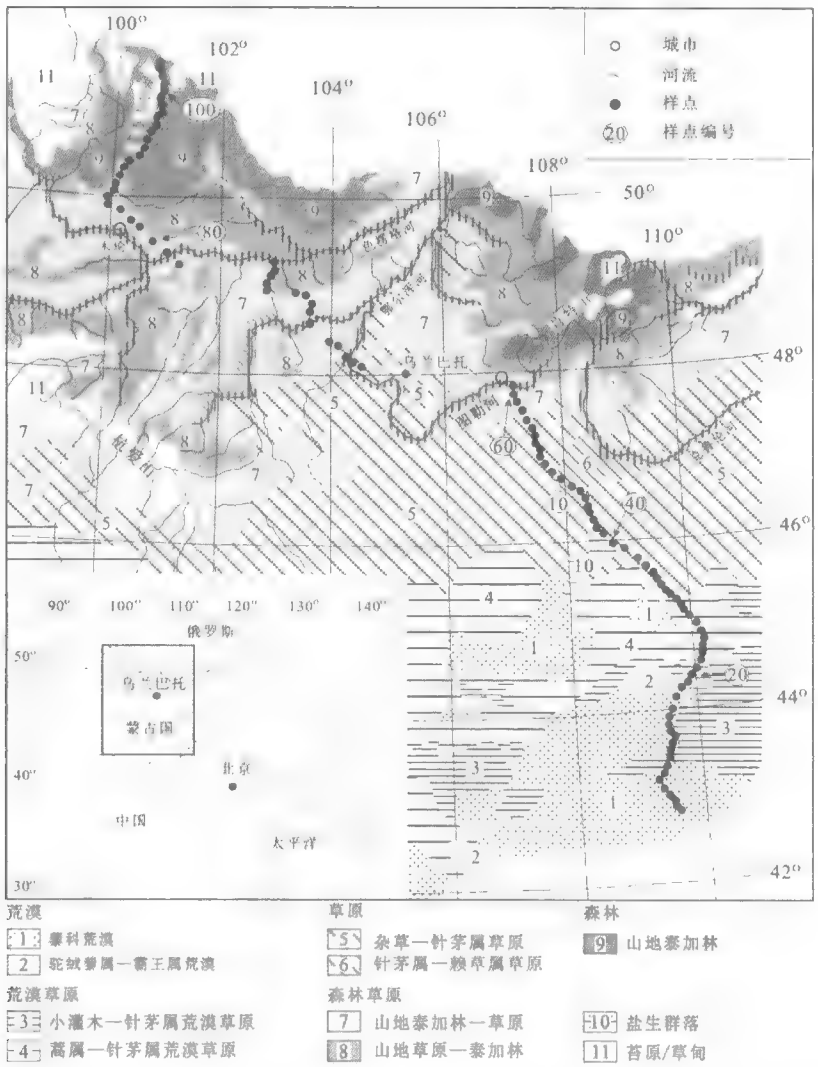

图1-1　蒙古国中东部的植被图(引自Lavrenko 等,1979;Lavrenko和Karamisheva,1990)和104个表土样点位置

3. 植被和气候

图1-1显示出蒙古国中东部的主要植被带分布区域（Lavrenko等,1979;Lavrenko和Karamisheva,1990）。从生物地理学的角度看,从南到北可划分出荒漠、荒漠草原、干草原、森林草原和西伯利亚泰加林五个主要植被带,而且草原和森林草原分布最广。上述五个植被带的分布完全受控于气候的南—北向梯度:温度由南向北递减,降水由南向北递增(图1-2)。我们从南到北跨越五个植被带系统的采集了表土样品，植物命名引自Hilbig(1995)。

3.1 荒漠植被

荒漠植被分布在东戈壁海拔750~1200m的地区，年平均气温4 ℃~6℃，7月气温＞24 ℃，1月气温＜-16℃。降水几乎全部发生在夏季，年降水量一般为50~150mm（图1-2），但是小于40mm的年份也屡见不鲜。冬季寒冷少雨。重要的荒漠植被由小灌木和半灌木植物组成，主要类型为藜科（Chenopodiaceae），如假木贼属（*Anabasis*）、梭梭属（*Haloxylon*）、盐爪爪属（*Kalidium*）、地肤属（*Kochia*）、戈壁藜属（*Iljinia*）、猪毛菜属（*Salsola*）、合头草属（*Sympegma*）和小蓬属（*Nanophyton*）；菊科（Asteraceae），包括亚菊属（*Ajania*）、蒿属（*Artemisia*）紫菀木属（*Asterothamnus*）和短舌菊属（*Brachanthemum*）；蓼科（Polygonaceae），如木藜属（*Atraphaxis*）和沙拐枣属（*Calligonum*）；蒺藜科（Zygophyllaceae），包括白刺属（*Nitraria*）和霸王属（*Zygophyllum*）；柽柳科（Tamaricaceae），如红砂属（*Reaumuria*）和柽柳属（*Tamarix*）；豆科（Fabaceae），包括锦鸡儿属（*Caragana*）和棘豆属（*Oxytropis*）；蔷薇科（Rosaceae），如锦刺属（*Potaninia*）；旋花科（Convolvulaceae），如旋花属（*Convolvulus*）等

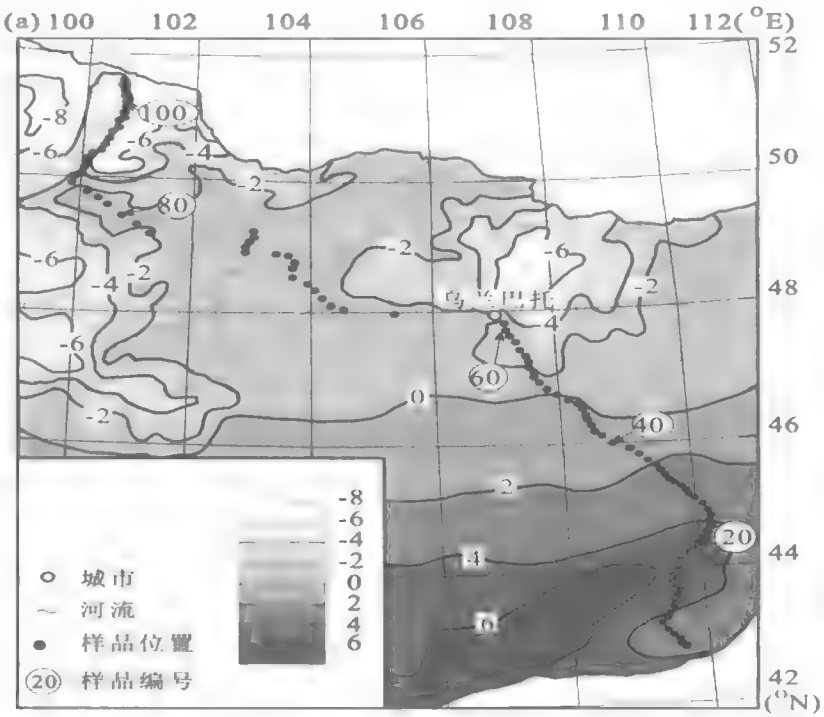

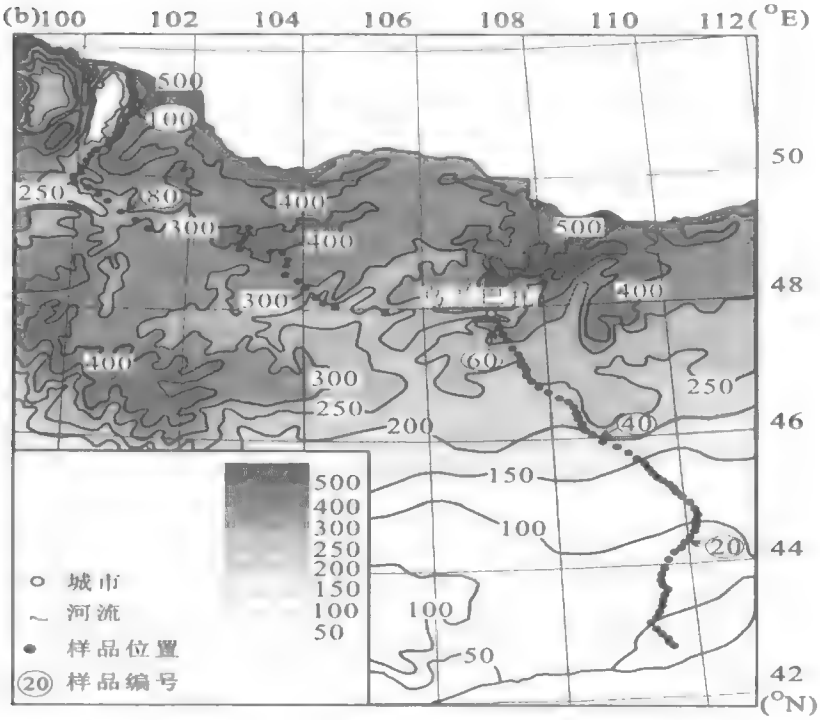

图1-2　蒙古国中东部气候：(a)年平均温度(℃)；(b)年平均降水(mm)
(引自Orshikh等，1990)

据植物组成可分出两个主要的荒漠群落(Hilbig，1995)，即藜科荒漠和驼绒藜属—霸王属(*Eurotia - Zygophyllum*)荒漠

藜科荒漠(图1-1；类型1)是荒漠中非常重要且广泛分布的植物群落，优势种为：短枝假木贼(*Anabasis brevifolia*)、珍珠柴(*Salsola passerina*)、小蓬(*Nanophyton erinaceum*)、梭梭(*Haloxylon ammodendron*)、细枝盐爪爪(*Kalidium gracile*)、木地肤(*Kochia prostrata*)、小果白刺(*Nitraria sibirica*)、泡泡刺(*Nitraria sphaerocarpa*)、木霸王(*Zygophyllum xanthoxylon*)、骆驼蓬(*Peganum nigellastrum*)、琵琶柴(*Reaumuria soogorica*)和膜果麻黄(Ephedra przewalskii)　伴生植物为：戈壁针茅(Stipa *gobica*)、中华隐子草(*Cleistogenes chinensis*)、三芒草(*Aristida adscensionis*)、白皮锦鸡儿(*Caragana leucophloea*)、茵陈蒿(*Artemisia scoparia*)、菴状亚菊(*Tanacetum achilleoides*)、亚菊属、猫头刺(*Oxytropis aciphylla*)、沙拐枣(*Calligonum mongolicum*)、紫菀木属、葱属(*Allium*)、戈壁短舌菊(*Brachanthemum gobicum*)、盐豆木属(*Halimodendron*)、野胡麻属(*Dodartia*)、旋花属、棉毛鸦葱(*Scorzonera capito*)和绵刺(*Potaninia mongolica*)(Hilbig，1995)

驼绒藜属—霸王属荒漠(图1-1；类型2)出现在荒漠带气候较湿润的地区，植被覆盖度为0~10%　灌木层由驼绒藜(*Eurotia ceratoides*)、木霸王、白皮锦鸡儿、内蒙古旱蒿(*Artemisia xerophytica*)、木蓼(*Atraphaxis frutescens*)、沙拐枣和麻黄属(*Ephedra*)组成　草

本层主要由沙生针茅(*Stipa glareosa*)、沙葱(*Allium mongolicum*)、银灰旋花(*Convolvulus ammanii*)、砂蓝刺头(*Echinops gmelinii*)、弯状鸦葱(*Scorzonera pseudodivaricata*)、兔唇花(*Lagochilus ilicifolius*)、燥原荠(*Ptilotrichum canescens*)、戈壁天冬(*Asparagus gobicus*)、菪状亚菊、无芒隐子草(*Cleistogenes songorica*)、短枝假木贼和细叶鸢尾(*Iris tenuifolia*)组成。

小灌木—沙生针茅荒漠草原(图1-1;类型3)主要分布在东戈壁地区。主要植物种类有旋花属、红砂属、霸王属、蒺藜属(*Tribulus*)、蒿属、骆驼蓬属(*Peganum*)、针茅属、画眉草属(*Eragrostis*)、三芒草属(*Aristida*)、驼绒藜属、沙拐枣属、锦鸡儿属和雾冰草属(*Bassia*)(Hilbig,1995)。

在东戈壁北部海拔750~1000m的地区生长着蒿属—针茅属(*Artemisia-Stipa*)荒漠草原(图1-1;类型4),该区年平均气温为3℃~4℃,7月气温22℃~24℃,1月气温-18℃~-16℃,年平均降水为100~150mm(图1-2)。禾本科(Poaceae)为主要建群种(如克氏针茅(*Stipa krylovii*)、戈壁针茅和无芒隐子草)、还有冷蒿(*Artemisia frigida*)、内蒙古旱蒿(*A. caespition*)、线叶菊(*Tanacetum sibiricum*)、乔状艾菊(*T. achillaeoides*)和三裂艾菊(*T. trifidum*)等亚灌木。其他常见的物种包括西伯利亚冰草(*Agropyrum sibiricum*)、沙葱、矮锦鸡儿(*Caragana pygmaea*)、白皮锦鸡儿、银灰旋花、狗娃花(*Heteropappus hispidus*)、白刺属、短枝假木贼、珍珠柴、木地肤、驼绒蒿(*Eurotia ceratoides*)、琵琶柴、刺叶柄棘豆(*Oxytropis aciphylla*)、骆驼蒿、戈壁短舌菊、绵刺和木霸王。

该植被类型主要由蒿属—针茅属(*Artemisia-Stipa*)禾草草原和针茅属—赖草属(*Stipa-Leymus*)草原群落组成,生长在海拔为950~1400m的蒙古国中部和东部广大地区。

非禾本草本—针茅属禾草草原(图1-1;类型5;Hilbig,1995)也以达乌里芯芭(*Cymbaria dahurica*)—克氏针茅(Stipa krylovii)群落而著称(Hilbig,1987),是该区草原植被的主要群落。为了与较湿润的山地草原区分,这类禾草草原常被称为干草原,主要生长在杭爱山东坡,肯特山的西、南和东南部。该区属于哈尔哈中部和蒙古—达斡尔地区南部,年均温为-2℃~3℃(图1-2),最低温为-20℃~-17℃,最高温为16℃~22℃,年平均降水量为150~300mm(图1-2)。禾草草原里禾本科植物发育良好,尤其是丛生禾草植物,优势种是针茅(克氏针茅)、糙隐子草(*Cleistogenes squarrosa*)和冷蒿(*Artemisia frigida*)。伴生种包括冰草(*Agropyrum cristatum*)、羊草(*Elymus chinensis*)、寸草苔(*Carex duriuscula*)、东北丝裂蒿(*Artemisia adamsii*)、滨蒿(*A. scoparia*)、黑蒿(*A. palustris*)、裂叶蒿(*A. tanacetifolia*)和芨芨草(*Achnatherum splendens*)。并伴生一些非禾本草本植物,如达乌里芯芭(*Cymbaria dahurica*)、驼舌草(*Goniolimon speciosum*)、木地肤、柳叶风毛菊(*Saussurea salicifolia*)和骆驼蓬及半灌木矮锦鸡儿(尤纳托夫,1959;Hilbig,1995)。此外,在农牧民居民点附近的针茅草原中,一些其他禾本和非禾本草本植物(如羊草、糙隐子草和冷蒿)占主导地位。针茅属—赖草属草原植被(图1-1,类型6)主要分布在较湿润的地区,优势种主要为针茅和羊草(Hilbig,1995)。

3.4. 森林—草原植被

该植被类型广泛分布在杭爱山的北部和东北部，肯特山的西北部、西部和南部；主要发育在色楞格和鄂尔浑河流域。北边与山地泰加林相邻，南边与草原和荒漠草原接壤。该区内，草原与其中的斑块状森林分界明显。具体来说，就是泰加林主要分布在低海拔山区的北坡和高海拔地区，而草原主要集中在南坡和山谷及周边地区。在东西向的山脉中，山顶经常是森林和草原的分界区(尤纳托夫，1959；Hilbig，1995)。

山地泰加林—草原植被(图1-1，类型7)主要由山地和高山草本—丛生禾草草原组成，局部有西伯利亚落叶松(*Larix sibirica*)林发育。该植被类型主要分布在海拔1000~1600m，年平均降水250~400mm，年平均气温-2℃~0℃，1月平均气温-24℃~-20℃，7月平均气温12℃~17℃(图1-2)。一些伴生种如桦木属(*Betula*)和杨属(*Populus*)生长在较高的山区中。

该区山地草原植被稀疏，一般覆盖度为60%~70%，从生禾草植物为建群种，如羊茅(*Festuca ovina*)、冷草(*Koeleria macrantha*)、纤细冷草(*K. gracilis*)、渐尖早熟禾(*Poa attenuata*)、冰草和克氏针茅。同时也出现一些蒿属植物，如冷蒿、银叶蒿(*A. argyrophylla*)和北极蒿(*A. borealis*)。其他伴生草本植物包括高山紫菀(*Aster alpinus*)、柳叶风毛菊(*Saussurea salicifolia*)、腺毛唐松草(*Thalictrum foetidum*)、小叶罗汉松(*Astragalus brevifolius*)、普米腊棘豆(*Oxytropis pumila*)、白头翁属(*Pulsatilla*)、红花百里香(*Thymus serpyllum*)、双齿葱(*Allium bidentatum*)、毛叶老牛筋(*Arenaria capillaris*)、锥叶柴胡(*Bupleurum bicaule*)、岩黄芪(*Hedysarum pumilum*)、卷鞘鸢尾(*Iris potaninii*)、黄花马先蒿(*Pedicularis flava*)、燥原荠、绢毛委陵菜(*Potentilla sericea*)、星毛委陵菜(*P. acaulis*)、岩生繁缕(*Stellaria petraea*)、瑞香狼毒(*Stellera chamaejasme*)和伏毛山莓草(*Sibbaldianthe adpressa*)(尤纳托夫，1959；Hilbig，1995)。

在过度放牧的地区，山地草原退化为由寸草苔(*Carex duriuscula*)占主导的短草甸草原。这些贫瘠的草原也发育有冷蒿，但除冰草外，禾草数量减少。随着海拔的增加，植被类型变为山地草原—泰加林植被(图1-1，类型8)，主要由西伯利亚落叶松林、欧洲赤松(*Pinus sylvestris*)林以及混有高山草甸的桦木属—西伯利亚落叶松(*Betula*—*Larix sibirica*)混交林组成(尤纳托夫，1959；Hilbig，1995)。

3.5. 山地泰加林植被

山地泰加林植被带(图1-1，类型9)主要分布在海拔1700~1950m的库苏古尔湖区域，年平均-6℃~-2℃，1月平均气温-24℃，7月平均气温12℃，年平均降水为300~500mm(图1-2)。山地泰加林优势种为落叶松和欧洲赤松。灌木层的特征种是刺蔷薇(*Rosa acicularis*)和圆叶桦(*Betula rotundifolia*)。在较高海拔地区，发育有高山绣线菊(*Spiraea alpina*)、金银花(*Lonicera altaica*)、西伯利亚刺柏(*Juniperus sibirica*)、细叶杜香(*Ledum palustre*)和杜鹃花属(*Rhododendron*)等。湿生草本和多年生禾草在这里发育良好，主要为异颖草属(*Calamagrostis obtusata*)、紫花党参(*C. purpurea*)、东北羊角芹(*Aegopodium alpestre*)、红三七(*Polygonum viviparum*)、三毛草属(*Trisetum*)、批碱草属(*Elymus*)、石竹科

(Caryophyllaceae)、莎草科(Cyperaceae)、毛茛科(Ranunculaceae)、虎耳草科(Saxifragaceae)以及伞形科(Apiaceae)(尤纳托夫,1959; Hilbig,1995)

4. 野外调查和室内实验方法

4.1. 野外调

样品采集断面从蒙古国东南部开始,向北跨越到蒙古国北部改为近东南—西北向(图1-1)。从低地荒漠到高山泰加林,以4°纬度为间隔,共采集了104个表土样品(表1-1)。其中,1~25号和90~104号在自然保护区内获得。每个样点采集10~20个表土子样品,为了确保其更具代表性,这些子样品随机在20m²的区域内采集(图1-1,表1-1)。部分样品取自苔藓,部分取自表层土壤(1cm深度)。

4.2. 室内实验方法

首先,对每个表土样品进行均质化处理。为了计算总孢粉浓度,在孢粉处理前,在每个样品中加入一粒石松孢子药片(含12542±414个石松孢子,由瑞典隆德大学Lund University制造,生产批号:124961)。使用10%~15%HCl(2h)、5%KOH(煮沸3~5min)以及醋酸和硫酸以9:1比例混合成的醋酸溶液对样品进行处理(Moore et al.,1991),然后,剩余样品用超声波清洗器震荡清洗过筛(7μm),最后,加入无水甘油保存制片。

孢粉鉴定参考已发表的孢粉学著作和文章(Moore等,1991; 王伏雄等,1995; 宛涛等,1999),及我们在该地和其他地区收集的超过500个花粉种属的现代花粉标准片。使用莱

表1-1 蒙古104个表土样点地理位置及植被概况(Ma等,2008)

序号	纬度(N)	经度(E)	海拔(m)	物质	植被类型	主要植物
1	42°45′55″	109°37′04″	1031	沙+落叶层	藜科荒漠	藜科、白刺属、麻黄属和蒺藜科
2	42°50′21″	109°36′02″	1104	沙+落叶层		
3	42°54′49″	109°31′11″	1147	沙+落叶层		
4	43°00′05″	109°24′49″	1195	沙+落叶层		
5	43°06′11″	109°21′41″	1217	沙+土壤层		
6	43°10′15″	109°08′51″	1100	沙+落叶层		
7	43°15′12″	109°13′05″	1070	沙+土壤层		
8	43°19′57″	109°20′50″	1014	沙+土壤层		
9	43°25′13″	109°29′20″	1000	沙+土壤层	针茅属荒漠草原	乔本科
10	43°30′22″	109°35′57″	979	沙+土壤层	藜科荒漠	藜科、白刺属、麻黄属和蒺藜科
11	43°35′03″	109°38′01″	950	沙+土壤层		
12	43°40′10″	109°37′43″	1011	沙+土壤层	针茅属荒漠草原	禾本科

续表1-1

序号	纬度(N)	经度(E)	海拔(m)	物质	植被类型	主要植物
13	43°45′06″	109°36′43″	937	沙+土壤层	藜科荒漠	藜科、白刺属、麻黄属、蒺藜科和禾本科
14	43°49′34″	109°35′51″	887	沙+土壤层		
15	43°54′55″	109°36′59″	884	沙+土壤层		
16	44°00′13″	109°38′22″	803	土壤+落叶层	驼绒藜属—霸王属荒漠	藜科、霸王属、禾本科、葱属、蒿属、锦鸡儿属、沙拐枣属和麻黄属
17	44°06′11″	109°40′40″	773	沙+土壤层		
18	44°12′13″	109°43′22″	754	土壤+落叶层		
19	44°16′39″	109°46′08″	751	土壤+落叶层		
20	44°20′19″	109°51′42″	782	沙+土壤层		
21	44°25′03″	109°57′27″	810	沙+土壤层	蒿属—禾本科荒漠草原	禾本科、蒿属、亚菊属、旋花属、藜科、霸王属和锦鸡儿属
22	44°31′25″	110°03′46″	748	沙+土壤层		
23	44°35′22″	110°05′47″	774	土壤+落叶层		
24	44°39′51″	110°07′20″	791	沙+土壤层		
25	44°45′10″	110°07′35″	848	土壤+落叶层		
26	44°49′52″	110°07′34″	889	土壤		
27	44°55′50″	110°06′32″	985	土壤		
28	45°00′05″	110°02′41″	931	沙+土壤层		
29	45°05′00″	109°58′54″	917	土壤+落叶层		
30	45°10′07″	109°54′50″	925	沙+土壤层		
31	45°15′13″	109°48′18″	964	土壤+落叶层	非禾本草本—针茅属草原	禾本科(针茅属、隐子草属、披碱草属、冰草属)、蒿属、锦鸡儿属、芯巴属和旋花属
32	45°20′05″	109°42′00″	991	土壤+落叶层		
33	45°25′22″	109°36′29″	988	土壤+落叶层		
34	45°30′06″	109°32′45″	988	土壤+落叶层		
35	45°35′27″	109°29′14″	1011	土壤+落叶层		
36	45°40′20″	109°26′13″	1012	土壤+落叶层		
37	45°45′26″	109°21′13″	1051	土壤+落叶层		

续表1–1

序号	纬度(N)	经度(E)	海拔(m)	物质	植被类型	主要植物
38	45°50′09″	109°09′57″	1066	土壤+落叶层		
39	45°55′05″	109°03′00″	1071	土壤+落叶层	非禾本草本—针茅草原	禾本科(针茅属、隐草属、披碱草属、冰草属)、蒿属、锦鸡儿属和芯巴属
40	46°00′01″	108°46′48″	1218	土壤+落叶层		
41	46°05′19″	108°38′07″	1154	土壤		
42	46°10′06″	108°33′49″	1178	土壤		
43	46°15′03″	108°29′16″	1191	土壤		
44	46°19′49″	108°24′22″	1277	土壤		
45	46°21′10″	108°21′01″	1288	土壤		
46	46°30′26″	108°19′12″	1292	土壤	针茅属—披碱草属草原	披碱草属、针茅属、狗娃花、蒿属、锦鸡儿属和葱属
47	46°34′50″	108°16′49″	1266	土壤		
48	46°40′02″	108°06′51″	1332	土壤+落叶层		
49	46°45′01″	107°56′13″	1240	土壤+落叶层	非禾本草本—针茅草原	禾本科(针茅属、隐草属、披碱草属、土壤冰草属)、蒿属、锦鸡儿属和芯巴属
50	46°50′08″	107°46′19″	1266			
51	46°55′07″	107°43′54″	1322	土壤+落叶层		
52	47°00′15″	107°38′20″	1312	土壤+落叶层		
53	47°05′09″	107°35′49″	1314	土壤+落叶层		
54	47°09′48″	107°34′09″	1358	土壤+落叶层		
55	47°15′07″	107°31′06″	1415	土壤+落叶层		
56	47°24′58″	107°25′50″	1415	土壤层		
57	47°30′03″	107°22′50″	1504	土壤层		
58	47°35′40″	107°16′29″	1581	土壤层	泰加林—山地非禾本草本/丛生禾草草原	蒿属、紫菀属、禾本科、委陵菜属、狼毒属、棘豆属、松属、落叶松属、云杉属和桦木属
59	47°40′37″	107°14′18″	1678	土壤层		
60	47°45′12″	107°14′33″	1568	土壤层		
61	47°50′24″	107°09′20″	1570	土壤层		

续表1-1

序号	纬度(N)	经度(E)	海拔(m)	物质	植被类型	主要植物
62	47°59′32″	105°26′06″	1231	土壤层	针茅草原	禾本科、蒿属，锦鸡儿和芯巴属
63	48°05′54″	104°24′00″	1080	土壤+落叶层	针茅草原	禾本科(针茅属、隐子草属、冰草属、
64	48°09′41″	104°20′43″	1042	土壤+落叶层		披碱草属)、蒿属、锦鸡儿属和芯巴属
65	48°14′49″	104°13′32″	1022	土壤+落叶层		
66	48°20′18″	106°06′49″	1120	土壤+落叶层	山地草原	禾本科、蒿属和桦木属
67	48°24′57″	103°59′22″	1222	土壤层	非乔本草本—针茅属草原	禾本科、蒿属、委陵菜属和狼毒属
68	48°29′42″	103°39′47″	1172	土壤+落叶层	针茅属草原	禾本科、蒿属、锦鸡儿属和芯巴属
69	48°34′00″	103°35′47″	1095	土壤+落叶层		
70	48°44′57″	103°34′29″	1170	土壤+落叶层	泰加林—山地非禾本草本/丛生禾草草原	禾本科、蒿属、紫菀属、委陵菜属
71	48°49′47″	103°30′30″	1255	土壤层		狼毒属、苔属、落叶松属、松属、云杉属和桦木属
72	48°55′00″	103°20′39″	1477	土壤+落叶层		
73	49°00′35″	102°47′59″	1422	土壤+落叶层		
74	49°05′09″	102°47′23″	1289	土壤+落叶层		
75	49°10′09″	102°51′27″	1161	土壤+落叶层	山地草原	禾本科、蒿属、锦鸡儿属和芯巴属
76	49°15′02″	102°57′16″	1035	土壤+落叶层		
77	49°19′57″	102°58′18″	944	土壤+落叶层	非乔本草本—针茅属草原	乔本科、蒿属、紫菀属、委陵菜属和狼毒属
78	49°24′57″	100°59′28″	1197	土壤+落叶层	山地草原	禾本科、蒿属、锦鸡儿属和芯巴属
79	49°30′28″	100°53′04″	1333	土壤层		
80	49°34′49″	100°49′14″	1516	土壤层	山地草原—泰加林	落叶松属、松属、桦木属、云杉属、蔷薇属、禾本科、蒿属、紫菀属、委陵菜属、狼毒属、苔草属和棘豆属

续表1-1

序号	纬度(N)	经度(E)	海拔(m)	物质	植被类型	主要植物
81	49°38′03″	100°13′10″	1338	100°49′14″		
82	49°45′02″	100°08′18″	1566	土壤+落叶层		
83	49°49′50″	100°06′22″	1840	土壤+落叶层		
84	49°56′56″	99°57′56″	1560	土壤	山地禾草草原	禾本科、蒿属、紫菀属、委陵菜属、
85	50°00′55″	99°58′15″	1677	土壤		蓼属、石竹科和毛茛科
86	50°05′02″	100°00′10″	1614	土壤+落叶层	山地草原—针叶林	落叶松属、松属、云杉属、蔷薇属、麻属、异颖草属、羊角芹属、羊茅草属、披碱草属、石竹科、莎草科和毛茛科
87	50°10′06″	100°01′19″	1588	土壤+落叶层		
88	50°14′33″	100°03′10″	1599	土壤+落叶层		
89	50°20′03″	100°06′25″	1646	土壤+落叶层		
90	50°25′08″	100°09′56″	1711	土壤+苔藓层	泰加林	落叶松属、松属和云杉属
91	50°30′00″	100°24′28″	1672	土壤+苔藓层		
92	50°35′01″	100°30′47″	1685	土壤+苔藓层		
93	50°40′01″	100°31′38″	1687	土壤+苔藓层	山地草原—泰加林	落叶松属、松属、云杉属、蔷薇属、桦木属和禾本科
94	50°44′59″	100°31′51″	1669	土壤+苔藓层		
95	50°50′04″	100°39′41″	1914	土壤+苔藓层	泰加林	落叶松属、松属和云杉属
96	50°54′40″	100°44′00″	1873	土壤+苔藓层		
97	50°59′56″	100°43′04″	1766	土壤+苔藓层		
98	51°05′41″	100°44′09″	1681	土壤+苔藓层		
99	51°10′13″	100°44′02″	1670	土壤+苔藓层		
100	51°15′13″	100°50′39″	1758	土壤+苔藓层	山地草原—泰加林	落叶松属、松属、云杉属、蔷薇属、桦木属和禾本科
101	51°20′24″	100°50′21″	1758	土壤+苔藓层		
102	51°25′06″	100°47′24″	1689	土壤+苔藓层	泰加林	落叶松属、松属和云杉属
103	51°30′23″	100°41′09″	1696	土壤+苔藓层	山地草原—泰加林	落叶松属、松属、云杉属、蔷薇属、桦木属和禾本科
104	51°35′08″	100°45′49″	1842	土壤+苔藓层		

卡光学显微镜进行孢粉鉴定和统计，常规鉴定用400倍放大率，必要时使用油镜放大1000倍。每个样品最少统计出500粒花粉。总孢粉数量除去孢子含量，以花粉总和为基数计算得出花粉百分比，并绘出花粉百分比曲线（图1-3）。在外加石松孢子计数的基础上，计算出花粉和孢子浓度，并表示为每克沉积物含多少粒（图1-4）。百分比低于2%的花粉和浓度低于100粒/克的孢粉属种不在孢粉图谱中出现。用Graph和CorelDraw软件绘制孢粉图谱。

4.3. 数值分析

基于植物种类在蒙古国主要植被带的重要性以及花粉组合特征，选出24个花粉类型进行数据分析。包括单束松型（*Pinus Haploxylon*-type）、双束松型（*Pinus Diploxylon*-Type）、云杉属（*Picea*）、冷杉属（*Abies*）、落叶松属、桦木属（*Betula*）、桤木属（*Alnus*）、蔷薇科（Rosaceae）、蒿属、紫菀型（*Aster*-type）、春黄菊型（*Anthemis*-type）、蒲公英型（*Taraxacum*-type）、禾本科、毛茛科（Ranunculaceae）、花葱科（Polemoniaceae）、百合科（Liliaceae）、石竹科、旋花属、藜科、黎科、蒺藜科、白刺属、麻黄属和莎草科。所有样点（104）都参与了数据分析。

4.3.1. 判别分析

理解现代花粉与相应植被间的定量关系对利用化石资料解译植被历史至关重要。判别分析（discriminant analysis，DA）在孢粉学上的应用源于：1）根据观测到的样品特征可得出观察样品属于某类型的预测判别模型；2）根据预测变量的线性组合建立的判别函数可以把不同的组区分开（SPSS Inc.，2001；McCune 和Grace，2002）。Liu和Lam（1985）运用判别分析作为一个推论统计方法，判定现代花粉和化石花粉组合的相似程度。此后，在基于植被带对每个表土花粉样品进行先验分类方面，判别分析已经被证明是一种有效的工具（Sugden和Meadows，1989；Liu，1990；Lynch，1996；Reese和Liu，2005；Graf和Chmura，2006）。本章运用判别分析来判定现代花粉组合能否代表特定的植被类型，并为该研究区建立从化石花粉谱中识别现代类似物的判别函数。

判别分析需要基于植被带对表土花粉样品进行先验分类（Liu和Lam，1985；Liu，1990；Lynch，1996）。基于104个现代花粉样品所属的地带性植被和局部植物群落将它们指派到5个主要的先验组（图1-1）。这5个现代花粉样品组以Z1、Z2、Z3、Z4、Z5命名，分别对应五个植被类型，即荒漠、荒漠草原、草原、森林草原和泰加林。

判别分析在SPSS11.0（SPSS Inc.，2001）的判别子程序内完成。用判别分析计算出两个有用的参数（Liu和Lam，1985）。第一，在每一个样点到每一个先验组的多维空间中心距离的远近基础上，建立植被指数。第二，从孢粉学角度来说，相似概率是将一个孢粉组合与其指派的植被的"孢粉特征"（同样由所属组的中心来代表）进行比较。一个低的相似概率说明：该样品尽管从地理学上来自或者在统计学上属于某一种植被，但实际上这个样品的孢粉组合与这个植被的孢粉特征明显不同（Liu和Lam，1985）。

4.3.2. 聚类分析

聚类分析（hierarchical cluster analysis，HCA）是将样品（案例）或类群（变量）按照它们

在性质上的亲疏程度进行分类的一种多元统计分析方法。在现代花粉数据分析中已得到广泛的应用（Birks，1973；Markgraf等，1981）。层序/等级聚类分析（Hierarchical cluster analysis，HCA）是一种探索性的方法，旨在揭示多元生态数据的自然分组（聚类），在生态学上的应用有着悠久的历史（McCune和Grace，2002），对小数量（小于数百个）的对象进行聚类最为有效。在本章中我们使用R模式中的层序聚类分析程序对主要花粉类群进行自然分组。

4.3.3. 非度量多维测度法

非度量多维测度法（non-metric multidimensional scaling，NMS）是近期发展起来的适用于非线性数据结构分析的一种复杂的迭代排序方法，用于判断类群对环境梯度（如湿度、温度和海拔）的响应。生境相似程度高，其类群的聚类和排序距离就小。本章选择NMS而不用其他排序方法（如：detrended correspondence analysis，DCA，即除趋势对应分析；principal components analysis，PCA，即主成分分析），主要是因为NMS更适于对非正态的或不连续的数据进行分析，其优势在于：1 不假设变量是线性相关的，更适应复杂的生态学数据分析；2 通过距离排列使花粉类型和环境空间的距离测量关系趋于线性化（Clarke，1993；McCune和Grace，2002）。为此，近年来NMS在生态学上已得到了广泛的应用，被认为是最有效的生态群落数据排序分析方法之一（Taylor等，2001；Enright 等，2005；Boucher和Mead，2006；Soh等，2006）。

层序聚类分析在SPSS11.0（SPSS Inc.，2001）中完成，选择适用于R性聚类的皮尔森（Pearson）积差相关分析系数作为距离测量技术，用平均连接（Between-groups linkage）法进行聚类。非度量多维测度法在pc-ord 4.14软件的“自动”（缓慢和彻底）模型中完成（McCune和Grace，2002）。用索伦森（Sorenon），又名布雷—柯蒂斯（Bray-Curtis），相似系数法计算矩阵距离排序。

所有结果都在Graph和CorelDraw11.0.中绘制成图

5. 结果

5.1. 花粉谱

依据104个表土样品（表1-1）的采样位置和当地的植物群落特征，其花粉谱被分成5个花粉组合带（图1-3，图1-4），分别对应5个主要的植被类型：1 荒漠；2 荒漠草原；3 草原；4 森林草原；5 泰加林。每个植被类型的花粉谱主要特征描述如下：

5.1.1. 带1（荒漠植被，样点1~19）：藜科—蒿藜科—白刺属—禾本科花粉组合

荒漠花粉组合中占优势的为藜科（20.35%~68.44%）、蒿藜科（1.36%~17.22%）、禾本科（3.29%~22.22%）和蒿属（3.07%~18.18%）。白刺属（1%~3%）、麻黄属、春黄菊型、花苞科和旋花属有一定的含量。木本植物花粉（松属、云杉属和桦木属）及毛茛科和石竹科的含量较低。

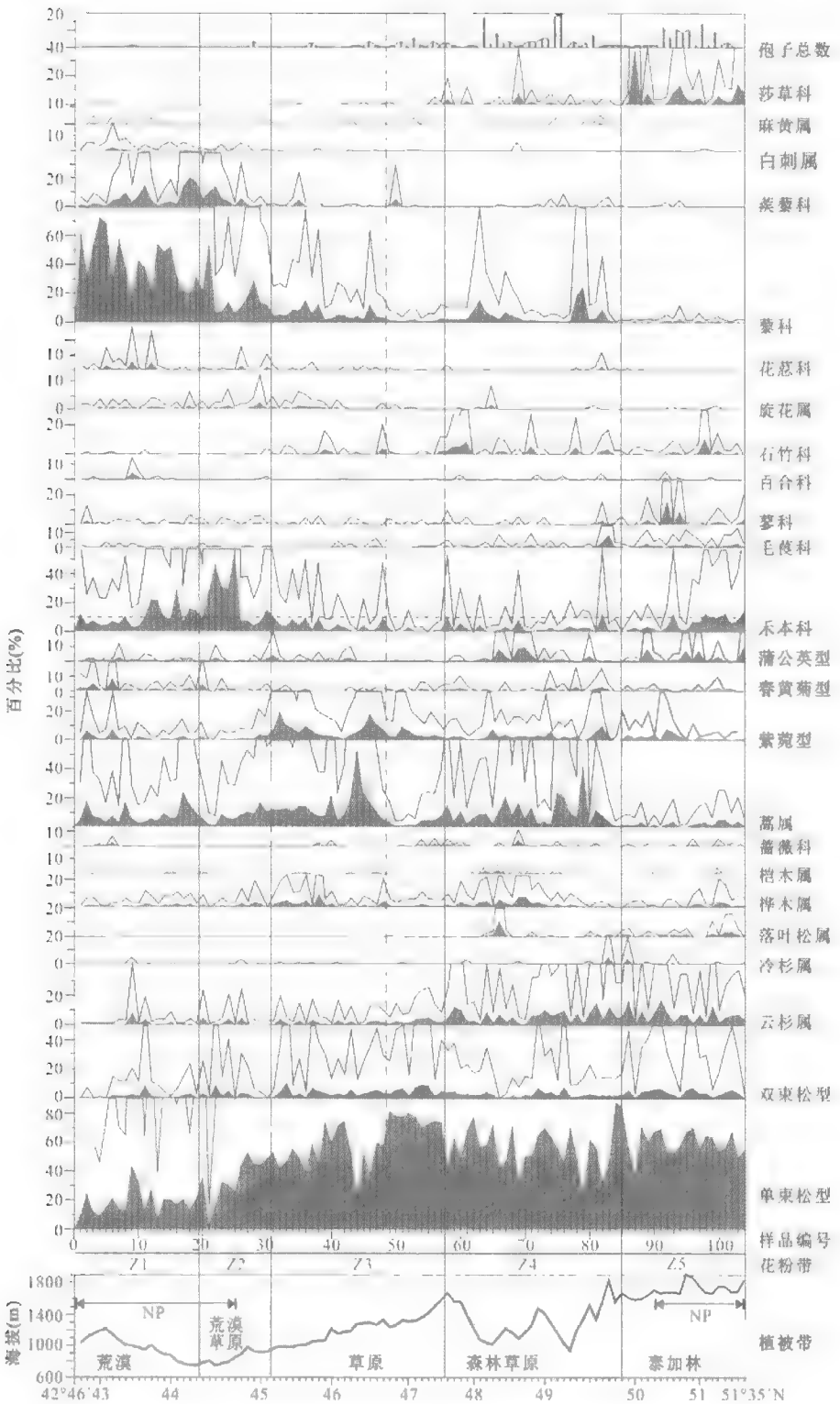

图1-3　蒙古国中东部南北横断面104个表土样品的花粉百分含量图(黑线:放大5倍)
最后图为沿横断面的植被带和海拔高度(NP:自然保护区)(Ma等,2008)

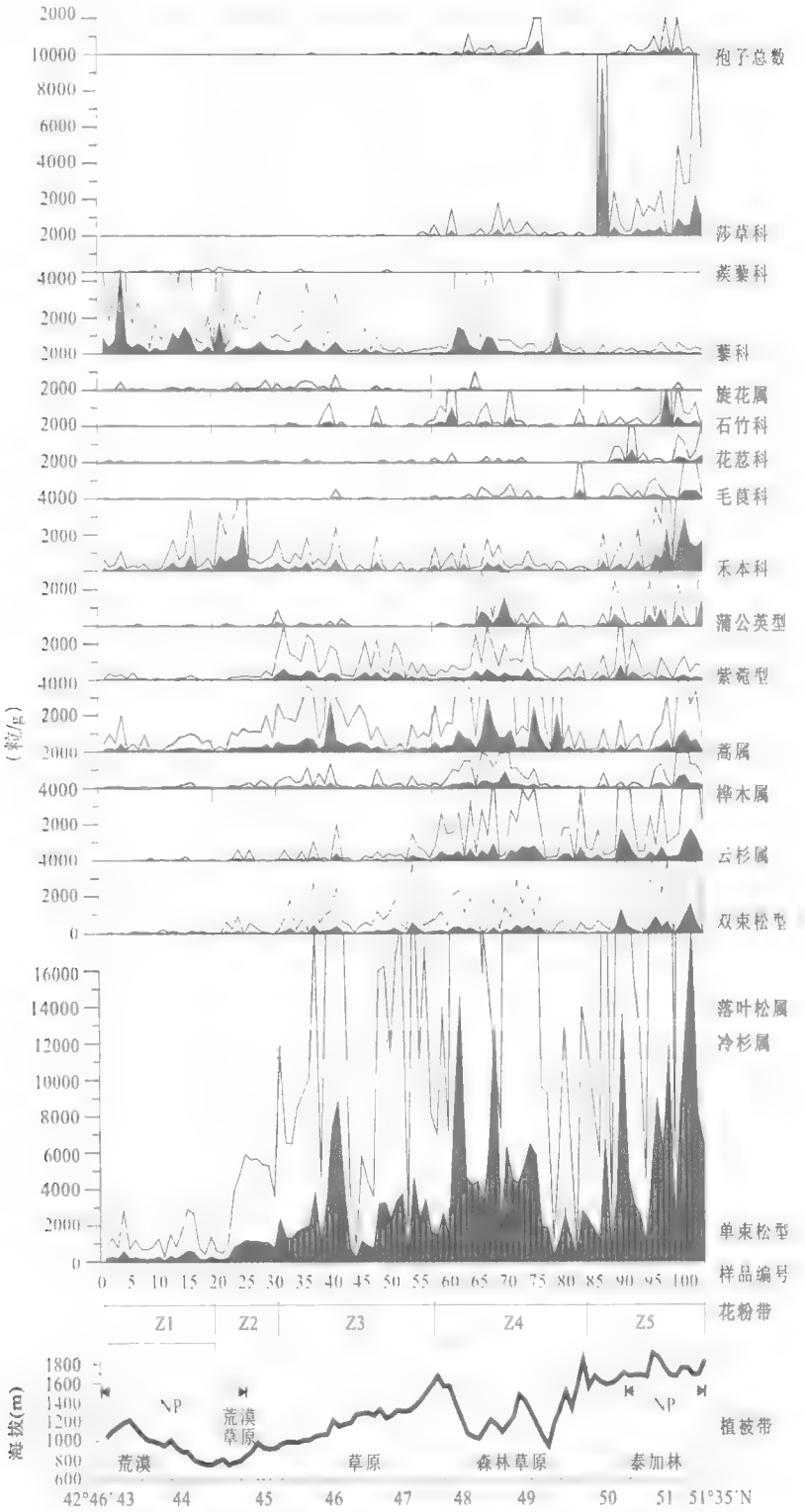

图1-4　蒙古国中东部南北横断面104个表土样点花粉浓度图(黑线:5倍放大)最后图显示沿横断面的植被带和海拔高度(NP:自然保护区)(Ma等,2008)

5.1.2. 带2(荒漠草原植被,样点20~30):禾本科—藜科花粉组合

荒漠草原的花粉组合特征是禾本科的百分比含量最高(7.03%~57.04%),其次为藜科(6.3%~22.18%)、蒿属(1.98%~10.61%)和蒺藜科(1.33%~10.07%),其他还有旋花属、白刺属、紫菀型、桦木属(<2.5%)和云杉属(<5%)。禾本科的花粉浓度相当高,而其他类型则很低。此外,在荒漠草原到荒漠的过渡区,藜科和蒺藜科的百分比含量有所增加。

5.1.3. 带3(草原植被,样点31~57):单束松型—蒿属—紫菀型-禾本科花粉组合

草原的花粉组合以单束松型(39.14%~78.44%)、蒿属(7.59%~23.57%)和紫菀型(0.91%~22.19%)百分含量较高,禾本科(1.08%~9.91%)、藜科和旋花属百分含量较低为特征。并含有少量的桦木属和云杉属。蒿属、紫菀型和旋花属的浓度较高,特别是在一些样品中(样点49~57)单束松型的百分含量非常高(71.70%~78.44%),但浓度非常低。而且,蒿属和禾本科的浓度也非常低。

5.1.4. 带4(森林草原,样点58~83):单束松型—云杉属—蒿属—桦木属花粉组合

森林草原的花粉组合(图1-3,图1-4)非常有特色,这是因为森林草原植被在生物地理学上的差异。在落叶松林附近(样点58~61,70~74,80~83),花粉组合中单束松型花粉百分含量较高(32.77%~70.16%),其次为云杉属(2.64%~15.32%)、蒿属(2.64%~15.53%)、禾本科(0.82%~12.26%)、石竹科(0.78%~8.16%)、桦木属(0.16%~7.32%)、蒲公英型和紫菀型。在河谷及其附近地带(样点62~65、68和77),花粉组合中单束松型百分含量非常高(56.98%~78.13%),其次为蒿属(2.82%~10.39%)、云杉属(0.57%~8.90%)、禾本科(0.52%~5.13%)、紫菀型(0.64%~8.53%)、藜科(1.30%~8.16%)、桦属(0.47%~4.19%)、蒲公英型、紫菀型、毛茛科、石竹科和莎草科。在距针叶林1~3km以外的高山草原区(样点66、67、69、75、76、78和79)的花粉组合中,单束松型花粉的百分含量较前两个地区有所减少(24.16%~56.31%),但蒿属(7.02%~23.92%)和藜科(0.53%~18.98%)的含量有所增加;其他还有云杉属(1.07%~7.55%)及桦木属(0.61%~7.21%)、禾本科(0.96%~8.41%)和紫菀型。

尽管如此,森林草原的花粉组合还是独具特色,即花粉组合主要由单束松型、云杉属、蒿属和桦木属组成,山地非禾本植物/灌木以及适中水分条件下的湿地植物(例如毛茛科、石竹科、蓼科和莎草科)也占有相当比例。蕨类植物孢子普遍存在,主要花粉类型的花粉浓度一般也比较高。

表1-2　用判别分析得到的24个花粉类型的标准化判别函数(Ma等,2008)

花粉类型	函数1	函数2	函数3	函数4
单束松型	1.460	4.683	0.452	2.094
双束松型	0.324	1.242	0.199	0.575
云杉属	0.486	0.286	0.355	0.371
冷杉属	-0.057	0.664	0.008	0.174
落叶松属	0.023	0.443	0.220	0.431

续表1-2

花粉类型	函数1	函数2	函数3	函数4
桦木属	0.366	0.847	-0.154	0.77
桤木属	0.038	-0.070	-0.156	-0.280
蔷薇科	0.185	-0.387	-0.096	0.068
蓼科	0.392	0.451	0.551	0.424
旋花属	-0.024	0.601	0.266	-0.131
禾本科	0.566	2.801	0.862	0.774
石竹科	0.243	0.102	-0.107	0.181
毛茛科	0.334	0.072	0.112	0.217
花葱科	0.347	0.692	0.504	-0.418
春黄菊型	0.230	0.389	0.139	-0.140
紫菀型	0.425	1.353	-0.383	0.662
蒲公英型	0.321	0.609	0.182	0.424
蒿属	0.950	2.387	0.132	0.780
藜科	-0.225	2.683	0.121	1.555
蒺藜科	-0.427	0.880	-0.086	0.480
门刺属	-0.756	0.131	0.177	0.358
麻黄属	-0.104	0.119	-0.274	0.071
百合科	-0.711	-0.148	-0.331	0.337
莎草科	0.667	1.657	0.553	1.157
贡献率百分比	75.40	15.40	5.70	3.50
变量累计百分比	75.40	90.80	96.50	100.00

5.1.5. 带5(针叶林,样点84~104):单束松型—云杉属—禾本科—莎草科花粉组合

泰加林花粉组合主要由单束松型(50.00%~84.72%),云杉属(2.21%~16.67%)和禾本科(1.10%~12.97%)组成,其他还有蒿属、紫菀型、蒲公英型、毛茛科、蓼科、石竹科、桦木属和蔷薇科。主要花粉类型的花粉浓度也非常高,对应于该区域有效湿度较高,花粉组合中山地非禾本植物/灌木(如毛茛科和石竹科),适中水分条件下的湿地植物(如莎草科和蓼科)的花粉含量也较高,蕨类植物也很丰富。值得注意的是,该森林群落的优势树种落叶松的花粉含量非常的低(<3%)。

5.2. 数值分析

5.2.1. 判别分析

判别分析的结果表明,判别函数1和2分别解释了数据集总方差的75.4%和15.4%(表

1–2）。在第一和第二判别函数轴（图1–5）上，5个组的几何中心明显相互分离。荒漠、荒漠草原和草原样品之间，及与其他植被类型的样品都可以很清楚地分开。然而，森林草原和泰加林的样品发生了一些重叠，森林草原和泰加林交错区的样品也反应出植被和孢粉谱的过渡性特征。判别分析，相似概率和植被指数的分类结果也显示出该过渡性特征（图1–6）。

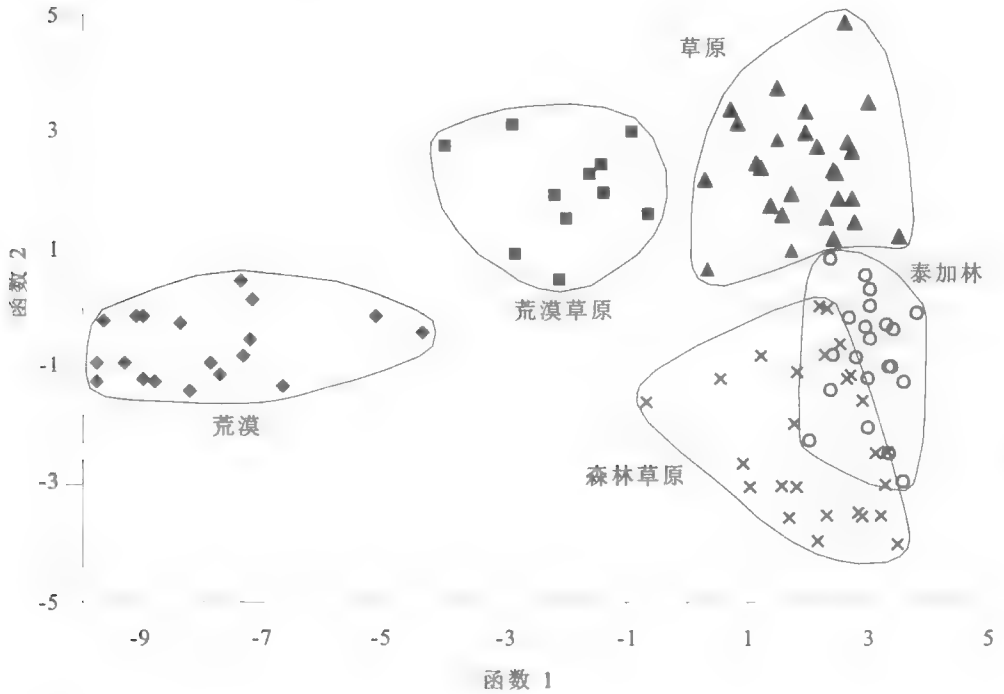

图1–5　104个表土样品沿判别分析第一函数轴和和第二函数轴的分类图（Ma等，2008）

观察样品所属预测植被类型（孢粉带）与先验组的对比表明97.1%的表土样品得到了正确分类（表1–3）。错误分类的样品相似概率一般非常低（<0.1），表明它们在特征上具有过渡性或者不同于所属组的其他成员（Liu和Lam，1985；Reese和Liu，2005）。例如，样点82和83位于森林草原和泰加林交错区，而样点12不同于花粉带1中其他样品。植被指数在植被间的边界地区一般会发生突然变化（图1–6）。

总之，判别分析的结果证实，5个植被带各自有着独特的孢粉学特征。正如5个花粉组合所表示的那样，除少数森林草原和泰加林的样品重叠外，大多数样品都与5个主要植被类型相匹配（图1–6）。统计分析也显示出在广阔的植被带内和群落交错带存在着小的非地带性植物群落。看来，数值方法在识别每个主要植被类型中的优势花粉类型及描绘过渡或独特样品时是非常有效的。

表1-3　判别分析对表土样品的分类结果表
显示97.1%的表土样品得到了正确划分(Ma等,2008)

分组	植被类型	样品号	预测观察样品所属植被类型荒漠				
			荒漠	荒漠草原	草原	森林草原	泰加林
原始	荒漠	19	19[a](100.0[b])	0(0.0)	0(0.0)	0(0.0)	0(0.0)
分组	荒漠草原	11	0(0.0)	11(100.0)	0(0.0)	0(0.0)	0(0.0)
	荒漠	27	0(0.0)	0(0.0)	27(100.0)	0(0.0)	0(0.0)
	森林草原	26	0(0.0)	0(0.0)	0(0.0)	25(96.2)	1(3.80)
	泰加林	21	0(0.0)	0(0.0)	0(0.0)	2(9.5)	19(90.5)

a判别分析分到组里的样品数;b正确分类的百分比

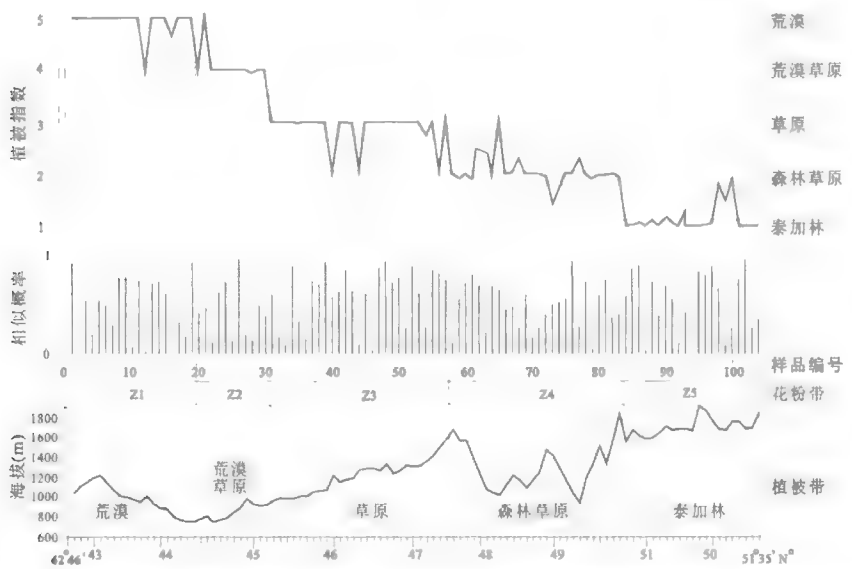

图1-6　104个表土样品的判别分析结果,显明了植被指数和相似概率值(Ma等,2008)

5.2.2. 层序聚类分析

图1-7显示了以树状图的形式呈现出的HCA结果。花粉类型沿左边纵轴排列。横轴表示群组之间重新标定的距离(SPSS Inc.,2001)。

HCA结果表明24个花粉类型可分为两个大组(A和B)(图1-7)。A组主要由山地乔木和非禾本草本/灌木植物组成,B组则由草本植物和灌木组成。在A组中,需要低温和较高湿度的山地针叶林和山地非禾本草本/灌木植物(单束松型、双束松型、冷杉属、云杉属、石竹科和毛茛科)为一个亚组(A1);正如落叶乔木/灌木和阳生植物(桦木属、桤木属、蔷薇科、蒲公英型和落叶松属)分为一亚组(A2)一样,适中水分条件下的湿生植物(莎草科和蓼科)被分为另一个亚组(A3)。B组可进一步分成4个亚组。B1亚组为草原中的非禾本草本植物/灌木(蒿属和紫菀型);B2亚组由花葱科、百合科和麻黄属组成;B3亚组为喜旱的荒漠非禾本草本植物/灌木(藜科、白刺属、蒺藜科和春黄菊型);B4亚组包括旋花属和禾本科

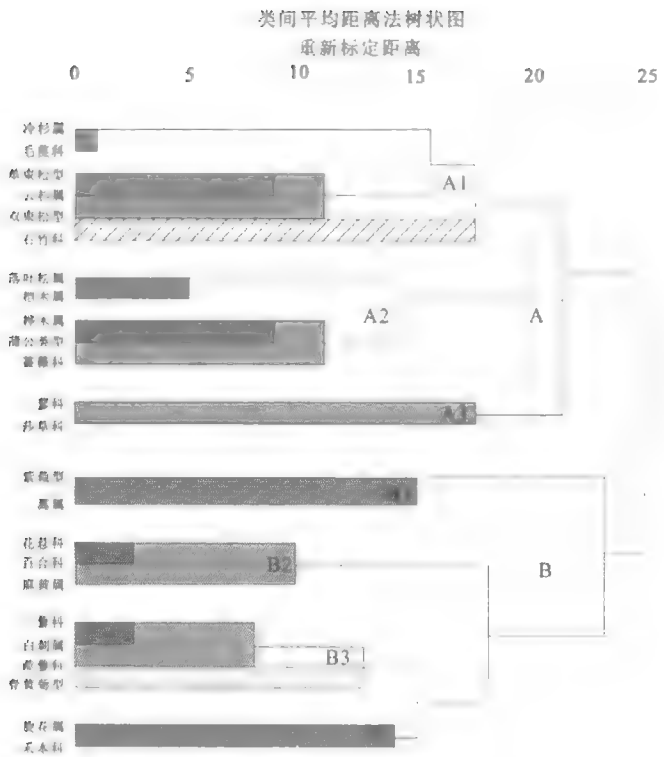

图1-7　24个花粉类型的层序聚类树状图(Ma等,2008)

菊科中的春黄菊型、蒲公英型、蒿属和紫菀型被聚类到三个不同的亚组中(图1-7)。春黄菊型与干旱类型一起聚类到亚组B3,蒲公英型与较喜湿类型聚类到亚组A2,蒿属和紫菀型聚类为亚组B1。这种分离似乎与它们所分布的小环境是一致的。这些亚组的孢粉学识别可为利用化石孢粉组合重建古环境打下有效的基础。

5.2.3. 非度量多维测度法

用NMS法对24个花粉种类进行了排序,结果以二维排序图表示(图1-8)。第一和第二轴的解译贡献率(variance explained)分别为74.2%和20.8%,这两轴的总解译贡献率共占95%,表明排序意义显著。有效性和可靠性评估显示,模型胁强系数(model stress)为12.7979,拟合效果较好(20为拟合较差;15为一般;5为好;2.5为优;0为完美);最终不稳定性/试验误差概率值(final instability)为0.00000887(< 0.00001),远远高于蒙特卡洛(Monte Carlo)检验预测值/显著水平(p=0.0196)。

在主要花粉类型的NMS排序图中,可以看出在第一排序轴中,藜科和藜科正值最高,云杉属和冷杉属负值最高。第一排序轴可能反映了温度梯度。山地森林乔木、山地非禾本草本植物/灌木和喜湿植物,如云杉属、冷杉属、松属、落叶松属、桦木属、桤木属、蔷薇科、毛茛科、石竹科、蒲公英型、莎草科和蓼科在第一轴中为负值;旱生荒漠非禾本草本植物/灌木和草原非禾本草本植物/灌木,例如藜科、白刺属、麻黄科、花葱科、禾本科、旋花属、春黄菊型、麻黄属、百合科和蒿属在第一轴中为正值。除了紫菀型,NMS和HCA结果一致。

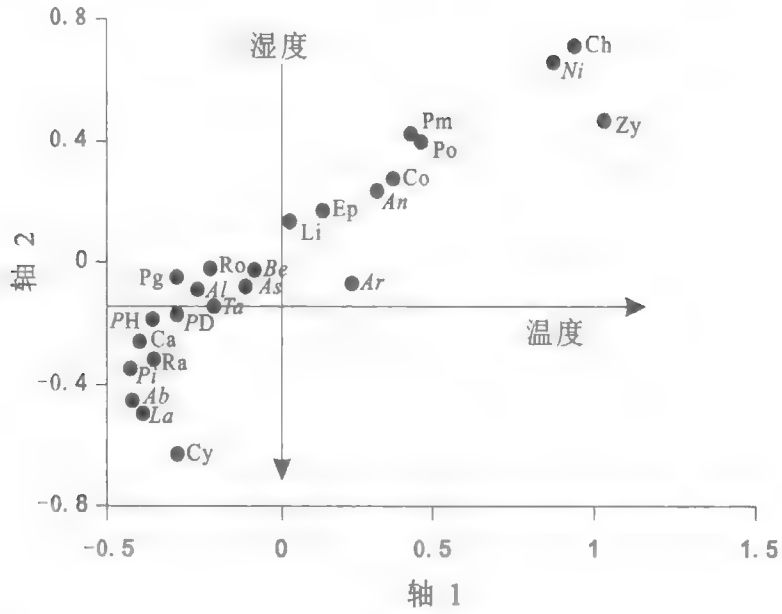

图1-8　24个花粉类型的非度量多维测度二维排序图(Ma等,2008)

其中:Ch.藜科;Ni.白刺属;Zy.蒺藜科;Pm.花葱科;Po.禾本科;Co.旋花属;An.春黄菊型;Ep.麻黄属;Li.百合科;Ar.蒿属;As.紫菀型;Be.桦木属;Ro.蔷薇科;Al.桤木属;Ta.蒲公英型;Pg.蓼科;Pi.云杉属;Ab.冷杉属;Ra.毛茛科;PD.双束松型;PH.单束松型;Ca.石竹科;La.落叶松属;Cy.莎草科

在NMS第二排序轴中,旱生植物(藜科和白刺属)正值最高,而湿生沼泽植物(莎草科)负值最高,第二排序轴可能反映了湿度梯度。图1-8也显示了桦林/灌木和冷湿针叶林的一个明显的分离,正如它们的现代地理分布一样,桦林/灌木生长所需的有效湿度似乎低于冷湿针叶林。

另外,沿对角线从右边的顶部到左角的底部,显示出一个从低海拔的荒漠(藜科和白刺属)到高山针叶林(落叶松属、冷杉属和云杉属)的排序,明确地反映了一个海拔逐渐上升的梯度。

6. 讨论

影响表土花粉与植被关系的因素很多,包括花粉产量和传播机制等。和其他地区一样,在蒙古国,我们也需要依据这些因素和过程来理解花粉与植被的复杂关系。

6.1. 花粉组合和植被

花粉带1最显著的特征是藜科百分含量最高而单束松型百分含量最低。旱生荒漠非禾本草本植物/灌木类型(藜科、蒺藜科和白刺属)的高含量表明这些花粉类型来源于当地植被,即荒漠。尽管荒漠中没有松树生长,单束松型花粉仍以较低的百分含量出现,这可能是松属花粉长距离传播的结果。

花粉带2的样品采自荒漠草原,在花粉组合中禾本科和单束松型的含量较高,其次为藜科、蒿属和蒺藜科。我们的样品中禾本科百分含量相当高(达到60%),与其他一些研究

结果形成鲜明对比。最近的研究表明，尽管在植被中禾本科植物发育较好，但中国荒漠草原的花粉组合仍以藜科和蒿属花粉为主（李月丛等，2005；Liu等，2006）。我们样品（样点21~25）中禾本科花粉含量丰富，可能源于这些样品采自自然保护区，在这里自然植被得到了很好的保护。相比之下，自然保护区以外的样品中禾本科花粉百分含量就相对较低，在那里植被受到了人类活动的干扰。值得注意的是，前人在中国荒漠草原研究中使用的大多数样品也来自受人类活动干扰的地区。

花粉带3中的样品采自蒿属—针茅属禾草草原，这里由于放牧，自然植被已经受到干扰。该带花粉组合以单束松型、蒿属和紫菀型的百分含量和浓度高为特征，但是禾本科百分含量较低。另一个有趣的现象是，在一些样品（样点49~57）中单束松型的百分含量非常高，而这些样品是在蒙古国首都（乌兰巴托）附近采集的，这里大部分草原已经转化成牧场。一些研究者认为禾草草原中蒿属花粉含量比禾本科更高，因为禾本科花粉代表性低，这就意味着草原孢粉组合以蒿属为主（Liu等，1999）。然而，Liu等的表土样品是在过度放牧的草原中采集的，而那里植物在开花前已经被食草动物有选择地吃掉了（禾本科柔嫩的叶片显然比有味道的蒿属受欢迎），因此，这些草原样品中蒿属的超代表性可能是人为干扰的结果。根据我们来自自然保护区内外的数据，我们认为在人类干扰较大的草原中，现代花粉谱中禾本科的含量趋于受到抑制。由此推论，花粉带3中单束松型花粉的高百分比含量很可能是人为干扰的结果（过度放牧）。

花粉带4（森林草原组）的花粉组合包含了三个子类型，反映了该区植被镶嵌式分布的特征（见图1-3、图1-4、图1-6）。该组合以单束松型、云杉属、蒿属和桦木属百分含量高为特征，但偶尔山地非禾本草本植物/灌木和蕨类植物在一些样品中含量也较高。主要花粉类型的浓度也较高。

在花粉带5（即针叶林组），值得注意的是，即使在以落叶松为主的泰加林，落叶松花粉的含量也非常低（样点102的含量最高，也仅为3.23%）。花粉组合中占主导地位的是单束松型、云杉属、禾本科、和莎草科，及一定量的山地非禾本草本植物/灌木、湿地植物和蕨类植物。

总之，我们的研究显示，蒙古国南北断面5个植被带都有着各自的现代花粉组合特征。在荒漠带，旱生荒漠类型（藜科、蒺藜科和白刺属）的花粉最为丰富，而荒漠草原中禾本科比较丰富。草原以蒿属和紫菀型百分含量高为特征，而禾草减少可能是过度放牧的结果。森林草原和泰加林中单束松型和云杉属花粉百分含量都很高，但在森林草原样点中，非禾本草本植物（蒿属和紫菀型）和温带夏季常绿树（桦木属和桤木属）的含量较高；而在泰加林样点中，山地非禾本草本植物/灌木和禾本植物的花粉（禾本科和莎草科）的含量较高。

6.2. 花粉传播和代表性

花粉的传播是现代花粉谱中影响各类花粉代表性的重要因素。本章选择了10种重要的类型来讨论其传播模式和代表性。

6.2.1. 松属

现今生长在蒙古国的松树有3个种：偃松(*Pinus pumila*)、西伯利亚松(*P. sibirica*)和欧洲赤松。其中，欧洲赤松产双束松型花粉，其他两种(偃松、西伯利亚松)产单束松型花粉。偃松和西伯利亚松生长在杭爱和肯特山以及库苏古尔湖流域。欧洲赤松则广泛分布在鄂尔浑、色楞格和鄂嫩河沿岸沙地阶地上(Hilbig, 1995)。

除了荒漠以外，在现代花粉谱中，松属花粉的含量在所有植被带都很丰富。松属花粉的百分含量在荒漠植被最低，而在过度放牧区的草原最高，在那里草原已变成了牧场。牧区松属花粉百分含量高的原因可能是两种因素叠加的结果，即森林草原带松属花粉的远距离传播和过度放牧导致的当地植物花粉产量下降。泰加林中松属花粉的百分含量和浓度都很高可能反映了泰加林中有松树生长，甚至比较繁茂。森林草原中松属花粉的百分含量和浓度较高，这些花粉就来自于当地在山地北坡和高海拔地区广泛发育的松林(见图1-3，图1-4)。荒漠和荒漠草原中松属花粉的百分含量和浓度最低，但即使是在这些没有松树存在的地区，有时松属花粉仍可占10%~50%，这可能是松属花粉可被风长距离传播的结果。尽管如此，花粉浓度可以进一步帮助解译，如草原带松属花粉浓度低，在森林草原中较高，在泰加林中最高。

一般来说，如果松属花粉含量小于50%的话，当地可能没有松树林存在。前人的研究显示，在花粉谱中松属花粉传播性好，具超代表性(如李文漪，1998；李文漪和姚祖驹，1993)，这与我们的结论相吻合。所以，在利用化石花粉数据进行古植被重建时，必须考虑到松属花粉的浓度。

6.2.2. 云杉属

在荒漠、荒漠草原和草原带，云杉属花粉零星出现，且含量小于5%。从森林草原(样点58)向北，云杉属花粉开始增加。在森林草原和泰加林中，云杉属花粉的高百分含量与这些地区云杉的良好发育相呼应。的确，云杉花粉的传播距离与松属花粉相比，十分有限。

6.2.3. 落叶松属

尽管落叶松是现代森林草原和泰加林中最常见的乔木，但其花粉丰度却非常低。许多研究表明落叶松属花粉具有低代表性且百分含量波动剧烈(Igarashi, 1996; Noshiro等1997; Minckley和Whitlock, 2000; Andreev等, 2001)。落叶松属花粉生产力很低且很难传播。在落叶松林中其花粉百分含量略微增加(5%~10%)，而落叶松林以外的地区，落叶松属花粉百分含量急剧下降，几乎为零(Noshiro等, 1997; Minckley和Whitlock, 2000)。Gunin等(1999)认为落叶松属花粉的传播距离一般小于200~300m，而且花粉易被水破坏。Andreev等(2001)指出，即使在落叶松林表土样品中，落叶松属花粉也相当稀少，正如东西伯利亚许多地区落叶松林的表土样品所证实的那样，在花粉谱中落叶松属花粉的低含量不能反映其真实的生长量。不少研究进一步指出，在化石孢粉谱中，落叶松属花粉含量虽低但连续存在，表明在样点附近有落叶松生长(Noshiro等, 1997; Gunin等, 1999; Minckley和Whitlock, 2000; Andreev等, 2001)。另外，贝加尔湖地区的表土样品也记录到落叶松属花粉具有普遍的低代表性(Kataoka等, 2003)。

6.2.4. 禾本科

从生态学的角度看，禾本科在荒漠、荒漠草原和泰加林中的发育程度低于草原和森林草原，但在我们的研究区中，荒漠、荒漠草原和泰加林中禾本科花粉百分含量高于草原和森林草原　这种现象的原因可能是荒漠、荒漠草原和泰加林都位于自然保护区，在自然植被样品中记录了禾本科真实的丰富度（可被高花粉浓度所证实）　相比之下，在草原和森林草原地区，由于牲畜有选择地以禾本科为食，样品的代表性已受到人类活动干扰

许多研究者发现，由于禾本科花粉的低代表性，在大多数样品中，其花粉百分含量一般低于5%，因而即使禾本科花粉百分含量很低（3%~10%），也可能表明发育有以禾草为优势种的草原植被（黄赐旋等，1993；王烽瑜等，1996；李文漪，1998；Liu等，1999；李月从等，2005）　然而，我们的数据显示，尽管由于禾本科花粉生产力低而导致其低代表性，但在自然植被保护较好的地区，禾本科花粉也可能达到较高的百分含量（大约10%~40%）

6.2.5. 桦木属、藜科、蒿属和紫菀型

除了森林草原以外，在所有植被带中都发现了桦木属花粉，百分含量为1%~8%　其广泛的分布指示其具有很好的传播性　藜科花粉在所有样品中都有发现，而且在荒漠、荒漠草原、草原和森林草原中特别丰富　因此，藜科花粉可能具有超代表性　蒿属花粉不仅存在于所有样品中，而且在大多数样品中都很丰富　无独有偶，紫菀型也存在于所有样品中　相对于它们在植被中的丰度，蒿属和紫菀型花粉可能具有超代表性

6.2.6. 莎草科和蔓藜科

莎草科花粉仅在森林草原和泰加林中发现，而蔓藜科花粉也仅在荒漠和荒漠草原中被观测到　这些花粉类型的出现区与它们母体的分布完全一致

为了定量重建古气候参数，已发展和验证了一些方法，如花粉—气候响应面分析和转换函数　然而，由于蒙古国现代气象站点和气候数据稀少，这些方法在该区不能得到有效的应用　花粉类型间的比值作为环境指标得到了有效的应用，并常常帮助识别环境变化趋势，而这种趋势仅用花粉百分含量和浓度很难被发现　如，Liu等（2005，2007）在南美洲阿尔蒂普拉诺高原（Altiplano）用禾本科/菊科（Poaceae/Asteraceae，P/A）花粉比值作为一种有效的湿度指标　同样，在中东（El-Moslimany，1990）和中亚（如，Van Campo等，1996；Liu等，1998；Demske和Mischke，2003；Herzschuh等，2004），蒿/藜（A/C）也作为一种湿度指标被广泛使用　Yu等（1998）和Cour等（1999）的研究认为中国干旱区A/C值小于0.5　Fowell等（2003）提出将荒漠草原（蒿属—藜科）与草原花粉类型（禾本科）的比值表示为一种半定量的“干旱花粉指数”，以便在蒙古国北部地区从草甸草原和森林草原中识别出干草原

如上所述，除一些被过度放牧干扰的地区外，荒漠、荒漠草原、草原、森林草原和泰加林中禾本科植物在非地带性植物群落中本可以很丰富　但是，由于在这些干旱半干旱环境中，禾本科花粉含量可能受到人类活动干扰而被扭曲，因此，荒漠草原（蒿属—藜科）与草原（禾本科）的比值作为“干旱花粉指数”对于古气候的重建可能不是非常有效　近年来

对阿拉善高原植被分析的结果(Herzschuh等,2004)也支持我们的认识。

根据我们获得的该区的现代花粉数据，本章建议了两个新的花粉—气候指数（表1-4），即湿度—指数(M)和温度—指数(T)。这两个指数是根据花粉类型组的比值计算得出的，这些花粉类型组指示了研究区不同的温度或者湿度条件。主要依据HCA(图1-7)和NMS(图1-8)的结果，将对气候敏感花粉类型组进行了分类，并参考从野外观察的生态环境条件和考虑特定类型花粉的代表性(如前面已讨论的禾本科)，对组中某些成分进行了微小的修正。

表1-4　组、类型、主要花粉类型和计算花粉—温度(T)和花粉—湿度指数(M)的算式(Ma等,2008)

组	类　型	主要花粉类型
S1	旱生荒漠	藜科,白刺属,蒺藜科
S2	荒漠—草原	花蒿科,春黄菊型,麻黄,百合科,旋花属
S3	中—旱生型草原	蒿属,紫菀型
S4	桦林/灌丛	桦木属,桤木属,蔷薇科,蒲公英型
S5	冷湿针叶林	云杉属,冷杉属,落叶松属,单束松型,双束松型,毛茛科,石竹科
S6	适中水分条件下的草原	莎草科,蓼科
	花粉气候指数	算式
T	温度指数	$T=(P_{S1}+P_{S2}+P_{S3})/(P_{S4}+P_{S5}+P_{S6})$
M	湿度指数	$(P_{S5}+P_{S6})/(P_{S1}+P_{S2}+P_{S3}+P_{S4})$

参考6种主要植物群落的生态特征，我们将主要花粉类型分成了六组(表1-4)。S1组包括藜科、白刺属和蒺藜科，是旱生荒漠的主要成分。S2组包含花蒿科、旋花属、春黄菊型、麻黄属和百合科，它们在荒漠草原中普遍存在。S3组包括蒿属和紫菀型，是中等旱生草原的代表植物。除了禾本科之外，这三组基本由HCA聚类的组B1到B4亚组的花粉类型所组成(图1-7,图1-8)，并与NMS排序基本一致。正如前面所讨论的，由于禾本科花粉的丰度受到了人类活动的干扰，因此禾本科被排除到所有组之外。S4到S6组分别代表冷湿针叶林、山地非禾草草原、桦林/灌木林和适中水分条件下的草原。这三个组包括的13个花粉类型，与由HCA聚类到A1、A2和A3亚组的类型一致，并与NMS排序相吻合(图1-7,图1-8)。

6.3.1. 温度指数

温度指数(T)的算式如下：

$$T=(P_{S1}+P_{S2}+P_{S3})/(P_{S4}+P_{S5}+P_{S6})$$

温度指数的基本原理是基于HCA和NMS的分析结果，HCA和NMS将花粉组合分成两个主要组。如上所述，上式中用到的花粉组S4~S6等于HCA描绘出的A1~A3,S1~S3来自B1~B4。因此，两组花粉百分含量(P)之间的比值可以作为一种温度指数——比值越高，表明温度越高。

6.3.2. 湿度指数

湿度指数(M)是由S1、S2、S3和S4组与S5和S6组的花粉百分含量(P)比值计算得出，算式如下：

$$M=(P_{S5}+P_{S6})/(P_{S1}+P_{S2}+P_{S3}+P_{S4})$$

湿度指数的基本原理是基于HCA和NMS的分析结果、现代生物地理学特征和野外植被分布观察。旱生荒漠、荒漠草原和中等旱生草原植被类型(S1,S2和S3)主要分布在海拔较低、温度较高的地区和研究区的南部(相对湿度较低)。主要生长在山地阳坡(南坡)的桦林/灌木(S4)，与蒙古的针叶林(S5)和适中水分条件下的草原(S6)相比较，则需要更低的湿度。

为了验证这两个新指数的有效性，我们计算了所有表土样品中每个花粉组(S1~S6)的花粉百分含量，并沿横断面标绘出所有样品的值来检测它们的区域差值(图1-9a~f)。同样，沿横断面也绘出了温度指数和湿度指数的曲线。显然，湿度指数在泰加林中最高，森林草原和草原中适中，荒漠草原和荒漠中最低(图1-9i)，而温度指数则在荒漠和荒漠草原中最高，草原和森林草原有所下降，泰加林中最低(图1-9h)。作为湿度指数的补充，沿着这一横断面我们又绘出了A/C值(Artemisia/Chenopodiaceae)变化曲线，这条曲线与我们的湿度指数曲线基本平行(图1-9g)。为了将花粉—气候指数与实际气候数据进行对比，我们从蒙古气候图中提取了年平均降水(MAP)和年均温(MAT)数据(Orshikh等，1990)，并沿着横断面绘制出平均降水(MAP)和年均温(MAT)(图1-9j,k)。

我们的湿度和温度指数的变化趋势很好地模拟了蒙古国中东部的降水和温度变化梯度。例如，降水从荒漠草原到草原稳定增长、在森林草原(样点72~75)达到峰值和在泰加林地区降水量最大都可以从湿度指数曲线获得(见图1-9i,k箭头)。同样，从南向北穿过草原地带，温度逐渐下降，而在森林草原和泰加林的群落过渡区，温度急速下降，温度指数曲线也有很好的对应(图1-9h,j)。

7. 总结和结论

本章展现了沿蒙古南北断面采集的104个表土样品的现代花粉谱。该断面横跨五个主要的植被，分别为荒漠、荒漠草原、草原、森林草原和泰加林。随着纬度升高，温度逐渐下降，降水逐渐增加，环境变化梯度显著。104个现代花粉谱表明每个植被带都有独特的花粉组合特征，具体如下：1.荒漠带：藜科—蒿藜科—白刺属—禾本科花粉组合；2)荒漠草原带：禾本科—单束松型—藜科花粉组合；3.草原带：单束松型—蒿属—紫菀型—禾本科花粉组合；4.森林草原带：单束松型—云杉属—蒿属—桦木属、山地非禾本草本植物/灌木花粉—蕨类孢子组合；5.山地泰加林地区：单束松型—云杉属—禾本科—莎草科、山地非禾本草本植物/灌木花粉—蕨类孢子组合。HCA将24种主要花粉类型分成了2个大组和7个亚组。两个大组中，组1主要包含荒漠和草原植被的旱生植物，而组2包括山地环境下的中生乔木、灌木和草本植物。判别分析将95.2%的表土样品正确地分到它们各自的先验组中，确认每个主要植被带均可被特有的孢粉谱定量的表示出来，从而为研究区基于化石

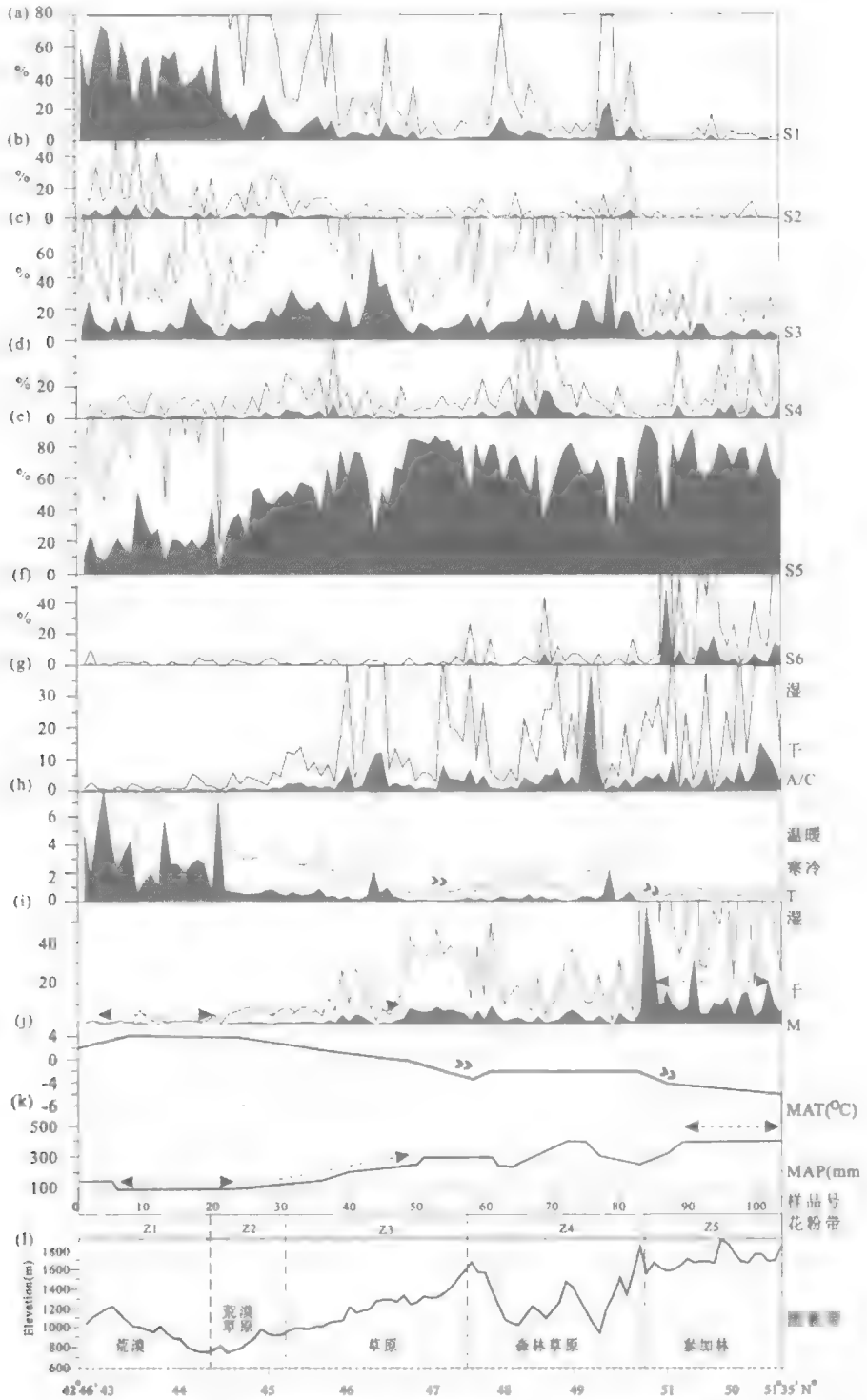

图1–9　用于计算花粉—气候指数的6个花粉组(S1~S6)的花粉百分含量(a~f);A/C值(g);温度指数,T(h);湿度指数,M(i);蒙古沿南北断面104表土样品的年平均温度[MAT(j)]、年平均降水[MAP(k)]和海拔(l)。黑线:放大5倍。(h),(i),(j),(k)中的虚线的单双箭头表示了花粉指数曲线(T和M)与相应的气候梯度(MAT和MAP)的类似趋势。MAP(mm)和MAT(℃)数据来自Orshikh等,(1990)

花粉组合进行古植被和古气候重建提供了依据

本章进一步阐述了在中亚干旱半干旱区中一些主要花粉的传播和代表性。在现代花粉谱中，松属花粉具有超代表性，如果在样品中松属花粉含量低于50%，特别是其花粉浓度较低时，样品所在的区域可能没有松树生长。在云杉林分布以外的地区，云杉属花粉可能具有微弱的超代表性，这归因于其囊状结构使其具有远距离传播的能力。相比之下，落叶松属具有非常低的代表性，即使在落叶松普遍存在的山地泰加林，其花粉含量也很低，仅大于3%。研究中一个有趣的发现是，与其他地区相比，在自然保护区的样品中，禾本科花粉百分含量较高。以往的孢粉文献记录的半干旱草原和草地的现代花粉谱中禾本科的超低代表性现象很可能是人类干扰所致。过度放牧使得禾本科植物开花的机会和数量显著下降，并降低了其花粉产量，从而导致了非禾本草原植物（如蒿属）花粉代表性过高。

根据研究区现代花粉数据建立的花粉—植被定量关系，我们还建议了两个能反映蒙古国降水和温度条件的花粉—气候指数。温度指数是根据10种花粉类型和13种花粉类型的百分含量比值计算得出的，其中的10种花粉类型是旱生荒漠和中旱生草原的特征分子，13种花粉类型是山地森林和草原的特征分子。湿度指数是根据14种花粉类型和9种花粉类型的百分含量比值得出的，其中的14种花粉类型是低地、温暖和阳生环境的特征分子，9种花粉类型是山地针叶林和适中水分条件下草原的特征分子。湿度指数（M）和温度指数（T）计算出的蒙古南北断面的温度和湿度变化趋势与从蒙古国现代气候图上提取的南北向的温度和降水变化梯度的对比分析表明，湿度和温度指数能够很好地模拟研究区域内的降水和温度变化梯度，因而，花粉—气候指数M和T可用于该区基于化石花粉数据的古气候重建。

致谢：廖淦标（Kam-biu Liu）教授在文章写作过程中给予指导和建议；李心清教授和汪卫国博士参加了野外工作；蒙红卫、桑艳礼和郭超博士参与了数据整理和绘图工作；蒙古国地质研究所的同事在野外考察的后勤方面提供了帮助。

参考文献

李文漪. 1998. 中国第四纪植被与环境. 北京：科学出版社.

李文漪，姚祖驹. 1993. 中国北、中亚热带晚第四纪植被与环境研究. 北京：海洋出版社.

李月丛，徐清海，阳小兰. 2005. 中国草原区主要群落类型花粉组合特征. 生态学报，25(3)：555~564.

黄赐旋，艾利斯·冯·康波，让·弗朗索瓦士·多布雷梅. 1993. 西藏西部表土花粉研究. 干旱区地理，16(4)：75~83.

苑涛，卫智军，杨静，赵晟，燕玲，张恩厚. 1999. 内蒙古草地现代植物花粉形态. 北京：中国农业出版社.

王伏雄，钱南芬，张玉龙，杨惠秋. 1995. 中国植物花粉形态. 第二版. 北京：科学出版社.

王璞瑜，宋长青，孙湘君. 1996. 内蒙古中部表土花粉研究. 植物学报，38(11)：902~909.

尤纳托夫. 1959. 蒙古人民共和国植被的基本特征. 北京：科学出版社.

Andreev, A.A., Klimanov, V.A. and Sulerzhitsky, L.D., 2001. Vegetation and climate history of the Yana

River lowland, Russia, during the last 6400 yr. Quaternary Science Reviews, 20: 259~266.

Birks, H.J.B., 1973. Modern pollen rain studies in some Arctic and Alpine environments. Quaternary plant ecology (ed. By H.J.B. Birks and R.G. West), pp. 143~168. Blackwell, Oxford.

Boucher, T.V. and Mead, B.R., 2006. Vegetation change and forest regeneration on the Kenai Peninsula, Alaska following a spruce beetle outbreak, 1987~2000. Forest Ecology and Management, 227: 233~246.

Clarke, K.R., 1993. Non-parametric multivariate analyses of changes in community structure. Australian Journal of Ecology, 18:117~143.

Cour, P., Zheng, Z., Duzer, D., Calleja, M. and Yao, Z., 1999. Vegetational and climatic significance of modern pollen rain in northwestern Tibet. Review of Palaeobotany and Palynology, 104: 183~204.

Demske, D. and Mischke, S., 2003. Palynological investigation of a Holocene profile section from the Palaeo- Gaxun-Nur- Basin. Chinese Science Bulletin, 48(14): 1418~1422.

Dorofeyuk, N.I. and Tarasov, P.E., 1998. Vegetation and lake levels of northern Mongolia since 12 500 yr B.P. based on the pollen and diatom records. Stratigraphy, Geological Correlation, 6: 70~83.

El-Moslimany, A.P., 1990. Ecological significance of common nonarboreal pollen: examples from drylands of the Middle East. Review of Palaeobotany and Palynology, 64: 343~350.

Enright, N.J., Miller, B.P. and Akhter, R., 2005. Desert vegetation and vegetation–environment relationships in Kirthar National Park, Sindh, Pakistan. Journal of Arid Environments, 61: 397~418.

Fowell, S.J.B., Hansen, C.S., Peck, J.A., Khosbayar, P. and Ganbold, E., 2003. Mid to late Holocene climate evolution of the Lake Telmen Basin, North Central Mongolia, based on palynological data. Quaternary Research, 59:353~363.

Graf, M.T. and Chmura, G.L., 2006. Development of modern analogues for natural, mowed and grazed grasslands using pollen assemblages and coprophilous fungi. Review of Palaeobotany and Palynology, 141: 139~149.

Gunin, P.D., Vostokova, E.A., Dorofeyuk, N.I., Tarasov, P.E. and Black, C.C., 1999. Vegetation dynamics of Mongolia. Geobotany 26, pp. 233~238. Kluwer Academic, Boston, MA.

Herzschuh, U., Tarasov, P., Wunnemann, B. and Hartmann, K., 2004. Holocene vegetation and climate of the Alashan Plateau, NW China, reconstructed from pollen data. Palaeogeography, Palaeoclimatology, Palaeoecology, 211: 1~17.

Hilbig, W., 1987. Changes in segetal vegetation under conditions of industrialized agriculture. Archiv fu¨r Naturschutz und Landschaftsforschung, 27: 229~249.

Hilbig, W., 1995. The vegetation of Mongolia. SPB Academic Publishing, Amsterdam.

Igarashi, Y., 1996. A Lateglacial climatic reversion in Hokkaido, Northeast Asia, inferred from the Larix pollen record. Quaternary Science Reviews, 15: 989~995.

Kataoka, H., Takahara, H., Krivonogov, S.K., Bezrukova, E.V., Orlova, L., Kropivina, S., Miyoshi, N. and Kawamuro, K., 2003. Pollen record from the Chivyrkui Bay Outcrop on the Eastern Shore of Lake Baikal since the Late Glacial. In: Kashiwaya, K. (eds.), Long continental record from Lake Baikal, 207~218. Springer-Verlag, Tokyo.

Lavrenko, E.M. and Karamisheva, Z.V. (eds.), 1990. Vegetation map of Mongolian People's Republic. 1: 3 000 000. In: Orshikh, N., Morgunova N.A. and Rodionov, M.N. (eds.), National atlas of the Mongolian People's

Republic, 72~73. Ulanbator, Moscow (in Russian).

Lavrenko, E.M., Iunatov, A.A., Aleksandr, A. and Dashniam, B., 1979. Vegetation map of Mongolian People's Republic (scale1: 1 500 000). GUGK, Moscow (in Russian).

Liu, H.Y., Cui, H., Pott, R. and Speier, M., 1999. Surface pollen of the woodland–steppe ecotone in southeastern Inner Mongolia, China. Review of Palaeobotany and Palynology, 105: 237~250.

Liu, H.Y., Wang, Y., Tian, Y.H., Zhu, J.L. and Wang, H.Y., 2006. Climatic and anthropogenic control of surface pollen assemblages in East Asian steppes. Review of Palaeobotany and Palynology, 138: 281~289.

Liu, K.–b., 1990. Holocene paleoecology of the boreal forest and Great Lakes~St. Lawrence forest on northern Ontario. Ecological Monographs, 60: 179~212.

Liu, K.–b. and Lam, S.–N.N., 1985. Paleovegetational reconstruction based on modern and fossil pollen data: an application of discriminant analysis. Annals of the Association of American Geographers, 17: 115~130.

Liu, K.–b., Yao, Z. and Thompson, L.G., 1998. A pollen record of Holocene climatic changes from the Dunde ice cap, Qinghai–Tibetan Plateau. Geology, 26: 135~138.

Liu, K.–b., Reese, C.A. and Thompson, L.G., 2005. Ice–core pollen record of climatic changes in the central Andes during the last 400 years. Quaternary Research, 64: 272~278.

Liu, K.–b., Reese, C.A. and Thompson, L.G., 2007. A potential pollen proxy for ENSO derived from the Sajama ice core. Geophysical Research Letters, 34, L09504, doi:10.1029/2006GL029018.

Lynch, E.A., 1996. The ability of pollen from small lakes and ponds to sense fine–scale vegetation patterns in the Central Rocky Mountains, USA. Review of Palaeobotany and Palynology, 94: 197~210.

Ma, Y.Z., Liu, K.–b., Feng, Z.D., Sang, Y.L., Wang, W. and Sun, A.Z., 2008. A survey of modern pollen and vegetation along a south–north transect in Mongolia. Journal of Biogeography, 35: 1512~1532.

Markgraf, V., DeAntoni, H.L. and Ager, T.A., 1981. Modern pollen dispersal in Argentina. Palynology, 5: 43~63.

McCune, B. and Grace, J.G., 2002. Analysis of ecological communities. MjM Software Design, Gleneden Beach, OR.

Minckley, T. and Whitlock, C., 2000. Spatial variation of modern pollen in Oregon and southern Washington, USA. Review of Palaeobotany and Palynology, 112: 97~123.

Moore, P.D., Webb, J.A. and Collinson, M.E., 1991. Pollen analysis. Blackwell Scientific Publications, Oxford.

Noshiro, S., Terada, K., Tsuji, S. and Suzuki, M., 1997.Larix~Picea forests of the Last Glacial Age on the eastern slope of Towada Volcano in northern Japan. Review of Palaeobotany and Palynology, 98: 207~222.

Orshikh, N., Morgunova, N.A. and Rodionov, M.N. (eds), 1990. The national atlas of the Mongolian People's Republic. Ulanbator~Moscow, Moscow (in Russian).

Reese, C.A. and Liu, K.–b., 2005. A modern pollen rain study from the central Anders region of South America. Journal of Biogeography, 32: 709~718.

Soh, M.C.K., Sodhi, N.S. and Lim, S.L.H., 2006. High sensitivity of montane bird communities to habitat disturbance in peninsular Malaysia. Biological conservation, 129, 149~166.

SPSS Inc. 2001. SPSS base 11.0 for Windows user's guide. SPSS Inc, Chicago.

Sugden, J.M. and Meadows, M.E., 1989. The use of multiple discriminant analysis in reconstructing recent vegetation changes on the Nuweveldberg, South Africa. Review of Palaeobotany and Palynology, 60: 131~147.

Tarasov, P.E., Webb, T., III, Andreev, A.A., Afanas'eva, N.B., Berezina, N.A., Bezusko, L.G., Blyakharchuk, T.A., Bolikhovskaya, N.S., Cheddadi, R., Chernavskaya, M.M., Chernova, G.M., Dorofeyuk, N. I., Dirksen, V.G., Elina, G.A., Filimonova, L.V., Glebov, F.Z., Guiot, J., Gunova, V.S., Harrison, S.P., Jolly, D., Khomutova, V.I., Kvavadze, E.V., Osipova, I.M., Panova, N.K., Prentice, I.C., Saarse, L., Sevastyanov, D.V., Volkova, V.S. and Zernitskaya, V.P., 1998. Present-day and mid-Holocene biomes reconstructed from pollen and plant macrofossil data from the former Soviet Union and Mongolia. Journal of Biogeography, 25: 1029~1053.

Tarasov, P.E., Peyron, O., Guio, J., Brewer, S., Volkova, V.S., Bezusko, L.G., Dorofeyuk, N.I., Kvavadze, E.V., Osipova, I.M. and Panova, N.K., 1999a. Last Glacial Maximum climate of the former Soviet Union and Mongolia reconstructed from pollen and plant macrofossil data. Climate Dynamics, 14: 227~240.

Tarasov, P.E., Guiot, J., Cheddadi, R., Andreev, A.A., Bezusko, L.G., Blyakharchuk, T.A., Dorofeyuk, N. I., Filimonova, L.V., Volkova, V.S. and Zernitskaya, V.P., 1999b. Climate in northern Eurasia 6000 years ago reconstructed from pollendata. Earth and Planetary Science Letters, 171: 635~645.

Tarasov, P., Dorofeyuk, N. and Metel'tseva, E., 2000a. Holocene vegetation and climate changes in Hoton-Nur basin, northwest Mongolia. Boreas, 29: 117~126.

Tarasov, P.E., Volkova, V.S., Webb, T., III, Guiot, J., Andreev, A.A., Bezusko, L.G., Bezusko, T.V., Bykova, G.V., Dorofeyuk, N.I., Kvavadze, E.V., Osipova, I.M., Panova, N.K. and Sevastyanov, D.V., 2000b. Last Glacial Maximum biomes reconstructed from pollen and plant macrofossil data from Northern Eurasia. Journal of Biogeography, 27: 609~620.

Taylor, F., Whitehead, J. and Domack, E., 2001. Holocene paleoclimate change in the Antarctic Peninsula: evidence from the diatom, sedimentary and geochemical record. Marine Micropaleontology, 41: 25~43.

Tuvdendorzh, D. and Myagmarzhav, B. (eds.), 1985. Atlas of the climate and ground water resources in the Mongolian People's Republic. GUGMS, Ulaan Bator.

Van Campo, E., Cour, P. and Huang, C.X., 1996. Holocene environmental changes in Bangong Co basin (Western Tibet). Part 2: the pollen record. Palaeogeography, Palaeoclimatology, Palaeoecology, 120: 49~63.

Webb, T., III, 1987. The appearance and disappearance of major vegetational assemblages: long term vegetational dynamics in eastern North America. Vegetatio, 69: 177~188.

Webb, T., III, Bartlein, P.J., Harrison, S. and Anderson, K.H., 1993. Vegetation, lake levels and climate in eastern United States since 18 000 yr B.P. In: Wright, H.E., Webb, T., III. and Kutzbach, J.E. (eds.), Global climates since the Last Glacial Maximum, 415~467. University of Minnesota Press, Minneapolis, MN.

Yu, G., Prentice, I.C., Harrison, S.P. and Sun, X., 1998. Pollenbased biome reconstruction for China at 0 and 6000 years. Journal of Biogeography, 25: 1055~1069.

第二章

蒙古高原表土有机质碳同位素与气候的关系

王丽霞[1]　郭兰兰[2]　冯兆东[3]

①环境保护部 南京环境科学研究所
②北京师范大学 环境演变与自然灾害教育部重点实验室
③中国科学院 新疆生态与地理研究所

本章通过对蒙古高原表土有机质碳同位素组成(即$\delta^{13}C$值)与气温、降水、干燥度等气候因子的统计分析,建立了本地区气候与有机质碳同位素组成(即$\delta^{13}C$值)关系的转化函数。分析结果显示:蒙古高原表土有机质$\delta^{13}C$值与年平均降水量分布呈显著的线性负相关关系(R^2=0.453;n=196;p<0.05);该区域表土有机质$\delta^{13}C$值同生长季(3~9月)降水量呈更显著的线性负相关关系(R^2=0.4966;n=196;p<0.05);该区域表土有机质$\delta^{13}C$值同生长季(3~9月)干燥度呈比较显著的线性正相关关系(R^2=0.5805;n=196;p<0.05),而且两者的正相关关系在滑动平均法降噪处理后显著提高(R^2=0.7784;n=192;p<0.05)。本研究结果表明:蒙古高原表土有机质碳同位素组成同区域降水和干燥度有显著的相关关系。我们认为,在研究蒙古高原及其他类似气候区域的风成沉积—古土壤序列时,可以用上述关系重建古降水和古湿度的变化。

关键词:蒙古高原;表土有机碳同位素;生物气候相关性;降水;干燥度

1. 引言

人类活动已经对全球气候产生了巨大影响,并对全球环境施加了巨大的负面影响,未来全球气候的稳定性和全球环境的可持续性是全人类共同关注的问题。但是,已有的气候和环境知识尚不足以支持我们对未来的气候与环境作出可靠的评价。例如,人类利用仪器观测记录全球气候和环境变化的历史仅一百多年。为了评价未来气候变化的自然趋势和人为影响,我们需要更长的记录作为气候和环境变化的"自然基线"。显然,实现百年以上尺度的过去气候和环境"自然基线"的重建,我们必须依赖气候和环境代用指标。代用指标指的是在自然档案里(如冰芯、树轮、湖芯、黄土等)记录了过去气候和环境变化的一些物理参数(如磁化率、粒度等)、化学参数(如稳定同位素组成、盐度等)、生物参数

（如孢粉、硅藻等）

风成沉积—古土壤序列中的有机质碳同位素组成（$\delta^{13}C$）作为一个重要的代用指标，被广泛用于过去植被演替以及相对应的气候变化历史的重建（如Cerling等，1989；Kelly等，1998；Goodfriend，1999；Gouveia等，2002）。陆生植物的$\delta^{13}C$值主要受光合作用方式控制，同时又受气候和环境因子的影响。按照光合作用方式，陆生植物可划分为C_3（卡尔文循环，Calvin cycle），C_4（C_4–二羧酸循环Hatch and Slack cycle），CAM（景天科酸代谢，Crassulacean Acid Metabolism）三种类型。其中C_3植物适宜于低温及水分相对充足的环境，其$\delta^{13}C$值为–33‰~–21‰；C_4植物适宜于高温干旱环境，其$\delta^{13}C$值介于–21‰~–10‰；CAM型植物光合作用兼具C_3、C_4途径，因此$\delta^{13}C$值介于两者之间，但CAM植物种属较少，仅包括部分沙漠肉质植物和热带雨林附生植物（Tieszen等，1997；Bird和Pousai，1997）。即使是同一种陆生植物，其碳同位素组成也会随生长区域温度（王国安等，2003；陈拓等，2002）、降水（王国安等，2001；Stuiver和Braunas，1987）、大气CO_2浓度（Leavitt，1994）等因子的波动而发生变化。同时，有充分证据显示，土壤有机质的碳同位素组成（即$\delta^{13}C$值）可以继承其上生长的有机体的碳同位素组成（即$\delta^{13}C$值）（见：Nadelhoffer和Fry，1988；Balesdent等，1993；Wedin等，1995；Bird和Pousai，1997）。气候因子对陆生植物碳同位素分馏过程的影响和土壤对陆生植物$\delta^{13}C$值的继承作用是应用风成沉积—古土壤序列中的有机质碳同位素组成（即$\delta^{13}C$值）进行古植被和古气候重建的理论依据。

遗憾的是，土壤有机质碳同位素组成的气候指代意义还远未明确。首先，土壤有机质$\delta^{13}C$值指标在不同生物气候分区的适用性是没有经过逐一的实验验证的。其次，即使在某一特定生物气候分区，也尚未建立得到广泛认可的定量或半定量的土壤有机质$\delta^{13}C$值与气候因子之间的关系。换句话说，我们还需要对土壤有机质$\delta^{13}C$值在现代不同生物气候分区的气候指代意义进行更广泛的检验。广袤的蒙古高原具有明显的生物气候地带性，为我们验证土壤有机质$\delta^{13}C$值的生物气候指代意义提供了理想的场所。

本研究沿纬度方向采集了蒙古高原表土样品，通过测定其有机质碳同位素组成，并整合区域气象观测资料，检验蒙古高原表土有机质$\delta^{13}C$值与各气候因子间的统计关系，厘定土壤有机质碳同位素的气候指代意义，为利用土壤有机质碳同位素组成提取全球干旱半干旱区风成沉积—古土壤序列中的古气候信息提供现代实验依据。

2. 区域地理背景及研究方法

2.1. 区域地理背景

本研究区位于蒙古高原以及它的南邻地区（中国黄土高原西部），包括中国北部和蒙古国南部的部分地区（见图2–1），以下简称为蒙古高原。蒙古高原的气候变化由大气环流主导。冬季时，蒙古高原受西伯利亚高压控制（冬季环流模式），气候寒冷干燥。夏季时，蒙古高原受亚洲低压和东亚季风控制（夏季环流模式），气候温暖湿润。春季和秋季是冬季环流和夏季环流的过渡季节。事实上，冬季环流和夏季环流系统的强弱直接决定了中亚干旱半干旱区（主要包括蒙古高原和南部毗邻的黄土高原）的南北边界。

冬季环流控制下，蒙古高压加强了温度的纬度地带性变化，即气温随纬度的增加而迅速地降低。夏季环流控制时间，蒙古高原中部（37°N~45°N）戈壁沙漠和毛乌素沙漠的高原热力作用破坏了气温的纬度地带性分布规律，蒙古高原中部出现一个典型的高原高温区域，由该区域向南、北两个方向气温依次降低。简言之，夏季环流系统下蒙古高原的气温分布整体呈现以中部地区为高温中心的南北对称格局（陈隆勋等，1991）。同时，夏季环流控制下的蒙古高原北部受来自大西洋、北冰洋的湿润气团的影响而产生降水，其南部受来自西太平洋和印度洋暖湿气团的影响而产生降水。南北两侧的海洋湿润气团都很难到达蒙古高原的中部地区，而且蒙古高原中部是夏季的高温区域，因此它成为了极端干旱区。也就是说，夏季环流控制下蒙古高原的降水分布也呈现以中部地区为干旱中心的南北对称格局（中国科学院，1984；Worden和Savada，1989；Zhang和Lin，1992）。

蒙古高原以及它的南邻地区（中国黄土高原西部）的现代植被和土壤经过对区域独

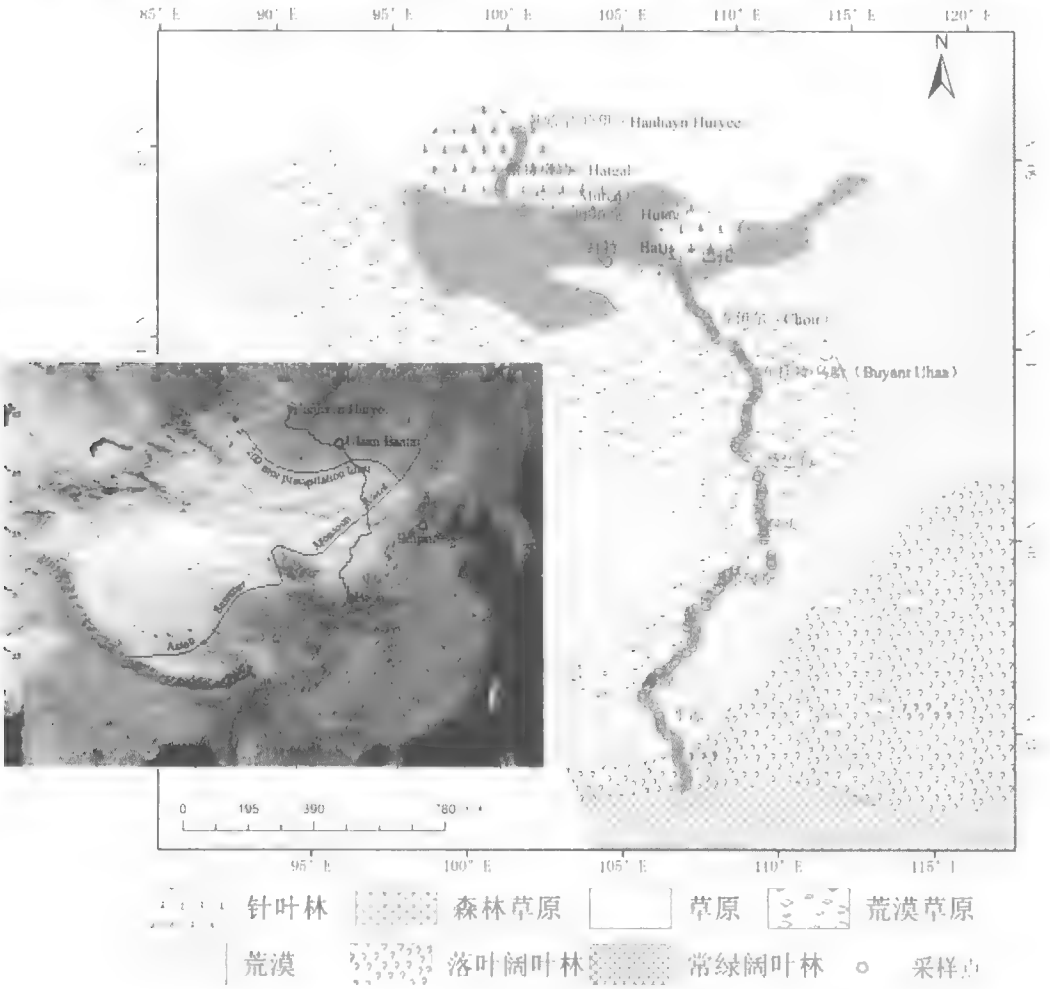

图2-1　研究区地貌、植被概况及采样路径（左图为中东亚遥感影像数据合成图，左图中西南—东北方向黑色实线为广泛认可的东亚夏季风影响范围界线。右图中南北向灰色圈线为采样路线）

特水热格局的长期适应，形成以中部戈壁荒漠为对称轴、沿南北方向基本对称的格局：由中部戈壁向北到西伯利亚，植被分布依次为蒙古高原南部荒漠草原、蒙古高原中部寒带草原、蒙古高原北部森林草原带以及蒙古高原最北部针叶林带；由中部戈壁向南至中国黄土高原西部，植被分布依次为内蒙古荒漠草原、黄土高原北部温带草原、黄土高原南部森林草原和秦岭山脉的落叶林一相对应，区域的地带性土壤分布模式为：由中部戈壁向北到西伯利亚，地带性土壤依次为蒙古高原中部风沙土、蒙古高原南部灰钙土、蒙古高原中部淡栗钙土、蒙古高原北部暗栗钙土（彼斯帕罗夫和方文哲，1959）；由中部戈壁向南至中国黄土高原，地带性土壤依次为蒙古高原中部风沙土、黄土高原北部灰钙土、黄土高原南部黄土或黑垆土和秦岭山脉的黄褐土（中国科学院内蒙古宁夏综合考察队，1978）。特别值得关注的是，该区域为C_4植物（猪毛蒿*Artemisia scoporia*和灌木亚菊*Ajania achilleides*为典型代表）和C_4植物（藜科Chenapodiaceae植物为典型代表）混合分布地区，由蒙古高原中部戈壁沙漠向南北两个方向，C_4植物的比重逐步降低（Pyankov等，2000；吴征镒，1980）。

2.2.1. 表土样品采集及实验方法

蒙古高原表土样品采集完成于2002年。采样路径开始于秦岭山脉北坡（34°14′24″N，106°55′30″E），结束于蒙古和俄罗斯边境的哈布尔（Khabur）城市附近（51°35′08″N，100°45′49″E）。采样剖面全长约3030km（采样路线见图2-1），共跨越了10个经度（100°E~110°E），17个纬度（34°N~52°N）。样品采集按照每隔5′N纬度设置一个采样点的密度进行，共设采样点196个。样品采集点选择不受人类干扰（主要在蒙古境内42°N~52°N区域）或少受人类干扰（如内蒙古和黄土高原地区38°N~42°N区域）的土壤表层，一般选在离耕作区和城市较远的有自然生长的天然植被覆盖的地区进行样品采集（由于中国内蒙古及黄土高原地区人类活动影响范围广阔，样品采集主要在秦岭、六盘山等还保留有部分天然植被的地区采集）。样品采集位置为地表以下10cm的土壤发生层的A层。样品采集后在兰州大学西部干旱环境教育部重点实验室完成室内分析测试工作，期间随机选取部分样品在中国科学院环境地球化学国家重点实验室测量进行交叉质量检测。

先将土壤在50℃下烘干，后用研钵磨碎后过孔径为0.105mm的分样筛，以去除残留的植物根系。然后用10%的稀盐酸除去样品中的碳酸盐矿物，用蒸馏水多次稀释土壤溶液至中性（pH值≈7），50℃下烘干后再次磨碎土壤样品至0.105mm备用。预处理后的样品采用高温灼烧氧化法制备CO_2气体：样品置于真空石英管内，通入高纯氧气在850℃条件下灼烧15min，采用液氮和酒精液氮等不同冷冻剂分离、净化土壤有机质燃烧生成的CO_2气体；并收集于集气管中，供德国生产的MAT252质谱仪进行稳定碳同位素分析（详细流程参阅Ehleringer和Cook，1998）。样品制备过程中，每5个样品加入一个国家标准炭黑GBW04407（$\delta^{13}C$：-22.43‰，Std：0.07‰）进行质量控制，运用该稳定碳同位素前处理系统对国家标准炭黑样品制备CO_2气体测量的$\delta^{13}C$值标准偏差小于0.2‰。稳定碳同位素测量结果依照国际PDB标准给出，$\delta^{13}C$的值由下式计算：

$$\delta^{13}C=[(^{13}C/^{12}C)样品-(^{13}C/^{12}C)PDB标准]/(^{13}C/^{12}C)PDB标准\times1000‰$$

2.2.2. 气象数据收集及分析方法

本项研究气象观测数据来自于两个渠道，包括中国部分和蒙古部分，其中中国部分选用中国国家气候资料中心1981~1990年共10年的气象资料（包括气温、降水和蒸发量等）在距各采样点经纬度1°的范围内共选出16个气象站点。蒙古部分是采用《MONTHLY CLIMATIC DATA FOR THE WORLD》中的1996~2000年共5年的气象资料，气象站点选择标准同中国部分相同，共选择10个气象站点。在这26个站点观测气象资料基础上（表2-1），根据气候分异规律，并基于站点的经纬度、气温和降水数据，采用Matlab二维插值方法计算得到所有196个采样点的气温和降水数据（插值方法详见王丽霞，2005）

3. 结果分析

3.1. 蒙古高原表土有机质δ13C值与气温的相关性

分析结果显示，尽管夏季时蒙古高原湿度分布具有南北对称的地带性分布规律，但蒙古高原全年平均温度由南向北逐步降低（见图2-2A），纬度地带性规律表现十分明显。沿纬度方向，蒙古高原表土有机质δ13C值与采样点的年平均气温值间不具有可通过检验的统计相关关系（R^2=0.001；n=196）。进一步地分析可以显示，由蒙古高原中部戈壁向北，表土有机质δ13C值同采样点年平均气温呈反相变化，即年平均气温升高时表土有机质δ13C值降低（即土壤有机质中富集轻碳同位素）；而由中部戈壁向南，表土有机质δ13C值与采样点年平均温度呈同相变化，即采样点气温增加时表土有机质δ13C值增高（即土壤有机质中富集重碳同位素）（见图2-2B）。

3.2. 蒙古高原表土有机质δ13C值与降水的相关性

表2-1　研究区内26个基准气象站基本信息

站点及名称	纬度(N)	经度(E)	海拔(m)	年均气温(°C)	降水量(mm)	蒸发量(mm)	生长季干燥度
57016宝鸡	34°21′	107°08′	613	12.96	632.35	772.47	1.055
53543东胜市	39°50′	109°59′	1459	5.9	363.36	586.25	1.613
53615陶乐	38°48′	106°42′	1099	8.41	159.61	673.1	4.216
53704中卫	37°32′	105°11′	1183	8.81	164.44	658.25	4.003
53705中宁	37°29′	105°40′	1184	9.35	192.6	678.86	3.525
53806海原	36°34′	105°39′	1697	7.03	340.48	583.08	1.713
53810同心	36°59′	105°54′	1111	8.99	262.86	668.23	2.542
53817固原	36°00′	106°16′	1752	6.15	438.95	557.36	1.27
53446包头	40°40′	109°51′	1069	6.86	620.62	638.13	2.33
53903西吉	35°58′	105°43′	1916	5.23	408.87	531.04	1.299

续表2-1

站点及名称	纬度(N)	经度(E)	海拔(m)	年均气温(°C)	降水量(mm)	蒸发量(mm)	生长季干燥度
53614银川市	38°29′	106°23′	1112	8.98	155.25	475.07	3.06
53723盐池	37°47′	107°24′	1348	8.31	227.92	462.68	2.93
53915平凉	35°33′	106°40′	1348	8.83	401.92	454.172	1.13
53336海流图	41°34′	108°31′	1289	5.27	166.5	469.53	2.82
53352百灵庙	41°42′	110°26′	1377	4.23	217.75	640.19	2.94
53529鄂托克旗	39°06′	107°59′	1381	7.07	220.42	672.5	3.051
44203R仁钦隆博(INCHINLHOMBE)	51°07′	99°40′	1583	-6.04	199.73	397.42	1.96
44207哈特嘎勒(HATGAL)	50°26′	100°09′	1687	-3.32	303.5	379.924	1.25
44230塔里爱兰(TARIALAN)	49°37′	102°00′	1236	0.61	316.72	492.04	1.55
44231木伦(MUREN)	49°38′	100°10′	1288	0.67	235.5	500.304	2.12
44232胡塔克(HUTAG)	49°23′	102°42′	933	0.84	278	518.39	1.86
44239布尔干(BULGAN)	48°48′	103°33′	1210	-0.28	307	467.94	1.52
44292乌兰巴托(ULAAN-BAATOR)	47°56′	106°59′	1338	-0.3	243.7	482.08	1.97
44294马安提(MAANTI)	47°18′	107°29′	1430	-0.7	197.65	468.57	2.37
44298乔伊尔(CHOIR)	46°27′	108°13′	1286	1.38	185	538	2.91
44358杂木因—乌迪(ZAMYN-UUD)	43°44′	111°54′	964	4.41	124.2	611.76	4.93

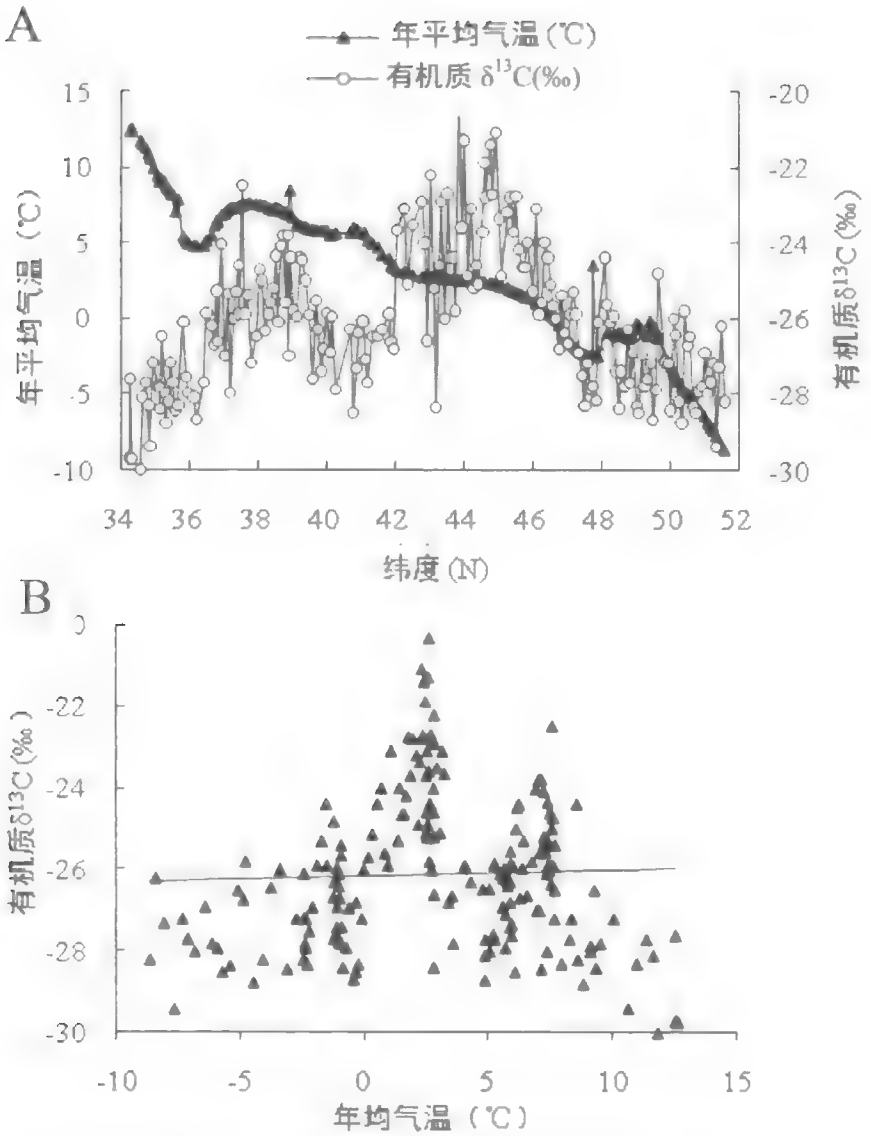

图2–2　蒙古高原年平均气温与表土有机质 δ ^{13}C值沿纬度方向变化曲线(A:上图)和蒙古高原年平均气温与表土有机质 δ ^{13}C值的散点图(B:下图)(Feng等,2008)

分析结果显示,蒙古高原多年平均降水量分布呈南北对称模式,该区域表土有机质δ ^{13}C值空间分布模式也呈南北对称模式,但变化趋势相反。换言之,以中部戈壁为中心向南北方向,随着年平均降水量升高,表土有机质δ ^{13}C值逐步降低(即土壤有机质中富集轻碳同位素)。需要补充的是,尽管蒙古高原降水分布主要受纬度地带性控制,但是海拔高度也对降水分布有重要影响(图2–3A)。我们对196个采样点多年平均降水量与采样点手持GPS测定的海拔高度进行了统计分析,结果显示多年平均降水量与海拔高度有显著相

关关系(R^2=0.42;n=196;p<0.05)，海拔越高，表土有机质碳同位素值越低(即土壤有机质中富集轻碳同位素)(图2-3B)。实际上，海拔高度对该区域降水纬度地带性分布规律的影响早有报道(陈隆勋等，1991；Worden 和 Savada，1989；Zhang和Lin，1992；中国科学院，1984)。尽管本研究没有将海拔高度作为单独变量进行考察，但我们考虑了海拔高度对表土有机质碳同位素值沿纬度方向的协相关影响(R^2=0.36;n=196;p<0.05)。

蒙古高原表土有机质δ^{13}C值与多年平均降水量的统计分析结果显示，蒙古高原年平

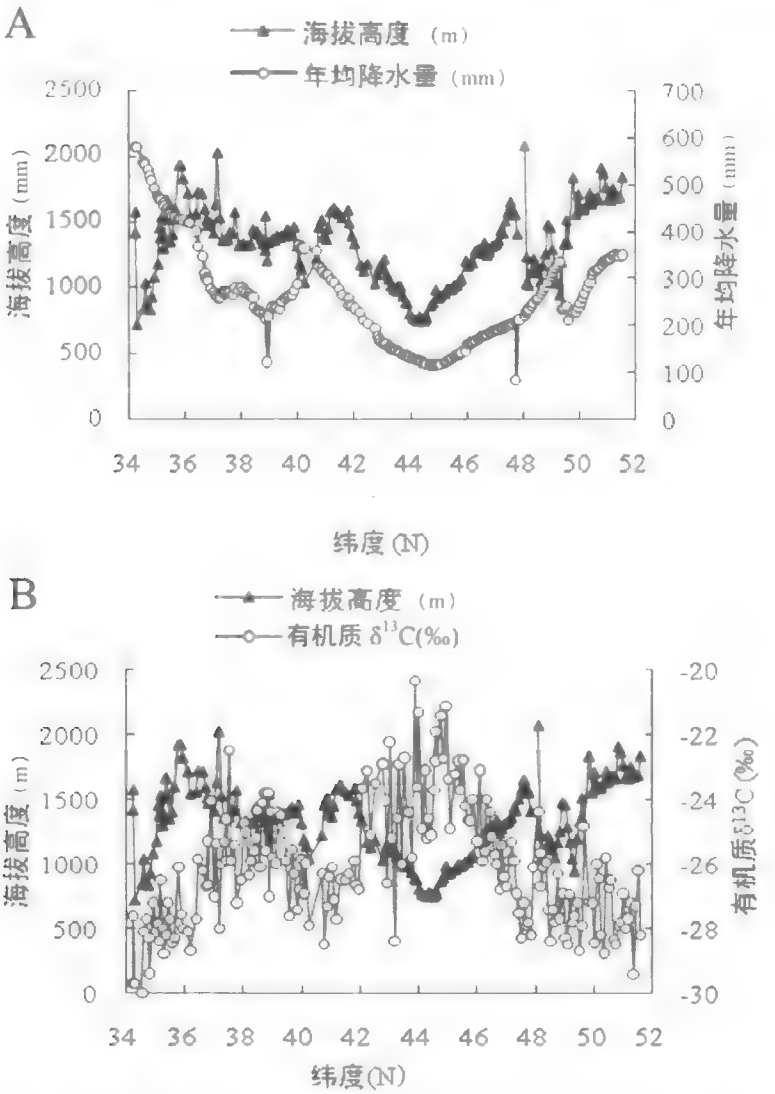

图2-3 蒙古高原年平均降水量与海拔高度沿纬度方向的相关曲线(A:上图)和蒙古高原海拔高度与表土有机质δ^{13}C值沿纬度方向的相关曲线(B:下图)(Feng等，2008)

均降水量最低的中部戈壁(44°N)地区，表土有机质δ¹³C值最高，表土有机碳中富集重碳同位素；由中部戈壁荒漠带向南北两个方向，随着年平均降水量的增加，表土有机质δ¹³C值逐渐偏轻，即表土有机质中富集轻碳同位素(图2-4A)。统计分析显示，沿纬度方向，蒙古高原表土有机质δ¹³C值与年降水量之间存在着明显的线性负相关关系(R^2=0.453；n=196；p<0.05)(图2-4B)。研究区年平均降水量每增加100mm，表土有机质δ¹³C值降低1.16‰。

通过对实验分析和观测数据的统计分析，我们建立了蒙古高原表土有机碳同位素与

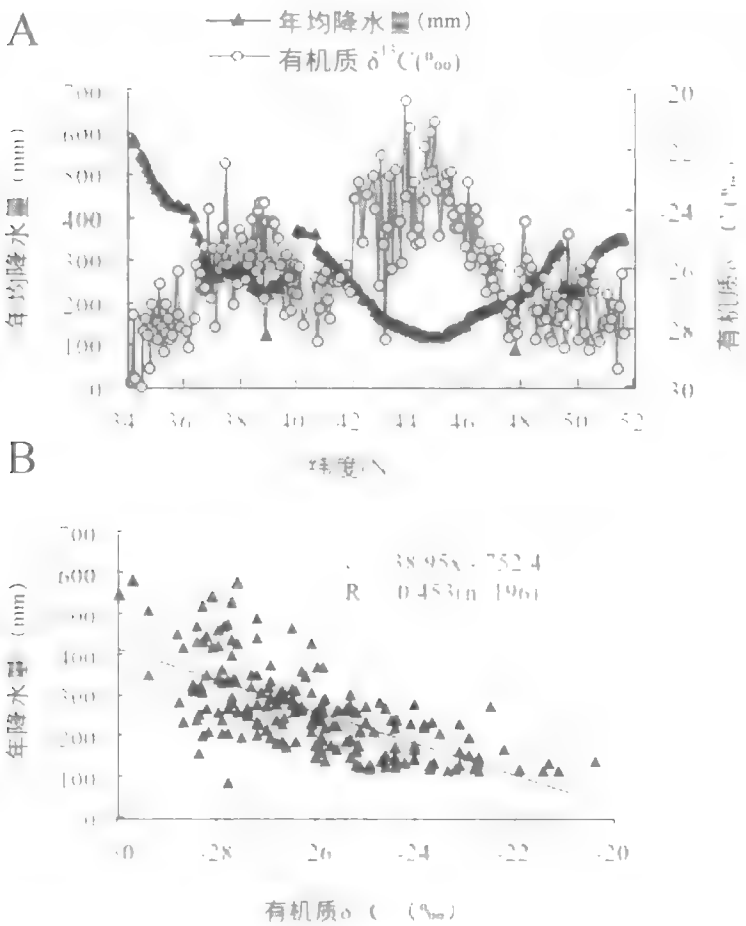

图2-4　蒙古高原年平均降水量与表土有机质δ¹³C值随纬度变化曲线(A：上图)和蒙古高原年平均降水量与表土有机质δ¹³C值的散点图(B：下图)(Feng等，2008)

年平均降水量的线性回归公式：

$$P_{年均}=35.958x-752.46$$

（其中：$P_{年均}$指年平均降水毫米数，x值指表土有机质的$\delta^{13}C$值(‰，PDB标准）

进一步的分析显示，由中部戈壁荒漠带向南北两个方向，生长季(4~9月)降水量与表土有机质$\delta^{13}C$值的关系更为密切，即生长季降水越多，对应的表土有机质$\delta^{13}C$值越偏负（图2-5A）。表土有机质$\delta^{13}C$值与蒙古高原生长季(4~9月)降水量有更显著的负相关性（$R^2=0.4966$；$n=196$；$p<0.05$）（图2-5B）。蒙古高原表土有机质碳同位素值与生长季(4~9月)降水量的线性回归公式为：

$$P_{生长季}=29.444x-546.01$$

（其中：$P_{生长季}$指生长季即4~9月的降水毫米数，x值指表土有机质$\delta^{13}C$值（‰，PDB标准）。

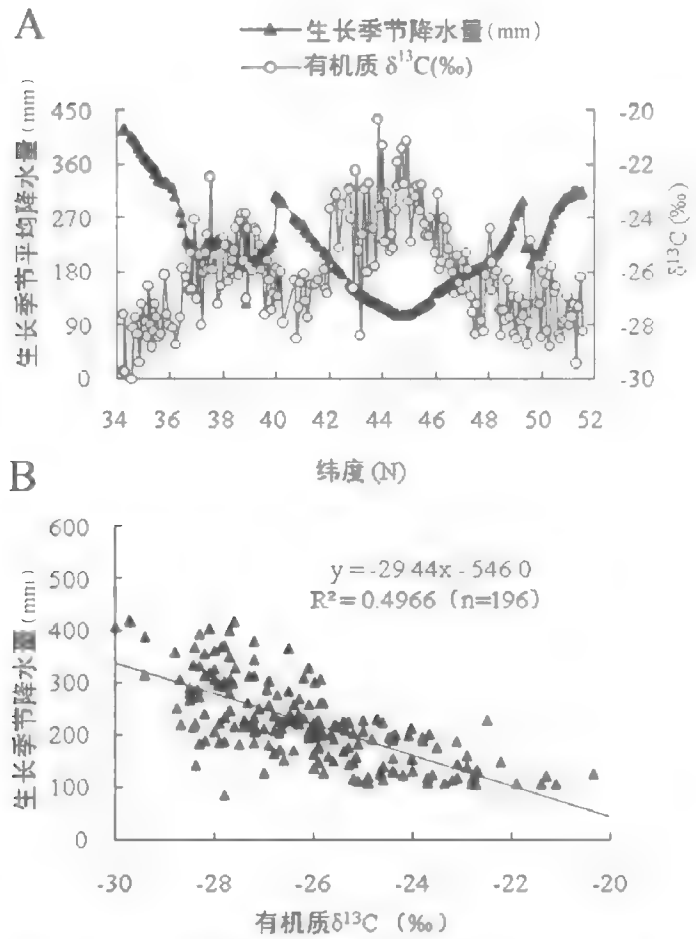

图2-5　蒙古高原平均生长季降水量与表土有机质$\delta^{13}C$值沿纬度变化曲线(A：上图）和蒙古高原平均生长季降水量与表土有机质$\delta^{13}C$值的散点图(B：下图)(Feng等，2008)

、蒙古高原表土有机质碳δ^{13}C值与生长季干燥度的相关性

为更准确地刻画蒙古高原水热配置条件对植物生长和表土有机质碳同位素组成的影响，我们定义了生长季干燥度指标，即将4~9月潜在蒸发量与降水量比值这一无量纲值定义为生长季干燥度，其中潜在蒸发量根据Thornwaite模型计算获得（计算方法详见赵传燕，2003），降水量来自气象观测和插值数据。

对蒙古高原干燥度和表土有机质δ^{13}C值的统计分析结果显示，沿纬度方向，蒙古高原生长季干燥度与表土有机质δ^{13}C值呈显著正相关关系（R^2=0.5805；n=196；p<0.05），即由蒙古高原中部戈壁沙漠向南北两个方向，生长季干燥度同表土有机质δ^{13}C值同步下降（图2-6A）。生长季干燥度每降低一个单位，表土有机质δ^{13}C值减小1.30‰，统计得到的蒙古高原生长季干燥度与表土有机质δ^{13}C值的线性回归公式为（图2-6B）：

$$A_{生长季}=0.4441x+14.137$$

（其中：$A_{生长季}$指生长季（即4~9月）平均干燥度（生长季潜在蒸发量与降水量比值，无量纲），x指表土有机质δ^{13}C值（‰，PDB标准））。

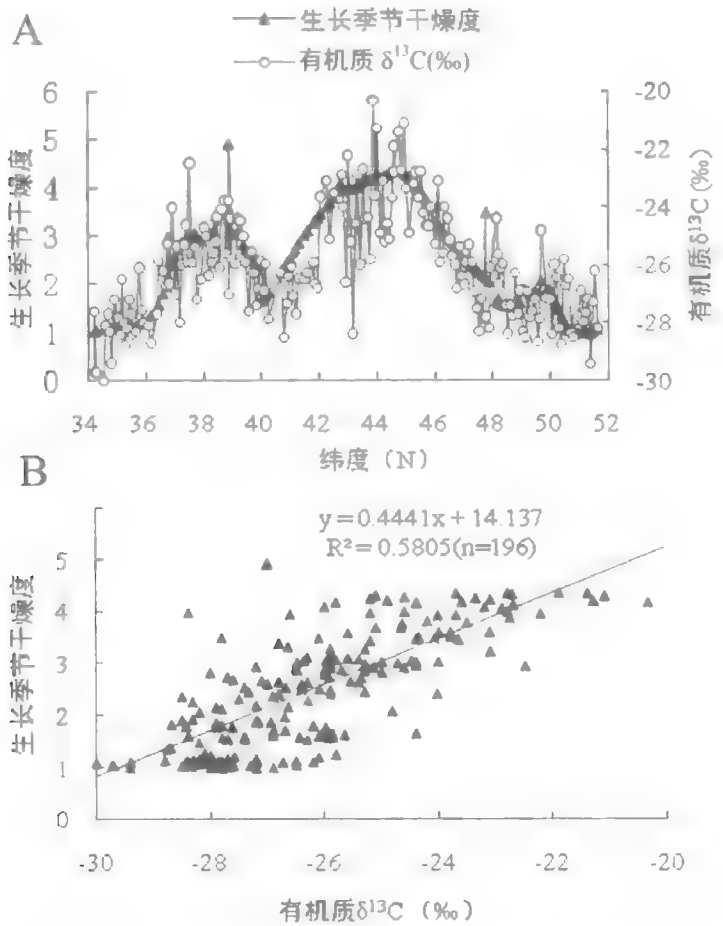

图2-6　蒙古高原平均生长季干燥度与表土有机质δ^{13}C值沿纬度变化曲线（A：上图）和蒙古高原平均生长季干燥度与表土有机质δ^{13}C值的散点图（B：下图）（Feng等，2008）

更进一步，我们将蒙古高原表土有机质δ¹³C值曲线和生长季干燥度曲线进行三点滑动平均以降低随机误差的影响。降噪处理后蒙古高原表土有机质δ¹³C值曲线与生长季干燥度曲线的同步变化趋势更加明显（图2-7A），统计分析结果也显示，经滑动平均后平均生长季干燥度与表土有机质δ¹³C值之间有更强的正相关性（R^2=0.7784；n=192；p<0.05）（滑动平均后比较分析的数据由原来的196对调整为192对）。三点滑动平均后蒙古高原生长季干燥度与表土有机质δ¹³C值的线性回归公式为（图2-7B）：

$$A_{滑动平均}=0.5872x+17.869$$

（其中：$A_{滑动平均}$指三点滑动平均处理后的生长季（4~9月）平均干燥度（生长季潜在蒸发量与降水量比值，无量纲），x指三点滑动平均处理后表土有机质δ¹³C值（‰，PDB标准）

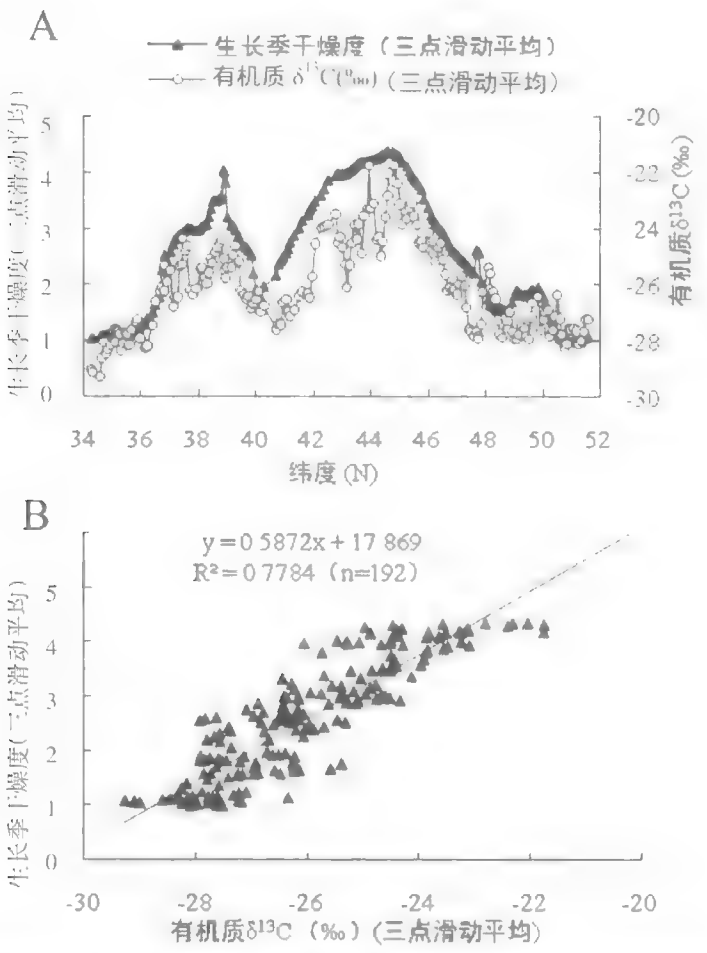

图2-7　三点滑动平均后蒙古高原生长季干燥度与表土有机质δ¹³C值随纬度变化曲线（A：上图）和三点滑动平均后蒙古高原生长季干燥度与表土δ¹³C值的散点图（B：下图）（Feng等，2008）

综上所述，我们的实验和分析结果证实，蒙古高原表土有机质$\delta^{13}C$值与采样点年平均降水量具有明显负相关关系（R^2=0.453），如果将降水量限制在生长季（4~9月），其负相关性有所提升（R^2=0.4966）。如果将生长季蒸发量一并考虑进来，生长季干燥度（生长季潜在蒸发量与降水量比值）与表土有机质$\delta^{13}C$值之间表现出很强的正相关性（R^2=0.5805），更进一步，通过三点滑动平均弱化生长季干燥度与表土有机质$\delta^{13}C$值的随机误差，可以获得生长季干燥度与表土有机质$\delta^{13}C$值极其显著的正相关关系（R^2=0.7784）。

4. 讨论

不同地区开展的植物有机质碳同位素组成实验结果表明，大气湿度会直接影响植物气孔导度和光合作用方式，并间接影响区域植物组成，从多个方面导致植被有机质碳同位素值发生变化（Bowling等，2002；刘卫国等，2002；Fessenden和Ehleringer，2003；Llorens等，2004）。首先，大气湿度不足导致的水分胁迫可以使植物叶片气孔关闭，气孔导通系数降低，使植物体吸收的CO_2中富集重碳同位素，使植物体和土壤有机质$\delta^{13}C$值偏高。其次，长期的水分胁迫环境会使一些原本采用C_3光合途径的植物将逐渐转向CAM光合途径，植物体因此也将富集重碳同位素，植物体和土壤有机质$\delta^{13}C$值偏高（Farquhar等，1989）。我们前期对蒙古高原C_3植物（猪毛蒿和灌木亚菊）的研究也显示，区内C_3植物在受水分胁迫后会富集重碳同位素（Lee等，2005）。另外，蒙古高原开展的另一项研究（Pyankov等，2000）也表明，区内C_4类型的藜科植物比重较大时，土壤有机质会富集重碳同位素，即有机质$\delta^{13}C$值偏高，而C_4植物的侵占通常在气候干旱条件下发生。显然，大气湿度降低会从多个方面（植物生理特征、植物光合作用方式和区域植物组成）使区域植被的$\delta^{13}C$值增高，而土壤又能够继承植物体的有机碳同位素组成变化。因此，区域大气湿度的降低将最终导致土壤有机质$\delta^{13}C$值增高（即土壤中富集重碳同位素）。

上述研究结果与我们的推断一致，蒙古高原表土有机质碳同位素组成主要由湿度控制。蒙古高原由南向北湿度条件的变化一方面会导致区域内占主导地位的C_3植物自身的碳同位素组成发生变化（气孔导度和光合作用效率发生变化），同时会调节区域内C_4植物的比重，两者的共同影响最终导致了区域表土有机质碳同位素组成的地理分异。具体地讲，区域内鄂尔多斯高原（37°N~39°N）和中部戈壁沙漠（42°N~46°N）在植物生长季气候温暖干燥，有利于灌木和草本植物繁盛，相应土壤有机质$\delta^{13}C$值偏高（即土壤有机质中富集重碳同位素）。研究区最南部的秦岭山脉（34°N~36°N）和最北部的Khanglas山脉（48°N~52°N）水分条件相对较好，土壤有机质$\delta^{13}C$值偏低（即土壤有机质中富集轻碳同位素）。同理，40°N附近土壤有机质的$\delta^{13}C$值偏低可能源于黄河湾湿地较好的水分条件。

本研究结果显示，区域内土壤表土有机质$\delta^{13}C$值与气候因子的相关关系可用一系列回归方程表达。1）年平均降水：$P_{年均}=-35.958x-752.46$（R^2=0.453；n=196；p<0.05）；2）平均生长季降水：$P_{生长季}=-29.444x-546.01$（R^2=0.4966；n=196；p<0.05）；3）平均生长季干燥度：$I_{年均}=0.4441x-14.137$（R^2=0.5805；n=196；p<0.05）；4）三点滑动平均生长季干燥度：$I_{滑动平均}=0.578x+17.869$（R^2=0.7784；n=192；p<0.05）（其中x指土壤有机质$\delta^{13}C$值，‰，PDB标准）。

假设蒙古高原所在的中东亚干旱半干旱区过去与现在植被组成是类似的，上述关系式就可以被应用于整个中东亚干旱半干旱区或者全球其他生物气候条件类似区域，重建这些地区风成沉积—古土壤序列中有机质 $\delta^{13}C$ 值记录的湿度和有效湿度的变化序列。

需要补充的是，大气 CO_2 浓度也会对植物的碳同位素组成产生显著影响，并将此影响遗传到土壤有机质碳同位素组成中（Pearman等，1976；Francey和Farquhar，1982；Leavitt，1994）。研究表明，大气 CO_2 浓度每增加100ml/m³会导致植物 $\delta^{13}C$ 值下降2.0‰，即土壤有机质中更加富集轻碳同位素（Feng和Epstein，1995）。假如这一结论可以在更大区域范围内得到证实，我们可以借助冰芯记录的大气 CO_2 浓度变化，来校正基于土壤有机质 $\delta^{13}C$ 值与气候因子（如降水、干燥度）之关系重建的过去降水量和干燥度变化序列。

致谢：李心清教授和汪卫国博士参加了野外工作，并感谢蒙古国地质研究所的同事在野外工作和后勤方面的帮助。

参考文献

彼斯帕罗夫，方文哲. 1959. 蒙古人民共和国的土壤. 北京：科学出版社.

陈隆勋，朱乾根，罗会邦等. 1991. 东亚季风. 北京：气象出版社.

陈拓，马健，冯虎元，何元庆，徐世健，强维亚，安黎哲. 2002. 阜康典型荒漠 C_4 植物稳定碳同位素值的环境分析. 干旱区地理，25(4)：342~345.

刘卫国，宁有丰，安芷生，吴振海，鹿化煜，曹蕴宁. 2002. 黄土高原现代土壤和古土壤有机碳同位素对植被的响应. 中国科学(D)辑，32(10)：832~836.

王国安，韩家懋，刘东升. 2003. 中国北方黄土区C-3草本植物碳同位素组成研究. 中国科学(D辑)，33(6)：550~556.

王国安，韩家懋. 2001. C_3 植物碳同位素在旱季和雨季中的变化. 海洋地质与第四纪地质，21(4)：43~47.

王丽霞. 2005. 蒙古高原南北断面有机质碳同位素、表土磁化率与现代环境转化函数的研究. 兰州大学硕士论文.

吴征镒. 1980. 中国植被. 北京：科学出版社.

赵传燕. 2003. 甘肃省祖厉河流域潜在生态条件的GIS辅助模拟. 兰州大学博士论文.

中国科学院. 1984. 中国自然地理. 北京：科学出版社.

中国科学院内蒙古与宁夏综合考察队，中国科学院南京土壤研究所. 1978. 内蒙古自治区与东北西部地区土壤地理. 北京：科学出版社.

Balesdent, J., Girardin, C. and Mariotti A., 1993. Site-related $\delta^{13}C$ of tree leaves and soil organic matter in a temperate forest. Ecology, 74: 1713~1721.

Bird, M.I. and Pousai, P., 1997. Variation of $\delta^{13}C$ in the surface soil organic carbon pool. Global Biogeochemical Cycles, 11: 313~322.

Bowling, D.R., McDowell, N.G., Bond, J.R., Law, B.E. and Ehleringer, J.R., 2002. $\delta^{13}C$ content of ecosystem respiration is linked to precipitation and vapor pressure deficit. Oecologia, 131: 113~124.

Cerling, T.E., Quade, J., Wang, Y. and Bowman, J.R., 1989. Carbon isotopes in soils and paleosols as

ecology and paleoecology indicators. Nature, 341: 138~139.

Ehleringer, G.R. and Cook, C.S., 1998. Carbon and oxygen isotope ratios of ecosystem respiration along an Oregon conifer transect: preliminary observations based on small flask sampling. Tree Physiology, 18: 513~519.

Farquhar G.D., Ehleringer J.R. and Hubick K.T., 1989. Carbon isotope discrimination and photosynthesis. Annual Review of Plant Physiology, 40: 503~537.

Feng, X. and Epstein, S., 1995. Carbon istopoes of trees from arid environments and implications for reconstructing atmospheric CO_2 concentration. Geochimica et CosmochimicaActa, 59: 2599~2608.

Feng, Z.-D., Wang, L.X., Ji, Y.H., Guo, L.L., Lee, X.Q. and Dworkin, S.I., 2008. Climatic dependency of soil organic carbon isotopic composition along the S-N Transect from 34° N to 52° N in central-east Asia. Palaeogeography, Palaeoclimatology, Palaeoecology, 257: 335~343.

Fessenden, J.E. and Ehleringer, J.R., 2003. Temporal variation in $\delta^{13}C$ of ecosystem respiration in the Pacific Northwest: link to moistures tress. Oecologia, 136: 129~136.

Francey, R.J. and Farquhar, G.D., 1982. An explanation of $^{13}C/^{12}C$ variations in tree rings. Nature, 297: 28~31.

Goodfriend, G.A., 1999. Terrestrial stable isotope records of Late Quaternary paleoclimates in the eastern Mediterranean region. Quaternary Science Reviews , 18: 501~513.

Gouveia, S.E.M., Pessenda, L.C.R., Aravena, R., Boulet, R., Scheel-Ybert, R., Bendassoli, J.A., Ribeiro, A.S. and Freitas, H.A., 2002. Carbon isotopes in charcoal and soils in studies of paleovegetation and climate changes during the late Pleistocene and the Holocene in the southeast and center-west regions of Brazil. Global and Planetary Change, 33: 95~106.

Kelly, E.F., Blecker, S.W., Yonker, C.M., Olson, C.G., Wohl, E.E. and Todd, L.C., 1998. Stable isotope composition of soil organic matter and phytoliths as paleoenvironmental indicators. Geoderma, 82: 59~81.

Leavitt, S.W., 1994. South American tree rings show declining $\delta^{13}C$ trend. Tellus 46(B): 152~157.

Lee, X. Q., Feng, Z.-D., Guo, L.L., Wang, L.X. and Jin, L.Y., 2005. Soil and plant-$\delta^{13}C$ variations along a N-S (32°N~55°N) transect in eastcentral Asia. Global Biogeochemical Cycles , 19: 1~8. doi:10.1029/2004GB2303 GB4010.

Llorens, L., Penuelas, J., Beier, C., Emmett, B., Estiarte, M. and Tietema, A., 2004. Effects of an experimental increase of temperature anddrought on the photosynthetic performance of two Ericaceous shrub species along a N-S European gradient. Ecosystems, 7: 613~624.

Nadelhoffer, K.J. and Fry, B., 1988. Controls on natural nitrogen-15 and carbon-13 abundances in forest soil organic matter. Soil Science Society of American Journal, 52: 1633~1640.

Pearman, G.I., Francey, R.J. and Fraser, P.J., 1976. Climatic implications of stable carbon isotopes in tree rings. Nature, 260: 771~773.

Pyankov, V.I., Gunin, P.D., Tsoog, S. and Black, C.C., 2000. C_4 plants inthe vegetation of Mongolia: their natural occurrence andgeographical distribution in relation to climate. Oecologia, 123: 15~31.

Stuiver M. and Braziunas T.F., 1987. Tree cellulose $^{13}C/^{12}C$ isotope ratios and climatic change. Nature, 328: 58~60.

Tieszen L.L., Reed B.C., Bliss N.B., Wylie B.K. and Dejong D.D., 1997. NDVI, C_3 and C_4 production and

distributions in the Great Plains grassland cover classes. Ecological Applications. 7: 59~78.

Wedin, D.A., Tieszen, L.L., Dewey, B. and Pastor, J., 1995. Carbon isotope dynamics during grass decomposition and soil organic matter formation. Ecology. 76: 1383~1392.

Worden, R.L. and Savada, A.M., 1989. Mongolia: A Country Study Federal Research Division, Library of Congress, Washington DC.

Zhang, J.C. and Lin, Z.G., 1992. Climate of China. Wiley, New York.

第三章

蒙古国北部夏马尔(Shaamar)风积剖面记录的过去近40 000年来植被与气候的变化

马玉贞[1]　　王　维[2]

①北京师范大学 环境演变与自然灾害教育部重点实验室

②内蒙古大学 环境与资源学院

本章以^{14}C年代为框架，基于夏马尔(Shaamar)风成—古土壤剖面的孢粉记录，通过数据统计分析和花粉气候指数分析重建了蒙古高原北部约38 000 cal. yr BP（cal.yr BP =校正的日历年前）以来的植被和气候变化。重建的古植被类型、温度和湿度指数显示：在约38 000~30 000 cal. yr BP夏马尔地区的植被是以云杉属、冷杉属和西伯利亚松型为主的泰加林，有效湿度很高；约30 000~23 000 cal. yr BP，植被为以蒿属和禾本科为建群的草原，温度和湿度都比较低；约23 000~10 000 cal. yr BP，植被演变的过程为泰加林—以禾本科为建群的草原—泰加林—森林草原—泰加林、早期气候（约23 000~20 000 cal. yr BP）冷干，晚期气候（约19 000~11 000 cal. yr BP）温暖略干；约10 000~3000 cal. yr BP，植被类型为森林草原，有效湿度较低，呈弓形的温度曲线在约6000 cal. yr BP达到最大值，约3000 cal. yr BP以来，植被为泰加林，气候凉湿。花粉记录与其他地区古气候记录的对比分析显示，蒙古高原北部的气候变化受北大西洋海—气耦合系统的控制或调整。

关键词：蒙古高原北部；植被和气候变化；花粉记录；数理统计；花粉气候指数

1. 引言

1.1. 研究蒙古高原北部气候变化的意义

地球气候系统在过去的40 000年经历了戏剧性的变化。在轨道和亚轨道时间尺度上，包括了末次冰期的间冰段（即深海氧同位素第三阶段MIS3，约57 000~25 000 yr BP；即距今约57 000~25 000年前）、末次冰期晚期（即深海氧同位素第二阶段MIS2，约25 000 ~ 11 500 cal. yr BP）和全新世（MIS1：约11 500 cal. yr BP以来）（Berger和Loutre，1991；Clemens等，1996；Bradley，1999；Ruddiman，2008）而且在亚轨道尺度上表现出较大的不稳定性，体现出千年或百年尺度的更为剧烈的波动（快速的、大幅度的冷暖变化事件）。例如，被广泛报道的海因里希事件（Heinrich Events），其准周期大约是5000~6000年；丹斯果—奥什格尔

波动（Dansgaard-Oeschger Oscillations，D-O旋回），其准周期大约为1300~1500年（Dansgaard等，1993；Bond等，1997；2001；Bard等，2000；Wang等，2001；Alley等，2002；Yuan等，2004）。

在过去的半个世纪里，轨道和亚轨道尺度的气候变化研究取得了突破性进展，但这些古气候（事件）记录存在着区域不均衡性，仍不足以全面科学地认识和理解全球气候系统变化的空间规律和调控机制。目前，在蒙古高原，对轨道和亚轨道尺度气候变化的研究还比较薄弱，特别是晚更新世以来的研究，有良好年代控制的高分辨率代用指标序列十分少见。近年来，几个团队对全新世气候环境变化进行了大量的调查研究（如Tarasov等，2000；Peck等，2002；Fowell等，2003；Feng等，2005；Prokopenko等，2007；Rudaya等，2009；Wang等，2009；2011；Zhang等，2012），但对该时期蒙古高原北部气候变化的时空格局和机制仍存在较大分歧。例如，Rudaya等（2009）支持早期Harrison等（1996）和Tarasov等（2000）提出的观点，即在全新世，东亚季风对蒙古高原北部大部分地区的气候产生了强烈的影响；而Chen等（2008）则认为，在全新世，包括蒙古高原北部在内的整个中亚干旱区被西风带控制。

蒙古高原北部厚达30m的夏马尔（Shaamar）风成—古土壤剖面为认识和理解晚更新世以来的环境变化提供了理想的物质基础。我们的跨越5个植被类型的蒙古国南北断面表土花粉组合与现代植被/气候间的关系研究（Ma等，2008）也为利用花粉代用指标正确解译植被和气候变化提供了参考依据。本章以较好的年代数据为框架，基于夏马尔风成—古土壤剖面的花粉记录，通过数据统计分析和花粉气候指数分析，重建蒙古高原北部约40 000 cal. yr BP以来的植被和气候变化，寻求较前人（如CLIMAP Members，1981；COHMAP Members，1988）更高分辨率的气候记录，并与中国季风区和北大西洋西风带的古气候记录进行对比，探讨过去约40 000 cal. yr BP来蒙古高原北部对全球变化的响应及其与高纬度和低纬度地区气候变化间的内在联系。

1.2. 研究区域

研究区位于亚洲大陆内部，南起乌兰巴托（Ulan Bator），北至贝加尔湖（Baikal Lake），东西介于杭爱山（Hentiy）和肯特山（Hangay）之间（48°N~53°N，104°E~108°E），在地形上为南北向的狭长谷地，形如走廊。这里风成沉积丰富（Khosbayar，1989；Logatchov，1989）（图3-1），冯兆东及其同事曾考察了十二个风成沉积剖面，并详细研究了其中的四个。其研究结果表明，风成沉积连续记录了晚更新世以来（距今50 000年）的生物/气候变化历史（Feng等，1998；2005；2007a；Feng，2001；Feng和Khosbayar，2004）。

乌兰巴托—贝加尔湖走廊区的年平均降水从南到北为250~400mm，年平均气温为-2℃~0℃，1月均温-24℃~-20℃，7月均温12℃~17℃。植被为森林草原，针叶林分布在山地的北坡和海拔较高处，草原和草甸草原发育在山地的南坡和海拔较低处。草原植被主要由丛生禾草和蒿属组成，有羊茅（*Festuca ovina*）、冷草（*Koeleria macrantha*）、纤细冷草（*K. gracilis*）、渐尖早熟禾（*Poa attenuata*）、冰草（*Agropyrum cristatum*）、克氏针茅（*Stipa krylovii*）、冷蒿（*Artmisia frigida*）、银叶蒿（*A. argyrophylla*）和北极蒿（*A. borealis*）。其他常见的草本植物

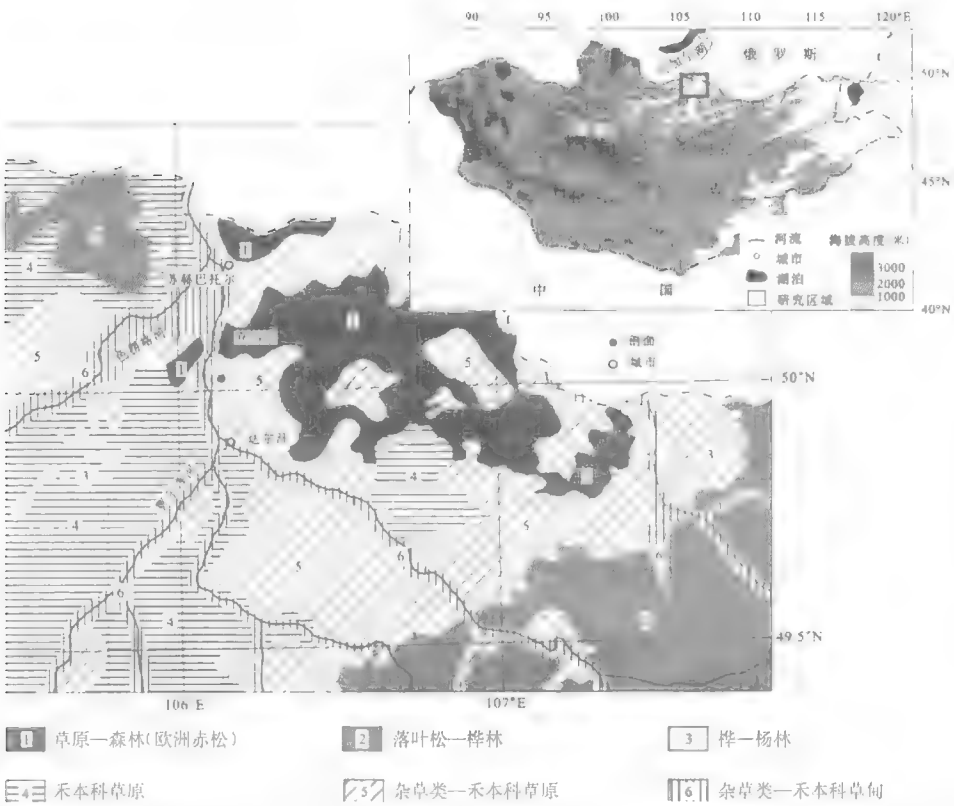

图3-1　研究区植被带分布(据Lavrenko等,1979; Hilbig,1995)及研究剖面位置图(自Ma等,2013)

有高山紫菀(*Aster alpinus*)、柳叶风毛菊(*Saussurea salicifolia*)、腺毛唐松草(*Thalictrum foetidum*)、蒙古黄芪(*Astragalus membranaceus*)、普米腊辣豆(*Oxytropis pumila*)、绢毛委陵菜(*Potentilla sericea*)、瑞香狼毒(*Stellera chamaejasme*)和花荵(*Polemonium coeruleum*)(Lavrenko等,1979; Hilbig,1995)。森林植被建群种为西伯利亚落叶松(*Larix sibirica*)、伴生种为西伯利亚松(*Pinus sibirica*)、欧洲赤松(*Pinus sylvestris*)、圆叶桦(*Betula rotundifolia*)、刺蔷薇(*Rosa acicularis*)、西伯利亚柏(*Juniperus sibirica*)、云杉属(*Picea*)和杨属(*Populus*)。湿生禾草和多年生杂草生长在河边和洼地,主要为珠芽蓼(*Polygonum viviparum*)、佛子茅属(Calamagrostis)、石竹科(Caryophyllaceae)、莎草科(Cyperaceae)、毛茛科(Ranunculaceae)、虎耳草科(Saxifragaceae)和伞形科(Umbelliferae)。富有特色的自然景观出现在色楞格(Selenga)和鄂尔浑(Orhon)河沿岸的砂地阶地上,那里发育着森林草原植被,以欧洲赤松为主,伴生有西伯利亚松、白榆(*Ulmus pumila*)、刺蔷薇、林地早熟禾(*Poa nemoralis*)、裂叶蒿(*Artemisia laciniata*)、黄囊苔草(*Carex korshinskyi*)、毛茛科和细叶蓼(*Polygonum angustifolium*)(Lavrenko等,1979; Hilbig,1995)。

2. 材料和方法

2.1. 地层和年代

夏马尔风成—古土壤天然露头剖面(50.2°N、105.2°E,海拔650 m)厚约30m,位于色楞格河南岸。根据岩性变化可分出3个地层单元(详见Feng等,2007a)。单元I(0~550cm)以砂层为主,单元II(550~1850cm)为粉砂层,单元III(1850~3090cm)为砂层(图3-2)。3个主要古土壤层(IIa、IIc 和 IIIa)中粉砂、黏土、有机质和碳酸盐的含量较高,六个弱发育古土壤层则以有机碳含量较高为主要特征(详见Feng等,2007a)

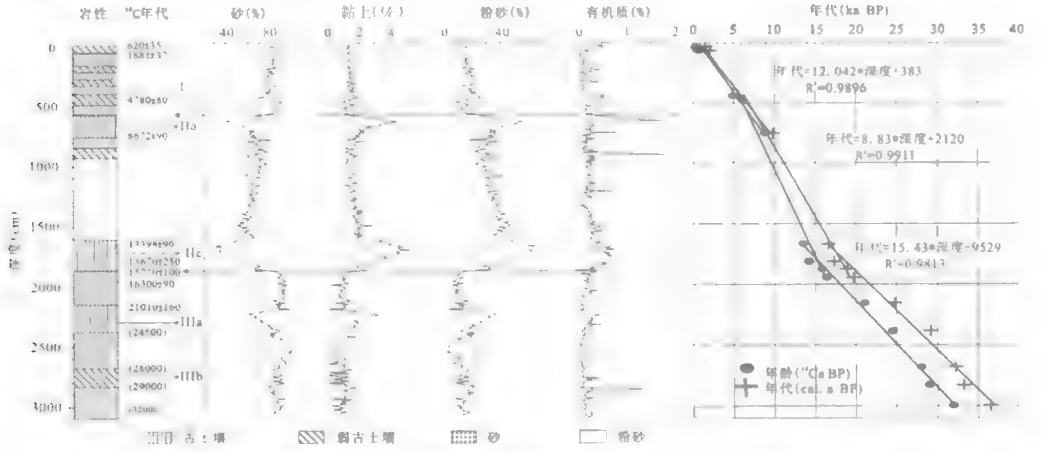

图3-2 夏马尔风成—古土壤剖面的地层岩性、年代、代用指标和年龄—深度模式
(砂、黏土、粉砂和有机质的百分含量引自Feng等,2007a),(Ma等,2013)

表3-1 夏马尔风成—古土壤剖面AMS及传统^{14}C测年数据(AMS 测年是指在美国亚利桑那大学的国家自然科学基金会加速器^{14}C实验室测得的年龄;传统^{14}C测年由兰州大学^{14}C测年实验室测定)(Feng等,2007a)

样品编号	实验编号	深度(cm)	测年材料	方法	δ ^{13}C值 (‰)	^{14}C年龄 (yr BP)	校正年代 (cal. yr BP)
SH02-C14-06	AA51936	50	炭屑	AMS	-24.8	620±35	620
SH02-C14-02	AA51935	60	炭屑	AMS	-23.1	1681±37	1608
4th Paleosol	CG-3465	450	全样	传统	常规	4780±-80	5542
MN-C14-14	AA519328	760	全样	AMS	-25.9	8672±-90	9076
MN-C14-11	AA519325	1680	全样	AMS	-24.4	13 398±-99	15 780
6th Paleosol	CG-3466	1850	全样	传统	常规	13 670±80	16 200
MN-C-14-9	AA519323	1890	全样	AMS	-22.8	15 770±90	18 900
MN-C-14-8	AA519322	1960	全样	AMS	-22.3	16 330±-100	19 000
MN-C-14-6	AA519320	2170	全样	AMS	-14.3	21 010±-160	24 610
7th Paleosol	CG9811	2400	全样	传统	常规	24 500±710	29 290
8th Paleosol	CG9812	2800	全样	传统	常规	28 900±1420	33 290

夏马尔风成—古土壤剖面共获得11个AMS和传统的^{14}C年代数据，AMS测年在美国亚利桑那大学的国家自然科学基金会加速器^{14}C实验室(NSF-Arizona Facility)完成；传统^{14}C测年在美州大学^{14}C测年实验室完成(表3-1)。显然，3090~2400cm的年代数据不够充足。

粒度分析显示地层单元III(1850~3090cm)的粒径变化不大(图3-2)，据此可假定整个单元III的沉积速率是基本不变的，那么，从最底部的3090cm到2400cm砂层的年代可由两个年代数据推测出来，即位于古古土壤IIIa层的顶部(2170 cm)的21 010 ^{14}C yr BP和位于古古土壤IIc层的底部(1890 cm)的15 771 ^{14}C yr BP，两者之间砂层的沉积速率推算为每18年沉积1cm(1cm =18年)。古古土壤IIc(1890cm处的年龄为15 770 ^{14}C yr BP，1680cm处的年龄为13 398 ^{14}C yr BP)的沉积速率为每11年沉积1cm(1cm =11年)，古古土壤IIIa和IIIb的年代可依此沉积速率推测出来，并且，可以通过和附近Bureghhanga剖面的古土壤年代对比进行验证(Feng等，2007a)。古古土壤层IIIa(2170~2400cm)顶部(2170cm)的年代数据为21 010 ^{14}C yr BP，据古古土壤层IIc沉积速率，古古土壤层IIIa底部的年龄推测为约24 500 ^{14}C yr BP，这个年龄和附近Bureghhang剖面的古土壤的年代数据(24 500 ^{14}C yr BP)非常接近(Feng等，2007a)。据砂层的沉积速率可推算出弱古土壤层(2700~2850cm)顶部(2700cm)的年龄为约28 000 ^{14}C yr BP。据沉积速率(1cm =11年)推算，弱古土壤层(2700~2850cm)底部(2850cm)的年龄为29 000 ^{14}C yr BP，这个年龄也很接近附近Bureghhang剖面的弱古土壤的年代数据(28 900 ^{14}C yr BP)(Feng等，2007a)。据砂层的沉积速率推算，剖面底部的年代(3020cm)为约32 000 ^{14}C yr BP。这样，2400~3090cm的年代数据不足得到了比较好的补充。

夏马尔剖面的全新世部分实际上是风成沉积和古土壤发育交替发生，其包含了一个古古土壤层(Ia)和四个弱古土壤层(Ia，Ib，Ic，Id)。古古土壤层Ia(550 ~ 760cm)的底部(760cm)的年代为8672 ^{14}C yr BP，弱古土壤层Id(450cm)的年代为4780 ± 80 ^{14}C yr BP。另外，在夏马尔山谷的丘陵山地上发现了相当于Ia的坡积土，此坡积土含有3个亚土壤层，其AMS年代(炭屑)分别为620 ± 35，1423 ± 35，和1681 ± 37 ^{14}C yr BP(Feng等，2007a)。

为了便于对比，本章用CALIB6.0和INTCAL 09校正程序(Reimer等，2009)对所有^{14}C年龄进行了日历年校正，用2 σ 的平均值作为校正年龄。与三个岩性地层单元相对应，采用三段式建立深度—年代模式。为了年代上的衔接，第一段从表层0cm到760cm，年代跨度为约0~8700 ^{14}C yr BP；第二段从450cm到1850cm，年代为约4800~15800 ^{14}C yr BP；第三段从1680cm到3090cm，年代为约13 400~32 000^{14}C yr BP。最后据深度—年代模式计算出65个样品采样深度所对应的年代。另外，如图3-2所示，单元I(砂层)和单元III(砂层)的沉降速率要比单元II(粉砂层)低，砂层较低的沉降速率可能要归因于以砂层为主的地层厚度被压实作用所压缩。

2.2. 孢粉分析

夏马尔风成—古土壤剖面共采集孢粉样品65个，采样间隔在3个主要古土壤层为25cm，其他层位为50cm。孢粉提取采用酸碱法结合筛滤法，即实验前加入一粒石松孢子(批号：938934，Lund University)，使用10%的HCL和36% HF对样品进行处理后，用超声波

清洗器清洗过筛(7μm筛布),然后用小管净化,最后用无水甘油保存制片鉴定。

参照正式出版的图版、手册和文章(Moore等,1991;王伏雄等,1995;马玉贞等,2009)及我们在中国北方和蒙古国收集的超过500个花粉种属的现代花粉标准片,在400倍莱卡光学显微镜下进行孢粉鉴定(必要时使用1000倍油镜),所有样品统计数量(不计孢子)均大于100粒。以陆生种子植物花粉总和为基数计算花粉百分比,以外加石松孢子法计算重量浓度。孢粉图谱使用Grapher和CorelDraw软件绘制。

2.3. 数据分析

2.3.1. 统计分析

判别分析(Discriminant analysis,DA)是多元统计分析中用于判别样品所属类型的一种统计分析方法,它首先依据各类型中已知样品建立每一类型的判别函数,然后计算新样品属于已知某类型的概率。最早将判别分析作为一种统计技术用于古植被重建,后来也有人将其用于表土花粉与植被关系研究(Liu和Lam,1985;MacDonald和Ritchie,1986;Sugden和Meadows,1989)。本章运用Ma等(2008)建立的现代植被类型判别函数去计算每个化石样品属于某植被类型的概率,重建植被历史。本章使用SPSS软件进行判别分析。

需说明的是,本章运用蒙古国南北断面表土花粉谱的植被类型判别函数(Ma等,2008)对夏马尔剖面化石花粉样品进行判别分析时,首先设定了两个假设:1 花粉谱中禾本科百分比较高时(>10%)可能指示草原植被的存在;2 云杉和冷杉比例较高时(>30%)可能表明泰加林存在。这两个假设是基于以下观察而得出的。首先,现代花粉雨的研究显示,禾本科花粉在过度放牧的草原、森林草原的现代花粉组合中呈现极端的低代表性(<5%~10%)是源于人类的干扰(Ma等,2008)。第二,夏马尔古风成—土壤剖面的花粉谱中云杉和冷杉的花粉百分比含量似乎远高于蒙古国南北断面表土花粉谱中的含量。

2.3.2. 花粉—温度(T)和花粉—湿度(M)指数

表3-2 组、类型、主要花粉类型和计算花粉—温度(T)和花粉—湿度指数(M)的算式(Ma等,2013)

组	类型	主要花粉类型
S1	旱生荒漠	藜科,白刺属,蒺藜科[蒺藜属(*Tribulus*),霸王属(*Zygophyllum*),骆驼蓬属(*Peganum*)]
S2	荒漠—草原	花葱科,春黄菊型,麻黄,旋花属(*Convolvulus*)
S3	中—旱生型草原	蒿属,紫菀型,狼毒属,桔梗科
S4	桦林/灌丛	桦木属,桤木属(*Alnus*),蔷薇科,柳属/榆属,蒲公英型
S5	冷湿针叶林	云杉属+冷杉属,刺柏属,西伯利亚松型,欧洲赤松型,毛茛科,石竹科
S6	适中水分条件下的草原	莎草科,蓼科
	花粉气候指数	算式
T	温度指数	$T=(P_{S1}+P_{S2}+P_{S3})/(P_{S4}+P_{S5}+P_{S6})$
M	湿度指数	$M=(P_{S5}+P_{S6})/(P_{S1}+P_{S2}+P_{S3}+P_{S4})$

Ma等(2008)依据蒙古国南北断面现代表土花粉资料建议了花粉—温度(T)和花粉—湿度(M)指数。Ma等首先使用聚类分析(hierarchical cluster analysis，HCA)和非度量多维测量(non-metric multidimensional scaling，NMS)方法对对气候敏感的花粉类型进行分类，并结合花粉种属母体植物的生态习性建立了六个组来代表不同的植被生态类型；然后根据花粉类型组的比值计算出T和M两个指数。而且，蒙古国南北断面上T和M指数计算出的温度和湿度的变化梯度与现代年均温和年均降水的变化梯度基本一致验证了这两个指数的有效性(Ma等，2008)。因此，基于化石花粉数据，利用花粉—气候指数去重建夏马尔地区历史上的温度和湿度是可行的。按照同样的方法，本章采用半定量的温度和湿度指数(表3-2)重建了夏马尔地区的花粉—温度(T)和花粉—有效湿度(M)序列。考虑到夏马尔地区花粉类型和地植物的特点，本章对Ma等(2008)文中的表4做了轻微的调整(见表3-2)。

3. 结果与分析

3.1. 孢粉谱

夏马尔风成—古土壤剖面的花粉主要有云杉属+冷杉属(*Picea*+*Abies*)、欧洲赤松型(*Pinus sylvestris*-type)、西伯利亚松型(*Pinus sibirica*-type)、落叶松属(*Larix*)、柏科(Cupressaceae)、蒿属(*Artemisia*)、紫菀型(*Aster*-type)、蒲公英型(*Taraxacum*-type)、禾本科(Poaceae)、狼毒属(*Stellera*)、藜科(Chenopodiaceae)、白刺属(*Nitraria*)、蒺藜科(Zygophyllaceae)、柽柳科(Tamaricaceae)、桔梗科(Campanulaceae)、罂粟科(Papaveraceae)、毛茛科(Ranunculaceae)和花荵科(Polemoniaceae)，其他还有榆属(*Ulmus*)、桦木属(*Betula*)、柳属(Salix)、春黄菊型(*Anthemis*-type)、蓼科(Polygonaceae)和莎草科(Cyperaceae)等。根据主要花粉类型百分比含量，将剖面孢粉谱从下到上划分七个组合带(图3-3)。

带1(2540~3100cm，约38 000~29 600 cal. yr BP)最显著的特征是泰加林植物花粉含量很高，为整个剖面最高值，且总花粉浓度也较高。泰加林花粉以云杉属+冷杉属(11.36%~60.66%)和西伯利亚松型(8.89%~40.71%)为主，欧洲赤松型、落叶松属和柏科有一定的含量。草本植物和夏绿阔叶树花粉的含量非常低。

带2(2150~2540cm，约29 600~23 400 cal. yr BP)中草本植物花粉的含量较带1有所增加，主要为蒿属(3.77%~43.01%)、禾本科(4.72%~27.27%)和藜科(3.03%~22.73%)；而泰加林花粉含量较带1有所减少，主要为西伯利亚松型(1.85%~11.61%)和云杉属+冷杉属(4.84%~35.53%)。其他特征包括：藜科花粉含量达到整个剖面最高值、夏绿落叶树花粉含量极低和总花粉浓度较低。

带3(1850~2150cm，约23 000~18 700 cal. yr BP)的明显特征是云杉属+冷杉属(9.93%~85.60%)花粉含量较带2有显著增加，禾本科(0.79%~15.79%)和蒿属(5.60%~17.88%)花粉含量较上带明显减少，夏绿落叶树花粉含量极低，总花粉浓度也很低。

带4(1610~1850cm，约18 700~16 200 cal. yr BP)的花粉组合中禾本科花粉含量高(5.91%~44.50%)且达到整个剖面最高值，总花粉浓度也较高。紫菀型和蒿属花粉有一定的含量，

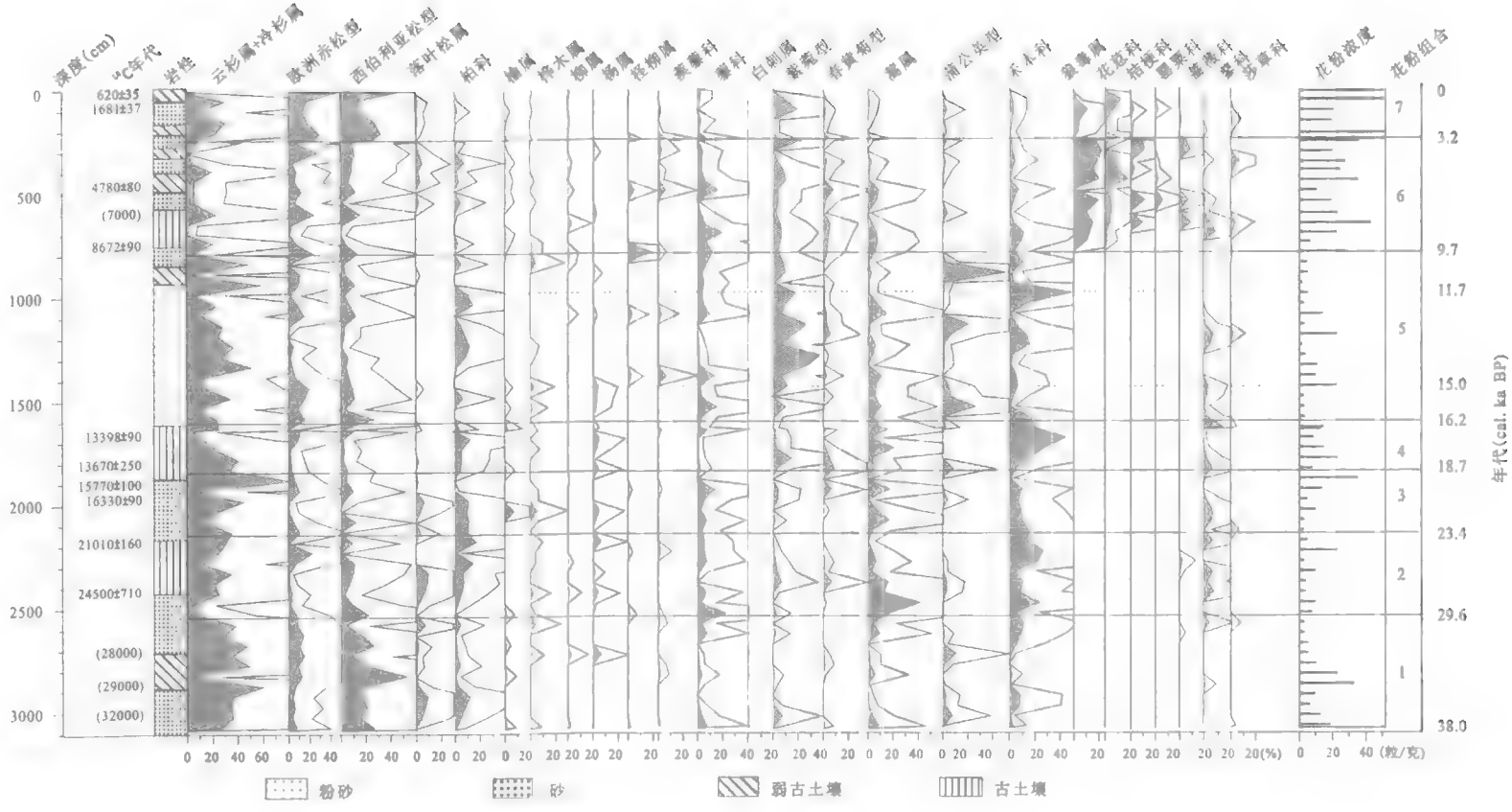

图3-3　夏马尔风成—古土壤剖面主要花粉类型百分比图(黑色实线:百分比扩大了5倍)(Ma等,2013)

旱生型植物花粉(如藜科、白刺属、蒺藜科和柽柳科)和夏绿落叶树花粉的含量极低。

带5(800~1610cm,约16 200 ~ 9700 cal. yr BP)的总花粉浓度较低,花粉组合以云杉属+冷杉属(4.48%~59.65%)、紫菀型(4.54%~37.61%)、禾本科(0.96%~49.44%)和蒲公英型(1.75%~52.99%)花粉含量具有高频率和高振幅的变化为特征。常见的草本植物还有蒿属和藜科。本带又分为三个亚带。

顶部(1450~1610cm,约16 200~15 000 cal. yr BP)和底部(1010~800cm,约11 700~9700 cal. yr BP)的花粉组合总花粉浓度极低,以云杉属+冷杉属(4.48%~59.65%)和松属(<30.00%)的花粉含量较高为特征。中间亚带(1450~1010cm,约15 000~11 700 cal. yr BP)总花粉浓度较高,且紫菀型花粉含量(6.94%~37.61%)远高于顶部和底部亚带,西伯利亚型和欧洲赤松型花粉含量较低,荒漠植物花粉如蒺藜科和柽柳属花粉含量甚微。

带6(240~800cm,约9700~3200 cal. yr BP)具有以下四个特征:1)云杉属+冷杉属花粉含量较低;2)几种中生草本植物(包括狼毒属、桔梗科、罂粟科、毛茛科和花葱科)突然出现;③总花粉浓度显著增加;④缺少夏绿乔木花粉。

带7(0~240cm,约3200~0 cal. yr BP)花粉组合中云杉属+冷杉属(10.21%~31.47%)、西伯利亚松型(14.15%~44.23%)和欧洲赤松型(14.47%~45.41%)花粉含量较上带(带6)显著上升,而旱生型草本植物(如藜科、蒺藜科和柽柳科)和中生草本植物(如桔梗科、罂粟科和毛茛科)花粉含量较带6急剧下降,紫菀型花粉含量较上带略有增加,而夏绿落叶树花粉含量几乎为零。总花粉浓度也较高。

3.2. 统计分析结果

图3-4显示了上述7个带的化石花粉样品的判别函数在第一轴和第二轴上的判别得分,及其与蒙古国南北断面5个植被带表土样品判别函数范围(图3-4中的黑色实线闭合圈)的比较。表土样品在第一轴和第二轴上的排序结果表明,尽管泰加林和森林草原的样品存在一些重叠,但五个植被带(泰加林、森林—草原、草原、荒漠草原和荒漠)的表土样品组可明显区分,且荒漠和其他植被的样品显著分离(Ma等,2008)。在夏马尔风成—古土壤剖面的化石花粉谱中,1、2、3、4和7花粉组合带的大多数样品属于或接近现代蒙古国南北断面的4个植被类型(荒漠除外),在某种程度上建议,化石花粉组合与代表现代植被类型的表土花粉组合的判别函数相类似,也就是说,现代花粉—植被关系可用于解释化石花粉。但有两点需要注意:1)第5化石花粉组合带的样品既与草原也与森林草原组合交叠;2)虽然第6化石花粉组合带的样品远离其他植被类型而靠近现代森林草原,但几乎没有样品落在现代森林草原的范围内。

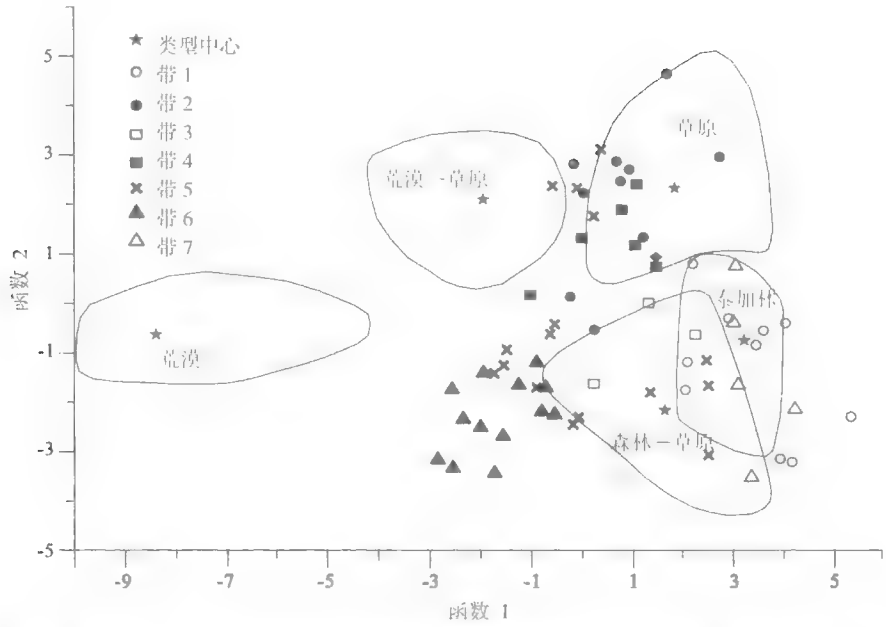

图3-4　夏马尔风成—古土壤剖面化石花粉样品的判别函数在第一和第二轴上的排序结果。基本上与代表蒙古国南北断面5个植被类型的表土样品组的判别函数范围(黑色实线闭合圈)相重叠(Ma等,2013)

图3-5显示了每一个化石样品花粉组合与现代表土样品花粉组合的相似概率及植被指数。大多数样品有较高的相似概率(>0.5),表明这些化石样品花粉组合所代表的植被类型与现代表土花粉组合所反映的植被类型相似。被错误分类的样品通常与现代相似物之间有非常低的相似概率值(<0.2),表明它们远离分类中心,与它们被指派的植被类型有一定的差距(Liu和Lam,1985;Reese和Liu 2005)。

综上所述,判别分析结果显明,通过与蒙古国南北断面现代花粉样品的比较,夏马尔剖面化石花粉谱基本可以用现代类似物进行解译,即依据地层化石花粉组合与现代相似物的相似概率和植被指数的变化可以重建植被的变化历史。

3.3. 气候解释

夏马尔风成—古土壤剖面的孢粉组合特征(图3-3)、半定量推断出的古植被和花粉—温度和花粉—湿度指数(图3-5)可以较为详尽地揭示蒙古高原北部过去38 000年来的植被及气候变化特征。

约38 000~30 000 cal. yr BP,花粉组合以云杉属+冷杉属(11.36%~60.66%)和西伯利亚松型(8.89%~40.71%)含量为整个剖面最高值及总花粉浓度较高为特征,植被景观很可能为泰加林。这样的解释是基于下面两点认识。首先,尽管松属花粉在现代花粉谱中显示出强扩散性和超代表性,但云杉属和冷杉属花粉的扩散能力却较低(Liu等,1999;Lu等,2008;Ma等,2008)。例如,在没有松树生长的地方,松属花粉的含量可能超过50%,但冷杉属和云杉属花粉的含量在冷杉和云杉林中一般为20%~50%,在林地外会显著下降。虽然在一些沙漠样品中,由于花粉浓度很低,导致云杉属和冷杉属的花粉百分比含量较高,但一般也不会超过10%(Liu等,1999;Lu等,2008;Ma等,2008)。第二,在蒙古高原北部的森林草原地区,流经乌兰巴托—贝加尔湖走廊谷地的色楞格河及其支流阶地的砂地上,生

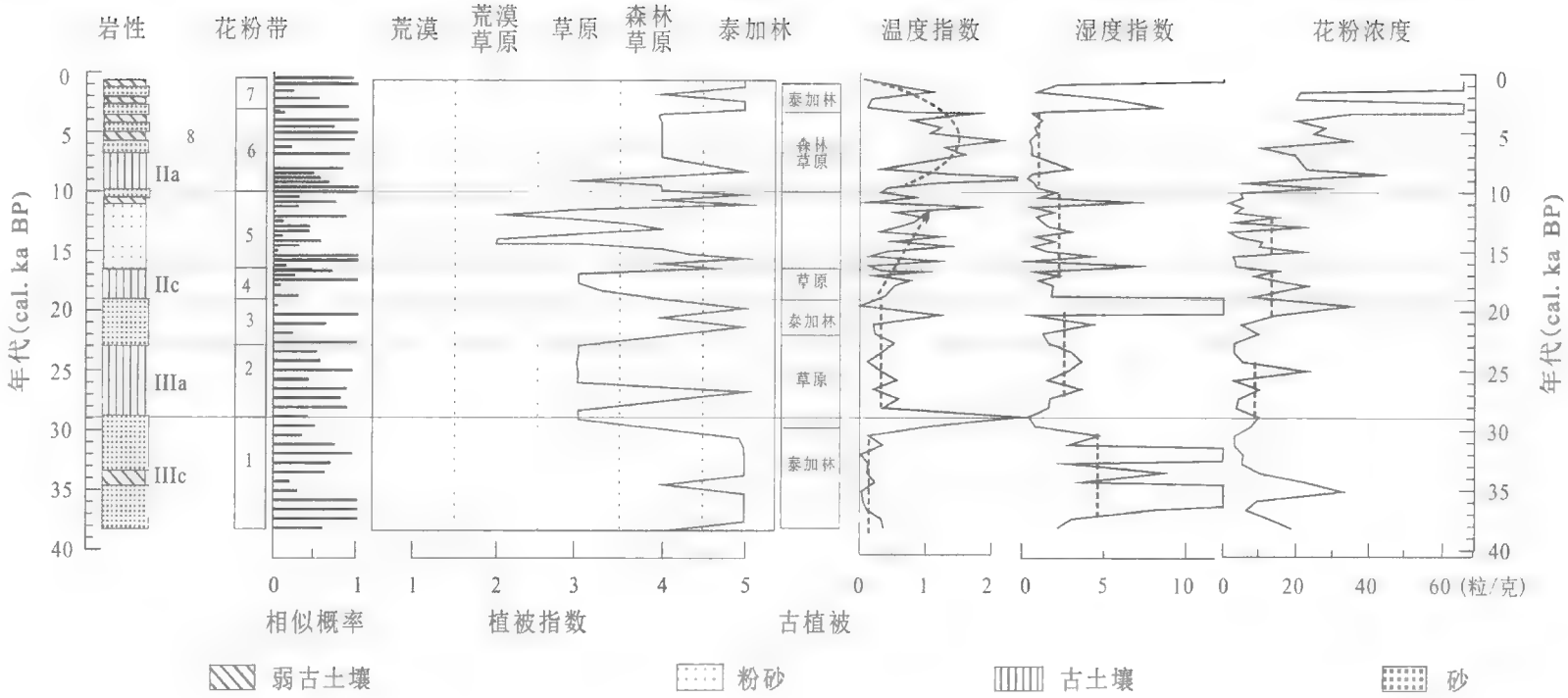

图3-5　夏马尔风成—古土壤剖面的气候和植被重建

左边:花粉数据判别分析结果显赤的相似、概率、植被指数和古植被;右边:花粉温度指数、花数—湿润度指数和总花数浓度(Ma等,2013)

长着以欧洲赤松和西伯利亚松为建群的泰加林(Lavrenko等,1979;Hilbig,1995),这说明夏马尔地区在38 000~30 000 cal. yr BP发育泰加林是非常可能的。另外,相似概率值也较高,植被指数指示的泰加林和花粉气候指数显示的低温高湿都进一步支持喜冷湿的泰加林在这个时期发育。

约30 000~23 000 cal. yr BP,以蒿属和禾本科花粉为主的花粉组合和较低的花粉浓度显示,当时草原植被在较冷干的气候条件下得到了发展。等于或接近于草原植被的植被指数和较高的相似概率也建议,这个时期的花粉组合所反映的草原植被可与蒙古高原北部的现代表土花粉组合所反映的草原植被相对比。另外,在29 000 cal. yr BP左右有一个温度高峰值,与其相伴随的是一个显著的低湿度值,但因仅有一个样品,这里不再讨论。

约23 000~19 000 cal. yr BP是另一个针叶林发育期,重建的温度和湿度较前期(约30 000~23 000 cal. yr BP)有所升高。接着,约19 000~16 500 cal. yr BP花粉组合中禾本科的花粉含量和总花粉浓度都显著增加,暗示了较温暖气候条件下的草原(以禾本科为建群)在该区扩张。植被指数也显示出植被类型是草原。但是,在19 000~17 500 cal. yr BP,部分样品的相似概率较低,可能用判别分析指派的重建植被与现代植被有一定的差距。

约16 500~15 000 cal. yr BP和约12 000~10 000 cal. yr BP,孢粉组合的特点是:云杉属+冷杉属(>15.00%)和松属(<30.00%)的百分比含量较高,但花粉浓度达到全剖面最低。如前所述,松属花粉很可能是被风长距离搬运来的。虽然花粉浓度很低,但综合考虑到云杉属和冷杉属较低的扩散能力(Liu等,1999;Lu等,2008;Ma等,2008),云杉属和冷杉属的花粉颗粒应来自附近的山地。在这两个时期(约16 500~15 000 cal. yr BP和约12 000~10 000 cal. yr BP),植被指数和相似概率值也显示出植被类型是泰加林,且重建的温度也很低。约15 000~12 000 cal. yr BP,部分样品的相似概率非常低(<0.2),暗示了用判别分析指派的重建植被与现代植被差距较大。该时段花粉组合以紫菀型和云杉属+冷杉属含量较高和总花粉浓度较高为主要特征,表明这个时期的植被类型为草原和森林草原。而且,重建的温度和有效湿度也可满足草原和森林草原植被发育的生态需求。

约10 000~3000 cal. yr BP,重建的温度较高,湿度较低。花粉组合和植被指数显示,这个时期的植被类型是森林草原。约3000 cal. yr BP以来,在凉湿条件下,泰加林在该区得到了发展。在整个全新世,地层化石花粉组合与现代相似物的相似概率值都比较高,这对全新世植被的重建提供了有力的支持。值得一提的是,约10 000 cal. yr BP年以来,重建的温度曲线呈马形,即从约10 000 cal. yr BP逐渐上升,到约6000 cal. yr BP达到最大值,然后开始逐渐下降。另外,约10 000~3000 cal. yr BP,重建的湿度值较低,约3000 cal. yr BP以来,重建的湿度值有显著的增加。

4. 讨论

4.1. 区域性比较

蒙古高原北部MIS3后期(约38 000~30 000 cal. yr BP)的极端湿润气候在中国北部也有报道。例如,MIS3的晚期(约40 000~30 000 cal. yr BP),在中国黄土高原,针叶林的急剧扩张反映了气候的极端湿润(Feng等,2007b);在蒙古高原南部,湖水面积和高度显著增

加(Pachur等,1995;Ma等,2003;Zhang等,2004)。另外,在该时段,在日本西部,温带针叶林也有所扩张(Hayashi等,2010)。

夏马尔地区重建的古气候显示,MIS2(约30 000~10 000 cal. yr BP)期间,早期(约30 000~20 000 cal. yr BP)比晚期(约20 000~10 000 cal. yr BP)更为寒冷,而且在约23 000~19 000 cal. yr BP,耐冷湿的泰加林在蒙古高原北部发育,耐寒的针叶林在日本西部生长(Gotanda和Yasuda,2008;Hayashi等,2010)。这在时间序列上与北大西洋冰盛期(Dansgaard等,1993;Bond等,1997;Alley等,2002)对应得很好。

夏马尔地区重建的过去约10 000 cal. yr BP来温度曲线呈一个弓形,约10 000~6000 cal. yr BP呈上升趋势(即变暖),约6000 cal. yr BP以来呈下降趋势(即变冷);重建的湿度值在约10 000~3000 cal. yr BP都是较低的,但从约3000 cal. yr BP开始,有一个明显的反弹。这个气候曲线与贝加尔湖重建的三条气候曲线基本一致。贝加尔湖重建的三条气候曲线显示,温度和湿度指数有相同的变化趋势(Demske等,2005),即在全新世的早期(约6000 cal. yr BP前),温度指数呈渐增(变暖)趋势而湿度指数呈下降(变干)趋势;在全新世的晚期(约6000 cal. yr BP后)湿度指数渐增(变湿)而温度指数下降(变凉)。由此看来,在乌兰巴托至贝加尔湖这个走廊地带,全新世最暖干的气候出现在中全新世,早全新世和晚更新世则较凉湿。

对比来看,重建的蒙古高原北部的全新世湿度变化与重建的中国北方全新世湿度变化似乎是相反的。在中国北方,中全新世是暖湿的,而晚全新世是凉干的(Feng和Khosbayar,2004;Feng等,2006a,2006b;2011;Ma等,2004;Xiao等,2004;Cao等,2010;Xu等,2010)。这种现象可能主要归因于东亚地区太阳辐射的变化。也就是说,在中全新世,全球的温度升高驱使东亚季风给中国北方带来更多的降水,因而导致了暖湿的气候。相反,中全新世的升温有效地导致了蒙古高原北部蒸发量的增强,且由于距离太远,东亚季风输送到蒙古国北部的水汽也非常有限,因而导致了暖干的气候(Wang等,2009;2011;Wang和Feng,2013)。晚全新世的低温有效地减少了蒙古高原北部的蒸发量,因而湿度增大。

4.2. 全球遥相关

本部分试图通过夏马尔剖面花粉记录与中国洞穴石笋和格陵兰冰芯(Greenland Ice core)的对比分析(图3-6)探讨蒙古高原北部过去约40 000年来气候变化的调控机制。葫芦洞(Hulu Cave)(Wang等,2001)石笋、董歌洞(Dongge Cave)(Yuan等,2004)石笋和格陵兰(Dansgaard等,1993)冰芯的δ¹⁸O数据来自NOAA网站(www.ngdc.noaa.gov/paleo/icecore/greenland/summit/index.html),太阳辐射量曲线来自Laskar等(2004)。在约38 000~30 000 cal. yr BP,夏马尔剖面记录显示了泰加林发育和气候极端湿润,这与格陵兰冰芯记录的温暖期和中国石笋记录的东亚夏季风强降水事件(Wang等,2001)在时间段上基本一致。我们推测,MIS3中期(约48 000~40 000 cal. yr BP)相对较高的冬季太阳辐射可能导致了北大西洋地区气候较温暖,从而使得蒙古高原北部地区得到足够多的西风环流携带来的水汽。MIS3晚期相对较低的夏季太阳辐射和有所增长的冰盖可能导致了蒙古高原北部的气温下降,低温又抑制了蒸发量,从而使有效湿度有所增加。

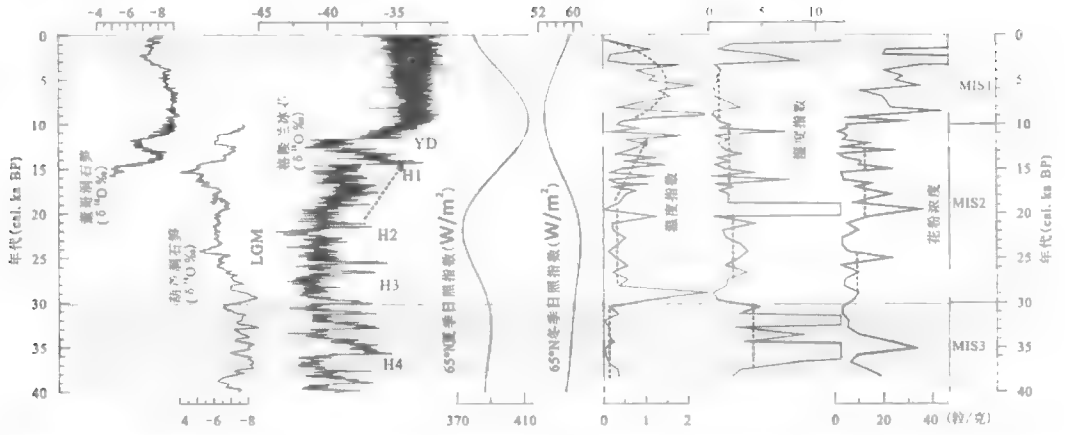

图3-6　夏马尔剖面花粉记录重建的温度、湿度指标和总花粉浓度与亚洲季风记录(Wang等,2001;Yuan等,2004),格陵兰冰芯记录(Dansgaard等,1993)和太阳辐射量的对比(Lasker等,2004)(Ma等,2013)

约30 000~20 000 cal. yr BP,夏季太阳辐射量下降,包括北格陵兰在内的北大西洋地区温度降低,可能导致了蒙古高原北部温度和湿度的降低。约19 000~11 000 cal. yr BP夏马尔剖面重建的气温有所上升,这似乎是对约21 000~13 000 cal. yr BP北大西洋地区氧同位素纪录的温度上升(Dansgaard等,1993;Bond等,1997;Dahl-Jensen等,1998;Bard等,2000;Alley等,2002)的延迟响应,再次支持了北大西洋地区和蒙古高原北部存在相关的猜测。另外,值得特别关注的是:从约19 000 cal. yr BP起,蒙古高原北部气温开始上升、北半球山地冰川和冰盖开始撤退(Rinterknecht等,2006;Clark等,2009)、热带大西洋和太平洋海平面开始上升且温度开始升高(Clark等,2004)、中纬度冰盛期(Last Glacial Maximum)结束(Schaefer等,2006),它们是否受同一机制的调控?

4.3. 两点说明

第一,三层主要古土壤层(Ⅲa、Ⅱc和Ⅰa)中的Ⅲa和Ⅱc是应该被特别关注的。在MIS2(约30 000~23 000 cal. yr B)早期,夏马尔剖面的古土壤层Ⅲa与草原植被对应,而不是与森林草原对应,这符合生物地理学中对于黑沃土/软土(Mollisol)的定义(Bhattacharyya等,2006;Feng等,2007a;2011)。而且,古土壤Ⅲa的形成年代与西伯利亚西南部灰化土的形成年代(约26 000~22 000 cal. yr BP)基本上是一致的(Melinikova,1991;Tarasov等,1997;Chlachula,2001;Velichko等,2002;Blyakharchuk等,2004)。与主要古土壤层Ⅲa非常相似,约19 000~16 500 cal. yr BP,主要古土壤层Ⅱc发育时的植被类型也为草原,无独有偶,西伯利亚西南部(Melinikova,1991;Tarasov等,1997;Velichko等,2002)和哈萨克斯坦东部(Feng等,2011)地区同期也发育了相应的古土壤。然而,在中国北部没有同时代的古土壤层记录被发现。还应指出的是,与上覆和下伏的砂层相比,在古土壤层中,产量低、扩散能力极差和不易保存的禾本科花粉的百分含量高,且总花粉浓度也较高。这些特征显示,主要古土壤层Ⅲa和Ⅱc形成的时期,草原植被繁茂,植被覆盖率高。

第二,在格陵兰冰芯记录和中国洞穴石笋记录中,波令/阿勒罗德(Bolling/Allerod,B/A)暖期(约15 000~13 000 cal. yr BP)和新仙女木(Younger Dryas,YD)冷事件(约13 000~10 000 cal. yr BP)的表现都很明显。B/A暖期在西伯利亚南部也被广泛发现(Horiuchi等,

2000; Blyakharchuk 等，2004; 2007; 2008; Demske 等，2005; Tarasov 等，2007; Rudaya 等，2008; 2009; Bezrukova等，2009）但在我们的记录里，这个事件只是微弱的和不确定的YD冷事件在西伯利亚南部也被大量发现（Blyakharchuk等，2004; 2007; 2008; Demske等，2005; Tarasov等，2007; Rudaya等，2008; 2009; Bezrukova等，2009）在夏马尔剖面记录里，位于约12 000~10 000 cal. yr BP的低温槽有可能是YD冷事件的表现。

致谢：廖淦标教授在文章写作过程中给予指导；蒙红卫博士、桑艳礼博士和李丹丹硕士参与了数据整理和绘图等工作；参加野外采样的有：张虎才教授，安成邦博士，Khosbaya教授，Narantsetseg教授。

参考文献

马玉贞，蒙红卫，桑艳礼，孙爱芝，伍婧，王维. 2009. 光学显微镜下松柏类和菊科花粉的分类、鉴定要点及生态意义. 古生物学报，48（2）：240~253.

Melinikova, A.P. 1991. 关于苏联北天山全新世冰川作用的退化问题. 冰川冻土 13(4): 291~298.

王伏雄，钱南芬，张玉龙，杨惠秋. 1995. 中国植物花粉形态. 第二版. 北京：科学出版社.

Alley, R.B., Brook, E.J. and Anandakrishnan, S., 2002. A northern lead in the orbital band: north - south phasing of Ice-Age events. Quaternary Science Reviews, 21: 431~441.

Bard, E., Rostek, F., Turon, J.L. and Gendreau, S., 2000. Hydrological Impact of Heinrich Events in the Subtropical Northeast Atlantic. Science, 289: 1321~1324.

Berger, A. and Loutre, M.F., 1991. Insolation values for the climate of the last 10 million years. Quaternary Science Reviews, 10: 297~317.

Bezrukova, E.V., Abzaeva, A.A., Letunova, P.P, Kulagina, N.V. and Orlova, L.A., 2009. Evidence of environmental instability of the Lake Baikal area after the last glaciations. Archaeology Ethnology & Anthropology of Eurasia, 37(3): 17~25.

Bhattacharyya, T., Pal, D.K., Lal, S., Chandran, P. and Ray, S.K., 2006. Formation and persistence of Mollisols on zeolitic Deccan basalt of humid tropical India. Geoderma, 136: 609~620.

Blyakharchuk, T.A., Wright, H.E., Borodavko, P.S. and van der Knaap, W.O., Ammann, B., 2004. Late Glacial and Holocene vegetational changes on the Ulagan high-mountain plateau, Altai Mountains, southern Siberia. Palaeogeography, Palaeoclimatology, Palaeoecology, 209: 259~279.

Blyakharchuk, T.A., Wright, H.E., Borodavko, P.S. and van der Knaap, W.O., Ammann, B., 2007. Late Glacial and Holocene vegetational history of the Altai Mountains (southwestern Tuva Republic, Siberia). Palaeogeography, Palaeoclimatology, Palaeoecology, 245: 518~534.

Blyakharchuk, T.A., Wright, H.E., Borodavko, P.S. and van der Knaap, W.O., Ammann, B., 2008. The role of pingos in the development of the Dzhangyskol lake-pingo complex, central Altai Mountains, southern Siberia. Palaeogeography, Palaeoclimatology, Palaeoecology, 257: 404~420.

Bond, G., Showers, W., Cheseby, M., Lotti, R., Almasi, P., deMenocal, P., Priore, P., Cullen, H., Hajdas, I. and Bonani, G., 1997. A Pervasive Millennial-Scale Cycle in North Atlantic Holocene and Glacial Climates. Science, 278: 1257~1266.

Bond, G., Kromer, B., Beer, J., Muscheler, R., Evans, M., Showers, W., Hoffmann, S., Lotti-Bond, R., Hajdas, I. and Bonani, G., 2001. Persistent Solar Influence on North Atlantic Climate during the Holocene. Science, 294: 2130~2136.

Bradley, R.S., 1999. Paleoclimatology: Reconstructing Climates of the Quaternary. 2nd Edition. Harcourt Academic Press, New York.

Cao, X.Y., Xua, Q.H., Jing, Z.C., Tang, J.G., Li, Y.C. and Tian, F., 2010. Holocene climate change and human impacts implied from the pollen records in Anyang, central China. Quaternary International, 227: 3~9.

Chen, F.H., Yu, Z.C., Yang, M.L., Ito, E., Wang, S.M., Madsen, D.B., Huang, X.Z., Zhao, Y., Sato, T., John, B., Birks, H., Boomer, I., Chen, J.H., An, C.B. and Wünnemann, B., 2008. Holocene moisture evolution in arid central Asia and its out-of-phase relationship with Asian monsoon history. Quaternary Science Reviews, 27: 351~364.

Chlachula, J., 2001. Pleistocene climate change, natural environments and palaeolithic occupation of the upper Yenisei area, south-central Siberia. Quaternary International, 80~81: 101~130.

Clark, P.U., Dyke, A.S., Shakun, J.D., Carlson, A.E., Clark, J., Wohlfarth, B., Mitrovica, J.X., Hostetler, S.W. and McCabe, A.M., 2009. The last Glacial Maximum. Science, 325: 710~714.

Clark, P.U., McCabe, A.M., Mix, A.C. and Weaver, A.J., 2004. Rapid rise of sea level 19 000 years ago and its global implications. Science, 304: 1141~1144.

CLIMAP Members, 1981. Seasonal reconstruction of the Earth's surface at the Last Glacial Maximum. GSA Map and Chart Series, MC-36. Geological Society of America.

Clemens, S.C., Murray, D.W. and Prell, W.L., 1996. Nonstationary phase of the Plio-Pleistocene Asian monsoon. Science, 274: 943~948.

COHMAP Members, 1988. Climatic changes of the last 18 000 years: observations and model simulations. Science, 241: 1043~1052.

Dahl-Jensen, D., Mosegaard, K., Gundestrup, N., Clow, G.D. and Johnsen, S.J., Hansen, A.W., Balling, N., 1998. Past Temperatures Directly from the Greenland Ice Sheet. Science, 282: 268~271.

Dansgaard, W., Johnsen, S.J., Clausen, H.B., Dahl-Jensen, D., Gundestrup, N.S., Hammer, C.U., Hvidberg, C.S., Steffensen, J.P., Sveinbjornsdottir, A.E., Jouzel, J. and Bond, G., 1993. Evidence for generalinstability of past climate from a 250-kyrice-core record. Nature, 364: 218~220.

Demske, D., Heumann, G., Granoszewski, W., Nita, M., Mamakowa, K., Tarasov, P.E. and Oberhansli, H., 2005. Late glacial and Holocene vegetation and regional climate variability evidenced in high-resolution pollen records from Lake Baikal. Global and Planetary Change, 46: 255~279.

Feng, Z.-D., Chen, F.H., Tang, L.Y. and Kang, J.C., 1998. East Asian monsoon climates and Gobi dynamics in marine isotope stages 4 and 3. Catena, 33: 29~46.

Feng, Z.-D., 2001. Gobi dynamics in the Northern Mongolian Plateau during the past 20 000+yr preliminary results. Quaternary International, 76/77: 77~83.

Feng, Z.-D. and Khosbayar, P., 2004. Paleosubarctic Eolian environments along the southern margin of the North American ice sheet and the southern margin of Siberia during the Last Glacial Maximum. Palaeogeography, Palaeoclimatology, Palaeoecology, 212: 265~275.

Feng, Z.-D., Wang, W.G., Guo, L.L., Khosbayar, P., Narantsetseg, T., Jull, A., An, C.B., Li, X.Q., Zhang, H.C. and Ma, Y.Z., 2005. Lacustrine and eolian records of Holocene climate changes in the Mongolian Plateau: preliminary results. Quaternary International, 136: 25~32.

Feng, Z.-D., An, C.B. and Wang, H.B., 2006a. Holocene climatic and environmental changes in the arid and semi-arid areas of China: a review. The Holocene, 16: 119~130.

Feng, Z.-D., Tang, L.Y., Wang, H.B., Ma, Y.Z. and Liu, K.B., 2006b. Holocene vegetation variations and

the associated environmental changes in the western part of the Chinese Loess Plateau. Palaeogeography, Palaeoclimatology, Palaeoecology, 241: 440~456.

Feng, Z.-D., Zhai, X.W., Ma, Y.Z., Huang, C.Q., Wang, W.G., Zhang, H.C., Khosbayar, P., Narantsetseg, T., Liu, K.B. and Rutter, N.W., 2007a. Eolian environmental changes in the Northern Mongolian Plateau during the past ~35,000 yr. Palaeogeography, Palaeoclimatology, Palaeoecology, 245: 505~517.

Feng, Z.-D., Tang, L.Y., Ma, Y.Z., Zhai, Z.X., Wu, H.N., Li, F., Zou, S.B., Yang, Q.L., Wang, W.G., Derbyshire, E. and Liu, K.B., 2007b. Vegetation variations and associated environmental changes during marine isotope stage 3 in the western part of the Chinese Loess Plateau. Palaeogeography, Palaeoclimatology, Palaeoecology, 246: 278~291.

Feng, Z.-D., Ran, M., Yang, Q.L., Zhai, X.W., Wang, W., Zhang, X.S. and Huang, C.Q., 2011. Stratigraphies and chronologies of late Quaternary loess-paleosol sequences in the core area of the central Asian arid zone. Quaternary International, 240: 156~166.

Fowell, S.J., Hansen, B.C.S., Peck, J.A., Khosbayar, P. and Ganbold, E., 2003. Mid- to late-Holocene climate evolution of the Lake Telmen Basin, north-central Mongolia, based on palynological data. Quaternary Research, 59: 353~363.

Gotanda, K. and Yasuda, Y., 2008. Spatial biome changes in southwestern Japan since the Last Glacial Maximum. Quaternary International, 184: 84~93

Harrison, S.P., Yu, G. and Tarasov, P.E., 1996. Late Quaternary lake-level record from northern Eurasia. Quaternary Research, 45: 138~159.

Hayashi, R., Takahara, H., Hayashida, A. and Takemura, K., 2010. Millennial-scale vegetation changes during the last 40,000 yr based on a pollen record from Lake Biwa, Japan. Quaternary Research, 74: 91~99.

Hilbig, W., 1995. The Vegetation of Mongolia. SPB Academic Publishing, Amsterdam.

Horiuchi, K., Minoura, K., Hoshino, K., Oda, T., Nakamura, T. and Kawai, T., 2000. Palaeoenvironmental history of Lake Baikal during the last 23 000 years. Palaeogeography, Palaeoclimatology, Palaeoecology, 157: 95~108.

Khosbayar, P., 1989. Map of Geological Complexes of Mongolia (1:500 000). Moscow Publishing House, Moscow (in Russian).

Laskar, J., Robutel, P., Joutel F., Gastineau M., Correia, A. C. M. and Levrard, B., 2004. A long-term numerical solution for the insolation quantities of the Earth. Astronomy & Astrophysics, 428(1): 261~285.

Lavrenko, E.M., Iunatov, A.A., Aleksandr, A. and Dashniam, B., 1979. Vegetation map of Mongolian People's Republic (Scale 1: 1 500 000). Moscow Publishing House, Moscow (in Russian).

Liu, K.B. and Lam, N.S.N., 1985. Paleovegetational reconstruction based on modern and fossil pollen data: an application of discriminant analysis. Annals of the Association of American Geographers, 75: 115~130.

Liu H.Y., Cui T., Pott R. and Speier M., 1999. The surface pollen of the woodland-steppe ecotone in southeastern Inner Mongolia, China. Review of Palaeobotany and Palynology, 105(3~4): 237~250.

Lu H.Y., Wu N.Q., Yang X.D., Shen C.M., Zhu L.P.,Wang L., Li Q. and Xu D.K., Tong G.B., Sun X.J., 2008. Spatial pattern of Abies and Picea pollen distribution along the elevation gradient in the Qinghai-Tibetan Plateau and Xinjiang, China. Boreas, 37: 254~262.

Logatchov N.A., 1989. Late Cenozoic of Mongolia (Stratigraphy and Paleogeography). The Joint Soviet-Mongolia Scientific Research Transaction, vol. 47. Moscow Publishing House, Moscow (in Russian).

Ma, Y.Z., Zhang, H.C., Pachur, H.J., Wünnemann, B., Li, J.J. and Feng, Z.-D., 2003. Late Glacial and

Holocene vegetation history and paleoclimate of the Tengger Desert, northwestern China. Chinese Science Bulletin, 48(14): 1457~1463.

Ma, Y.Z., Zhang, H.C., Pachur, H.J., Wunnemann, B., Li, J.J. and Feng, Z.-D., 2004. Modern pollen-based interpretations of mid-Holocene palaeoclimate (8500 to 3000 cal., BP)at the southern margin of the Tengger Desert, northwestern China. The Holocene, 14(6): 841~850.

Ma, Y.Z., Liu, K.B., Feng, Z.-D., Sang, Y.L., Wang, W. and Sun, A.Z., 2008. A survey of modern pollen and vegetation along a south-north transect in Mongolia. Journal of Biogeography, 35: 1512~1532.

Ma, Y.Z., Liu, K.-b., Feng, Z.D., Meng, H.W., Sang, Y.L., Wang, W. and Zhang, H.C., 2013. Vegetation changes and associated climate variations during the past ~38 000 years reconstructed from the Shaamar eolian-paleosol section in northern Mongolia. Quaternary International, 311: 25~35.

MacDonald, G.M. and Ritchie, J.C., 1986. Modern pollen spectra from the western interior of Canada and the interpretation of Late Quaternary vegetation development. New Phytologist, 103: 245~268.

Moore P.D. and Webb J.A., Collinson M.E., 1991. Pollen analysis. Blackwell Scientific Publications, Oxford.

Pachur, H.J., Wünemann, B. and Zhang, H.C., 1995. Lake evolution in the Tengger Desert, Northwestern China, during the last 40 000 years. Quaternary Research, 44: 171~180.

Peck, J.A., Khosbayar, P., Fowell, S.J., Pearce, R.B., Ariunbileg, S., Hansen, B.C. and Soninkhishig, N., 2002. Mid to Late Holocene climate change in north central Mongolia as recorded in the sediments of Lake Telmen. Palaeogeography, Palaeoclimatology, Palaeoecology, 183: 135~153.

Prokopenko, A.A., Khursevich, G.K., Bezrukova, E.V., Kuzmin, M.I., Boes, X., Williams, D.F., Fedenya, S.A., Kulagina, N.V., Letunova, P.P. and Abzaeva, A.A., 2007. Paleoenvironmental proxy records from Lake Hovsgol, Mongolia, and a synthesis of Holocene climate change in the Lake Baikal watershed. Quaternary Research, 68: 2~17.

Reese, C. A. and Liu, K-b., 2005. A modern pollen rain study from the central Anders region of South America. Journal of Biogeography, 32: 709~718.

Reimer, P.J., Baillie, M.G.L., Bard, E., Bayliss, A., Beck, J.W., Blackwell, P.G., Ramsey, C.B. and Buck, C.E., 2009. Intcal09 and marine09 radiocarbon age calibration curves 0-50 000 years Cal BP. Radiocarbon, 51: 1111~1150.

Rinterknecht, V.R., Clark, P.U., Raisbeck, G.M., Yiou, F., Bitinas, A., Brook, E.J., Marks, L., Zelcs, V., Lunkka, J.P., Pavlovskaya, I.E., Piotrowski, J.A. and Raukas, A., 2006. The last deglaciation of the southeastern sector of the Scandinavian Ice Sheet. Science, 311: 1449~1452.

Rudaya, N.A., Tarasov, P.E., Dorofeyuk, N.I., Kalugin, I.A., Andreev, A.A., Diekmann, B. and Daryin, A. V., 2008. Environmental Changes in the Mongolian Altai during the Holocene. Archaeology, Ethnology and Anthropology of Eurasia, 36(4): 2~14.

Rudaya, N., Tarasov, P., Dorofeyuk, N., Solovieva, N., Kalugin, I., Andreev, A., Daryin, A., Diekmann, B., Riedel, F., Tserendash, N. and Wagner, M., 2009. Holocene environments and climate in the Mongolian Altai reconstructed from the Hoton-Nur pollen and diatom records: a step towards better understanding climate dynamics in Central Asia. Quaternary Science Reviews, 28: 540~554.

Ruddiman, W.F., 2008. Earth's Climate: Past and Future. Freeman W. H., New York.

Schaefer, M.J., Denton, G.H., Barrell, J.A., Ivy-Ochs, S., Kubik, P., Andersen, B.G., Phillips, M.K., Lowell, T.V. and Schluchter, C., 2006. Near-Synchronous Interhemispheric Termination of the Last Glacial Maximum in Mid-Latitudes. Science, 312: 1510~1513.

Sugden, J.M. and Meadows, M.E., 1989. The use of multiple discriminant analysis in reconstructing recent vegetation changes on the Nuwelveldverg, South Africa. Review of Palaeobotany and Palynology, 60(1~2): 131~147.

Tarasov, P.E., Jolly, D. and Kaplan, J.O., 1997. A continuous Late Glacial and Holocene record of vegetation changes in Kazakhstan. Plaeogeography, Palaeoclimatology, Palaeoecology, 136: 281~292.

Tarasov, P., Dorofeyuk, N. and Metel'Tseva, E., 2000. Holocene vegetation and climate changes in Hoton Nuur Basin, northwest Mongolia. Boreas, 29: 117~126.

Tarasov, P., Bezrukova, E., Karabanov, E., Nakagawa, T., Wagner, M., Kulagina, N., Letunova, P., Abzaeva, A., Granoszewski, W. and Riedel, F., 2007. Vegetation and climate dynamics during the Holocene and Eemian interglacials derived from Lake Baikal pollen records. Palaeogeography, Palaeoclimatology, Palaeoecology, 252: 440~457.

Velichko, A.A., Catto, N., Drenova, A.N., Klimanov, A.V., Kremenetski, K.V. and Nechaev, V.P., 2002. Climate changes in East Europe and Siberia at the late glacial–Holocene transition. Quaternary International, 91: 75~99.

Wang, W., Ma, Y.Z., Feng, Z.-D., Meng, H.W., Sang, Y.L. and Zhai, X.W., 2009. Vegetation and climate changes during the last 8660 cal. a BP in central Mongolia, based on a high-resolution pollen record from Lake Ugii Nuur. Chinese Science Bulletin, 54(9): 1579~1589.

Wang, W., Ma, Y.Z. and Feng, Z.-D., Narantsetseg, T., Liu, K.B., Zhai, X.W., 2011. A prolonged dry mid-Holocene climate revealed by pollen and diatom records from Lake Ugii Nuur in central Mongolia. Quaternary International, 229: 74~83.

Wang W. and Feng, Z.-D., 2013. Holocene moisture evolution across the Mongolia Plateau and its surrounding areas: a synthesis of climatic records. Earth-Science Reviews, 122: 38~57.

Wang, Y.J., Cheng, H., Edwards, R.L., An, Z.S., Wu, J.Y., Shen, C.C. and Dorale, J.A., 2001. A high-resolution absolute-dated late Pleistocene Monsoon record from Hulu Cave, China. Science, 294: 2345~2348.

Xiao, J.L., Xu, Q.H., Nakamura, T., Yang, X.L., Liang W.D. and Inouchi Y., 2004. Holocene vegetation variation in the Daihai Lake region of north-central China: a direct indication of the Asian monsoon climatic history. Quaternary Science Reviews, 23: 1669~1679.

Xu, Q.H., Xiao, J.L., Li, Y.C., Tian, F. and Nakagawa, T., 2010. Pollen-Based Quantitative Reconstruction of Holocene Climate Changes in the Daihai Lake Area, Inner Mongolia, China. Journal of Climate, 23: 2856 ~ 2868.

Yuan, D., Cheng, H., Edwards, R.L., Dykoski, C.A., Kelly, M.J., Zhang, M., Qing, J., Lin, Y., Wang, Y., Wu, J., Dorale, J.A., An, Z. and Cai, Y., 2004. Timing, duration, and transitions of the last interglacial Asian monsoon. Science, 304: 575~578.

Zhang, C.J., Zhang, W.Y., Feng, Z.-D., Mischke, S., Gao, X., Gao, D. and Sun, F.F., 2012. Holocene hydrological and climatic change on the northern Mongolian Plateau based on multi-proxy records from Lake Gun Nuur. Palaeogeography, Palaeoclimatology, Palaeoecology, 323~325: 75~86.

Zhang, H.C., Peng, J.L., Ma, Y.Z., Chen, G.J., Feng, Z.-D., Li, B., Fan, H.F., Chang, F.Q., Lei, G.L. and Wünnemann, B., 2004. Late Quaternary palaeolake levels in Tengger Desert, NW China. Palaeogeography, Palaeoclimatology, Palaeoecology, 211: 45~58.

第四章

蒙古国西部阿奇特湖(Achit Nuur)湖芯记录的过去20 000多年来植被与气候的变化

孙爱芝[1]　　冉　敏[2]

①中国科学院大学 地球科学学院

②西南大学 地理科学学院

本章对蒙古国西部阿奇特湖(Achit)湖芯91个沉积样品进行了孢粉分析,结合10个AMS ^{14}C测年数据,重建了该地区过去约22 600年以来植被及气候变化的历史。对阿奇特湖流域植被的重建显示:约22 600~13 200 cal. yr BP,高海拔地区主要为森林植被,低海拔地区主要为草原植被;约13 200~6400 cal. yr BP,高海拔地区主要为草原植被,低海拔地区主要为荒漠植被;约6400~1600 cal. yr BP,高海拔地区泰加林扩张;过去约1600年以来以该流域植被主要为禾本科草原植物。基于孢粉资料重建的年均温度显示,阿奇特湖地区约22 600~13 200 cal. yr BP气候寒冷,约13 200~6400 cal. yr BP气候温和,过去约5000年以来气候相对温暖。基于孢粉重建的年降水量显示,约22 600~13 200 cal. yr BP气候相对湿润,约13 200~6400 cal. yr BP气候相对干旱,约6400~1600 cal. yr BP气候相对湿润,过去约1600年以来气候相对干旱。

关键词:孢粉;植被变化;气候变化;蒙古高原西部;阿奇特湖

1.引言

蒙古高原西部,即蒙古国西部(即阿奇特湖所在地区,见图4-1),位于北大西洋气候系统和太平洋气候系统的相互作用区,具有重要的气候学意义。近二十年来,许多科学家已对该地区及其周边区域(如阿尔泰山、蒙古高原北部及中部、中国新疆地区)的古气候变化做了大量的研究(Gunin,1999;Grunert 等,2000;Harrison 等,1996;Rudaya 等,2009;Tarasov 等,1998,2000)。然而,已有的研究对该地区气候变化,特别是全新世气候变化的认识还存在较为明显的争议。总的来讲,对该地区全新世气候变化的认识主要有以下三种观点。第一种观点认为,蒙古高原西部全新世气候主要受东亚季风影响,且影响强度在全新世中期(即全新世气候最宜期)达到最高(Harrison 等,1996;Tarasov 等,2000)。第二种观点认为,包括蒙古高原西部的中亚干旱区(西至咸海、东至杭爱山地区)在内的区域

全新世气候主要受北大西洋气候系统影响，且其全新世湿度变化与亚洲季风区具有相位差(Chen 等，2008)。第三种观点认为，干旱半干旱的蒙古高原(包括蒙古高原西部)全新世湿度变化主要受温度控制，即高温的中全新世时期蒙古高原也是干燥的，而早全新世时段和晚全新世时段的气候相对湿润(Wang 等，2009，2011；Wang 和 Feng，2013)。上述争论说明，仍需要对该地区全新世气候变化做深入地研究。

Gunin(1999)曾基于孢粉资料对阿奇特湖流域的全新世气候变化进行了初步研究，但该研究的年代控制和样品分辨率都不理想。本章基于 10 个 AMS ¹⁴C 年龄数据，对阿奇特湖 200cm 的岩芯(91 个样品)进行孢粉分析，尝试较高分辨率地重建该地区过去约 22 600 年以来的植被以及气候变化历史。

2. 研究区地理概况

阿奇特湖(49°25′N，90°31′E，海拔 1444m)为一位于山间盆地的淡水湖，西边为蒙古阿尔泰山，北边为摩根泰加山，东边为呼麦图尔根山(图 4-1 中的点位 1)。湖泊面积 297km²，最长处为 24km，最宽处为 18km，湖水平均深度为 2m，最深为 5m。该淡水湖有两条入湖河流(Huv-Usny-Gol 河和摩根布伦河)和一条出湖河流(科布多河)，后者最终流入其东南面封闭的哈尔乌苏湖。

阿奇特湖地区气候属典型的大陆型气候，冬季冷干且持续时间长，夏季凉湿且持续时间较短。1 月平均气温-21℃~-16℃，7 月平均气温 15℃~20℃；年均降水量为 200~300mm。阿奇特湖周围的植被以荒漠草原为主，湖泊北岸主要为低矮的沼泽植物，南岸主要为盐沼植物，东岸和西岸主要为荒漠植物。植物种类主要有克氏针茅(*Stipa krylovii*)、戈壁针茅(*Stipa gobica*)、无芒隐子草(*Cleistogenes songorica*)等，同时还混杂着冷蒿(*Artemisia frigida*)、旱蒿(*A. xerophytica*)、艾菊(*Tanacetum sibiricum*)、乔状交菊(*T. achilleoides*)、二裂交菊(*T. trifidum*)等。此外，水生植物(轮藻和眼子菜)广泛分布于湖泊周围阴凉地带(Hilbig，1995)，泰加林植被(乔木如落叶松属、松属)主要分布在邻近的蒙古阿尔泰山高海拔地区，森林草原分布在中海拔地区，草原分布在低海拔地区，而低地一般为荒漠草原植被。

3. 材料和方法

3.1. 野外采样及地层划分

我们于 2010 年 8 月在阿奇特湖(Achit)靠近中心位置水深约 3.8 m 处利用奥地利活塞钻成功钻取长 200cm 的湖芯样，并就地进行地层描述和划分，同时完成分样。分样间距为 2cm，获得孢粉样品 91 个，年代样品 10 个，之后将样品密封冷冻保存，运送回实验室进行理化指标分析。实验室分析指标主要包括粒度和总有机质含量。粒度样品分析间距为 2cm，在马尔文激光粒度分析仪(Mastersizer 2000)上分析测量，该仪器测量范围为 2~2000μm。粒度分析步骤如下：1 加过量双氧水去除有机质以及溶解盐；2 加入盐酸去除碳酸盐；3 用偏磷酸钠溶液对样品进行充分分解；4 将处理好的样品送入马尔文激光粒度仪进行粒度分析。总有机质含量的测定采用硫酸亚铁—重铬酸钾滴定法完成。上述

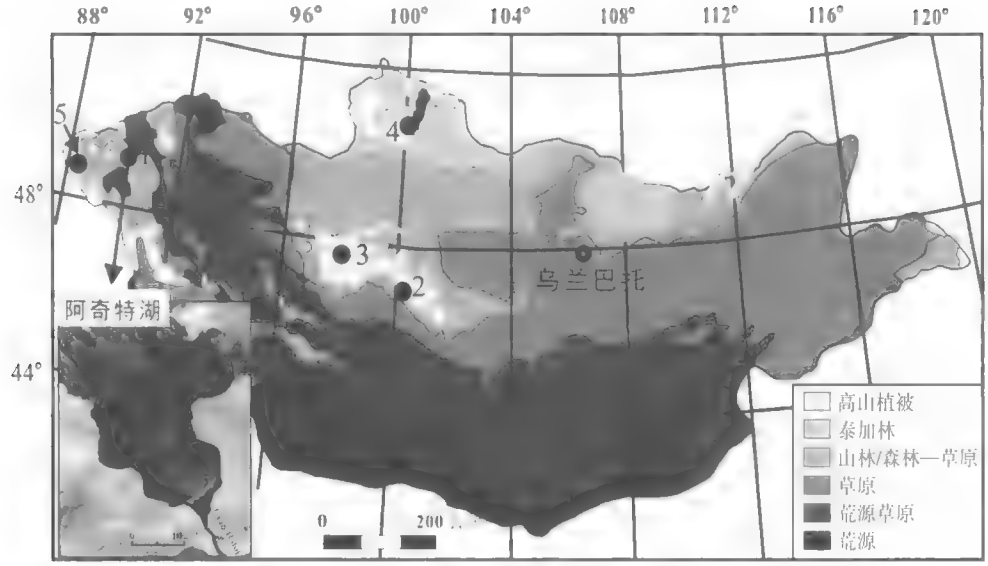

图4-1　样点位置及蒙古植被图(Hilbig,1995)。1. 阿奇特(Achit)湖;2. Ugii湖;3. Telmen湖;4. Hovsgol湖;5. Hoton湖。左下角插图为取样点在阿奇特湖的位置(来自于http://maps.google.com)

指标的分析均在兰州大学西部环境教育部重点实验室完成。

根据沉积物有机质含量以及平均粒径的变化可将阿奇特湖(Achit)200cm湖芯分为5个地层单元(图4-2)。地层单元1(165~200cm)为浅灰色黏土层,平均有机质含量为约2.5%,平均粒径为约5μm。地层单元2(150~165cm)为黑色黏土细砂层,平均有机质含量为约5%,平均粒径为约120μm。地层单元3(130~150cm)为浅灰色粉砂层,平均有机质含量为约7.5%,平均粒径为约18μm。地层单元4(112~130cm)为灰褐色层,平均有机质含量为约5%,平均粒径为约90μm。地层单元5(0~112cm)为灰色粉砂层,内夹两层砂质层(105~112cm和52~62cm)。与下覆地层单元4相比,地层单元5以高的有机质含量(约10%)和细的沉积物颗粒(约22μm)为特征。

本研究对Achit湖湖芯10个沉积物样品进行了AMS ^{14}C测年,测年分析在美国亚尼桑那大学AMS ^{14}C年代实验室(NSF-AMS Facility)完成,结果见表4-1。为了判定该地区湖泊沉积物的碳库效应,本章对湖芯表层沉积物进行了测年,测得的表层沉积物年龄为2099 ^{14}C yr BP(碳库效应)。据此,我们将所有的原始AMS ^{14}C年龄减去该年龄,再通过CALIB 6.0年代校正软件校正得到日历年龄(以1950年为基准)(Reimer等,2009)。最后假设相邻两个年代点间的沉积物沉积速率保持不变,采用线性内插外推方式建立了阿奇特湖岩芯年龄—深度模式(图4-2)。年龄模式显示,阿奇特湖长200cm岩芯的沉积物主要形成于过去约22 600年以来,沉积速率变化较大,从3mm/年到90mm/年不等。为了便于讨论和比较,本章接下来所用的年龄均为校正年龄。

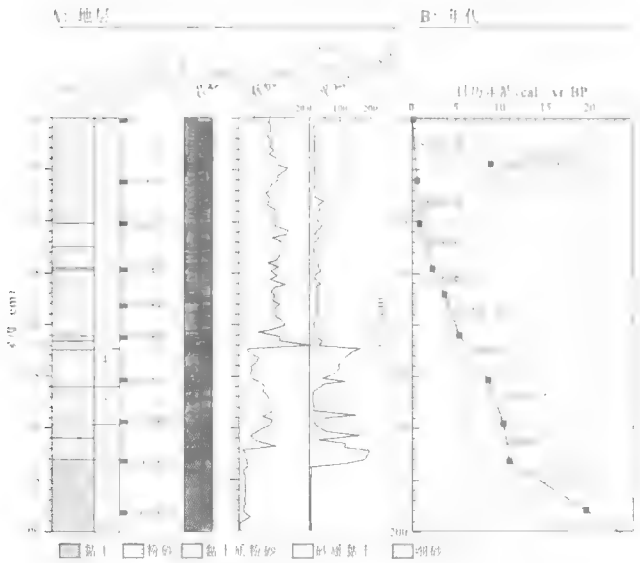

图4–2　阿奇特湖湖芯地层、照片、有机质含量(%)、平均粒径(m)及年龄—深度模式图(Sun等,2013)

表4–1　阿奇特湖湖芯沉积物AMS ^{14}C测年结果

实验编号	深度(cm)	测年材料	δ ^{13}C值(‰)	测年结果 (^{14}C yr BP)	去碳库效应后的校正年龄 (2δ, cal. yr BP)
AA94349	0~2	有机质	–13.3	2099±35	0
AA94350	30~31	有机质	–13.0	2673±38	524~652
AA94351	51~52	有机质	–11.7	2981±39	725~926
AA94352	73~74	软体动物	–8.3	4421±38	2180~2460
AA94353	85~86	有机质	–9.0	5497±40	3488~3823
AA94354	105~106	有机质	–7.9	6717±61	5258~5478
AA94355	127~128	树根	–7.9	9971±52	8547~8795
AA94356	148~149	有机质	–7.6	11 300±62	10 235~10 519
AA94357	165~167	有机质	–6.9	11 796±92	10 755~11 247
AA94358	190~191	有机质	–3.7	18 600±110	19 463~19 875

3.3 孢粉分析和孢粉指标

阿奇特湖岩芯共获得 91 个孢粉样品，样品分析采用酸碱法和过筛法。实验室处理前每个样品加入一片石松孢子药片（每片 27 637±563 粒石松孢子）以便计算孢粉浓度（Moore 等，1991）。根据样品岩性的差异，每样取 5~10g，分别进行了去碳酸盐(10% HCl)、去有机质(10% KOH)和去硅酸盐(36% HF)处理，然后通过超声波过筛(网布孔径 7~

10μm)，收取网布上的残留物，最后将样品转入小指管，离心脱水加甘油保存。孢粉的鉴定根据相关孢粉书籍(王伏雄等，1997；Erdtman，1978；摩尔和韦布，1987)以及研究组采集的200多种现代花粉标准片进行，每个样品至少鉴定出300粒以上的花粉。花粉百分含量的计算是以所有陆生植物花粉总数(不包括孢子)为基数，孢粉图谱通过Garpher 8.0软件运行得出。

在北半球干旱半干旱地区，许多孢粉指标被用来指示生物气候的变化。如非木本植物花粉和木本植物花粉的比值(NAP/AP)被用来指示半湿润半干旱地区有效湿度的变化(Moore等，1991)，该指标的有效性在俄罗斯阿尔泰(Blyakharchuk等，2007)、蒙古北部(Dorofeyuk和Tarasov，1998)以及中国黄土高原地区得到了进一步地证明(Feng等，2004，2006；Prokopenko等，2007)。Prokopenko等人(2007)利用SFI指数，即草原森林指数=(蒿属+藜科+麻黄属+石竹科)/乔木，来指示Hovsgol湖地区草原面积扩张历史。此外，尽管在整个蒙古高原现代孢粉谱中，禾本科被认为是超级低代表性类型(Gunin，1999；Ma等，2008)，但在蒙古中部的Telmen湖地区，(C+A)/P，即(藜科+蒿属)/禾本科比值仍被用来反映全新世气候的干燥度(Fowell等，2003)。

3.4 植被和环境重建

孢粉资料的定量解译可以通过孢粉生物群区重建来完成(Prentice等，1996)。根据现代植物的生物地理学特征和分布将植物划分为不同的植物功能型和植被类型(表4-2)。然后，根据Prentice等(1996)描述的方法，计算出化石孢粉组合与用来做比较的生物群区类型的近似程度。在进行计算时，本章主要采用的是Yu等人(2000)文中列举的花粉类型—植物功能型类型归属关系，而且根据Herzschuh等(2004)和Tarasov等(1998)的研究结果对部分关系进行了修改(表4-2)。

为了定量重建古气候参数(温度和降水)，本章采用了植物功能型—现代类比法(PFT-MAT)。PFT-MAT方法是通过计算被选择的花粉类型与现代花粉类型之间的弦距比来确定化石花粉谱与现代花粉谱之间的差异(Davis等，2003；Jiang等，2006，2009；Nakagawa等，2002；Sun和Feng，2013)。我们参照的现代花粉数据集共有2066个花粉数据，包括中国北方211个(Members of China Quaternary Pollen Data Base，2001)，俄罗斯和欧洲1855个(Guiot等，1993；Tarasov等，1998)。表土孢粉样点气象数据是5°×5°栅格点内相邻气象站点的多年平均值(Guiot和Goeury，1996)。对每一个化石孢粉样品，均选择8个最近距离的现代花粉样品代表"最佳的现代类比样品"。每个地层样品的平均气候参数值均通过Guiot等(1993)和Magny等(2001)描述的方法进行了校正。所有的数据计算是用PPPBASE软件(Guiot和Goeury，1996)完成。本章计算了两个气象参数值：年均温度(MAT)和年均降水量(MAP)。

表 4-2　中国北方植物花粉种类以及植物功能型划分 (来自于Yu等,2000;Tarasov等,1998)

简称	植物功能型	花粉种类
Bec	北方常绿针叶树	冷杉属,云杉属
Bs	北方夏绿乔木/灌木	桦木属,柳属
Ctc	冷温性针叶树	冷杉属
Df	荒漠灌木/草本	菊科,十字花科,石竹科,藜科,胡颓子科,麻黄属,百合科,蓼科,蓼属,委陵菜属
Ec	广温性针叶树	松属
Es	广温性夏绿乔木/灌木	椴木属
G	草本/灌木	禾本科
S	莎草植物	莎草科
Sf	草原草/灌木	伞形科,蒿属,菊科,十字花科,石竹科,藜科,胡颓子科,豆科,唇形科,百合科,桑科,葎草属,车前属,蓼科,蓼属,唐松草属,蔷薇科,委陵菜属,地榆属,拉拉藤属,酸模属,荨麻属,败酱科
Ts	暖温带夏绿乔木/灌木	槭属,桦木属,白蜡树属,栎属,茜草属,柳属
Ts1	冷温带夏绿乔木/灌木	鹅耳枥属,榛属,椴树属,榆属
Ts2	过渡带夏绿乔木/灌木	朴属,胡桃属,枫杨属,瑞香科

4. 结果

4.1. 孢粉分析结果

阿奇特湖湖芯孢粉样品中共鉴定出 49 种不同的陆生植物孢粉,其中包括 14 种木本和 33 种草本及灌木花粉(图 4-3)。如松属(*Pinus*)、云杉属(*Picea*)、柏科(Cupressaceae)、桦木属(*Betula*)、栎属(*Quercus*)、榆属(*Ulmus*)、柳属(*Salix*)、杨属(*Populus*)、榛属(*Corylus*)、蔷薇科(Rosaceae)、麻黄属(*Ephedra*)、白刺属(*Nitraria*)、柽柳属(*Tamarix*)、禾本科(Gramineae)、蒿属(*Artemisia*)、藜科(Chenopodiaceae)、紫菀型(*Aster*-type)、蒲公英型(*Taraxacum*-type)、春黄菊型(*Anthemis*-type)、葎草属(*Humulus*)、毛茛科(Ranunculaceae)、蓼属(*Polygonum*)、莎草科(Cyperaceae)等。此外,还鉴定出了四种水生植物(香蒲属(*Typha*)、黑三棱属(*Sparganium*)、泽泻属(*Alisma*)和狐尾藻属(*Myriophyllum*))花粉和一种藻类植物盘星藻属(*Pediastrum*)。根据主要孢粉百分含量及孢粉组合特征,将阿奇特湖湖芯的孢粉组成变化划分为 3 个带和 5 个亚带,其中 5 个孢粉亚带与上述的 5 个地层单元有较好的对应关系(图 4-3)。

孢粉带 1(172 ~ 200cm;约 22 600~13 200 cal. yr BP)对应于地层单元 1。该带花粉主要为草本,其含量高达约 65%~80%,主要包括莎草科(约 12%~35%)、禾本科(约 7%~20%)、紫菀型(约 3%~6%)、蒲公英型(约 2%~8%)和春黄菊型(约 1%~10%)。针叶树花粉含量为约 20%,主要有松属(约 10%~20%)、云杉属(约 2%~7%)、柏科(0%~7%)以及落叶松属

(0%~2%)。该带阔叶树花粉百分含量以及孢粉总浓度均极低。该带另外一个显著特征是水生植物花粉含量极高,为整个湖芯的最高值段

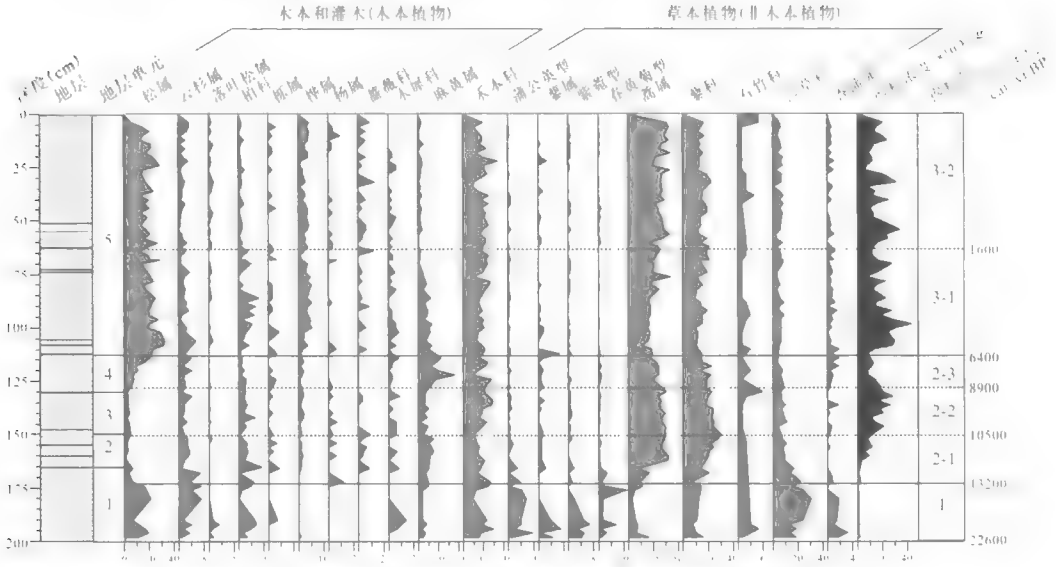

图4-3 阿奇特湖主要孢粉百分含量及孢粉浓度图(Sun等,2013)

孢粉带2(112~172cm;约13 200~6400 cal. yr BP)对应于地层单元2、3和4。该带最显著的特征是具有较高含量的禾本科花粉和相对较高的孢粉浓度,可进一步划分为三个亚带。孢粉亚带2-1(150~172cm;约13 200~10 500 cal. yr BP)对应于地层单元2。该亚带孢粉谱主要由草本及灌木花粉组成,包括蒿属(约35%~45%)、藜科(约20%~30%)、禾本科(约8%~17%)和麻黄属(约1%~8%)。针叶树花粉(主要有松属、云杉属和柏科)含量明显下降(<10%)。阔叶树花粉开始出现,主要包括栎属、桦木属、杨属及榆属。孢粉亚带2-2(130~150cm;约10 500~8900 cal. yr BP)对应于地层单元3。与上一个孢粉亚带(即孢粉亚带2-1)相比,该亚带禾本科和桦属花粉含量上升,麻黄属含量下降。孢粉亚带2-3(112~130cm;约8900~6400 cal. yr BP)对应于地层单元4。该亚带最显著的特征是耐旱植物花粉(如麻黄属)含量明显增加,松属花粉显著增加,而孢粉浓度显著下降。

孢粉带3(0~112cm;约6400~0 cal. yr BP)对应于地层单元5。该带主要的特征为松属和阔叶树花粉含量显著增加(分别高达约45%和约10%),同时草本花粉含量明显下降(约50%~70%)。针叶树主要包括松属(约20%~35%)、云杉属(约1%~5%)、柏科(约0%~9%)以及落叶松属(约0%~5%),其中松属为针叶树成分的主要组成。阔叶树花粉主要包括桦属(约2%~6%)、杨属(约0%~2%)以及栎属(约0%~1%)。与孢粉亚带2-3相比,该带孢粉浓度明显上升,可进一步划分为两个亚带:孢粉亚带3-1(62~112cm;约6400~1600 cal. yr BP)和孢粉亚带3-2(0~62cm;约1600~0 cal. yr BP)。与孢粉亚带3-2相比,亚带3-1具有较高的木本花粉含量(如松属、云杉属、桦属、柏科)和较高的孢粉浓度(约20000粒/g)。

4.2. 植被与环境重建

总的来说，对阿奇特湖地区植被历史的定性解译与利用生物群区模型定量重建的结果是一致的(图 4–4)。尽管本章所使用的生物群区化方法无法准确地重建过渡性植被类型(如森林草原或荒漠草原)，但是通过分析森林和非森林带的生物群区得分仍然可以得到一些植被过渡类型的信息。如，阿奇特湖湖芯顶部(约 1600~0 cal. yr BP)和底部(约 22 600~13 200 cal. yr BP)的草原类型分值和泰加林接近，说明这两个阶段植被可能为森林草原过渡类型；湖芯中部(约 13 200~6400 cal. yr BP)的荒漠植被和草原植被分值接近，说明该阶段极有可能为荒漠草原植被；其上部(约 6400~1600 cal. yr BP)植被重建显示主要为泰加林。重建的生物群区类型和主要的孢粉组合(例如针叶林、阔叶林和草本植物百分含量)的变化具有较好的对应关系(图 4–4)。

基于孢粉数据定量重建的温度变化很好地响应了末次盛冰期及末次冰消期的寒冷气候(约 22 600~13 200 cal. yr BP)，之后约 13 200~10 500 cal. yr BP 相对温暖的气候又与北大西洋地区的温度记录一致(Davis 等，2003；Moros 等，2004)。重建的温度最高时段发生在约 10 500~6400 cal. yr BP，这正好对应了早中全新世的高温期(Harrison 等，1996；Tarasov 等，2000；Rudaya 等，2009)。接下来气温总体呈下降趋势(约 6400~2000 cal. yr BP)，这与北半球大尺度的降温趋势是一致的(Wanner 等，2008)。此外，西太平洋暖池以及印度洋的阿拉伯海记录到的过去约 1000 年以来气温呈上升趋势(Gupta 等，2003；Stott 等，2004)似乎也在阿奇特湖地区有所反映(图 4)。基于孢粉定量重建的年均降水量显示，阿奇特湖地区在过去约 22 600 年以来经历了两次气候相对湿润期(约 22 600~13 200 cal. yr BP 和约 6400~1600 cal. yr BP)和两次相对干旱期(约 13 200~6400 cal. yr BP 和过去 1600 年以来)。

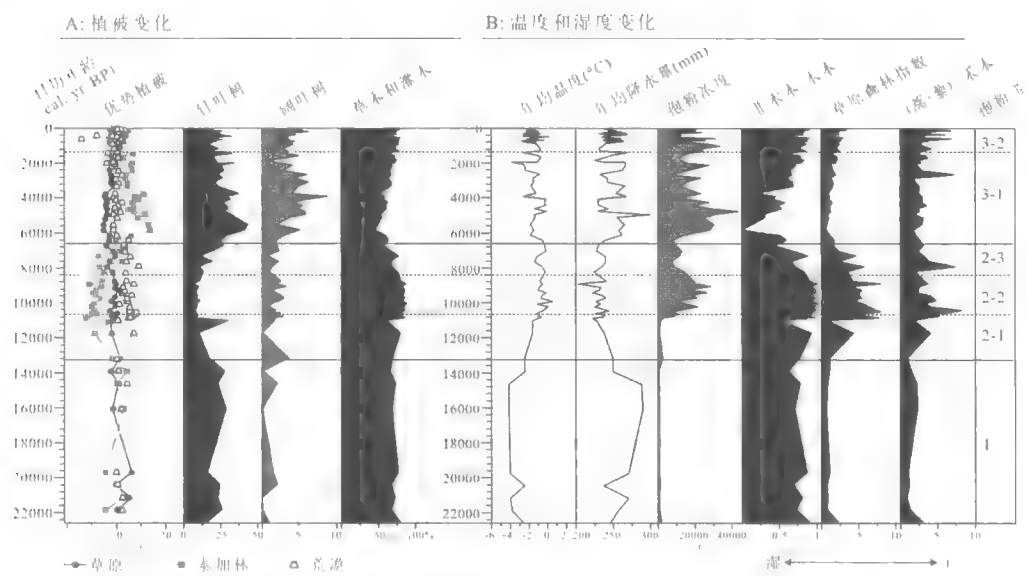

图4–4　植被和气候重建结果。A代表植被的变化，包括生物群系重建的优势植被、针叶林、阔叶林、禾本和灌木孢粉百分含量；B代表重建的年均温度和年均降水量的变化，也包括孢粉浓度、非木本和木本花粉比值、草原森林指数以及(蒿属+藜科)/禾本科值(Sun等，2013)

5. 讨论和结论

5.1. 植被变化及其相应的气候

总的来说，阿奇特湖湖芯孢粉组合揭示了该地区约 22 600 cal. yr BP 以来的植被和气候变化（图 4–3、图 4–4）。具体地讲，约 22 600~13 200 cal. yr BP，湿地植物（如莎草科和香蒲属）孢粉含量最高，显示该时段植被主要以草甸草原为主，气候相对湿润。并且该时段较低的草原森林指数（SFI 指数）和（A+C）/P 值进一步表明，该时段的气候是湿润的。与接下来的时段相比，该时期较高的针叶林花粉百分含量指示周围山地上暗针叶林可能在不断扩张。

接下来的时段（约 13 200~6400 cal. yr BP）植被主要为荒漠草原植被，主要有蒿属、藜科、麻黄属、禾本科等，具有较高的草本植物孢粉含量。较高的森林草原指数（SFI 指数）以及较高的（A+C）/P 值均显示，该时段气候温干且湖泊水位呈下降趋势。所有与孢粉有关的数据（包括定量重建的年均温度、年均降水量、非木本和木本比值、（A+C）/P 值、森林草原指数等）均显示，约 10 500~6400 cal. yr BP 研究区湿度最低而温度最高。

约 6400~1600 cal. yr BP，生物群区结果显示，阿奇特湖流域高海拔地区植被主要为泰加林，中海拔地区植被主要为落叶林，这与孢粉谱中含量增加的针叶树和阔叶树花粉的解译是一致的。该时期湖泊周围山地森林的扩张以及相对较低的 NAP/AP 值和森林草原指数显示，随着气温的逐渐下降，湿度是逐渐增加的。过去约 1600 年以来，由于温度的上升，阿奇特湖地区湿度下降，气候变干，植被主要为草原。

5.2. 区域气候对比

为了从较大的地理空间尺度来理解蒙古高原西部全新世植被以及气候的变化，本章将阿奇特湖岩芯孢粉记录与周边地区 5 个湖芯孢粉记录进行了对比。所选取 5 个湖泊中的 3 个来自于蒙古高原北部，包括 Ugii 湖（Wang 等，2009，2011；图 4–1 中点位 2）、Telmen 湖（Peck 等，2002；Fowell 等，2003；图 4–1 中点位 3）和 Hovsgol 湖（Prokopenko 等，2007；图 4–1 中点位 4），1 个来自于阿尔泰山脉的 Hoton Nuur 湖（Rudaya 等，2009；图 4–1 中点位 5），1 个来自于中国新疆的 Wulungu 湖（肖霞云等，2006；Liu 等，2008；图 4–1 中点位 6）。

Ugii 湖的多指标分析结果显示，该地区约 9100~6700 cal. yr BP 气候温和，湿度适中，植被主要为荒漠草原；接下来的中全新世（约 6700~3300 cal. yr BP）气候干旱，藜科花粉含量相对较高；约 2600~1000 cal. yr BP 气候相对湿润；过去 1000 年以来气候相对干旱（Wang 等，2009，2011；图 4–1 点位 2）。基于孢粉重建的 Telmen 湖全新世干燥度显示，该地区中全新世（约 7100~4600 cal. yr BP）气候干旱，这大致上可与前述的 Ugii 湖中全新世干旱气候相对应；约 4600 cal. yr BP 以来气候总体湿润，并经历了两个气候相对干旱期（距今 3000 年左右和距今 1800 年左右）（Peck 等，2002；Fowell 等，2003；图 4–1 中点位 3）。基于孢粉重建的 Hovsgol 湖地区草原森林指数显示，该地区早全新世（约 9500~6000 cal. yr BP）气候相对湿润，中全新世（约 6000~3500 cal. yr BP）气候相对干旱，晚全新世（约 3500~0 cal. yr BP）气候相对湿润（Prokopenko 等，2007；图 4–1 中点位 4）。总的来说，上述

三个湖泊所记录的蒙古高原北部全新世气候变化可大致分为以下三个阶段：早全新世相对湿润(约 9500~7000 cal. yr BP)、中全新世气候干旱(约 9500~6000 cal. yr BP)以及晚全新世气候相对湿润(过去约 3500 年以来)。

与早期的研究(Tarasov 等,2000)相比，由于具有更高的地层分辨率和更可靠的年代，Rudaya 等人(2009)对蒙古阿尔泰地区的 Hoton 湖的研究大大提高了对该地区全新世气候变化的理解。后者基于孢粉资料重建的 Hoton 湖地区全新世降水历史显示，该地区气候在约 10 500 cal. yr BP 以前是干旱的，全新世前半期(约 10 500~5000 cal. yr BP)气候逐渐变湿润，全新世后半期(即约 6500 cal. yr BP 至今)气候逐渐又变干旱。植被重建结果显示，Hoton 湖地区在约 10 500 cal. yr BP 以前主要为冷草原植被，约 10 500~6500 cal. yr BP 植被主要为北方乔木以及开放的阔叶树林地，约 6500 cal. yr BP 至今草原植物花粉含量明显上升(Rudaya 等,2009)。

位于新疆北部的乌伦古湖孢的粉记录显示，早全新世(约 10 000~6700 cal. yr BP)湖泊周围主要为浅湖或者湿地环境。约 6700 cal. yr BP 至今 A/C 值逐渐上升，荒漠植被得分逐渐下降，暗示气候逐渐变湿润，气候最湿润期发生在约 4200~500 cal. yr BP 间(肖霞云等,2006；Liu 等,2008；图 4–1 中点位 6)。

综上所述，蒙古高原北部地区(即 Ugii 湖、Telmen 湖和 Hovsgol 湖)全新世气候大致可分为相对湿润的早全新世、相对干旱的中全新世和相对湿润的晚全新世三个阶段。蒙古阿尔泰地区(即 Hoton 湖)全新世气候可以分为相对湿润的全新世前半期(约 10 500~5000 cal. yr BP)和相对干旱的全新世后半期(约 5000 cal. yr BP 至今)两个阶段。新疆北部(即乌伦古湖)全新世气候变化历史可以分为干旱的全新世前期(约 10 000 ~ 6700 cal. yr BP)和湿润的全新世后期(约 6700~0 cal. yr BP)两个阶段。

阿奇特湖湖芯孢粉资料记录到的蒙古高原西部过去约 22 600 年以来气候变化在大区域尺度上与其周边地区湖泊孢粉记录到的气候变化历史具有较好的一致性，这在一定程度上增加了我们对本章孢粉重建结果的信心。然而，阿奇特湖所记录的全新世小区域尺度气候变化却与其相邻的湖泊(Hoton 湖和乌伦古湖)具有较为明显的差异，反而与蒙古高原北部(即 Ugii 湖、Telmen 湖和 Hovsgol 湖)的全新世气候变化历史更为相似，这在一定程度上支持了 Wang 等人(2009,2011)、Wang 和 Feng(2013)关于蒙古高原北部全新世湿度变化受温度控制的观点。他们认为，蒙古高原中全新世的气候干旱主要是由于高温导致蒸发加剧从而导致了湿度降低引起的。该结论得到了阿奇特湖湖芯基于孢粉组合定性分析和生物群区化定量分析结果的支持。本研究的结果面临的一个矛盾，即本章基于孢粉定量重建的降水量与定性和半定量获得的湿度变化结果是一致的，这似乎说明降水(而不是温度)仍然是控制该地区湿度变化的主要因素。这就与前述的温度控制湿度变化的观点相冲突。此外，如果本章定量重建的年均温和年均降水量是经得起检验的，那么该地区的气候变化则基本遵循冷—湿和暖—干的水热组合模式，这种水热组合又具有典型的西风带气候特征(Aizen 等,2001；Bothe 等,2011；Bridgman 和 Oliver,2006)。当然，这还需要更进一步地深入研究。

5.3. 结论

基于阿奇特湖孢粉资料重建的结果显示，约 22 600~13 200 cal. yr BP，气候冷湿，流域植被主要为森林和草原，湖泊周围植被主要为草原而周围山地主要为森林；约 13 200~6400 cal. yr BP，气候温干，流域高海拔地区主要为草原植被，低海拔地区则主要为荒漠植被；约 6400~1600 cal. yr BP，流域高海拔地区泰加林扩张，气候冷湿；过去约 1600 年以来，该流域植被又以森林草原植被为主。

基于孢粉数据重建的温度和降水量结果显示：1 阿奇特湖地区末次冰期以来温度和湿度变化是不同步的；2 约 22 600 cal. yr BP 以来，研究区气候在约 22 600~13 200 cal. yr BP 最湿润，在约 10 500 ~7000 cal. yr BP 温度最高；3 在约 13 200~6400 cal. yr BP 的高温阶段尽管可能带来了更多的降水，但也大大增加了蒸发，从而导致这一时段区域有效湿度反而相对较低。

致谢：张成君教授、张妮娟女士和孙非非女士参加了野外工作，并感谢蒙古国地质研究所的同事在野外工作和后勤方面的帮助

参考文献

Erdtman, G.主编，中国科学院植物研究所古植物室孢粉组译. 1978. 孢粉学手册. 北京：科学出版社.

P.D., 摩尔, J.A., 韦布著；李文漪, 肖向明, 刘光锈译. 1987. 孢粉分析指南. 南宁：广西人民出版社.

王伏雄, 钱南芬, 张玉龙, 杨惠秋. 1997. 中国植物孢粉形态(第二版). 北京：科学出版社.

肖霞云, 蒋庆丰, 刘兴启, 肖海丰, 沈吉. 2006. 新疆乌伦古湖全新世以来高分辨率的孢粉记录与环境变迁. 微体古生物学报, 23 (1): 77~86.

Aizen, E.M., Aizen, V.B., Melack, J.M., Nakamura, T. and Ohta, T., 2001. Precipitation and atmospheric circulation patterns at mid~latitudes of Asia. International Journal of Climatology, 21: 535~556.

Blyakharchuk, T.A., Wright, H.E., Borodavko, P.S., van der Knaap, W.O. and Ammann, B., 2007. Late Glacial and Holocene vegetational history of the Altai Mountains (southwestern Tuva Republic, Siberia). Palaeogeography, Palaeoclimatology, Palaeoecology, 245: 518~534.

Bothe, O., Fraedrich, K. and Zhu, X., 2011. Precipitation climate of Central Asia and the large~scale atmospheric circulation. Theoretical Applied Climatology. http:// dx.doi.org/10.1007/s00704~011~0537~2.

Bridgman, B.H. and Oliver, J.E., 2006. The Global Climate System: Patterns, Processes, and Teleconnections. Cambridge University Press, New York.

Chen, F.H., Yu, Z.C., Yang, M.L., Ito, E.,Wang, S.M., Madsen, D.B., Huang, X.Z., Zhao, Y., Sato, T., Birks, H.J.B., Boomer, I., Chen, J.H., An, C.B. and Wünnemann, B., 2008. Holocene moisture evolution in arid central Asia and its out~of~phase relationship with Asian monsoon history. Quaternary Science Reviews, 27 (3~4): 351~364.

Davis, B.A.S., Brewer, S., Stevenson, A.C., Guiot, J. and other data contributors. 2003. The temperature of Europe during the Holocene reconstructed from pollen data. Quaternary Science Reviews, 22: 1701~1716.

Dorofeyuk, N.I. and Tarasov, P.E., 1998. Vegetation and lake levels in Northern Mongolia in the last 12 500 years as indicated by data of pollen and diatom analyses. Stratigraphy and Geological Correlation, 6(1):

70~83.

Feng, Z.-D., An, C.B., Tang, L.Y. and Jull, A.J.T., 2004. Stratigraphic evidence of a Megahumid climate between 10,000 and 4000 years BP. in the western part of the Chinese Loess Plateau. Global and Planetary Change, 43 (3-4): 145~155.

Feng, Z.-D., Tang, L.Y., Wang, H.B., Ma, Y.Z. and Liu, K.B., 2006. Holocene vegetation variations and the associated environmental changes in the western part of the Chinese Loess Plateau. Palaeogeography, Palaeoclimatology, Palaeoecology, 241: 440~456.

Fowell, S.J., Hansen, B., Peck, J.A., Khosbayar, P. and Ganbold, E., 2003. Mid to late Holocene climate evolution of the Lake Telmen Basin, North Central Mongolia, based on palynological data. Quaternary Research, 59 (3): 353~363.

Grunert, J., Lehmkuhl, F. and Walther, M., 2000. Paleoclimatic evolution of the Uvs Nuur basin and adjacent areas (Western Mongolia). Quaternary Internarional, 65/66: 171~191.

Guiot, J., Harrison, S.P. and Prentice, T.C., 1993. Reconstruction of Holocene patterns of moisture in Europe using pollen and lake~level data. Quaternary Research, 40: 139~149.

Guiot, J. and Goeury, C., 1996. PPPBASE, a software for statistical analysis of paleoecological and paleoclimatological data. Dendrochronologia, 14: 295~300.

Gunin, P.D., 1999. Vegetation dynamics of Mongolia. Kluwer Academic Publisher, Copenhagen, 238 pp.

Gupta, A.K., Anderson, D.M. and Overpeck, J.T., 2003. Abrupt changes in the Asian southwest monsoon during the Holocene and their links to the North Atlantic Ocean. Nature, 421: 354~357.

Harrison, S.P., Yu, G. and Tarasov, P.E., 1996. Late Quaternary Lake~Level Record from Northern Eurasia. Quaternary Research, 45 (2): 138~159.

Herzschuh, U., Tarasov, P., Wünemann, B. and Hartmann, K., 2004. Holocene vegetation and climate of the Alashan Plateau, NW China, reconstructed from pollen data. Palaeogeography, Palaeoclimatology, Palaeoecology, 211 (1-2): 1~17.

Hilbig, W., 1995. The vegetation of Mongolia. SPB Academic Publishing, Amsterdam.

Jiang, W.Y., Guo, Z.T., Sun, X.J., Wu, H.B., Chu, G.Q, Yuan, B.Y, Hatté, C. and Guiot, J., 2006. Reconstruction of climate and vegetation changes of Lake Bayanchagan (Inner Mongolia): Holocene variability of the East Asian monsoon. Quaternary Research, 65 (3): 411~420.

Jiang, W.Y., Guiot, J., Chu, G.Q., Wu, H.B., Yuan, B.Y., Hatté, C. and Guo, Z.T., 2009. An improved methodology of the modern analogues technique for palaeoclimate reconstruction in arid and semi~arid regions. Boreas, 39: 145~153.

Liu, X.Q., Herzschuh, U., Shen, J., Jiang, Q.F. and Xiao, X.Y., 2008. Holocene environmental and climatic changes inferred from Wulungu Lake in northern Xinjiang, China. Quaternary Research, 70(3): 412~425.

Ma, Y.Z., Liu, K.~B., Feng, Z.D., Sang, Y.L., Wang, W. and Sun, A.Z., 2008. A survey of modern pollen and vegetation along a south~north transect in Mongolia. Journal of Biogeography, 35: 1512~1532.

Magny, M., Guiot, J. and Schoellammer, P., 2001. Quantitative reconstruction of Younger Dryas to Mid-Holocene paleoclimates at Le Locle, Swiss Jura, using pollen and lake~level data. Quaternary Research, 56: 170~180.

Members of China Quaternary Pollen Data Base, 2001. Simulation of China biome reconstruction based

on pollen data from surface sediment samples. Acta Botanica Sinica, 43: 201~209.

Moore, P.D., Webb, J.A. and Collinson, M.E., 1991. Pollen Analysis, second ed. Blackwell Scientific Publication, Oxford, p. 216.

Moros, M., Emeis, K., Risebrobakken, B., Snowball, I., Kuijpers, A., Mcmanus, J. and Jansen, E., 2004. Sea surface temperature and ice rafting in the Holocene North Atlantic: climate influences on northern Europe and Greenland. Quaternary Science Reviews, 23: 2113~2160.

Nakagawa, T., Tarasov, P.E., Nishida, K., Gotanda, K. and Yasuda, Y., 2002. Quaternary pollen-based climate reconstruction in central Japan: application to surface and Late Quaternary spectra. Quaternary Science Reviews, 21: 2099~2113.

Peck, J.A., Khosbayar, P., Fowell, S.J., Pearce, R.B., Ariunbileg, S., Hansen, B. and Soninkhishig, N., 2002. Mid to Late Holocene climate change in north central Mongolia as recorded in the sediments of Lake Telmen. Palaeogeography, Palaeoclimatology, Palaeoecology, 183 (1~2): 135~153.

Prentice, I.C., Guiot, J., Huntley, B., Jolly, D. and Cheddadi, R., 1996. Reconstructing biomes from palaeoecological data: a general method and its application to European pollen data at 0 and 6 ka. Climate Dynamics, 12: 185~194.

Prokopenko, A.A., Alexander, A., Khursevich, G.K., Bezrukova, E.V., Kuzmin, M.I., Boes, X., Williams, D.F., Fedenya, S.A., Kulagina, N.V., Letunova, P.P. and Abzaeva, A.A., 2007. Paleoenvironmental proxy records from Lake Hovsgol, Mongolia, and a synthesis of Holocene climate change in the Lake Baikal watershed. Quaternary Research, 68 (1): 2~17.

Reimer, P.J., Baillie, M.G.L., Bard, E., Bayliss, A., Beck, J.W., Blackwell, P.G., Ramsey, C.B., Buck, C. E., Burr, G.S. and Edwards, R.L., 2009. IntCal09 and Marine09 radiocarbon age calibration curves, 0~50 000 years cal BP. Radiocarbon, 51: 1111~1150.

Rudaya, N., Tarasov, P., Dorofeyuk, N., Solovieva, N., Kalugin, I., Andreev, A., Daryin, A., Diekmann, B., Riedel, F., Tserendash, N. and Wagner, M., 2009. Holocene environments and climate in the Mongolian Altai reconstructed from the Hoton-Nur pollen and diatom records: a step towards better understanding climate dynamics in Central Asia. Quaternary Science Reviews, 28 (5~6): 540~554.

Stott, L., Cannariato, K., Thunell, R., Haug, G.H., Koutavas, A. and Lund, S., 2004. Decline of surface temperature and salinity in the western tropical Pacific Ocean in the Holocene epoch. Science, 431: 56~59.

Sun, A.Z. and Feng, Z.-D., 2013. Holocene climatic reconstructions from the fossil pollen record at Qigai Nuur in the southern Mongolian Plateau. The Holocene, 23: 1391~1402.

Sun, A.Z., Feng, Z.-D., Ran, M. and Zhang, C.J., 2013. Pollen-recorded bioclimatic variations of the last ~22 600 years retrieved from Achit Nuur in the western part of the Mongolian Plateau. Quaternary International, 311: 36~43.

Tarasov, P.E., Webb, III. T., Andreev, A.A., Afanas'eva, N.B., Berezina, N.A., Blyakharchuk, T.A., Bolikhovskaya, N.S., Cheddadi, R., Chernavskaya, M.M. and Chernova, G.M., 1998. Present-day and mid-Holocene biomes reconstructed from pollen and plant macrofossil data from the former Soviet Union and Mongolia. Journal of Biogeography, 25: 1029~1053.

Tarasov, P., Dorofeyuk, N. and Metl'tseva, E., 2000. Holocene vegetation and climate changes in Hoton-Nur basin, northwest Mongolia. Boreas, 29 (2): 117~126.

Wang, W., Ma, Y.Z., Feng, Z.D., Meng, H.W., Sang, Y.L. and Zhai, X.W., 2009. Vegetation and climate changes during the last 8660 cal. a BP in central Mongolia, based on a high-resolution pollen record from Lake Ugii Nuur. Chinese Science Bulletin, 54 (9): 1579~1589.

Wang, W., Ma, Y.Z., Feng, Z.D., Narantsetseg, Ts., Liu, K.B. and Zhai, X.W., 2011. A prolonged dry mid-Holocene climate revealed by pollen and diatom records from Lake Ugii Nuur in central Mongolia. Quaternary International, 229 (1~2): 74~83.

Wang, W. and Feng, Z.-D., 2013. Holocene moisture evolution across the Mongolian Plateau and its surrounding areas: a synthesis of climatic records. Earth-Science Reviews, 122: 38~57.

Wanner, H., Beer, J., Bütikofer, J., Crowley, T.J., Cubasch, U., Flückiger, J., Goosse, H., Grosjean, M., Joos, F., Kaplan, J.O., Küttel, M., Müller, S.A., Prentice, I.C., Solomina, O., Stocker, T.F., Tarasov, P., Wagner, M. and Widmann, M., 2008. Mid-to Late-Holocene climate change: an overview. Quaternary Science Reviews, 267: 1791~1828.

Yu, G., Chen, X.D., Ni, J., Cheddadi, R., Guiot, J., Han, H., Harrison, S.P., Huang, C., Ke, M., Kong, Z., Li, S., Li, W., Liew, P., Liu, G., Liu, Q. and Liu, K-B., 2000. Palaeovegetation of China: a pollen data-based synthesis for the mid-Holocene and last glacial maximum. Journal of Biogeography, 27: 635~664.

第五章

蒙古国北部岗湖(Gun Nuur)湖芯记录的过去10 000年植被与气候的变化

冯兆东[1]　　马玉贞[2]

①中国科学院 新疆生态与地理研究所

②北京师范大学 环境演变与自然灾害教育部重点实验室

本章利用岗湖湖芯的孢粉资料重建了蒙古高原北部全新世以来的温度和湿度变化历史。结果显示:全新世早期(约11 000~8000 cal. yr BP),蒙古高原北部的温度和湿度都比较低;随后的2000年里(约8000~6000 cal. yr BP)温度和湿度逐步上升;全新世晚期(即6000 cal. yr BP之后)气候波动频繁,但以暖湿为主,较高的乔木/非乔木比、孢粉浓度、有机质含量和硅藻丰度均表达了这一时期偏湿的气候特征。全新世早期较低的冬季太阳辐射和残存的大面积冰盖很可能有效地阻滞了欧亚大陆内部的温度上升。较低的气温也很可能有效地抑制了局地的水汽蒸发,从而有效地减少了区域降水。同时,注入到北大西洋的冰雪融水也很可能有效地抑制了北大西洋水汽的蒸发,从而减少了对其下游(包括蒙古高原北部)的水汽供给。过去6000年来冬季太阳辐射的逐渐增加、冰盖的最终消融、大气CO_2浓度的上升及由此导致的大气水分的增加都可能使蒙古高原北部的温度偏高。此外,过去6000年来冰盖的最终消融和海平面的不断上升也可能导致了亚洲大陆内部冬季风的减弱,从而诱使相对暖湿的大西洋气团进一步东侵,导致蒙古高原降水有所增加。

关键词:气候变化;全新世;蒙古高原;孢粉分析

1. 引言

对不同时间尺度气候变化规律的研究可以为我们评估某一区域未来环境(包括水资源和生态系统)对全球气候变化的响应提供科学参照。从这个意义上讲,全新世(即:现代间冰期或过去一万年)的气候变化特别值得关注,因为我们仍然处在全新世时段,而且目前和将来一段时间的气候边界条件仍然是全新世气候边界条件的延续(Wanner等,2008)。全新世气候变化主要受控于四个驱动因子:1-冬季太阳辐射;2-夏季太阳辐射;3-大气CO_2浓度;4-冰盖的范围。从本章研究区(即:蒙古高原北部)的角度看,早全新世较低的冬季太阳辐射和较大的冰盖范围(包括较长时间覆盖的大面积冰雪和较大面积的永久冻土)可能是影响本研究区全新世早期气候变化的高纬驱动力。过去7000年以来,在全球冰盖面积缩小和海洋表层的升温条件下,增加的大气CO_2浓度(Bush,2005)和适中的夏

季辐射(Ruddiman,2008)可能是影响本研究区全新世中期和晚期气候变化的低纬度驱动力

已有的研究表明,本章研究点岗湖(Gun Nuur)所在的蒙古高原北部的全新世气候变化主要受控于东亚季风影响(Harrison等,1996;Tarasov等,2000)　也有人认为,整个亚洲干旱、半干旱区(包括蒙古高原北部)的全新世气候主要受西风系统控制(Chen等,2008)而Wang等人(Wang等,2013;Wang和Feng,2013)则认为亚洲中部与东部干旱和极端干旱区(包括蒙古高原北部)全新世湿度的变化主要受控于温度的变化(如高温导致干旱)　这些分歧说明,在蒙古高原北部建立更高分辨率的气候序列是十分必要的

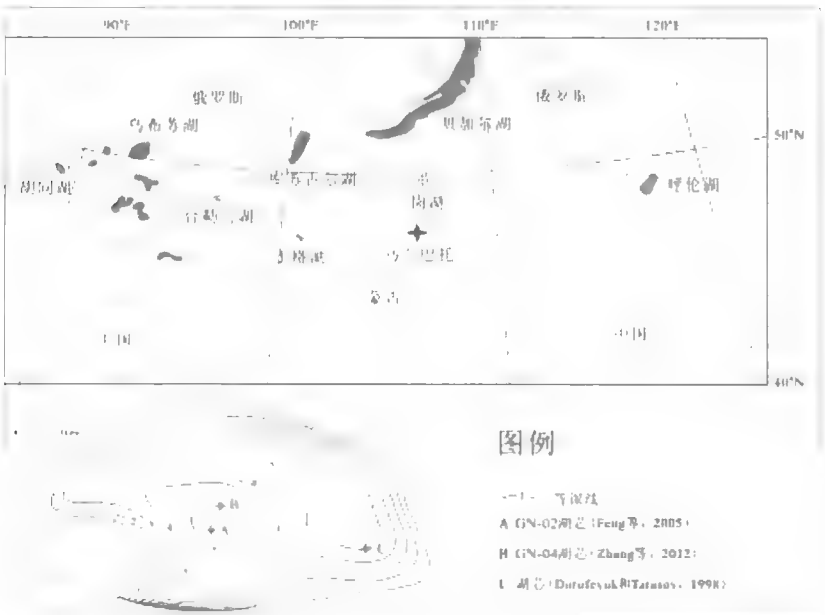

图5-1　岗湖位置和等深线图(Zhang等,2012)

关于岗湖气候变化重建的文章共有四篇　第一篇是1998年苏联学者(Dorofeyuk和Tarasov,1998)的文章,他们利用有限的测年数据和有限的硅藻资料建立了全新世气候变化序列(图5-1等深线图上的C);第二篇是2005年冯兆东等人发表的GN-02孔不包含孢粉数据的文章(Feng等,2005);第三篇是Zhang等人的文章(Zhang等,2012),他们基于对2004年钻取GN-04孔碳酸盐(矿物、同位素)的分析,重建了全新世岗湖水位和盐度变化的历史(图5-1等深线图上的B)　基于孢粉的岗湖气候变化重建是第四篇文章(Feng等,2013),其选取2002年在蒙古高原北部岗湖(Gun Nuur)在GN-02孔采集的样品为研究对象(图5-1等深线图上的A),用49个AMS ¹⁴C测年作年代支持,基于372个孢粉样品的分析资料,重建岗湖(Gun Nuur)的气候变化历史

首先必须指出的是,欧洲赤松(*Pinus sylvestris*)孢粉在岗湖孢粉谱中占绝对主导地位,而且欧洲赤松孢粉在孢粉谱中一般具有超代表性,因而它的气候归属就显得十分重要　我们的观点是,欧洲赤松孢粉含量的增加在岗湖所在地区不仅仅反映温度的上升,而

且反映湿度的增加(见:4.1.温度和湿度指数的重建)。因此,在我们构建新的用以指示温度(T)和湿度(M)变化的气候指数中(表5-1),欧洲赤松(表5-1中的S4)既是升温因子,也是增湿因子。值得提及的是,我们构建孢粉气候指数的思路和Demske等(2005)完全相同,表5-1中的S1、S2、S4三种类型代表"温暖",而S3、S5、S6三种代表"寒冷";S4、S5、S6三种类型代表"增湿",而S1、S2、S3三种代表"变干"。

表5-1 本章孢粉群组(S1~S6)与孢粉气候指数的计算

组号	类型	典型孢粉类型
S1	旱生荒漠	藜科、白刺属、蒺藜科、麻黄属
S2	中、旱生草原	蒿属、紫菀属
S3	冷温性针叶树	冷杉属
S4	桦木灌丛/森林	桦木灌丛/森林 桦属、栒木属、蔷薇科、榆属、蒲公英属 亮针叶林 欧洲赤松、柏属
S5	暗针叶林	云杉属、冷杉属、西伯利亚松、毛茛科、石竹科、蓝盆花属、罂粟科
S6	喜湿草甸草原	莎草科、蓼科
T	温度指数	T=(S1+S2 +S4)/(S3+S5+S6)
M	湿度指数	M=(S4+S5+S6)/(S1+S2+S3)

2. 地理背景及研究方法

岗湖(50°15′N,106°37′E,海拔600m)位于蒙古高原北部乌兰巴托—贝加尔湖走廊(48°N~56°N,104°E~108°E)中部的森林草原植被带(图5-1),是鄂尔浑河(Orhon River)东支流布林河(Buryn River)中游的一个封闭湖泊,湖水面积约为2.5km²,最大水深5m(图5-1)。鄂尔浑河东支流下游为草原植被,上游为森林草原植被。值得提及的是,欧洲赤松不仅发育在山地阳坡(Dumamsuren等,2009),而且也分布在岗湖周边冲积平原的沙丘(Dorofeyuk和Tarasov,1998)上。研究区现代气候属于温带大陆性气候,冬季气候寒冷干燥,夏季温暖湿润。年均气温-2℃,年均降水量350mm,降水主要集中在7~9月(Zhang等,2012)。

2002年,我们在岗湖(UN-02孔)中心的水深5m处用Livingstone活塞钻成功地钻取了745cm长的连续湖芯(图5-1等深线图上的A点)。湖芯取回后,在实验室以2cm间隔分样,共获得372个孢粉样品。孢粉提取采用酸碱法,程序为:实验前加入石松孢子以计算孢粉浓度,然后用10%的盐酸和39%的氢氟酸处理。我们在孢粉鉴定过程中参照了正式出版的孢粉图版和手册(如Moore等,1991;王伏雄等,1995)以及我们自己在中国北方收集的500多个现代花粉标本。孢粉鉴定是在400倍Leica光学显微镜下完成的,所有样品统计花粉数量均大于300粒(不包括孢子),以陆生种子植物花粉总和为基数计算孢粉百分比。

3. 结果

3.1 地层与年

岗湖湖芯(即:GN-02 孔)按地层可划分为四个沉积单元(图 5-2)。单元 A(720~745cm)为有机质和碳酸钙含量均较低的黑色黏土质粉砂层;单元 B(720~570cm)为富含碳酸钙的灰褐色纹泥层;单元 C(240~570cm)为三个中粉砂—细粉砂交替层,其中细砂粉层的有机质含量和碳酸钙含量比中粉砂层的较高;单元 D(0~240cm)为砂质粉砂层,其中 205~234cm 富含软体动物壳体,有机质含量达到整个湖芯最高,碳酸钙含量也很高。

我们共获得 49 个 AMS ^{14}C 年代,其中 48 个为沉积物全样年代,1 个为碳屑年代(表 5-2)。年代资料已经在 Zhang 等(2012)的文章中发表,其年代的可靠性和可能存在的问题在 Chang 等人(2011)的文章中进行了比较全面地阐述。年代模式是通过以下几个步骤建立的。首先,采用多项式回归方法建立 48 个年代样品的年龄—深度模式(图 5-2)。该模式显示,湖芯顶部(即:0cm)年龄为 1060 ^{14}C yr BP(^{14}C yr BP = 距今的 ^{14}C 年龄)。我们实测的顶层 0~5cm 处的年龄为 1200 ± 40 ^{14}C yr BP。考虑到该样品是湖芯表层 5cm 的混合体,实测的 0~5cm 深度的年龄(1200 ± 40 ^{14}C yr BP)与由 48 个年代样品获得的年龄—深度模式给出的 0cm 的年龄(1060 ^{14}C yr BP)是互相支持的,都表明湖芯上部的碳库效应大约为 1000 年。此外,湖芯下部 743~744cm 处碳屑(碳屑无碳库效应)测得的年龄与由年代模式推出的该深度年龄(含碳库效应)也相差约 1000 年,表明湖泊下部的碳库效应也为 1000 年左右,其与湖芯上部的碳库效应相近。据此我们假设:湖泊碳库效应在整个 GN-02 孔序列中变化不大,可将 1060 ^{14}C yr BP 应用到每个孢粉样点深度(即,模式年龄减去碳库效应)。最后,我们将经过碳库效应校正的年龄—深度模式(其仍为碳 ^{14}C 年龄)使用 CALIB 6.0 程序包中的 INTCAL09 数据库进行了日历年校正(Reimer 等,2009),得到了日历年代。

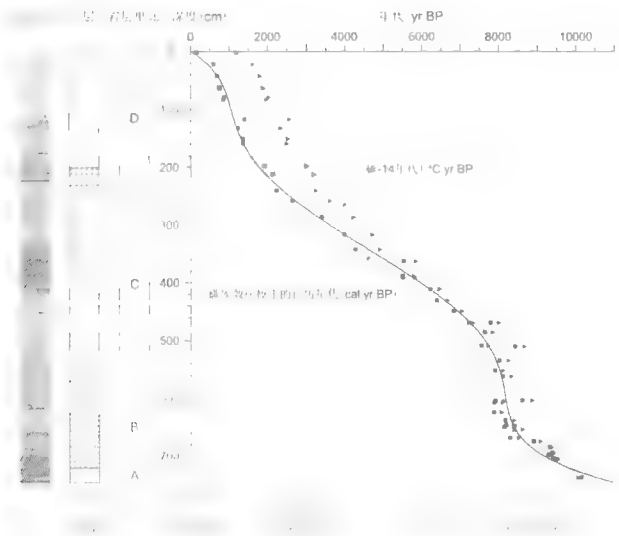

图5-2　GN-02孔年龄—深度模式(Feng等,2013)

表5-2 GN-02孔AMS ^{14}C测年数据

实验编号	样品号	深度(cm)	测年材料	δ ^{13}C (‰)	^{14}C年龄 (yr BP)	碳库效应校正后的^{14}C年龄	日历年龄 (cal. yr BP)	平均值
Beta-182732	GN 01	0~5	沉积物全样	-18.2	1200±40	140	3~282	139
Beta-182733	GN 02	20~25	沉积物全样	-20.2	1620±40	560	515~648	587
Beta-182734	GN 03	40~45	沉积物全样	-21.4	1800±40	740	568~734	682
Beta-182735	GN 04	60~65	沉积物全样	-22.1	1870±40	810	673~788	721
Beta-171822	GN 05	64~65	沉积物全样	-23.1	1900±40	840	678~900	748
Beta-171823	GN 06	151~152	沉积物全样	-24.1	2530±40	1470	1294~1479	1355
Beta-171824	GN 07	240~242	沉积物全样	-21.0	3250±40	2190	2068~2331	2225
Beta-171825	GN 08	342~344	沉积物全样	-22.7	4910±40	3850	4152~4410	4268
Beta-171826	GN 09	391~392	沉积物全样	-20.9	5820±50	4760	5326~5591	5504
Beta-198046	GN 10	469~470	沉积物全样	-21.2	7330±50	6270	7014~7301	7200
Beta-198047	GN 11	607~608	沉积物全样	-23.5	8080±50	7020	7730~7951	7856
Beta-198048	GN 12	649~650	沉积物全样	-25.9	8380±50	7320	8008~8292	8114
Beta-198049	GN 13	697~698	沉积物全样	-24.5	9330±50	8270	9091~9428	9260
Beta-171827	GN 14	743~744	沉积物全样	-26.8	9500±50	—	10 588~11 079	10786
KIA25401	GN 15	388~389	沉积物全样	-17	5795±30	4735	5326~5583	5484
KIA25402	GN 16	430~431	沉积物全样	-20.81	6670±30	5610	6310~6444	6371
KIA25403	GN 17	508~509	沉积物全样	22.82	7725±35	6665	7472~7589	7535
KIA25404	GN 18	551~552	沉积物全样	-22.92	8105±35	7045	7794~7950	7885
KIA23783	GN 19	604~605	沉积物全样	-23.93	8135±45	7075	7794~7977	7898
KIA23782	GN 20	624~625	沉积物全样	-25.14	8065±40	7005	7735~7936	7842
KIA23781	GN 21	646~647	沉积物全样	-25.32	8415±45	7355	8029~8311	8164
KIA23780	GN 22	654~655	沉积物全样	-24.3	8610±45	7550	8212~8422	8368
KIA23779	GN 23	674~675	沉积物全样	-26.8	9075±45	8015	8662~9016	8879
KIA23778	GN 24	694~695	沉积物全样	-21.13	9409±46	8349	9154~9479	9367
AA51939	GN 25	79~80	沉积物全样	-15.8	2030±37	970	790~952	861
AA51940	GN 26	83~84	沉积物全样	-17.0	1975±41	915	741~919	838
AA51941	GN 27	117~118	沉积物全样	-17.4	2560±37	1500	1306~1420	1379
AA51942	GN 28	132~133	沉积物全样	-20.9	2338±37	1278	1089~1290	1220
AA51943	GN 29	159~160	沉积物全样	-16.1	2500±140	1440	1018~1691	1352
AA51944	GN 30	198~199	沉积物全样	-21.6	3016±39	1956	1824~1988	1905

续表5-2

实验编号	样品号	深度(cm)	测年材料	δ ^{13}C (‰)	^{14}C年龄 (yr BP)	碳库效应校正后的^{14}C年龄	日历年龄 (cal. yr BP)	平均值
AA51945	GN 31	212~214	沉积物全样	−16.2	3201±38	2141	1999~2304	2126
AA51946	GN 32	258~260	沉积物全样	−19.9	3617±40	2557	2490~2756	2631
AA51947	GN 33	286~288	沉积物全样	−17.4	4226±42	3166	3269~3469	3391
AA51948	GN 34	316~318	沉积物全样	−14.8	4721±44	3661	3863~4142	3983
AA51949	GN 35	363~364	沉积物全样	−9.4	5843±47	4783	5329~5600	5515
AA51950	GN 36	411~412	沉积物全样	−15.1	6458±47	5398	6009~6291	6208
AA51951	GN 37	448~450	沉积物全样	−10.3	7040±61	5980	6667~6955	6817
AA51952	GN 38	469~470	沉积物全样	−8.0	7991±69	6931	7624~7931	7765
AA51953	GN 39	485~486	沉积物全样	−5.2	7836±63	6776	7509~7733	7626
AA51954	GN 40	509~510	沉积物全样	−11.5	8660±66	7600	8214~8544	8403
AA51955	GN 41	533~534	沉积物全样	−5.6	8242±63	7182	7871~8163	7999
AA51956	GN 42	561~562	沉积物全样	−5.6	8324±63	7264	7962~8184	8085
AA51957	GN 43	603~604	沉积物全样	−11.0	8858±83	7798	8408~8972	8585
AA51958	GN 44	638~639	沉积物全样	−16.4	8397±62	7337	8014~8313	8137
AA51959	GN 45	668~669	沉积物全样	−15.0	8500±60	7440	8070~8385	8264
AA51960	GN 46	684~685	沉积物全样	−21.09	356±64	8296	9091~9466	9297
AA51961	GN 47	703~704	沉积物全样	−14.79	439±88	8379	9136~9530	7373
AA51962	GN 48	705~706	沉积物全样	−28.99	9528±58	8468	9320~9544	9484
AA51963	GN 49	737~738	沉积物全样	−27.6	10047±70	8987	9893~10 254	10118

注：编号Beta表示测年在Beta实验室完成，KIA在基尔大学Leibniz实验室完成，AA在美国基金委支持的亚利桑那大学AMS实验室完成

3.2. 孢粉组合

我们用聚类分析划分出的 4 个孢粉带与上述的 4 个地层单元有很好的对应关系。孢粉带 GN-A 和 GN-B 以草本花粉为主，孢粉带 GN-C 和 GN-D 以乔木花粉(特别是欧洲赤松)为主(图 5-3)。

孢粉带 GN-A(720~745cm，约 10 800~9800 cal. yr BP)。该孢粉带以草本花粉(65%)占绝对优势为特征，夏绿树花粉(15%)含量也比较高。草本花粉主要由藜科(30%)、蒿属(20%)和禾本科(10%)组成，其他的草本花粉还有麻黄属、紫菀属和石竹科。夏绿树主要有桦属和榆属。针叶树花粉的平均百分比低于 20%，其组分包括落叶松(*Larix*)、云杉、冷杉(*Abies*)、西伯利亚松(*Pinus sibirica*)和欧洲赤松。值得注意的是，本孢粉带涉草科花粉

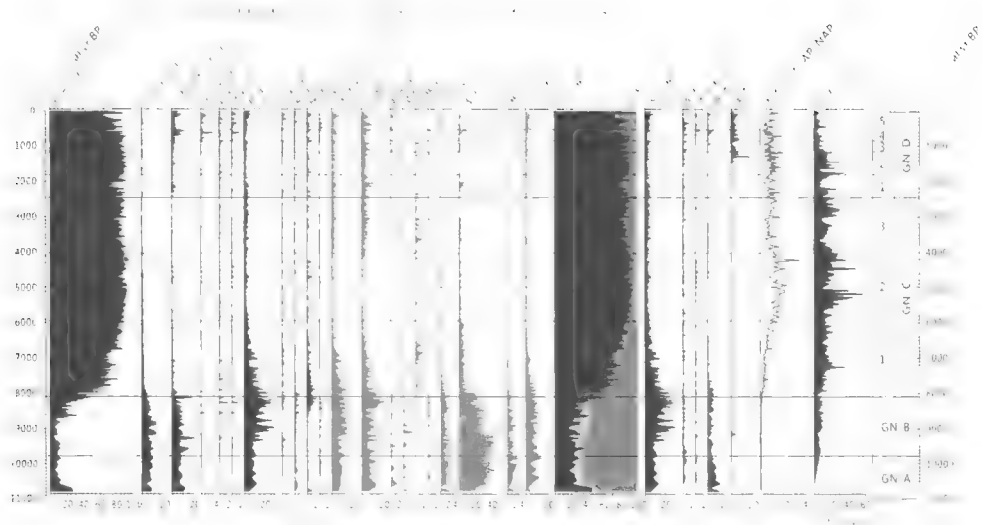

图5-3 GN-02孔孢粉百分比图(Feng等,2013)

和蕨类孢子的含量相对较高

孢粉带GN-B(570~720cm,约9800~8100 cal. yr BP)与孢粉带GN-A相比,该孢粉带桦属花粉含量明显增加,藜科和麻黄属含量有所降低。然而,两个孢粉带(GN-A和GN-B)的相同之处要比差异更加明显,其共同特征是落叶松、西伯利亚松、云杉和冷杉属花粉含量相对较高,蒿属和禾本科花粉含量都保持在一个较高的水平上。

孢粉带GN-C(240~570cm,约8100~2400 cal. yr BP)欧洲赤松花粉含量由GN-A和GN-B带的10%左右猛增到GN-C带的70%左右。相应地,该孢粉带的草本花粉(主要包括藜科、蒿属、禾本科和莎草科)显著减少,落叶松、西伯利亚松、云杉和冷杉的花粉几乎完全消失,乔木/非乔木比(AP/NAP)和孢粉浓度显著增加。根据带内乔木和草本花粉含量的波动情况,可将孢粉带GN-C分为3个亚带(即图3中的GN-C1、GN-C2、GN-C3)。

孢粉带GN-D(0~240cm,约2400~0 cal. yr BP)如同孢粉带GN-C一样,孢粉带GN-D的欧洲赤松花粉仍占绝对优势。与孢粉带GN-C不同的是:1暗针叶树花粉再现(包括西伯利亚松、云杉和冷杉);2夏绿树花粉再现(包括榛属、桦属和榆属);3铁杉属和柏科植物开始出现;4一些主要草本植物的花粉含量上升(藜科、蒿属、紫菀属、禾本科和莎草科)。根据西伯利亚松和蒿属花粉含量的变化可将本带分为5个亚带,即图3中的GN-D1、GN-D2、GN-D3、GN-D4、GN-D5。

4. 讨论和结论

4.1. 温度和湿度指数的重建

首先,我们检验了两套已经发表了的用于指示温度和有效湿度变化的孢粉气候指数,探讨它们是否可以被应用到我们的研究中。第一套是由Demske等人(2005)根据西伯利亚南部现代植被分布和气候要素之间的关系构建的(表5-3)。第二套是由Ma等人(2008)根据蒙古国境内表土(沿一条南北断面采集)孢粉组合与相应的气候要素之间的关系构建的(表5-4)。

表5-3　孢粉群组(S1-S7)与孢粉气候指数的计算(Demske等,2005)

组号	类型	典型孢粉类型
S1	草原	蒿属、菊科、藜科、麻黄属、禾本科、毛茛科、唐松草属、蔷薇科、委陵菜属、地榆属、葱属、伞形科、紫草科、十字花科、石竹科、豆科、拉拉藤属、唇形科、罂粟科、车前属、蓝雪科、景天属、蔊菜
S2	桦木灌丛/森林	桦木属、桑科、榆属(乔木)
S3	亮针叶林	落叶松属、欧洲赤松、刺柏属(乔木)
S4	暗针叶林	西伯利亚云杉、西伯利亚松、冷杉属、花楸属、接骨木属、忍冬属(乔木)
S5	亚高山灌丛	桤木、杜鹃属(乔木)
S6	其他灌丛	柳属、白桦
S7	北方高山种属	杜鹃花科、虎耳草属、仙女木属、马先蒿属、龙胆科、莎草科、蓼科、酸模属、山蓼属(非乔木)
T	温度指数	T= sqr[(S2+S3+S4+S6)/(S5+S7)]
M	湿度指数	M=sqr[(S4+S5+S6+S7)/(S1+S2+S3)]

利用 Demske 等人(2005)的气候指数重建的温度指数(T)曲线显示(图 5-4A):约 11 000~7000 cal. yr BP 的温度非常低,过去 7000 年以来,温度明显升高。重建的湿度指数(M)曲线则显示:约 11 000~8000 cal. yr BP 气候最为湿润;在随后的约 8000~6000 cal. yr BP 里,气候变干;约 6000~2500 cal. yr BP 气候持续干旱;在过去的大约 2500 年里,湿度一直在上升。

利用 Ma 等(2008)的气候指数重建的温度指标(T)曲线显示(图 5-4B):约 11 000~8000 cal. yr BP 温度非常高,约 8000 cal. yr BP 之后持续偏低。重建的湿度指数(M)曲线则显示:约 11 000~8000 cal. yr BP 气候非常干燥,经过大约 2000 年(即:约 8000~6000 cal. yr BP)的过渡,过去 6000 年(即:6000 cal. yr BP 以来)的气候一直比较湿润。显而易见,使用 Demske 等(2005)的方法重建的温度指数(T)和湿度指数(M)序列(图 5-4A)与使用 Ma 等(2008)的方法重建的温度指数(T)和湿度指数(M)序列(图 5-4B)完全相反

表5-4　孢粉群组(S1-S6)与孢粉气候指数的计算(Ma等,2008)

组号	类型	典型孢粉类型
S1	旱生荒漠	藜科、白刺属、麻黄科
S2	荒漠草原	花葱科、春黄菊属、百合科、麻黄、旋花属
S3	中、旱生草原	蒿属、紫菀属
S4	桦木灌丛/森林	桦木属、桤木属、蔷薇科、蒲公英属
S5	冷湿针叶林	云杉、冷杉、落叶松属、西伯利亚松、欧洲赤松、毛茛科、石竹科
S6	适中水分条件下的草原	莎草科、蓼科
T	温度指数	T=(S1+S2+S3)/(S4+S5+S6)
M	湿度指数	M=(S5+S6)/(S1+S2+S3+S4)

上述两套指数(Demske 等,2005;Ma 等,2008)为什么会导致完全相反的结论呢?因为上述两套指数对占绝对优势的花粉——欧洲赤松的生物气候属性做了完全相反的归类。具体地说,在 Demske 等人(2005)建立温度(T)和湿度(M)指数的西伯利亚地区,温度是由北向南递增的,湿度是由北向南递减的,该地区由北向南逐渐增多的欧洲赤松自然被归类为"暖干"属性(见表 5-3)。与此相反,在 Ma 等人(2008)建立温度(T)和湿度(M)指数的蒙古国境内,温度是由南向北递减的,湿度是由南向北递增的,该地区由南向北逐渐增多的欧洲赤松自然被归类为"冷湿"属性。

欧洲赤松是广泛分布于欧洲和亚洲的广温性和广湿性植物,其分布范围西起爱尔兰半岛,东至东西伯利亚,南起中国内蒙古,北达北极圈(Zhang,2007)。在贝加尔湖地区的山地,欧洲赤松与落叶松混交泰加林占据了干暖的南坡和东坡以及干暖的低海拔区域,而西伯利亚松、冷杉和西伯利亚云杉(*Picea obovata*)混交泰加林则占据了湿冷的北坡、西坡和高海拔地区。因此,在贝加尔湖区全新世气候变化重建中,欧洲赤松被认为指示暖干环境(如:Bezrukova 等,2009,2011;Demske 等,2005;Tarasov 等,2005,2007,2009)。我们的研究区(即:岗湖所在的区域))位于鄂尔浑河的一个支流,鄂尔浑河是色楞格河(Selenga River)的一个支流(注:色楞格河是直接流入贝加尔湖的)。在色楞格河流域的山地阳坡和岗湖附近的冲积平原沙丘上,欧洲赤松都占绝对优势(Dorofeyuk 和 Tarasov,1998;Dumamsuren 等,2009)。这确实可以说明,欧洲赤松是非常耐旱的(Dumamsuren 等,2009)。

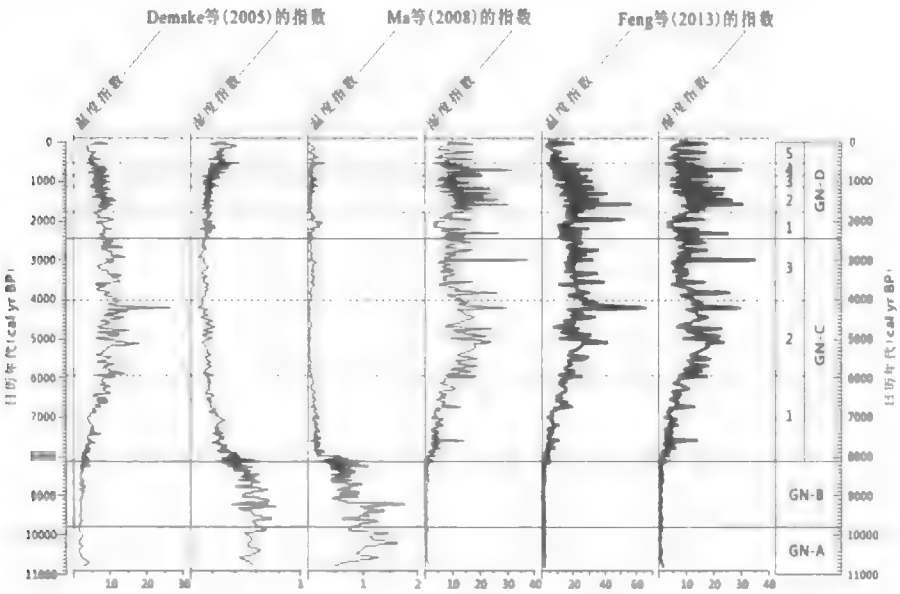

图5-4　基于孢粉资料重建的温度指数(T)和湿度指数(M)(A:采用Demske等的指数计算的结果;B:采用Ma等的指数计算的结果;C:采用Feng等设计的指数计算的结果)

但是，欧洲赤松并非是喜旱的。在贝加尔湖区(西伯利亚泰加林中部)和岗湖地区(森林草原带中部)出现了完全相反的情形：在贝加尔湖所在地区，如果土壤水分下降，欧洲赤松一定会替代暗针叶林(如西伯利亚松、冷杉和云杉)。相反，在岗湖所在的地区，如果土壤水分下降，欧洲赤松则一定会被草本植物所替代。换言之，与森林草原的主要草本植物相比，欧洲赤松生长过程中对土壤水分是有最低要求的。因此，森林草原中的欧洲赤松比森林草原中的草本植物需要更多的土壤水分(Dumamsuren 等，2009；Zhang，2007)。如果全新世以来岗湖所在地区的植被以森林草原为主，欧洲赤松扩张的限制因子应该是土壤有效湿度。实际上这种假设被本研究孢粉资料所证实：过去 7000 年以来，以欧洲赤松为主(不是以暗针叶林为主)的景观占绝对优势，这种景观很可能是森林—草原景观(图 5-3)。因此，在岗湖湖芯的研究中，我们将欧洲赤松归类为"高湿"属性，这与 Ma 等人(2008)的归类是一致的(见表 5-4)。

由于西伯利亚南部地区的欧洲赤松是由北向南递增的，因此，在古气候重建研究中，欧洲赤松在该地区被广泛认定为指示气候变暖(如：Bezrukova 等，2009；Demske 等，2005；Prokopenko 等，2007；Tarasov 等，1997，2007，2009)。我们在这里提供三套资料以支持欧洲赤松的"喜暖"属性。首先，几乎所有西伯利亚南部的晚冰期和全新世孢粉记录均揭示，晚冰期的草原植被景观逐渐地被全新世早期以欧洲赤松为主的森林—草原景观所替代，这很可能表明，欧洲赤松的扩张是由冰后期气候的变暖所导致的(Blyakharchuk 等，2004，2007；Kremenetski 等，1997；Rudaya 等，2009；Tarasov 等，1997，2000)。其次，从纬度上来讲，以下两点可以证明欧洲赤松与升温有关。第一，蒙古高原北部和西伯利亚南部的孢粉记录显示，全新世早期欧洲赤松是由南向北逐渐扩张的，这很可能表明，欧洲赤松的向北扩张与永久冻土南界的向北撤退导致的土壤升温有关(Bezrukova 等，2009，2011；Demske 等，2005；MacDonald 等，2000；Prokopenko 等 2007；Tarasov 等，2000)。第二，从西伯利亚南部到蒙古高原北部，随着温度由北向南的增加，现代欧洲赤松在植被中的比例大幅度增加，这很可能是与温度由北向南的递增相关的。最后，从地形和海拔上看，欧洲赤松和落叶松广泛生长在贝加尔湖地区较温暖的由地南坡和东坡以及较温暖的低海拔区域(Demske 等，2005；Prokopenko 等，2007；Tarasov 等，2000)，这似乎也表明了欧洲赤松的"喜暖"属性。需要补充说明的是，Ma 等人(2008)认为欧洲赤松指示低温环境的说法是有待商榷的，因为他们数据库中的 108 个现代表土样中，仅有 10 个采自有欧洲赤松生长的景观带(森林和森林草原景观)，并且这 10 个表土样只来自蒙古高原北缘相对狭小的库苏古尔湖地区(Lake Hovsgol)，所以不具有统计学意义。

综上所述，在岗湖所在的区域(即：森林—草原带)欧洲赤松应该是指代高湿环境的，在乌兰巴托—贝加尔湖走廊应该是指代高温环境的。根据以上讨论，我们构建了新的温度(T)和湿度(M)指数(见表 5-1；Feng 等，2013)。根据新建指数重建的气候序列显示：全新世早期(约 10 000~8000 cal. yr BP)的温度指数(T)和湿度指数(M)均较低；随后的大约 2000 年里(即：约 8000~6000 cal yr BP)温度和湿度均逐渐上升；约 6000~1000 cal. yr BP 气候相对暖湿；最近一千年的温度略有下降，但湿度仍然较高(图 5-4C)。

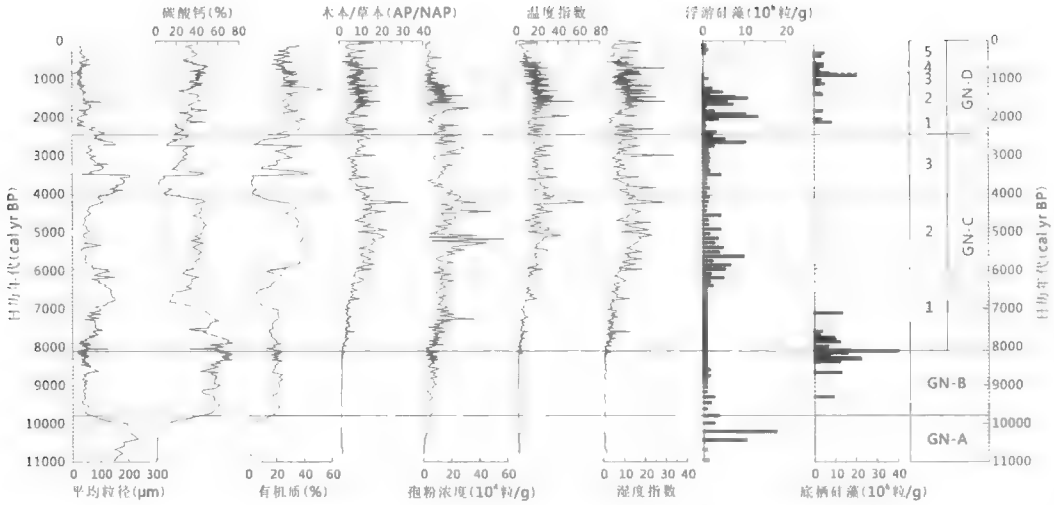

图5-5　根据新建指标重建的温度指数(T)和湿度指数(M)与有机质、乔木/非乔木值、孢粉浓度、浮游类硅藻丰度、底栖类硅藻丰度(注:图中粒度、碳酸钙和有机质含量的数据源自GN-04孔(Zhang等,2012))

值得提醒的是,我们用新建的指数(表5-1)重建的湿度曲线与乔木/非乔木比值曲线和孢粉浓度曲线几乎完全平行(图5-5),这进一步印证了新建湿度指数的可接受性。而且,反映流域和湖泊初级生产力的有机质含量(Shen等,2010)曲线也与我们用新建的指数重建的湿度曲线平行,这也进一步印证了新建湿度指数的可接受性。另外,GN-02孔的浮游硅藻丰度(图5)在约6500~1500 cal. yr BP的增加也显示这一时期是湖水位较高的时段(Dorofeyuk和Tarasov,1998;Shen等,2010),与该时段较高的湿度指数相对应。在约9000~7000 cal. yr BP和约1500~500 cal. yr BP,指示低湖面的底栖硅藻丰度增加,它们对应于湿度指数较低的时段。值得注意的是,在湖芯底部的黑灰色黏土质粉砂层中(GN-A),有两个样品的浮游硅藻丰度较高,该黏土质粉砂层的风积相和河流相成因(Dorofeyuk和Tarasov,1998;Zhang等,2012)可能意味着,这两个样品的硅藻很有可能是外源的。

此外,以莎草科、藜科和麻黄属为主的孢粉组合表明,全新世早期(约11 000~8000 cal. yr BP)的湖泊水位较低,湖泊周围发育了大面积沼泽植物(如莎草科)(图5-3)。与约11 000~6500 cal. yr BP和约2000~0 cal. yr BP两个阶段相比,约6500~2000 cal. yr BP的莎草科含量明显降低,很可能反映当时湖水位较高,湖泊周围的沼泽面积较小。这里需要进一步指出的是,在半干旱和半湿润地区,山地莎草对低地孢粉的贡献可以忽略的情况下,莎草科花粉的大量增加被认为是湖泊水位显著降低和沼泽大量发育的证据(Shen等,2010;Wang等,2011)。另外,在约3900~3500 cal. yr BP出现的粒度峰值也可能代表浅水沉积环境(Zhang等,2012),与之相对应的有机质含量减少和重建湿度指数的下降也支持这一解译。总之,用新建指数重建的湿度指数得到其他气候代用指标的很好印证,因此重建的结果是可信的。特别需要提及的是,Zhang等人(2012)认为GN-04孔的280~450cm

非常低的黄铁矿含量反映了约 6000~2500 cal. yr BP(全新世中期)的气候干旱,这与我们的解译是相反的。然而,作为海洋有机物分解代用指标的黄铁矿在湖泊研究中的气候和水文指示意义仍需要进一步求证(Berner,1984,1985)。

4.2. 区域古气候对比

为了从更大空间尺度来审视岗湖湖芯孢粉资料记录到的气候变化,我们先回顾一些最近发表的关于岗湖周边地区全新世气候重建的资料。首先,我们回顾一下蒙古高原北部西缘的阿尔泰山脉的文献,该地许多湖泊,包括乌布苏湖(Uvs Nuur)和胡同湖(Hoton Nuur)在内,已被深入地研究过(位置见图 5-1)。Rudaya 等人(2009)对胡同湖的全新世气候序列进行了重建,并且重新审视了其他人的文献(Blyakharchuk 等,2004,2007;Dorofeyuk 和 Tarasov,1998;Grunert 等,2000;Tarasov 等,2000)。Rudaya 等人(2009)的归纳是:阿尔泰东部(即蒙古国境内的阿尔泰)全新世早期(约 11 000 ~ 5000 cal. yr BP)为暖湿期,晚期(约 5000~0 cal. yr BP)为冷干期,其与东亚季风主导的气候模式一致;阿尔泰西部(即哈萨克斯坦境内的阿尔泰)全新世早期为暖干期,晚期为冷湿期,其与西风主导的气候模式一致;阿尔泰北部(即俄罗斯境内的阿尔泰)全新世早期为暖湿期,晚期为冷湿期。他们猜测,阿尔泰北部全新世早期的气候受东亚季风的影响,而全新世晚期的气候受西风系统的影响。

在蒙古高原北部东缘(即:靠近大兴安岭一侧),Wen 等人(2010a,2010b)重建了中国东北呼伦湖(Lake Hulun)全新世的气候序列(位置见图 5-1)。他们的结果显示:全新世早期(约 8000 cal. yr BP 之前)气候暖干;全新世中期(约 8000~4500 cal. yr BP)温度下降,但湿度达到全新世的最高值;约 4500~3500 cal. yr BP 气候温凉干旱;约 3500~1500 cal. yr BP 的气候逐渐转暖变湿;约 1000~500 cal. yr BP 是一个偏冷偏干的时段;约 500~0 cal. yr BP 的气候以暖湿为基本特征。而且,重建的呼伦湖全新世气候变化历史与邻近的哈尼泥炭 $\delta^{13}C$ 记录(Hong 等,2005)的变化历史相一致。

岗湖南边的优贵湖(Ugii Nuur)和台勒门湖(Telmen)(位置见图 5-1)记录了全新世中期(约 6500~3500 cal. yr BP)的气候干旱(Fowell 等,2003;Peck 等,2002;Wang 等,2009;Wang 等,2011),约 6500 cal. yr BP 之前及约 3500 cal. yr BP 之后的气候相对湿润。但是,岗湖记录的全新世中期气候变干的趋势与研究区北边的西伯利亚南部(Demske 等,2005)和南边的中国北方(Shi 等,1993)的全新世中期暖湿的气候模式有很好的一致性。这个一致性暗示,蒙古高原干旱、半干旱区全新世中期偏干的气候很可能是由全球或北半球范围的中全新世高温导致的(Wang 等,2011;Wang 和 Feng,2013)。

岗湖北边的贝加尔湖盆地的湖泊和泥炭已被广泛而系统地研究过(如:Bezrukova 等,2009;Bezrukova 等,2011;Demske 等,2005;Fukumoto 等,2012;Horiuchi 等,2000;Prokopenko 等,1999,2004,2007;Shichi,2009;Tarasov 等,2005,2007,2009)。这些重建结果显示,全新世早期植被由高属草原植被演替为以桦木属、云杉属为主的混交林和灌丛植被。同时,欧洲赤松开始发育并逐渐扩张,至约 7000 cal. yr BP,欧洲赤松取得优势地位(Demske 等,2005)。然而,上述的重建结果也存在明显的矛盾,例如,从三个不同的湖芯

获取的半定量重建具有很好的一致性(Demske 等,2005),但从另一个湖芯获取的定量重建却显示了明显的不一致(Tarasov 等,2007)。具体地讲,Demske 等人(2005)的重建显示,约 6000 cal. yr BP 之前温度升高,湿度降低;约 6000 cal. yr BP 之后湿度有增加趋势,而温度则有明显的下降趋势。但是,Tarasov 等人(2007)的定量重建结果显示,年降水和冬季温度的变化都有 3 个明显的阶段:第一阶段(约 11 100~8000 cal. yr BP)气候暖湿;第二阶段(约 8000~6000 cal. yr BP)气候温凉干旱;第三阶段(即:过去约 6000 年以来),气候又转向暖湿。

如前所述,用我们新建的孢粉气候指数(表 5-1)重建的气候变化序列显示,全新世早期(约 10 000~8000 cal. yr BP)温度和湿度都较低;之后的大约 2000 年里(约 8000~6000 cal. yr BP)温度和湿度逐渐上升;过去的约 6000 年来,气候以暖湿为主,但波动频繁。此外,我们在岗湖揭示的全新世湿度变化与贝加尔湖记录到的全新世湿度变化有很好的对应,贝加尔湖地区也是从全新世早期(约 11 500~6000 cal. yr BP)的偏干转向晚期(约 6000~0 cal. yr BP)的偏湿的(Demske 等,2005;Tarasov 等,2007)。总之,我们在岗湖重建的湿度变化与西风控制的阿尔泰西部的湿度变化是比较一致的,即全新世早期(约 11 500~5000 cal. yr BP)气候偏干旱,全新世晚期(自约 5000 cal. yr BP)气候偏湿润(Rudaya 等,2009)。还有,Wen 等人(2010)在呼伦湖揭示的第二湿润期(约 3500~1000 cal. yr BP)似乎也与岗湖重建的全新世晚期的湿润气候相吻合。

最后,我们不得不承认,岗湖孢粉资料所揭示的全新世早期(即:约 6000 cal. yr BP 之前)的寒冷、晚期(即约 6000 cal. yr BP 之后)的温暖气候特征与上述周边地区的记录(Demske 等,2005;Rudaya 等,2009;Tarasov 等,2007;Tarasov 等,2009)存在明显的地理不连贯性(即 geographic incoherency)。周边地区的气候重建都表明,早全新世是温暖的,而晚全新世是寒冷的。但是,贝加尔湖记录到的全新世暖期(约 6500~2500 cal. yr BP)(Demske 等,2005)与岗湖记录到的全新世暖期(约 6000~1000 cal. yr BP)(Feng 等,2013)是基本一致的。还需指出的是,Tarasov 等人(2007)在贝加尔湖所做的定量重建也显示,约 8000~6000 cal. yr BP 是温凉干旱的,随后的 6000 年是渐趋暖湿的,这一重建与我们在岗湖的重建也是比较一致的。此外,Prokopenko 等(2007)在重新审定年代序列和评价气候代用指标的基础上,归纳了贝加尔湖地区的全新世气候重建。他们的归纳显示,自约 7000 cal. yr BP 以来贝加尔湖地区的冬季和夏季温度均有升高趋势,这也与我们在岗湖重建的温度指数变化是一致的。

4.3. 区域气候变化的驱动机制

如果我们对岗湖所在地区的全新世气候重建(Feng 等,2013)和 Prokopenko 等人(2007)对贝加尔湖地区的归纳是经得起检验的,以下两个方面的原因可能导致了乌兰巴托—贝加尔湖走廊全新世早期(约 11 000~6000 cal. yr BP)的冷干和晚期(即:过去约 6000 年来)的暖湿特征:第一,全新世早期较低的冬季太阳辐射和大面积的冰盖(CLIMAP Members,1981;Ruddiman,2008;Tarasov 等,1997,2007);第二,过去约 7000 年以来,在全球冰盖面积缩小和海洋表层的升温条件下,增加的大气 CO_2 浓度和适中的夏季辐射

(Bush, 2005; COHMAP Members, 1988; Peltier 和 Fairbanks, 2006; Prokopenko 等, 2007; Ruddiman, 2008)。也就是说，较低的冬季太阳辐射和残存的冰盖(包括较长时间覆盖的大面积雪盖和较大面积的永久冻土)可能抑制了全新世早期大陆内部温度的上升。全新世早期相对较低的温度可能有效地减弱了西伯利亚南部局地水汽的蒸发，导致了区域降水也随之减少(Lydolph, 1977)。与西伯利亚南部毗邻的蒙古高原北部也很自然地被"干冷化"了。与此同时，全新世早期大量冰雪融水向北大西洋的注入也可能抑制了洋面水汽的蒸发，因而输送到包括蒙古高原北部在内的下风区的水汽减少。但是，约 7000 cal. yr BP 之后冰盖面积的缩小及由此导致的全球海平面上升可能使亚洲内陆冬季季风逐渐减弱，诱使相对暖湿的大西洋气团进一步向东侵入(Moros 等, 2004; Peltier 和 Fairbanks, 2006; Rudaya 等, 2009)，使得亚洲中东部(包括蒙古高原北部)的降水增多(Bai 等, 2010)。另外，我们在岗湖重建的过去约 7000 年的"高温"趋势也是有解的：冬季辐射的攀升、冰盖的逐渐消失、大气 CO_2 和水汽含量的回升都可能导致过去约 7000 年以来的温度增加(Bush, 2005)。

5. 总结

虽然我们在这里提供了三套资料以支持欧洲赤松的"喜暖"属性，但是我们不得不承认：将欧洲赤松的温度信号从湿度信号中区分开来是很难的。例如：欧洲赤松在贝加尔湖地区分布在山地的阳坡和低海拔地区，与其他针叶树相比，它绝对指示高温和低湿环境。然而，山地阳坡和低海拔地区的较低湿度主要是由这些地区本身的相对高温导致的较高蒸发引起的。此外，与湿度指数重建不同，我们的温度指数重建缺乏其他代用指标的佐证。简而言之，我们对岗湖温度重建的可靠性仍然没有十足的信心，我们不但需要深入调查孢粉与气候之间的关系，也需要更进一步理解欧洲赤松的生物气候学意义。

致谢：成文过程中得到了以下人士的帮助：张晓森先生，潘燕芳女士，兰波先生，张东良先生，杨运鹏先生。2002年参加野外采样的有：张虎才教授、安成帮教授、Khosbaya教授、Narantsetseg教授。

参考文献

白庆梅，田文寿，冯兆东，王澄海，靳立亚，2010. 亚洲干旱/半干旱区降水与大洋暖池气候的相关特征研究，冰川冻土，32(2)：295~308.

沈吉，薛滨，吴敬禄，吴艳宏，刘兴起，羊向东，刘健，王苏民，2010. 湖泊沉积与环境演化，北京：科学出版社.

王伏雄，钱南芬，张玉龙，杨惠秋，1995. 中国植物花粉形态(第二版)，北京：科学出版社.

张新时，2007. 中国植被及其地理格局，北京：地质出版社.

Berner, R.A., 1984. Sedimentary pyrite formation: an update. Geochimica et Cosmochimica Acta, 48: 605~615.

Berner, R.A., 1985. Sulphate reduction, organic matter decomposition and pyrite formation. Philosophical Transactions of the Royal Society of London, A315: 25~38.

Bezrukova, E.V., Abzaeva, A.A., Letunova, P.P., Kulagina, N.V. and Orlova, L.A., 2009. Evidence of environmental instability of the Lake Baikal after the last glaciations (based on pollen records from peatlands). Archaeology, Ethnology & Anthropology of Eurasia, 37(3):17~24.

Bezrukova, E.V., Belov, A.V. and Orlova, L.A., 2011. Holocene vegetation and climate variability in North Pre-Baikal region, East Siberia, Russia. Quaternary International, 237:74~82.

Blyakharchuk, T.A., Wright, H.E., Borodavko, P.S., van der Knaap, W.O. and Ammann, B., 2004. Late glacial and Holocene vegetation changes on the Ulagan high-mountains plateau, Altai Mountains, southern Siberia. Palaeogeography, Palaeoclimatology, Palaeoecology, 209:259~279.

Blyakharchuk, T.A., Wright, H.E., Borodavko, P.S., van der Knaap, W.O. and Ammann, B., 2007. Late glacial and Holocene vegetation history of the Altai Mountains (southwestern Tuva Republic, Siberia). Palaeogeography, Palaeoclimatology, Palaeoecology, 245:518~534.

Bush, A.B.G., 2005. CO_2/H_2O and orbitally driven climate variability over central Asia through the Holocene. Quaternary International, 136:15~23.

Chang, F.Q., Zhang, H.C., Ming, Q.Z., Chen, C.J., Zhang, W.X., Shi, Z.T. and Feng, Z.-D., 2011. AMS radiocarbon dating problems between 10 and 8 ka BP in lacustrine deposits from Gun Nuur, Northern Mongolia. Radiocarbon, 53: 501~509.

Chen, F.H., Yu, Z.C., Yang, M.L., Ito, E., Wang, S.M., Madsen, D.B., Huang, X.Z., Zhao, Y., Sato, T., Birks, H.J.B., Boomer, I., Chen, J., An, C. and Wünnemann, B., 2008. Holocene moisture evolution in arid central Asia and its out-of-phase relationship with Asian monsoon history. Quaternary Science Reviews, 27: 351~364.

CLIMAP Members, 1981. Seasonal reconstruction of the Earth's surface at the Last Glacial Maximum. GSA Map and Chart Series, MC-36. Geological Society of America.

COHMAP Members, 1988. Climatic changes of the last 18 000 years: observation and modeling. Science, 241:1043~1052.

Demske, D., Heumann, G., Granoszewski, W., Nita, M., Mamakowa, K., Tarasov, P.E. and Oberhänsli, H., 2005. Late glacial and Holocene vegetation and regional climate variability evidenced in high-resolution pollen records from Lake Baikal. Global and Planetary Change, 46:255~279.

Dorofeyuk, N.I. and Tarasov, P.E., 1998. Vegetation and lake levels in northern Mongolia in the last 12,500 years as indicated by data of pollen and diatom analyses. Stratigraphy and Geological Correlation, 6: 70~83.

Dulamsuren, C., Hauck, M., Bader, M., Oyungerel, S., Osokhjargal, D., Nyambayar, S. and Leuschner, C., 2009. The different strategies of Pinus sylvestris and Larix sibirica to deal with summer drought in a northern Mongolian forest-steppe ecotone suggest a future superiority of pine in a warming climate. Canadian Journal of Forest Research, 39:2520~2528.

Feng, Z.D., Ma,Y.Z., Zhang, H.C., Narantsetsega,T. and Zhang, X.S., 2013. Holocene climate variations retrieved from Gun Nuur lake-sediment core in the northern Mongolian Plateau. The Holocene, 23 (12):1721~1730.

Feng, Z.D., Wang, W.G., Guo, L.L., Khosbayar, P., Narantsetseg, T., Jull, A.J.T., An, C.B., Li, X.Q., Zhang, H.C. and Ma, Y.Z., 2005. Lacustrine and eolian records of Holocene climate changes in the Mongolian

Plateau: Preliminary results. Quaternary International, 136:25~32.

Fowell, S.J., Hansen, B.C.S., Peck, J.A., Khoshbayar, P. and Ganbold, E., 2003. Mid to late Holocene climate evolution of the Lake Telmen Basin, North Central Mongolia, based on palynological data. Quaternary Research, 59:353~363.

Fukumoto, Y., Kashima, K., Orkhonselenge, O. and Ganzorig, U., 2012. Holocene environmental changes in northern Mongolia inferred from diatom and pollen records of peat sediment. Quaternary International, 254: 83~91.

Grunert, J., Lehmkuhl, F. and Walther, M., 2000. Paleoclimatic evolution of the Uvs Nuur basin and adjacent areas (western Mongolia). Quaternary International, 65:171~192.

Harrison, S.P., Yu, G. and Tarasov, P.E., 1996. Late Quaternary lake-level record from Northern Eurasia. Quaternary Research, 45:138~159.

Hong, Y.T., Hong, B., Lin, Q.H., Shibata, Y., Hirota, M. and Zhu, Y.X., 2005. Inverse phase oscillations between the East Asian and Indian Ocean summer monsoons during the last 12 000 years and paleo-El Nino. Earth and Planetary Science Letters, 231:337~346.

Horiuchi, K., Minoura, K., Hoshino, K., Oda, T., Nakamura, T. and Kawai, T., 2000. Palaeoenvironmental history of Lake Baikal during the last 23,000 years. Palaeogeography, Palaeoclimatology, Palaeoecology, 157: 95~108.

Kremenetski, C.V., Tarasovt, P.E. and Cherkinsky, A.E., 1997. The latest Pleistocene in southwestern Siberia and Kazakhstan. Quaternary International, 41/42:125~137.

Lydolph, P.E., 1977. Climates of the Soviet Union. Elsevier Scientific Publishing Co. New York.

Ma, Y.Z., Liu, K.B., Feng, Z.D., Sang, Y.L., Wang, W. and Sun, A.Z., 2008. A survey of modern pollen and vegetation along a south-north transect in Mongolia. Journal of Biogeography, 35:1512~1532.

MacDonald, G.M., Velichko, A.A., Kremenetski, C.V., Borisova, O.K., Goleva, A.A., Andreev, A.A., Cwynar, L.C., Riding, R.T., Forman, S.L., Edwards, T.W.D., Aravena, R., Hammarlund, D., Szeicz, J.M. and Gattaulin, V.N., 2000. Holocene treeline history and climate change across Northern Eurasia. Quaternary Research, 53:302~311.

Moore, P.D., Webb, J.A. and Collinson, M.E., 1991. Pollen analysis. Blackwell Scientific Publications, Oxford.

Moros, M., Emeis, K., Risebrobakken, B., Snowball, I., Kuijpers, An., McManus, J. and Jansen, E., 2004. Sea surface temperature and ice rafting in the Holocene North Atlantic: climate influences on northern Europe and Greenland. Quaternary Science Reviews, 23:2113~2160.

Peck, J.A., Khosbayar, P., Fowell, S.J., Pearce, R.B., Ariunbileg, S., Hansen, B.C.S. and Soninkhishig, N., 2002. Mid to Late Holocene climate change in north central Mongolia as recorded in the sediments of Lake Telmen. Palaeogeography, Palaeoclimatology, Palaeoecology, 183:135~153.

Peltier, W.R. and Fairbanks, R.G., 2006. Global glacial ice volume and Last Glacial Maximum duration from an extended Barbados sea level record. Quaternary Science Reviews, 25:3322~3337.

Prokopenko, A.A., Khursevich, G.K., Bezrukova, E.V., Kuzmin, M.I., Boes, X., Williams, D.F., Fedenya, S.A., Kulagina, N.V., Letunova, P.P. and Abzaeva, A.A., 2007. Paleoenvironmental proxy records from Lake Hovsgol, Mongolia, and a synthesis of Holocene climate change in the Lake Baikalwatershed. Quaternary Re-

search, 28:2~17.

Prokopenko, A.A. and Williams, D.F., 2004. Deglacial methane emission signals in the carbon isotopic record of Lake Baikal. Earth and Planetary Science Letters, 218: 135~147.

Prokopenko, A.A., Williams, D.F., Karabanov, E.B. and Khursevich, G.K., 1999. Response of Lake Baikal ecosystem to climate forcing and pCO_2 change over the last glacial/interglacial transition. Earth and Planetary Science Letters, 172: 239~253.

Reimer, P.J., Baillie, M.G.L., Bard, E., Bayliss, A., Beck, J.W., Blackwell, P.G., Bronk Ramsey, C., Buck, C.E., Burr, G.S., Edwards, R.L., Friedrich, M., Grootes, P.M., Guilderson, T.P., Hajdas, I., Heaton, T.J., Hogg, A.G., Hughen, K.A., Kaiser, K.F., Kromer, B., McCormac, F.G., Manning, S.W., Reimer, R.W., Richards, D. A., Southon, J.R., Talamo, S., Turney, C.S.M., van der Plicht, J. and Weyhenmeyer, C.E., 2009. IntCal09 and Marine09 radiocarbon age calibration curves, 0~50 000 years cal BP. Radiocarbon, 51:1111~1150.

Rudaya, N., Tarasov, P., Dorofeyuk, N., Solovieva, N., Kalugin, I., Andreev, A., Daryin, A., Diekmann, B., Riedel, F., Tserendash, N. and Wagner, M., 2009. Holocene environments and climate in the Mongolian Altai reconstructed from the Hoton-Nur pollen and diatom records: a step towards better understanding climate dynamics in Central Asia. Quaternary Science Reviews, 28:540~554.

Ruddiman, W.F., 2008. Earth's climate: past and future (Second edition). Freeman and Company, New York.

Shi, Y.F., Kong, Z.C., Wang, S.M., Tang, L.Y., Wang, F.B., Yao, T.D., Zhao, X.T., Zhang, P.Y. and Shi, S., 1993. Mid-Holocene climates and environments in China. Global and Planetary Change, 7:219~233.

Shichi, K., Takahara, H., Krivonogov, S.K., Bezrukova, E.V., Kashiwaya, K., Takehara, A. and Nakamura, T., 2009. Late Pleistocene and Holocene vegetation and climate records from Lake Kotokel, central Baikal region. Quaternary International, 205:98~110.

Tarasov, P.E., Granoszewski, W., Bezrukova, E. V., Brewer, S., Nita, M., Abzaeva, A. A. and Oberhänsli, H., 2005. Quantitative reconstruction of the Last Interglacial vegetation and climate based on the pollen record from Lake Baikal, Russia, Climate Dynamics, 25:625~637.

Tarasov, P., Bezrukova, E., Karabanov, E., Nakagawa, T., Wagner, M., Kulagina, N., Letunova, P., Abzaeva, A., Granoszewski, W. and Riedel, F., 2007. Vegetation and climate dynamics during the Holocene and Eemian interglacials derived from Lake Baikal pollen records. Palaeogeography, Palaeoclimatology, Palaeoecology, 252:440~457.

Tarasov, P.E., Bezrukova, E.V. and Krivonogov, S.K., 2009. Late glacial and Holocene changes in vegetation cover and climate in southern Siberia derived from a 15 kyr long pollen record from Lake Kotokel. Climate of the Past, 5:1~11.

Tarasov, P.E., Dorofeyuk, N.I. and Meteltseva, E., 2000. Holocene vegetation and climate changes in Hoton-Nuur basin, northwestern Mongolia. Boreas, 9: 117~126.

Tarasov, P.E., Jolly, D. and Kaplan, J.O., 1997. A continuous Late Glacial and Holocene record of vegetation changes in Kazakhstan. Palaeogeography, Palaeoclimatology, Palaeoecology, 136:281~292

Wang, W. and Feng, Z.D., 2013. Holocene moisture evolution across the Mongolia Plateau and its surrounding areas: a synthesis of climatic records. Earth-Science Reviews, 122:38~57.

Wang, W., Ma, Y.Z. and Feng, Z.D., 2009. A high-resolution-Holocene climate reconstruction based on

pollen and diatom data from central Mongolia. Chinese Science Bulletin, 543:1579~1589.

Wang, W., Ma, Y.Z., Feng, Z.D., Narantsetseg, Ts., Liu, K.B. and Zhai, X.W., 2011. A prolonged dry mid-Holocene climate revealed by pollen and diatom records from Lake Ugii Nuur in central Mongolia. Quaternary International, 229:74~83.

Wanner, H., Beer, J., Bütikofer, J., Crowley, T.J., Cubasch, U., Flückiger, J., Goosse, H., Grosjean, M., Joos, F., Kaplan, J.O., Küttel, M., Müller, S.A., Prentice, I.C., Solomina, O., Stocker, T.F., Tarasov, P., Wagner, M. and Widmann, M., 2008. Mid- to Late Holocene climate change: An overview. Quaternary Science Reviews, 267: 1791~1828.

Wen, R., Xiao, J., Chang, Z., Zhai, D., Xu, Q., Li, Y., Itoh, S. and Lomtatidze, Z., 2010a. Holocene climate changes in the mid-high-latitude-monsoon margin reflected by the pollen record from Hulun Lake, northeastern Inner Mongolia. Quaternary Research, 73:293~303.

Wen, R.L., Xiao, J.L., Chang, Z.G., Zhai, D.Y., Xu, Q.H. and Li, Y.C., 2010b. Holocene precipitation and temperature variations in the East Asian monsoonal margin from pollen data from Hulun Lake in northeastern Inner Mongolia, China. Boreas, 39:262~272.

Zhang, C.J., Zhang, W.Y., Feng, Z.D., Mischke, S., Gao, X., Gao, D. and Sun, F.F., 2012. Holocene hydrological and climatic change on the northern Mongolian Plateau basedon multi-proxy records from Gun Nuur. Palaeogeography, Palaeoclimatology, Palaeoecology, 323~325:75~86.

第六章

蒙古国中部优贵湖(Ugii Nuur)湖芯记录的过去近9000年来植被和气候的变化

王 维[1] 马玉贞[2]

① 内蒙古大学 环境与资源学院

② 北京师范大学 环境演变与自然灾害教育部重点实验室

本章以蒙古国中部优贵湖(Ugii Nuur)湖泊沉积物为研究对象,以AMS ^{14}C年代为框架,利用沉积物孢粉、硅藻及粒度等代用指标重建了蒙古国中部优贵湖地区过去近9000年来的植被和气候变化。结果显示,8120~5830 ^{14}C yr BP(约9070~6620 cal. yr BP),孢粉组合以蒿属、藜科及松属主导,流域植被为山地草原,孢粉温度指数适中,湿度指数较高,浮游类硅藻与底栖类硅藻比值较高,沉积物粒度较小,反映湖泊水位较深,研究区气候总体温和湿润;5830~3080 ^{14}C yr BP(约6620~3280 cal. yr BP),旱生藜科花粉含量剧烈增加并维持峰值,松属、禾本科以及莎草科花粉含量降低,植被退化为荒漠草原,孢粉温度指数增高,湿度指数降低,浮游类硅藻与底栖类硅藻比值降低,沉积物粒度变粗,湖泊水位下降,气候干旱;3080 ^{14}C yr BP(约3280 cal. yr BP)以来,藜科花粉含量降低,孢粉温度指数降低,湿度指数升高,浮游类硅藻与底栖类硅藻比值增加,粒度变细,均表明气候变湿润。区域气候记录对比表明,中全新世中东亚干旱和极干旱地区可能存在持续的干旱气候,该干旱气候可能由温度升高导致的蒸发增强所致。

关键词:蒙古国中部;孢粉记录;硅藻记录;全新世;植被和气候变化

1. 引言

全新世植被和气候变化本底规律和机制的研究对于预测和理解将来变暖情形下的气候变化趋势和区域生态响应等具有重要意义(Wanner 等,2008)。研究表明,地球气候系统在中全新世(约 5000~6000 cal. yr BP)经历了深刻的变化并导致了较大尺度的海洋—大气系统重组(Steig,1999;Ruddiman,2001;Broecker,2003;Oppo 等,2003)。因此,探讨中全新世气候变化的时空分布规律,对于理解过去气候变化机制具有重要意义。然而,目前学界对于中全新世气候变化及其机制的认识仍十分有限,需要更多来自气候敏感地带的高质量地质记录提供帮助。蒙古高原处于东亚冬、夏季风和西风带气候系统的交互作用地带,对过去气候变化响应敏感,区域内广泛分布的湖泊沉积序列记录了过去气候变化的

历史。

已有研究表明，中国北方半干旱地区中全新世气候温暖湿润(见Feng等，2006及引用的相关文献)，蒙古国北部(Harrison等，1996；Tarasov等，2000)及毗邻的南西伯利亚地区(Velichko等，1997；Demske等，2005)中全新世气候也比较湿润(或温暖)。然而，近年来相继发表的中国新疆北部、内蒙古西部和鄂尔多斯高原等地中全新世干旱气候记录的证据(Rhodes等，1996；Chen C.-T.A.等，2003；Chen等，2003，2006；Li等，2003；Hartmann等，2009)似乎表明，中全新世期间在上述两个区域之间的蒙古高原核心干旱和半干旱区存在干旱气候。蒙古国也有类似的证据，如Tarasov等(1999)的研究认为，6000 ^{14}C yr BP左右蒙古国中部地区夏季温度较现今高约2℃，有效湿度较现今低约10%；蒙古国偏北地区Telmen(48°50′N，97°20′E，海拔1789m)湖的孢粉记录也表明存在中全新世干旱气候(Peck等，2002；Fowell等，2003)。尽管如此，蒙古高原中全新世气候时空分布规律和驱动机制的研究仍需要更多来自关键区域的高质量气候记录。为此，本章以蒙古国中部优贵湖湖泊沉积物为研究对象，以AMS ^{14}C年代为框架，利用湖泊沉积物地球物理和地生态代用指标，高分辨率地重建了蒙古国中部杭爱山北侧优贵湖(47°46′N，102°46′E，海拔1330m)过去近9000年来的植被及气候变化，以期揭示蒙古国中部地区全新世气候变化的时空规律和驱动机制。

2. 研究区概况

优贵湖(Ugii Nuur)位于蒙古国中部地区杭爱山北侧山麓地带(图6-1)，现代气候为大陆性干旱气候，冬季寒冷干燥，夏季相对温暖湿润，年均温度约0℃，年均降水量约250 mm(Tuvdendorzh和Myagmarzhav，1985)。据2004年野外观测，优贵湖现代湖泊水域面积约12km^2，最大水深约17m。发源于杭爱山东侧的鄂尔浑河的无名支流流经山地草原后从西南部注入优贵湖，并由西北方向流出汇入鄂尔浑河。

优贵湖附近及其东南部地带性植被为典型针茅(*Stipa*)草原，向北和西北方向依次过渡为山地羊茅(*Festuca*)草原和山地落叶松(*Larix sibirica*)/松属(*Pinus*)/桦木属(*Betula*)—羊茅森林草原(Lavrenko等，1979；Tuvdendorzh和Myagmarzhav，1985；Hilbig，1995)。优贵湖流域植被垂直分异显著，山地羊茅草原主要分布在流域上游海拔略高地带，以针茅为建群并伴生糙隐子草(*Cleistogenes squarrosa*)和冷蒿(*Artemisia frigida*)的典型草原发育在流域海拔略低的中下游地区。此外，下游地区山地上的针茅草原也可以细分为两个亚类：1)山地水分条件略差的阳坡上发育伴生地肤(*Kochia*)和猪毛菜(*Salsola*)的针茅草原；2)海拔较高的山顶或水分条件较好的阴坡发育以羊茅为主的山地草原(Lavrenko等，1979；Tuvdendorzh和Myagmarzhav，1985；Hilbig，1995)。

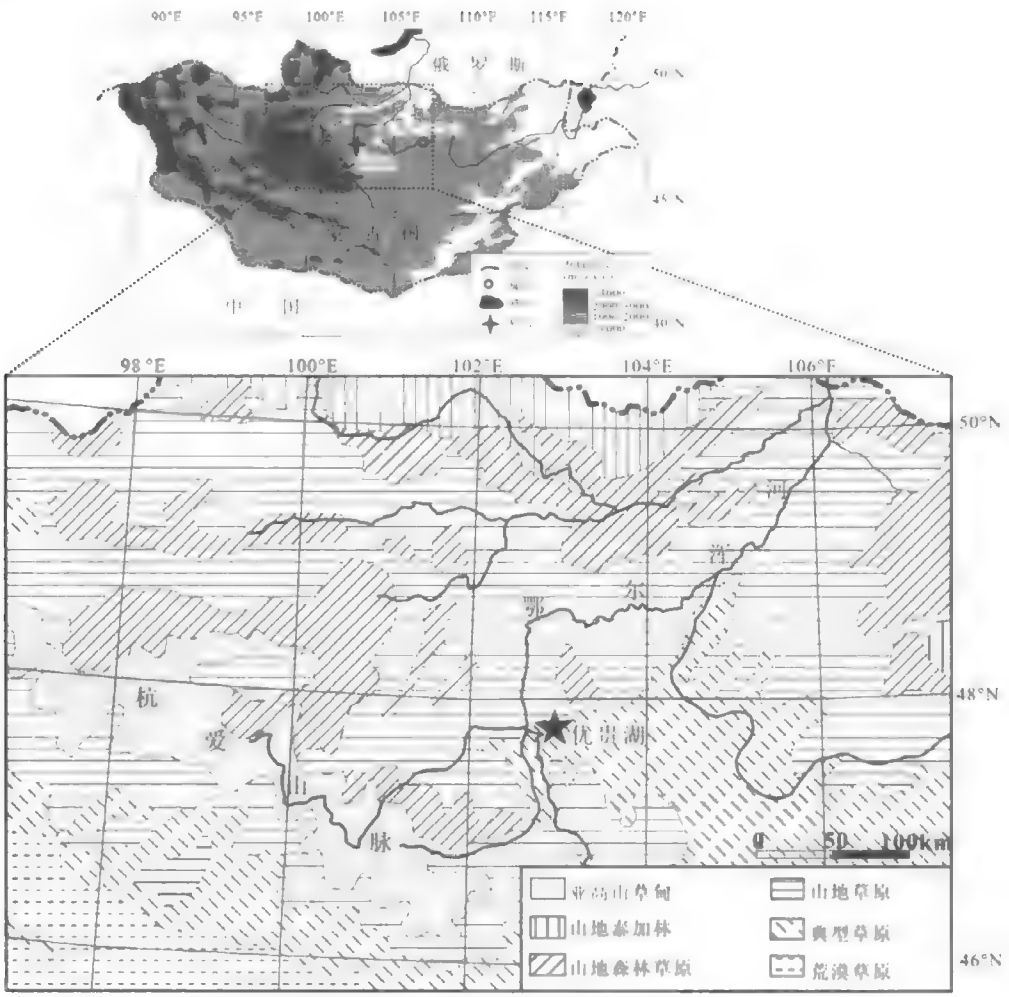

图6-1 优贵湖位置及区域植被概况(Lavrenko等,1979)

3. 方法

3.1. 现代花粉样品采集

为给岩芯孢粉数据的解译提供孢粉来源、传播过程以及气候环境意义方面的依据，本章采集并分析了研究区入湖河流表层沉积物样品(图 6-2 中 1~4 号)、湖心表层沉积物样品(图 6-2 中 5 号,即岩芯表层样品)、湖泊北侧山地山麓地带针茅草原现代表土花粉样品(图 6-2 中 6、7 号)及山顶附近山地草原现代花粉样品(图 6-2 中 8、9 号)的孢粉组成。

3.2. 岩芯钻取和样品采集

2004 年 8 月，在优贵湖中心偏东水深约 14.5m 处(47°46′N、102°46′E、海拔 1330m)，我们使用奥地利活塞钻钻取了约 854cm 长的沉积物岩芯。孢粉样品以约 2cm 间距分取，共获得样品 384 个(部分层位全样用于测年或代用指标测试造成样品缺失)。硅藻样品以 10cm 间距采集，共获样品 75 个(硅藻样品在蒙古国地质科学院分取，上部 100cm 岩芯完

整带间国、未分样）　粒度和磁化率等代用指标样品也以 2cm 间距采集

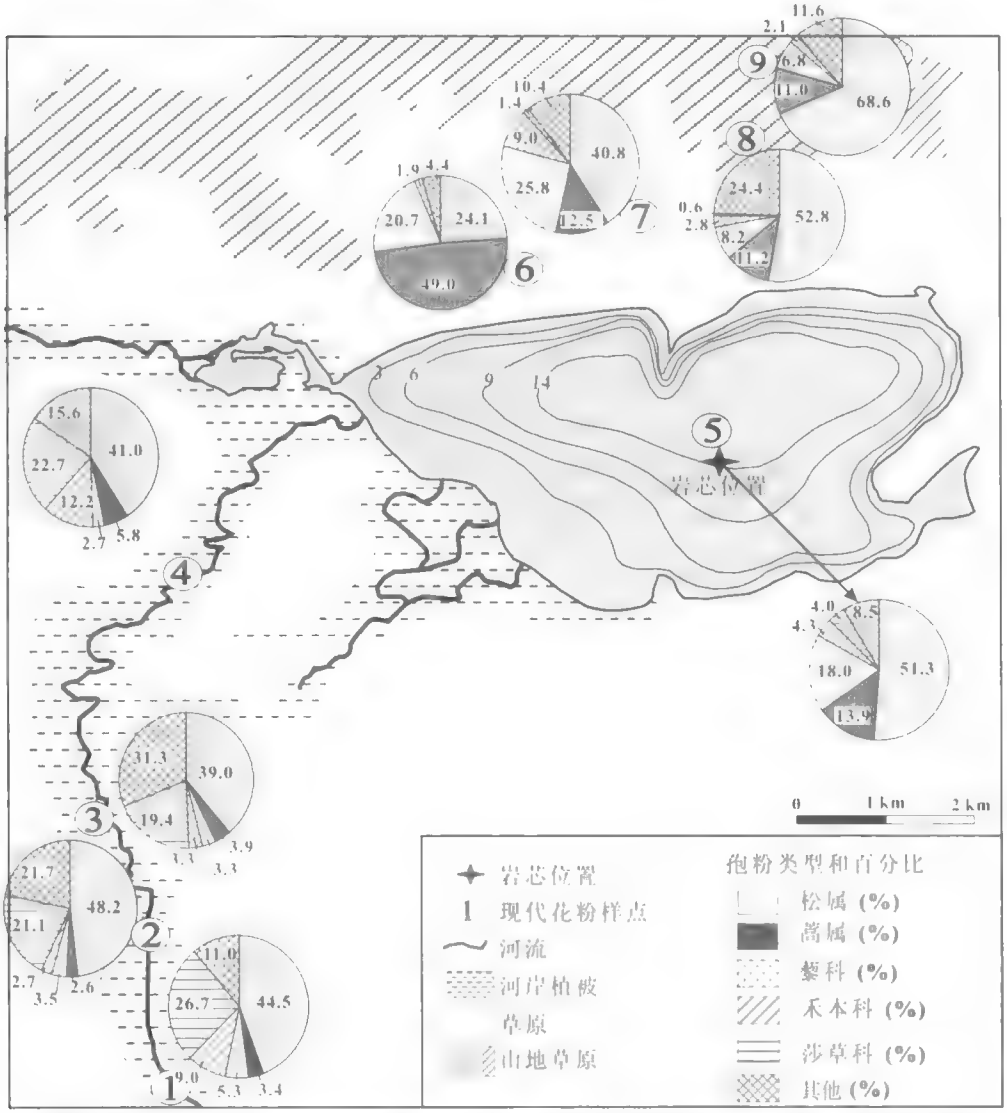

图6-2　现代花粉采样点及百分比组成。1~4号：入湖河流表层沉积物；5号：湖心表层沉积物；6~7号：低海拔山麓带针茅草原表土样品；8~9号：高海拔山地草原表土样品(Wang 等，2011)

3.3. 实验方法

使用酸碱法(Faegri 和 Iversen, 1975)并结合筛滤法提取孢粉样品　依次使用氢氧化钠、盐酸以及氢氟酸处理样品以去除有机质、碳酸盐和硅酸盐，残余物超声振荡过 7μm 筛布去除杂质，于指管富集保存于甘油溶液中　所有处理进行前，于指管样品中加入已知数量的石松孢子片剂（瑞典隆德大学，批号：938934）用于计算孢粉浓度(Stockmarr, 1971)　使用和参考已有的图册、书籍以及实验室内存有的现代花粉标准片，在 400 倍显微镜下进行花粉鉴定(Erdtman, 1969; Moore, 1991; 王伏雄等，1995)，共鉴定出花粉类型 52 科属　单样统计数量大于 350 粒(不包括孢子类型)，以陆生植物花粉总数为基数计算

花粉百分比。使用 Grapher 2.0 绘制孢粉百分比对深度和孢粉浓度对深度图。使用时序群组分析(CONISS)为孢粉带划分提供参考(Bennett,1996)。参考 Stoermer 和 Smol(1999)的方法进行硅藻提取,主要步骤包括盐酸处理、蒸馏水漂洗、倾滤、浮选等。参考出版的文献和书籍进行硅藻鉴定及环境意义将解释(Gasse,1986;Krammer 和 Lange-Bertalot,1986~1991;Camburn 和 Charles,2000)。随机选取 10 个断面进行硅藻鉴定,统计数量大于 300 个 / 样(Schrader 和 Gersonde,1978)。使用马尔文公司 Mastersizer 2000 型激光粒度分析仪进行沉积物粒度分析。沉积物全样的放射性碳测年在美国亚利桑那州立大学完成。

3.4. 孢粉气候定量重建

参考 Ma 等(2008)利用中国二连至蒙古国库布苏湖(Hovsgol)南北断面 104 个表土现代花粉建立的温度和湿度指标,重建了优贵湖温度和湿度序列。上述两个指标由代表不同生态气候的花粉类群计算而来。即依据现代表土花粉数量分析结果(层序聚类分析和非尺度多维标度),并参考各花粉类型母体植物生境,将蒙古高原主要花粉类型划分并组成 6 个生态气候类群(S1、S2、S3、S4、S5 和 S6),经过运算得到孢粉温度指标(T)和湿度指标(M)(见表 6-1)。

表6-1　孢粉类群(S1-S6)与孢粉气候指数的计算(Ma等,2008)

组号	类型	典型孢粉类型
S1	旱生荒漠	藜科、白刺属、蒺藜科
S2	荒漠草原	花葱、春黄菊型、百合科、麻黄属、旋花属
S3	中、旱生草原	蒿属、紫菀型
S4	桦木灌丛/森林	桦属、榛木属、蔷薇科、蒲公英型
S5	冷湿针叶林	云杉属、冷杉属、单束松型、双束松型、落叶松属、毛茛科、石竹科
S6	喜湿草甸草原	莎草科、蓼科
T	温度指数	T=(S1+S2+S3)/(S4+S5+S6)
M	湿度指数	M=(S5+S6)/(S1+S2+S3+S4)

4. 结果

4.1. 现代花粉—植被—气候关系研究

松属花粉在研究区各类型现代沉积物花粉组合中含量均较高,变化于 30%~70%。然而,现代湖泊附近以及流域内并无松属植物发育。因此可以推断,现代沉积物中松属花粉具有超代表性,为风力搬运的来自北部森林草原地带的松属花粉,该松属森林草原植被位于优贵湖西北方向 80km 以外。由此可见,优贵湖岩芯中高含量的松属花粉不能代表当地有松属植物发育。上述结果也得到了前人研究的支持(吴玉书等,1995;王琫瑜等,1996;Ma 等,2008)。

藜科(Chenopodiaceae)花粉含量在相对干燥的山麓带表土样品(图6-2中6、7号)花粉组合中较高，而在研究区河流表层沉积物样品(图6-2中1~4号)和山地草原表土样品(图6-2中8、9号)中含量较低，表明藜科花粉含量在一定程度上可以反映有效湿度状况。这与前人研究主张藜科含量或藜科与其他类型花粉的比值可以指示干旱程度的观点一致。例如，蒙古高原现代花粉研究结果显示，从草原到荒漠草原藜科花粉含量及其母体植物相对丰度呈增加趋势(Gunin 等，1999；Pyankov 等，2000；Ma 等，2008)。还如，中东地区和中国青藏高原地区的研究也表明，蒿属与藜科花粉含量的比值(A/C)可以用来指示气候干旱程度(El-Moslimany，1990；Van Campo 等，1996；Liu，K.-B 等，1998)。然而，Fowell 等(2003)使用(藜科 + 蒿属)/ 禾本科[(C+A)/G]值重建了 Telmen 湖干旱程度序列。看来，使用藜科花粉相关的指标时仍需谨慎，尤其是在长距离空气传播花粉主导或河流搬运花粉主导的情形下，该指标可能不能反映气候的真实状况(孙湘君等，1994；Ma 等，2005)。

众多研究表明，禾本科(Poaceae)花粉具有较低的代表性，蒙古高原南部(Liu 等，1999)和北部(Gunin 等，1999)的研究得出了类似的结论。本章现代花粉的研究结果也表明：禾本科花粉具有较低的代表性，在禾本科植物建群的植被中含量通常在10%以下(4号样品是个例外)。

莎草科(Cyperaceae)植物是山地草甸和湿地草甸的典型成分(Hilbig，1995；Gunin 等，1999)，其花粉含量的变化应该可以指示母体植物建群的植被群落的扩张或退缩，含量增加可能指示湿地草甸和/或山地草甸的扩张，进而反应凉/湿的气候(Fowell 等，2003)。

综上所述，湖芯中各类型花粉可能具有不同的来源和指示意义。松属来源于长距离空气传播，具超代表性；藜科和蒿属花粉来源于草原和荒漠草原；禾本科代表草原，但具有较低的代表性；莎草科花粉来源于河岸、湖岸或山地草甸。

4.2. 岩性和年代

根据野外观察和室内粒度分析数据，将优贵湖岩芯分为3个沉积单元(图6-3)：单元1(484~854cm)由灰褐色黏土质粉砂组成，中值粒度变化于5~20μm，砂含量小于2%；单元2(242~484cm)为浅灰色粉砂，含有两个富碳酸盐亚层(450~492cm 和348~368cm)，中值粒度变化于15~50μm，平均约30μm，砂含量增高至16%(平均约8%)；单元3(0~242cm)为灰色黏土质粉砂，中值粒度5~15μm，砂含量小于1%。

优贵湖岩芯共获得14个 AMS ^{14}C 年代(表6-2)。根据岩性和粒度变化，分三段回归建立了岩芯的年代—深度模式，在此基础上计算各段的沉积速率(图6-3)，外推获得底部年龄为8120 ^{14}C yr BP。三段的沉积速率分别为：单元3(0~242cm)为0.20 cm/yr、单元2(242~484cm)为0.076 cm/yr、单元1(484~854cm)为0.15 cm/yr。

表6-2 优贵湖AMS 14C测年数据

实验编号	样品号	深度(cm)	测年材料	^{13}C(‰)	^{14}C 年龄
AA81667	UG3	3~5	沉积物全样	-4.8	756±36
AA81668	UG4545	46	沉积物全样	-25.9	1929±39
AA81669	UG86	87	沉积物全样	-26.1	2014±38
AA64246	UG224	224~225	沉积物全样	-28.7	2228±36
AA64247	UG260	260~261	沉积物全样	-20.9	2117±38
AA64248	UG290	290~291	沉积物全样	-25	2549±36
AA64249	UG330	330~331	沉积物全样	-26.7	3283±43
AA64250	UG360	360~361	沉积物全样	-18.7	3260±44
AA64256	UG533	533~534	沉积物全样	-28.8	6091±49
AA64260	UG630	630~631	沉积物全样	-26.5	6727±45
AA64262	UG700	700~701	沉积物全样	-27.2	7325±70
AA64263	UG730	730~711	沉积物全样	-27.9	7077±53
AA64264	UG760	760~761	沉积物全样	-28	7341±54

注:编号AA表示测年在美国基金委支持的亚利桑那大学AMS实验室完成

4.3 孢粉和硅藻记录

4.3.1. 孢粉记录

根据观察和时序聚类分析(CONISS)结果,将优贵湖岩芯孢粉组合划分为3个孢粉组合带(图6-4)。

孢粉组合带1(530~854cm;8120~5830 ^{14}C yr BP;约9070~6620 cal. yr BP):基本上与沉积单元1(484~854cm)相对应,孢粉组合中藜科花粉含量适中,禾本科和莎草科含量较高,中生杂类草花粉[如毛茛科(Ranunculaceae)、唐松草属(*Thalictrum*)、地榆属(*Sanguisorba*)、蒲公英型(*Taraxacum*-type)、紫菀型(*Aster*-type)等等]表现较为突出,相对含量较高

孢粉组合带2(320~530cm;5830~3080 ^{14}C yr BP;约6620~3280 cal. yr BP):基本对应于沉积单元2(242~484cm),沉积速率(0.076cm/yr)为整个序列最低。孢粉组合的显著特征是:藜科花粉含量达整个序列峰值,莎草科和禾本科花粉含量为最低值,孢粉总浓度达整个序列最大,中生杂类草花粉的种数和百分含量较上带均显著减少,麻黄属花粉含量较上带有所增加。

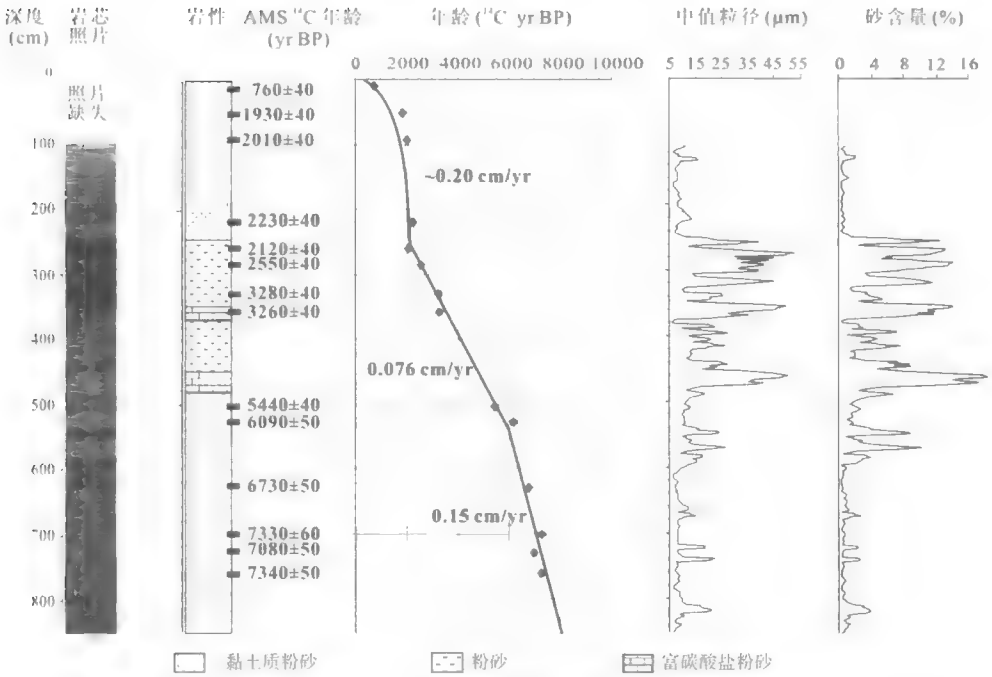

图6-3　优贵湖岩芯岩性(岩芯照片)、年代及粒度(中值粒度和砂含量)(Wang等,2011)

注:岩芯上部6个年代(760、1930、2010、2230、2120、2550 ^{14}C yr BP)非线性回归得到上部(0~242 cm)年代模式(R2=0.9259);中段7个年代(2230、2120、2550、3280、3260、5440、6090 ^{14}C yr BP)线性回归得到中段年代—深度模式(R2=0.974);底部6个年代(5440、6090、6730、7330、7080、7340 ^{14}C yr BP)线性回归得到下部年代—深度模式(R^2=0.879)

孢粉组合带3(0~320cm;3080~0 ^{14}C yr BP;约3280 cal. yr BP以来):基本对应沉积单元3(0~242cm),松属、蒿属、莎草科以及禾本科花粉含量显著增加,同时藜科花粉含量减少,中生杂类草花粉的类型数量和百分含量均显著增加,麻黄属花粉基本消失

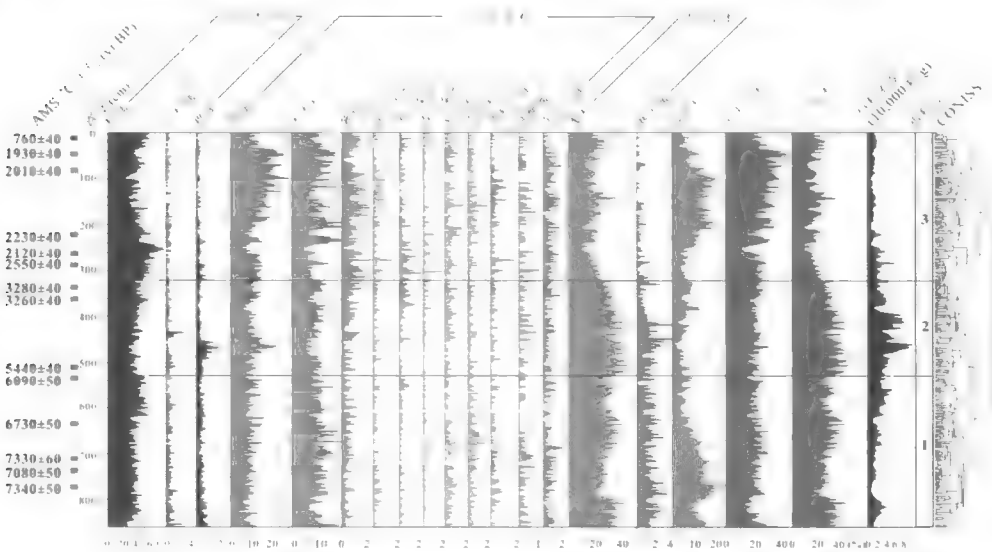

图6-4　优贵湖孢粉百分比图谱(Wang等,2009;2011)

4.3.2. 硅藻记录

根据浮游类硅藻和底栖类硅藻丰度变化，将优贵湖硅藻组合序列划分为 3 个组合带（图 6–5）。

硅藻组合带 1（575~854cm；8120~6200 ^{14}C yr BP）：基本对应于岩性沉积单元 1（484~854cm），硅藻组合主要由浮游类和底栖类组成，附生类不多。浮游类硅藻主要有：Aulacoseira granulata（Ehr.）Simonsen、A. alpigena（Grunow）Krammer，Stephanodiscus spp. 和 Cyclotella ocellata。底栖类种属有 Ellerbeckia arenaria（Moore）Crawford、Cocconeis（3种）和 Epithemia（3 种）。浮游类硅藻与底栖类硅藻比值（以下简称浮游/底栖比）较高，变化于10~40，平均约 20。

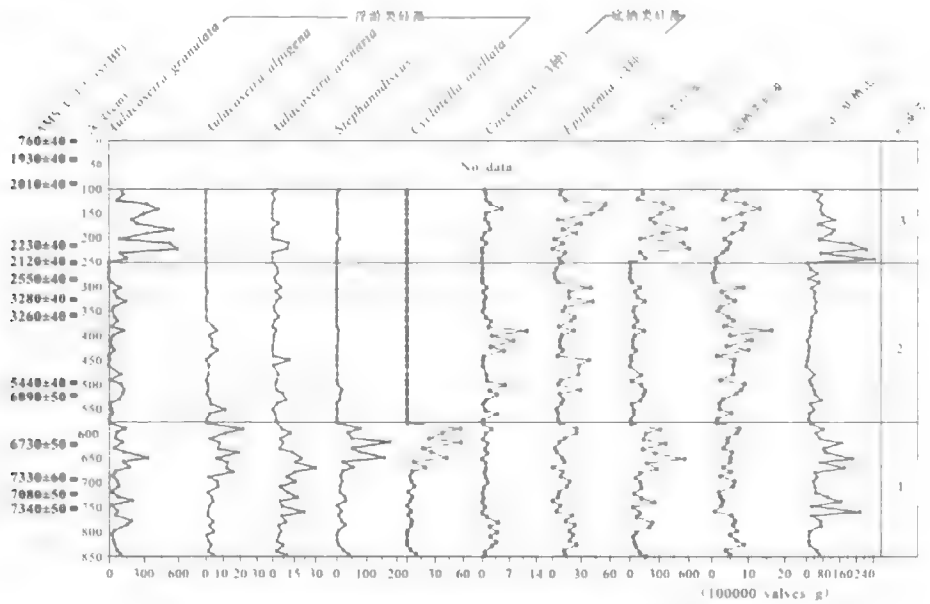

图6–5　优贵湖岩芯硅藻丰度图谱（Wang等，2011）

硅藻组合带 2（250~575cm；6200~2340 ^{14}C yr BP）：基本对应于沉积单元 2（242~484cm），浮游类硅藻丰度大幅减少，其中 *Aulacoseira alpigena*（*Grunow*）*Krammer*，*Stephanodiscus spp.* 和 *Cyclotella ocellata*）几近消失，*Aulacoseira granulata*（*Ehr.*）*Simonsen* 仅零星出现。相反，本带两大底栖类硅藻种属（*Cocconeis* 和 *Epithemia*）显著增加，导致浮游/底栖比剧烈降低，达整个序列最低水平（平均不足 5）。

硅藻组合带 3（100~250cm；2340~2010 ^{14}C yr BP）：基本对应于沉积单元 3（0~242cm），浮游类硅藻（主要是 *Aulacoseira granulate*（*Ehr.*）*Simonsen*）丰度显著增加，浮游/底栖比增加至 40 左右。

5. 讨论与结论

5.1. 蒙古国中部优贵湖地区过去近9000年来的植被和气候变化

基于 14 个 AMS ^{14}C 测年构建的年代框架，本章利用孢粉、硅藻和粒度等代用指标重

建了蒙古国中部优贵湖地区过去近 9000 年来的植被和气候变化。8120~5830 ¹⁴C yr BP(约 9070~6620 cal. yr BP),孢粉组合以蒿属、藜科及松属主导,研究区植被为山地草原,浮游/底栖比较高,沉积物粒度较小,均反映湖泊水位较深,研究区气候总体上温和湿润。5830~3080 ¹⁴C yr BP(约 6620~3280 cal. yr BP),旱生藜科花粉含量剧烈增加并维持峰值,松属、禾本科以及莎草科花粉含量降低,研究区植被退化为草原或荒漠草原,浮游/底栖比降低,沉积物粒度变粗,均指示湖泊水位下降,研究区气候干旱。3080 ¹⁴C yr BP(约 3280 cal. yr BP)以来,藜科花粉含量降低,禾本科、松属以及蒿属花粉含量增加,研究区植被好转,浮游/底栖比增加,粒度变细,反映湖泊水位增加,气候变湿润。

5.2. 蒙古国中部优贵湖多指标重建的中全新世干旱气候

关于蒙古国中部是否存在中全新世干旱气候这一问题,Tarasov 等(1999)曾指出蒙古国中部地区在中全新世(约 6000 ¹⁴C yr BP)经历了高温干旱的夏季气候,Fowell 等(2003)研究 Telmen 湖孢粉记录后提出约 6090~4100 ¹⁴C yr BP 气候干旱。为验证上述观点,本章对比研究了前人构建的 3 类基于孢粉的干旱指数,并结合岩芯粒度及硅藻指标,确定是否存在中全新世干旱气候。

首先,我们讨论 Fowell 等(2003)在 Telmen 湖孢粉序列研究中构建的(C+A)/P(C 为藜科,A 为蒿属,P 为禾本科)干旱指数在优贵湖序列的表现。尽管该指数重建的优贵湖干旱指数序列显示了中全新世(5400~4800 ¹⁴C yr BP)干旱气候(图 6-6 中 C),但重建结果是否可靠值得商榷。我们认为 Fowell 等(2003)的(C+A)/P 不适用于优贵湖孢粉序列,原因如下:Telmen 湖和优贵湖地理的位置差异导致了地带性植被的不同,Telmen 湖位于优贵湖以北约 200km 处,地带性植被为山地草原,蒿属和藜科被界定为干旱组分,蒿属花粉含量的增加指示了干旱加剧(Hilbig,1995;Fowell 等,2003)。然而,优贵湖地区地带性植被为干草原和荒漠化草原,藜科代表了干旱组分,蒿属代表了相对湿润组分,蒿属花粉含量增加指示了气候湿润。也就是说,蒿属含量的增加在 Telmen 湖地区指示了干旱,而在优贵湖则指示了湿润。

其次,藜科/蒿属值(C/A 值)作为湿度指标在优贵湖孢粉记录中的适用性又如何呢?干旱区和半干旱区现代花粉研究表明:该指标可以用来指示区域气候干旱程度(El-Mosliney,1990)。本研究优贵湖孢粉序列中,蒿属和藜科花粉百分含量变化亦呈现出反相位变化趋势(图 6-4),似乎支持 C/A 值可作为干旱指数,并表明约 5920~3400 ¹⁴C yr BP 气候干旱(图 6-6 中 D)。然而,优贵湖孢粉序列的孢粉带 1 中蒿属花粉百分含量通常低于 10%,这种情形下 C/A 值的适用性可能就存在问题了。通常该指标适用的前提是:蒿属和藜科花粉在花粉组合中占据主导地位时,蒿属花粉代表了较为湿润的组分,而藜科花粉代表了较为干旱的组分,因此用 C/A 值指示气候干旱程度。而对于优贵湖孢粉带 1 而言,不足 10%的蒿属与藜科都代表了相对干旱的组分,而含量较高的莎草科、禾本科以及杂类草花粉含量才正真代表了湿润组分,因此 C/A 值不能用以指示带 1 的真实干旱程度。但是,这似乎并不影响 C/A 值指示孢粉带 2 和 3 的干旱程度,因为在这两个孢粉带湿润组分中蒿属花粉占据了主导。

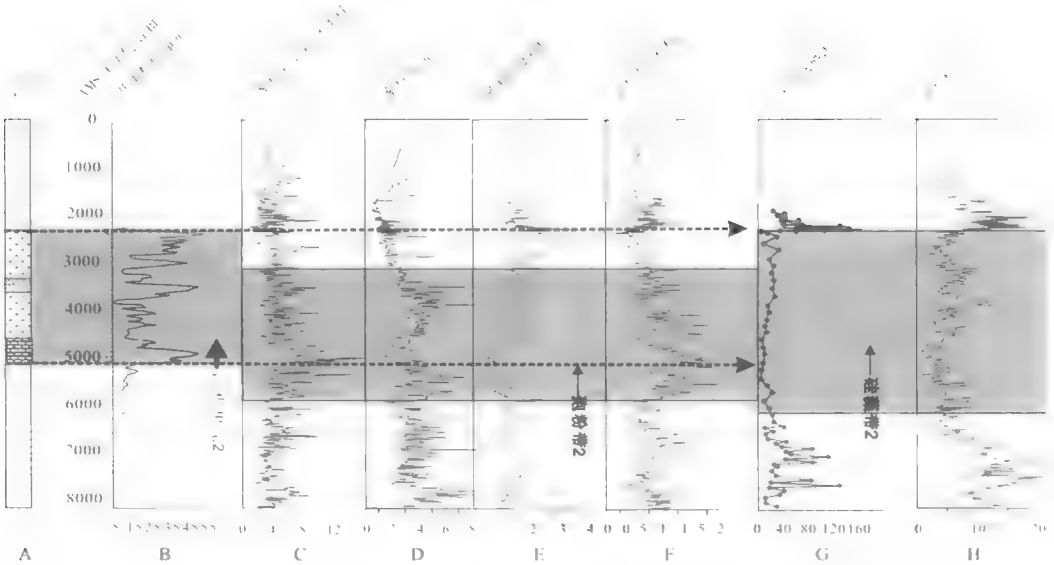

图6-6 优贵湖岩芯3类基于孢粉的生物气候代用指标序列
[(C+A)/G、C/A、孢粉湿度和温度指标](Wang等,2011)

最后,来看一下蒙古国南北断面上建立的半定量转换函数的表现(Ma 等,2008)。我们认为基于孢粉的温度指标和湿度指标(Ma 等,2008)可能最适用于优贵湖孢粉序列,原因如下:第一,该函数是在研究蒙古国南北断面上穿越荒漠、荒漠草原、草原、山地草原、山地森林草原、森林的不同植被群落的 104 个现代表土花粉样品的基础上获得的;第二,优贵湖研究点正好位于该断面的中间位置,现代植被类型为荒漠化草原或典型草原。本章使用这套温度指标和湿度指标(Ma 等,2008)重建的优贵湖温度和湿度序列(图 6 中的 E 和 F)表现出两个显著特征:第一,相比于孢粉带 1(530~854cm;8120~5830 ^{14}C yr BP)和孢粉带 3(0~320cm;3080~0 ^{14}C yr BP),孢粉带 2(320~530cm;5830~3080 ^{14}C yr BP)具有更高的温度指标和更低的湿度指标;第二,湿度指标的变化与温度指标的变化总体上呈反相位关系。这表明蒙古国中部地区在 5830~3080 ^{14}C yr BP(约 6620~3280 cal. yr BP)经历了持久干旱的气候。这还可能表明湿度的变化可能完全受控于温度变化(即受温度决定的蒸发强度控制)。

为深入研究优贵湖孢粉序列揭示的中全新世干旱气候的细节,本章对比了优贵湖岩性记录(沉积单元 2:242~484cm;5120~2330 ^{14}C yr BP)、孢粉记录(孢粉带 2:320~530cm;5830~3080 ^{14}C yr BP)和硅藻记录(硅藻带 2:250~575cm;6200~2340 ^{14}C yr BP)指示的干旱时段的共性和差异性。首先,三种指标均揭示了中全新世干旱气候。硅藻数据中较低的浮游/底栖比(250~575cm)揭示优贵湖 6200~2340 ^{14}C yr BP 为低水位,气候干旱。孢粉记录中 6200 ~2340 ^{14}C yr BP 莎草科花粉含量的急剧降低(图 6-6 中 H),间接支持了硅藻重建的结果,反映了干旱气候条件下湖岸和/或河岸沼生草甸的退缩(抑或包括山地亚高山草甸的退缩)。5920~3400 ^{14}C yr BP 孢粉湿度指数的低值也基本上支持了中全新世气候干旱(图 6-6 中 E)。优贵湖中值粒度在 5120~2330 ^{14}C yr BP 为峰值,揭示了水位降低气候

持续干旱，进一步支持了硅藻与孢粉数据揭示的中全新世干旱气候。第二，岩性、硅藻和孢粉数据揭示的干旱时段在起讫时间上存在显著的位相差异。硅藻记录揭示的干旱起始时间最早，始于6200 ¹⁴C yr BP，而孢粉记录的植被退化则相对滞后了370年(始于5830 ¹⁴C yr BP)，岩性沉积记录变化的转折时间则为5120 ¹⁴C yr BP，相比植被变化又晚了近700年。岩性记录的干旱时段的结束年代和硅藻指示的时间基本一致，在2330 ¹⁴C yr BP左右，而孢粉记录的植被好转的时间则早于上述约750年，位于3080 ¹⁴C yr BP左右。尽管存在可能因指标敏感性不同造成的差异，但硅藻记录、岩性记录和孢粉记录的干旱时段在5120~3080 ¹⁴C yr BP重叠，证实了该时段蒙古国中部优贵湖地区干旱气候的存在。

此外，我们发现孢粉浓度记录和沉积速率记录似乎并没有表现出中全新世气候的干旱，中全新世的孢粉浓度表现出异乎寻常的高值，对应时段的沉积物沉积速率表现出最低值(0.076 cm/yr)，而沉积物粒度却显著大于上覆的单元3与下伏的单元1。我们认为，孢粉浓度的高值可能和较低的沉积速率有关，也可能和干旱时期湖泊的退缩有关。一方面沉积速率降低导致了孢粉浓度增加；另一方面湖泊退缩二次悬移作用在湖泊中心富集了更多的花粉。然而，粒度增粗与沉积速率降低之间的矛盾，似乎需要更深入地研究。

5.3. 蒙古国中部中全新世干旱气候的地理分布

已有研究表明，中国北方半干旱区中全新世气候温暖湿润(Feng 等，2006)，蒙古高原北部及毗邻的南西伯利亚半湿润地区中全新世气候湿润(Harrison 等，1996；Tarasov 等，1999，2000；Horiuchi 等，2000；Demske 等，2004)。然而，对于位于其间的蒙古高原中部戈壁荒漠以及中亚核心干旱带，最近发表的一些序列可能表明存在中全新世干旱气候。诚如上述，这种中全新世干旱气候的地理分布如何？本章通过对蒙古高原北部半干旱区(4个序列)和蒙古高原南部干旱区及中亚干旱区东部(4个序列)共8个具有良好年代控制的全新世气候序列的对比研究(图6-7)，揭示中东亚地区中全新世干旱气候的地理分布。

蒙古高原北部全新世生物气候序列主要有：蒙古国中部的优贵湖孢粉和硅藻序列(本文)、蒙古国偏北位置的Telmen湖孢粉序列、蒙古国北部乌兰巴托—贝加尔走廊地带的夏玛尔(Sharmmar)风成序列和蒙古国北部库布苏湖孢粉序列。优贵湖(本文，图6-7A)孢粉记录、硅藻以及沉积物粒度组成表明5830~3080 ¹⁴C yr BP(约6620~3280 cal. yr BP)气候持久干旱；略偏北的Telmen湖孢粉干旱指数序列显示约6090~4100 ¹⁴Cyr BP(约7000~4670 cal. yr BP)气候干旱(图6-7B，Fowell 等，2003；Peck 等，2002)；蒙古国北部夏玛尔(Sharmmar)风成序列的地层和孢粉数据也揭示贝加尔—乌兰巴托走廊地带7000~3000 ¹⁴C yr BP(约7820~3200 cal. yr BP)以干旱气候为主(图6-7C；Feng 等，2007)；库布苏湖泊沉积孢粉记录也显示约5300~3300 ¹⁴C yr BP(约6000~3500 cal. yr BP)森林退缩、草原扩张、干旱程度增加(图6-7D；Prokopenko 等，2007)。尽管上述序列在起讫年代上存在一定差异，但时间交叠在中全新世，表明蒙古国中部和北部地区经历了中全新世干旱气候。

蒙古高原南部干旱区和中亚东部干旱区的全新世生物气候记录包括：新疆北部玛纳

斯湖孢粉序列、内蒙古阿拉善西部的居延泽气候序列、内蒙古阿拉善东部的潴野泽孢粉序列和内蒙古鄂尔多斯高原西部的盐海子序列。新疆北部玛纳斯湖沉积记录中 A/C 值低值表明 6000~4500 ^{14}C yr BP(约 6850~5170 cal. yr BP)经历了较为严重的干旱(图 6-7E, Rhodes 等,1996);内蒙古阿拉善地区西端的居延泽岩芯的多指标气候记录显示 6700~4700 ^{14}C yr BP(约 7600~5400 cal. yr BP)湖泊水位指标和径流量指标均位于低值,指示了干旱气候(图 6-7F;Hartmann 等,2009);内蒙古阿拉善地区东部的潴野泽孢粉记录中,白刺花粉含量的峰值可能揭示了 6200~3500 ^{14}C yr BP(约 7100~3800 cal. yr BP)湖泊干涸,湖底发育白刺荒漠,气候持续干旱(图 6-7G,Chen 等,2006);内蒙古鄂尔多斯高原西北部盐海子的湖泊沉积记录也指示了约 8000~4000 ^{14}C yr BP(约 8850~4460 cal. yr BP)的干旱气候(图 6-7H;Chen C. T. A.等,2003)。

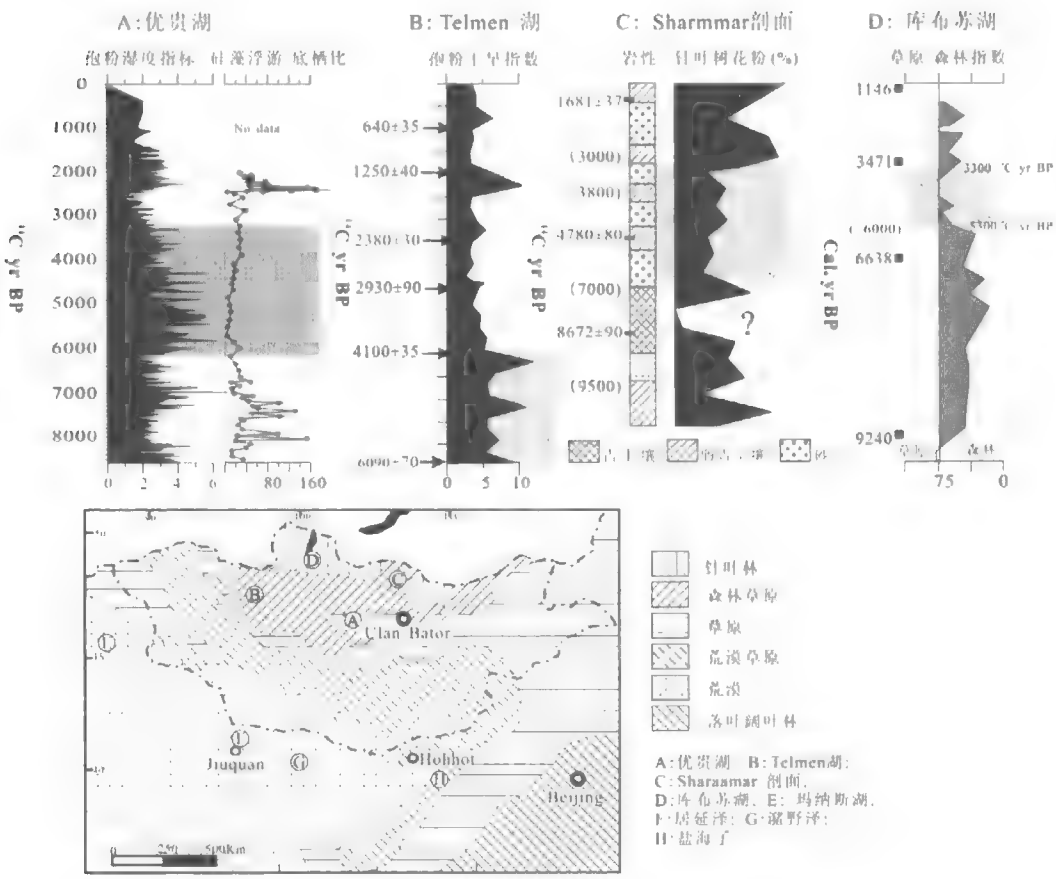

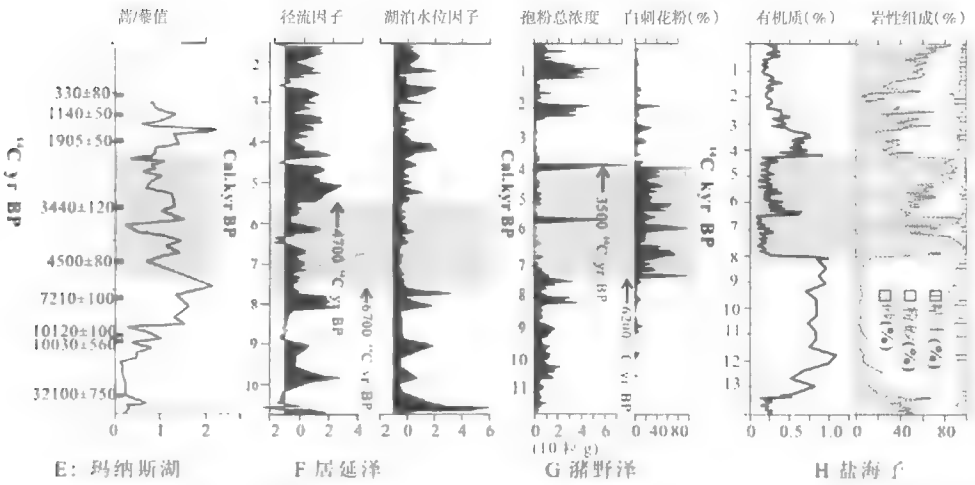

图6-7 蒙古国和中国西北干旱区中全新世气候记录(上图:蒙古国全新世气候记录;中图:生物气候略图及样点分布;下图:中国西北干旱区气候记录)。A:优贵湖孢粉湿度指标和硅藻记录(本章);B:Telmen湖孢粉干旱指数;C:蒙古国北部Sharmmar风成序列岩性组成和针叶树花粉含量;D:蒙古国北部库布苏湖草原/森林指数;E:玛纳斯湖蒿/藜;F:居延泽径流因子和水位因子指标;G:猪野泽孢粉总浓度和白刺花粉含量;H:盐海子总有机质含量和岩性组成。(Wang等,2011)

通过对上述蒙古高原干旱和极干旱区的全新世气候记录的对比研究,可以得出两个初步结论:第一,蒙古高原干旱和极干旱区可能经历了持久的中全新世(约6000~3000 ^{14}C yr BP;约6850~3200 cal. yr BP)干旱气候;第二,该中全新世干旱气候可能向北延伸到了蒙古高原北部(即蒙古国北部)半干旱地区,但并未向南扩展到中国北方半干旱地区(该地区众多记录表明中全新世气候温暖湿润)。

探讨上述中全新世干旱气候的成因机制,首要考虑的因素是大尺度的温度变化。中国北方地区众多气候记录表明中全新世为温度最高时段(也称大暖期)(Shi等,1993),蒙古国和西伯利亚南部地区的研究也表明蒙古高原北部和南西伯利亚也经历了中全新世的温暖气候(Tarasov等,1999;Demeske等,2005)。对于蒙古高原干旱和极干旱区而言,大尺度升温导致的蒸发增强可能超过了区域降水的可能增加,进而导致了干旱程度的增加。而对于蒙古高原南侧的中国北方季风边缘区,季风增强导致降水增加效果显著,温度增加导致的蒸发增强并未成为干旱气候发育的主要因素,气候依旧温暖湿润(Feng等,2006,2007)。与干旱区和极干旱地区不同的是,蒙古国北部和南西伯利亚地区似乎并不缺乏可用于蒸发的水源(包括水体和土壤水分),中全新世的升温导致了有效蒸发增强,为气候系统注入了更多的水汽,进而促进了降水的增加,导致了湿润气候。最后需要说明的是,本章初步得到了中亚干旱和极干旱地区中全新世气候干旱的观点存在一定的不足,全新世气候记录均分布在蒙古高原的南北两侧,而核心的蒙古国南戈壁地区没有全新世气候记录。

致谢:感谢已故蒙古国科学院地质研究所Khosbayar教授在野外和数据收集方面提供的帮助

参考文献

孙湘君, 杜乃秋, 翁成郁, 林瑞芬, 卫克勤. 1994. 新疆玛纳斯湖盆周围近14000年以来的古植被古环境. 第四纪研究, 3: 239~248.

王璮瑜, 宋长青, 孙湘君. 1996. 内蒙古中部表土花粉研究. 植物学报, 38(11): 902~909

王伏雄, 钱南芬, 张玉龙, 杨慧秋. 1995. 中国植物花粉形态(第二版). 北京: 科学出版社.

吴玉书, 萧家仪. 1995. 西藏扎布耶盐湖地区现代花粉雨的初步研究. 云南植物研究, 17, 1: 72~78.

Bennett, K.D., 1996. Determination of the number of zones in a biostratigraphical sequence. New Phytologist, 132: 155~170.

Broecher, W.S., 2003. Does the trigger for abrupt climate change reside in the ocean or in the atmosphere? Science, 300: 1519~1922.

Camburn, K.E. and Charles, D.F., 2000. Diatoms of Low-alkalinity Lakes in the Northeastern United States. The Academy of Natural Sciences of Philadelphia, Philadelphia.

Chen, C.-T.A., Lan, H.-C., Lou, J.-Y. and Chen, Y.-C., 2003. The dry Holocene Megathermal in Inner Mongolia. Palaeogeography Palaeoclimatology Palaeoecology, 193: 181~200.

Chen, F.H., Cheng, B., Zhao, Y., Zhu, Y. and Madsen, D.B., 2006. Holocene environmental change inferred from a high-resolution pollen record, Lake Zhuyeze, arid China, The Holocene, 16(5): 675~684.

Chen, F.H., Wu, W., Holmes, J.A., Madsen, D.B., Zhu, Y., Jin, M. and Oviatt, C.G., 2003. A mid-Holocene drought interval as evidenced by lake desiccation in the Alashan Plateau, Inner Mongolia, China. Chinese Science Bulletin, 48: 1401~1410.

Demske, D., Heumann, G., Granoszewski, W., Nita, M., Mamakowa, K., Tarasov, P.E. and Oberhänsli, H., 2005. Late glacial and Holocene vegetation and regional climate variability evidenced in high-resolution pollen records from Lake Baikal. Global and Planetary Change, 46: 255~279.

El-Mosilimany, A.P., 1990. Ecological significance of common non-arboreal pollen: Examples from drylands of the Middle East. Review of Palaeobotany and Palynology, 64: 343~350.

Erdtman, G., 1969. Handbook of Palynology. Munksgaard, Copenhagen.

Faegri, K. and Iversen, J., 1975. Textbook of Pollen Analysis. Munksgaard, Copenhagen.

Feng, Z.-D., An, C.B. and Wang, H.B., 2006. Holocene climatic and environmental changes in the arid and semi-arid areas of China: a review. The Holocene, 16(1): 1~12.

Feng, Z.-D., Zhai, X.W., Ma, Y.Z., Huang, C.Q., Wang, W.G., Zhang, H.C., Khosbayar, P., Narantsetseg, T., Liu, K.-B. and Rutter, N.W., 2007. Eolian environmental changes in the Northern Mongolian Plateau during the past ~35,000 yr. Palaeogeography, Palaeoclimatology, Palaeoecology, 245: 505~517.

Fowell, S.J.B., Hansen, B.C.S., Peck, J.A., Khosbayar, P. and Ganbold, E., 2003. Mid to late Holocene climate evolution of the Lake Telmen Basin, North Central Mongolia, based on palynological data. Quaternary Research 59, 353~363.

Gasse, F., 1986. East African diatoms: taxonomy, ecological distribution. Bibliothecta Diatomologica. Band 11. Berlin, J. Cramer.

Gunin, P.D., Vostokova, E.A., Dorofeyuk, N.I., Tarasov, P.E. and Black, C.C., 1999. Vegetation dynamics of Mongolia. In Geobotany 26. Dordrecht, Kluwer Academic Publishers.

Harrison, S.P., Yu, G. and Tarasov, P.E., 1996. Late Quaternary lake-level record from northern Eurasia. Quaternary Research, 45: 138~159.

Hartmann, K. and Wünnemann, B., 2009. Hydrological changes and Holocene climate variations in NW China, inferred from lake sediments of Juyanze palaeolake by factor analyses. Quaternary International, 194: 28~44.

Hilbig, W., 1995. The vegetation of Mongolia. SPB Academic publishing, Amsterdam.

Horiuchi, K., Minoura, K., Hoshino, K., Oda, T., Nakamura, T. and Kawai, T., 2000. Palaeoenvironmental history of Lake Baikal during the last 23000 years. Palaeogeography, Palaeoclimatology, Palaeoecology, 157: 95~108.

Krammer, K. and Lange-Bertalot, H., 1986-1991. Bacillariophyceae. In: Ettl, H., Gerloff, J., Heynig, H., Mollenhauser, D., (eds), Süβwasserflora von Mitteleuropa Band 2(1-4). Gustav Fisher Verlag, Stuttgrat/Jena.

Lavrenko, E.M., Iunatov, A.A., Aleksandr, A. and Dashniam, B., 1979. Vegetation map of Mongolian People's Republic (scale 1: 1 500 000). Moscow.

Li, X.Q., Zhou, W.J., An, Z.S. and Dodson, J., 2003. The vegetation and monsoon variations at the desert loess transition belt at Midiwan in northern China for the last 13 ka. The Holocene, 13(5): 779~784.

Liu, H.Y., Cui, H.T., Pott, R. and Speier, M., 1999. The surface pollen of the woodland-steppe ecotone in southeastern Inner Mongolia, China. Review of Palaeobotany and Palynology, 105: 237~250.

Liu, K.-B., Reese, C.A. and Thompson, L.G., 1998. A pollen record of Holocene climatic changes from the Dunde ice cap, Qinghai-Tibetan Plateau. Geology, 26: 135~138.

Lydolph, P.E., 1977. Climates of the Soviet Union. In Landsberg, H. E., editor, World Survey of Climatology 7, Elsevier Publishing Company, Amsterdam.

Ma, Y.Z., Fang, X.M., Li, J.J., Wu, F.L. and Zhang, J., 2005. The vegetation and climate change during Neocene and Early Quaternary in Jiuxi Basin, China. Science in China (series D), 48(5): 676~688.

Ma, Y.Z., Liu, K.-B., Feng, Z.D., Sang, Y.L., Wang, W. and Sun, A.Z., 2008. A survey of modern pollen and vegetation along a south-north transect in Mongolia. Journal of Biogeography, 35: 1512~1532.

Moore, P.D., Webb, J.A. and Collinson, M.E., 1991. Pollen Analysis, 2nd edition, Blackwell Scientific Publications, Oxford.

Oppo, D.W., McManus, J.E. and Cullen, J.L., 2003. Deepwater variability in the Holocene epoch. Nature, 422: 277~278.

Peck, J.A., Khosbayar, P., Fowell, S.J., Pearce, R.B., Ariunbileg, S., Hansen, B.C.S. and Soninkhishig, N., 2002. Mid to Late Holocene climate change in north central Mongolia as recorded in the sediments of Lake Telmen. Palaeogeography, Palaeoclimatology, Palaeoecology, 183: 135~153.

Prokopenko, A.A., Khursevich, G.K., Bezrukova, X.B., Kuzmin, M.I., Boes, X., Williams, D.F., Fedenya, S.A., Kulagina, N.V., Letunova, P.P. and Abzaeva, A.A., 2007. Paleoenvironmental proxy records from Lake Hovsgol, Mongolia, and a synthesis of Holocene climate change in the Lake Baikal watershed. Quaternary Research, 68: 2~17.

Pyankov, V.I., Gunin, P.D., Tsoog, S. and Black, C.C., 2000. C4 plants in the vegetation of Mongolia: their natural occurrence and geographical distribution in relation to climate. Oecologia, 123: 15~31.

Rhodes, T.E., Gasse, F., Lin, R.F., Fontes, J.-C., Wei, K.Q., Bertrand, P., Gibert, E., Mélières, F., Tucholka,

P. and Wang, Z.X., 1996. A late Pleistocene-Holocene lacustrine record from Lake Manas, Zunggar (northern Xinjiang, western China). Paleogeography, Palaeoclimatology, Palaeoecology, 120: 105~121.

Ruddiman, W. F., 2001. Earth's Climate: past and future. Freeman W H and Company, New York.

Schrader, H.J. and Gersonde, R., 1978. Diatoms and silicoflagellates in the eight metres section of the lower Pliocene of Capo Rossello. Utrecht Micropaleontological Bulletin, 17: 129~176.

Shi, Y.F., Kong, Z.C. and Wang, S.M., 1993. Mid-Holocene climates and environments in China. Global and Planetary Change, 7: 219~233.

Steig, E.J., 1999. Mid-Holocene climate change. Science, 286: 1485~1487.

Stockmarr, J., 1971. Tablets with spores used in absolute pollen analysis. Pollen and Spores, 13: 615~621.

Stoermer, E.F. and Smol, J.P. 1999. The Diatoms: Applications for the Environmental and Earth Sciences, Cambridge University Press, Cambridge.

Tarasov, P.E., Dorofeyuk, N. and Metel'tseva, E., 2000. Holocene vegetation and climate changes in Hoton-Nur basin, northwest Mongolia. Boreas, 29: 117~126.

Tarasov, P.E., Guinot, J., Cheddadi, R., Andreev, A., Bezusko, L.G., Blyakharchuk, T.A., Dorofeyuk, N.I., Filimonova, L.V., Volkova, V.S. and Zernitskaya, V.P., 1999. Climate in northern Eurasia 6000 years ago reconstructed from pollen data. Earth and Planetary Science Letters, 171: 635~645.

Tuvdendorzh, D. and Myagmarzhav, B., 1985. Atlas of the climate and ground water resources in the Mongolian People's Republic. Ulan Bator: GUGMS of Mongolia.

Van Campo, E., Cour, P. and Hang, S.X., 1996. Holocene environmental changes in Bangong Co basin (Western Tibet). Part 2: The pollen record. Palaeogeography, Palaeoclimatology, Palaeoecology, 120: 49~63.

Velichko, A.A., Andreev, A.A. and Klimanov, V.A., 1997. Climate and vegetation dynamics in the tundra and forest zone during the late glacial and Holocene. Quaternary International, 41/42: 71~96.

Wang, W., Ma, Y.Z., Feng, Z.D., Meng, H.W., Sang, Y.L. and Zhai, X.W., 2009. Vegetation and climate changes during the last 8660 cal. a BP in central Mongolia based on a high-resolution pollen record from Lake Ugii Nuur. Chinese Science Bulletin, 54(9): 1579~1589.

Wang, W., Ma Y.Z., Feng Z.D., Ts Narantsetseg,, Liu K.-b. and Zhai X.W., 2011. A prolonged dry mid-Holocene climate revealed by pollen and diatom records from Lake Ugii Nuur in central Mongolia. Quaternary International, 229: 74~83.

Wanner, H., Beer, J., Bütikofer, J., Crowley, T.J., Cubasch, U., Flückiger, J., Goosse, H., Grosjean, M., Joos, F., Kaplan, J.O., Küttel, M., Müller, S.A., Prentice, I.C., Solomina, O., Stocker, T.F., Tarasov, P., Wagner, M. and Widmann, M., 2008. Mid- to Late Holocene climate change: an overview. Quaternary Science Reviews, 27: 1791~1828.

第七章

中国内蒙古中部柒盖淖尔(Qigai Nuur)湖芯记录的过去 10 000 年以来植被与气候的变化

孙爱芝[①]　　冯兆东[②]

① 中国科学院大学 地球科学学院

② 中国科学院 新疆生态与地理研究所

本章基于222个柒盖淖尔湖芯(QGN-2004)孢粉数据重建了蒙古高原南部过去约11 000年以来的植被和气候变化。孢粉定量重建古气候的方法采用的是植物功能型—现代类比法(PFT-MAT)。重建结果显示,约9200 cal. yr BP以前柒盖淖尔地区温度偏低,降水波动明显,区域植被在森林草原和干草原间波动。约9200~2800 cal. yr BP,森林草原植被占优势,气候温暖湿润,但存在两次明显的冷干阶段,分别为约7400~6000 cal. yr BP和约4000~2800 cal. yr BP。约2800~850 cal. yr BP,气候变冷变干,干草原植被占优势。过去约850年以来,植被中包含了丰富的草本植物,重建的气候变化结果显示温度逐渐上升,降水量波动变化。柒盖淖尔地区孢粉资料定量重建的年平均降水量与中国南部季风强度记录有很好的可比性,这表明研究区降水的主要变化可能受控于夏季太阳辐射驱动的赤道辐合带的南北摆动,而次一级的降水波动则受控于由厄尔尼诺引起的赤道西太平洋海水表面温度的变化。

关键词:东亚夏季风;全新世;蒙古高原;古气候;孢粉;植被

1. 前言

蒙古高原南部是研究过去气候变化的关键地区之一。第一,作为中亚干旱带(Central Asian Arid Zone,CAAZ)的一部分,它对自然变化和人类活动的影响反应非常敏感(IPCC,2007)。而且,在过去的100年中CAAZ地区气候变暖引起的干旱趋势警示我们,未来的气候变暖会使包括蒙古高原南部的CAAZ地区的水资源短缺和生态退化问题更加严重。第二,蒙古高原南部位于现代东亚季风边缘区(高由禧,1962),由于该区对气候变化的敏感性,使它成为了现代气候和古气候变化研究的焦点之一。当然,其气候敏感性也与该地区将来的社会、经济发展密切相关(Huang等,2004;徐国昌等,1997)。由于最近地质时期

（如全新世，过去约 11 500 年以来）的气候边界条件与我们正在或将要经历的气候边界条件存在很大的相似性，对该时段气候变化的研究备受关注。

本研究将基于位于蒙古高原南部季风边缘区（图 7-1A）的柒盖淖尔（QGN）湖芯孢粉资料，定量地重建全新世气候变化历史，希望我们的重建结果可以化解现有的关于东亚季风边缘区全新世气候变化的争议。这些争议主要围绕以下三个问题：①温度和降水变化是同步还是异步的（如：Chen 等，2006；Feng 等，2006；Shi 等，1993；Xiao 等，2004）？②全新世气候适宜期的时间偏早还是偏晚（如：An 等，2000；Feng 等，2006；Xiao 等，2004；Zhou 等，2001）？③季风边缘区气候变化的动力学机制如何（如：An，2000；Hartmann 和 W ü nemann，2009；Herzschuh 等，2004；Zhao 等，2008）？

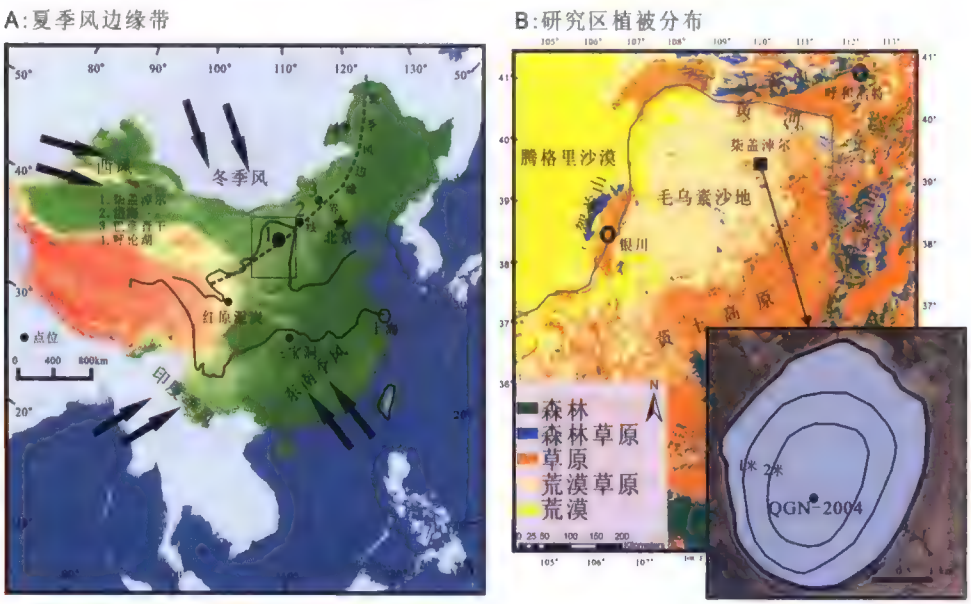

图7-1　现代夏季风边缘界线（高由禧，1962）（A：左图）和研究区植被分布图（张新时，2007）（B：右图）。右下角为柒盖淖尔湖水深及岩芯位置。左图（A）还标注了四个湖泊的位置。1. 柒盖淖尔湖；2. 岱海；3. 巴彦查干湖；4. 呼伦湖

2. 研究区概况及剖面位置

柒盖淖尔（109°22′ E，39°22′ N）位于毛乌素沙地中部（图 7-1B），行政上属于鄂尔多斯市伊金霍洛旗西南的纳林希里镇。气候上属典型的大陆性气候，春季干旱多风，夏季气候温和，秋季多雨凉爽，冬季干燥寒冷。距离柒盖淖尔约 20km 的乌审旗气象站点的数据显示，多年年平均气温约 7℃，年平均降水量约 300mm，潜在蒸发量约 1000mm。柒盖淖尔是毛乌素沙地上古河谷侵蚀而成的七个串珠状湖盆的第六个。湖泊水面面积 5km^2，最大水深 3m。现代植被以草原为主（图 7-1B），主要包括猪毛菜属（*Salsola spp.*）、锦鸡儿属（*Caragana*）、沙蒿（*Artemisia arenaria*）、藜科（Chenopodiaceae）、沙蓬（*Agriophyllum squarrosum*）和虫实属（*Corispermum spp*）。草甸草原和湿地沼泽则主要分布在低洼、湖岸和河谷地带（张新时，2007）。

3. 研究方法

3.1. 岩芯提取和样品分析

湖泊沉积物岩芯是用奥地利 UWITEC 公司生产的 Niederreiter 深水平台钻采集，为保证钻取岩芯的完整性，在湖心相距 3m 处钻取了两根平行岩芯，同时考虑到样品接头处可能出现的扰动和污染，采用不同长度的样管进行钻取。柒盖淖尔共取得 8.2m 的连续样芯，湖芯钻取后就地分样。通过沉积物标志层（如纹层和颜色变化）的对比衔接两支平行样管钻取的样芯，剔除钻管接头部位受污染和扰动的部分，从而得到完整的沉积序列。湖芯样品上部 220cm 采用 1cm 间隔分样，其余 600cm 采用 2cm 间隔分样。样品分别用于孢粉、地球化学和地球物理学指标分析。此外，不等间隔的从岩芯的中心部位分出部分样品用作 AMS ^{14}C 测年。

除孢粉分析外，本章对柒盖淖尔沉积物还进行了粒度（Grain Size）和有机质含量（OM）分析。粒度分析是在英国 MALVEN 公司生产的 Mastersizer 2000 型激光粒度仪上进行的，有机质含量实验采用重铬酸钾—硫酸氧化法，所有实验均在兰州大学西部环境教育重点实验室完成。

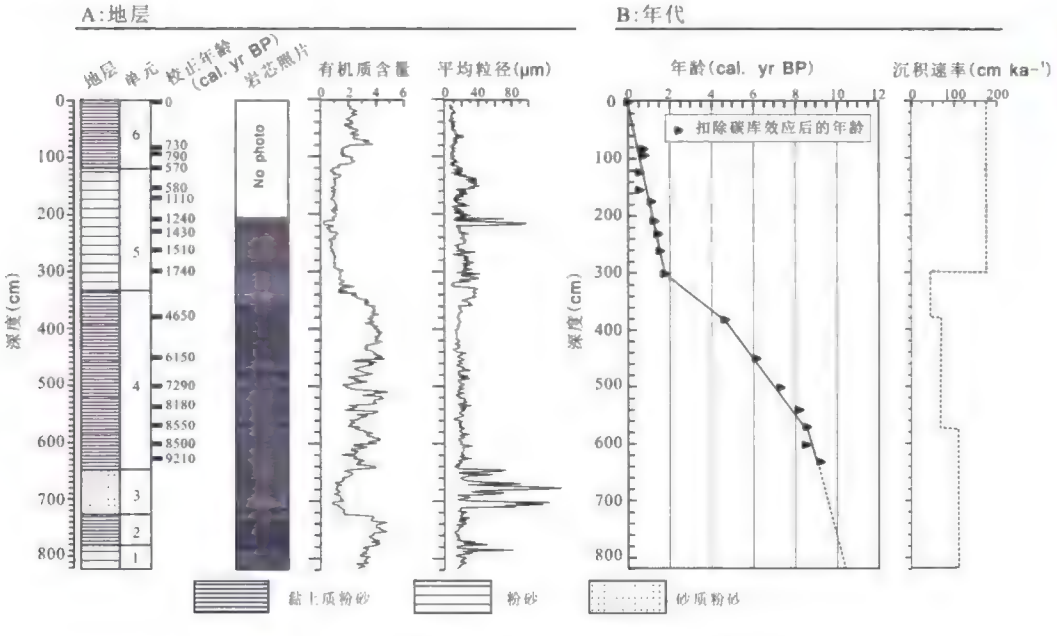

图7-2　柒盖淖尔岩芯地层、照片、有机质含量(OM,%)、中值粒径(μm)、年龄—深度模式和沉积速率(Sun等,2013)

3.2. 年代

我们总共从柒盖淖尔湖芯获得了 17 个 AMS ^{14}C 年龄，均由美国亚利桑那大学的国家自然科学基金会 AMS ^{14}C 实验室（NSF AMS Facility at University of Arizona）测定（表 7-1）。为了确定该湖的碳库效应，我们在湖芯上部 0 ~ 2cm 处获得一个 1947 ± 50 ^{14}C yr BP 的年

龄。此外，根据岩芯 0~300cm 获得的 9 个年龄线性外推得到最顶部的年龄（0cm）约为 2020 ^{14}C yr BP，这与实际测得的年龄基本一致，说明柒盖淖尔存在约 1950 年的碳库效应。为了消除碳库效应，本章将测得的 17 个 ^{14}C 年龄均减去 1950 年，然后利用 Reimer 等（2009）提供的方法校正为日历年龄。整个湖芯年龄是采用四段式线性年龄—深度模式建立起来的，这四段的对应的深度分别为 0~302cm、302~382cm、382~572cm 和 572~820cm。需要注意的是，老于 9000 cal. yr BP 的年龄是通过深度 572~632cm 层位间建立的线性年龄—深度模式外推获得的（图 7-2）。本章所有的年龄均为校正年龄（注：cal. yr BP 代表校正日历年）。

表7-1　柒盖淖尔岩芯AMS ^{14}C测年数据和校正年龄

实验室编号	深度(cm)	测年材料	δ ^{13}C (‰)	测年数据 (yr BP，± error)	校正后 ^{14}C 年龄（yr BP）	校正年龄 (cal. yr BP)
AA64196	0~2	有机质	−11.2	1950±50	0±50	0
AA64201	84~85	有机质	−9.0	2700±70	750±70	557~893
AA64202	94~95	有机质	−8.9	2780±60	830±60	671~906
AA64204	124~125	有机质	−7.7	2480±60	530±60	508~636
AA64205	154~155	有机质	−4.2	2490±40	540±40	505~652
AA64206	174~175	有机质	−5.2	3120±60	1170±60	962~1257
AA64208	209~210	有机质	−3.8	3280±40	1340±40	1178~1309
AA64209	231~232	有机质	−6.0	3490±60	1540±60	1318~1536
AA64210	261~262	有机质	−6.3	3540±60	1590±60	1349~1680
AA64211	301~302	有机质	−3.1	3760±40	1820±40	1624~1865
AA64214	381~382	有机质	−9.6	6120±70	4170±70	4455~4853
AA64216	450~451	有机质	−10.6	7340±60	5390±60	6000~6293
AA64217	501~502	有机质	−8.1	8340±110	6390±110	7019~7553
AA64218	541~542	有机质	−10.4	9320±60	7370±60	8036~8327
AA64219	571~572	有机质	−9.0	9670±90	7720±90	8349~8749
AA64220	601~602	有机质	−7.4	9650±50	7700±50	8406~8586
AA64221	631~632	有机质	−6.0	10170±60	8230±60	9024~9401

3.3. 孢粉分析

按照 2 ~ 4cm 间隔共获得 222 个孢粉样品。孢粉样品的分析采用酸碱法和过筛法。为了计算孢粉浓度，实验室处理前每个样品均加入一片石松孢子药片（每片 27 637 ± 563 粒石松孢子）（Moore 等，1991）。根据样品岩性的差异，每个样品取 5 ~ 10g，分别经过去碳酸盐（10% HCl）、去有机质（10% KOH）和去硅酸盐（36%HF）的处理，然后通过超声波过筛

(网布孔径 7～10 μm),收取网布上的残留物。最后将样品转入小指管,离心脱水加甘油保存。孢粉的鉴定是在光学显微镜(Olympus BX 51)400~1000 倍下进行的,每样鉴定花粉数超过 300 粒(不包括孢子)。孢粉的鉴定主要依据已经出版的描述我国植物孢粉形态的相关文献和书籍(王伏雄等,1997;Erdtman,1978;摩尔和韦布,1987),以及研究组采集的 200 多种现代孢粉标准片。孢粉百分含量的计算是以所有陆生植物花粉总数(不包括孢子)为基数的。孢粉图谱用 Tilia(1.7.16)软件(Grimm,1990)完成,其中孢粉带划分是用聚类分析(CONISS)完成的。

在古气候重建中有几种孢粉指标常被用来指示气候湿度变化。如 C/A 值(藜科与蒿属孢粉含量比值)已被证明是反映干旱和半干旱地区干燥度指数的有效指标(El-Moslimany,1990;Liu 等,1998;Van Campo 等,1996;Zhao 等,2009a)。值得注意的是,该指标的应用也是存在争议的,如在蒙古高原北部干旱地区的孢粉谱中藜科孢粉占绝对主导地位时(Wang 等,2011),或者在半干旱地区中禾本科孢粉有足够的代表性时(Fowell 等,2003),C/A 值的指示意义就失去了它的有效性。另外一个孢粉指标[(C+A)/P](藜科和蒿属孢粉含量总和与禾本科的比值)亦被用来重建蒙古国中部全新世干燥度的变化(Fowell 等,2003)。不过,由于禾本科的低代表性(Gunin,1999;Ma 等,2008),这个指标的应用也有争议(Wang 等,2011)。本章则利用另一个指标[A/(E+N)](其中 A 为蒿属;E 为麻黄属;N 为白刺属)来指示柒盖淖尔地区全新世湿度的变化。这个指标的指示意义在于:在干旱环境下,麻黄属和白刺属植物随着干燥度的增加而增加(孙湘君等,1994;许清海等,2009;Li 等,2005;Zhao 等,2008),而蒿属的数量则随着湿度的增加而增加(Ma 等,2008;Wang 等,2011;Wen 等,2010a,2010b)。因此,A/(E+N)值可作为湿度变化的指标。此外,本章还采用 Br/Co 值(其中 Br 指阔叶树孢粉含量;Co 指针叶树孢粉含量)来指示研究区全新世温度的变化。该指标主要是基于普遍使用的全球植物功能类型(Prentice 等,1996)和蒙古高原植物地理分布的特征(Demske 等,2005;Ma 等,2008;Tarasov 等,2007;Xu 等,2010)建立的,即针叶树主要生长在较冷的环境中,而阔叶树主要生长在较暖的环境中。

3.4. 孢粉古气候定量重建方法

在重建东亚季风边缘区古气候变化研究中,常用的基于孢粉资料的定量方法有三种:①孢粉响应面函数(PRS)(许清海等,2003);②转换函数(TF)(Wen 等,2010a,2010b);③植物功能型—现代类比法(PFT-MAT)(Jiang 等,2006,2009)。孢粉响应面函数是基于中国北方 215 个表土孢粉数据建立的(Sun 等,1996),转换函数是基于中国北方至蒙古国北部南北断面上的 646 个表土孢粉数据建立的(Wen 等,2010b),植物功能型—现代类比法(PFT-MAT)则是基于化石孢粉组合与现代孢粉数据集的相似程度的比较而运行的(Prentice 等,1992,1996;Tarasov 等,2000)。植物功能型—现代类比法(PFT-MAT)的现代孢粉数据集来自 Jiang 等人(2006,2009)描述的 2066 个孢粉数据,其中包括中国北方的 211 个数据(Members of China Quaternary Pollen Data Base,2001)和俄罗斯与欧洲的 1855 个数据(Guiot 等,1993;Tarasov 等,1998)。我们用上述三种方法对采自柒盖淖尔湖周围的

表上孢粉数据进行了重建。三种重建结果显示(表 7-2),用 PFT-MAT 方法表现最好,用 PFT-MAT 重建的年均降水量和年均温度与附近的气象站点的器测数据相比,分别相差只有 20mm 和 1℃。因此,本章采用 PFT-MAT 方法来定量重建柒盖淖尔地区全新世气候的变化。

基于植物的生活型、叶型、物候和植物生态环境将不同的孢粉类型归类到不同植物功能型(PFT)(Prentice 等,1996)。每个孢粉类型的 PFT 归类主要是基于 Jiang 等人(2006)的分类方案进行的。PFT 得分是基于孢粉百分含量高于 0.5%的所包含的孢粉含量的平方根总和计算得到的(Prentice 等,1996)。本研究利用现代孢粉数据集中的 50 个孢粉类型进行了植被和气候重建。

表7-2 利用三种不同孢粉定量重建方法计算得到的现代年均降水量和年均温度的对比
(注:离柒盖淖尔仅20km的乌审旗气象站点的多年年均温度约为7℃,多年年均降水量约为300mm)

	年均降水量MAP (mm)			年均温度MAT (℃)		
	孢粉响应面函数(PRS)	转换函数(TF)	植物功能型—现代类比法(PFT-MAT)	孢粉响应面函数(PRS)	转换函数(TF)	植物功能型—现代类比法(PFT-MAT)
现代孢粉定量重建结果	250	171	279	9.32	5.28	7.95
重建值与气象站点观测数据的差值	-50	-130	-21	+2.32	-1.72	+0.95

PFT-MAT 方法则是以现代孢粉样品计算出 PFT 组合为基础,通过相异系数评测化石 PFT 组合与现代 PFT 组合之间的相似程度,获得与 PFT 组合最相似的一个或几个现代 PFT 组合,这样的一个或几个现代 PFT 组合即为化石 PFT 组合的最佳类比。据此而推测:化石点的古植被和古气候与其最佳类比的相应的采样点上的植被与气候类似,进而可定量估计古气候参数(Davis 等,2003;Nakagawa 等,2002)。对每一个地层孢粉样品,我们都选择 8 个最近距离的现代孢粉样品代表"最佳的现代类比样品"。每个地层样品的平均气候参数值均通过 Guiot 等人(1993)和 Magny 等人(2001)描述的方法进行了校正。所有的数据计算是在 PPPBASE 软件(Guiot 和 Goeury,1996)中进行。表上孢粉样点气象数据是 5°×5°栅格点内相邻气象站点的多年平均值(Guiot 和 Goeury,1996)。

4. 研究结果

4.1. 年代结果

柒盖淖尔湖芯长 8.2m,为过去约 10 700 年以来的沉积(图 7-2A)。我们通过年龄—深度模式计算获得了不同层位沉积物沉积速率。深度 0~302cm 的沉积速率约为

175cm/kyr，深度 302~382cm 约为 35cm/kyr，382~572cm 约为 50cm/kyr，深度 572~820cm 约为 90cm/kyr(图 7-2B)。值得提及的是，深 632~820cm 的年龄是通过 570~632cm 年龄—深度关系线性外推获得的。尽管年龄的外推存在误差，但是该段地层沉积物较粗也反映这一时期沉积速率较快，即对应的年龄—深度模式斜率较大。

4.2. 地层岩性和组成

根据沉积物平均粒径和有机质含量(OM)的特征，柒盖淖尔湖芯地层可划分为 6 个单元(图 7-2A)。沉积单元 1(780~820cm)为灰褐色粉砂层，平均粒径约 15μm，平均有机质含量约 3%。沉积单元 2(720~780cm)为深褐色黏土质粉砂层，平均粒径约 10μm，该层明显的特征是有机质含量增加(可达 4%)。沉积单元 3(650~720cm)为浅灰色黏土质粉砂层，平均粒径约 60μm，低的有机质含量(低至约 1%)和波动的粗粒径(8~20μm)是该层最明显的特征。沉积单元 4(340~650cm)为深色黏土质粉砂层，属于湖相沉积，平均粒径小于 10μm，该层以有较大波动的有机质含量(从 1%到 5%)为特征。沉积单元 5(120~340cm)为灰褐色黏土质粉砂层，平均粒径约 20μm，平均有机质含量约 1%。沉积单元 6(0~120cm)为灰褐色黏土质粉砂层，平均粒径约 15μm，平均有机质含量约 2%。

4.3. 地层孢粉结果

从柒盖淖尔湖芯孢粉样品中共鉴定出56个陆生种子植物花粉类型，包括16种乔木、40种草本和灌木类型。此外，也鉴定出了水生藻类盘星藻。根据主要孢粉含量变化和聚类分析的结果，柒盖淖尔岩芯孢粉组合被划分为6个孢粉带(图7-3)。

孢粉带1(780~820cm；约10 700~10 300 cal. yr BP)：对应于地层单元1。孢粉组合以草本为主，包括藜科(30%~50%)、蒿属(7%~20%)和麻黄属(5%~12%)。针叶树花粉含量约20%，主要有松属(10%~30%)、柏科(1%~6%)和云杉属(1%~5%)。阔叶树花粉含量和孢粉总浓度都非常低。

孢粉带2(720~780cm；约10 300~9800 cal. yr BP)：对应于地层单元2。孢粉组合以阔叶树花粉的增加(达20%)、草本花粉的减少为特征。阔叶树花粉主要有栎属(5%~10%)、桦属(0.3%~1.6%)、榛木属(0%~1%)、榆属(0%~2%)和胡桃属(0%~1.3%)，其中，栎属花粉增加最为显著。与孢粉带1相比，陆地湿生草本类型(如莎草科和毛茛科)和水生香蒲属均有明显增加。

孢粉带3(650~720cm；约9800~9200 cal. yr BP)：对应于地层单元3。该带最明显的特征是旱生灌木花粉(如麻黄属、门刺属和紫菀型)快速增加，孢粉浓度和莎草科、栎属花粉含量快速下降。

孢粉带4(330~650cm；约9200~2800 cal. yr BP)：对应于地层单元4。该带具有较高的孢粉浓度和相对高的阔叶树花粉含量(如栎属、桦属和榆属)，草本和灌木花粉含量(如蒿属、莎草科、藜科、蔷薇科、榛属和柽柳属)较孢粉带3高。该带可进一步划分为3个孢粉亚带(孢粉亚带4-1、孢粉亚带4-2和孢粉亚带4-3)。

孢粉亚带4-1(580~650cm；约9200~8500 cal. yr BP)：以草本和阔叶树花粉含量的增加、针叶树花粉含量的下降为特征。阔叶树花粉的增加主要是由栎属(可达 6%)和榆属

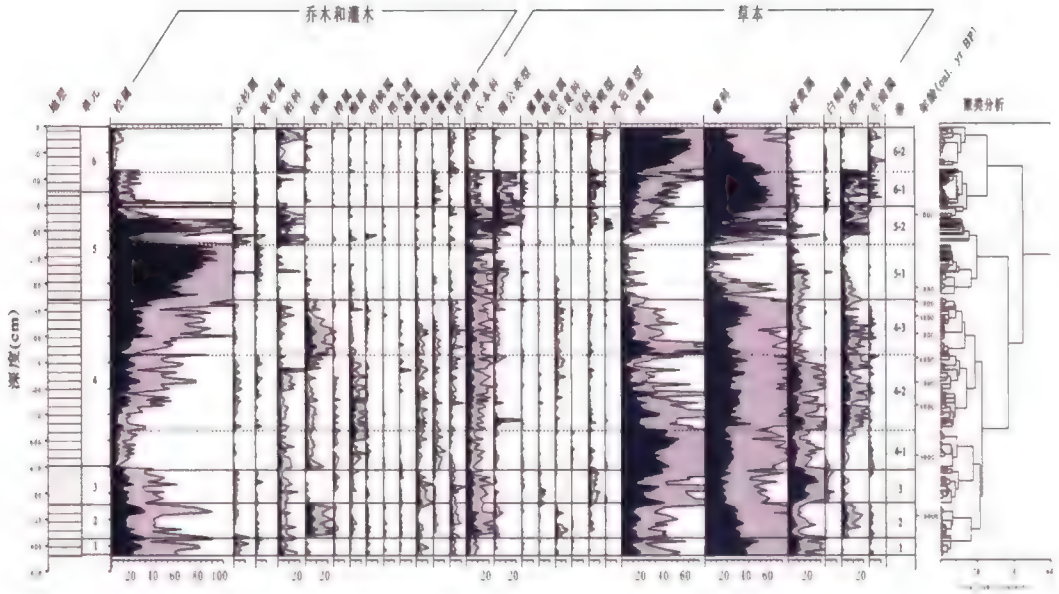

图7-3　柒盖淖尔孢粉图谱及孢粉带(Sun等,2013)

(可达7%)贡献的。草本花粉的增加主要由中生类型(如蒿属、蔷薇科和沙棘属)贡献的。与孢粉带3相比,旱生花粉类型(如麻黄属和白刺属)含量下降。

孢粉亚带4-2(430~580cm;约8500~5800 cal. yr BP):以草本花粉含量的逐渐下降(特别是蒿属)和针叶树花粉含量的逐渐升高(特别是松属)为特征。该亚带最明显的特征是藜科和麻黄属花粉含量增加。

孢粉亚带4-3(330~430cm;约5800~2800 cal. yr BP):与孢粉亚带4-2相比,孢粉亚带4-3有三个特征:①较高的孢粉浓度;②快速增加的栎属花粉;③略有增加的毛茛科花粉。

孢粉带5(140~330cm;约2800~850 cal. yr BP):对应于地层单元5。孢粉组合以高含量的针叶树花粉(40%~95%)和较低的孢粉浓度为特征。草本植物花粉(特别是藜科和蒿属)和阔叶树花粉(特别是栎属)含量下降。另一个明显的特征是湿生和水生植物花粉含量都较低。该带可进一步划分为2个孢粉亚带(孢粉亚带5-1、孢粉亚带5-2)。

孢粉亚带5-1(220~330cm;约2800~1300 cal. yr BP):以全剖面整个湖芯最高含量的针叶树花粉和最低含量的藜科和蒿属花粉为特征。

孢粉亚带5-2(140~220cm;约1300~850 cal. yr BP)以草本花粉的增加和针叶树花粉的减少为特征,该亚带增加的草本花粉类型主要有禾本科(5%~17%)、莎草科(3%~15%)、藜科(10%~50%)和凤毛菊型(5%~18%)。

孢粉带6(0~140cm;约850~0 cal. yr BP):大致对应于地层单元6。该带孢粉组合以草本植物为主,又可进一步划分为两个孢粉亚带。

孢粉亚带6-1(80~140cm;约850~450 cal. yr BP):以高含量的藜科和莎草科花粉和较低的孢粉浓度为特征。

孢粉亚带6-2(0~80cm;约450~0 cal. yr BP):以高含量的蒿属花粉(可达70%)、相对高含量的柏科花粉(可达12%)和逐渐增加的孢粉浓度为特征。

4.4. 古气候定量重建

基于 PFT-MAT 方法定量重建的柒盖淖尔地区年均温和年均降水量结果显示(图 7-4),约 10 700~9200 cal. yr BP 该地区气候存在三个不同阶段的变化:冷干(孢粉带 1)、暖湿(孢粉带 2)和冷干(孢粉带 3)。约 9200~2800 cal. yr BP(孢粉带 4),柒盖淖尔地区的气候较温暖湿润,而且降水量的波动是比较明显的。约 2800~1400 cal. yr BP,研究区气候开始变冷变干,而过去约 1400 年以来温度呈上升趋势,降水偏低且有明显波动。

其中,约 9200~2800 cal. yr BP 的气候重建包含更详细的信息。经过短暂的气候湿润(约 9200~8500 cal. yr BP)后,第一个明显的暖期开始于约 8500 cal. yr BP,而且一直持续到约 7400 cal. yr BP。约 7400~6000 cal. yr BP 气候明显的凉爽和干燥。约 6000~2800 cal. yr BP 气候出现明显的波动变化,期间的气候变化主要有三个特征:①约 6000~4000 cal. yr BP 气候温暖而湿润;②约 4000~2800 cal. yr BP 气候较温凉和干燥;③约 6000~2800 cal. yr BP 温度和降水呈下降趋势。

本章基于 PFT-MAT 方法定量重建的年均温和年均降水量与其他指标数据揭示的气候变化的结果是一致的。例如,有机质含量(图 7-4 中的 OM 变化曲线)与重建的年均降水量曲线变化非常相似;A/(E+N)值和孢粉总浓度的变化与年均降水量变化曲线的主要变化一致,与孢粉带对应的主要气候阶段也与孢粉总浓度的变化基本对应;而 Br/Ca 值的变化则与年均温的主要变化一致。换句话说,Br/Ca 值很好地记录到了研究区温度的主要变化被 Br/Ca 值较好的记录到了,而降水的主要变化则被 A/(E+N)值较好地记录到了。

综上所述,末次冰消期以来柒盖淖尔地区经历了三次大的冷干阶段,对应于孢粉带 1、3 和 5;两次大的温暖湿润阶段,对应于孢粉带 2 和 4。最后阶段(孢粉带 6,过去约 850 年以来)的气候特征是温度呈上升趋势而降水存在明显波动。约 9200~2800 cal. yr BP,气候温暖湿润,但也出现两次冷干阶段,分别发生在约 7400~6000 cal. yr BP 和约 4000~3000 cal. yr BP,这两次事件在图 7-4 中被清楚地标示出来了(浅灰色框)。柒盖淖尔湖芯孢粉资料的结果证实,首先,全新世期间的温度和降水的变化基本上是同步的;其次,温度和降水在约 6000 ~ 1400 cal. yr BP 下降趋势很明显。

5. 讨论

5.1. 柒盖淖尔地区植被和气候的变化

柒盖淖尔湖芯孢粉和有机质含量资料(图 7-4)显示,约 10 700~9200 cal. yr BP 区域植被发生了显著的变化。特别是,约 10 700~10 300 cal. yr BP(孢粉带 1)湖泊沉积物以粉砂为主,植被为藜科建群的荒漠草原。约 10 300~9800 cal. yr BP(孢粉带 2),湖泊接受粉砂质黏土沉积,植被大大改善,可能为森林草原。约 9800~9200 cal. yr BP(孢粉带 3),旱生

灌木(如麻黄属和白刺属)成为区域优势植物,此时湖泊沉积物为砂质

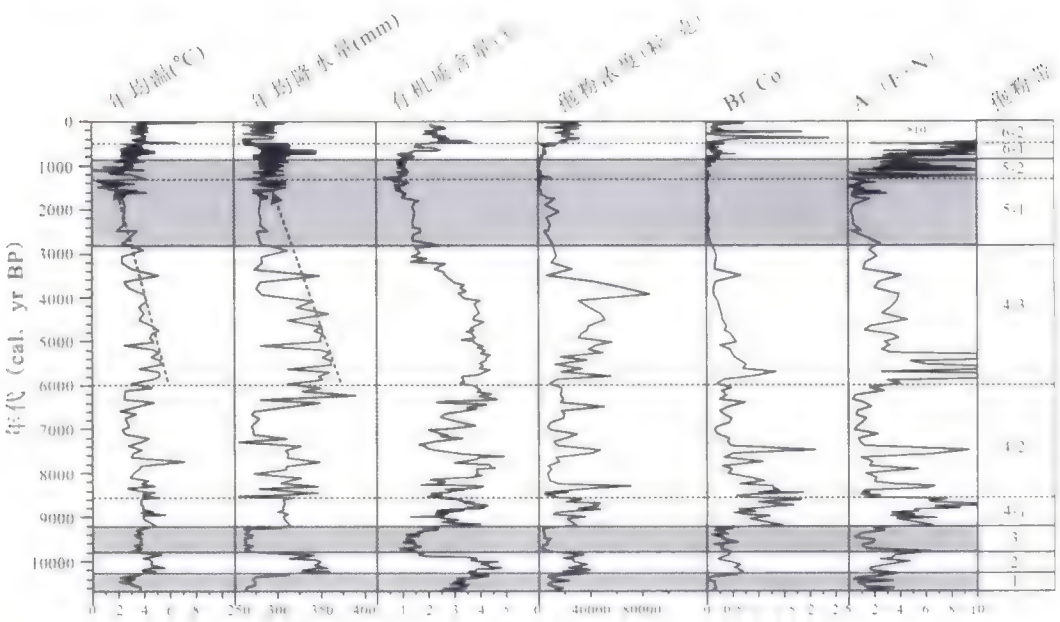

图7-4 利用孢粉资料定量重建的年均温(MAT)和年均降水量(MAP)以及它们与OM(%)、孢粉浓度(粒/g)、Br/Co值(Br指阔叶树花粉含量,Co指针叶树花粉含量)、(E+N)/A值(E代表麻黄属花粉含量,N代表白刺属花粉含量,A代表蒿属花粉含量)的对比。图中深灰色框代表全新世冷干阶段(如孢粉带1、3和5),浅灰色框代表中全新世冷干阶段,带箭头断线代表MAT和MAP的变化趋势(Sun等,2013)

约 9200~2800 cal. yr BP(孢粉带 4)较高的孢粉浓度和阔叶树花粉含量显示,湖泊水位升高、区域植被覆盖度增加,植被以森林草原为主。然而,这一时期植被类型和覆盖度出现明显的变化(图 7-3)。特别是,约 9200~8500 cal. yr BP(孢粉亚带 4-1)植被可能开始发育为生长有栎属植物的灌丛类型,气候温和且相对湿润。随后,约 8500~6000 cal. yr BP(孢粉亚带 4-2)在相对温暖湿润气候下,植被发展为以榆树为主的灌丛。但在约 7400~6000 cal. yr BP 草原植被扩张,气候变冷干。约 6000~2800 cal. yr BP(孢粉亚带 4-3)以栎属和毛茛科花粉含量和孢粉浓度的增加为特征,表明气候再次变温暖和湿润。但约 4000~2800 cal. yr BP 植被再一次退化为草原。值得注意的是,自约 4000 cal. yr BP 开始柒盖淖尔地区气候变冷变干,这与被广泛报道的"4000 cal. yr BP 事件"(Perry 和 Hsu,2000)或 Bond 等人(2001)报道的"全新世事件 3"或我国北方新石器文化重要的"4.2 ka 事件"(Liu 和 Feng,2012;Wu 和 Liu,2004)有所对应。

约 2800~850 cal. yr BP(孢粉带 5),松属花粉(40% ~ 95%)占优势,阔叶树花粉和部分草本花粉含量较低。值得一提的是,松属花粉是在现代孢粉谱中被广泛报道的超代表性类型(李文漪,1998;Ma 等,2004),它的超代表性会造成植被恢复和气候重建上的困难,而且特别值得注意的是,在中国北方和蒙古地区没有松树出现的表土样品中松属花粉含量可高达 55%,平均含量 30%(Ma 等,2004;Ma 等,2008)。我们在柒盖淖尔地区采集和分

析了 30 个表土孢粉样品，结果显示松属花粉确属超代表性类型，在没有松树生长的地方，松属花粉含量最高可达 70%，平均为 35%。这些松属花粉很可能是远距离传播来的，如距离湖泊有约 200km 的大青山、贺兰山、吕梁山等(见图 7-1)。我们推测，柒盖淖尔地区约 2800~850 cal. yr BP 周围山地可能分布着以松属植物为主的针叶林，气候较冷。同时，较低的孢粉浓度和低的阔叶树花粉含量揭示，该时期研究区气候较干燥，植被稀疏。约 850~450 cal. yr BP，孢粉组合以高含量的禾本科、蒲公英型、莎草科和藜科花粉为主，之后的约 450~0 cal. yr BP 孢粉组合则以高含量的蒿属、车前属和柏科花粉为主。过去约 850 年以来，定量重建的年均温略微增加，而与约 850~450 cal. yr BP 相比，约 450~0 cal. yr BP 的年均降水量略有减少。

5.2. 区域对比

Shi 等人(1993)曾报道，我国全新世大暖期(最高温度)发生在约 9500~3300 cal. yr BP，其中最温暖时期发生在约 8000~6850 cal. yr BP。An 等人(2000)则报道，全新世大暖期开始于约 10 000~7 500 ^{14}C yr BP，结束于约 5 000~2 000 ^{14}C yr BP。之后，Feng 等人(2004)的研究结果显示，在我国北方全新世大暖期应该被表达为全新世最适宜期(最大降水量)，发生的时间为约 10 000~4000 cal. yr BP，其中最湿润时期发生在约 8400~6000 cal. yr BP。此外，在一些文献中，全新世大暖期或/和全新世适宜期还被翻译成全新世东亚夏季风最盛期(Herzschuh，2006；Zhao 等，2009b)，这些研究结果显示，最盛期发生在约 10 000~3500 cal. yr BP (Herzschuh，2006)，或约 10 000~4000 cal. yr BP(Zhao 等，2009b)，或约 7000~4500 cal. yr BP(Wang 等，2010)。

本章将基于最新发表的气候定量重建结果，重点讨论我国北方夏季风边缘区全新世最湿润期(最大降水量)的持续时间(图 7-5)。柒盖淖尔湖芯孢粉资料显示，全新世最湿润期发生在约 6000~4000 cal. yr BP，第二湿润期发生在约 9200~7000 cal. yr BP(图 7-1 中的研究点 1)。基于转换函数方法，Xu 等人(2010)定量重建了位于柒盖淖尔东北方向岱海地区(图 7-1 中的研究点 2)的全新世气候，结果显示，全新世最适宜期发生在约 7500~3500 cal. yr BP。Jiang 等人(2009)则利用 PFT-MAT 方法定量重建了位于岱海东北方向的巴彦淖尔(图 7-1 中的研究点 3)的全新世气候，结果显示，全新世大暖期发生在约 10 500~8000 cal. yr BP，而全新世最湿润期发生在约 10 500~5500 cal. yr BP。Wen 等人(2010b)也利用转换函数方法定量重建了位于巴彦淖尔东北方向的呼伦湖(图 7-1 中的研究点 4)地区的全新世气候，结果则显示，全新世最适宜期发生在约 7500~5000 cal. yr BP，第二适宜期发生在约 3400~1500 cal. yr BP。

很显然，上述四个基于孢粉资料定量重建的年均温和年均降水量的结果(图 7-5)，没有在表达全新世最适宜期发生的时间上达成共识。四个重建不一致的原因可能是由于年代(如测年误差、测年数量、年代—深度模式等)、或/和不同方法(如两种不同的定量重建方法)、或地区差异(气候可能在不同地区有所不同)造成的。但是，我们的重建结果与被广泛接受的能反映东亚夏季风强度的南方洞穴石笋(图 7-1A 中的三宝洞)(Dong 等，

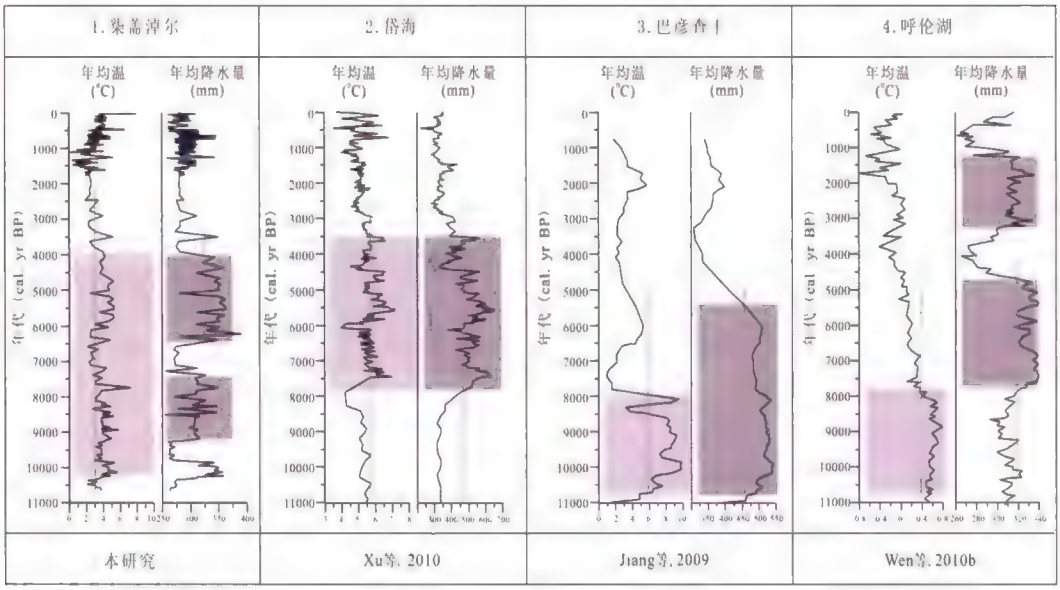

图7-5　柒盖淖尔孢粉数据定量重建的年均温(MAT)和年均降水量(MAP)结果与岱海、巴彦查干和呼伦湖重建结果的对比。图中浅灰色代表全新世大暖期(高的温度)发生的时段,深灰色代表全新世最适宜期(高的降水)发生的时段,灰色的线代表不同阶段的平均值(Sun等,2013)

2010;Hu 等,2008)、泥炭序列(图 7-1A 中的红原泥炭)(Hong 等,2003)的结果是一致的。这种一致性与观察到的我国南方现代季风强度和季风边缘区的气候的关系是对应的(张家琴等,1994;Liu 等,2008;Wang 等,1981)。此外,柒盖淖尔地区的年均降水量的变化与重建的赤道南太平洋表面海水温度的变化较为一致(见 Stott 等,2004),后者也成为影响研究区降水量的一个驱动因素。本章重建的柒盖淖尔地区的气候变化结果显示:①温度和降水的变化基本是同步的;②全新世适宜期出现在早中全新世,其中最湿润期为约 6000~4000 cal. yr BP,第二湿润期为约 9200~7400 cal. yr BP;③较高的温度下强季风可能给季风边缘区带来更多的降水,导致气候湿润。当然,上述四个序列(柒盖淖尔、岱海、巴彦查干、呼伦湖)定量重建的不一致性问题还需要更进一步地深入研究。

5.3. 可能的气候变化机制

全球温度变化的主要驱动因素是北半球夏季太阳辐射,其自约 20 000 cal. yr BP 开始增加,于约 10 000 cal. yr BP 达最高并开始逐渐下降(图 7-6,Kutzbach 和 Gallimore,1988)。夏季太阳辐射强度的变化被全球许多沉积序列记录到了(见:An 等,2000;Feng 等,2006;Koutavas 等,2002;Kutzbach 和 Gallimore,1988;Kutzbach 和 Liu,1997;Shi 等,1993)。能反映东亚夏季风强度变化的我国南方三宝洞石笋氧同位素组成被认为是精准地记录了夏季太阳辐射强度的变化(Dong 等,2010;图 7-6)。位于东亚季风边缘区的柒盖淖尔地区的温度可能也是受控于全新世东亚夏季风强度变化的影响,所以定量重建的年均温与三宝洞重建的季风强度的变化非常一致也就不足为奇。这种一致性暗示,研究区全新世降水

的主要变化可能受控于夏季太阳辐射控制的但有些滞后的东亚夏季风变化的影响，即"海洋缓冲效应"。海洋缓冲效应的意思是，低纬海洋在太阳辐射最强（约 10 000~9000 cal. yr BP）和全新世气候最适宜（约 9000~6000 cal. yr BP）的时候逐渐变暖，导致更多的水汽进入东亚夏季风系统（见 Feng 等，2006）。研究区降水的主要变化更可能与夏季太阳辐射变化影响的赤道辐合带（ITCZ）的南北摆动有关，即：向北摆动（变湿）或向南摆动（变干）决定了东亚夏季风的强度变化（An 等，2000；Chiang 和 Kushnir，2000）。然而，研究区降水的次一级变化则与赤道西太平洋海水表面温度变化更为相像（MD81 站，5°N，127°E，见图 7-1A），即降水的次一级变化主要受控于西太平洋海水表面温度的变化（Stott 等，2004）。特别值得指出的是，柒盖淖尔定量重建的年均降水量曲线中的 Q1 部分（约 10 300~4000 cal. yr BP）与赤道西太平洋海水表面温度曲线的 W1 部分（约 11 000~4400 cal. yr BP），Q2 与 W2、Q3 与 W3 部分都能一一对应，这更说明了东亚季风边缘区高的降水是由较高的赤道西太平洋地区海水表面温度控制的。两者的因果关系可能与受厄尔尼诺（ENSO）影响的赤道西太平洋海水表面温度（SST）的变化有关（Higginson 等，2004；Ju 和 Slingo，2006）。也就是说，ENSO 的频繁变动将更温暖的水带到太平洋东部（美洲一边），导致赤道西太平洋（亚洲一边）表面海水温度变低，进一步导致较少的水汽被输送到东亚季风边缘区（如柒盖淖尔地区）。

虽然赤道辐合带的南北移动可以很好地解释柒盖淖尔湖芯孢粉资料记录到的第一级降水变化，赤道西太平洋海水温度的变化可以很好地解释柒盖淖尔湖芯孢粉资料记录到的次一级降水变化，但仍然有两个重要变化得不到解释。柒盖淖尔湖芯孢粉资料和其他指标（如有机质含量和粒度）揭示的全新世两次明显的干旱事件分别发生在约 9800~9200 cal. yr BP 和约 7400~6000 cal. yr BP，但从时间上看，这两次干旱事件却对应于赤道西太平洋海水表面温度（SST）的高温期（图 7-6）。坦率地讲，我们目前还不能给这两次"特殊的干旱事件"提供解释。

6. 结论

蒙古高原南部柒盖淖尔地区的孢粉数据显示，约 10 700~9200 cal. yr BP 区域植被在森林草原和干草原之间波动；约 9200~2800 cal. yr BP 植被以森林草原为主；约 2800~850 cal. yr BP 植被出现退化，干草原广泛分布；过去约 850 年以来，植被中出现大量的草本植物。PFT-MAT 定量重建结果揭示，约 9200 cal. yr BP 以前研究区气候出现三次明显的波动：①约 10 700~10 300 cal. yr BP 冷干；②约 10 300~9800 cal. yr BP 温湿；③约 9800~9200 cal. yr BP 冷干。约 9200~2800 cal. yr BP，气候温暖湿润，期间存在两次冷干事件，分别发生在约 7400~6000 cal. yr BP 和约 4000~2800 cal. yr BP。约 2800~1400 cal. yr BP，气候又开始变冷变干，过去约 1400 年以来气候的特点表现为温度逐渐上升和降水偏低而且波动较大。本章的气候定量重建结果证实：①温度和降水的变化基本是同步的；②全新世适宜期出现在早中全新世；③研究区降水量的第一级变化主要受控于夏季太阳辐射主控的赤

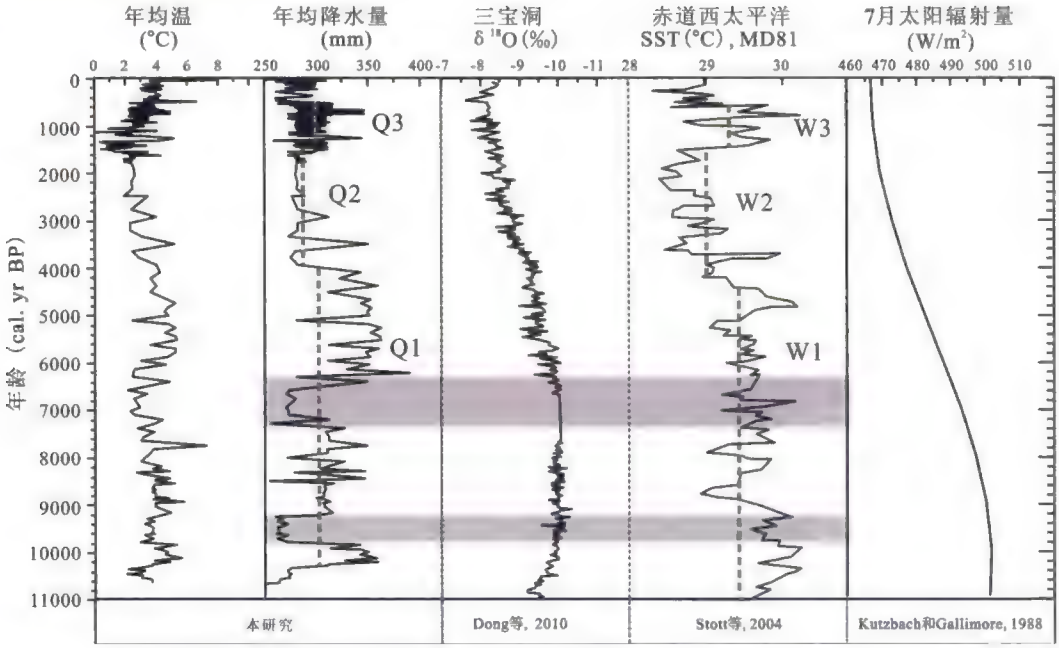

图7-6　柒盖淖尔岩芯孢粉数据定量重建的年均温(MAT)和年均降水量(MAP)变化与三宝洞石笋 $\delta^{18}O$、赤道西太平洋海水表面温度(SST)(MD81站,5°N,127°E)和北纬25°7月太阳辐射量的对比。图中灰色断线代表不同阶段的平均值,浅灰色框代表早中全新世两次明显的变干事件(Sun等,2013)

道辐合带的南北摆动;④降水量的次一级变化则主要受控于厄尔尼诺—南方涛动的东西移动。

另外,我们在本章中增加的两个孢粉—气候指标也得到其他指标的印证。Br/Co 值曲线与重建的年均温的变化基本一致,A/(E+N)比值曲线与重建的年均降水量具有相似的变化趋势,说明这两个孢粉指标可以分别用来半定量的代表温度和降水的变化。

致谢:马玉贞教授、张成君教授、翟新伟副教授、仵慧宁博士、王维博士、杨奇丽博士、胡轶鑫硕士参与野外采集工作。

参考文献

额瑞德曼·G,1978,孢粉学手册.中国科学院植物研究所古植物室孢粉组译,北京:科学出版社.

高由禧.1962.东亚季风的若干问题.北京:科学出版社,pp:49~63.

李文漪.1998.中国第四纪植被与环境.北京:科学出版社.

摩尔P.D,韦布 J.A,1987. 孢粉分析指南. 李文漪,肖向明,刘光锈等译.南宁:广西人民出版社.

孙湘君,杜乃秋,翁成郁,林瑞芬,卫克勤.1994. 新疆玛纳斯湖盆周围近14000年以来的古植被古环境.第四纪研究,14(3):239~248.

王伏雄,钱南芬,张玉龙,杨惠秋.1997. 中国植物孢粉形态(第二版). 北京:科学出版社.

徐国昌,姚辉,董安祥.1997.中国干旱半干旱气候变化.北京:气象出版社.

许清海,肖举乐,中村俊夫,阳小兰,杨振京,梁文栋,井内美郎,杨素叶.2003.孢粉资料定量重建全新

世以来岱海盆地的古气候.海洋地质与第四季地质,23(4):99~108.

许清海,田芳,李月丛,阳小兰.2009.中国北方草原区捕捉器样品与表土样品孢粉组合及其与植被和气候的关系.古地理学报,11(1):81~90.

张素琴,任振球,李松勤.1994.全球温度变化对我国降水的影响.应用气象学报,5(3):333~339.

张新时. 2007.中华人民共和国植被图(1:100 000).北京:地质出版社.

An, Z.S., 2000. The history and variability of the East Asian paleomonsoon climate. Quaternary Science Reviews, 19: 171~187.

An, Z.S., Porter, S.C., Kutzbach, J.E., Wu, X.H., Wang, S.M., Liu, X.D., Li, X.Q. and Zhou, W.J., 2000. Asynchronous Holocene optimum of the East Asian monsoon. Quaternary Science Reviews, 19(8): 743~762.

Bond, G., Kromer, B., Beer, J., Muscheler, R., Evans, M.N., Showers, W., Hoffmann, S., Lotti-Bond, R., Hajdas, I. and Bonani, G., 2001. Persistent solar influence on north Atlantic climate during the Holocene. Science, 294: 2130~2136.

Chen, F.H., Cheng, B., Zhao, Y., Zhu, Y. and Madsen, D.B., 2006. Holocene environmental change inferred from a high-resolution pollen record, Lake Zhuyeze, arid China. The Holocene, 16: 675~684.

Chiang, J., Kushnir, Y., 2000. Interdecadal changes in eastern Pacific ITCZ variability and its influence on the Atlantic ITCZ. Geophysical Research Letters, 27: 3687~3690.

Davis, B.A.S., Brewer, S., Stevenson, A.C., Guiot, J. and other data contributors, 2003. The temperature of Europe during the Holocene reconstructed from pollen data. Quaternary Science Reviews, 22: 1701~1716.

Demske, D., Heumann, G., Granoszewski, W., Nita, M., Mamakowa, K., Tarasov, P. and Oberh?nsli, H., 2005. Late glacial and Holocene vegetation and regional climate variability evidenced in high-resolution pollen records from Lake Baikal. Global and Planetary Change, 46: 255~279.

Dong, J.G., Wang, Y.J., Cheng, H., Hardt, B., Lawrence Edwards, R., Kong, X.G., Wu, J.Y., Chen, S.T., Liu, D.B., Jiang, X.Y. and Zhao, K., 2010. A high-resolution stalagmite record of the Holocene East Asian monsoon from Mt Shennongjia, central China. The Holocene, 20(2): 257~264.

El-Mosilimany, A.P., 1990. Ecological significance of common non-arboreal pollen: examples from drylands of the Middle East. Review of Palaeobotany and Palynology, 64: 343~350.

Feng, Z.-D., An, C.B., Tang, L.Y. and Jull, A.J.T., 2004. Stratigraphic evidence of a Megahumid climate between 10,000 and 4000 years B.P. in the western part of the Chinese Loess Plateau. Global and Planetary Change 43(3~4): 145~155.

Feng, Z.-D., An, C.B. and Wang, H.B., 2006. Holocene climatic and environmental changes in the arid and semi-arid areas of China: a review. The Holocene, 16 (1):119~130.

Fowell, S.J., Hansen, B., Peck, J.A., Khosbayar, P. and Ganbold, E., 2003. Mid to late Holocene climate evolution of the Lake Telmen Basin, North Central Mongolia, based on palynological data. Quaternary Research, 59 (3): 353~363.

Grimm, E.C., 1990. Tilia and Tilia graph PC spreadsheet and graphics software for pollen data. INQUA, Working Methods, Newsletter, 4: 5~7.

Guiot, J., Harrison, S.P. and Prentice, T.C., 1993. Reconstruction of Holocene patterns of moisture in Europe using pollen and lake-level data. Quaternary Research, 40: 139~149.

Guiot, J. and Goeury, C., 1996. PPPBASE, a software for statistical analysis of paleoecological and

paleoclimatological data. Dendrochronologia, 14: 295~300.

Gunin, P.D., 1999. Vegetation dynamics of Mongolia. Kluwer Academic Publisher, Copenhagen, pp238.

Hartmann, K. and Wünemann, B., 2009. Hydrological changes and Holocene climate variations in NW China, inferred from lake sediments of Juyanze palaeolake by factor analyses. Quaternary International, 194: 28~44.

Herzschuh, U., Tarasov, P., Wünemann, B. and Hartmann, K., 2004. Holocene vegetation and climate of the Alashan Plateau, NW China, reconstructed from pollen data. Palaeogeograph, Palaeoclimatology Palaeoecology, 211(1~2): 1~17.

Herzschuh, U., 2006. Palaeo-moisture evolution in monsoonal Central Asia during the last 50 000 years. Quaternary Science Reviews, 25(1~2): 163~178.

Higginson, M.J., Altabet, M.A., Wincze, L., Herbert, T.D. and Murray, D.W., 2004. A solar (irradiance) trigger for millennial-scale abrupt changes in the southwest monsoon. Paleoceanography, 19: PA3015, doi: 10.1029/2004PA001031.

Hong, Y.T., Hong, B., Lin, Q.H., Zhu, Y.X., Shibata, Y., Hirota, M., Uchida, M., Leng, X.T., Jiang, H.B., Xu, H., Wang, H. and Yi, L., 2003. Correlation between Indian Ocean summer monsoon and North Atlantic climate change during the Holocene. Earth and Planetary Science Letters, 211: 371~380.

Hu, C.Y., Henderson, G.M., Huang, J.H., Xie, S., Sun, Y. and Johnson, K., 2008. Quantification of Holocene Asian monsoon rainfall from spatially separated cave records. Earth and Planetary Science Letters, 266: 221~232.

Huang, F., Lisa, K., Xiong, S.F. and Huang, F.B., 2004. Vegetation, environment and human activity since Holocene in east Inner Mongolia. Science in China (series D), 34(11): 1029~1040.

IPCC, 2007. Climate Change 2007: The Physical Science Basis. Contribution of Working Group I to the Fourth Assessment Report of the Intergovernmental Panel on Climate Change, S. Solomon, D. Qin, M. Manning, Z. Chen, M. Marquis, K.B.Averyt, M. Tignor and H.L. Miller, Eds., Cambridge: Cambridge University Press.

Jiang, W.Y., Guo, Z.T., Sun, X.J., Wu, H.B., Chu, G.Q., Yuan, B.Y., Hatté, C. and Guiot, J., 2006. Reconstruction of climate and vegetation changes of Lake Bayanchagan (Inner Mongolia): Holocene variability of the East Asian monsoon. Quaternary Research, 65 (3): 411~420.

Jiang, W.Y., Guiot, J., Chu, G.Q., Wu, H.B., Yuan, B.Y., Hatté, C. and Guo, Z.T., 2009. An improved methodology of the modern analogues technique for palaeoclimate reconstruction in arid and semi-arid regions. Boreas, 39: 145~153

Ju, J. and Slingo, J., 2006. The Asian summer monsoon and ENSO. Quarterly Journal of the Royal Meteorological Society, 121: 1133~1168.

Koutavas, A., Lynch-Stieglitz, J., Marchitto, T.W. and Sachs, J.P., 2002. El Nino-like pattern in ice age Tropical Pacific sea surface temperature. Science, 297: 226~229.

Kutzbach, J.E. and Gallimore, R.G., 1988. Sensitivity of a coupled atmosphere mixed layer ocean model to changes in orbital forcing at 9000 years BP. Journal of Geophysical Research, 93: 803~821.

Kutzbach, J.E. and Liu, Z., 1997. Response of the African monsoon to orbital forcing and ocean feedbacks in the middle Holocene. Science, 278: 440~443.

Li, Y.C., Xu, Q.H., Zhao, Y.K., Yang, X.L., Xiao, J.L., Chen, H. and Lu, X.M., 2005. Pollen indication to

vegetation in the eastern part of desert China. Chinese Science Bulletin, 50(13): 1356~1364.

Liu, F.G. and Feng, Z.-D., 2012. A dramatic climatic transition at ~4000 cal. yr BP and its cultural responses in Chinese cultural domains. The Holocene, 22(10): 1181~1197.

Liu, J.H., Zhang, P.Z., Cheng, H., Chen, F.H., Yang, X.L., Zhang, D.Z., Zhou, J., Jia, J.H., An, C.L., Sang, W.C. and Johnson, K.R., 2008. Asian summer monsoon precipitation recorded by stalagmite oxygen isotopic composition in the western Loess Plateau during AD 1875~2003 and its linkage with ocean-atmosphere system. Chinese Science Bulletin, 53(13): 2041~2049.

Liu, K.B., Yao, Z.J. and Thompson, L.G., 1998. A pollen record of Holocene climatic changes from the Dunde ice cap, Qinghai-Tibetan Plateau. Geology, 26: 135~138.

Ma, Y.Z., Zhang, H.C., Pachur, H.J., Wünnemann, P., Li, J.J. and Feng, Z.-D., 2004. Modern pollen-based interpretations of mid-Holocene palaeoclimate (8500 to 3000 cal. BP) at the southern margin of the Tengger Desert, northwestern China. The Holocene, 14(6): 841~850.

Ma, Y.Z., Liu, K.B., Feng, Z.D., Sang, Y.L., Wang, W. and Sun, A.Z., 2008. A survey of modern pollen and vegetation along a south-north transect in Mongolia. Journal of Biogeography, 35: 1512~1532.

Magny, M., Guiot, J. and Schoellammer, P., 2001. Quantitative reconstruction of Younger Dryas to Mid-Holocene paleoclimates at Le Locle, Swiss Jura, using pollen and lake-level data. Quaternary Research, 56: 170~180.

Members of China Quaternary Pollen Data Base, 2001. Simulation of China biome reconstruction based on pollen data from surface sediment samples. Acta Botanica Sinica, 43: 201~209.

Moore, P.D., Web, J.A. and Collinson, M.E., 1991. Pollen Analysis, 2nd edition. Oxford: Blackwell Scientific Publication.

Nakagawa, T., Tarasov, P.E., Nishida, K., Gotanda, K. And Yasuda, Y., 2002. Quaternary pollen-based climate reconstruction in central Japan: application to surface and Late Quaternary spectra. Quaternary Science Reviews, 21: 2099~2113.

Perry, C.A. and Hsu, K.J., 2000. Geophysical, archaeological, and historical evidence support a solar-output model for climate change. Proceedings of the National Academy of Sciences, 97: 12 433~12 438.

Prentice, I.C., Cramer, W., Harrison, S.P., Leemans, R., Monserud, R.A. and Solomon, A.M., 1992. A global biome model based on plant physiology and dominance, soil properties and climate. Journal of Biogeography, 19: 117~134.

Prentice, I.C., Guiot, J., Huntley, B., Jolly, D. and Cheddadi, R., 1996. Reconstructing biomes from palaeoecological data: a general method and its application to European pollen data at 0 and 6 ka. Climate Dynamics, 12: 185~194.

Reimer, P.J., Baillie, M.G.L., Bard, E., Bayliss, A., Beck, J.W., Blackwell, P.G., Ramsey, C.B., Buck, C. E., Burr, G.S. and Edwards, R.L., 2009. IntCal09 and Marine09 radiocarbon age calibration curves, 0~50 000 years cal BP. Radiocarbon, 51: 1111~1150.

Shi, Y.F., Kong, Z.C., Wang, S.M., Tang, L.Y., Wang, F.B., Yao, T.D., Zhao, X.T., Zhang, P.Y. and Shi, S., 1993. Mid-Holocene climates and environments in China. Global and Planetary Change, 7: 219~233.

Stott, L., Cannariato, K., Thunell, R., Haug, G.H., Koutavas, A. and Lund, S., 2004. Decline of surface temperature and salinity in the western tropical Pacific Ocean in the Holocene epoch. Nature, 431: 56~59.

Sun, A.Z. and Feng, Z.D., 2013. Pollen-recorded bioclimatic variations of the last 15,000 years retrieved from Lake Qigai Nuur in the southern Mongolian Plateau of China. The Holocene, 23: 1391~1402.

Sun, X.J., Wang, B.Y. and Song, C.Q., 1996. Pollen-climate response surfaces of selected taxa from Northern China. Science in China (Series D), 26(5): 431~436.

Tarasov, P.E., Webb, III. T., Andreev, A.A., Afanas'eva, N.B., Berezina, N.A., Blyakharchuk, T.A., Bolikhovskaya, N.S., Cheddadi, R., Chernavskaya, M.M. and Chernova, G.M., 1998. Present-day and mid-Holocene biomes reconstructed from pollen and plant macrofossil data from the former Soviet Union and Mongolia. Journal of Biogeography, 25: 1029~1053.

Tarasov, P.E., Volkova, V.S., Webb, Ⅲ. T., Guiot, J., Andreev, A.A., Bezusko, L.G., Bezusko, T.V., Bykova, G.V., Dorofeyuk, N.I., Kvavadze, E.V., Osipova, I.M., Panova, N.K. and Sevastyanov, D.V., 2000. Last glacial maximum biomes reconstructed from pollen and plant macrofossil data from northern Eurasia. Journal of Biogeography, 27: 609~620.

Tarasov, P., Bezrukova, E., Karabanov, E., Nakagawa, T., Wagner, M., Kulagina, N., Letunova, P., Abzaeva, A., Granoszewski, W. and Riedel, F., 2007. Vegetation and climate dynamics during the Holocene and Eemian interglacials derived from Lake Baikal pollen records. Palaeogeography, Palaeoclimatology, Palaeoecology, 252 (3~4): 440~457.

Van Campo, E., Cour, P. and Sixuan, H., 1996. Holocene environmental changes in Bangong Co. Basin (western Tibet): Part 2. the pollen record. Palaeogeography, Palaeoclimatology, Palaeoecology, 120: 49~63.

Wang, S.W., Zhao, Z.C. and Chen, Z.H., 1981. Reconstruction of the summer regime for the last 500 years in China. Geojournal, 5:117~122.

Wang, Y.B., Liu, X.Q. and Herzschuh, U., 2010. Asynchronous evolution of the Indian and East Asian Summer Monsoon indicated by Holocene moisture patterns in monsoonal central Asia. Earth-Science Reviews, 103: 135~153.

Wang, W., Ma, Y.Z., Feng, Z.D., Narantsetseg, T., Liu, K.B. and Zhai, X.W., 2011. A prolonged dry mid-Holocene climate revealed by pollen and diatom records from Lake Ugii Nuur in central Mongolia. Quaternary International, 229(1~2): 74~83.

Wen, R.L., Xiao, J.L., Chang, Z.G., Zhai, D.Y., Xu, Q.H., Li, Y.C., Itoh, S. and Lomtatidze, Z., 2010a. Holocene climate changes in the mid-high-latitude- monsoon margin reflected by the pollen record from Hulun Lake, northeastern Inner Mongolia. Quaternary Research, 73: 293~303.

Wen, R.L., Xiao, J.L., Chang, Z.G., Zhai, D.Y., Xu, Q.H. and Li, Y.C., 2010b. Holocene precipitation and temperature variations in the East Asian monsoonal margin from pollen data from Hulun Lake in northeastern Inner Mongolia, China. Boreas, 39: 262~272.

Wu, W.X. and Liu, T.S., 2004. Possible role of the "Holocene Event 3" on the collapse of Neolithic Cultures around the Central Plain of China. Quaternary International, 117: 153~166.

Xiao, J.L., Xu, Q.H., Nakamura, T., Yang, X.L., Liang, W.D. and Inouchi, Y., 2004. Holocene vegetation variation in the Daihai Lake region of north-central China: a direct indication of the Asian monsoon climatic history. Quaternary Science Reviews, 23: 1669~1679.

Xu, Q.H., Xiao, J.L., Li, Y.C., Tian, F. and Nakagawa, T., 2010. Pollen-Based Quantitative Reconstruction of Holocene Climate Changes in the Daihai Lake Area, Inner Mongolia, China. Journal of Climate, 23(11):

2856~2868.

Zhao, Y., Yu, Z.C., Chen, F.H. and Li, J.J., 2008. Holocene vegetation and climate change from a lake sediment record in the Tengger sandy desert, northwest China. Journal of arid environments, 72: 2054~2064.

Zhao, Y., Xu, Q.H., Huang, X.Z. and Tao, S.C., 2009a. Differences of modern pollen assemblages from lake sediments and surface soils in arid and semi-arid China and their significance for pollen-based quantitative climate reconstruction. Review of Palaeobotany and Palynology, 159: 519~524.

Zhao, Y., Yu, Z.C., Chen, F.H., Zhang, J.W. and Yang, B., 2009b. Vegetation response to Holocene climate change in monsoon-influenced region of China. Earth-Science Reviews, 97 (1~4): 242~256.

Zhou, W.J., Head, M.J. and Lin, D., 2001. Climate changes in northern China since the late Pleistocene and its response to global change. Quaternary International, 83~85: 285~292.

第八章

中国新疆北部湖芯记录的过去8000年气候与水文的变化

冉　敏[1]　　冯兆东[2]

① 西南大学 地理科学学院

② 中国科学院 新疆生态与地理研究所

本章首先述评了有关新疆北部过去8000年来气候和水文变化的文献，然后归纳了这些文献中所包含的地理一致性(Geographic Coherency)信息，并回答了一些有关新疆北部全新世气候变化的焦点问题。首先采用湖芯孢粉蒿/藜值(A/C值)作为湿度指标，然后将每个孢粉序列的A/C值标准化为湿度指标(SMI)，最后获得所有参与序列SMI的平均值，即平均标准化湿度指数(Mean SMI)。我们获得的平均标准化湿度指数显示，过去8000年来区域湿度总体呈现增加趋势，这一结论也得到了其他孢粉指标的支持。气候驱动机制分析显示，过去8000年来北大西洋地区冬季温度的上升和北大西洋涛动(NAO)的正相趋势及高活动频率的厄尔尼诺—南方涛动(ENSO)很可能导致了新疆北部过去8000年来湿度的增加。同时，采用湖芯碳酸盐$\delta^{18}O$值作为湖水的盐度指标，用同样的方法获得所有参与序列的标准化的盐度指数，即平均标准化盐度指数(Mean SSI)。我们获得的平均标准化盐度指数显示，过去8000年来新疆北部湖水盐度持续上升。湖水盐度的增加主要归咎于全新世以来天山和阿尔泰山冰川面积的持续减小。也就是说，山区持续减小的冰川面积使得流入湖泊的冰川融水持续减少，最终导致湖水的咸化。可是，流域湿度的增加和湖水的咸化似乎是矛盾的。一个可以解开这个矛盾的解释是：尽管过去8000年来在温度总体下降背景下降水的增加或/和蒸发的减少可能导致了新疆北部土壤有效湿度的增加，但山地冰川融水的持续减少使得湖水补给量越来越少，因而引起湖水盐度越来越高。

关键词：新疆北部、A/C值、$\delta^{18}O$值、全新世、湿度变化、盐度变化

1. 引言

亚洲干旱区(Asian Arid Zone: AAZ)是指西起里海，东达大兴安岭(35°N~55°N、50°E~120°E)的广大地区。该地区暖季降水主要是向北移动的西风带来的北大西洋水汽所致，冷季降水主要是南移的西风带来的地中海水汽所致(Azien等，2001；Bothe等，2012)。冷季

气候主要受控于西风带和北大西洋涛动相互作用，而暖季气候主要受占据亚洲内陆的亚洲低压和延伸至亚洲干旱区的亚速尔高压相互作用的影响（Aizen等，2001；Meeker和Mayewski，2002）。

阿尔泰山脉将亚洲干旱区分为两半，我们的研究区（新疆北部）位于西半部的最东边。东—西走向的天山阻挡了其南侧阿拉伯海水汽的进入，而阿尔泰山和天山之间的东—西向山坳却允许盛行西风所带水汽进入新疆北部（Azien等，2001；Staubwasee和Weiss，2006）。西欧全新世气候记录和亚洲干旱区西半部（即阿尔泰山以西）全新世气候的时空一致性表明，亚洲干旱区西半部全新世气候是受西风气候系统主控的（Chen等，2008；Ran和Feng，2013；Wang和Feng，2013）。但是，也有研究认为，亚洲季风在全新世暖期推进到了新疆北部（Wingkler和Wang，1993），这一观点得到了来自玛纳斯湖和伊犁河谷记录的支持（孙湘君等，1994；林瑞芬等，1996；Rhodes 等，1996；Li 等，2011；Cheng等，2012）。

尽管上述资料及其解译之间存在的不一致和相互矛盾问题十分严重，但是如果考虑不同的控制因子，这些不一致和相互矛盾就可能得到和解。例如，如果湖泊主要依靠冰川融水补给，则其盐度首先取决于受控于温度的冰川融水，其次是残留的冰川面积的大小（Zhang等，2010；Feng等，2013），可能与流域降水量无关（Sorrel等，2007）。我们倾向于接受下列主张：流域植被能够真实地反映流域的气候变化，因此封闭和半封闭湖泊中的孢粉记录可以追溯过去的气候变化（Demske等，2005；Tarasov等，2006；Blyakharchuk等，2007；Ma等，2008；Rudaya等，2009；Zhao等，2012）。本章通过综述已发表的关于新疆北部过去8000年的气候和水文资料，谋求解决部分先前提到的分歧和矛盾。

2. 地理背景

新疆北部包括准噶尔盆地、天山北坡和阿尔泰山西南坡（图8-1a），以大陆性气候为特征，年日温度变化均较大。盆地到山区具有明显的垂直气候差异。例如，低海拔盆地（海拔200m）年平均温度（MAT）>8℃，年平均降水（MAP）<100mm；高海拔山地（海拔4000m）MAT<-15℃，MAP>600mm（胡汝骥，2004；陈曦，2010）。山地（天山和阿尔泰山）的植被垂直带明显，由上而下依次为：山地森林、森林草原、草原和沙漠（图8-1b），泰加林分布在中国阿尔泰山北部的高海拔区域。

本章选择的八个湖泊沉积序列中的六个位于新疆北部，一个位于南疆（博斯腾湖），一个位于吉尔吉斯斯坦（伊塞克湖），这八个湖泊的地理属性见表8-1。我们选择过去8000年作为本章的讨论时段是由于上述八个湖泊沉积序列中记录最短的是8000年，即八个序列对过去8000年均有比较完整的记录。另外一个值得提及的问题是所选序列的年代问题。若原文献只给出了^{14}C年代而没有给出年代—深度模式，我们首先使用CALIB 6.0中INTCAL09程序对给出的^{14}C年代进行校正，得到日历校正年龄（cal. yr BP = 即距离1950年的年代）（Reimer等，2009），然后用两个邻近点的测年线性插值，建立整个序列的年龄—深度模式。

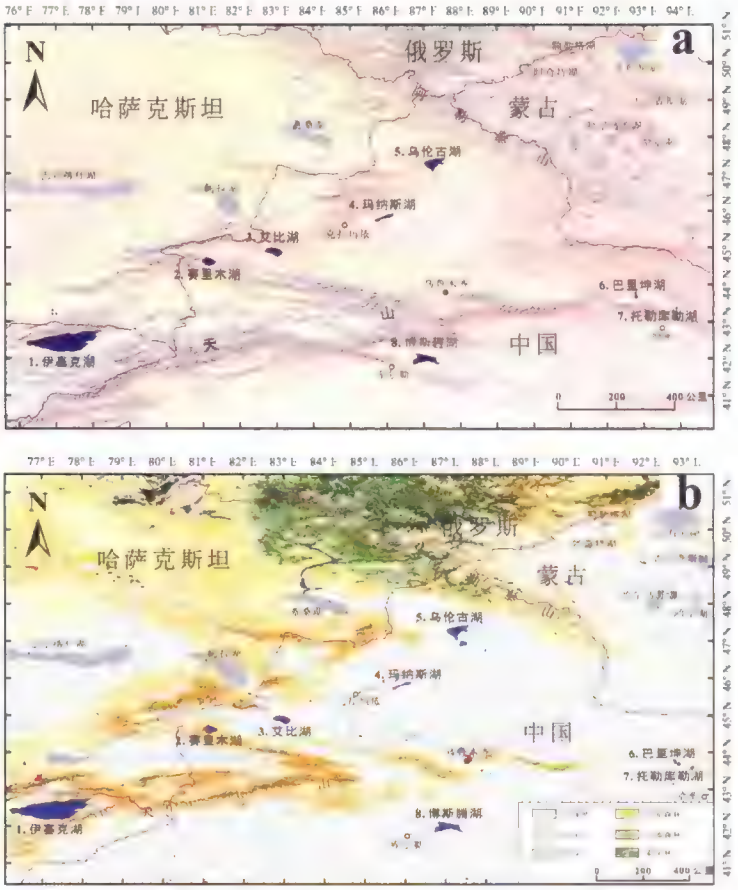

图8-1　本文所选八个湖泊的位置和它们的地形背景(a:上图)以及它们的植被分布背景(b:下图)

表8-1　本章所选八个湖泊的地理位置(包括吉尔吉斯斯坦的伊塞克湖)

序号	湖名	纬度(°)	经度(°)	海拔(m)	年均温(℃)	年均降水量(mm)	年均蒸发量(mm)
1	伊塞克	42.5	76.5	1600	10.0	250	820
2	赛里木	44.6	81.2	2072	0.5	350	550
3	艾比	44.9	82.6	200	7.8	95	1315
4	玛纳斯	45.8	85.9	257	6.1	100	2100
5	乌伦古	47.2	87.4	479	3.4	117	1844
6	巴里坤	43.7	92.8	1575	1.0	210	1638
7	托勒库勒	43.6	92.9	1575	1.3	211	16.3
8	博斯腾	42.1	86.9	1048	8.3	141	2039

3. 代用指标的气候意义

3.1. 孢粉A/C值：流域湿度指标

孢粉指标是古气候重建研究中最常用的指标之一，因为孢粉指标的气候指代性已在现代气候条件下得到了广泛的检验。孢粉组合中的A/C值早就被认为是可以指示干旱半干旱地区湿度的变化（El-Moslimany，1990），因为在干旱半干旱地区蒿属（A）一般随湿度的增加而增加，而藜科（C）则随湿度的增加而减少。为进一步检验A/C值作为湿度指标的可靠性，Zhao等（2012）基于中国北方的608个孢粉组合资料对A/C的适用性进行了统计检验。Zhao等的结果显示，草原植被A/C值的中值和平均值分别为3.05和6.03，草原沙漠植被为1.54和3.26，沙漠植被为0.47和0.62。他们的结论是，A/C值在中国干旱半干旱地区仍然是一个可以接受的湿度指标。但是，在使用A/C值时必须注意以下两点：①由于河流会将周围山体的蒿属带进湖泊，湖芯孢粉中A/C值可能会低估流域的干旱程度；②在盐碱地广布的盆地中耐盐和耐旱的藜科可能主导孢粉谱，从而使得A/C值作为湿度指标的有效性大打折扣（Zhao等，2012）。

为了使所有参与的湖芯序列的A/C值具有时间上的可比性，我们首先将每一个序列的A/C值转换为标准湿度指数。具体地讲，每一个序列中我们对200年时间段赋予一个表示湿度的序数值。该200年时间段的A/C平均值和整个序列（即8000年）的最高A/C值的比值便是这个时间段的序数值。所赋的序数值划分为0（最低值）至4（最高值）五个等级。一般来讲，某个序列的A/C值可能与这个序列所在流域的绝对湿度相关。但是，将所有参与序列的A/C值标准化为序数值后（即标准化湿度指数，SMI），这些序数值就可能反映大范围湿度变化的时间规律。也就是说，如果所有参与序列的序数值（即标准化湿度指数）表现出了地理上的连贯性或一致性，那么平均标准化湿度指数（即Mean SMI）就可以被用来描述大范围湿度变化的时间规律（Davis等，2003；Herzschuh，2006；Zhao等，2009；Ran和Feng，2013；Wang和Feng，2013）。

3.2. 碳酸盐 $\delta^{18}O$ 值：湖水盐度指标

湖芯碳酸盐和介形类壳体的氧同位素信号（即 $\delta^{18}O$）受控于多种因素，其中盐度和湖水温度最为重要。一般来讲，氧同位素信号受溶解的 CO_2 的氧同位素影响，而后者直接与湖水盐度相关（Fontes等，1996）。毫不夸张地讲，蒸发/降水值是控制干旱半干旱区封闭和半封闭湖泊碳酸盐的氧同位素信号的最重要因素，因为湖水盐度主要受控于蒸发（盐度浓缩过程）与降水（盐度稀释过程）的比值（Mischke和Wünnemann，2006；Zhang等，2010）。但是，在新疆北部，山区（天山和阿尔泰山）大量冰雪融水控制着封闭和半封闭湖泊的水平衡和盐度，导致氧同位素组成更为复杂。通常情况下，封闭和半封闭湖泊碳酸盐 $\delta^{13}C$ 和 $\delta^{18}O$ 同步变化，均受控于蒸发/降水值（Leng和Marshall，2004；沈吉等，2010）。若 $\delta^{13}C$ 和 $\delta^{18}O$ 反向变化，则表明 $\delta^{18}O$ 比 $\delta^{13}C$ 对温度变化更为敏感（Wu和Wang，1997）。另外，伊塞克湖碳酸盐 $\delta^{13}C$ 主要受控于湖泊生产力，$\delta^{13}C$ 与 $\delta^{18}O$ 没有成因上的任何关联（Ricketts等，2001）。

与上述计算平均标准化湿度指数的过程相同，我们也计算了平均标准化盐度指数。具体地讲，每一个序列中我们对200年时间段赋予一个表示盐度的序数值。该200年时间段的$\delta^{18}O$平均值和整个序列（即8000年）的最高$\delta^{18}O$值的比值便是这个时间段的序数值。所赋的序数值划分为0（最低值）至4（最高值）五个等级。一般来讲，某个序列的$\delta^{18}O$值可能与这个湖的绝对盐度相关。但是，将所有参与序列的$\delta^{18}O$值标准化为序数值后（即标准化盐度指数，SSI），这些序数值就可能反映大范围盐度变化的时间规律。也就是说，如果所有参与序列的序数值（即标准化盐度指数）表现出了地理上的连贯性或一致性，那么平均标准化盐度指数（即Mean SSI）就可以被用来描述大范围盐度变化的时间规律。

4. 各湖芯过去8000年以来气候记录综述

4.1. 伊塞克湖

伊塞克湖（位置见图8–1）位于吉尔吉斯斯坦境内的西天山海拔1600m处，湖区年平均温度（MAT）为10.0℃，年平均降水（MAP）为250mm，潜在蒸发量为820mm（见表8–1）。伊塞克湖中没有孢粉资料发表，本章仅关注湖芯介形壳体的$\delta^{18}O$和元素资料（Ricketts等，2001）。基于$\delta^{18}O$资料和元素指标的重建显示，该地区早全新世气候湿润，晚全新世气候干旱。在约8.7~6.9 cal. ka BP（cal. ka BP = 距今千年前，为校正日历年）时段湖泊呈开放状态（即外溢），湖水盐度很低。约6.9 cal. ka BP之后湖泊变为封闭性湖泊，湖水盐度随之上升（图8–2）。如前所述，伊塞克湖碳酸盐$\delta^{13}C$主要受控于湖泊生产力。湖芯上部介形壳体$\delta^{13}C$的下降主要归答于湖泊生产力的增加，这一结论得到了有机质含量和硅藻丰富度增加的支持（Ricketts等，2001）。

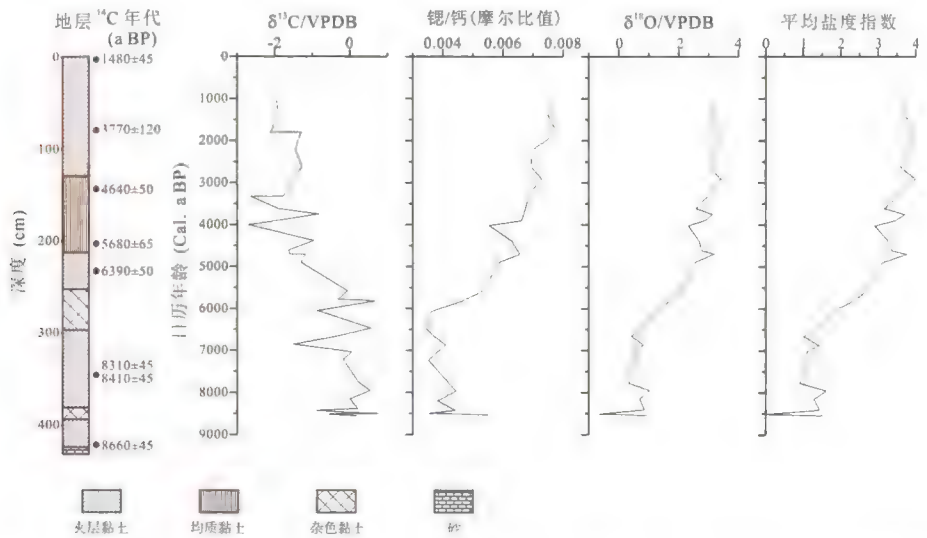

图8–2　吉尔吉斯斯坦境内伊塞克湖数据（Ricketts等，2001）：碳酸盐$\delta^{13}C$、Sr/Ca、$\delta^{18}O_{carb}$和基于$\delta^{18}O$值的SSI（标准化盐度指数）（Ran and Feng, 2014）

4.2. 赛里木湖

赛里木湖(海拔2072m)年平均温度(MAT)为0.5℃,年平均降水(MAP)为350mm,潜在蒸发量为550mm(见表8-1)。赛里木湖没有碳酸盐$\delta^{18}O$资料发表,本章仅关注孢粉资料(Jiang等,2013)。作者采用孢粉A/C值和孢粉数据的主成分分析推断了流域湿度的变化。结果显示(图8-3),约9.6 cal. ka BP之前荒漠植被占主导;在约9.6~5.5 cal. ka BP时段湿度明显增加,草原植被占主导;在约5.5~3.5 cal. ka BP时段湿度不断下降,植被以荒漠草原为主;在约2.5~0.2 cal. ka BP时段草甸草原植被占主导;A/C值表达了过去约200年的干旱化趋势,但是这个时段偏低的A/C值很可能是人类活动或人类活动对表层湖芯扰动的结果。

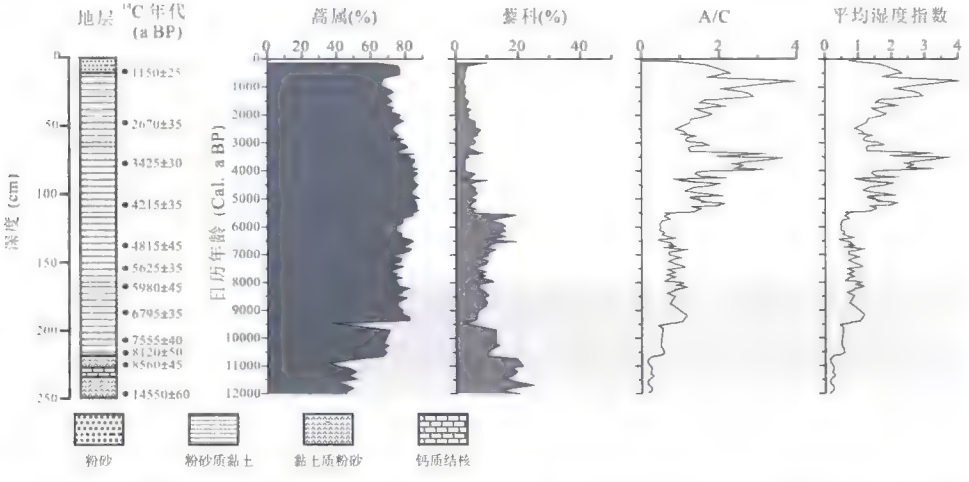

图8-3　赛里木湖数据(Jiang等, 2013):蒿属孢粉百分比、藜科孢粉百分比、A/C值和基于A/C值的SMI(标准化湿度指数)(Ran and Feng, 2014)

4.3. 艾比湖

艾比湖(海拔200m)平均年温度(MAT)为7.8℃,年平均降水(MAP)为95mm,潜在蒸发量高达1315mm(见表8-1)。本章中使用Wang等(2013)的孢粉资料和张成君(未发表数据)的碳酸盐$\delta^{18}O$资料。孢粉和地层资料显示,在约13.9~7.4 cal. ka BP湖区植被主要以草原和湿地为主,在约7.4~3.6 cal. ka BP有效湿度逐渐增加。约3.6 cal. ka BP以来有效湿度进一步增加,流域内植被得到进一步改善。碳酸盐$\delta^{18}O$和$\delta^{13}C$资料显示,自约8.0 cal. ka BP以来(即过去8000年)艾比湖湖水盐度基本上处于上升状态,仅在约2.5 cal. ka BP和约1.0 cal. ka BP出现两个短暂的淡水时段(图8-4)。

4.4. 玛纳斯湖

玛纳斯湖(海拔257 m)年平均温度(MAT)为6.1℃,年平均降水(MAP)为100mm,潜在蒸发量高达2100mm(见表8-1)。本章中使用的孢粉资料来自于孙湘君等(1994),碳酸盐$\delta^{18}O$资料来自Rhodes等(1996)。地球化学指标和地层显示(Rhodes等,1996),在约10.0~6.0 ^{14}C ka BP湖水位逐渐上升,在约6.0~4.5 ^{14}C ka BP流域湿度突然下降,伴随着的是湖水位的急剧下降。在约4.5~2.5 ^{14}C. ka BP湖水位有所回升。过去约2500年来玛纳斯湖水

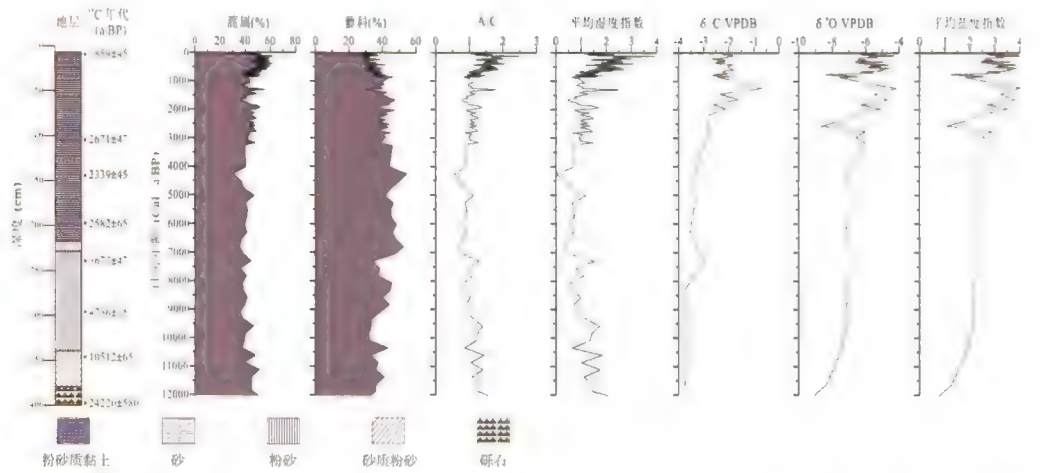

图8-4　艾比湖孢粉数据(Wang等,2013)和稳定同位素数据(张成君,未发表数据)。孢粉数据包括蒿属孢粉百分比、藜科孢粉百分比、A/C值和基于A/C值的SMI(标准化湿度指数)。稳定同位素数据包括碳酸盐 $\delta^{13}C$、$\delta^{18}O$和基于 $\delta^{18}O$值的SSI(标准化盐度指数)(Ran and Feng, 2014)

逐渐变为过咸水(即hyper-saline)。孢粉资料揭示(孙湘君等,1994),在约11.0~9.0 ^{14}C ka BP时段湖区植被主要以沙漠植被为主,在约9.0~4.0 ^{14}C ka BP时段主要以草原植被为主,约4.0 ^{14}C ka BP之后又恢复为沙漠植被(图8-5)。碳酸盐 $\delta^{18}O$和 $\delta^{13}C$数据揭示(Rhodes等,1996),过去约12 000年来湖水盐度基本呈现增加趋势,仅在约6.5~5.0 ^{14}C ka BP出现盐度低值,对应着约6.0~4.5 ^{14}C ka BP的低湖水位。同时,在约6.0~4.5 ^{14}C ka BP湖芯夹杂有河流相沉积,进一步支持湖水位急剧下降的推论。

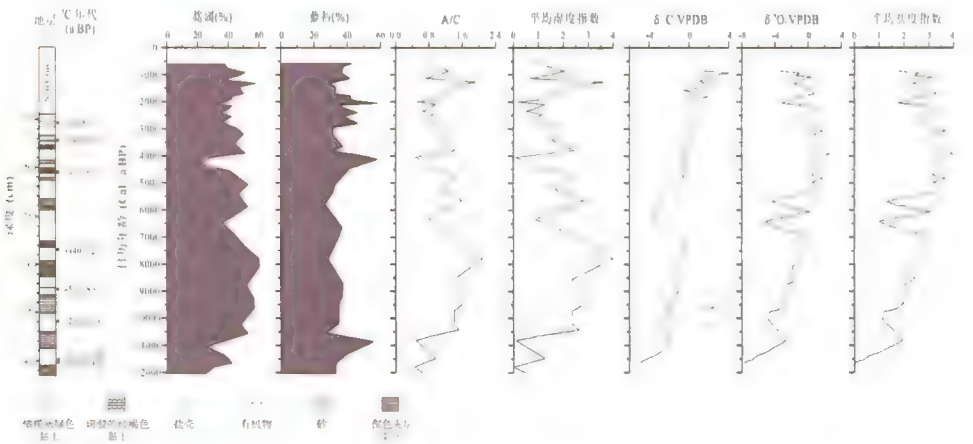

图8-5　玛纳斯湖孢粉数据(孙湘君等, 1994)和稳定同位素数据(Rhodes等,1996)。孢粉数据包括蒿属孢粉百分比、藜科孢粉百分比、A/C值和基于A/C值的SMI(标准化湿度指数)。稳定同位素数据包括碳酸盐 $\delta^{13}C$、$\delta^{18}O$和基于 $\delta^{18}O$值的SSI(标准化盐度指数)(Ran and Feng, 2014)

4.5. 乌伦古湖

乌伦古湖(海拔479m)位于准噶尔盆地北部,由源自阿尔泰山的河流补给。湖区年平均温度(MAT)为3.4℃,年平均降水(MAP)为117mm,潜在蒸发量高达1844mm(见表8-1)。本章中使用的孢粉资料来自Liu等(2008),介形壳体的δ^{18}O资料来自Jiang等(2007)。Liu等(2008)利用孢粉解译指出:在约6.7 cal. ka BP以前湿地植被对孢粉的大量贡献导致孢粉资料失去了气候学意义。在约6.7 cal. ka BP之后荒漠植被组分的下降表明了流域湿度的增加(图8-6)。另外,Jiang等(2007)综合了多项指标(如孢粉组合、地球化学指标、介形壳体组合)后认为:全新世早期(约10.0~7.6 cal. ka BP)气候冷干,全新世中期(约7.6~5.3 cal. ka BP)气候冷湿,全新世晚期气候波动剧烈,可以分为四个阶段:约5.3~3.6 cal. ka BP暖干,约3.6~2.1 cal. ka BP冷干,约2.1~1.3 cal. ka BP冷湿,约1.3 cal. ka BP之后(即过去1300年以来)气候冷干。

如果Liu等(2008)的解译是可以接受的,那么约6.7 cal. ka BP以前的孢粉很可能大多来自湖周围的大面积湿地,即湿地面积的扩张导致蒿属孢粉含量过高,从而使得A/C值不能指示流域湿度。图8-6显示,孢粉的A/C值自约6.7 cal. ka BP以来几乎没有变化。介形壳体δ^{18}O及δ^{13}C指示的盐度变化可以分为两个阶段:约10.0~6.0 cal. ka BP和约6.0~0 cal. ka BP,这两个时段的盐度均呈现上升趋势(Jiang等,2007)。

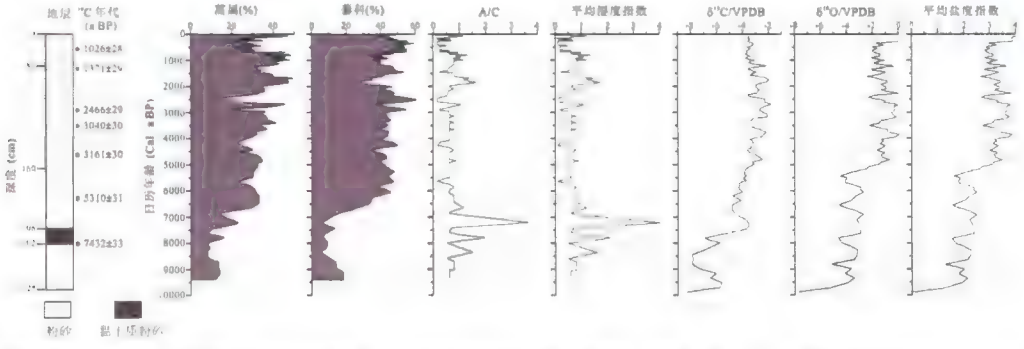

图8-6　乌伦古湖孢粉数据(Liu等, 2011)和稳定同位素数据(Jiang等,2011)。孢粉数据包括蒿属孢粉百分比、藜科孢粉百分比、A/C值和基于A/C值的SMI(标准化湿度指数)。稳定同位素数据包括碳酸盐δ^{13}C、δ^{18}O和基于δ^{18}O值的SSI(标准化盐度指数)(Ran and Feng, 2014)

4.6. 巴里坤湖

巴里坤湖(海拔1575m)位于准噶尔盆地的东缘,湖区年平均温度(MAT)为1.0℃,年平均降水(MAP)为210mm,潜在蒸发量高达1638mm(见表8-1)。本综述中使用的孢粉资料来自An等(2011),碳酸盐δ^{18}O资料来自Xue和Zhong (2011)。由孢粉A/C值得到的标准化湿度指数(SMI)显示,自约10.0 cal. ka BP以来湿度基本处于增加状态,在约2.5~0.8 cal. ka BP出现最高值,在约4.5~3.0 cal. ka BP出现低值(图8-7)。碳酸盐δ^{18}O值显示,自约7.5 cal. ka BP以来湖水盐度基本处于上升状态,仅在约1.0 cal. ka BP之后有所下降。在巴里坤湖芯中观测到的δ^{13}C和δ^{18}O的相反变化被归咎于大气与水体交换过程的加强(Xue和Zhong, 2011)。

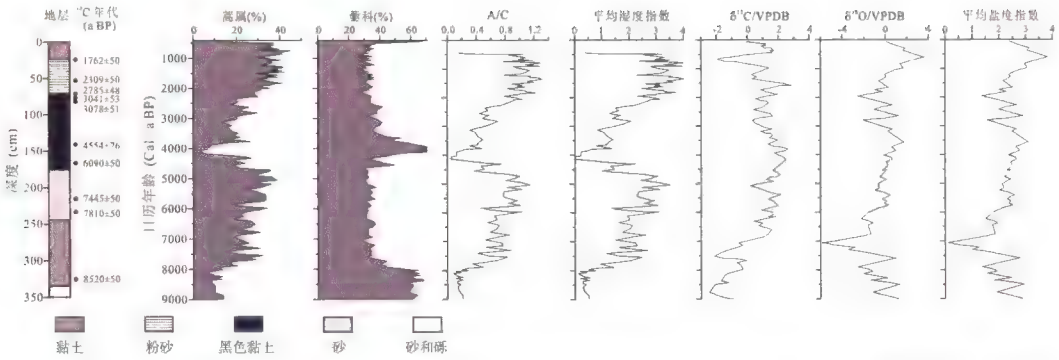

图8–7　巴里坤湖孢粉数据(An等, 2011)和稳定同位素数据(Xue和Zhong,2011)。孢粉数据包括蒿属孢粉百分比、藜科孢粉百分比、A/C值和基于A/C值的SMI(标准化湿度指数)。稳定同位素数据包括碳酸盐 $\delta^{13}C$、$\delta^{18}O$和基于 $\delta^{18}O$值的SSI(标准化盐度指数)(Ran and Feng, 2014)

4.7. 托勒库勒湖

托勒库勒湖(海拔1575m)距巴里坤湖150km(见图8–8),湖区年平均温度(MAT)为1.3℃,年平均降水(MAP)为211mm,潜在蒸发量高达1603mm(见表8–1)。托勒库勒湖没有碳酸盐 $\delta^{18}O$数据发表,本章中的孢粉数据来自陶士臣(2011)。托勒库勒湖芯孢粉A/C值与巴里坤湖芯孢粉A/C值均显示,流域湿度均在约4.0 cal. ka BP突然增加(图8–8)。但是,托勒库勒湖芯孢粉A/C值并没有显示约8.0~5.0 cal. ka BP湿度的增加(Xue和Zhong,2011)。

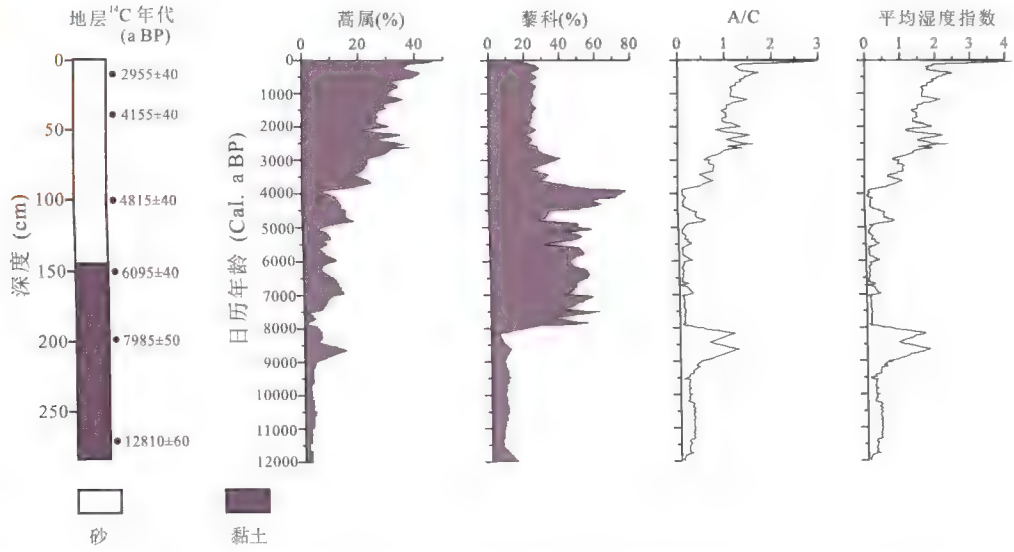

图8–8　托勒库勒湖孢粉数据(陶士臣,2011):蒿属孢粉百分比、藜科孢粉百分比、A/C值和基于A/C值的SMI(标准化湿度指数)(Ran and Feng, 2014)

4.8. 博斯腾湖

博斯腾湖(海拔1048m)位于天山南坡,湖区(海拔1048m)年平均温度(MAT)为8.4℃,年平均降水(MAP)为141mm,潜在蒸发量高达1048mm(见表8–1)。博斯腾湖的全新世气候

重建研究工作开始于1980s，Feng等（2006）系统地述评了对2005年之前的重建文献。最近发表的资料有陈发虎等（2006）、Mischke和Wünnemann（2006）、Wünnemann等（2006）和Huang等（2009）。Zhang等（2010）对这些最新工作的重建成果（2005~2009年）进行了系统的评述。本章使用的孢粉资料来自黄小忠（2006），碳酸盐$\delta^{18}O$资料据来自Mischke和Wünnemann（2006）。黄小忠的孢粉研究结果表明，在约8.0~6.0 cal. ka BP孢粉A/C值较低，在约6.0~0.5 cal. ka BP孢粉A/C值较高（图8-9），在约0.5 cal. ka BP孢粉A/C值出现低值后又开始回升。介形壳体$\delta^{18}O$和$\delta^{13}C$资料显示，博斯腾湖水盐度在过去8000年来呈波动上升状态，盐度的上升得到了碳酸盐矿物资料的支持（Zhang等，2010）。

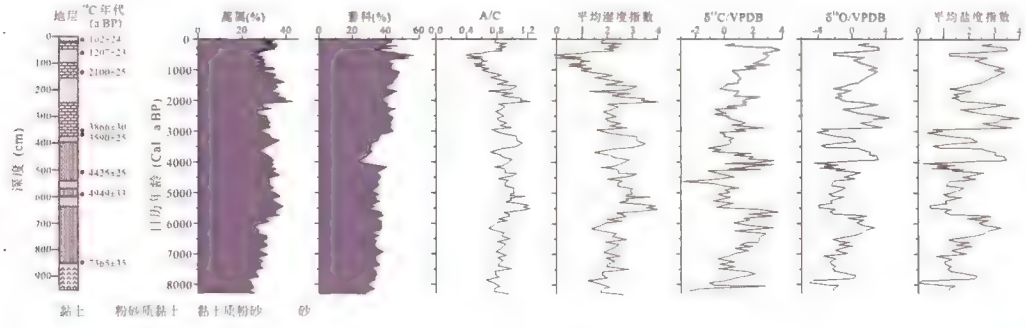

图8-9　博斯腾湖孢粉数据（黄小忠，2006）和稳定同位素数据（Mischke和Wünnemann，2006）。孢粉数据包括蒿属孢粉百分比、藜科孢粉百分比、A/C值和基于A/C值的SMI（标准化湿度指数）。稳定同位素数据包括碳酸盐$\delta^{13}C$、$\delta^{18}O$和基于$\delta^{18}O$值的SSI（标准化盐度指数）（Ran and Feng, 2014）

5. 区域对比和讨论

5.1. A/C值指示的流域湿度变化

值得再次提及的是，中国干旱半干旱区孢粉A/C值和生物气候之间的关系是经得起检验的（Zhao等，2012）。但是，以下两个方面需要特别注意：①由于周围山地的蒿属孢粉（即A/C值的分子）被河流带入湖泊，湖芯孢粉的A/C值可能会低估流域的干旱程度；②在盐碱地广布的流域内，占据主导的耐盐和耐旱的藜科孢粉（即A/C值的分母）可能会使A/C值作为湿度指标的有效性大打折扣。另外，湖区湿地的扩张和缩小也可能使A/C值作为湿度指标的有效性受到影响（Liu等，2008）。需要进一步说明的是，湿地的扩张（或缩小）与湖泊水位的升降没有固定的关系。例如，湖水位升高引起湖岸线的延长可能导致湿地面积增加，但是，湖水位下降导致的湖滩面积增加也会引起湿地面积的扩张（Charman，2002）。

我们重建的七个标准化湿度指数（SMI）曲线未能体现新疆北部全新世湿度变化的地理空间一致性，尤其是玛纳斯湖和乌伦古湖孢粉A/C值揭示，全新世早期湿度大于全新世晚期湿度，这个趋势与其他五个SMI曲线的趋势几乎是相反的。玛纳斯湖在约10.0~6.0 cal. ka BP出现过第一次湖进（Rhodes等，1996），与此同时（即约10.5~6.5 cal. ka BP）孢粉A/C值也很高（孙湘君等，1994），这一结果导致作者（Rhodes等，1996）认为，新疆北部全新

世气候主要受控于东亚季风系统而非西风系统。乌伦古湖自约6.7 cal. ka BP以来荒漠孢粉组分的下降被认为指示湿度的下降。但是，孢粉A/C值并未显示出这种变化。我们认为，乌伦古湖盆地大面积的盐碱地可能导致了孢粉A/C值的失效，即盐碱地广布的流域内，占据主导的耐盐和耐旱的藜科孢粉（即A/C值的分母）可能会使A/C值作为湿度指标的有效性大打折扣。实际上，目前的乌伦古湖盆地就发育大面积的盐碱地（见图8-1a）。需要指出的是，目前玛纳斯湖盆的盐碱地比乌伦古湖盆地的盐碱地更加发育，如此大面积分布的盐碱地也可能是玛纳斯湖芯孢粉A/C值失效的原因。

我们计算了七条标准化湿度指数（SMI）曲线（包括玛纳斯湖和乌伦古湖）的平均值（即Mean SMI），该平均值所表示的有效湿度在全新世早期（约8.0~5.0 cal. ka BP）和晚期（约2.0~0 cal. ka BP）都相对较高，而在中期（约5.0~2.0 cal. ka BP）相对较低（图10的倒数第二条曲线）。很显然，约8.0~5.0 cal. ka BP较高的平均湿度（即Mean SMI）是由玛纳斯湖和乌伦古湖较高的Mean SMI值导致的。我们重新计算了五条标准化湿度指数（SMI）曲线（不包括玛纳斯湖和乌伦古湖）的平均值（即Mean SMI）。该平均值所显示的湿度有明显的增加趋势（图8-10的最后一条曲线和图8-11的第一条曲线）。值得提及的是，上述五个湖芯（赛里木湖、艾比湖、巴里坤湖、托勒库勒湖和博斯腾湖）的其他孢粉资料都一致地支持基于A/C值重建的有效湿度的变化。

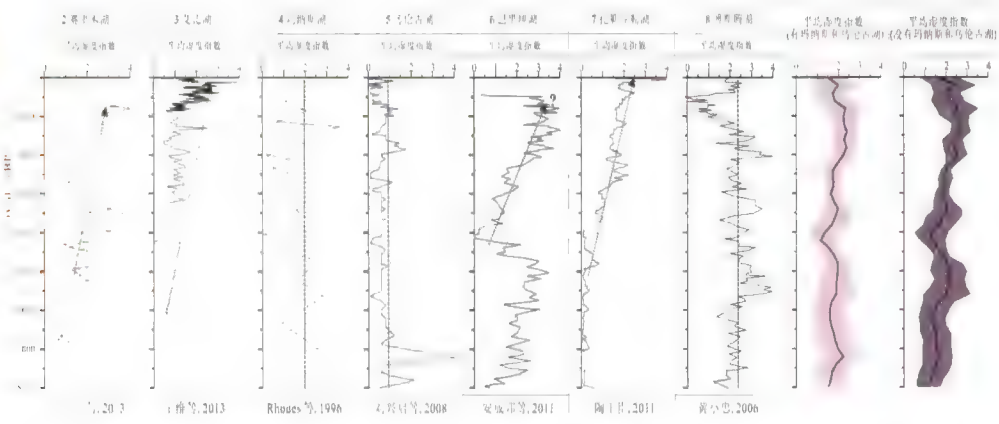

图8-10　七条基于A/C值的标准化湿度指数（SMI）曲线，没有包括玛纳斯湖和乌伦古湖曲线的平均指数曲线（倒数第二条曲线），和包括玛纳斯湖和乌伦古湖曲线的平均湿度指数曲线（最后一条曲线）（Ran and Feng, 2014）

为什么新疆北部过去8000年来的湿度呈增加趋势？原因可能有二。第一，全新世以来新疆北部有效湿度的增加可能与北大西洋地区的冬季温度的上升有关（图8-11）。过去8000年来北半球冬季太阳辐射的增加（Berger 和Loutre，1991）驱使北大西洋地区冬季温度的增加（Davis等，2003），导致了挪威冬季降雪的增加（Bakke等，2008）。与此同时，在冬季条件下盛行西风可能将更多的北大西洋水汽输送到新疆北部，导致新疆北部湿度的增加。第二，北大西洋涛动（NAO）和厄尔尼诺—南方涛动（ENSO）可能共同影响新疆北部的湿度变化。首先，当NAO正相时，盛行西风会从北大西洋输送更多的水汽到中亚地区（包括

新疆)(Aizen等,2001;Bother等,2012)。实际上,过去5000年来一直趋于正相的NAO(Olsen等,2012)可能是新疆北部湿度增加的直接驱动力(图8-11)。其次,最近观测到的ENSO活动和中亚西部(包括里海及其下风区)之间的关联也可以解释新疆北部湿度的增加。具体地讲,在ENSO活动时,在太平洋西部和印度洋北部上空形成一个强高压,该高压的反气旋作用与副热带急流共同作用,将阿拉伯海湾和赤道非洲的水汽注入到中亚西南部(即:里海附近及下风区)(Mariotti,2007)。同时,冬季南移的西风会将这股水汽从西中亚带到新疆北部。因此,过去6000年来ENSO活动增加趋势(Rein等,2005)也可能是造成新疆北部湿度增加的原因之一。

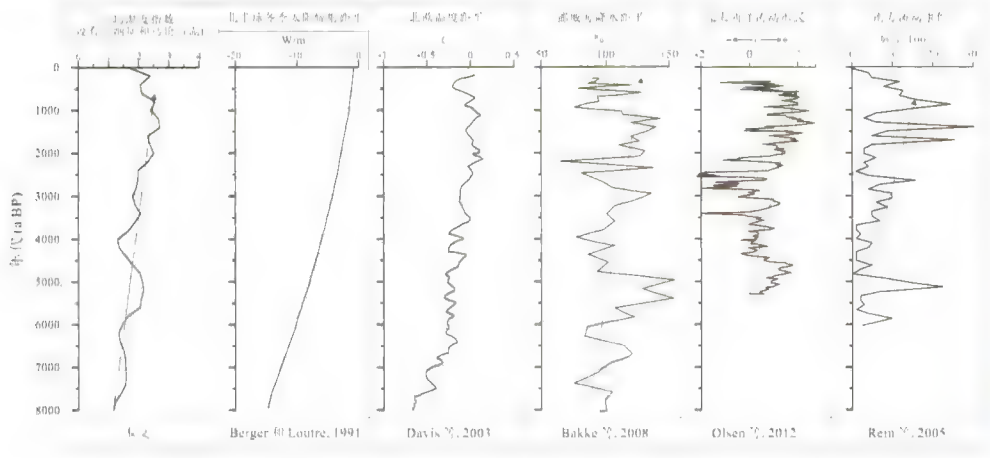

图8-11　新疆北部过去8000年平均湿度指数(Mean SMI)变化的可能驱动机理:北半球冬季辐射量(Berger和Loutre,1991)、北欧冬季温度(Davis等,2003)、挪威冬季降水(Bakke等,2008)、过去5000年北大西洋涛动(NAO)的变率(Olsen等,2012)、过去6000年的厄尔尼诺—南方涛动(ENSO)的变率(Rein等,2005)(Ran and Feng, 2014)

5.2. $\delta^{18}O$指示的湖水盐度变化

通常来说,干旱半干旱区封闭或半封闭湖泊湖水的盐度主要受控于蒸发/降水值,因而湖芯碳酸盐同位素组成($\delta^{18}O_{carb}$)主要受控于蒸发/降水值。但是,以冰川融水补给为主的封闭—半封闭湖泊湖水的盐度则是受融水多寡控制的,因而$\delta^{18}O_{carb}$记录的受控因子可能会比较复杂。玛纳斯湖$\delta^{18}O_{carb}$记录被认为是受东亚季风降水控制的(Lin和Wei,1998),而巴里坤湖和其他湖泊的$\delta^{18}O_{carb}$记录被认为是受西南季风和西风系统共同影响的(Zhong等,2010)。也就是说,$\delta^{18}O_{carb}$记录可能主要受控于降水水汽的来源。但是,在干旱半干旱区封闭或半封闭湖泊中,碳酸盐$\delta^{18}O_{carb}$总是与湖水盐度相关的(Fontes等,1996;Leng和Marshall,2004;Zhang等,2010)。本综述利用发表的$\delta^{18}O_{carb}$记录计算的六条标准化盐度指数(SSI)曲线显示(注:赛里木湖没有盐度资料),自8000年以来几乎所有曲线都呈上升趋势(图8-12),它们一致表明,新疆北部湖泊湖水盐度在过去8000年以来一直处于上升状态。

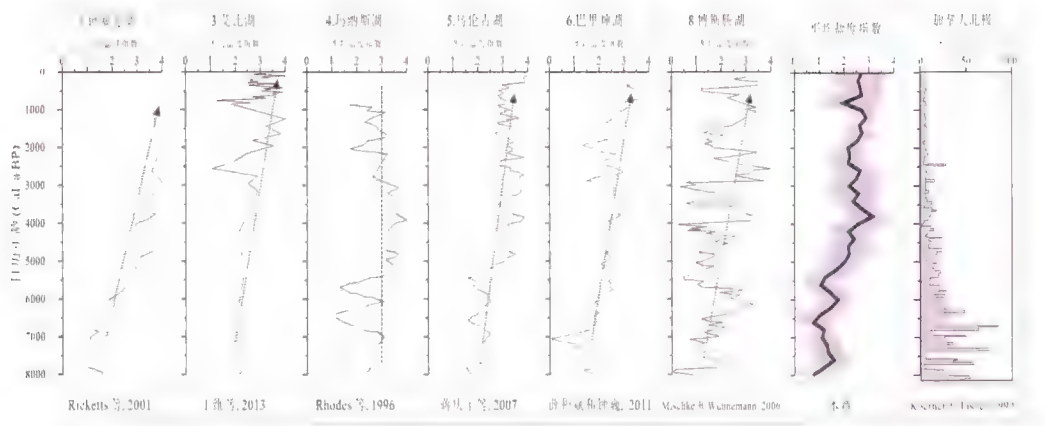

图8-12　六条基于δ ^{18}O值的标准化盐度指数(SSI)曲线和平均标准化盐度指数(Mean SSI),以及平均曲线与加拿大北极地区全新世冰盖残留面积(Koerner和Fisher,1990)的对比(Ran and Feng, 2014)

现在有一个突出的矛盾摆在我们面前：由孢粉A/C值反映的湿度在过去8000年一直是增加的,但由δ $^{18}O_{carb}$值表达的湖泊湖水盐度在过去8000年却也一直是增加的。也就是说，过去8000年以来新疆北部在气候变得越来越湿润的情况下湖水盐度变得越来越高。这个矛盾不能被温度的降低或降水的增加或者二者共同作用来解决。令人欣喜的是,全新世以来山区(天山和阿尔泰山)冰川面积的变化似乎能够提供一条解决途径。具体地讲,全新世冰川面积的变化可能控制了湖水盐度变化。这里,我们用加拿大北极地区全新世冰川的退缩历史(图8-12的最后一条曲线)(Koerner和Fisher,1990)来替代新疆北部全新世冰川的退缩历史(新疆北部没有这样的记录发表)。我们如此的替代应该是可以接受的，因为全新世新疆北部的冰川面积和加拿大冰盖面积均受北半球太阳辐射量的控制(Ruddiman,2008)。也就是说,全新世以来不断缩小的山地冰川面积导致了冰川融水的不断减少,继而引起湖水盐度的不断升高。孢粉A/C值所表达的过去8000年湿度的增加很可能是由变冷背景下降水的增加所致(Wanner等,2008)。总之,在变冷的条件下降水的增加导致了新疆北部湿度的增加,但是流域内湿度的增加未能弥补由于冰川面积减小所引起的湖水位的下降。换句话说,即使全新世流域内湿度不断增加,冰川融水的减少仍然使得湖泊湖水的盐度持续上升。

最后需要注意的是,乌伦古湖和玛纳斯湖在过去8000年湖水盐度的上升意味着湖水位一直是下降的(Liu等,2008)。这里我们提出两点质疑:第一,孢粉指标仅仅指示流域内湿度的变化，而以冰川融水补给为主的湖泊水位与流域湿度是没有关联的(Zhang等,2010;Feng等,2013);第二,湖相沉积物粒度组成可能指示湖水位的高低(即采样点距入水口的距离),也可以指示河流的动力的状况(即进水量的大小)(沈吉等,2010)。换句话说,较粗的颗粒可能指示湖水位下降(即:距离入水口更近),也可能指示河流流量的增加。看来,全新世乌伦古湖水位的上升推论值得商榷。虽然最近发表的资料都支持"西风主导新疆北部全新世气候变化"的说法(见Chen等,2008;Ran和Feng,2013;Wang和Feng,2013),但是基于玛纳斯湖记录推断的"东亚季风影响新疆北部全新世气候变化"的早期

说法(Rhodes等,1996;孙湘君等,1994)仍然受到最近来自伊犁河谷资料的支持(Li等,2011;Cheng等,2012)。

6. 结论

五个湖泊序列中(赛里木湖、艾比湖、巴里坤湖、托勒库勒湖、博斯腾湖)基于A/C值的标准化湿度指数曲线比较结果揭示,过去8000年以来区域湿度呈增加趋势,这一趋势很可能与北大西洋地区的冬季温度和北大西洋涛动(NAO)有直接的关联,即过去8000年来逐渐趋于正相的北大西洋涛动NAO和逐渐升高的北大西洋地区的冬季温度通过盛行西风向新疆北部输送更多水汽。

七个湖泊序列中(除上述五个湖泊外,还有玛纳斯湖和乌伦古湖)基于碳酸盐 $\delta^{18}O_{carb}$ 值的标准化盐度指数曲线比较结果揭示,过去8000年来新疆北部湖泊盐度不断增加。盐度不断增加的原因很可能是由天山和阿尔泰山冰川面积不断减小所致。具体地讲,全新世山区的冰川面积不断减小,导致补给湖泊的冰川融水持续下降,最终引起湖水盐度的持续上升。

不过,我们遇到了一个突出的矛盾是:为什么过去8000年新疆北部在湿度增加背景下湖水盐度却越来越高?最令人信服的解释是:在温度下降的条件下降水增加可能导致了新疆北部湿度的增加。但是,冰川融水的不断减少使得湖水的盐度持续上升。

致谢:成文过程中得到了以下人士的帮助:张东良先生,兰波先生,杨运鹏先生,王艳楠先生。

参考文献

陈发虎,黄小忠,杨美林,杨勋林,范育新,赵晖. 2006. 亚洲中部干旱区全新世气候变化的西风模式. 第四纪研究,26:881~887.

陈曦. 2010. 中国干旱区自然地理. 北京:科学出版社.

黄小忠. 2006. 新疆博斯腾湖记录的亚洲中部干旱区全新世气候变化研究[博士论文], 兰州大学

胡汝骥. 2004. 中国天山自然地理. 北京: 中国环境科学出版社.

林瑞芬,卫克勤,程致远,Gasse, F., Fontes,J.C., Gibert, E. 1996. 新疆玛纳斯湖沉积柱样的古气候古环境研究. 地球化学,25: 63~72.

林瑞芬, 卫克勤. 1998. 新疆玛纳斯湖沉积物氧同位素记录的古气候信息探讨——与青海湖的色林错比较. 第四纪研究,4:308~318.

沈吉,薛滨,吴敬禄,吴艳宏,刘兴起,羊向东,刘健,王苏民. 2010. 湖泊沉积与环境演化. 北京: 科学出版社,pp 473.

孙湘君, 杜乃秋, 翁成郁, 林瑞芬, 卫克勤. 1994. 新疆玛纳斯湖盆周围近14000年以来的古植被古环境. 第四纪研究,3:239~248.

陶士臣. 新疆东部湖泊沉积花粉记录的全新世植被与环境 [博士论文], 兰州大学,2011.

Aizen, E.M., Aizen, V.B., Melack, J.M., Nakamura, T. and Ohta, T., 2011. Precipitation and atmospheric circulation patterns at mid-latitudes of Asia. International Journal of Climatology, 21: 535~556.

An, C.B., Lu, Y.B., Zhao, J.J., Tao, S.C., Dong, W.M., Li, H., Jin, M. and Wang, Z.L., 2011. A high-resolution

record of Holocene environmental and climatic changes from Lake Balikun (Xinjiang, China): Implications for central Asia. The Holocene, 22: 43~52.

Bakke, J., Lie, O., Dahl, S., Nesje, A. and Bjune, A.E., 2008. Strength and spatial patterns of the Holocene wintertime westerlies in the NE Atlantic region. Global and Planetary Change, 60: 28~41.

Berger, A. and Loutre, M.F., 1991. Insolation values for the climate of the last 10 million years. Quaternary Science Reviews, 10: 297~317.

Blyakharchuk, T.A., Wright, H.E., Borodavko, P.S., van der Knaap, W.O. and Ammann, B., 2007. Late Glacial and Holocene vegetational history of the Altai Mountains (southwestern Tuva Republic, Siberia). Palaeogeography, Palaeoclimatology, Palaeoecology , 245 (3~4): 518~534.

Bothe, O., Fraedrich, K. and Zhu, X., 2012. Precipitation climate of Central Asia and the large-scale atmospheric circulation. Theoretical and Applied Climatology, 108: 345~354.

Charman, D.J., 2002. Peatland Systems and Environmental Change. John Wiley&Sons, New York.

Chen, F.H., Yu, Z.C., Yang, M.L., Ito, E., Wang, S.M., Madsen, D.B., Huang, X.Z., Zhao, Y., Sato, T., Birks, H.J.B., Boomer, I., Chen, J.H., An, C.B. and Wünnemann, B., 2008. Holocene moisture evolution in arid central Asia and its out-of-phase relationship with Asian monsoon history. Quaternary Science Reviews, 27: 351~364.

Cheng, H., Zhang, P.Z., Spotl, C., Edwards, R.L., Cai, Y.J., Zhang, D.Z., Sang, W.C., Tan, M. and An, Z. S., 2012. The climatic cyclicity in semiarid-arid central Asia over the past 500,000 years. Geophysical Research Letters, 39: L01705.

Davis, B.A.S., Brewer, S., Stervenson, A.C., Guiot, J. and other data contributors, 2003. The temperature of Europe during the Holocene reconstructed from pollen data. Quaternary Science Reviews, 22: 1701~1706.

Demske, D., Heumann, G., Granoszewski, W., Nita, M., Mamakowa, K., Tarasov, P.E. and Oberhensli, H., 2005. Late glacial and Holocene vegetation and regional climate variability evidenced in high-resolution pollen records from Lake Baikal. Global. Planetary Change, 46: 255~ 279.

El-Moslimany, A.P., 1990. Ecological significance of common non-arboreal pollen: examples from drylands of the Middle East. Review of Palaeobotany and Palynology, 64: 343~350.

Feng, Z-.D., An, C.B. and Wang, H.B., 2006. Holocene Climatic and Environmental Changes in the Arid and Semiarid Regions of China: A Review. The Holocene, 16: 1~12.

Feng, Z.-D., Wu, H.N., Zhang, C.J., Ran, M., and Sun, A.Z., 2013. Bioclimatic change of the past 2500 years within Balkhash Basin in the eastern Kazakhstan of Central Asia. Quaternary International, 311: 63~70.

Fontes, J.C., Gasse, F. and Gibert, E., 1996. Holocene environmental changes in Lake Bangong basin (Western Tibet). Part1: Chronology and stable isotopes of carbonates of a Holocene lacustrine core. Palaeogeography, Palaeoclimatology, Palaeoecology, 24:25~47.

Herzschuh, U., 2006. Palaeo-moisture evolution in monsoonal Central Asia during the last 50,000 years. Quaternary Science Reviews, 25: 163~178.

Huang, X.Z., Chen, F.H., Fan, Y.X. and Yang, M.L., 2009. Dry late-glacial and early Holocene climate in arid central Asia indicated by lithological and palynological evidence from Bosten Lake, China. Quaternary International, 194: 19~27.

Jiang,Q.F., Shen, J., Liu, X.Q.,Zhang, E.L. and Xiao, X.Y., 2007. A high-resolution climatic change since Holocene inferred from multi-proxy of lake sediment in westerly area of China. Chinese Science Bulletin, 52

(14): 1970~1979.

Jiang, Q.F., Ji, J.F., Shen, J., Matsumoto, R.Y.O., Tong, G.B., Qain, P., Ren, X.M. and Yan, D.Z., 2013. Holocene vegetational and climatic variation in westerly-dominated areas of Central Asia inferred from the Sayram Lake in northern Xinjiang, China. Science China: Earth Sciences, 56: 339~353.

Koerner, R.M. and Fisher, D.A., 1990. A record of Holocene summer climate from a Canadian high-Arctic ice core. Nature, 343: 630~31.

Leng, M.J. and Marshall, J.D., 2004. Palaeoclimate interpretation of stable isotope data from lake sediment archives. Quaternary Science Reviews, 23: 811~31.

Li, X.Q., Zhao, K.L., Dodson, J. and Zhou, X.Y., 2011. Moisture dynamics in central Asia for the last 15kyr: new evidence from Yili Valley, Xinjiang, NW China. Quaternary Science Reviews, 30: 3457~3466.

Liu, X.Q., Herzschuh, U., Shen, J., Jiang, Q. and Xiao, X., 2008. Holocene environmental and climatic changes inferred from Wulungu Lake in northern Xinjiang, China. Quaternary Research, 70: 412~425.

Ma, Y.Z., Liu, K.B., Feng, Z.-D., Sang, Y.L., Wang, W. and Sun, A.Z., 2008. A survey of modern pollen and vegetation along a south-north transect in Mongolia. Journal of Biogeography, 35: 1512~1532.

Mariotti, A., 2007. How ENSO impacts precipitation in southwest central Asia. Geophysical Research Letters, 34: L16706.

Meeker, L.D. and Mayewski, P.A., 2002. A 1400-year high-resolution record of atmospheric circulation over the North Atlantic and Asia. The Holocene, 12: 257~266.

Mischke, S. and Wünnemann, B., 2006. The Holocene salinity history of Bosten Lake (Xinjiang, China) inferred from ostracod species assemblages and shell chemistry: possible palaeoclimatic implications. Quaternary International, 154-155: 100~112.

Olsen, J., Anderson, N.J. and Knudsen, M.F., 2012. Variability of the North Atlantic Oscillation over the past 5, 200 years. Nature Geoscience, 5: 808~812.

Ran, M., Feng, Z.-D., 2013. Holocene moisture variations across China and driving mechanisms: a synthesis of climatic records. Quaternary International, 313/314: 179~193.

Ran, M. and Feng, Z.D., 2014. Climatic and Hydrological Variations during the Past 8000 Years in Northern Xinjiang of China and the Associated Mechanisms. Quaternary International, http://dx.doi:10.1016/j.quaint.2014.07.056.

Reimer, P.J., Baillie, M.G.L. and Bard, E., 2009. IntCal09 and Marine radiocarbon age calibration curves, 0-50 000 years cal BP. Radiocarbon, 51: 1111~1150.

Rein, B., Luckge, A., Reinhardt, L., Sirocko, F., Wolf, A. and Dullo, W.C., 2005. El Nino variability off Peru during the last 20,000 years. Paleoceanography, 20: 4003.

Ricketts, R.D., Johnson, T.C., Brown, E.T., Rasmussen, K.A. and Romanovsky, V.V. , 2001. The Holocene paleolimnology of Lake Issyk-Kul, Kyrgyzstan: trace element and stable isotope composition of ostracodes. Palaeogeography, Palaeoclimatology, Palaeoecology, 176: 207~227.

Rhodes, T.E., Gasse, F., Lin, R. F., Fontes, J.C., Wei, K.Q., Bertrand, P., Gibert, E., Melieres, F., Tucholka, P., Wang, Z.X. and Cheng, Z.Y., 1996. A late Pleistocene-Holocene lacustrine reocrd from Lake Manas, Zunggar (northern Xinjiang, western China). Palaeogeography, Palaeoclimatology, Palaeoecology, 120: 105~121.

Rudaya, N., Tarasov, P., Dorofeyuk, N., Solovieva, N., Kalugin, I., Andrew, A., Dryin, A., Diekmann, B.,

Riedel, F.,Tserendash,N. and Wagnere, M., 2009. Holocene environments and climate in the Mongolian Altai reconstructed from the Hoton-Nur pollen and diatom records: a step towards better understanding climate dynamics in central Asia. Quaternary Science Reviews, 28: 540~554.

Ruddiman, W.F., 2008. Earth's Climate: Past and Future. Freemand and Company, New York.

Staubwasse, M. and Weiss, M., 2006. Holocene climate and cultural evolution in late prehistoric-early historic West Asia. Quaternary Research, 66: 372~387.

Sorrel, P., Popescu, S.M., Klotz, S., Suc, J.P. and Oberhansli, H., 2007. Climate variability in the Aral Sea basin (Central Asia) during the late Holocene based on vegetation changes. Quaternary Research, 67: 357~370.

Tarasov, P., Jin, G.Y. and Wagner, M., 2006. Mid-Holocene environmental and human dynamics in northeastern China reconstructed from pollen and archaeological data. Palaeogeography, Palaeoclimatology, Palaeoecology, 241: 284~300.

Wang, W. and Feng, Z.-D. Holocene moisture evolution across the Mongolian Plateau and its surrounding areas: A synthesis of climatic records. Earth-Science Reviews, 122: 38~57.

Wang, W., Feng, Z.-D., Ran, M. and Zhang, C.J., 2013. Holocene climate and vegetation changes inferred by pollen records from Lake Aibi of northern Xinjiang, China. Quaternary International, 311: 54~62.

Wanner, H., Beer, J., Bütikofer, J., Growley, T.J., Cubasch, U., Flückiger, J., Goosse, H., Grosjean, M., Joos, F., Kaplan, J.O., Küttel, M., Müller, S.A., Prentice, I.C., Solomina, O., Stocker, T.F., Tarasov, P., Wagner, M. and Widmann, M., 2008. Mid- to Late Holocene climate change: an overview. Quaternary Science Reviews, 27: 1791~1828.

Winkler, M.G. and Wang, P.K., 1993. The late-Quaternary vegetation and climate of China. In: Wright Jr., H.E.,Kutzbach, J.E., Webb III, T., Ruddiman, W.F., Street- Perrott, F.A., Bartlein, P.J. (Eds.), Global Climates Since The Last Glacial Maximum. University of Minnesota Press, Minneapolis, pp 2210~261.

Wu, J.L. and Wang, S.M., 1997. Carbonate 18O- and 13C-recorded environmental changes in RM lake core in Zioge of the eastern Tibetan Plateau. Marine Geology and Quaternary Geology, 17: 63~71 (in Chinese).

Wünnemann, B., Mischke, S. and Chen, F., 2006. A Holocene sedimentary record from Bosten lake, China. Palaeogeography, Palaeoclimatology, Palaeoecology, 234: 223~238.

Xue, J.B. and Zhong, W., 2011. Holocene climate variation denoted by Barkol Lake sediments in northeastern Xinjiang and its possible linkage to the high and low latitude climates. Science China Earth Science, 54: 603~614.

Zhang,C.J., Feng,Z.-D., Yang,Q.L. ,Guo,X.H. and Sun,F.F., 2010. Holocene environmental variations recorded by organic-related and carbonate-related proxies of the lacustrine sediments from Bosten Lake, northwestern China. The Holocene, 20: 363~373.

Zhao, Y., Yu, Z.C., Chen, F.H., Zhang, J.W. and Yang, B., 2009. Vegetation response to Holocene climate change in monsoon-influenced region of China. Earth-Science Reviews, 97: 242~256.

Zhao, Y., Liu, H.Y., Li, F.R., Huang, X.Z., Sun, J.H., Zhao, W.W., Herzschuh, U. and Tang, Y., 2012. Application and limitations of the Artemisia/Chenopodiaceae pollen ratio in arid and semi-arid China. The Holocene, 22: 1385~1392.

Zhong, W., Xue, J.B., Li, X.D., Xu, H.J. and Jun, O.A., 2010. Holocene Climatic Record Denoted by Geochemical Indicators from Barkol Lake in the Northeastern Xinjiang, NW China. Geochemistry International, 48: 792~800.

第九章

哈萨克斯坦东部巴尔喀什湖(Balkhash Lake)湖芯记录的过去2500年气候与水文的变化

冯兆东[①]　　冉　敏[②]

① 中国科学院 新疆生态与地理研究所

② 西南大学 地理科学学院

我们从巴尔喀什湖获取了一根850cm长的湖芯钻孔，测定了17个AMS年代，利用碳酸盐含量以及$\delta^{18}O$重建了湖水盐度，利用孢粉的A/C值和孢粉浓度重建了流域湿度。我们还采用气候—孢粉响应面的方法重建了流域年平均温度(MAT)和年平均降水(MAP)。我们的重建支持以前盛行的观点：西风带主导区的气候变化基本上是以冷湿模式和暖干模式为特征的。巴尔喀什盆地在过去约2500年经历了3个阶段的气候变迁：约2500~1800 cal. yr BP为冷湿，约1800~650 cal. yr BP相对暖干，约650~0 cal. yr BP为冷湿，其中最近100年来呈现暖干趋势。重建的流域湿度与年平均降水(MAP)的变化趋势是基本一致的。但是，年平均温度(MAT)也明显地影响了流域湿度，例如，高温导致蒸发加强，从而使流域湿度下降。湖泊盐度则主要受控于区域温度，例如，低温导致山区冰川融水减少，入湖淡水量下降，湖水的盐度因此而增加。其次，湖泊盐度也受控于较大幅度的流域湿度变化。值得指出的是，较小幅度的流域湿度波动对盐度的影响微乎其微。

1. 前言

过去约2500年来全球的气候变化主要受控于叠加于轨道驱道因子上的太阳活动(Ruddiman，2008；Mann 等，2009)。较小空间尺度上的陆—气相互作用和较短时间尺度上的人类活动与火山喷发都被确认为是影响气候变化的扰动因子(Anderson，2002；Bridgman 和 Oliver，2006；Bauer 等，，2003；Maasch 等，2005)。

巴尔喀什流域(我们的研究区)所在的中亚干旱区(CAAZ)指西起里海，东至阿尔泰山脉的广大干旱地区(图 9-1)。由于其南边东—西走向的天山山脉(北纬 40°附近)阻挡了阿拉伯海的气候影响，巴尔喀什流域的气候主要受西风带的控制(Gong 等，2001；Heorling 等，2001；Staubwasse 和 Weiss，2006)。巴尔喀什流域位于中亚干旱区(CAAZ)东部，其降水受到多个因素调控：暖季由于西风带北移，降水的水汽主要来自北大西洋；而冷季由于西风带南移，降水的水汽主要来自地中海 (Aizen 等，2001；Bridgman 和 Oliver，2006；

Bothe 等，2011）。特别值得提及的是，极锋的频繁南侵是促成该流域形成降水最为重要的机制（Lydolph，1997；Aizen 等，2001）。进而，巴尔喀什流域冷季气候受到西风带和北大西洋涛动（NAO）相互作用的影响，而暖季气候受控于占据亚洲内陆的亚洲低压和延伸至中亚干旱区的亚速尔高压的调控（Aizen 等，2001；Meeker 和 Mayewski，2002）（图 9–2）。整个全新世（过去约 11 500 年以来）期间的中亚干旱区气候也被认为是由西风带主导的。如此认为的理由是：重建的中亚干旱区全新世气候记录与重建的西欧全新世气候记录有很好的一致性，也就是说，与东亚季风区暖湿模式和冷干模式（Shi 等，1993；Holme 等，2009）不同，西风带主导区全新世气候变化主要以暖干模式或冷湿模式为特征（见 Geel 等，2004；Yang 等，2002，2009；Kroonenberg 等，2007；Boomer 等，2009）。

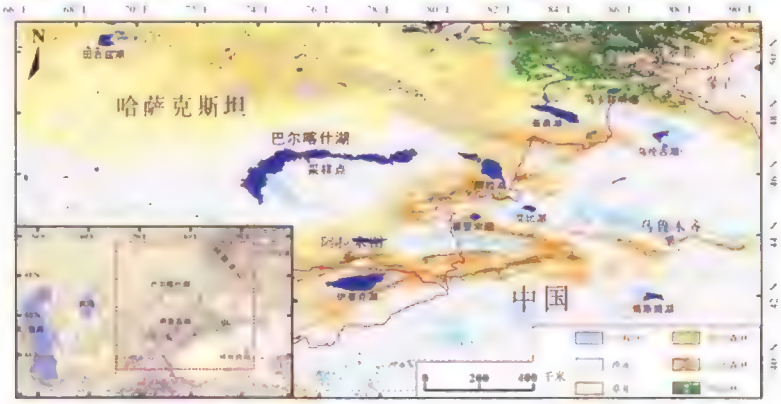

图9–1　巴尔喀什湖流域植被图。左下角小图显示巴尔喀什湖与里海和咸海的位置关系

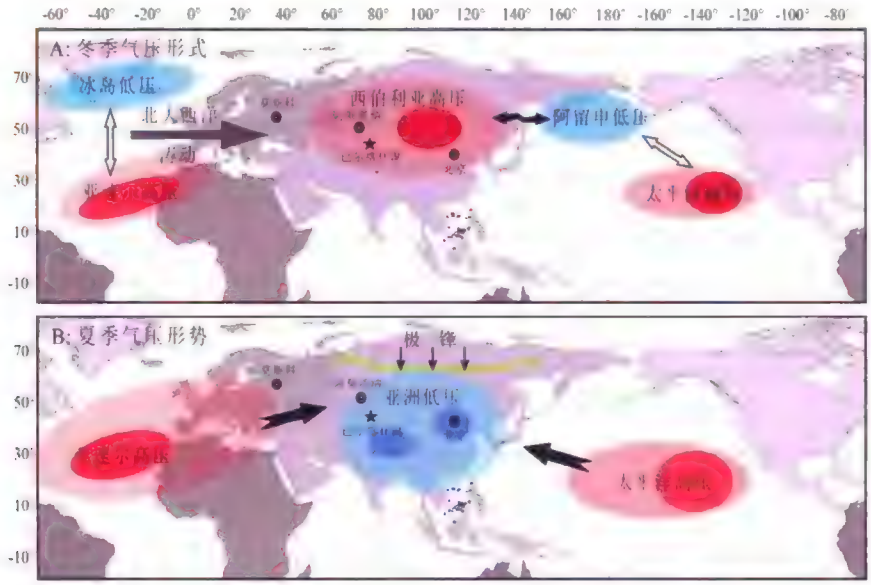

图9–2　冬季气压系统（A）：西伯利亚高压强度取决于两个因子：1 亚洲大陆内部和太平洋的气压差，2 西伯利亚高压—阿留申低压系统与西伯利亚—冰岛低压系统之间的空间动力反差。夏季气压系统（B）：亚洲低压不仅诱使太平洋高压深入亚洲内部形成东亚夏季季风，还诱使了亚速尔高压对中亚干旱区的渗透（注意：a. 浅红色大圈中的深红色小圈为高压气团中心；b. 浅蓝色大圈中的深蓝色小圈为低压气团中心）

然而，已有的资料和解译都不能明确地支持中亚干旱区全新世暖干和冷湿的气候模式。先举两个支持暖干和冷湿模式的例子。里海湖岸阶地记录到的两个高湖水位期发生在大约 2600 cal. yr BP 和大约公元 1600 年，正好对应于太阳活动较弱的全球变冷期(Kroonenberg 等，2007；Boomer 等，2000，2009)。由鞭毛藻记录到的过去约 2000 年咸海高盐度期(干旱期)均发生在较温暖时期(如 AD 0~400，AD 900~1350，AD1800 至今)。上述证据似乎都支持暖干或冷湿气候模式。然而，咸海也存在高盐度期出现在较寒冷时期(AD 1500 和 AD 1650)的情形，这一情形对暖干—冷湿气候模式构成了挑战。另外，在咸海重建的风尘历史表明，较寒冷时期更强的西伯利亚高压将更多的风成沙带到了咸海(Huang 等，2011)。进而，咸海的风尘记录和土耳其湖芯 $\delta^{18}O$(Jones 等，2006)的对比显示，冷期既是咸海的多风沙期，也是地中海水汽向中亚西部输送水汽较少的时期，这与亚洲季风区的暖湿—冷干气候模式完全一致，而与已被广泛接受的暖干—冷湿中亚气候模式完全相反。还有，咸海的孢粉资料表明，该地区的气候既不符合暖干—冷湿模式，也不遵从"太阳活动主导大范围温度变化"的模式。具体地讲，孢粉资料显示，AD 0~400、AD 900~1150、AD 1500~1650 气候冷干，沙漠植被扩张；AD 400~900、AD 1150~1450 气候暖湿，干草原植被扩张(Sorrel 等，2006)。需要指出的是，大范围地讲，AD 900~1150 应为中世纪大暖期，而 AD 1150~1450 已经进入了小冰期。

然而，尽管上述的资料和资料解译之间的不一致和相互矛盾问题十分严重，但如果我们能更周全地考虑到控制盐度、植被、风沙等因子，这些不一致和相互矛盾的问题也许可能得到和解。例如，如果湖水主要由冰川融水供给，其盐度则受控于温度，与流域降水无关(Sorrel 等，2007)。如果向湖输送沙子源区的沙量不是限制因子，入湖的风沙量可能主要受控于大气环流，与流域植被覆盖度的关系不大(Huang 等，2011)。我们倾向于接受下列主张：流域植被也许最能真实地反映流域气候，因此流域内封闭湖泊的孢粉记录能够追溯过去气候的变化(Blyakharchuk 等，2007；Tarasov 等，2007；Rudaya 等，2009)。本章重建了巴尔喀什流域过去约 2500 年的生物气候变化，谋求解决上述资料和资料解译之间不一致和矛盾问题的一部分。

2. 区域概况

巴尔喀什湖是亚洲最大的湖泊之一(坐标范围为 73°N~80°N，44°E~47°E)，有七条河流补给该湖，其中来自天山的伊犁河是最主要的补给河流。巴尔喀什湖的面积为 16 400km^2，根据水文特征可将其划分为两个部分：西部的淡水区和东部的咸水区。自有观测记录以来，湿润年份的湖泊面积超过 18 000km^2，而干旱年份的湖泊面积则不到 16 000km^2(Petr，1992)。湖泊所在的区域为温带大陆性气候，7 月的平均温度为 30℃，1 月的平均温度为 -14℃。年平均温度为(MAT)6℃，年平均降水量(MAP)为 150mm，年平均蒸发量高达 1000mm(Propastin，2011)。盆地范围的年平均温度为 3℃~10℃，盆地范围的年平均降水量为 130~450mm(郭利丹等，2008)。湖滨的植被是以科杨属为主的河岸森林，以及包括芦苇和印度香蒲属在内的湿地种属。巴尔喀什盆地东北部的植被为针叶林(例如阿勒泰

山)、东南部为山区森林(例如天山)、北部为草原森林、西部为沙漠(ESA UCLouvain, 2010)。山区植被的垂直带由上而下为:苔原、高山草甸、针叶林、森林—草原(落叶树—灌木—草原混合体)、干草原、沙漠。

3. 材料和方法

3.1. 采样及组分分析

我们于2007年夏天在巴尔喀什湖西侧淡水区最东端利用Livingtone型活塞钻获取了一根850cm的湖芯(46.4°N, 75.6°E)，并对选取的17个全样在亚利桑那大学的NSF-AMS加速质谱仪进行了AMS ^{14}C测年(表9-1)。我们对湖芯按2cm间隔分样(共计389个样品)，测定了它们的总有机碳(TOC)、碳酸钙($CaCO_3$)和氧同位素($\delta^{18}O_{calc}$)。总有机碳用酸式反滴定法(主要试剂为浓H_2SO_4和$K_2Cr_2O_7$)测定。碳酸盐含量的测定是通过以下两个步骤完成的:先用稀释的1N HCl释放样品中的CO_2，然后计算释放的CO_2体积。氧同位素测定程序如下:先筛选出小于40μm的细颗粒，再加入磷酸酸化以释放CO_2，最后将收集到的CO_2进行纯化，并转入Finnigan Delta plus质谱仪进行氧同位素的分析。粒度分析仅选取了190个样品(注:完成其他代用指标的测定后，400~250cm段的样品因样品量不足而无法完成粒度分析)，利用Malvern Mastersizer 2000激光衍射粒度分析仪完成了测定。粒度分析的前处理包括:①用H_2O_2除去有机质和溶解盐;②用1N HCl除去碳酸盐;③用($NaPO_3$)分解(解散)样品的颗粒团聚体。上述所有理化指标的测定均在兰州大学西部环境教育部重点实验室完成。

表9-1 巴尔喀什湖湖芯沉积物AMS ^{14}C测年结果

样品编号	深度(cm)	测年材料	$\delta^{13}C$(‰)	^{14}C年代 (yr BP)	去碳库效应后校正年代 (2δ) (cal. yr BP)
BK-A-1	0~2	沉积物	-24.1	910±40	0
BK-A-2	50~52	沉积物	-24.7	1151±33	265~331
BK-A-3	100~102	沉积物	-23.6	1390±40	475~556
BK-A-4	150~152	沉积物	-25.6	1336±33	434~529
BK-A-5	200~202	沉积物	-23.7	1570±40	553~612
BK-A-6	248~250	沉积物	-24.2	1640±33	652~728
BK-A-7	300~302	沉积物	-23.9	1410±40	496~559
BK-A-8	350~352	沉积物	-25.5	1473±34	585~646
BK-A-9	400~402	沉积物	-23.6	1870±40	784~938
BK-A-10	450~452	沉积物	-24.7	2134±34	1168~1291
BK-A-11	500~502	沉积物	-23.9	2624±34	1545~1703
BK-A-12	550~552	沉积物	-25.4	2736±40	1692~1869
BK-A-13	600~602	沉积物	-23.6	2920±40	1876~2061
BK-A-14	610~612	沉积物	-23.6	3040±40	1995~2180

续表9-1

样品编号	深度(cm)	测年材料	δ ^{13}C(‰)	^{14}C年代 (yr BP)	去碳库效应后校正年代 (2δ) (cal. yr BP)
BK-A-15	650~652	沉积物	−25.4	3061±40	2038~2184
BK-A-16	750~752	沉积物	−24.7	3239±35	2307~2460
BK-A-17	850~852	沉积物	−11.7	3271±34	2330~2488

3.2. 孢粉分析

我们对湖芯按4cm间隔分样，共获取207个孢粉样品。孢粉分析预处理的流程如下：称取5~10g干样，加入一片已知浓度的石松孢子，用于计算孢粉浓度(Moore等，1991)，用10%的HCl除去碳酸盐，用10%的KOH除去腐殖酸，用36%的HF除去硅酸盐；余留沉淀物中的孢粉是经过超声波配合下的7μm筛选获得的；将获取的孢粉(实际上是孢粉浓缩液)用无水甘油制成电镜薄片；孢粉鉴定是在400~1000倍偏光显微镜下完成的，每个样品至少鉴定了300粒孢粉。在孢粉鉴定过程中，我们参照了工具书中的孢粉图谱(王伏雄等，1995)以及我们自己从中国北方采集到的200多种植物的孢粉样片。孢粉浓度是根据外加石松孢子的浓度进行计算(用粒/g表示)。孢粉制图是借助Tilia软件完成的，孢粉组合带的划分是借助CONISS程序完成的。

首先，我们计算了A/C值，因为该比值是一个被广泛用来评估亚洲干旱半干旱地区湿度(干旱度)变化的半定量指数(El-Mosilimany，1990；Liu等，2008；Van Campo等，1996；Zhao，2009，2012)。然后，我们用下列3种孢粉定量重建方法重建了年均温(MAT)和年均降水(MAP)：1.气候—孢粉响应面法(CPRS)；2.气候—孢粉转化函数法(CPTF)；3.植物功能型—现代类似法(PFT-MAT)。CPRS方法是基于采自中国北方(包括毗邻我们研究区——巴尔喀什湖盆地的新疆)的215个现代表层土样孢粉数据库构建的(宋长青等，1997)；CPTF方法是基于蒙古国和中国华北东部646个表层土样孢粉数据库构建的(Wen等，2013)；PFT-MAT方法是通过比较现代孢粉数据库和化石孢粉数据库的亲缘关系构建的，它所依赖的现代孢粉数据库包括211个中国的表层土样孢粉和1855个欧洲及苏联的表层土样孢粉(Jiang等，2009；Guiot等，1993；Tarasov等，1998)。

4. 结果

4.1. 地层和年代

巴尔喀什湖芯的地层可分为三个沉积单元(图9-3)，第一单元(650~850cm)为黏土质粉砂，有机质和碳酸盐的含量高于平均值；第二单元(120~650cm)为粉砂质黏土，有机质含量(2%)、碳酸盐含量(55%)接近平均值；第三单元(0~120cm)为砂质黏土，有机质含量和碳酸盐含量低于平均值。湖芯最上部的测年为910 ^{14}C yr BP(0~2cm)，我们认为这是"碳库效应"造成的，假设"碳库效应"在整个湖芯的差别并不明显，我们对每个碳^{14}C年龄

都进行了校正(即消除"碳库效应"造成的年龄误差)。所有年代(已经消除"碳库效应"的影响)应用 CALIB 6.0 INTCAL 程序进行了校正,得到了日历校正年龄。最后,通过最佳拟合法建立了年龄—深度的线性关系(图 9–3)。

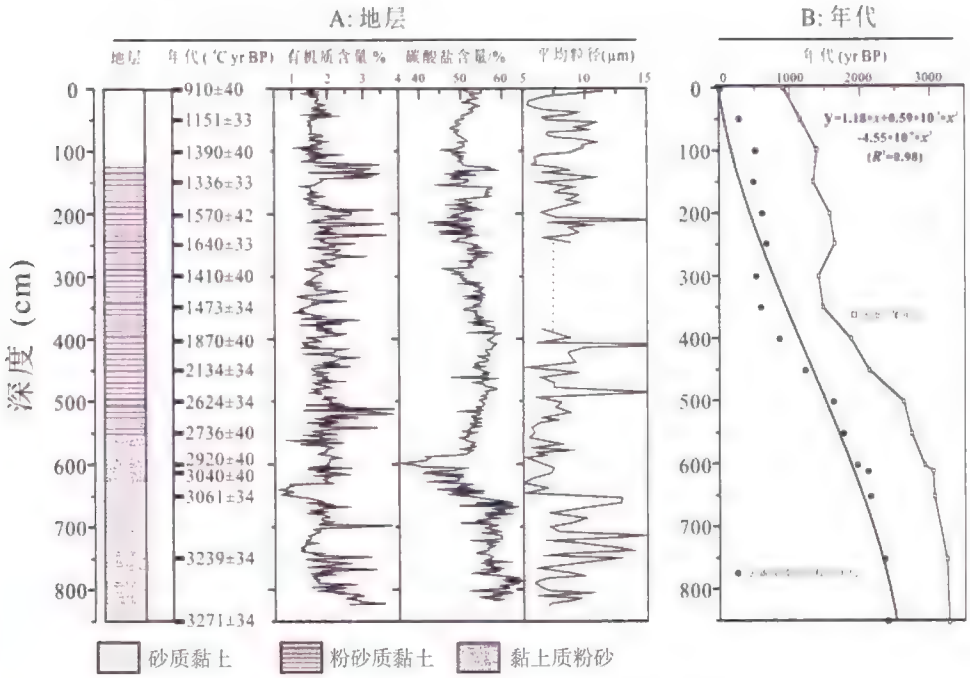

图9–3 巴尔喀什湖芯的岩性和年代(Feng等,2013)

4.2. 孢粉资料

我们采用基于约束最小二乘增量总和的群组分析法(CONISS)对巴尔喀什湖芯的孢粉资料进行了孢粉学聚类分带,聚类分带(即孢粉组合带)将巴尔喀什湖芯划分为 4 个孢粉带(图 9–4)。总体来说,孢粉谱中草本植物的孢粉主导着孢粉谱,乔木的孢粉不占优势。由于采用 CONISS 法划分的孢粉亚带之间的差别并不明显,我们的讨论仅仅关注主要孢粉带(如图 9–4 中的孢粉带 1~4)。

孢粉带1(588~850cm;约2500~1830 cal. yr BP):与上覆带(即孢粉带2)的孢粉组合相比,该组合的特点是:①喜湿植物的孢粉含量较高(如蔷薇科,柽柳科,十字花科,蒿属,乔木科);②喜旱植物的孢粉含量较少(如蒺藜科,藜科,麻黄属);③孢粉浓度相当高。

孢粉带2(288~588cm;约1830~725 cal. yr BP):该组合中喜湿植物的孢粉含量有所下降(例如蔷薇科,柽柳科,蒿属,十字花科,乔木科),而喜旱植物的孢粉有所增加(例如蒺藜科,藜科,麻黄属),孢粉的浓度明显低于孢粉带 1。

孢粉带3(40~288cm;约725~60 cal. yr BP):该组合中喜旱植物的群孢粉含量持续增加(如蒺藜科,藜科,麻黄属),孢粉浓度持续下降。同时,喜湿植物的孢粉含量持续减少(如蔷薇科,柽柳科,十字花科,乔木科)。

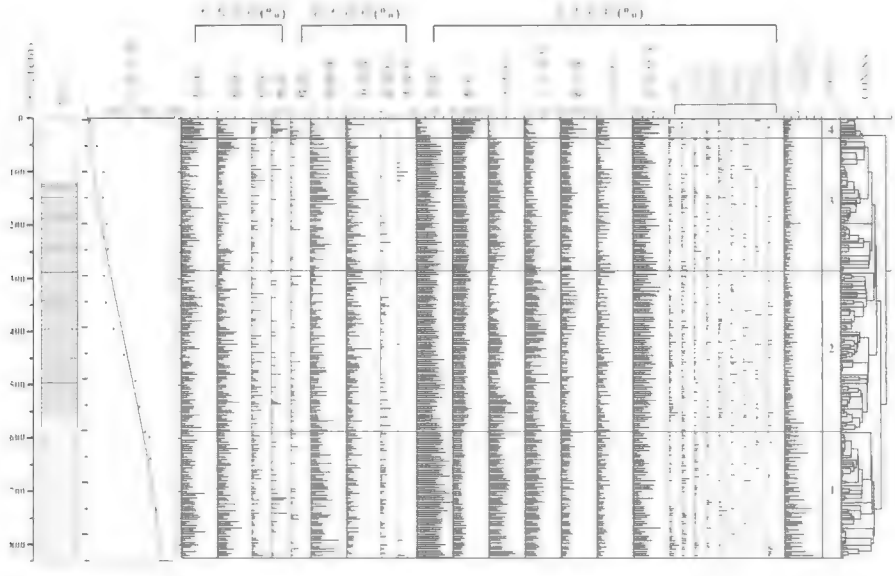

图9-4　巴尔喀什湖芯的孢粉谱自(Feng等,2013)

孢粉带4(0~40cm;约60~0 cal. yr BP):该组合中藜科孢粉含量显著增加,蒿藜科霸王属孢粉含量略有增加,而蒿属和禾本科孢粉含量随之减少。造成这些变化的原因是干旱度的增加,而导致干旱度增加的原因可能是过去 60 年气候的迅速变暖(Lioubimtseva 等,2006;郭利丹等,2008)。需要特别指出的是,所有的校正日历年龄都是距离 1950 年的年代,所以此处的过去 60 年应该是没有意义的。但是,因为 ^{14}C 测年具有较大的误差(理论误差和技术误差),而且 1950 年以后该湖泊的沉积是连续的,我们认为,湖芯顶部 40cm 的沉积物应该是在过去 60 年间沉积的。

4.3. 湖泊盐度和盆地气候重建

我们利用三种基于孢粉的定量方法对研究区温度和降水量进行了重建:①气候—孢粉反应面法(CPRS);②气候—孢粉转换函数法(CPTF);③与现代植物类比的植物功能类型法(PFT-MAT)。显然,这三种方法得到的结果并不相同(图 9-5)。这里我们较为信任利用 CPRS 法得到的结果,理由如下:第一,CPRS 法所依据的表层孢粉谱的来源包含了与本研究区(巴尔喀什湖)相邻的区域;第二,过去 100 年变暖的趋势(Lioubimtseva 等,2006;郭利丹等,2008)在 CPRS 法所得到结果中得到了体现;第三,与利用另外两种方法(即 CPTF 和 PFT-MAT)的重建结果相比,利用 CPRS 法重建的年平均温度(MAT)(4.6℃~5.2℃)与现代盆地范围年平均温度(3℃~10℃)较为接近;第四,根据 CPRS 法得到的 MAP 曲线与作为湿度指数的 A/C 值曲线很相似,这表明利用该方法得到的结果或许更为合理。

基于 CPRS 法的重建结果表明,过去约 2500 年来巴尔喀什盆地经历了三个阶段的气候变化(图 9-6),第一阶段(约 2500~1800 cal. yr BP)为低温和多降水阶段,其中穿插了一个短暂的少降水时段(出现在大约 2150 cal. yr BP 左右)。第二阶段(约 1800~650 cal. yr BP)的年平均降水量(MAP)低于第一阶段,而年平均温度(MAT)高于第一阶段。值得注意

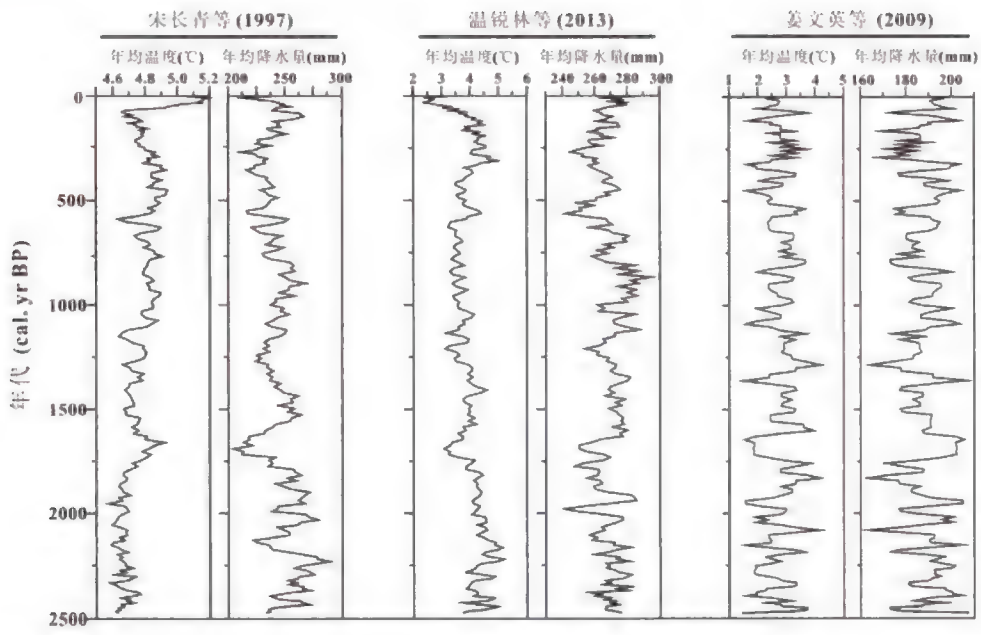

图9-5　基于孢粉资料的年平均温度(MAT)和年平均降水量(MAP)的定量重建。左图:采用孢粉响应面法(宋长青等,1997);中图:采用年转换函数法(Wen等,2013);右图:采用改进的PAT-MAT法(Jiang等,2009)

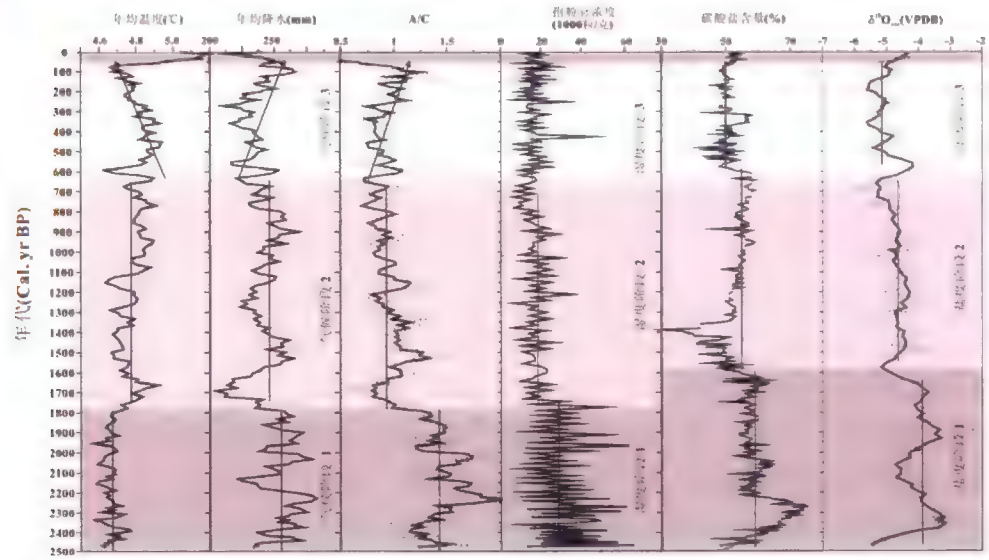

图9-6　三组代用指标。①利用孢粉响应面法重建的年平均温度(MAT)和年平均降水量(MAP)变化;②盐度指标:碳酸盐含量(%)、$\delta^{18}O_{carb}$;③湿度指标:A/C值和孢粉浓度(Feng等,2013)

的是:年平均降水量(MAP)在第二阶段伊始(约 1800 cal. yr BP)就开始大幅减少,并在约 1700 cal. yr BP 达到最小。第三阶段(约 650~0 cal. yr BP)是一个冷湿阶段,但是最近的 100 年有变暖和变干的趋势。应该指出的是:在约 250~100 cal. yr BP(相当于 17 世纪中叶到 19 世纪末),温度明显降低而降水明显增加。

作为一个湿度指标,A/C 值也表明,巴尔喀什盆地过去 2500 年经历了三个阶段的湿

度演化：第一阶段(约2500~1800 cal. yr BP)的湿度较高，并在约2200~2100 cal. yr BP达到最大；第二阶段(约1800~650 cal. yr BP)的湿度较前期(即第一阶段)有明显下降；第三阶段(约650~0 cal. yr BP)的湿度有明显的回升，而且湿度的增加趋势与年平均降水量的增加趋势非常相似。进而，基于A/C值所划分的湿度阶段也得到了孢粉浓度资料的有力支持。需要提及的是：巴尔喀什湖芯的A/C值均落在荒漠草原植被A/C值的范围内(0.5~2.0)(Zhao等，2012)，这说明，过去2500年来巴尔喀什盆地的景观一直由荒漠草原主导。

我们也对巴尔喀什湖芯样品的碳酸盐含量和碳酸盐中氧同位素($\delta^{18}O_{carb}$)进行了测试。湖中碳酸盐的沉淀主要是由湖水温度和生物生产量来控制的。温度增加，蒸发量增加，导致了碳酸盐的溶解度减小。从生物生产量的角度来讲，水生植物通过光合作用吸收水中的CO_2，导致湖水pH值的上升，进而影响碳酸盐的沉淀。一般来讲，干旱半干旱区封闭湖泊中碳酸盐的沉淀量与湖水的盐度有着密切的关系(Gasse等，1987；Aravena等，1992；Zhang等，2010)，因此我们(本章)把碳酸盐的含量作为湖泊盐度的指标。干旱—半干旱区封闭湖泊碳酸盐中的氧同位素含量取决于蒸发量和降水量的比率(Gasse等，1987；Li和Ku，1997；Zhang等，2010)，蒸发是富集重氧同位素($\delta^{18}O_{carb}$)的过程，因此我们也将$\delta^{18}O_{carb}$作为衡量湖泊盐度的指标。

作为湖泊盐度的指标，碳酸盐含量和氧同位素含量($\delta^{18}O_{carb}$)都显示，巴尔喀什湖经历了3个阶段的盐度变化：第一阶段(约2500~1600 cal. yr BP)的$CaCO_3$含量(%)和$\delta^{18}O_{carb}$都相当高，期间约2200~2000 cal. BP时段的盐度有所下降；第二阶段(约1600~650 cal. yr BP)的盐度比第一阶段有明显的下降，且在约1600~1400 cal. yr BP时段出现整个湖芯(即过去约2500年)的盐度最低值；第三阶段(约650~0 cal. yr BP)的平均盐度略低于第二阶段。

5. 讨论

巴尔喀什湖芯的资料似乎是支持先前盛行的观点的：西风带主导区的气候变化是遵从“冷湿”(低MAT，高MAP)和“温干”(高MAT，低MAP)模式的。我们的重建显示，巴尔喀什盆地经历了三个阶段的气候变化：约2500~2800 cal. yr BP为冷湿阶段，约1800~650 cal. yr BP气候适中(稍暖稍干)，过去约650年为冷湿阶段(其中，约100年有变暖和变干的趋势)。

正如我们所期望的那样，湿度的变化与年平均降水量(MAP)的变化是一致的。但是，年平均温度(MAT)也通过控制蒸发量调控了盆地的湿度。例如，第一阶段的高湿度很可能既是年平均降水量(MAP)增加的结果，也是平均温度(MAT)下降的结果。第三阶段中约650~100 cal. yr BP时段的湿度增减趋势既与年平均降水量(MAP)增加趋势平行，也与平均温度(MAT)下降趋势平行。但是，第二阶段湿度变化的细节似乎与平均降水量(MAP)变化的细节很相似，可能表明第二阶段的湿度变化是由降水变化主导的。

如前所述，巴尔喀什湖泊盐度也经历了三个阶段的变化。第一个阶段(约2500~1600 cal. yr BP)为高盐度阶段，这个高盐度阶段出现在高湿度阶段(即气候变化第一阶段)，这

说明盆地范围的湿度和降水量并没有控制湖泊的盐度。我们认为，该时期（约 2500~1600 cal. yr BP）盆地范围的低温可能是造成湖泊高盐度的主要因素。也就是说，气候第一阶段（约 2500~1600 cal. yr BP）的低温减少了山区冰川的融化，导致湖泊的补给量较少，进而造成了湖泊盐度的升高。还需提及的是，盆地范围的低温和湖泊的高盐度之间存在约 200 年的时间差，我们认为这 200 年是湖泊盐度对低温响应的时滞。

值得注意的是，叠加于第一阶段高盐度背景上的次一级（secondary）低 $\delta^{18}O_{carb}$ 值代表了湖泊的一个盐度相对较低的时段（约 2200~2000 cal. yr BP），这个低盐度时段（约 2200~2000 cal. yr BP）可能是湖泊盐度对低湿度（约 2500~2300 cal. yr BP）的延迟响应。还有，在约 1600~1400 cal. yr BP 碳酸盐含量处于谷低水平，$\delta^{18}O_{carb}$ 值也偏低，这个谷底水平（约 1600~1400 cal. yr BP）可能是对约 1800~1600 cal. yr BP 阶段低湿度的延迟响应。还值得注意的是，湖泊的盐度对于湿度的低幅振动反应并不敏感。

综上所述，孢粉资料显示，巴尔喀什盆地经历了三个阶段的气候变化：约 2500~1800 cal. yr BP 为冷湿阶段，约 1800~650 cal. yr BP 为适中阶段（稍暖稍干），过去约 650 年为冷湿阶段（注：最近 100 年有变暖和变干的趋势）。第一阶段的湖泊盐度变化的主控因素为盆地范围的温度变化，而且存在约 200 年左右的盐度对温度响应的时间滞后。盆地范围的低温减少了冰川的融水量，导致了湖泊的供给减少，进而造成湖泊盐度的升高。盆地范围湿度的大幅度变化似乎主控了次一级的湖泊盐度的变化，而且也存在约 200 年左右的盐度对湿度响应的时间滞后。再次，湖泊的盐度对于湿度的低幅振动反应并不敏感。

致谢：参与了野外采样和室内分析的同行还有：忭惠宁博士，张成君博士，翟新伟博士，王维博士，杨奇丽博士，黄昌庆博士。成文过程中还得到了以下人士的帮助：兰波先生，张东良先生，杨运鹏先生，王艳楠先生。

参考文献

郭利丹，夏自强，李捷，唐志坚. 2008. 巴尔喀什湖流域气候变化特征分析. 河海大学学报，3:316~321.

宋长青，孙湘君，吕厚远，1997. 中国北方花粉—气候因子转换函数建立及应用. 科学通报，20:2182~2186.

王伏雄，钱南芬，张玉龙，杨惠秋. 1995. 中国植物花粉形态. 第二版. 北京：科学出版社.

Aizen, E.M., Aizen, V.B., Melack, J.M., Nakamura, T. and Ohta, T., 2001. Precipitation and atmospheric circulation patterns at mid-latitudes of Asia. International Journal of Climatology, 21: 535~556.

Anderson, D.M., Overpeck, J.T. and Gupta, A.K., 2002. Increase in the Asian Southwest Monsoon during the past four centuries. Science, 297: 596~599.

Aravena, R., Warner, B.G., MacDonald, G.M. and Han, K.I., 1992. Carbonate isotope composition of lake sediments in relation to lake productivity and radiocarbon dating. Quaternary Research, 37: 333~345.

Bauer, E., Claussen, M. and Brovkin, V., 2003. Assessing climate forcing of the Earth system for the past millennium. Geophysical Research Letters. 30(6): 1276, doi:10.1029/2002GL016639.

Blyakharchuk, T.A., Wright, H.E., Borodavko, P.S., van der Knaap, W.O. and Ammann, B., 2007. Late Glacial and Holocene vegetational history of the Altai Mountains (southwestern Tuva Republic, Siberia). Palaeogeography, Palaeoclimatology, Palaeoecology, 245 (3~4): 518~534.

Boomer, I., Aladin, N., Plotnikov, I., Whatley, R., 2000. The palaeolimnology of the Aral Sea: a review. Quaternary Science Reviews, 19: 1259~1278.

Boomer, I., Wunnemann, B., Mackay, A.W., Austin, P., Sorrel, P., Reinhardt, C., Keyser, D., Guichard, F. and Fontugne, M., 2009. Advances in understanding the late Holocene history of the Aral Sea region. Quaternary International, 194: 79~90.

Bothe, O., Fraedrich, K. and Zhu, X., 2011. Precipitation climate of Central Asia and the large-scale atmospheric circulation. Theoretical Applied Climatology, DOI: 10.1007/s00704-011-0537-2.

Bridgman, B.H. and Oliver, J.E., 2006. The global climate system: patterns, processes, and teleconnections. Cambridge University Press, New York.

El-Mosilimany, A.P., 1990. Ecological significance of common non-arboreal pollen: examples from drylands of the Middle East. Review of Palaeobotany and Palynology, 64: 343~350.

ESA and UCLouvain, 2010. The Globe Coverage 2009 Project (http://dup.esrin.esa.it/globcover).

Feng, Z.D., Wu, H.N., Zhang, C.J., Ran, M., and Sun, A.Z., 2013. Bioclimatic change of the past 2500 years within Balkhash Basin in the eastern Kazakhstan of Central Asia. Quaternary International, 311: 63~70.

Gasse, F., Fontes, J.C., Plaziat, P., Carbonel, P., Kaczmarska, I., De Deckker, P., Soulie-Marsche, I., Callot, Y. and Dupeuble, P.A. 1987. Biological remains, geochemistry and stable isotope for the reconstruction of environmental and hydrological changes in the Holocene lakes from north Sahara. Palaeogeography, Palaeoclimatology, Palaeoecology, 60: 1~46.

Geel, B.V., Bokovenko, N.A., Burova, N.D., Chugunov, K.V., Dergachev, V.A., Dirksen, V.G., Kulkova, M., Nagler, A., Parzinger, H., van der Plicht, J., Vasiliev, S.S. and Zaittseva, G.I., 2004. Climate changes and the expansion of the Scythian culture after 850 BC: a hypothesis. Journal of Archaeological Sciences, 31: 1753~1742.

Gong, D.Y., Wang, S.W. and Zhu, J.H., 2001. East Asian winter monsoon and Arctic Oscillation. Geophysical Research Letters, 28: 2073~2076.

Grimm, E.C., 1990. Tilia and Tilia graph PC spreadsheet and graphics software for pollen data. INQUA Working Methods Newsletter, 4:5~7.

Guiot, J., Harrison, S.P. and Prentice, T.C., 1993. Reconstruction of Holocene patterns of moisture in Europe using pollen and lake-level data. Quaternary Research, 40: 139~149.

Heorling, M.P., Hurrell, J.W. and Xu, T., 2001. Tropical origins for recent North Atlantic climate change. Science, 292: 90~92.

Holme, J.A., Cook, E.R. and Yang, B., 2009. Climate change over the past 2000 years in Western China. Quaternary International, 194: 91~107.

Huang, X.T., Oberhänsli, H., von Suchodoletz, H. and Sorrel, P., 2011. Dust deposition in the Aral Sea: implications for changes in atmospheric circulation in central Asia during the past 2000 years. Quaternary Science Reviews, 30: 3661~3674.

Jiang, W.Y., Guiot, J. and Chu, G.Q., 2009. An improved methodology of the modern analogues technique for palaeoclimate reconstruction in arid and semi-arid regions. Boreas, 39: 145~153.

Jones, M.D., Roberts, C.N., Leng, M.J. and Turkes, M., 2006. A high-resolution late Holocene lake isotope record from Turkey and links to North Atlantic and monsoon climate. Geology, 34: 361~364.

Kroonenberg, S.B., Abdurakhmanov, G.M., Badyukova, E.N., van der Borg, K., Kalashnikov, A., Kasimov, N.S., Rychagov, G.I., Svitoch, A.A., Vonhof, H.B. and Wesselingh, F.P., 2007. Solar-forced 2600 BP and Little Ice Age highstands of the Caspian Sea. Quaternary International, 173/174: 137~143.

Li, H.C. and Ku, T.L., 1997. δ13C and δ18O covariance as a paleohydrological indicator for closed-basin lakes. Palaeogeography, Palaeoclimatology, Palaeoecology, 133: 69~80.

Liu, X.Q., Herzschuh, U., Shen, J., Jiang, Q.F. and Xiao, Y.X., 2008. Holocene environmental and climatic changes inferred from Wulunggu Lake in northern Xinjiang, China. Quaternary Research, 70: 412~425.

Lioubimtseva, E. and Cole, A., 2006. Uncertainties of climate change in arid environments of Central Asia. Reviews of Fisheries Science, 14: 14~29.

Lydolph, P.E., 1977. Climates of the Soviet Union. Elsevier Scientific Publishing Co. New York.

Maasch, K.A., Mayewski. P.A., Rohling, E.J., Stager, J.C., Karilen, W, Meeker, L.D. and Meyerson, E.A., 2005. A 2000-year context for modern climate change. Geografiska Annaler. 87(A): 1~15.

Mann, M.E., Zhang, Z.H. and Rutherford, S., 2009. Global signature and dynamical origins of the Little Ice Age and Medieval Climate Anomaly. Science, 326: 1256~1260.

Meeker, L.D. and Mayewski, P.A., 2002. A 1400-year high-resolution record of atmospheric circulation over the North Atlantic and Asia. The Holocene, 12: 257~266.

Moore, P.D., Webb, J.A. and Collinson, M.E., 1991. Pollen Analysis. Blackwell Science, Oxford.

Petr, T., 1992. Lake Balkhash, Kazakhstan. International Journal of Salt Lake Research, 1(1): 21~46.

Propastin, P., 2011. Patterns of Lake Balkhash water level changes and their climatic correlation during the period of 1992-2010. Lakes and Reservoirs Research and Management, 17: 161~169.

Reimer, P.J., Baillie, M.G.L.and Bard, E., 2009. IntCal09 and Marine09 radiocarbon age calibration curves, 0-50,000 years cal BP. Radiocarbon, 51: 1111~1150.

Rudaya, N., Tarasov, P., Dorofeyuk, N., Solovieva, N., Kalugin, I., Andrew, A., Dryin, A., Diekmann, B., Riedel, F., Tserendash, N. and Wagnere, M., 2009. Holocene environments and climate in the Mongolian Altai reconstructed from the Hoton-Nur pollen and diatom records: a step towards better understanding climate dynamics in central Asia. Quaternary Science Reviews, 28: 540~554.

Ruddiman, W.F., 2008. Earth's climate, past and future (Third Edition). Freeman and Company, New York.

Shi, Y.F., Kong, Z.C., Wang, S.M., Tang, L.Y., Wang, F.B., Yao, T.D., Zhao, X.T., Zhang, P.Y. and Shi, S., 1993. Mid-Holocene climates and environments in China. Global and Planetary Change, 7: 219~233.

Sorrel, P., Popescu, S.M., Head, M.J., Suc, J.P., Klotz, S. and Oberhänsli, H., 2006. Hydrographic development of the Aral Sea during the last 2000 years based on quantitative analyses of dinoflagellate cysts. Palaeogeography, Palaeoclimatology, Palaeoecology, 234: 304~327.

Sorrel, P., Popescu, S.M., Klotz, S., Suc, J.P. and Oberhänsli, H., 2007. Climate variability in the Aral Sea basin (Central Asia) during the late Holocene based on vegetation changes. Quaternary Research, 67: 357~370.

Staubwasse, M. and Weiss, M., 2006. Holocene climate and cultural evolution in late prehistoric-early

historic West Asia. Quaternary Research, 66: 372~387.

Tarasov, P.E., Webb, III T. and Andreev, A.A., 1998. Present-day and mid-Holocene biomes reconstructed from pollen and plant macrofossil data from the former Soviet Union and Mongolia. Journal of Biogeography, 25: 1029~1053.

Tarasov, P., Bezrukova, E., Karabanov, E., Nakagawa, T., Wagner, M., Kulagina, N., Letunova, P., Abzaeva, A., Granoszewski, W. and Riedel, F., 2007. Vegetation and climate dynamics during the Holocene and Eemian interglacials derived from Lake Baikal pollen records. Palaeogeography, Palaeoclimatology, Palaeoecology, 252: 440~457.

Van Campo, E., Cour, P. and Sixuan, H., 1996. Holocene environmental changes in Bangong Co. Basin (western Tibet): Part 2. the pollen record. Palaeogeography, Palaeoclimatology, Palaeoecology, 120: 49~63.

Wen, R.L., Xiao, J.L., Ma, Y.Z., Feng, Z.-D., Li, Y.C. and Xu, Q.H., 2013. Pollen-climate transfer functions intended for temperate eastern Asia. Quaternary International, 311: 3~11.

Yang, B., Brauning, A., Johnson, K.R. and Shi, Y., 2002. General characteristics of temperature variation in China during the last two millennia. Geophysical Research Letters, 29 (9): doi:10.1029/ 2001GL014485.

Yang, B., Wang, J.S., Brauning, A., Dong, Z.B. and Esper, J., 2009. Late Holocene climatic and environmental changes in arid central Asia. Quaternary International, 194: 68~78.

Zhang, C.J., Feng, Z.-D., Yang, Q.L. and Gou, X.H., 2010. Carbon-and carbonate-related proxies-recorded Holocene climatic variations in Bosten Lake of the Tarim Basin. The Holocene, 20: 263~273.

Zhao, Y., Yu, Z.C., Chen, F.H., Zhang, J.W. and Yang, B., 2009. Vegetation response to Holocene climate change in monsoon-influenced region of China. Earth-Science Reviews, 97: 242~256.

Zhao, Y., Liu, H.Y., Li, F.R., Huang, X.Z., Sun, J.H., Zhao, W.W., Herzschuh, U. and Tang, Y., 2012. Application and limitations of the Artemisia/Chenopodiaceae pollen ratio in arid and semi-arid China. The Holocene, 22: 1385~1392.

第十章

蒙古高原及其周边地区全新世湿度演化及其机制研究

王　维[①]　冯兆东[②]

①内蒙古大学 环境与资源学院

②中国科学院 新疆生态地理研究所

本章对蒙古高原及其周边地区的全新世气候序列进行了综述，集成研究了蒙古高原及其周边地区全新世湿度演化的时空分布规律，并探讨了气候变化的联系和响应机制。首先，我们构建了基于研究区自然条件（湖泊大小、水深、代表性等）和沉积物序列质量要素（测年、分辨率、沉积连续性等）的评价体系，对蒙古高原及其周边地区（A区：蒙古高原南侧中国季风边缘区；B区：蒙古高原北部西伯利亚南侧的贝加尔地区和阿尔泰地区；C区：蒙古高原西侧中国新疆北部；D区：包括蒙古国南部干旱区和中国内蒙古北部干旱区在内的蒙古高原核心地区）的87个全新世气候序列进行筛选，进而对入选的26个高质量的全新世孢粉生物气候序列进行了系统的综述，使用区域加权平均法获得了上述4个地区的全新世区域湿度演化序列，并对其联系和响应机制进行了讨论。结果表明：①中国夏季风影响的半干旱区（A区）全新世湿度演化曲线与前人获得的东亚夏季风强度曲线基本一致，二者都是对北半球夏季日辐射变化以及与之相关的热带西太平洋表层海水升温的延迟响应；②冬季风主导的西伯利亚南部（B区）全新世湿度演化表现出自10.6~9.6 cal. kyr BP开始的持续降低，与俄罗斯平原地区的年降水变化和北大西洋地区暖季温度变化一致，这表明俄罗斯平原及西伯利亚南部地区全新世气候变化与北大西洋地区暖季温度变化有关；③新疆北部地区（C区）全新世湿度演化表现出自8.0 cal. kyr BP以来的逐渐增加趋势，这可能归因于北半球冬季辐射的增加以及由此导致的北大西洋冷季温度升高所致的表层海水蒸发增强；④蒙古高原核心干旱区（D区）全新世湿度演化的最低时段和温度的最高时段在年代上基本对应，均位于中全新世，表明暖季温度的增加导致了蒸发增强，从而形成了中全新世的干旱气候。

关键词：蒙古高原；全新世气候变化；湿度演化；生物气候重建

1. 引言

蒙古高原以蒙古国和内蒙古自治区为中心，占据以蒙古国南戈壁为中心的西起蒙古阿尔泰地区、东至内蒙古大兴安岭地区、北到贝加尔湖南部、南邻中国黄土高原的广大地区。蒙古高原位于极锋南侵的前沿，极锋位置及其两侧高低压气候系统的变化实现了高低纬物质和能量的交换。因此，蒙古高原全新世气候变化研究具有重要的气候学意义（Aizen等，2001；Visbeck，2002）。欧亚地区极锋两侧的高低压系统主要包括：位于蒙古国北部和俄罗斯西伯利亚南部的西伯利亚—蒙古高压、位于南欧的亚速尔高压和位于亚洲中东部的亚洲低压。一方面，蒙古高压控制和影响着欧亚地区中东部的冬季气候，亚速尔高压控制和影响着中亚西部地区的夏季气候，亚洲低压控制和影响着亚洲东部地区的夏季气候（Bridgman和Oliver，2006；Lydolph，1977）。蒙古高压的时空变化与其西部的亚速尔高压和其南部的亚洲低压的变化息息相关（Bridgman和Oliver，2006；Gong等，2001）。另一方面，在半球尺度上，蒙古高压与东亚地区海陆气压差和大气长波（即罗斯贝波）波动造成的高低压气候系统（冰岛低压及阿留申低压）的变化有关（Bridgman和Oliver，2006；Lydolph，1977；Meeker和Mayewski，2002）。研究表明，与冰岛低压相关的北大西洋涛动（North Atlantic Oscillation，NAO）和与阿留申低压相关的北太平洋涛动（North Pacific Oscillation，NPO）呈反相位变化，北太平洋涛动（NPO）正相与北大西洋涛动（NAO）的负相对应（Bridgman和Oliver，2006；Kim等，2004），呈遥相关的跷跷板关系。这种遥相关的跷跷板关系可能控制了蒙古高压气候系统，抑或被蒙古高压气候系统所调控（Gong等，2001；Kutzbach和Liu，1997）。

蒙古高原及其周边地区的古气候序列记录了上述气候子系统的相互作用历史，具有重要的古气候意义。在过去的11 500年里（即全新世），上述气候子系统的变化与相互作用受以下四个因子的驱动和控制：①冬季辐射；②夏季辐射；③大气CO_2浓度；④北半球冰川覆盖范围（Ruddiman，2007）。早全新世较低的冬季辐射和大范围的冰雪覆盖（包括冰川、积雪以及冻土覆盖范围）可能是驱动全球气候变化的高纬度驱动因子。约在7000 cal. yr BP左右大气CO_2浓度和冰雪覆盖达到现今水平（Ruddiman，2007），其后较高的大气CO_2浓度、适中的夏季辐射和温暖的海洋表层的联合作用成为了驱动全球气候变化的低纬度驱动因子。此外，Bush（2005）和Prokopenko等（1999）利用大气CO_2和水汽的反馈作用机制解释了俄罗斯西伯利亚和中亚地区中晚全新世以来的增暖。蒙古高原及其周边地区相互作用的三个气候子系统（与大西洋联系的西风带、与高纬度地区相联系的蒙古高压以及与低纬度地区相联系的夏季风）的时空演化及其遥相关机制，以及前面述及的海气耦合作用机制，可能共同控制和影响了蒙古高原地区全新世的气候变化。

过去二十年来，蒙古高原及其周边地区的全新世湿度演化成为学界争论的焦点。如，Harrison等（1996）和Tarasov等（2000）认为，蒙古高原北部和西伯利亚南部全新世最湿润期与中国暖湿的大暖期对应，年代上均介于9.5~3.3 cal. kyr BP（Shi等，1993），该时期亚洲夏季风增强，向西可能深入到蒙古阿尔泰地区。Herzschuh（2006）对中东亚地区75个古气

候序列对比综合研究认为，西风带主导的中亚地区全新世气候变化模式与季风主导的东亚地区相似，早全新世湿润（约10.5~6.5 cal. kyr BP）、中全新世变干（约6.5~4.5 cal. kyr BP）和晚全新世干旱（约4.5 cal. kyr BP以来）（Herzschuh，2006；Wang等，2010；Zhang等，2011；Zhao等，2009）。但是，Chen等（2008）通过中亚地区11个高质量全新世气候序列集成研究，提出了和季风区全新世气候变化反相位的气候变化模式（以下简称西风模式），他们主张中亚地区早全新世气候干旱（约12.0~8.0 cal. kyr BP），中晚全新世气候湿润（约8.0 cal. kyr BP）。然而，无论是西风模式还是季风模式都没有表达出蒙古高原核心干旱半干旱地区记录的中全新世干旱气候（An等，2008；Feng，2001；Feng等，2005；Wang等，2009，2011）。

蒙古高原气候学上的复杂性和古气候记录的矛盾性意味着：学界应以更加严厉的标准和更为宽阔的视野重新审视和研究已有的全新世古气候序列，以期在更大地理范围内理解气候变化的时空规律及其背后的驱动和联系机制。为此，本章对比综合研究的气候序列不仅来自于蒙古高原地区（D区）（蒙古国和中华人民共和国内蒙古自治区），还包括毗邻的蒙古高原东南部中国夏季风边缘区（A区）、蒙古高原北部冬季风主导的贝加尔地区和阿尔泰地区（B区）、蒙古高原西部西风带影响的中国新疆维吾尔自治区北部地区（C区）（图10-1）。

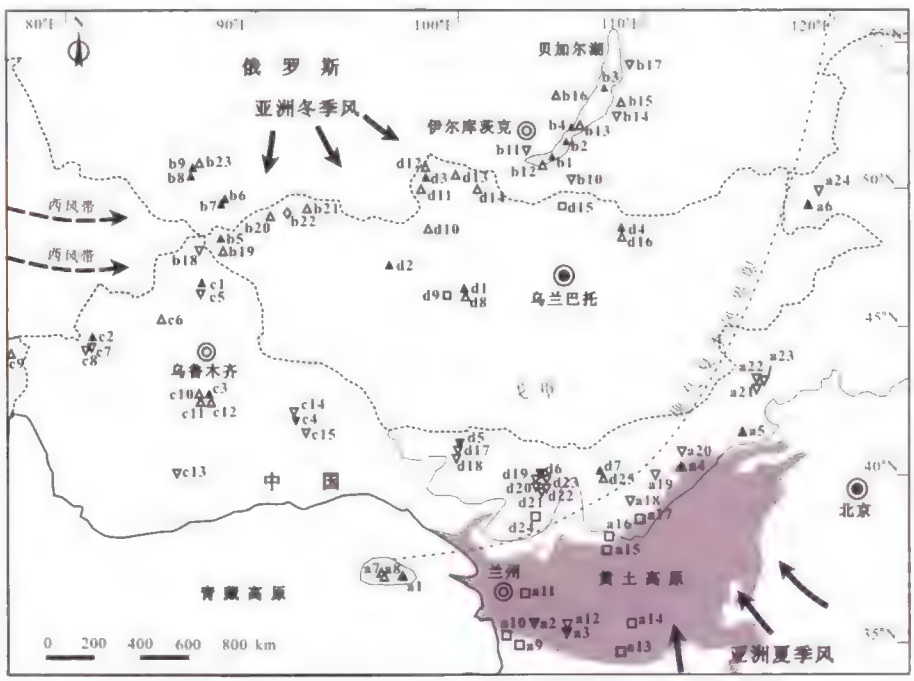

图10-1 研究区概况及综述的研究点（据高由禧，1962；Lydolph，1977；Visbeck，2002修改）

a1-a6，b1-b9，c1-c4 和d1-d7为通过质量筛选入选区域平均湿度构建的样点序列；注：▲通过质量筛选的湖泊钻孔序列；□通过质量筛选的湖相剖面或泥炭剖面；△未通过质量筛选的湖泊钻孔序列；▽未通过质量筛选的湖相剖面或泥炭剖面；□未通过质量筛选的风成、风成/湖相、泥炭/风成复合序列；◇未通过质量筛选的古湖岸阶地序列

2. 研究方法

2.1. 代用指标

现代花粉—植被—气候关系研究结果表明，孢粉作为古植被古气候重建的代用指标环境指示意义明确，因此，本研究首选孢粉代用指标序列。基于孢粉组合的气候代用指标可分为半定量和定量两类，半定量的孢粉代用指标主要有A/C值、乔木花粉百分比（AP）以及基于孢粉类群的温度和湿度的比值（如干旱指数、湿度指数、温度指数、草原/森林指数以及孢粉群区值等），定量的孢粉代用指标主要指利用转换函数建立的气候因子序列。

El-Mosilimany（1990）通过对中东干旱和半干旱地区现代花粉研究，基于随着干旱程度增加藜科花粉百分比增加而蒿属百分比含量降低的事实，构建了指示湿度状况的A/C值，该指标被广泛地应用于地层序列古气候重建中。本章综述的26个孢粉生物气候序列中，艾比湖（Wang等，2013）、博斯腾湖（黄小忠，2006；Huang等，2009）、巴里坤湖（Tao等，2010）以及居延泽（Herzschuh等，2004）孢粉生物气候序列中均使用A/C值重建了过去湿度变化。乔木花粉百分比（AP）是半湿润和半干旱地区指示有效湿度的理想指标（Moore，1991）。本章采纳的孢粉生物气候序列中，使用该指标作为区域有效湿度的序列中，5个来自俄罗斯阿尔泰和蒙古阿尔泰地区（Blyakharchuk等，2004，2007），3个来自于中国受夏季风影响的半干旱区（Feng等，2004，2006b；Liu H.Y.等，2002；Shen等，2005），1个来自于蒙古国北部（Doroyefuk和Tarasov，1998）。本章中使用的基于孢粉类群的比值包括干旱指数、湿度指数、草原—森林指数以及孢粉群区值，其中Fowell等（2003）构建了孢粉干旱指数[即（C+A）/P，C为藜科含量，A为蒿属含量，P为禾本科含量]，并利用该指数重建了蒙古国中部Telmen地区全新世的湿度演化历史（Fowell等，2003）。Demske等（2005）在综合研究贝加尔湖地区植被垂直带谱的基础上，提出了指示湿度变化的孢粉湿度指数并重建了贝加尔湖南部、中部、北部3个地区的湿度演化序列；Ma等（2008）在对蒙古国南北断面表土花粉研究的基础上，提出了用于指示湿度变化的孢粉湿度指数，Wang等（2011）利用该指数重建了蒙古国中部优贵湖（Ugii Nuur）地区全新世湿度演化序列；草原—森林指数（SFI）是草原类型孢粉含量与森林类型孢粉含量的比值，在Hovsgol湖全新世研究中被用来重建区域草原扩张的程度进而间接指示了区域有效湿度（Prokopenko等，2007）。孢粉群区化（Biome）依据现代植被的植物功能型（PFT）划分，赋以化石花粉类型特定的植物功能型，并据此计算得出不同植被类型（如苔原、泰加林、草原、荒漠等）的孢粉群区分值，用以指示该植被类型存在的可能性（Prentice等，1996），本章综述的孢粉生物气候序列中，贝加尔湖的Buguldeika序列（Tarasov等，2007）、蒙古阿尔泰的Hoton序列（Rudaya等，2009）以及中国季风边缘区的巴彦查干序列（Jiang等，2006）均使用了该指标重建了区域有效湿度。

对关键气候因子进行定量重建一直以来都是古气候学家追求的目标之一。对现代植被分布和气候关系的定量化表述是构建基于孢粉定量气候因子的前提。研究学者已先后使用回归模型法（Birks，1995；ter Braak和Juggins，1993）、最佳类比法（Guiot，1990；Overpeck等，1985）以及信息统计法（Klimanov，1984）发展和构建了现代花粉—气候转换函数，并将

这些函数应用于地层花粉数据，定量重建全新世的降水和温度变化。本章综述的全新世气候序列中，贝加尔湖Buguldeika序列（Tarasov等，2007）、蒙古阿尔泰地区Hoton Nuur序列（Rudaya等，2009）、中国北方巴彦查干序列（Jiang等，2006）以及岱海序列（Xu等，2010）和呼伦湖序列（Wen等，2010a）均使用了孢粉转换函数定量地重建了全新世降水变化。

此外，本章还综述了一些非孢粉代用指标序列，来验证和支持孢粉指标重建的湿度序列的可接受性。需要说明的是，这些非孢粉指标序列并未参与到区域平均湿度的计算中。这些非孢粉指标包括指示水动力状况的粒度指标、指示水深状况的硅藻浮游类/底栖类比值、指示水温的硅藻暖水种/冷水种比值、指示流域植被发育状况或湖内生产力水平有机质含量、指示湖泊水量平衡及盐度状况沉积物元素和矿物组成指标及指示流域植被的有机碳同位素指标等。

2.2. 数据筛选

参考前人研究成果，本章构建了全新世气候序列评价体系，对近期已发表的全新世气候序列在以下5个方面进行了全面的考量和评估（Feng等，2006a；Mayewski等，2004；Morrill等，2003；Wanner等，2008）：①年代序列的可靠性；②代用指标指示意义的确定性；③样品分辨率；④沉积环境的稳定性；⑤代用指标代表性（地理尺度）。考虑到不同序列间的相互对比，在考虑上述5个方面（共计9个指标）的基础上，构建了无量纲的指标来反映某一序列的综合质量。显然，这种做法具有一定的主观性，但它是建立在一些理论和实践经验基础之上，在没有更好的方法时，也不失为一种选择。具体而言，依据文献和前人的研究经验，赋予每个序列的上述9个指标无量纲值，其总和得分用以指示该序列的综合质量（表10-1）。表10-1中每列对应的是每个序列具体指标的表述（数值或描述），后面括弧内是赋以该指标的无量纲值，1代表最低，3代表最高。这9个指标分别为：①沉积序列类型：一般而言，湖泊和泥炭沉积物因连续性好且利于孢粉保存被赋予最高分（即3分），风成/古土壤序列和风成/湖沼相复合沉积序列被赋以2分；②地理代表性：具有全球或大陆尺度的气候序列被赋予最高分（即3分），山间盆地湖泊沉积一般而言具有区域意义，被赋以分值2，仅具地方代表性的序列分值为1；③现在湖泊水深：一般而言，现在湖泊水深可能与该湖泊全新世历史时期的湖泊水位有一定关系，现代水深越大，全新世历史时期湖泊干涸的可能性就越小。据此，现代水深5m以上的湖泊沉积物序列被赋予最高分（即3分），2～5m水深湖泊序列分值为2，2m以内以及干涸湖泊序列分值为最低1；④测年材料：从沉积物中挑出的孢粉浓缩物、腐殖酸以及陆生植物残体（包括种子、炭屑、叶片等），因不受湖泊碳库效应的影响，年代较为可靠，被赋予最高分（即3分），其他用于放射性测年的材料如软体动物壳体、沉积物总有机质等可能受到碳库效应的影响，赋予值取2分；⑤年代控制数量：年代控制数量越多，序列的年代精度越大，对于全新世时段而言，超过8个年代控制的序列被赋予最高分（即3分），5～8个年代控制得分值取2，5个以下为1；⑥测年方法和碳库效应评价：科学评估碳库效应的AMS ^{14}C测年序列被赋予最高分（即3分），基于孢粉浓缩物、腐殖酸以及陆生植物残体AMS ^{14}C测年序列因无需进行碳库效应评估也被赋值3，没有进行碳库效应评估的序列取值2；⑦沉积序列的连续性：不存在沉积间断的序列

被赋予最高分(即3分),存在显著沉积间断的序列取值1;⑧样品分辨率:分辨率<100年/样的序列取值3,100~300年/样取值2,>300年/样取值为1;⑨代用指标质量:主要考虑代用指标环境指示意义的确定性,孢粉指标分值取3,多指标重建序列取值也为3,其他单一指标赋值为2。

对于具有不同代用指标且均通过质量评估的序列,仅选取孢粉生物气候序列进行区域湿度序列重建。需要说明的是,尽管鄂尔多斯北部库不齐沙漠的盐海子序列(Chen C.T.A.等,2003)没有孢粉指标序列,但其综合气候序列通过了质量评估,考虑其地理位置上的不可或缺性,本章区域湿度重建时采用了该序列。而对于位于夏季风边缘区的黑地湾孢粉序列(Li等,2003a),尽管通过了质量考察,但考虑到其重建的湿度完全依赖于孢粉浓度的变化,这在沉积速率变化较大的风成/古土壤沉积序列中不确定性较大,因此本章没有采纳该序列。

本章对蒙古高原及其周边地区的87个全新世气候序列(73个湖沼相序列、12个风成/古土壤/湖沼相复合沉积序列、2个古湖岸阶地序列)进行了质量评价和筛选,对选取质量总分值大于或等于22的26个序列进行了区域全新世有效湿度的综合重建。

2.3. 区域平均湿度指数构建

本章使用区域平均法计算全新世区域平均有效湿度指数。具体来讲,对于每个气候序列,依据原作者的表述并结合前人的综合研究,选取一个最为可靠的指示有效湿度的指标序列(如A/C值、乔木花粉含量、基于孢粉的湿度指标、干旱指数等),以200年间隔计算该指标的湿度指数。该指数由每个时段(200年)内具体指标的平均值和该指标在整个序列的最高值的比值生成,分为四级,无量纲,变化于0~4,其中0指示湿度最低,4指示湿度最高。计算每个地区内多个序列湿度指数的平均值即得到区域平均湿度指数序列,该指数也是无量纲的,而且可以进行区域间的相互比较。为了科学表达综合重建结果的可靠性和重建方法的一致性,本章给出了每个地区区域平均湿度指数序列的平均误差和参与重建的每个序列的湿度曲线。需要特别说明的是,这种区域平均方法可能平滑掉了一些细节,但它的确可以表达一个地区全新世湿度演化的一般性规律(Davis等,2003;Herzshuh,2006;Wang等,2010;Zhao等,2009)。

3. 蒙古高原及周边地区全新世湿度演化的时空变化规律

为在大尺度上理解蒙古高原全新世湿度演化的时空规律,本研究首先从蒙古高原周边地区展开(即夏季风影响的半干旱地区、冬季风主导的西伯利亚南部、西风带主导的新疆北部),然后转入本章的核心地区(即蒙古高原),以期揭示大尺度气候变化时空分布规律和驱动联系机制。

表10-1　蒙古高原及其周边地区全新世气候序列及质量指数

序号	序列名称	经度(°)	纬度(°)	海拔(m)	序列类型	分值	代表性	分值	湖泊水深(m)	分值	测年材料	分值	测年数量	分值	测年方法和碳库评价(年)	分值	连续性(千年)	分值	分辨率(年)	分值	代用指标	分值	质量指数	参考文献
A: 夏季风影响的半干旱区																								
a1	青海湖(QH-2000)	36.70	100.60	3194	▲	3	大陆	3	22.3	3	OM	2	7	2	AMS ^{14}C, 1039	3	0~15	3	约 50	3	P, GC	3	25	Liu 等,2002b; Shen 等,2005
a2	苏家湾	35.53	104.52	1700	▼	3	区域	2	干涸	1	Ch, HM	3	7	2	AMS ^{14}C, —	3	0~14.8	3	约 140	2	P,L, GC, GS	3	22	Feng 等,2004; 2006b
a3	大地湾	35.00	105.92	1400	▼	3	区域	2	干涸	1	Ch, HM	3	9	3	AMS ^{14}C, —	3	0~13.7	3	约 60	3	P,L, GC, GS	3	24	Feng 等,2004; 2006b
a4	岱海	40.58	112.68	1221	▲	3	区域	2	13.1	3	OM	2	8	3	AMS ^{14}C, 360	3	0~10.2	3	约 40	3	P, GC, GS	3	25	Xiao 等,2004; Xu 等,2010
a5	巴彦查干	41.65	115.21	1335	▼	3	区域	2	干涸	1	OM, Pr	3	9	3	AMS ^{14}C, 570	3	0~12.5	3	约 140	2	P	3	23	Jiang 等,2006
a6	呼伦湖	49.13	117.50	545	▲	3	大陆	3	5.1	3	OM	2	14	3	AMS ^{14}C, 685	3	0~11	3	约 60	3	P, GS	3	26	Wen 等,2010a b
a7	青海湖(1F)	36.80	100.15	3194	△	3	大陆	3	26	3	OM, Pr	2	41	3	AMS ^{14}C, —	3	0~32	3	约 20	3	GC. GS	2	26	An 等,2012
a8	青海湖(14B)	~36.8	~100.1	3194	△	3	大陆	3	26	3	OM	2	3	1	AMS ^{14}C, —	2	0~12	3	约 60	3	GC, GS	2	22	Lister 等,1991

续表10-1

序号	序列名称	经度(°)	纬度(°)	海拔(m)	序列类型	分值	代表性	分值	湖泊水深(m)	分值	测年材料	分值	测年数量	分值	测年方法和碳库评价(年)	分值	连续性(千年)	分值	分辨率(年)	分值	代用指标	分值	质量指数	参考文献
A: 夏季风影响的半干旱区																								
a9	合作	~34.5	~103.2	2915	□	2	大陆	3	—	1	OM	2	1	1	^{14}C, —	3	0~80	3	约100	2	GC, M, GS	3	20	Fang等,2003
a10	塬堡	~35.0	~103.0	n.d.	□	2	大陆	3	—	1	OM	2	2	1	^{14}C, —	3	3.2~75	1	约200	2	MS, GS, L	3	18	Chen等,1997
a11	沙井坪	36.0	103.83	n.d.	□	2	区域	2	—	1	OM	2	4	1	^{14}C, IRSL —	3	0~60	3	约150	2	MS, L	2	18	Fang等,1999
a12	大地湾	35.77	105.82	1400	□	3	区域	2	—	1	OM	2	4	1	^{14}C, —	3	0~11	3	约130	2	P	3	20	夏敦胜等,1998
a13	耀县	34.93	108.83	n.d.	□	2	当地	1	—	1	Q&F	2	2	1	TL	3	0~12	3	约170	2	P	3	18	Li等,2003b
a14	黑木沟	35.75	109.42	n.d.	□	2	大陆	3	—	1	Q&F	2	2	1	TL	3	0~50	3	约670	1	MS, L	2	18	An等,1991
a15	靖边	37.50	108.33	1400	□	2	大陆	3	—	1	OM	2	11	3	AMS ^{14}C, —	3	0~10	3	约100	2	GS, MS	2	21	Xiao等,2002
a16	糜地湾	37.65	108.62	1400	□	2	当地	1	—	1	Ch, OM	3	11	3	AMS ^{14}C, —	3	0~15.8	3	约100	2	P, GS, L	3	21	Li等,2003a
a17	杨桃峁	38.80	110.45	1400	□	2	当地	1	—	1	P, HM	3	5	2	AMS ^{14}C, —	3	0~15.8	3	约100	2	P, GS, L	3	18	Zhou等,1996
a18	巴汗淖尔	39.32	109.27	1278	▽	3	区域	2	干涸	1	OM	2	12	3	^{14}C, —	3	4~9	1	约50	3	GS, GC	3	21	Guo等,2007

续表10-1

序号	序列名称	经度(°)	纬度(°)	海拔(m)	序列类型	分值	代表性	分值	湖泊水深(m)	分值	测年材料	分值	测年数量	分值	测年方法和碳库评价(年)	分值	连续性(千年)	分值	分辨率(年)	分值	代用指标	分值	质量指数	参考文献
A: 夏季风影响的半干旱区																								
a18	巴汗淖尔	39.32	109.27	1278	▽	3	区域	2	干涸	1	OM	2	12	3	^{14}C, —	3	4~9	1	约 50	3	GS, GC	3	21	Guo 等,2007
a19	察素齐	40.67	111.13	1000	▽	3	当地	1	—	1	OM	2	4	1	^{14}C, —	3	0~9.1	1	约 70	3	P	3	18	王琦瑜和孙湘君,1997
a20	调角海子	41.30	112.35	1221	▽	3	区域	2	干涸	1	OM	2	13	3	AMS ^{14}C, —	2	2~11.5	1	约 70	3	P	3	20	张兰生等,1997
a21	好鲁库	42.95	116.75	1295	▽	3	区域	2	干涸	1	OM	2	4	1	AMS ^{14}C, —	2	0~11	3	约 200	2	P, D, etc	3	19	Liu 等,2002a
a22	小牛场	42.62	116.82	1460	▽	3	区域	2	干涸	1	OM	2	3	1	AMS ^{14}C, —	2	3~11	1	约 280	2	P, D	3	17	Liu 等,2002a
a23	柳州湾	42.70	116.67	1365	▽	3	区域	2	干涸	1	OM	2	2	1	AMS ^{14}C, —	2	0~14	3	约 350	1	P, etc	3	18	Wang 等,2001
a24	扎赉淖尔	49.33	117.53	n.d.	▽	3	区域	2	干涸	1	OM	2	4	1	^{14}C, —	2	3.2~23.5	1	约 160	2	P	3	17	童国榜等,1997
B:冬季风主导的南西伯利亚地区																								
b1	Vydrino Shoulder (贝加尔湖)	51.58	104.85	340	▲	3	大陆	3	665	3	P	3	12	3	AMS ^{14}C, —	3	1~16	3	约 130	2	P	3	26	Demske 等,2005

续表10-1

序号	序列名称	经度(°)	纬度(°)	海拔(m)	序列类型	分值	代表性	分值	湖泊水深(m)	分值	测年材料	分值	测年数量	分值	测年方法和碳库评价(年)	分值	连续性(千年)	分值	分辨率(年)	分值	代用指标	分值	质量指数	参考文献
B:冬季风主导的南西伯利亚地区																								
b2	Posolskoe-High(贝加尔湖)	52.08	105.87	340	▲	3	大陆	3	130	3	P	3	12	3	AMS ^{14}C,—	3	0.7~24.4	3	约 90	3	P	3	27	Demske 等,2005
b3	Continent Ridge(贝加尔湖)	53.95	108.91	340	▲	3	大陆	3	386	3	P	3	10	2	AMS ^{14}C,—	3	0.9~14.4	3	约 80	3	P	3	27	Demske 等,2005
b4	Buguldeika	52.52	106.51	340	▲	3	大陆	3	355	3	OM	2	10	2	AMS ^{14}C,1160	2	0.6~15	3	约 250	2	P	3	25	Tarasov 等,2007
b5	Hoton Nuur-2	48.62	88.33	2083	▲	3	区域	2	32	3	Pr	3	1**	2	AMS ^{14}C,—	2	0~11.5	3	约 110	2	P	3	23	Rudaya 等,2009
b6	Akkol 湖	50.25	89.62	2204	▲	3	区域	2	2.8	2	Pr、OM	3	12	3	AMS ^{14}C,—	3	0~10	3	约 150	2	P	3	24	Blyakharchuk 等,2007
b7	Grusha 湖	50.38	89.42	2413	▲	3	区域	2	3.5	2	OM	2	10	3	AMS ^{14}C,—	3	0~12	3	约 460	1	P	3	22	Blyakharchuk 等,2007
b8	Uzunkol 湖	50.48	87.10	1985	▲	3	区域	2	5.9	3	HA	3	5	2	AMS ^{14}C,—	3	0~6	3	约 160	2	P	3	23	Blyakharchuk 等,2004

续表10-1

序号	序列名称	经度(°)	纬度(°)	海拔(m)	序列类型	分值	代表性	分值	湖泊水深(m)	分值	测年材料	分值	测年数量	分值	测年方法和碳库评价(年)	分值	连续性(千年)	分值	分辨率(年)	分值	代用指标	分值	质量指数	参考文献
B:冬季风主导的南西伯利亚地区																								
b8	Uzunkol 湖	50.48	87.10	1985	▲	3	区域	2	5.9	3	HA	3	5	2	AMS ^{14}C, —	3	0~6	3	约 160	2	P	3	23	Blyakharchuk 等,2004
b9	Kendegelukol 湖	50.50	87.63	2050	▲	3	区域	2	5.5	3	HA	3	6	2	AMS ^{14}C, —	3	0~15	3	约 260	2	P	3	24	Blyakharchuk 等,2004
b10	Sphagnum(贝加尔地区)	49.65	107.80	1348	▲	3	当地	1	干涸	1	OM	2	4	1	AMS ^{14}C, —	2	0~9	1	约 100	3	P, D	3	17	Fukumoto 等,2012
b11	Dulikha(贝加尔地区)	51.08	104.97	524	▽	3	当地	1	干涸	1	Pr, OM	3	3	1	AMS ^{14}C, —	3	0~16	3	约 130	2	P	3	17	Bezruko-va 等,2009
b12	Vydrino Shoulder(贝加尔湖)	51.58	104.87	n.d.	△	3	大陆	3	675	3	P	3	10	3	AMS ^{14}C, —	3	0~16	3	约 120	2	D, GC	3	26	Morley 等, 2005
b13	BDP-93-2(贝加尔湖)	n.d.	n.d.	n.d.	△	3	大陆	3	>300	3	OM	2	4	2	AMS ^{14}C, —	2	0~18	3	约 110	2	D	2	22	Karabanov 等,2000

续表10-1

序号	序列名称	经度(°)	纬度(°)	海拔(m)	序列类型	分值	代表性	分值	湖泊水深(m)	分值	测年材料	分值	测年数量	分值	测年方法和碳库评价(年)	分值	连续性(千年)	分值	分辨率(年)	分值	代用指标	分值	质量指数	参考文献
B:冬季风主导的南西伯利亚地区																								
b14	CHM-3(贝加尔地区)	52.75	108.8	458	▽	3	当地	1	干涸	1	OM	2	2	1	AMS ^{14}C,—	2	0~12	3	约 340	1	P	3	17	Shichi 等, 2009
b15	Kotokel 湖	52.78	108.12	458	△	3	区域	2	3.5	2	OM	2	3	1	AMS ^{14}C,—	2	0~15	3	约 120	2	P	3	20	Tarasov 等, 2009
b16	Tsagan_Tyrm lake	52.87	106.58	n.d.	△	3	区域	2	2.6	2	OM	2	4	1	AMS ^{14}C,—	2	0~6.3	1	约 140	2	P, D, M, GC	3	18	Sklyarov 等, 2010
b17	Duguldzora(贝加尔地区)	54.35	109.55	478	▽	2	当地	1	干涸	1	Pr, OM	3	5	2	AMS ^{14}C,—	2	0~16	3	约 160	2	P	3	19	Bezrukova 等, 2009
b18	大罗坝	48.03	88.03	2082	▽	3	区域	2	干涸	1	OM	2	1	1	^{14}C,—	2	0~7	1	约 410	1	P	3	16	阎顺和许英勤, 1992
b19	Hoton Nuur-1	48.67	88.30	2083	▽	3	区域	2	4.8	2	OM	2	6	2	AMS ^{14}C—	2	0~11	3	约 600	1	P	3	20	Tarasov 等, 2000
b20	Achit 湖	49.50	90.60	1435.	▽	3	区域	2	10	3	OM	2	4	1	^{14}C,—	2	0~14.6	3	约 500	1	P	3	20	Gunin, 1999
b21	Bayan 湖	50.00	94.02	932	▽	3	区域	2	>5	3	OM	2	4	1	^{14}C,—	2	0~15.4	3	约 150	2	P	3	21	Grunert 等, 2000

续表10-1

序号	序列名称	经度(°)	纬度(°)	海拔(m)	序列类型	分值	代表性	分值	湖泊水深(m)	分值	测年材料	分值	测年数量	分值	测年方法和碳库评价(年)	分值	连续性(千年)	分值	分辨率(年)	分值	代用指标	分值	质量指数	参考文献
b22	Uvs 湖	50.38	92.20	759	◇	2	区域	2	6	3	OM	2	3	1	AMS ^{14}C, —	2	0~11.5	3	—	3	Ter-race	2	20	Grunert 等, 2000
b23	Tashkol 湖	50.45	87.67	2150	▽	3	区域	2	6.25	3	HA	3	6	2	AMS ^{14}C, —	3	4~16	1	约 300	1	P	3	21	Blyakharchuk 等, 2004
C: 西风带影响的新疆北部地区																								
c1	乌伦古湖 (WLG2004)	47.17	87.22	478	▲	3	区域	2	12	3	OM	2	6	2	AMS ^{14}C, 760	3	0~9.5	3	约 80	3	P, GC, L	3	24	Jiang 等, 2007; Liu 等, 2008
c2	艾比湖 (A2009)	45.03	82.91	200	▲	3	区域	2	2.5	2	OM	2	7	2	AMS ^{14}C, 1800	3	0~15	3	约 80	3	P	3	23	Wang 等, 2013
c3	博斯腾湖 (BSTC04)	42.10	87.18	1048	▲	3	区域	2	15	3	TOC, Pr	3	6	2	AMS ^{14}C, OSL, 1140	3	0~9	3	约 140	2	P, D, GC	3	24	黄小忠, 2006; Huang 等, 2009
c4	巴里坤湖 (BLK06E)	43.67	92.80	1585	▼	3	区域	2	干涸	1	P, Pr, OM	3	13	3	AMS ^{14}C, 790	3	0~16.7	3	约 80	3	P	3	23	Tao 等, 2010
c5	乌伦古湖	n.d.	n.d.	478.6	▽	3	区域	2	干涸	1	OM	2	2	1	^{14}C, —	2	0~12	3	约 600	1	P	3	18	羊向东和王苏民, 1994

续表10-1

序号	序列名称	经度(°)	纬度(°)	海拔(m)	序列类型	分值	代表性	分值	湖泊水深(m)	分值	测年材料	分值	测年数量	分值	测年方法和碳库评价(年)	分值	连续性(千年)	分值	分辨率(年)	分值	代用指标	分值	质量指数	参考文献
C:西风带影响的新疆北部地区																								
c6	玛纳斯湖	45.75	86.00	251	△	3	区域	2	干涸	1	Ca, OM	2	8	3	AMS ^{14}C, —	2	0~11	3	约 250	2	P, GS, GC	3	21	Rhodes 等, 1996; 孙湘君等, 1994
c7	艾比湖 (AZ section)	44.87	82.73	195	▽	3	区域	2	干涸	1	OM	2	2	1	^{14}C, —	2	2.9~10	1	约 350	1	P	3	16	吴进禄, 1995; 吴进禄等, 1996
c8	艾比湖 (ZkooB)	n.d.	n.d.	195	▽	3	区域	2	干涸	1	OM	2	6	2	^{14}C, —	2	0~12	3	约 600	1	GC	2	18	李国胜, 1993
c9	伊塞克湖	42.50	77.17	1606	△	3	区域	2	240	3	OM	2	8	3	AMS ^{14}C, —	3	1~8.7	1	约 190	2	GC	2	21	Ricketts 等, 2001
c10	博斯腾湖 (BSTC01)	41.93	86.75	1046	△	3	区域	2	15	3	Pr	3	4	2	AMS ^{14}C, —	3	0~8.5	1	约 20	3	GC, GS, M	3	23	Zhang等, 2010
c11	博斯腾湖 (XBWu46)	41.90	86.75	1046	△	3	区域	2	15	3	HA, Pr	3	6	2	AMS ^{14}C, —	3	0~8.5	1	约 20	3	GC, GS, M	3	23*	Wünnemann 等, 2006

续表10-1

序号	序列名称	经度(°)	纬度(°)	海拔(m)	序列类型	分值	代表性	分值	湖泊水深(m)	分值	测年材料	分值	测年数量	分值	测年方法和碳库评价(年)	分值	连续性(千年)	分值	分辨率(年)	分值	代用指标	分值	质量指数	参考文献
c12	博斯腾湖(XBWu46)	41.90	86.72	1046	△	3	区域	2	15	3	Pr	3	6	2	AMS ^{14}C,—	3	0~8.4	1	约 50	3	GC	2	22	W ü nne-mann 等,2003
c13	塔里木	39-41	82-84	~815	▽	3	区域	2	干涸	1	Ch, Pr	3	4	1	AMS ^{14}C,—	3	0~12	3	约 1000	1	P, GC, GS, MS	3	20	Feng 和 Liu, 2005
c14	巴里坤湖(BLK-1)	43.70	92.83	1580	▽	3	区域	2	干涸	1	OM	2	7	2	^{14}C,750	3	0~9.4	3	约 40	3	GC, GS. MS	3	22	Xue等,2008; Zhong 等,2010
c15	托勒库勒湖	43.33	43.33	1890	▽	3	区域	2	干涸	1	OM	2	6	2	AMS ^{14}C,200	3	0~15	3	约 340	1	P, GS	3	20	An 等,2011
D:蒙古高原核心干旱区																								
d1	额吉湖	47.77	102.77	1330	▲	3	区域	3	14.5	3	OM	2	14	3	AMS ^{14}C,87	3	0~8.6	1	20~50	3	P, D, GS	3	23	Wang等,2009;2011
d2	Telmen 湖	48.83	97.33	1789	▲	3	区域	2	24.5	3	P, HA	3	9	3	AMS ^{14}C,—	3	0~7.5	1	约 200	2	P, GC, L	3	23	Fowell 等,2003;Peck 等,2002

续表10-1

序号	序列名称	经度(°)	纬度(°)	海拔(m)	序列类型	分值	代表性	分值	湖泊水深(m)	分值	测年材料	分值	测年数量	分值	测年方法和碳库评价(年)	分值	连续性(千年)	分值	分辨率(年)	分值	代用指标	分值	质量指数	参考文献
D:蒙古高原核心干旱区																								
d1	额吉湖	47.77	102.77	1330	▲	3	区域	3	14.5	3	OM	2	14	3	AMS ^{14}C, 87	3	0~8.6	1	20~50	3	P, D, GS	3	23	Wang等, 2009; 2011
d2	Telmen 湖	48.83	97.33	1789	▲	3	区域	2	24.5	3	P, HA	3	9	3	AMS ^{14}C, —	3	0~7.5	1	约 200	2	P, GC, L	3	23	Fowell 等, 2003; Peck 等, 2002
d3	Hovsgol 湖	51.08	100.75	1641	▲	3	区域	2	200	3	OM	2	5	2	AMS ^{14}C, 500	3	0~13.7	3	约 300	1	P,D	3	22	Prokopenko 等, 2007
d4	Gun 湖	50.25	106.60	600	▲	3	区域	2	5.5	3	OM	2	7	2	AMS^{14}C, —	2	0~11	3	约 280	2	P,D	3	22	Dorofeyuk和 Tarasov,1998
d5	居延泽	41.88	101.85	907	▼	3	区域	2	干涸	1	OM, HA	3	7	2	AMS ^{14}C, 1890	3	1.5~ 10.7	3	30~80	3	P	3	22	Herzschuh 等, 2004
d6	潴野泽	39.00	103.33	1320	▼	3	区域	2	干涸	1	Ch, OM	3	9	3	AMS ^{14}C, 540	3	0~11.6	3	约 50	3	P, L	3	24	Chen 等, 2003; 2006

续表10-1

序号	序列名称	经度(°)	纬度(°)	海拔(m)	序列类型	分值	代表性	分值	湖泊水深(m)	分值	测年材料	分值	测年数量	分值	测年方法和碳库评价(年)	分值	连续性(千年)	分值	分辨率(年)	分值	代用指标	分值	质量指数	参考文献
D:蒙古高原核心干旱区																								
d7	盐海子	40.10	108.43	1180	▼	3	区域	2	0.5	1	OM, P	3	8	3	AMS ^{14}C, —	3	0~15	3	约 100	2	GC, GS, M	3	23	Chen C.T.A. 等,2003
d8	额吉湖	47.73	102.77	1330	△	3	区域	2	16	3	OM	2	3	1	AMS ^{14}C, —	2	1~11	3	约 180	2	GC, M	3	21	Schwanghart 等,2009
d9	Karakourum S4	~47.0	~102.0	n.d.	□	2	当地	1	干涸	1	Q&F	3	8	3	OSL	3	1~11	3	约 500	1	GC	2	19	Lehmkuhl 等,2011
d10	大坝湖	48.20	98.78	2465	△	3	区域	2	4.5	2	OM	2	5	2	^{14}C,—	2	0~12	3	约 500	1	P, D	3	20	Gunin,1999
d11	Yamant 湖	49.90	102.6	1000	△	3	区域	2	>5	3	OM	2	0	1	AMS ^{14}C, —	2	0~16	3	约 400	1	P	3	20	Gunin,1999
d12	Hovsgol 湖	50.53	101.17	1645	△	3	区域	2	>5	3	OM	2	2	1	AMS ^{14}C, —	2	0~7	2	约 470	1	P,D	3	19	Dorofeyuk 和 Tarasov,1998
d13	Hovsgol 湖	51.88	100.35	1641	△	3	区域	2	236	3	OM	2	4	1	AMS^{14}C, 500	3	0~27	3	约 330	1	GC	2	20	Murakami等 2010

续表10-1

序号	序列名称	经度(°)	纬度(°)	海拔(m)	序列类型	分值	代表性	分值	湖泊水深(m)	分值	测年材料	分值	测年数量	分值	测年方法和碳库评价(年)	分值	连续性(千年)	分值	分辨率(年)	分值	代用指标	分值	质量指数	参考文献
D:蒙古高原核心干旱区																								
d14	Dood 湖	51.33	99.38	1538	△	3	区域	2	>5	3	OM	2	2	1	AMS ^{14}C, 500	2	0~14.6	3	约 660	1	P, D	3	20	Dorofeyuk 和 Tarasov,1998
d15	Shaamar	50.20	105.20	650	△	2	当地	1	—	1	Ch, OM	3	8	3	AMS ^{14}C, —	3	0~11	1	约 300	1	P, L, GC	3	20	Feng,等, 2007
d16	Gun 湖	50.25	106.07	600	△	3	区域	2	5	3	OM	2	9	3	AMS^{14}C, 1200	3	0~9	1	约 30	3	GC, GS	2	22	Feng 等, 2005;Zhang 等,2012
d17	居延泽	41.83	101.63	898	▽	3	区域	2	干涸	1	Pr	2	4	1	AMS ^{14}C, 500	3	2.7~5.5	1	30	3	GC, GS, MS	3	20	Mischke 等, 2002
d18	居延泽	41.88	101.85	907	▽	3	区域	2	干涸	1	OM, HA	3	7	2	AMS ^{14}C, 1890	3	1.5~10.7	1	30~80	3	GC, GS, M	3	21	Hartmann 和 W ü nne-mann,2009
d19	潴野泽	39.07	103.60	1302	▽	3	区域	2	干涸	1	OM	2	5	2	AMS ^{14}C, —	2	0~13.3	3	约 140	2	P	3	20	Zhao等,2008

续表10-1

序号	序列名称	经度(°)	纬度(°)	海拔(m)	序列类型	分值	代表性	分值	湖泊水深(m)	分值	测年材料	分值	测年数量	分值	测年方法和碳库评价(年)	分值	连续性(千年)	分值	分辨率(年)	分值	代用指标	分值	质量指数	参考文献
D:蒙古高原核心干旱区																								
d20	潴野泽	39.05	103.67	1309	▽	3	区域	2	干涸	1	OM 壳	2	11	3	AMS ^{14}C, —	2	0~1	3	约 200	2	P, GS	3	21	Li 等,2009
d21	潴野泽	39.05	103.67	1309	▽	3	区域	2	干涸	1	OM	2	6	2	^{14}C, —	2	0~6.8	1	约 160	2	GC, GS, MS	3	18	Shi 等,2002
d22	白碱湖	39.15	103.15	1280	◇	2	区域	2	干涸	1	Ca 壳	2	7	2	^{14}C, —	2	0~42.4	3	—	2	Ter-race, L	3	19	Pachur 等, 1995
d23	野马湖	39.10	103.67	1306	▽	3	区域	2	干涸	1	OM	2	6	2	^{14}C, —	2	0~16	3	约 200	3	GC, GS, MS	3	21	Chen 等, 1999;Shi 等, 2002
d24	红水河	38.17	102.75	1460	□	2	区域	2	干涸	1	Pr, OM	3	9	3	AMS ^{14}C, —	3	3~8	1	约 40	3	P	3	21	Ma 等,2004
d25	盐海子	40.10	108.43	1180	△	3	区域	2	0.5	1	OM	2	5	2	AMS ^{14}C, —	3	0~22	3	约 100	2	GC	2	20	钱作华等, 2002

注：各分项分值加和为质量指数，表征序列的总体质量；

* 因同一样点入选孢粉气候序列，未入选序列；

** 与6个年代控制的Hoton Nuur-1孔的主要花粉曲线对比，得到了较为可信的年代—深度模式；

缩写：OM——有机质；HM——胡敏素；HA——胡敏酸；Pr——植物残体；Ch——碳屑；Ca——碳酸盐；Q&F——石英和长石；P——孢粉；D——硅藻；GS——粒度；MS——磁化率；M——矿物组分；GC——地球化学指标；L—岩性；

符号及代表意义：▲通过质量筛选的湖泊钻孔序列；▼通过质量筛选的出露湖相和泥炭剖面；△未通过质量筛选的湖泊钻孔序列；▽未通过质量筛选的出露湖相和泥炭剖面；□未通过质量筛选的风成剖面、风成-湖相复合剖面、泥炭-风成复合剖面；◇未通过质量筛选的古湖泊阶地记录

3.1. 夏季风影响的半干旱地区（A区）

中国夏季风影响的半干旱地区，主要分布在图10–1所示的现今夏季风界限以内的狭长的草原或农牧交错地带，年降水量变化于100~400mm（高由禧，1962）。该地区全新世气候变化研究较为成熟，成果颇丰。施雅风等集成了前人对全新世动植物化石、土壤、冰川进退以及历史记载等的研究成果后指出，中国北方地区以暖湿水热组合为特征的气候适宜期（即全新世大暖期）发生于约8.5~3.0 ^{14}C kyr BP（约9.5~3.3 cal. kyr BP），其中最为暖湿的时段发生于约7.2~6.0 ^{14}C kyr BP（约8.0~6.8 cal. kyr BP）（Shi等，1993）。此后，陆续有学者对中国北方季风区全新世气候变化进行了综述和研究（如An等，2000；An等，2006；Feng等，2006a；He等，2004；Wang等，2010；Zhang等，2011；Zhao等，2009）。尽管如此，统一的认识似乎仍未达成。

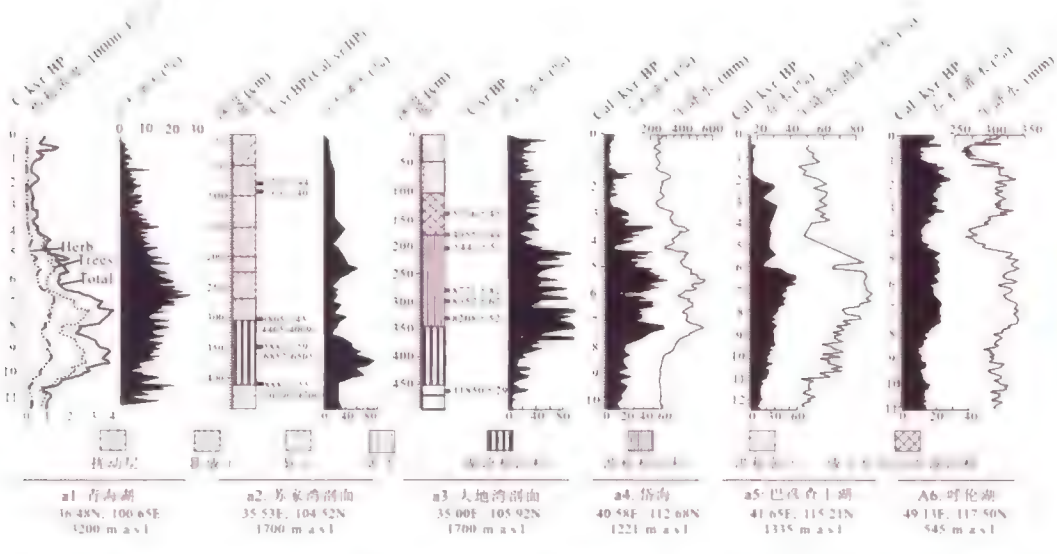

图10–2　中国夏季风影响的半干旱区全新世湿度序列：青海湖（Liu等，2002；Shen等，2005）；苏家湾和大地湾剖面（Feng等，2004，2006b）；岱海（Xiao等，2004；Xu等，2010）；巴彦查干湖（Jiang等，2006）；呼伦湖（Wen等，2010a，2010b）

本地区综述的第一个序列来自于青藏高原东部的青海湖（图10–2，对应图10–1和表10–1中的a1点），其孢粉序列中乔木和灌丛花粉百分比含量在约7.2 ^{14}C kyr BP（约8.0 cal. kyr BP）到约6.0 ^{14}C kyr BP（约6.8 cal. kyr BP）期间达到峰值（Liu等，2002a；Shen等，2005），指示了温暖湿润气候条件下森林的扩张。尽管这与最近发表的基于地球化学指标的青海湖全新世气候序列表现出显著差异（图10–1中a7点；An等，2012），但考虑到本章更看重孢粉生物指标序列，故未采纳地球化学指标序列。

位于黄土高原的河谷阶地的苏家湾和大地湾剖面，为黄土/古土壤/湖沼相复合沉积，上部为黄土—古土壤沉积，下部是湿地沼泽相沉积，他们是黄土高原地区迄今为止仅有的高质量全新世气候序列。苏家湾剖面（图10–2，图10–1中的a2点）地层和年代表明，8885 ± 55 14C yr BP至3805 ± 45 ^{14}C yr BP（约10.0~4.2 cal. kyr BP）期间为湿地沼泽相沉积，

之前和之后均为黄土沉积(Feng等,2004,2006b)。大地湾湿地沼泽相—冲积相—风成相复合剖面(图10-2;图10-1中的a3点)在地层和年代上与苏家湾剖面具有较好的可比性(Feng等,2004,2006b),细节上二者又可相互补充,完整地提供了黄土高原地区全新世植被、气候以及环境演化序列。即苏家湾剖面提供的晚全新世(3.8 ¹⁴C kyr BP或约4.2 cal. kyr BP以来)信息较为详尽,而大地湾剖面早中全新世(约8.9~3.8 ¹⁴C kyr BP或约10.0~4.2 cal. kyr BP)的记录完善且分辨率较高。两个剖面的地层和乔木及灌丛花粉百分比均指示了早中全新世湿润和晚全新世变干的趋势,其中乔木花粉峰值指示的森林扩张时期(全新世气候最宜期)介于约7.5~5.8 ¹⁴C kyr BP(约8.3~6.6 cal. kyr BP),而早全新世(约8.9 ¹⁴C kyr BP以前)和晚全新世(3.8 ¹⁴C kyr BP以后)地层为风成黄土,气候干旱。

第4个序列来自于内蒙古自治区岱海(图10-2;图10-1中的a4样点),孢粉记录表明,中全新世(约7.9~4.4 cal. kyr BP)为针阔混交林主导的暖湿气候(Xiao等,2004;Xu等,2010),约4.4~4.2 cal. kyr BP以后,乔木花粉含量骤减指示了气候变干。岱海附近大青山调角海子的孢粉气候序列(张兰生等,1997)(图10-1中a20样点)和鄂尔多斯高原巴汗淖尔气候序列(Guo等,2007)(图10-1中a18样点)基本上支持岱海重建的植被和气候序列,尽管后两个剖面的质量指数略低(<22),没能够参与到区域平均湿度指数的构建中。

第5个序列来自于内蒙古自治区巴彦查干湖相孢粉沉积序列(图10-2;图10-1中a5样点)。该序列基于孢粉定量重建的有效湿度表明,全新世有效湿度的峰值时段位于约8.4~5.4 cal. kyr BP,自5.4 cal. kyr BP以来有效湿度波动地降低(Jiang等,2006)。

最后一个序列来自内蒙古自治区呼伦湖(图10-2;图10-1中a6样点),孢粉序列中乔木和灌丛花粉百分比以及基于孢粉定量重建的降水量均在约7.9~4.7 cal. kyr BP时段表现为峰值,指示了有效湿度的最大时期,之前和之后均为相对干旱时段(Wen等,2010a,2010b)。

综上,季风边缘区半干旱地带经历了十分显著的全新世气候适宜期,该适宜期发生在约8.5~4.5 cal. kyr BP。此外,晚全新世变干可能伴有湿度波动回返现象,6个序列中有5个序列显示,自4.5 cal. kyr BP以来气候逐渐变干的过程伴有变湿的波动,只有青海湖序列没有记录到这些波动,纬度偏高的呼伦湖和巴彦查干序列似乎更为敏感地记录了这些波动。

3.2. 冬季风主导的西伯利亚南部(B区)

本地区分为东部的贝加尔湖地区和西部的阿尔泰地区,全新世气候序列均来自于湖泊沉积或泥炭沉积。

3.2.1. 贝加尔湖地区

贝加尔湖南北跨越4个纬度,区域植被主要以云杉、冷杉和西伯利亚松主导的暗针叶林为主,向南随着温度升高,植被中以欧洲赤松和落叶松建群的亮针叶林成分逐渐增多(Demske等,2005)。区域山地海拔为340~2850m,植被垂直带谱发育,自下而上依次分布亮针叶疏林、暗针叶疏林、亚高山灌丛、高山草甸和高山苔原。前人对贝加尔湖及其周边的湖泊和泥炭地进行了广泛的研究(Bezrukova等,2005,2009;Demske等,2005;Horiuchi

等，2000；Karabanov 等，2000；Prokopenko 等，1999，2007；Shichi 等，2009；Tarasov 等，2005，2007，2009）。这些结果表现出了很高的相似性，早全新世桦属和云杉属针阔混交林替代了先前的蒿草草原，中全新世（约7 cal. kyr BP）欧洲赤松疏林扩张并取代了桦—云杉针阔混交林，这种演化表现出了自北而南的穿时性（Prokopenko等，2007）。

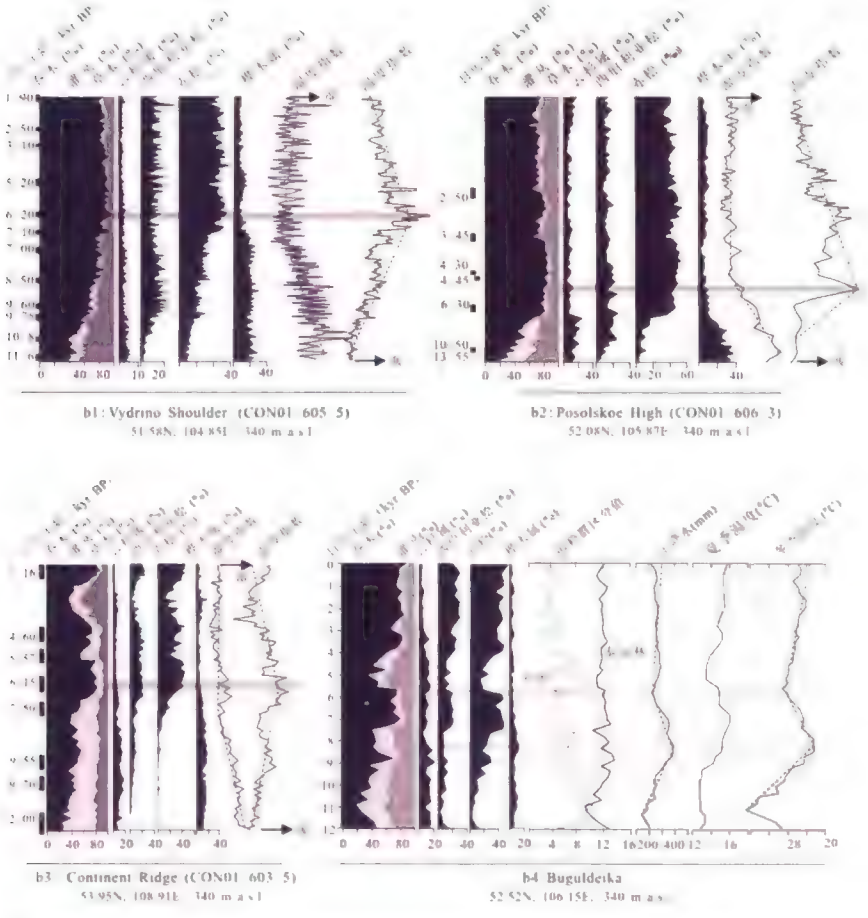

图10-3　冬季风主导的贝加尔湖地区全新世湿度演化序列（虚线为添加的趋势线）。资料来源：Vydrino Shoulder，Posolskoe High，Continental Ridge（Demske等，2005）；Buguldeika（Tarasov等，2007）

本章对贝加尔湖地区12个已发表的孢粉生物气候序列进行了考察（图10-1和表10-1中b1~b4和b10~b17样点），其中4个通过了质量筛查（图10-3）而进入到后续的区域平均湿度因子的构建当中（Vydrino Shoulder，Posolskoe High，Continental Ridge，Buguldeika；样点b1~b4）。这4个全新世气候序列在空间上覆盖了整个贝加尔湖地区，均为基于孢粉数据的定量和半定量重建序列。样点b1~b3的半定量重建气候序列（图10-3，图10-1中的b1~b3）使用孢粉植物功能型（PFT）生物气候分类法获得，即依据孢粉母体植物生境（温度和湿度）赋以孢粉类型不同的PFT类群，计算不同类群的比值获得温度和湿度指数（Demske等，2005）。样点b4（图10-3，图10-1中样点b4）的全新世湿度定量重建序列是通过最佳类比法（MAT）获得的（Tarasov等，2007）。由图10-3可以看出，3个半定量重建序列均显示出相似

的变化趋势，即早中全新世（约6.0 cal. kyr BP以前）温度增加湿度降低，中晚全新世（约6.0 cal. kyr BP以来）温度大幅降低和湿度小幅增加。然而，样点b4的定量重建序列（Tarasov等，2007）展示了和上述三个半定量序列不同的变化趋势，全新世年降水量和冬季温度序列展示出3段式变化趋势：约11.0~8.3 cal. kyr BP暖湿，约8.3~5.8 cal. kyr BP凉干，5.8 cal. kyr BP以来暖湿。

尽管如此，b1~b3的3个半定量重建序列和b4的定量重建序列还是具有两个相同之处：①约6.0 cal. kyr BP为温度的转折点；②约6.0 cal. kyr BP以后湿度均小幅增加。但是，相比之下差异更为突出，主要集中表现在以下两个方面：①b1~b3半定量序列中约6.0 cal. kyr BP以后温度降低，而b4点约6.0 cal. kyr BP以后无论是夏季温度还是冬季温度均表现出小幅上升；②3个半定量序列（b1~b3）早中全新世以暖干趋势主导，而定量序列（b4）早中全新世则展示出2段式变化，早期暖湿后期凉干。

3.2.2. 阿尔泰地区

阿尔泰地区现代植被分布表现出两大特点，其一是由北向南气候有效湿度降低，植被覆盖减少；其二为由西向东气候变干，植被恶化。现代植被分布基本上印证了该地区现代气候受大西洋水汽输送和西伯利亚高压的影响。具体而言，阿尔泰地区位于中纬度森林草原和草原地带，受西风带水汽输送和山地地形影响，阿尔泰山地西坡和北坡发育以冷杉、云杉和西伯利亚松为主的暗针叶林，而阿尔泰地区东南部山地，受西伯利亚高压控制和地形下沉气流影响，大气水汽含量减少，气候大陆度增加，现代植被为以西伯利亚松和西伯利亚落叶松为主的亮针叶林（Blyakharchuk等，2004，2007）。过去几十年，学者对阿尔泰地区全新世气候变化开展了较为深入地研究。Rudaya和他的同事对该地区的研究（Blyakharchuk.等，2004，2007；Dorofeyuk和Tarasov，1998；Tarasov等，2000，等）进行了综述（Rudaya等，2009），认为阿尔泰地区东部蒙古国境内早全新世（约11.0~5.0 cal. kyr BP）气候暖湿，晚全新世（约5.0~0 cal. kyr BP）气候变凉干，与东亚地区以及全球气候变化模式具有可比性；哈萨克斯坦境内的阿尔泰西部地区早全新世气候暖干，晚全新世气候冷湿，与西风带气候影响地区的全新世气候变化模式一致；俄罗斯境内的阿尔泰北部地区早全新世经历了和阿尔泰东部地区相似的暖湿气候，晚全新世气候变化与阿尔泰西部地区相似（凉湿）（Rudaya等，2009）。

本章综述了该地区内的11个全新世气候变化序列，其中5个（图10-1和表10-1中的b5~b9点位）通过了质量筛选。阿尔泰东部地区蒙古国境内Hoton Nur的孢粉气候序列（图10-4，图10-1中b5点位）和年代框架参考了Tarasov等（2000）的模式，在样品分辨率方面得到了较大的提升。孢粉气候序列指示，约10.5 cal. kyr BP以前，Honton Nur地区植被以冷草原主导，气候凉干；约10.5~6.5 cal. kyr BP植被演化为北方泰加疏林，气候暖湿；约6.5 cal. kyr BP以来植被退化为草原，气候变冷干。最佳类比法（MAT）定量重建的Honton Nuur全新世降水序列也表明，约10.5 cal. kyr BP以前气候干旱，约10.5~5.0 cal. kyr BP气候湿润，约5.0 cal. kyr BP以来气候变干（Rudaya等，2009）。

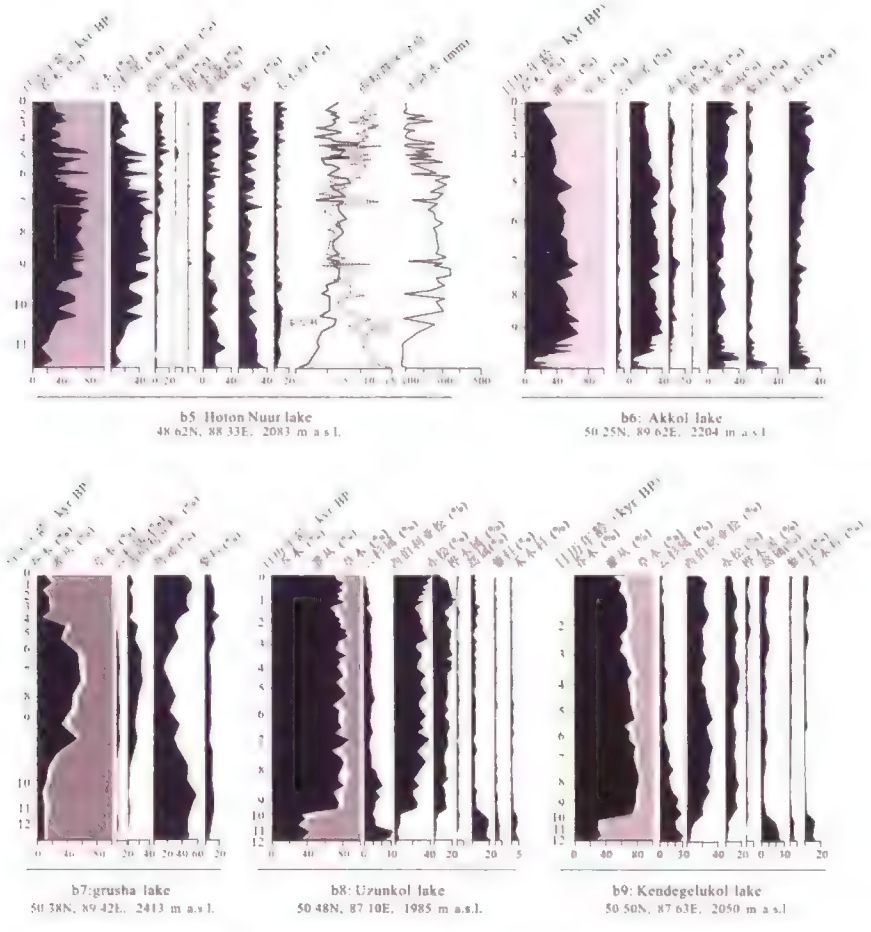

图10–4　冬季风主导的阿尔泰地区全新世湿度变化。资料来源：Hoton湖（Rudaya等，2009）；Akkol湖和Grusha湖（Blyakharchuk等，2004）；Uzunkol湖和Kendegelukol湖（Blyakharchuk等，2007）

Akkol和Grusha是本章在该地区综述的另外两个序列，均位于阿尔泰地区北部俄罗斯境内，流域内的植被为草原和森林，其中最近的森林（西伯利亚松和西伯利亚落叶松）距离湖泊约30km　考虑到落叶松属花粉的超代表性（Andreev等，2001；Ma等，2008；Minckley和Whitelock，2000），单束松型花粉增加可能指示了亮针叶林的扩张，进而反映区域有效湿度增加　上述两个序列（图10–4；图10–1中b6和b7点位）单束松型花粉的变化表现出相似的趋势，均揭示了早全新世气候暖湿和晚全新世气候变干的趋势，与Honton Nuur定量重建的全新世湿度序列具有一致性　Uzunkol和Kendegelukol（图10–4；图10–1中b8和b9点位）位于阿尔泰地区的西北部俄罗斯境内，　者的孢粉生物气候序列与前述3个序列不同，全新世双束松型花粉和单束松型花粉变化相似，与云杉属花粉变化趋势相反　如果说云杉属花粉含量增加可以指示温度升高的话（Demske等，2005，Rudaya等，2009；Tarasov等，2000），那么整个阿尔泰地区全新世温度的变化应该是一致的，即早全新世升温，晚全新世降温

3.3. 西风带影响的新疆北部(C区)

新疆北部地区位于中国西北部，其北侧和东侧为阿尔泰山脉，西侧和南侧为天山山脉，年均降水量约100 mm，潜在蒸发量达到了2000 mm以上，由此导致了极为干旱的大陆性气候。植被景观以典型荒漠和草原化荒漠主导（程曦，2010；胡汝骥，2004；吴征镒，1980）。由于气温垂直递减的原因，北侧中国阿尔泰山地和南侧天山山地植被均表现出显著的垂直分带性，在阿尔泰地区为草原、森林草原、针叶林、亚高山草甸，在天山山地为荒漠、荒漠草原、森林、亚高山草甸。

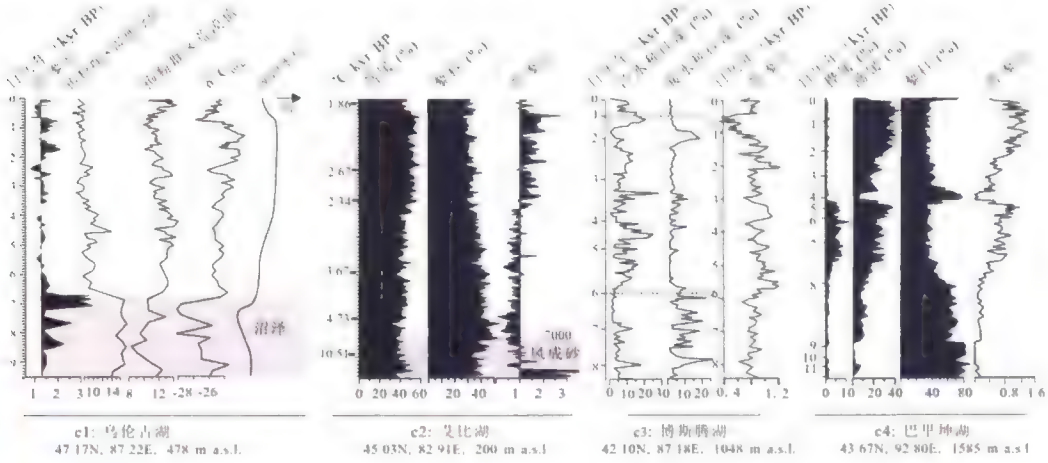

图10-5　西风带影响的新疆北部地区全新世湿度变化。资料来源：乌伦古湖(Jiang等，2007；Liu等，2008；Xiao等，2006)；艾比湖(Wang等，2013)；博斯腾湖(黄小忠，2006；Huang等，2009；Yang，2008)；巴里坤(Tao等，2010)

已有研究认为该地区冷季降水与西风带有关，暖季降水与亚洲夏季风有关，西风区气候变化以暖干/冷湿气候模式为特征(Mangerud等，1974；Wendland和Bryson，1974)，季风区气候变化以暖湿/冷干的水热组合主导(Shi等，1993)。20世纪90年代以来，关于新疆北部地区全新世气候变化模式及水热组合已成为研究者争论的热点，形成两大主流观点，即亚洲夏季风模式(林瑞芬等，1996；林瑞芬和卫克勤，1998；Rhodes等，1996；孙湘君等，1994；文启忠和乔玉楼，1990)和西风模式(韩嫩媞，1992；韩嫩媞和袁玉江，1990；李吉均，1990)。尽管有报道称新疆北部(至少是新疆北部的偏东地区)的暖季降水的水汽来自太平洋或印度洋夏季的水汽蒸发，与亚洲夏季风相关(陈添宇等，2005；李江风，1991；王克丽等，2005；魏文寿等，2003；周琴南等，1983)，但最近中亚地区的观测和研究的结果却表明情况可能并非如此(Aizen等，2001；陈曦，2010)，他们认为包括新疆北部及其以西的西天山地区冷季降水与极锋压迫导致西风带的南移有关(Aizen等，2001)，暖季降水也与亚速尔高压加强导致的西风带的北移有关。也就是说，新疆北部地区冷暖两季的降水可能都与高纬度冷空气活动有关，在夏季表现为降水过程，在冬季则为降雪过程(陈曦，2010；胡汝骥，2004；卫克勤等，2003；张家宝等，2002)。

本章综述了新疆北部通过质量考察的4个湖相沉积序列(c1：乌伦古湖；c2：艾比湖；

c3：博斯腾湖；c4：巴里坤湖），以期能够回答上述争论的核心问题。首先，位于准噶尔盆地北缘的乌伦古湖全新世沉积记录中，孢粉记录可能并不能真实地反映区域的植被和气候状况，这主要是因为沼泽沉积环境下，当地花粉占据主导（Prentice，1985；Sugita，1994），孢粉谱严重地被当地非地带隐域性湿地植被花粉（黑三棱和芦苇）所歪曲（Liu等，2008）。而基于有机碳同位素和沉积物粒度以及孢粉等多指标综合重建的湖泊水位变化曲线则显示，乌伦古湖早全新世（约10~6.7 cal. kyr BP）为浅水或沼泽环境，气候干旱（Jiang等，2007；Liu等，2008；肖霞云等，2006）；约6.7~4.0 cal. kyr BP水位上升，约4.0~0.5 cal. kyr BP维持高湖面，孢粉A/C值增加，孢粉群区荒漠指数降低，反映了气候渐湿润（Jiang等，2007；Liu等，2008）（图10-5及图10-1中c1）。第2个序列来为准噶尔盆地西缘的艾比湖序列（图10-5及图10-1中c2），孢粉记录中反映区域有效湿度的A/C值表现出自约7.0 cal. kyr BP持续升高的趋势（Wang等，2013）。塔里木盆地北侧博斯腾湖序列是本地区综述的第3个序列（图10-5及图10-1中c3），硅藻组合中冷水种丰度增加和暖水种丰度降低指示，约5.7~1.5 cal. kyr BP气候变冷（杨美临，2008），同期孢粉组合中A/C值升高（黄小忠，2006）。硅藻和孢粉资料都指示，约5.7cal. kyr BP以来区域有效湿度增加，气候总体上变冷湿。第4个序列来自于准噶尔盆地东侧天山地区的巴里坤湖（图10-5及图10-1中c4），孢粉组合中A/C值的持续增加也指示了全新世逐渐变湿的趋势，但巴里坤湖A/C值的增加表现两段式增加，前段对应时间为约7.5~4.3 cal. kyr BP，后段对应时间为近2200年以来，中间可能相对比较干旱。需要说明的是，巴里坤序列反映的约7.5 cal. kyr BP以来新疆北部地区持续变湿的气候变化得到了托勒库勒湖孢粉序列的支持（图10-1和表10-1中c5），该序列位于巴里坤湖附近，由于质量略差未能入选本文综述行列（An等，2011）。

综上，新疆北部地区全新世气候变化表现出早全新世干旱和中晚全新世变湿的特点，与陈发虎等提出的西风模式（Chen等，2008）既有相似之处，也有不同。相同的是都主张早全新世干旱和中全新世湿润。不同之处在于对晚全新世湿度的认识上，陈发虎等主张晚全新世变干趋势，而本文综述结果显示晚全新世湿度持续变湿。

3.4. 蒙古高原核心干旱区（D区）

蒙古高原中部的蒙古国南戈壁地区是蒙古高原现代气候最为干旱的地区。由蒙古国南戈壁向北，受太阳辐射量减小和西风带作用影响，年均温减小，年降水量增加，气候变冷变湿（Hilbig，1995；Tuvdendorzh和Myagmarzhav，1985）。植被自南向北依次分布：戈壁荒漠、荒漠化草原、典型草原、森林草原、针叶林（Hilbig，1995）。由蒙古国南戈壁向南，受太阳辐射量增加和亚洲夏季风降水的影响，年均温增加，年降水量增多，气候变暖变湿。相应植被由南向北依次分布：戈壁荒漠、荒漠化草原、典型草原、阔叶森林草原、阔叶森林（Hilbig，1995；吴征镒，1980）。本章综述分上述两个地区展开，即①蒙古高原北部，包括蒙古国南戈壁以北蒙古国境内地区；②蒙古高原南部，包括中国内蒙古自治区境内的干旱和超干旱地区。

3.4.1. 蒙古高原北部

本章在该地区共考察了13个全新世气候序列，其中4个通过了本章构建的质量筛查、

这4个气候序列是：①蒙古国中部地区的Ugii湖（图10-1和表10-1的d1；Wang等，2009，2011）；②蒙古国中部偏西地区的Telmen湖（图10-1和表10-1中d2；Peck等，2002；Fowell等，2003）；③蒙古国北部Hovsgol湖（图10-1和表10-1中d3；Prokopenko等，2007）；④蒙古国北部Gun湖（图10-1和表10-1中d4；Doroyefuk 和Tarasov，1998）

蒙古国中部的Ugii湖（图10-6；图10-1中d1）全新世气候序列的气候指标包括孢粉、硅藻以及粒度等。孢粉组合中适中的旱生藜科花粉和中等偏高的孢粉湿度指数，以及较高的浮游/底栖硅藻比值均表明，蒙古国中部Ugii湖地区8.1~5.8 ^{14}C kyr BP（约9.1~6.7 cal. kyr BP）植被为草原，气候略温和，有效湿度条件适中；5.8~3.1 ^{14}C kyr BP（约6.7~3.3 cal. kyr BP）可能经历了极干旱的气候，其中孢粉组合中藜科含量持续维持峰值，同时孢粉湿度指数为低值，浮游/底栖比降至最低；近3300年以来，孢粉组合中的藜科含量变化、孢粉湿度指数以及浮游/底栖比均反映了湿度先增加后降低的趋势，其中约2.6~1.0 cal. kyr BP湿度最大（Wang等，2009，2011）。Telmen序列（图10-6；图10-1中d2）仅重建了过去7100年以来的植被和气候变化，基于孢粉的干旱指数[(A+C)/P；A为蒿属含量，C为藜科含量，P为木本科含量]反映了中全新世干旱的气候特征，在约7.1~4.6 cal. kyr BP表现为峰值；约4.6~0 cal. kyr BP孢粉干旱指数表现出低值（Peck等，2002；Fowell等，2003）。上述两个序列反映的中全新世干旱气候还得到了其他序列的印证。蒙古国北部Hovsgol孢粉序列草原—森林指数[SFI=(A+C+E+Ca)/T；其中A为蒿属花粉含量，C为藜科花粉含量，E为麻黄属花粉含量，Ca为石竹科花粉含量，T为乔木花粉含量]也指示了中全新世干旱气候（图10-6；图10-1中d3），该指数显示约6.0~3.5 cal. kyr BP区域植被由森林草原退化为草原，气候干旱化，同期硅藻组合中冷水种（*Cyclotella bodaniza*）的消失可能指示了温度增加，表明该干旱时段可能为暖干水热组合。然而，蒙古国北部的Gun Nuur（即岗湖）孢粉序列（图10-6；图10-1中d4）展示出了与上述不同的全新世湿度变化趋势。具体而言，Dorofeyuk和Tarasov（1998）的孢粉序列中，约9.5 cal. yr BP以前草本花粉主导，反映了较为干旱的气候环境；约9.5~8.0 cal. kyr BP乔木花粉增长，反映区域森林覆盖增加，气候逐渐变湿；约8.0 cal. kyr BP以来，乔木花粉稳定为峰值，反映植被为森林草原，气候湿润。同时，我们也注意到了最近发表的Gun Nuur的非孢粉气候记录（图10-1中d16；Zhang等，2012），该基于地球化学指标的气候序列似乎与Gun Nuur孢粉序列重建的结果不同，似乎支持本区域前三个序列反映的中全新世干旱气候，即约7.0~2.5 cal. kyr BP，高盐度和较粗的沉积物可能反映了较低的湖泊水位和干旱的气候。实际上，孢粉和地球化学以及地球物理指标重建结果之间的矛盾，可能源自于孢粉记录对欧洲赤松生境及其花粉（双束松型）代表性的解译。即如果如Demske等（2005）所述将欧洲赤松的单束松型花粉归入指示干旱花粉类型的话，那么孢粉记录的中全新世双束松型花粉峰值可能就指示了相对干旱的环境。但Ma等（2008）以及Dorofeyuk和Tarasov（1998）无论是对现代表土的研究还是对岩芯中花粉的研究，均将此类型花粉定为反映湿度增加的乔木类型，这样一来，中全新世的峰值自然就成为湿度最大的时段。我们分析后发现，造成上述差异的根本原因在于，Gun Nuur位于蒙古国与俄罗斯交界处的色楞格河流域，现代植被为森林草原，向北过渡为森林，向南过渡为山地草原。俄罗斯研究

学者是从北往南看，欧洲赤松就分布在湿度较低的生境中了，而中国和蒙古国学者是从南往北看，赤松森林草原生长在最为湿润的环境中。究竟哪种重建的结果更为合理，可能只能通过现代花粉—植被—气候关系研究和区域对比研究予以证实。可能离Gun Nuur比较近的位于色楞格河流域的Shammar（即夏玛尔）风成地层气候记录（Feng和Khosbayar，2004；Feng等，2007）可以提供区域对比的证据，尽管该序列没能通过本文构建的质量考察。Shammar序列中基于14C的风成砂/古土壤地层、有机碳含量及孢粉数据均指示了干旱的中全新世气候（约7.8~3.1 cal. kyr BP），该时段以前和以后均为古土壤和针叶松属主导的相对湿润阶段。

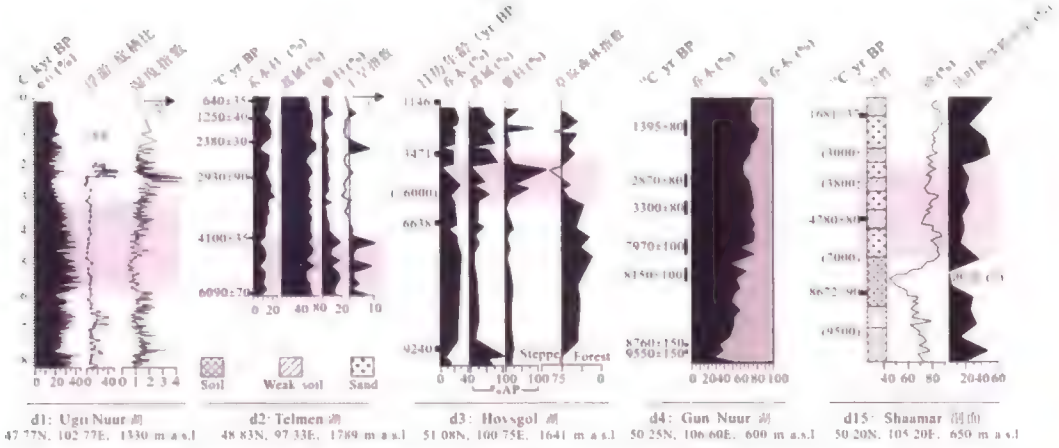

图10-6　蒙古高原北部全新世湿度变化。文献来源：Ugii 湖（Wang等，2009；2011）；Telmen湖（Fowell等，2003；Peck等，2002）；Hovsgol湖（Prokopenko等，2007）；Gun Nuur 湖（Dorofeyuk and Tarasov，1998）；Shaamar剖面（Feng等，2005）数据仅提供作为参考，未参加区域平均湿度构建

综上，蒙古高原北部可能经历了中全新世干旱气候，该干旱气候可能伴随着温度升高，气候水热组合特征表现为暖干，而早、晚全新世气候相对凉湿。需要说明的是，尽管上述4个序列得出了蒙古高原北部中全新世干旱的论点，但各序列所反映的干旱气候的起讫时间具有显著的差异，这可能归因于：①年代不确定性；②样品分辨率不一致；③代用指标的敏感性不同。此外，本集成研究得出的蒙古国中全新世干旱气候与此前蒙古国中部中全新世干旱气候一致（Tarasov等，1999），而与最近发表的一些气候记录存在矛盾，如Ugii Nuur湖泊沉积物中矿物学和地球化学沉积记录表明约8.0~4.0 cal. kyr BP为全新世最为湿润阶段（Schwangart等，2009），其临近的鄂尔浑河谷风成古土壤序列测年结果为5530 cal. yr BP，可能指示了气候湿润（Lehmkuhl等，2011）。但上述序列可能在年代和地层稳定和连续方面均存在严重缺陷。

3.4.2. 蒙古高原南部

蒙古高原南部全新世环境变化研究主要集中在内蒙古西部和甘肃河西走廊地区，在内蒙古额济纳的居延泽（Chen等，2003；Hartmann和W ü nnemann，2009；Herzschuh等，2004；Mischke等，2002）、甘肃民勤的潴野泽（Chen等，2003，2006；Li等，2009；Long等，

2010；Zhao等，2008）和内蒙古杭锦旗的盐海子（Chen C.T.A.等，2003）开展了较多的工作。居延泽和潴野泽的地层和测年记录可能最早地揭示中全新世的干旱气候。该记录表明，7.0~4.6 ka cal. BP（约7.8 ~5.2 cal. kyr BP）为中全新世干旱气候时段（Chen F.H.等，2003），盐海子的粒度和TOC记录（Chen C.T.A.等，2003）以及潴野泽的孢粉记录（Chen等，2006）也揭示了中全新世的干旱气候。具体来讲，居延泽地层和孢粉记录显示，约7.5~5.4 cal. kyr BP为风成砂沉积（Chen F.H.等，2003），相应的孢粉记录中A/C值较前期和后期均有所降低，荒漠群区指数也略有升高（Herzschuh等，2004），这些都指示了中全新世的干旱的气候（图10-7，图10-1中d5）。此外，居延泽地球化学和矿物学序列（未能入选区域平均湿度构建）也表明存在中全新世干旱气候，基于主成分分析得出的径流因子和湖泊水位因子指标均表明中全新世湖泊为径流量较低的低水位，气候干旱（Hartmann和W ü nnemann，2009；图10-7，图10-1中d18）。潴野泽剖面中约7.0~3.8 cal. kyr BP风成砂地层揭示的干旱与孢粉序列中白刺花粉占据主导的层位相对应（Chen等，2006；图10-7，图10-1中d6点）。我们最近开展的额济纳—阿尔山断面现代表土花粉研究表明，白刺花粉在额济纳荒漠戈壁中占据优势，进而支持了潴野泽白刺花粉主导时气候干旱化的说法。向东跨越贺兰山至库不齐沙漠的盐海子，中全新世（8.0~4.3 ka cal. kyr BP）砂含量峰值对应TOC含量的低值，与该湖泊沉积序列无机碳同位素反映的中全新世高盐度湖水一致（钱作华等，2002；图10-1和表10-1中d25），揭示了中全新世的干旱气候（Chen C.T.A.等，2003；图10-7，图10-1中d7）。考虑到样品分辨率和年代误差，上述3个序列所反映的中全新世干旱气候在时相上具有可比性，可能表明中全新世干旱气候具有较大的地理分布。

然而，伴随着该地区全新世研究的深入和全新世气候序列的继续发表，中全新世气候是否干旱的争论仍在继续。潴野泽地区最近发表的两个孢粉序列（图10-7；图10-1中d19和d20）均未反映出中全新世的干旱气候（Li等，2009；Zhao等，2008）。据我们判断，地层和年代揭示的中全新世干旱气候（Chen等，2003，2006；Chen C.T.A.等，2003）比其他指标所指示的中全新世湿润气候（Li等，2009；Zhao等，2008）可靠性可能大一些。我们的判断主要基于以下依据：①湖相沉积序列中砂质沉积主要反映了水动力条件较强的浅水沉积环境（Peng等，2005；W ü nnemann等，2006）；②内蒙古自治区西部阿拉善高原潴野泽和居延泽湖相沉积序列中指示干旱环境的风成砂沉积对应年代为中全新世（Chen等，2003）；③由于风成砂和冲洪积砂中孢粉含量极低，外来花粉可能占据了主导，这导致了风成砂和冲洪积砂层位孢粉谱严重偏离实际，反映的可能是区域外的背景花粉，并不能反映区域植被和气候的真实面貌（Bennett，1983）。

4. 综合与讨论

4.1. 夏季风边缘区（夏季风影响的半干旱地区）

如前所述，使用区域平均的方法集成得到某一地区的平均有效湿度变化的方法的确降低了各序列的分辨率，掩盖了一些细节。然而，该区域平均的方法有效地体现了共性的特征，可以揭示该整个区域湿度变化趋势。本区域中参与区域平均有效湿度构建的序列

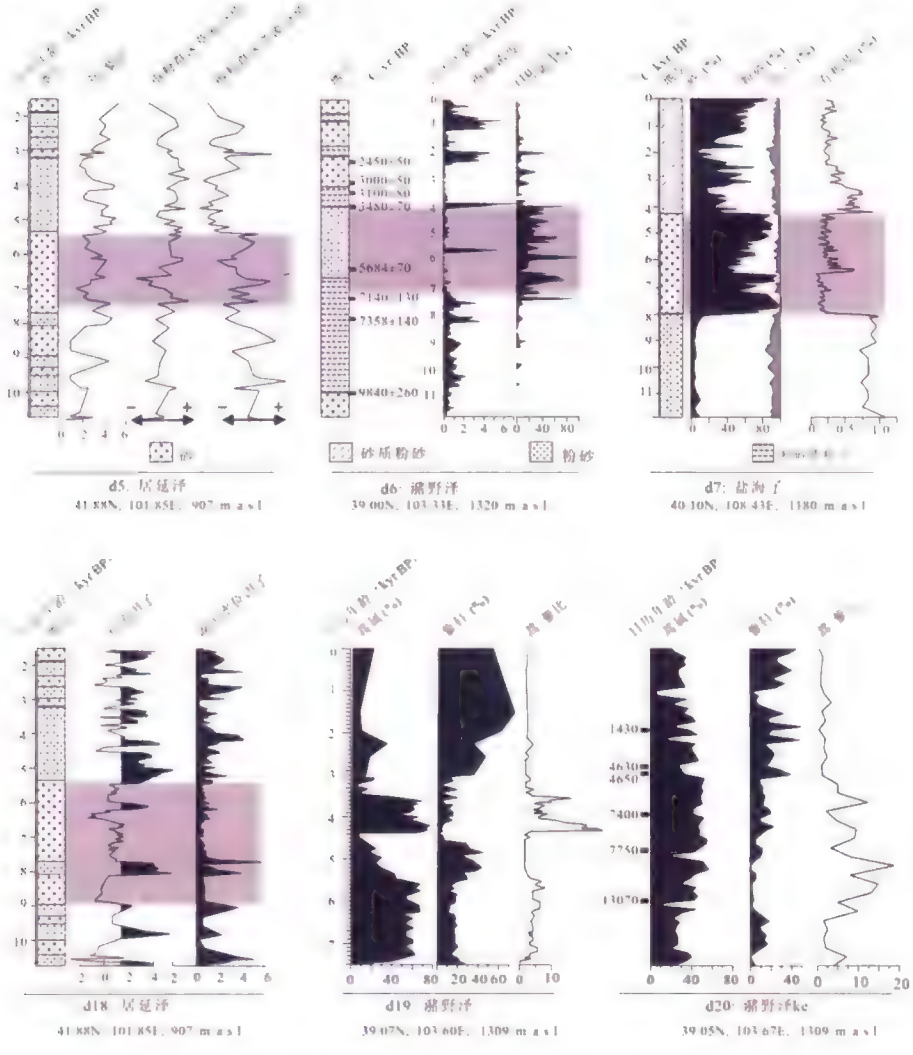

图10-7　蒙古高原南部全新世湿度代用指标序列。资料来源：居延泽（Herzschuh等，2004）；猪野泽（Chen F.H.等，2003，2006）；盐海子（Chen C.T.A.等，2003）。下部为未参加区域平均湿度构建的序列：居延泽（Hartmann和W ü nnemann.，2009）、猪野泽（Li等，2009；Zhao等，2008）

和代用指标有：青海湖孢粉序列中乔木和灌丛花粉百分比、苏家湾和大地湾孢粉序列中乔木和灌丛花粉百分比、岱海孢粉序列中基于孢粉重建的年均降水量序列、巴彦查干孢粉序列中基于孢粉的降水与潜在蒸发比值、呼伦湖基于孢粉记录重建的年降水量。由上述6个序列区域得到的季风边缘区区域平均湿度指数变化曲线（图10-8右下角A）表现出与东亚夏季风强度变化曲线（图10-8中A1；Herzschuh，2006；Zhao等，2009）相同的趋势，均表现出与西太平洋表层水温（Stott等，2004；图10-8中A2）和北半球岁差导致的夏季辐射变化（Berger，1991；COMHAP Members，1988；图10-8中A2）相似的变化趋势。这表明整个太平洋洋流和水温的变化，尤其是热带太平洋地区表层水温的变化（可能受控于东西赤道太平洋厄尔尼诺环流变化）可能影响和控制了亚洲夏季风变化。即早全新世北半球夏

季辐射增强(COMHAP Members,1988),赤道辐合带(ITCZ)向北迁移(Liu等,2000),向亚洲季风系统中带入了更多的水汽。此外,早全新世北半球夏季辐射增加导致海陆热力差异的增加,也同样促进了亚洲夏季风增强,给亚洲大陆带来了更多的降水和湿润的气候环境。需要注意的是,本章季风边缘区区域平均湿度指数变化趋势与前人集成研究的结果也存在一定的差异性,主要体现在季风进退的时间上。相比于Zhao等(2009)和Herzschuh(2006)的曲线,本章区域平均湿度曲线指示的亚洲夏季风增强的时间略晚,衰退的时间略早。此外,上述湿度增强或夏季风增强的时间基本上位于约9.5 cal. kyr BP,同西太平洋表层水温增加的时间(约10.5 cal. kyr BP)相比约滞后1000年左右,表明早全新世亚洲夏季风增强可能显著滞后于热带西太平洋表层的升温。

4.2. 冬季风主导的西伯利亚南部地区

冬季风主导的西伯利亚南部地区参与区域平均湿度指数构建的序列和指标有:贝加尔湖三个序列(Vydirino Shoulder、Posolskoe High、Continental Ridge)基于孢粉的湿度指数、贝加尔湖Buguldeika孢粉序列基于孢粉重建的年降水量、阿尔泰地区Hoton Nuur基于孢粉定量重建的年降水量、俄罗斯阿尔泰地区四个湖泊(Akkol、Grusha、Uzunkol、Kendegelukol)孢粉序列中乔木百分含量。贝加尔地区全新世区域平均湿度序列(图10-8中左上部B1)显示,早全新世约12.0~10.0 cal. kyr BP区域有效湿度呈增加趋势,约10.0~5.6 cal. kyr BP逐渐降低,约5.6 cal. kyr BP以后的晚全新世为低值。阿尔泰地区全新世区域平均湿度曲线(图10-8中B2)显示,约11.0~9.6 cal. kyr BP区域有效湿度显著增加,并于约9.6~6.6 cal. kyr BP维持峰值,约6.6 cal. kyr BP之后逐渐降低。

受地轴倾斜控制的大气径圈环流位置季节性北移(即与西风带相关的弗雷尔环流)和夏季亚速尔高压的扩张北移(Bridgman和Oliver,2006)的控制和影响,暖季北半球西风带向北迁移,俄罗斯平原和其东部的西伯利亚南部地区(阿尔泰地区和贝加尔地区)同处于西风带控制之下,西风带气候系统便成为两地气候变化的纽带和联系机制(Aizen等,2001)。此外,暖季发育成熟的亚洲低压系统向东向北延伸到西伯利亚东南部地区,有效地"吸引"西风带向东延伸,也促进了西风带气候系统对中亚地区的控制(从咸海到兴安岭)(Aizen等,2001)。而Velichko和他的同事认为俄罗斯平原地区的夏季温度以及年均降水量(主要发生在暖季)(图10-8中B3;Velichko等,2002)与格陵兰地区的暖季温度(图10-8中B4;Stuiver等,1995)密切相关。因此,本章将西伯利亚南部阿尔泰地区和贝加尔地区的全新世湿度曲线与西风带上游俄罗斯平原全新世暖季温度和年均降水序列(图10-8中B3;Velichko等,2002)以及北大西洋地区暖季温度进行了对比。对比结果显示,阿尔泰地区和贝加尔地区全新世湿度变化与北大西洋地区暖季温度变化和俄罗斯平原地区暖季温度及降水变化相关,可能北大西洋暖季温度变化导致的洋面蒸发增强,通过北移的西风带控制和影响了下游的俄罗斯平原以及本文综述的阿尔泰和西伯利亚地区。指标序列间的差异可能表明:①早全新世初期贝加尔地区的湿度变化快速响应于俄罗斯平原和北大西洋地区温度的上升和降水的增加,而阿尔泰地区似乎响应略显迟滞,这可能归因于两个地区海拔高度的不同(阿尔泰地区海拔约2000m,贝加尔地区平均海拔在340m左

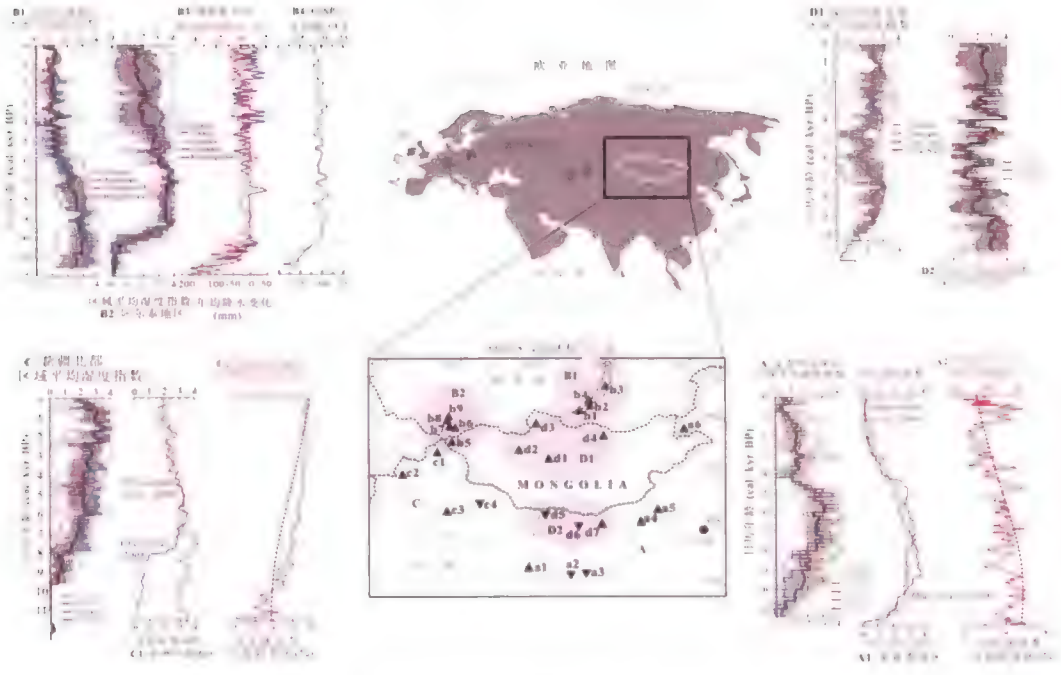

图10-8　区域平均湿度指数及与相关气候系统序列或驱动因子的比较(自Wang和Feng,2013)。注:1夏季风影响的季风边缘区区域平均湿度指数与东亚夏季风强度指数(Zhao等,2009)、季风区平均有效湿度指数(Herzschuh,2006)、热带西太平洋表层水温变化(Stott等,2004)以及北半球夏季日辐射变化(Berger,1991;COHMAP members,1988)进行比较;2西伯利亚南部地区区域平均湿度指数比较于俄罗斯平原暖季温度和年均降水量(Velichko等,2002)、格陵兰温度变化(Stuiver等,1995);3新疆北部区域平均湿度指数序列比较于亚洲中部地区平均湿度指数序列(Chen等,2008)、亚洲中部地区平均有效湿度序列(Herzschuh,2006)、欧洲西北地区冷季温度变化(Davis等,2003)和北半球冬季日辐射变化(Berger,1991)

右);(2)约6000年以来,阿尔泰地区和贝加尔地区湿度呈明显降低趋势,而俄罗斯平原地区的暖季温度和年降水以及格陵兰地区的温度变化均未表现出该趋势,这表明约6000年以来阿尔泰地区和贝加尔地区受北大西洋影响或控制减弱、更多地受北半球温度降低的影响;3阿尔泰地区区域平均湿度因子序列显示,约4000年以来标准误差较大,这主要源自Uzunkol序列中乔木花粉含量的异常高值,可能这种高含量的乔木花粉仅体现了森林覆盖条件较好情况下的总体面貌,不能反映区域湿度本质变化。

4.3. 西风带影响的新疆北部地区

西风带影响的新疆北部地区参与区域平均湿度因子构建的序列和指标有:乌伦古湖多指标综合重建的湖泊水位变化(包括孢粉)、艾比湖、博斯腾湖以及巴里坤湖孢粉记录的A/C值。新疆北部地区全新世区域平均湿度序列(图10-8中左下C)最为突出的特点是,约8.0 cal. kyr BP以来呈持续增加趋势,约6.0~0.5 cal. kyr BP为峰值。本章集成得到了新疆北部区域平均湿度变化序列(图10-8中C)与Chen等(2008)和Herzschuh(2006)总结的有效湿度变化序列(图10-8中C1),既有相同也有差异。具体来说,首先,本集成得到的区域平

均湿度和Chen等(2008)重建的平均有效湿度均表现出早全新世(8.0 cal. kyr BP以前)干旱气候,而Herzschuh(2006)重建的平均有效湿度序列则指示了较为湿润的早全新世。其次,约8.0 cal. kyr BP以来,本集成的区域湿度因子表现出持续增加的趋势,仅在600年以来表现出显著降低,而Chen等(2008)和Herzschuh(2006)构建的区域有效湿度变化则展示出约6.0 cal. kyr BP以后逐渐降低的趋势。我们将本章新疆北部地区区域平均湿度变化曲线与北半球冬季日辐射曲线(图10-8中C2;Berger,1991)和欧洲西北部冷季温度变化(图10-8中C2;Davis,2003)进行了对比,结果显示二者具有相似的变化趋势。这种相同的变化趋势可能揭示,北半球冬季辐射增加导致了北大西洋地区冬季温度升高,洋面蒸发增强,在冷季给西风带注入了更多的水汽,导致下风地区冬季降水主导的地区湿度增加。

4.4. 蒙古高原核心干旱区

蒙古高原核心干旱区区域平均湿度构建使用的序列和代用指标有,蒙古高原北部的Ugii湖(即优贵湖)孢粉湿度指数、Telmen湖孢粉干旱指数、Hovsgol湖孢粉草原/森林指数(SFI)和Gun Nuur(即岗湖)乔木花粉含量;蒙古高原南部的居延泽孢粉A/C值、内蒙古潴野泽孢粉记录中白刺花粉含量和内蒙古库不齐沙漠盐海子TOC含量。

如图10-8D(右上部)所示,蒙古高原北部的区域平均湿度曲线显示,约7.0~3.8 cal. kyr BP为干旱气候时段,之前和之后均为气候湿润时段。考虑各序列分辨率差异和年代不确定性后,该干旱时段的起讫时间基本上对应于贝加尔湖地区孢粉记录重建的高温时段(约6.5~2.5 cal. kyr BP;Demske等,2005)。我们注意到蒙古高原北部的Gun Nuur孢粉序列并不支持本章区域平均湿度主张的中全新世干旱气候,在没有理由剔除该序列(>22)的前提下,本章蒙古高原北部区域平均湿度构建时使用了该序列,这也就造成了中全新世干旱时段的标准误差略显偏大。蒙古高原南部区域平均湿度序列基本上支持了Chen等依据地层和年代数据提出的中全新世干旱主张(Chen F.H.等,2003),表现出约8.0~4.0 cal. kyr BP为湿度最低值的特征(图10-8中D2),指示了中全新世干旱。该中全新世干旱气候在年代上对应于西伯利亚南部孢粉序列揭示的中全新世暖期(Demske等,2005)和中国季风区的中全新世大暖期(Shi等,1993),表明蒙古高原干旱区中全新世干旱气候可能与中全新世暖季温度升高有关(Bush,2005;Wang等,2011)。即:升温导致的蒸发增强超过了降水增加(如果中全新世降水有增加的话),导致了干旱气候的生成。早、晚全新世该地区湿度的增加很可能和较低的暖季温度有关(即低温导致蒸发降低)。

5. 结论

(1)亚洲夏季风边缘区全新世湿度演化与东亚夏季风强度演化历史(Zhao等,2009;Herzschuh,2006)基本同步,二者均滞后于热带西太平洋表层水温变化和北半球夏季辐射变化。

(2)西伯利亚南部全新世湿度演化历史是整个欧亚大陆中纬度西风带影响区域气候变化的一部分,大西洋地区暖季温度和洋面蒸发可能影响该区的气候变化。

(3)新疆北部全新世以来湿度增加可能和欧洲北部地区和大西洋地区冷季温度增加有关,北半球冬季辐射增强可能导致了上述地区温度的增加。

(4)蒙古高原北部和南部的中全新世干旱气候,在年代上可以和西伯利亚南部及中国季风区暖期对应,进而支持了干旱气候可能归因于暖季温度增加导致的蒸发增强的假说。

致谢:感谢国家自然科学基金(No. 40930102, No. 40331102, No.41162004)和内蒙古教育厅高等学校青年科技英才领军项目A类(NYNT-14-01)的支持

参考文献

陈添宇,李照荣,陈乾,李宝梓. 2005. 用GMS5卫星反演水汽场分析中国西北地区大气水汽分布的气候特征.大气科学,29(6):864~871.

陈曦. 2010.中国干旱区自然地理.北京:科学出版社.

高由禧. 1962.东亚季风的若干问题.北京:科学出版社.

韩淑媞. 1992.新疆巴里坤湖全新世环境变迁序列.地质科学,12: 247~260.

韩淑媞,袁玉江. 1990.新疆巴里坤湖35000年来古气候变化序列.地理学报,45(3):350~362.

胡汝骥. 2004.中国天山自然地理.北京: 中国环境科学出版社.

黄小忠. 2006.新疆博斯腾湖记录的亚洲中部干旱区全新世气候变化研究.兰州大学博士论文.

李国胜. 1993.艾比湖最近20ka的氧碳同位素记录与气候突变. 海洋地质与第四纪地质,13:75~64.

李江凤. 1991.新疆气候.北京:气象出版社.

李吉均. 1990.中国西北地区晚更新世以来环境变迁模式.第四纪研究,3: 197~204.

林瑞芬,卫克勤. 1998.新疆玛纳斯湖沉积物氧同位素记录的古气候信息探讨—与青海湖和色林错比较.第四纪研究,4:308~318.

林瑞芬,卫克勤,程志远,王志祥,Gasse, F., Fontes, J.-C., Gibert, E., Tucholka, P. 1996.新疆玛纳斯湖沉积柱样的古气候古环境研究.地球化学,25(1):63~72.

吴敬禄. 1995.新疆艾比湖全新世沉积特征及古环境演化.地理学报,15:39~47.

夏敦胜,马玉贞,陈发虎,王建民. 1998. 甘肃大地湾剖面全新世植被演替与气候变化. 兰州大学学报(自),34(1):119~127.

肖霞云,蒋庆丰,刘兴起,肖海丰,沈吉. 2006. 乌伦古湖全新世以来高分辨率的孢粉记录与环境变迁. 微体古生物,23(1):77~86.

阎顺,许英勤. 1992. 新疆阿尔泰山大罗坝盆地全新世植被与环境.新疆地质,10:279~284

杨美临. 2008.博斯腾湖多代用指标(侧重硅藻)记录的全新世气候变化模式.兰州大学博士论文.

羊向东,王苏民. 1994.一万多年来乌伦古湖地区花粉组合及其古环境.干旱区研究,11:7~10.

张家宝,史玉光. 2002,新疆气候变化及短期气候预测研究.北京:气象出版社.

张兰生,方修琦,任国玉,索秀芬. 1997.我国北方农牧交错带的环境演变.地学前缘,1:127~136.

周琴南. 1983.关于新疆降水水汽来源问题的研究.北方天气文集.北京:北京大学出版社.

Aizen, E.M., Aizen, V.B., Melack, J.M., Nakamura, T. and Ohta, T., 2001. Precipitation and atmospheric circulation patterns at mid-latitudes of Asia. International Journal of Climatology, 21:535~556.

An, C.B., Chen, F.H. and Barton, L., 2008. Holocene environmental changes in Mongolia: A review. Global and Planetary Change, 63: 283~289.

An, C.B., Feng, Z.-D. and Barton, L., 2006. Dry or humid? Mid-Holocene humidity changes in arid and

semi-arid China. Quaternary Science Reviews, 25(3~4): 351~361.

An, C.B., Zhao, J.J., Tao, S.C., Lv, Y.B., Dong, W.M., Li, H., Jin, M. and Wang, Z.L., 2011. Dust variation recorded by lacustrine sediments from arid Central Asia since ~15 cal ka BP and its implication for atmospheric circulation. Quaternary Research, 75: 566~573.

An, Z.S., Colman, S.M., Zhou, W.J., Li, X.Q., Brown, E.T., Jull, A.J.T., Cai, Y.J., Huang, Y.S., Lu, X.F., Chang, H., Song, Y.G., Sun, Y.B., Xu, H., Liu, W.G., Jin, Z.D., Liu, X.D., Cheng, P., Liu, Y., Ai, L., Li, X.Z., Liu, X.J., Yan, L.B., Shi, Z.G., Wang, X.L., Wu, F., Qiang, X.K., Dong, J.B., Lu, F.Y., and Xu, X.W., 2012. Interplay between the Westerlies and Asian monsoon recorded in Lake Qinghai sediments since 32 ka. Scientific Reports, 2: 1~7.

An, Z.S., Kukla, G. J., Porter, S. C. and Xiao, J., 1991. Magnetic susceptibility evidence of monsoon variation on the Loess Plateau of central China during the last 130,000 years. Quaternary Research, 36: 29~36.

An, Z.S., Porter, S.C., Kutzbach, J.E., Wu, X.H., Wang, S.M., Liu, X.D., Li, X.Q. and Zhou, W.J., 2000. Asynchronous Holocene optimum of the East Asian monsoon. Quaternary Science Reviews, 19(8): 743~762.

Andreev, A.A., Klimanov, V.A. and Sulerzhitsky, L.D., 2001. Vegetation and climate history of the Yana River lowland, Russia, during the last 6400 yr. Quaternary Science Reviews, 20: 259~266.

Bennett, K.D., 1983. Devensian late-glacial and flandrian vegetational history at Hockham mere, Norfolk, England. II. Pollen accumulation rates. New Phytol. 95: 489~504.

Berger, A. and Loutre, M.F., 1991. Insolation values for the climate of the last 10 million years. Quaternary Science Reviews, 10: 297~317.

Bezrukov, E.V., Abzaeva, A.A., Letunova, P.P., Kulagina, N.V. and Orlova, L.A., 2009. Evidence of environmental instability of the lake Baikal area after the last glaciation (based on pollen records from peatlands). Archaeology, Ethnology and Anthropology of Eurasia, 37(3): 17~25.

Bezrukov, E.V., Abzaeva, A.A., Letunova, P.P., Kulagina, N.V., Vershinin, K.E., Belov, A.V., Orlova, L. A., Danko, L.V. and Krapinina, S.M., 2005. Post-glacial history of Siberian spruce (Picea obovata) in the Lake Baikal area and the significance of this species as a paleo-environmental indicator. Quaternary International, 136: 47~57.

Birks, H.J.B., 1995. Quantitative palaeoenvironmental reconstructions. Statistical modeling of quaternary science data (ed. by D. Maddy and J.S. Brew), Quaternary Research Association, Cambridge.

Blyakharchuk, T.A., Wright, H.E., Borodavko, P.S., van der Knaap, W.O. and Ammann, B., 2004. Late Glacial and Holocene vegetational changes on the Ulagan high-mountain plateau, Altai Mountains, southern Siberia. Palaeogeography, Palaeoclimatology, Palaeoecology, 209(1): 259~279.

Blyakharchuk, T.A., Wright, H.E., Borodavko, P.S., van der Knaap, W.O. and Ammann, B., 2007. Late Glacial and Holocene vegetational history of the Altai Mountains (southwestern Tuva Republic, Siberia). Palaeogeography, Palaeoclimatology, Palaeoecology, 245(3): 518~534.

Bridgman, B.H. and Oliver, J.E., 2006. The global climate system: patterns, processes, and teleconnections. Cambridge University Press, New York.

Bush, A.B.G., 2005. CO_2/H_2O and orbitally driven climate variability over central Asia through the Holocene. Quaternary International, 136: 15~23.

Chen, C.T.A., Lan, H.C., Lou, J.Y. and Chen, Y.C., 2003. The dry Holocene Megathermal in Inner Mongolia. Palaeogeography, Palaeoclimatology, Palaeoecology, 193: 181~200.

Chen, F.H., Bloemendal, J., Wang, J.M., Li, J.J. and Oldfield, F., 1997. High-resolution multi-proxy climate records from Chinese loess: evidence for rapid climatic changes over the last 75 kyr. Palaeogeography, Palaeoclimatology, Palaeoecology, 130: 323~335.

Chen, F.H., Cheng, B., Zhao, Y., Zhu, Y. and Madsen, D.B., 2006. Holocene environmental change inferred from a high-resolution pollen record, Lake Zhuyeze, arid China. The Holocene, 16: 675~684.

Chen, F.H., Shi, Q. and Wang, J.M., 1999. Environmental changes documented by sedimentation of Lake Yiema in arid China since the Late Glaciation. Journal of Paleolimnology, 22: 159~169.

Chen, F.H., Wu, W., Holmes, J.A., Madsen, D.B., Zhu, Y., Jin, M. and Oviatt, C.G., 2003. A mid-Holocene drought interval as evidenced by lake desiccation in the Alashan Plateau, Inner Mongolia, China. Chinese Science Bulletin, 48: 1401~1410.

Chen, F.H., Yu, Z.C., Yang, M.L., Ito, E., Wang, S.M., Madsen, D.B., Huang, X.Z., Zhao, Y., Sato, T., Birks, H.J.B., Boomer, I., Chen, J.H., An, C.B., and Wünnemann, B., 2008. Holocene moisture evolution in arid central Asia and its out-of-phase relationship with Asian monsoon history. Quaternary Science Reviews, 27(3~4): 351~364.

COHMAP Members, 1988. Climatic changes of the last 18 000 years: observations and model simulations. Science, 241: 1043~1052.

Davis, B.A.S., Brewer, S., Stervenson, A.C., Guiot, J. and Contributors, D., 2003. The temperature of Europe during the Holocene reconstructed from pollen data. Quaternary Science Reviews, 22: 1701~1706.

Demske, D., Heumann, G., Granoszewski, W., Nita, M., Mamokowa, K., Tarasov, P.E. and Oberhansli, H., 2005. Late glacial and Holocene vegetation and regional climate variability evidenced in high-resolution pollen records from Lake Baikal. Global and Planetary Change, 46: 255~279.

Dorofeyuk, N.I. and Tarasov, P.E., 1998. Vegetation and lake levels in Northern Mongolia in the last 12,500 years as indicated by data of pollen and diatom analyses. Stratigraphy and Geological Correlation, 6 (1): 70~83.

El-Mosilimany, A.P., 1990. Ecological significance of common non-arboreal pollen: examples from drylands of the Middle East. Review of Palaeobotany and Palynology, 64: 343~350.

Fang, X.M, Lv, L.Q., Mason, J.A., Yang, S.L., An, Z.S., Li, J.J. and Guo, Z.L., 2003. Pedogenic response to millennial summer monsoon enhancements on the Tibetan Plateau. Quaternary International, 106: 79~88.

Fang, X.M., Ono, Y., Fukusawa, H., Pan, B.T., Li, J.J., Guan, D.H., Oi, K., Tsukamoto, S., Torii, M. and Mishima, T., 1999. Asian summer monsoon instability during the past 60 000 years: magnetic susceptibility and pedogenic evidence from the western Chinese Loess Plateau. Earth and Planetary Science Letters, 168: 219~232.

Feng, Q. and Liu, W., 2005. Environmental conditions leading to the formation of Holocene soil layers in the Northern Taklimakan Desert, Tarim Basin, Northwest China. Geological Journal, 40(1): 23~34.

Feng, Z.-D., 2001. Gobi dynamics in the Northern Mongolian Plateau during the past 20 000+ yr: preliminary results. Quaternary International, 76: 77~83.

Feng, Z.-D., An, C.B., Tang, L.Y. and Jull, A.J.T., 2004. Stratigraphic evidence of a Megahumid climate

between 10 000 and 4000 years B.P. in the western part of the Chinese Loess Plateau. Global and Planetary Change, 43(3~4): 145~155.

Feng, Z.-D., An, C.B. and Wang, H.B., 2006a. Holocene climatic and environmental changes in the arid and semi-arid areas of China: a review. The Holocene, 16(1): 119~130.

Feng, Z.-D. and Khosbayar, P., 2004. Paleosubarctic Eolian environments along the southern margin of the North American Icesheet and the southern margin of Siberia during the Last Glacial Maximum. Palaeogeography, Palaeoclimatology, Palaeoecology, 212(3~4): 265~275.

Feng, Z.-D., Tang, L.Y., Wang, H.B., Ma, Y.Z. and Liu, K.B., 2006b. Holocene vegetation variations and the associated environmental changes in the western part of the Chinese Loess Plateau. Palaeogeography, Palaeoclimatology, Palaeoecology, 241: 440~456.

Feng, Z.-D., Wang, W.G., Guo, L.L., Khosbayar, P., Narantsetseg, T., Jull, A.J.T, An, C.B., Li, X.Q., Zhang, H.C. and Ma, Y.Z., 2005. Lacustrine and eolian records of Holocene climate changes in the Mongolian Plateau: preliminary results. Quaternary International, 136(1): 25~32.

Feng, Z.-D., Zhai, X.W., Ma, Y.Z., Huang, C.Q., Wang, W.G., Zhang, H.C., Khosbayar, P., Narantsetseg, T., Liu, K.B. and Rutter, N.W., 2007. Eolian environmental changes in the Northern Mongolian Plateau during the past 35,000 yr. Palaeogeography, Palaeoclimatology, Palaeoecology, 245(3~4): 505~517.

Fowell, S.J., Hansen, B., Peck, J.A., Khosbayar, P. and Ganbold, E., 2003. Mid to late Holocene climate evolution of the Lake Telmen Basin, North Central Mongolia, based on palynological data. Quaternary Research, 59(3): 353~363.

Fukumoto, Y., Kashima, K., Orkhonselenge, A. and Ganzorig, U., 2012. Holocene environmental changes in northern Mongolia inferred from diatom and pollen records of peat sediment. Quaternary International, 254: 83~91.

Gong, D.Y., Wang, S.W. and Zhu, J.H., 2001. East Asian winter monsoon and Arctic Oscillation. Geophysical Research Letters, 28(10): 2073~2076.

Grunert, J., Lehmkuhl, F. And Walther, M., 2000. Paleoclimatic evolution of the Uvs Nuur basin and adjacent areas (Western Mongolia). Quaternary International, 65/66: 171~192.

Guiot, J., 1990. Methodology of the last climatic cycle reconstruction from pollen data. Palaeogeography, Palaeoclimatology, Palaeoecology, 80: 49~69.

Gunin, P.D., 1999. Vegetation dynamics of Mongolia. Kluwer Academic Publisher, Copenhagen.

Guo, L.L., Feng, Z.D., Li, X.Q., Liu, L.Y. and Wang, L.X., 2007. Holocene climatic and environmental changes recorded in Baahar Nuur Lake core in the Ordos Plateau, Inner Mongolia of China. Chinese Science Bulletin, 52(7): 959~966.

Harrison, S.P., Yu, G. and Tarasov, P.E., 1996. Late Quaternary Lake-Level Record from Northern Eurasia. Quaternary Research, 45(2): 138~159.

Hartmann, K. and Wünemann, B., 2009. Hydrological changes and Holocene climate variations in NW China, inferred from lake sediments of Juyanze palaeolake by factor analyses. Quaternary International, 194: 28~44.

He, Y., Theakstone, W. H., Zhang, Z. L., Zhang, D. A., Yao, T. D., Chen, T., Shen, Y. P. and Pang, H. X., 2004. Asynchronous Holocene climatic change across China. Quaternary Research, 61(1): 52~63.

Herzschuh, U., 2006. Palaeo-moisture evolution in monsoonal Central Asia during the last 50 000 years. Quaternary Science Reviews, 25(1~2): 163~178.

Herzschuh, U., Tarasov, P., Wünemann, B. and Hartmann, K., 2004. Holocene vegetation and climate of the Alashan Plateau, NW China, reconstructed from pollen data. Palaeogeography, Palaeoclimatology, Palaeoecology, 211(1~2): 1~17.

Hilbig, W., 1995. The vegetation of Mongolia. SPB Academic Publishing, Amsterdam.

Horiuchi, K., Minoura, K., Hoshino, K., Oda, T., Nakamura, T. and Kawai, T., 2000. Palaeoenvironmental history of Lake Baikal during the last 23 000 years. Palaeoclimatology Palaeoecology, 157(1~2): 95~108.

Huang, X.Z., Chen, F.H., Fan, Y.X. and Yang, M.L., 2009. Dry late-glacial and early Holocene climate in arid central Asia indicated by lithological and palynological evidence from Bosten Lake, China. Quaternary International, 194: 19~27.

Jiang, Q.F., Shen, J., Liu, X.Q., Zhang, E.L. and Xiao, X.Y., 2007. A high-resolution climatic change since Holocene inferred from multi-proxy of lake sediment in westerly area of China. Chinese Science Bulletin, 52(14): 1970~1979.

Jiang, W.Y., Guo, Z.T., Sun, X.J., Wu, H.B., Chu, G.Q., Yuan, B.Y., Hatte, C. and Guiot, J., 2006. Reconstruction of climate and vegetation changes of Lake Bayanchagan (Inner Mongolia): Holocene variability of the East Asian monsoon. Quaternary Research, 65(3): 411~420.

Karabanov, E.B., Prokopenko, A.A., Williams, D.F. and Khursevich, G.K., 2000. A new record of Holocene climate change from the bottom sediments of Lake Baikal. Palaeogeography, Palaeoclimatology, Palaeoecology, 156 (3~4): 211~224.

Kim, J.-H., Rumbu, N., Lorenz, S.J., Lohmann, G., Nam, S.-Il., Schouten, S., Ruhlemann, C. and Schneider, R.R., 2004. North Pacific and North Atlantic sea-surface temperature variability during the Holocene. Quaternary Science Reviews, 23: 3141~2154.

Klimanov, V.A., 1984. Paleoclimatic reconstruction based on the information statistical method. In Velichko A.A., H.E. Wright & C.W. Barnosky (eds.), Late Quaternary Environments of the Soviet Union. University of Minnesota Press, Minneapolis.

Kutzbach, J.E. and Liu, Z., 1997. Response of the African monsoon to orbital forcing and ocean feedbacks in the middle Holocene. Science, 278: 440~443.

Lehmkuhl, F., Hilgers, A., Fries, S., Hulle, D., Schlutz, F., Shumilovskikh, L., Felauer, T. and Protze, J., 2011. Holocene geomorphological processes and soil development as indicator for environmental change around Karakorum, Upper Orkhon Valley (Central Mongolia). Catena, 87: 31~44.

Li, X.Q., Zhou, W.J., An, Z.S. and Dodson, J., 2003a. The vegetation and monsoon variations at the desert-loess transition belt at Midiwan in northern China for the last 13 ka. The Holocene, 13(5): 779~784.

Li, X.Q., Zhou, W.J. and Dodson, J., 2003b. The vegetation characteristics of the Yuan area at Yaoxian on the Loess Plateau in China over the last 12 000 years. Review of Palaeobotany and Palynology, 124: 1~7.

Li, Y., Wang, N., Cheng, H., Long, H. and Zhao, Q., 2009. Holocene environmental change in the marginal area of the Asian monsoon: a record from Zhuye Lake, NW China. Boreas, 38: 349~361.

Lister, G. S., Kelts, K., Zao, C. K., Yu, J.-Q. and Niessen, F., 1991. Lake Qinghai, China: closed-basin like levels and the oxygen isotope record for ostracoda since the latest Pleistocene. Palaeogeography, Palaeoclimatology,

Palaeoecology, 84: 141~162.

Liu, H.Y., Xu, L.H. and Cui, H.T., 2002a. Holocene history of desertification along the woodland-steppe border in northern China. Quaternary Research, 57: 259~270.

Liu, X. Q., Shen, J., Wang, S. M., Yang, X. D., Tong, G. B. and Zhang, E.L., 2002b. A 16 000-year pollen record of Qinghai Lake and its paleoclimate and paleoenvironment. Chinese Science Bulletin, 47: 1931~1936.

Liu, X.Q., Herzschuh, U., Shen, J., Jiang, Q.F. and Xiao, X.Y., 2008. Holocene environmental and climatic changes inferred from Wulungu Lake in northern Xinjiang, China. Quaternary Research, 70(3): 412~425.

Liu, Z., Kutzbach, J. and Wu, L., 2000. Modeling climate shift of El Nino variability in the Holocene. Geophysical Research Letters, 27: 2265~2268.

Long, H., Lai, Z.P., Wang, N.A. and Li, Y., 2010. Holocene climate variations from Zhuyeze terminal lake records in East Asian monsoon margin in arid northern China. Quaternary Research, 74(1): 46~56.

Lydolph, P. E., 1977. Climates of the Soviet Union in World Survey of Climatology, Volume 7. Elsevier Scientific Publishing, New York.

Ma, Y.Z., Liu, K.-B., Feng, Z.-D., Sang, Y.L., Wang, W. and Sun, A.Z., 2008. A survey of modern pollen and vegetation along a south-north transect in Mongolia. Journal of Biogeography, 35: 1512~1532.

Ma, Y.Z., Zhang, H.C., Pachur, H.J., Wünnemann, B., Li, J.J. and Feng, Z.-D., 2004. Modern pollen-based interpretations of mid-Holocene palaeoclimate (8500 to 3000 cal. BP) at the southern margin of the Tengger desert, northwestern China. The Holocene, 14(6): 841~850.

Mangerud, J., Andersen, S.T., Berglund, B.E. and Donner, J.J., 1974. Quaternary stratigraphy of Norden, a proposal for terminology and classification. Boreas, 3(3): 109~126.

Mayewski, P.A., Rohling, E.E., Stager, J.C., Karlén, W., Maasch, K.A., Meeker, L.D., Meyerson, E.A., Gasse, F., van Kreveld, S., Holmgren, K., Lee-Thorp, J., Rosqvist, G., Rack, F., Staubwasser, M., Schneider, R.R. and Steig, E.J., 2004. Holocene climate variability. Quaternary Research, 62(3): 243~255.

Meeker, L.D. and Mayewski, P.A., 2002. A 1400-year high-resolution record of atmospheric circulation over the North Atlantic and Asia. The Holocene, 12(3) : 257~266.

Minckley, T. and Whitlock, C., 2000. Spatial variation of modern pollen in Oregon and southern Washington, USA. Review of Palaeobotany and Palynology, 112: 97~123.

Mischke, S., Fuchs, D., Riedel, F. and Schudack, M.E., 2002. Mid to Late Holocene palaeoenvironment of Lake Eastern Juyanze (north-western China) based on ostracods and stable isotopes. Geobios, 35: 99~110.

Moore P.D., Webb J.A. and Collinson M.E., 1991. Pollen Analysis, 2nd edition. Blackwell Scientific Publication, Oxford.

Morley, D.W., Leng, M.J., Mackay, A.W. and Sloane, H.J., 2005. Late glacial and Holocene environmental change in the Lake Baikal region documented by oxygen isotopes from diatom silica. Global and Planetary Change, 46: 221~233.

Morrill, C., Overpeck, J.T. and Cole, J.E., 2003. A synthesis of abrupt changes in the Asian summer monsoon since the last deglaciation. The Holocene, 13(4): 465~467.

Murakami, T., Katsuta, N., Yamamoto, K., Takamatsu, N., Takano, M., Oda, T., Matsumoto, G. I., Horiuchi, K. and Kawai, T., 2010. A 27-kyr record of environmental change in central Asia inferred from the sediment

record of Lake Hovsgol, northwest Mongolia. Journal of Paleolimnology, 43: 369~383.

Overpeck, J.T., Webb, T. and Prentice, I.C., 1985. Quantitative interpretation of fossil pollen spectra: dissimilarity coefficients and the method of modern analogs. Quaternary Research, 23: 87~108.

Pachur, H.-J., Wünemann, B. and Zhang, H., 1995. Lake Evolution in the Tengger Desert, Northwestern China, during the Last 40 000 Years. Quaternary Research, 44: 171~180.

Peck, J.A., Khosbayar, P., Fowell, S.J., Pearce, R.B., Ariunbileg, S., Hansen, B. and Soninkhishig, N., 2002. Mid to Late Holocene climate change in north central Mongolia as recorded in the sediments of Lake Telmen. Palaeogeography, Palaeoclimatology, Palaeoecology, 183(1~2): 135~153.

Peng, Y., Xiao, J., Nakamura, T., Liu, B. and Inouchi, Y., 2005. Holocene East Asian monsoonal precipitation pattern revealed by grain-size distribution of core sediments of Daihai Lake in Inner Mongolia of north-central China. Earth and Planetary Science Letters, 233(3~4): 467~479.

Prentice, I. C., 1985. Pollen representation, source area, and basin size: toward a unified theory of pollen analysis. Quaternary Research, 23: 76~86.

Prentice, I.C., Guiot, J., Huntley, B., Jolly, D. and Cheddadi, R., 1996. Reconstructing biomes from palaeoecological data: a general method and its application to European pollen data at 0 and 6 ka. Climate Dynamics, 12: 185~194.

Prokopenko, A.A., Alexander, A., Khursevich, G.K., Bezrukova, E.V., Kuzmin, M.I., Boes, X., Williams, D.F., Fedenya, S.A., Kulagina, N.V., Letunova, P.P., and Abzaeva, A.A., 2007. Paleoenvironmental proxy records from Lake Hovsgol, Mongolia, and a synthesis of Holocene climate change in the Lake Baikal watershed. Quaternary Research, 68(1): 2~17.

Prokopenko, A.A., Williams, D.F., Karabanov, E.B. and Khursevich, G.K., 1999. Response of Lake Baikal ecosystem to climate forcing and pCO_2 change over the last glacial/interglacial transition. Earth and Planetary Science Letters, 172 (3~4): 239~253.

Rhodes, T.E., Gasse, F., Lin, R. F., Fontes, J.-C., Wei, K.Q., Bertrand, P., Gibert, E., Melieres, F., Tucholka, P., Wang, Z.X. and Cheng, Z.-Y., 1996. A late Pleistocene-Holocene lacustrine record from Lake Manas, Zunggar (northern Xinjiang, western China). Palaeogeography, Palaeoclimatology, Palaeoecology, 120: 105~121.

Ricketts, R.D., Johnson, T.C., Brown, E.T., Rasmussen, K.A. and Romanovsky, V.V., 2001. The Holocene paleolimnology of Lake Issyk-Kul, Kyrgyzstan: trace element and stable isotope composition of ostracodes. Palaeogeography, Palaeoclimatology, Palaeoecology, 176: 207~227.

Rudaya, N. Tarasov, P., Dorofeyuk, N., Solovieva, N., Kalugin, I., Andreev, A., Daryin, A., Diekmann, B., Riedel, F., Tserendash, N. and Wagner, M., 2009. Holocene environments and climate in the Mongolian Altai reconstructed from the Hoton-Nur pollen and diatom records: a step towards better understanding climate dynamics in Central Asia. Quaternary Science Reviews, 28(5~6): 540~554.

Ruddiman, W.F., 2008. Earth's climate, past and future (Second Edition). Freeman and Company, New York.

Schwanghart, W., Frechen, M., Kuhn, N.J. and Schütt, B., 2009. Holocene environmental changes in the Ugii Nuur basin, Mongolia. Palaeogeography, Palaeoclimatology, Palaeoecology, 279(3~4): 160~171.

Shen, J., Liu, X. Q., Wang, S. M. and Ryo, M., 2005. Palaeoclimatic changes in the Qinghai Lake area

during the last 18,000 years. Quaternary International, 136: 131~140.

Shi, Q., Chen, F.H., Zhu, Y., and Madsen, D., 2002. Lake evolution of the terminal area of Shiyang River drainage in arid China since the last glaciations. Quaternary International, 93/94: 31~43.

Shi, Y.F., Kong, Z.C., Wang, S.M., Tang, L.Y., Wang, F.B., Yao, T.D., Zhao, X.T., Zhang, P.Y. and Shi, S., 1993. Mid-Holocene climates and environments in China. Global and Planetary Change, 7(1~3): 219~233.

Shichi, K., Takahara, H., Krivonogov, S.K., Bezrukova, E.V., Kashiwaya, K., Takehara, A. and Nakamura, T., 2009. Late Pleistocene and Holocene vegetation and climate records from Lake Kotokel, central Baikal region. Quaternary International, 205: 98~110.

Sklyarov, E.V., Solotchina, E.P., Vologina, E.G., Ignatova, N.V., Izokh, O.P., Kulagina, N.V., Sklyarova, O.A., Solotchin, P.A., Stolpovskaya, V.N., Ukhova, N.N., Fedorovskii, V.S. and Khlystov, O.M., 2010. Detailed Holocene climate record from the carbonate section of saline Lake Tsagan-Tyrm (West Baikal area). Russian Geology and Geophysics, 51: 237~258.

Stott, L., Cannariato, K., Thunell, R., Haug, G.H., Koutavas, A. and Lund, S., 2004. Decline of surface temperature and salinity in the western tropical Pacific Ocean in the Holocene epoch. Nature, 431: 56~59.

Stuiver, M., Grootes, P.M. and Braziunas, T.F., 1995. The GISP2 δ18O record of the past 16,500 years and the role of the sun, ocean and volcanoes. Quaternary Research, 4: 341~354.

Sugita, S., 1994. Pollen representation of vegetation in Quaternary sediments: theory and method in patchy vegetation. The Journal of Ecology, 82(4): 881~897.

Tao, S.C., An, C.B., Chen, F.H., Tang, L.Y., Wang, Z.L., Lu, Y.B., Li, Z.F., Zheng, T.M. and Zhao, J.J., 2010. Pollen-inferred vegetation and environmental changes since 16.7 ka BP at Balikun Lake, Xinjiang. Chinese Science Bulletin, 55(22): 2449~2457.

Tarasov, P., Bezrukova, E., Karabanov, E., Nakagawa, T., Wagner, M., Kulagina, N., Letunova, P., Abzaeva, A., Granoszewski, W. and Riedel, F., 2007. Vegetation and climate dynamics during the Holocene and Eemian interglacials derived from Lake Baikal pollen records. Palaeogeography, Palaeoclimatology, Palaeoecology, 252 (3~4): 440~457.

Tarasov, P., Bezurkova, E. and Krivonogov, S., 2009. Late Glacial and Holocene changes in vegetation cover and climate in southern Siberia derived from a 15 kyr long pollen record from Lake Kotokel. Climate of Past Discussion, 5: 127~151.

Tarasov, P., Dorofeyuk, N. and Metl'tseva, E., 2000. Holocene vegetation and climate changes in Hoton-Nur basin, northwest Mongolia. Boreas, 29(2): 117~126.

Tarasov, P., Granoszewski, W., Bezrukova, E., Brewer, S., Nita, M., Abzaeva, A., and Oberhansli, H., 2005. Quantitative reconstruction of the last interglacial vegetation and climate based on the pollen record from Lake Baikal, Russia. Climate Dynamic, 25: 625~637.

Tarasov, P.E., Guiot, J., Cheddadi, R., Andreev, A.A., Bezusko, L.G., Blyakharchuk, T.A., Dorofeyuk, N. I., Filimonova, L.V., Volkova, V.S. and Zernitskaya, V.P., 1999. Climate in northern Eurasia 6000 years ago reconstructed from pollen data. Earth and Planetary Science Letters, 171(4): 635~645.

ter Braak, C.J.F. and Juggins, S., 1993. Weighted averaging partial least squares regression (WA-PLS): an important method for reconstructing environmental variable from species assemblages. Hydrobiologia, 269~270: 4855~4502.

Tuvdendorzh, D. and Myagmarzhav, B., 1985. Atlas of the Climate and Ground Water Resources in the

Mongolian People's Republic. Ulan Bator: GUGMS of Mongolia.

Velichko, A.A., Catto, N., Dernova, A.N., Klimanov, V.A. Kremenetski, C. and Nechaev, V.P., 2002. Climate changes in East Europe and Siberia at the Late Glacial–Holocene transition. Quaternary International, 91: 75~99.

Visbeck, M., 2002. The ocean's role in Atlantic climate variability. Science, 297: 2223~2224.

Wang, H., Liu, H., Cui, H. and Abrahamsen, N., 2001. Terminal Pleistocene/Holocene palaeoenvironmental changes revealed by mineral-magnetism measurements of lake sediments for Dali Nor area, southeastern Inner Mongolia Plateau, China. Palaeogeography, Palaeoclimatology, Palaeoecology, 170: 115~132.

Wang, W. and Feng, Z-.D., 2013. Holocene moisture evolution across the Mongolian Plateau and its surrounding areas: A synthesis of climatic records. Earth-Science Reviews, 122: 38~57.

Sun, A.Z. and Feng, Z.D., 2013. Pollen-recorded bioclimatic variations of the last 15,000 years retrieved from Lake Qigai Nuur in the southern Mongolian Plateau of China. The Holocene, 23: 1391~1402.

Wang, W., Feng, Z.-D., Ran, M. and Zhang, C.J., 2013. Holocene climate and vegetation changes inferred from pollen records of Lake Aibi, northern Xinjiang, China: A potential contribution to understanding of Holocene climate pattern in East-central Asia. Quaternary International, 311: 54~62.

Wang, W., Ma, Y.Z., Feng, Z.-D., Meng, H.W., Sang, Y.L. and Zhai, X.W., 2009. Vegetation and climate changes during the last 8660 cal. a BP in central Mongolia, based on a high-resolution pollen record from Lake Ugii Nuur. Chinese Science Bulletin, 54(9): 1579~1589.

Wang, W., Ma, Y.Z., Feng, Z.-D., Narantsetseg, Ts., Liu, K.B. and Zhai, X.W., 2011. A prolonged dry mid-Holocene climate revealed by pollen and diatom records from Lake Ugii Nuur in central Mongolia. Quaternary International, 229(1~2): 74~83.

Wang, Y.B., Liu, X.Q. and Herzschuh, U., 2010. Asynchronous evolution of the Indian and East Asian Summer Monsoon indicated by Holocene moisture patterns in monsoonal central Asia. Earth-Science Reviews, 103: 135~153.

Wanner, H., Beer, J., Bütikofer, J., Crowley, T.J., Cubasch, U., Flückiger, J., Goosse, H., Grosjean, M., Joos, F., Kaplan, J.O., Küttel, M., Müller, S.A., Prentice, I.C., Solomina, O., Stocker, T.F., Tarasov, P., Wagner, M. and Widmann, M., 2008. Mid- to Late Holocene climate change: an overview. Quaternary Science Reviews, 27(19~20): 1791~1828.

Wen, R.L., Xiao, J.L., Chang, Z.G., Zhai, D.Y., Xu, Q.H., Li, Y.C. and Itoh, S., 2010a. Holocene precipitation and temperature variations in the East Asian monsoonal margin from pollen data from Hulun Lake in northeastern Inner Mongolia, China. Boreas, 39(2): 262~272.

Wen, R.L., Xiao, J.L., Chang, Z.G., Zhai, D.Y., Xu, Q.H., Li, Y.C., Itoh, S. and Lomtatidze, Z., 2010b. Holocene climate changes in the middle high-latitude monsoon margin reflected by the pollen record from Hulun Lake, northeastern Inner Mongolia. Quaternary Research, 73(2): 293~303.

Wendland, W.M. and Bryson, R.A., 1974. Dating climatic episodes of the Holocene. Quaternary Research, 4(1): 9~14.

Wünnemann, B., Chen, F.H., Riedel, F., Zhang, C.J., Mischke, S., Chen, G.J., Demske, D. and Ming, J., 2003. Holocene lake deposits of Bosten Lake, southern Xinjiang, China. Chinese Science Bulletin, 48: 1429~1432.

Wünnemann, B., Mischke, S. Abd Chen, F.H., 2006. A Holocene sedimentary record from Bosten lake,

China. Palaeogeography, Palaeoclimatology, Palaeoecology, 234 (2~4): 223~238.

Xiao, J.L., Nakamura, T., Lu, H.Y. and Zhang, G.Y., 2002. Holocene climate changes over the desert/loess transition of north-central China. Earth and Planetary Science Letters, 197: 11~18.

Xiao, J.L., Xu, Q.H., Nakamura, T., Yang, X.L., Liang, W.D. and Inouchi, Y.W., 2004. Holocene vegetation variation in the Daihai Lake region of north-central China: a direct indication of the Asian monsoon climatic history. Quaternary Science Reviews, 23(14~15): 1669~1679.

Xu, Q.H., Xiao, J.L., Li, Y.C., Tian, F. and Nakagawa, T., 2010. Pollen-Based Quantitative Reconstruction of Holocene Climate Changes in the Daihai Lake Area, Inner Mongolia, China. Journal of Climate, 23(11): 2856~2868.

Xue, J.B., Zhong, W., Zhao, Y.J. and Peng, X.Y., 2008. Holocene abrupt climate shifts and mid-holocene drought intervals recorded in Barkol Lake of northern Xinjiang of China. Chinese Geographical Science, 18: 54~61.

Zhang, C.J., Feng, Z.-D., Yang, Q.L., Gou, X.H. and Sun, F.F., 2010. Holocene environmental variations recorded by organic-related and carbonate-related proxies of the lacustrine sediments from Bosten Lake, northwestern China. The Holocene, 20: 363~373.

Zhang, C.J., Zhang, W.Y., Feng, Z.-D., Mischke, S., Gao, X., Gao, D. and Sun, F.F., 2012. Holocene hydrological and climatic change on the northern Mongolian Plateau based on multi-proxy records from Lake Gun Nuur. Palaeogeography, Palaeoclimatology, Palaeoecology, 323~325: 75~86.

Zhang, J.W., Chen, F.H., Holmes, J.B., Li, H., Guo, X.Y., Wang, J.L., Li, S., Lv, Y.B., Zhao, Y. and Qiang, M.R., 2011. Holocene monsoon climate documented by oxygen and carbon isotopes from lake sediments and peat bogs in China: a review and synthesis. Quaternary Science Reviews, 30: 1973~1987.

Zhao, Y., Yu, Z.C., Chen, F.H. and Li, J.J., 2008. Holocene vegetation and climate change from a lake sediment record in the Tengger sandy desert, northwest China. Journal of arid environments, 72: 2054~2064.

Zhao, Y., Yu, Z.C., Chen, F.H., Zhang, J.W. and Yang, B., 2009. Vegetation response to Holocene climate change in monsoon-influenced region of China. Earth-Science Reviews, 97(1~4):242~256.

Zhong, W., Xue, J.B., Li, X.D., Xu, H.J. and Jiang, O.Y., 2010. A Holocene climatic record denoted by geochemical indicators from Barkol Lake in the northeastern Xinjiang, NW China. Geochemistry International, 48: 792~800.

Zhou, W.J., Donahue, D.J., Porter, S.C., Jull, T.A., Li, X.Q., Stuiver, M., An, Z.S., Matsumoto, E. and Dong, G.R., 1996. Variability of Monsoon Climate in East Asia at the End of the Last Glaciation. Quaternary Research, 46: 219~229.

后序

蒙古高原与地中海全新世气候的可能联系

冯兆东

中国科学院 新疆生态与地理研究所

关于蒙古高原全新世以来气候变化的解释已经有了几种不同的观点。第一种观点认为，盛行西风一直在主导着蒙古高原的大部分地区及其西侧的全部地区（如：Chen等，2008；Ran和Feng，2013；Wang和Feng，2013）。第二种观点认为，亚洲季风的主导作用曾到达蒙古高原北侧的西伯利亚南部和西侧的阿尔泰山脉（如：Harrison等，1996；Tarasov等，2000）。第三种观点认为，约7000年之前的低海平面、仍然广泛分布的冰川和冻土、较低的海洋表层温度、较低的冬季太阳辐射等因素很可能抑制了欧亚大陆中心部分（包括蒙古高原北部）的温度和降水；而约7000年之后海平面的上升、冰川和冻土面积的萎缩、海洋表层温度的增加、冬季太阳辐射量的增强、大气CO_2浓度的上升（可能也包括与之相关的大气水分的上升）很可能促成了欧亚大陆中心部分（包括蒙古高原北部）温度和降水的上升（如：Bush，2005；Prokopenko等，2007；Feng等，2013）。第四种观点认为（Rudaya等，2009），蒙古高原西侧的阿尔泰山脉一直是全新世气候的天然界限。阿尔泰山脉东侧的早全新世（约11 500~5000年前）是暖湿的，晚期（即过去5000年）是冷干的（与东亚季风气候模式一致）。阿尔泰山脉西侧的早全新世是暖干的，晚期是冷湿的（与欧洲西风气候模式一致）。阿尔泰山脉北部的早全新世是暖湿的（与东亚季风气候模式一致），晚期是冷干的（与欧洲西风气候模式一致）。

但是，我们最近在阿尔泰山脉南部（中国境内）的定量重建给了我们一个与上述不同的和令我们自己迷恋的视角。我们在娜仁夏湿地（喀纳斯湖附近）采集了一个约4m长的泥炭芯，分析了188个样品的孢粉组合。我们采用植物功能型—现代类似法（PFT-MAT）进行了气候的定量重建。我们的重建显示（Feng等，未发表；图1），阿尔泰山脉南部的早全新世（约11 500~7000年前）和晚全新世（过去约4000年）都是暖湿的，而中全新世（约7000~4000年前）是冷干的。这一结论与贝加尔湖地区的定量重建比较相近（见Tarasov等，2007；图1）。我们的文献跟踪还提醒我们：地中海北部与阿尔泰山脉南部的全新世气候情形更为相近（Peyron等，2011，2013；图1）。地中海北部最具代表性的样点要算位于意大利境内的艾克瑟撒湖。艾克瑟撒湖的定量重建显示，约10 000~7200年前地中海北部是暖湿

的，约7200~4400年前地中海北部是冷干的，过去约4400年来的地中海北部又是暖湿的

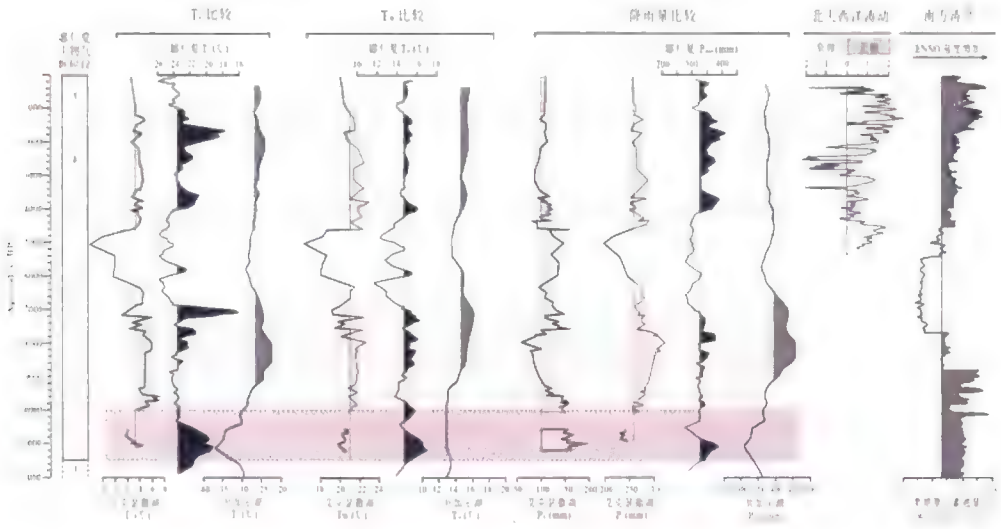

图1　重建的贝加尔、娜仁夏、艾克瑟撒记录与重建的ENSO强度记录的比较（注：T_c：冷季温度，T_w：暖季温度，P_c：冷季降水，P_w：暖季降水，P_{ann}：年降水）

我们对全新世北大西洋涛动（NAO）和南方涛动（ENSO）变化文献的跟踪，让我们对上述的地中海北部与阿尔泰南部全新世气候记录的相似性有了猜想。具体地讲，实测资料显示，过去60年（自1950起）北大西洋的NAO正相期与赤道太平洋的ENSO暖期（即厄尔尼诺期）具有同步性（Syed等，2006）。重建资料显示，过去约5200年来NAO正相期与ENSO暖期也具有同步性（Olsen等，2012；Rein等，2005）。我们的猜想实际上是受到了Syed等的工作的启发。他们的研究显示（Syed等，2006，2010），中亚南部（或称CSWA；包括巴基斯坦北部、乌茨别克北部、阿富汗、塔吉克斯坦）地区冬季和春季降水的剧增与西部扰动（Western Disturbances）的加强密切相关（图2），该西部扰动起源于地中海并从里海和阿拉伯海获得更多的水汽。而且，NAO正相期和ENSO暖期时西部扰动的增强又进一步加深了CSWA以及以北地区的低压槽，从而加强了SCWA地区（可能也包括以北地区）的降水机制。另外，最近的研究显示（Mariotti，2007），ENSO暖期和CSWA地区的降水之间还存在着直接关联。即：ENSO暖期印度洋北部的高压得以加强，该高压所致的反气旋与亚热带急流一起将阿拉伯海的水汽直接带到CSWA地区，从而导致该区秋季和冬季降水的明显增多。图1显示，三地（贝加尔、娜仁夏、艾克瑟撒）的全新世重建记录与重建的ENSO强度很相似（Rein等，2005）。因此，我们假想：阿尔泰南部（娜仁夏）早全新世（约11 000~7000年前）和晚全新世（过去约4000年来）的湿润气候很可能是ENSO（加强）和NAO（正相）二者密切配合的结果。与湿润相伴随的温暖也应该与ENSO和NAO的密切配合有关。例如，观测资料显示，NAO正相期欧亚大陆约45°N以北地区的对流加强是西伯利亚地区冬半年升温的一个重要原因。另外，ENSO暖期西伯利亚高压的减弱也可能是西伯利亚地区冬季升温的又一重要因素。我们进一步假想：早全新世和晚全新世ENSO与NAO联合影响的范围

很可能从中亚南部(即CSWA)向东北方向扩展到了阿尔泰山脉,甚至扩展到了贝加尔湖地区(见图2)。

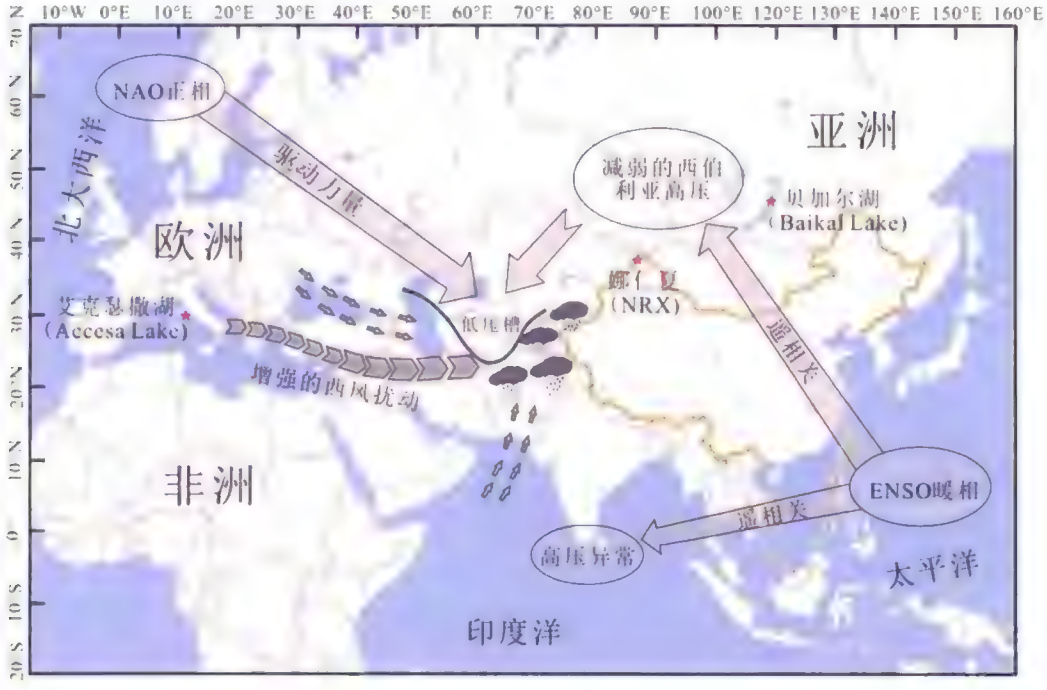

图2　北大西洋涛动(NAO)和南方涛动(ENSO)共同影响着中亚南部(CSWA)的气候。早全新世(约11 000~7000年前)和晚全新世(过去约4000年来)时段,ENSO(暖相)与NAO(正相)联合影响的范围从中亚南部(即CSWA)向东北方向扩展到了阿尔泰山脉,甚至扩展到了贝加尔湖地区

参考文献

Bush, A.B.G., 2005. CO_2/H_2O and orbitally driven climate variability over central Asia through the Holocene. Quaternary International, 136: 15~23.

Chen, F.H., Yu, Z.C., Yang, M.L., Ito, E., Wang, S.M., Madsen, D.B., Huang, X.Z., Zhao, Y., Sato, T., Birks, H.J.B., Boomer, I., Chen, J.H., An, C.B., Wunnemann, B., 2008. Holocene moisture evolution in arid central Asia and its out-of-phase relationship with Asian monsoon history. Quaternary Science Reviews, 27, 351~364.

Feng, Z.-D., Ma, Y.Z., Zhang, H.C., Narantsetsega, Ts., Zhang, X.S., 2013. Holocene climate variations retrieved from Gun Nuur core in the Northern Mongolian Plateau. The Holocene, 23(12): 1719 ~ 1728.

Harrison, S.P., Yu, G., Tarasov, P.E., 1996. Late Quaternary lake-level record from Northern Eurasia. Quaternary Research, 45: 138~159.

Mariotti, A., 2007. How ENSO impacts precipitation in southwest central Asia. Geophysical Research Letters, 34: L16706.

Olsen, J., Anderson, N.J., Knudsen, M.F., 2012. Variability of the North Atlantic Oscillation over the past 5,200 years. Nature Geoscience, 5: 808~812.

Peyron, O., Goring, S., Dormoy, I., Kotthoff, U., Pross, J., de Beaulieu, J.-L., Drescher-Schneider, R., Vanniere, B., Magny, M., 2011. Holocene seasonality changes in the central Mediterranean region reconstructed from the pollen sequences of Lake Accesa (Italy) and Tenaghi Philippon (Greece). The Holocene, 21(1): 131~146.

Peyron, O., Magny, M., Goring, S., Joannin, S., de Beaulieu, J.-L., Brugiapaglia, E., Sadori, L., Garfi, G., Kouli, K., Ioakim, C., Combourieu-Nebout, N., 2013. Contrasting patterns of climatic changes during the Holocene across the Italian Peninsula reconstructed from pollen data. Climate of the Past 9: 1233~1252.

Prokopenko, A.S., Khursevich, G.K., Bezrukova, E.V., Kuzmin, M.I., Boes, X., Williams, D.F., Fedenya, S.A., Kulagina, N.V., Letuniva, P.P., Abzaeva, A.A., 2007. Paleoenvironmental proxy records from lake Hovsgol, Mongolia, and a synthesis of Holocene climate change in the Lake Baikal Watershed. Quaternary Research, 68: 2~17.

Ran, M., Feng, Z.-D., 2013. Holocene moisture variations across China and driving mechanisms: a synthesis of climatic records. Quaternary International, 313/314: 179~193.

Rein, B., Lückge, A., Reinhardt, L., Sirocko, F., Wolf, A. And Dullo, W.C., 2005. El-El Niño variability off Peru during the last 20 000 years. Paleoceanography, 20: PA4003.

Rudaya, N., Tarasov, P., Dorofeyuk, N., Solovieva, N., Kalugin, I., Andrew, A., Dryin, A., Diekmann, B., Riedel, F., Tserendash, N., Wagnere, M., 2009. Holocene environments and climate in the Mongolian Altai reconstructed from the Hoton-Nur pollen and diatom records: a step towards better understanding climate dynamics in central Asia. Quaternary Science Reviews, 28: 540~554.

Syed, F.S., Giorgi, F., Pal, J.S.,King, M.P., 2006. Effect of remote forcings on the winter precipitation of central southwest Asia part 1: observations. Theoretical and Applied Climatology, 86: 147~160.

Syed, F.S., Giorgi, F., Pal, J.S., Keay, K., 2010. Regional climate model simulation of winter climate over Central-Southwest Asia, with emphasis on NAO and ENSO Effects. International Journal of Climatology, 30: 220~235.

Tarasov, P., Bezrukova, E., Karabanov, E., Nakagawa, T., Wagner, M., Kulagina, N., Letunova, P., Abzaeva, A., Granoszewski, W., Riedel, F., 2007. Vegetation and climate dynamics during the Holocene and Eemian interglacials derived from Lake Baikal pollen records. Palaeogeography, Palaeoclimatology, Palaeoecology, 252 (3~4): 440~457.

Tarasov, P., Dorofeyuk, N., Metel'tseva, E., 2000. Holocene vegetation and climate changes in Hoton-Nuur basin, northwest Mongolia. Boreas, 9: 117~126.

Wang, W., Feng, Z.D., 2013. Holocene moisture evolution across the Mongolian Plateau and its surrounding areas: A synthesis of climatic records. Earth-Science Reviews, 122: 38~57.

附录一

Available online at www.sciencedirect.com

SCIENCE DIRECT

ELSEVIER

Palaeogeography, Palaeoclimatology, Palaeoecology 212 (2004) 265–275

PALAEO

www.elsevier.com/locate/palaeo

Paleosubarctic Eolian environments along the southern margin of the North American Icesheet and the southern margin of Siberia during the Last Glacial Maximum

Z.-D. Feng[a,b,*], P. Khosbayar[c]

[a]National Laboratory of Western China's Environmental Systems, MOE, Lanzhou University, Lanzhou 730000, China
[b]Department of Earth and Environmental Studies, Montclair State University, Upper Montclair, New Jersey 07043, USA
[c]Institute of Geology and Mineral Resources, Mongolian Academy of Sciences, Ulaan Baatar, Mongolia

Received 3 June 2002; received in revised form 1 June 2004; accepted 1 June 2004

Abstract

Based on a negative correlation of magnetic susceptibility with organic matter content and the degree of gleying documented both in North American and southern Siberian eolian sequences, the authors propose that reducing conditions of incipient histosol development contributed to the alteration of magnetic minerals from strongly magnetic forms of oxidized iron to weakly magnetic forms. Therefore, the magnetic susceptibility is basically an indicator of redox cycles. Well-vegetated conditions generally dominated the later part of the Last Glacial Maximum (LGM; ~15,000 – ~8000 ^{14}C years BP) and poorly vegetated conditions the early part (~21,000– ~15,000 ^{14}C years BP), with a rapid transition around 15,000 ^{14}C years BP chronologically corresponding to many well-documented rapid transitions around the world. The magnetic susceptibility signatures indicate approximately 1000-year-long cycles of environmental changes during the Last Glacial Maximum (~21,000–10,000 ^{14}C years BP) in North America. The initial perturbation of these ~1000-year-long cycles might have started in the Tropical Pacific and then been promptly transferred to the North Atlantic via the North American Icesheet. The southern Siberian eolian sequence recorded approximately 1400-year cycles. These ~1400-year cycles might have been associated with the thermal variations in the Arctic Ocean that was directly linked with the thermal variations in the North Atlantic Ocean. To sum up, our research suggests that the North American eolian sequence recorded ~1000-year cycles and the southern Siberian eolian sequence recorded ~1400-year cycles, although it is not able to propose plausible mechanisms controlling the ~1000- or/and ~1400-year cycles.
© 2004 Elsevier B.V. All rights reserved.

Keywords: Paleoclimate change; Last glacial maximum; North American; Mongolian Plateau; Abrupt events; Eolian sequence

* Corresponding author. Department of Earth and Environmental Studies, Montclair State University, Upper Montclair, New Jersey 07043, USA.
E-mail addresses: fengzd@lzu.edu.cn, fengz@mail.montclair.edu (Z.-D. Feng), P_khosbayar@yahoo.com (P. Khosbayar).

0031-0182/$ - see front matter © 2004 Elsevier B.V. All rights reserved.
doi:10.1016/j.palaeo.2004.06.004

1. Introduction

Abrupt shifts in climatic conditions at high latitudes in the Northern Hemisphere have captured the attention of climate scientists. Based on modeled binge/purge oscillations of the North American Ice-sheet (MacAyeal, 1993), Broecker (1995) proposed that massive iceberg discharges from the North American Icesheet into the North Atlantic triggered the abrupt climatic events (known as Heinrich Events). Also noted was the repeated pattern that each one of Heinrich events occurred at the end of a sequence of Dansgaad–Oeschger (D–O) Oscillations during a prolonged cold period, and the sequence of D–O Oscillations tend to follow a saw-tooth Bond Cycle (Clarke and Marshall, 1999). These Atlantic-related events are argued to have driven global abrupt events at millennial–centennial timescales via the North Atlantic Deep Water (NADW) conveyor belt (Bond and Lotti, 1995). A plausible interpretation is that Heinrich Events initiate the Bond Cycles with the ocean subsequently responding like a damped oscillator to larger initial perturbations (Weaver, 1999). The large initial perturbations are likely fast and cumulative responses of the North American Icesheet to external atmospheric changes and the D–O Oscillations are likely regular responses to the atmospheric changes with a periodicity of 1000–2000 years (Clarke and Marshall, 1999).

The Atlantic-centered theory of global abrupt climatic shifts, however, may be the result of biased databases because much paleoclimatic research has focused on the North Atlantic and adjacent areas (Stocker, 1998). In terms of D–O Oscillations, Cane (1998) and Cane and Clement (1999) proposed, according to modeling results, that the Tropical Pacific might have been much more important than the North Atlantic in perturbing global climates. That is, possible long-term (millennial–centennial) El Niño variations in the Tropical Pacific can generate 3–5 times more energy than North Atlantic sea-surface temperature variations. Sirocko et al. (1999) have further elaborated the significance of the tropics. They calculated that high latitudes represent only about 8.2% of the area of the globe, while the tropics and subtropics represent about 57%. Their calculated annual energy received is 130 kcal/cm^2 for the high latitudes (polar regions) and 300 kcal/cm^2 for the low latitudes (tropics and subtropics). In total, the annual heat input of the tropics and subtropics is about 16 times higher than in the polar regions. In fact, data from many sites in low latitudes and the southern hemisphere exhibiting D–O oscillations seems favor a low-latitude forcing over a high-latitude one (Leuschner and Sirocko, 2000).

Ocean-surface currents and atmospheric currents transport heat from low latitudes to high latitudes and also water vapor from oceans to continental interiors through the middle latitudes that represent about 35% of the area of the globe. Furthermore, cold air masses from high latitudes and warm air masses from low latitudes interact violently in the middle latitudes and the violent natural history of the interactions may be documented in the middle latitudes. By defining and quantifying the specific responses of continental environmental systems in the middle latitudes to global changes and linking these responses to those in high and low latitudes, will major uncertainties about the mechanisms of global change be understood. This paper uses published and newly obtained data from the Northern Mongolian Plateau, near the southern margin of Siberia (Feng et al., 1998; Feng, 2001), and published data from the central Great Plains, near the southern margin of the North American Icesheet (Feng et al., 1994a; Feng, 1998), to reconstruct the paleo-subarctic (presently temperate) environments of the continental interior during the Last Glacial Maximum (LGM).

2. Climatic proxy data from the Southern Margin of Siberia

Numerous eolian/paleosol sequences have been reported (Khosbayar, 1989) in the topographical corridor from Ulaanbaatar to Lake Baikal in the interior of the Asian continent (dotted area in Fig. 1). The data show that this forest-steppe area was occupied by active sand dunes many times during the late Pleistocene and Holocene. The change from a desert to a forest-steppe environment may explain why the eolian/soil sequences in this area are well developed and preserved. To decipher the paleoenvironmental records, we focus on Khyaraany (50.2°N, 106.7°E; site A in Fig. 1) and Shaamar (50.2°N, 104.2°E; site B in Fig. 1) sections located near the physiographic boundary between the Mongolian Plateau and Siberia.

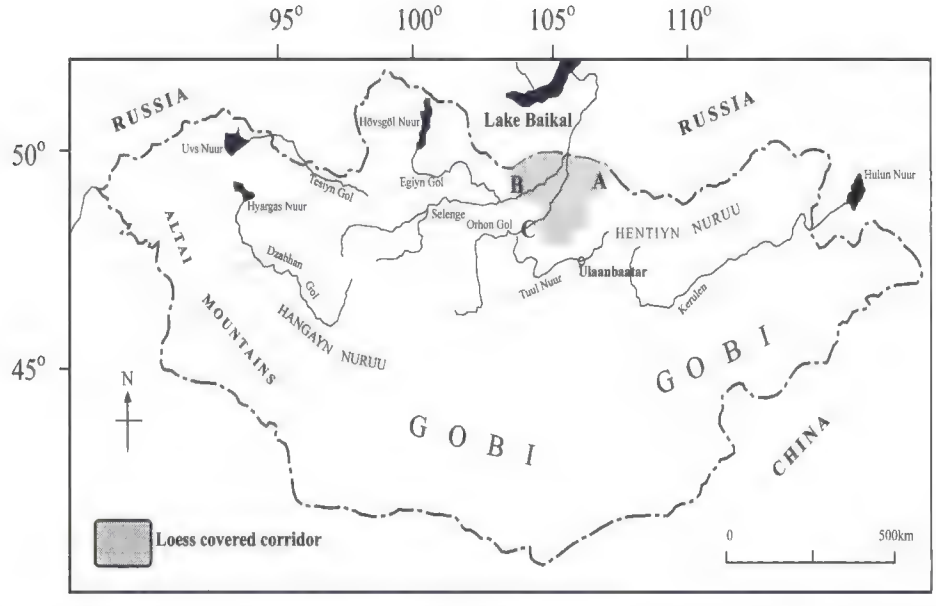

Fig. 1. Map of the Mongolian Republic showing the three study sites. (A) Khyaraany sand/silt/soil section; (B) Shaamar loess–soil section; (C) Buregkhanga loess–soil section. Dotted is the loess-covered corridor from Lake Baikal to Ulaabaatar.

A third section in Buregkhanga area (48.1°N, 103.8°E; site C in Fig. 1) recorded the environmental events during Marine Isotope Stage (MIS) 3 (~20,000–~40,000+ ^{14}C years BP) (see Feng et al., 1998). The data from Khyaraany section was already published (Feng, 2001) and the Shaamar section was recently sampled at 5-cm intervals for particle size and magnetic analyses. The particle size of bulk samples was measured using a Malvern Mastersizer 2000 laser diffraction particle size analyzer. The magnetic susceptibility (SI) was measured by the procedure of Thompson and Oldfield (1986) using a Bartington MS 2B susceptibility meter and the frequency-dependent susceptibility was calculated based on the high-frequency and low-frequency susceptibility measurements. Some of radiocarbon dating samples were conventionally dated in the Radiocarbon Dating Laboratory of Lanzhou University (CG samples) and others were AMS analyzed in the Radiocarbon Dating Facility of Arizona State University (AA samples).

2.1. Stratigraphy and chronology

A meandering river (i.e., Gun Nuur River) in the Khyaraany area exposed a sand/loess/soil section. Observed were three major units, i.e., 0–400 cm a sandy unit, 400–800 cm a silty (loess) unit, and 800–1200 cm a sandy unit (Fig. 2). Multiple loess layers occur in the two sandy units and multiple sand layers occur in the silty unit. The bottom of the topsoil (at a depth of 85 cm) was dated at 2720±70 ^{14}C years BP (CG-3641). A second organic enriched (i.e., histosol normally formed under tundra conditions) at a depth of 175 cm was dated at 4070±70 ^{14}C years BP (CG-3454). A third organic matter enriched layer at a depth of 450 cm was dated at 8300±100 ^{14}C years BP (CG-3462). A fourth organic enriched layer at a depth of 670 cm was dated at 13,030±120 ^{14}C years BP (CG-3464). And, a fifth organic enriched layer at a depth of 755 cm was dated at 15,090±110 ^{14}C years BP (CG-3463). Based on two observed facts that these two sandy units are horizontally laminated and that the sandy units can be traced to crossbedded dune sand 30–40 km away, we assumed that the sandy units were gradually deposited. An age extrapolation suggests that the bottom of the section (1200 cm) is about 22,000 ^{14}C years BP.

A 31-m eolian/paleosol section is exposed in Shaamar area by a major gully of the Selenge River. Three major stratigraphic units, each being separated by a major paleosol (see Fig. 2), were field observed and further supported by laboratory analyses. The first one (0–600 cm) is a sandy unit. The second one (600–

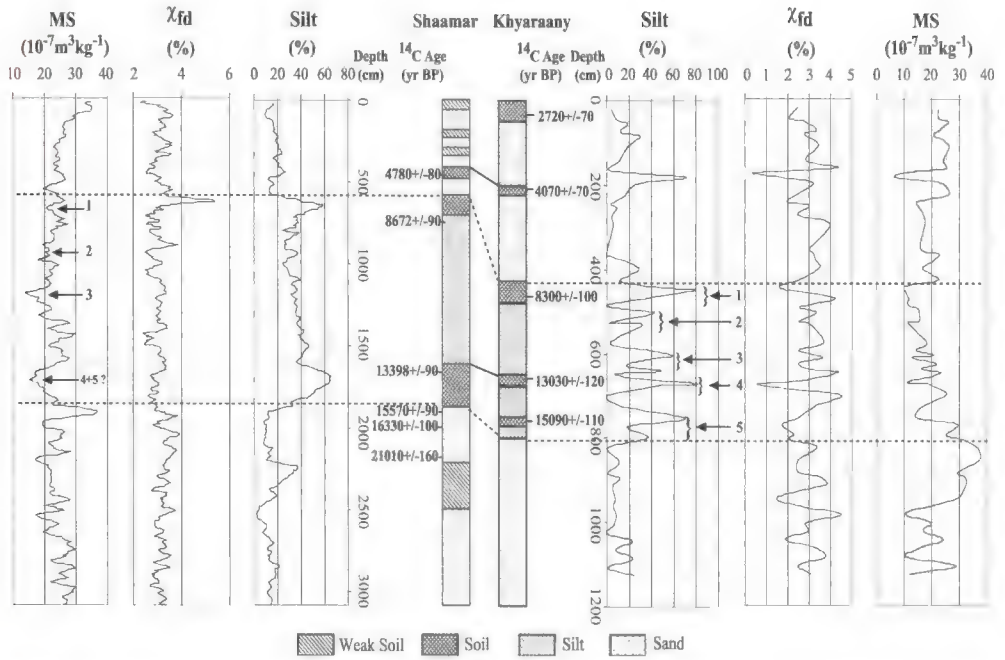

Fig. 2. General characteristics of Khyaraany and Shaamar sand/silt/soil sections: silt percentage, frequency-dependent magnetic susceptibility (Fx), and specific magnetic susceptibility (MS).

1850 cm) is a silty unit and bracketed by two paleosols. The third one (1850–3100 cm) is a sandy unit containing a weak paleosol in the middle (2250–2600 cm). Six radiocarbon dates were obtained mainly from paleosols. The middle of a sandy paleosol at a depth of 350–450 cm was dated at 4780±80 ^{14}C years BP (CG-3465). The bottom of a well-developed silty paleosol (at a depth of 600–800 cm) overlying the second stratigraphic unit was dated at 8672±90 ^{14}C years BP (AA51928). A second well-developed silty paleosol underlying the second stratigraphic unit (at a depth of 1600–1850 cm) was bracketed by two dates: 13,398±90 ^{14}C years BP (AA51925) at the top and 15,570±90 ^{14}C years BP (AA51923) at the bottom. A date of 16,330±100 ^{14}C years BP (AA51922) was also obtained immediately below the second silty paleosol. The top of a weak paleosol (at a depth of 2250–2600 cm) in the middle of the third stratigraphic unit was dated at 21,010±160 ^{14}C years BP (AA51920).

2.2. Silt percentage and magnetic susceptibility

The silt content, as well as the sand content, varies widely throughout the Khyaraany section with the clay content being negligible (Fig. 2). Because the ^{14}C samples obtained exclusively from organic matter-enriched layers are characteristically high in silt content and low in sand content, we examined the relationship between the silt percentage and organic matter content on 14 samples from the top portion of the section. The correlation is strongly positive (r=0.85) (Feng, 2001). The frequency-dependent magnetic susceptibility identifies the organic-enriched layers by low values (Fig. 2). The specific magnetic susceptibility is high in the upper sandy portion (0–400 cm: 0–~8000 ^{14}C years BP) and even higher in the lower sandy portion (800–1200 cm: ~8000–~15,000 ^{14}C years BP). The lowest susceptibility occurs in the middle silty portion (400–800 cm: ~15,000–~22,000 ^{14}C years BP). Also noticeable is apparently negative correlation between the silt percentage and the specific magnetic susceptibility. At the Shaamar section, the silt content, as well as the sand content, also varies widely with the clay content also being negligible. The first unit (0–600 cm: 0–~8000 ^{14}C years BP) and third unit (1850–3100: ~15,000–~21,000+ ^{14}C years BP) are apparently coarser than the second unit (600–1850 cm: ~8000–

~15,000 ^{14}C years BP), being similar to the Khyaraany section. The second unit is also characterized by a slightly lower frequency-dependent susceptibility and specific susceptibility (Fig. 2).

At both the Khyaraany and Shaamar sections, gleyed and non-gleyed alternating couplets were observed and further supported by the laboratory data for the deglacial portions (~8000–15,000 ^{14}C years BP). At the Khyaraany section, five filed-observed yellowish gleyed layers (numbered as 1, 2, 3, 4, and 5 in Silt diagram of Fig. 2) were characterized by higher silt contents and lower frequency-dependent magnetic susceptibility values. Four yellowish gleyed layers (numbered as 1, 2, 3, 4 in MS diagram of Fig. 2) were field observed at the Shaamar section and further supported by stratigraphically corresponding troughs in the specific magnetic susceptibility. It should be noted here that the two field-observed organic-enriched gleyed layers dated at 13,030 and 15,090 ^{14}C years BP, respectively, at the Khyaraany section are corresponding to just one organic-enriched gleyed layer (i.e., a paleosol) bracketed by two dates (13,398 and 15,570 ^{14}C years BP) at the Shaamar section, and we thus interpret that the fourth and fifth gleyed layers found at the Khyaraany section might have been merged at the Shaamar section during the paleosol formation. It should be added that the alternating couplets of gleyed and non-gleyed layers were also observed in the third stratigraphic units formed before 15,000 ^{14}C years BP at both sections, but the pattern is not well expressed. We have also noticed that frequency-dependent susceptibility expresses the gleyed layers at the Khyaraany section, while specific magnetic susceptibility indicates the gleyed layers at the Shaamar section. Unfortunately, our data do not allow us further explore why frequency-dependent susceptibility does a better job in indicating the gleyed layers at the Khyaraany section.

2.3. Discussions

Two observations can be made based on the data from the two sections. First, lower magnetic signatures than the two sandy units characterize the middle silty unit at both sections. Second, the field-observed gleyed layers in the middle unit formed between ~8000 and ~15,000 ^{14}C years BP, which are normally finer in particle size and higher in organic matter content, are characterized by lower magnetic signatures than the non-gleyed layers. These two observations imply that the magnetic signatures in this paleo-subarctic environment were primarily controlled by redox cycles. That is, during less-windy (more silt deposit) and better-vegetated (more organic matter) periods, waterlogged conditions of the land-surface reduced some minerals of strongly magnetic forms to weakly magnetic forms. Based on ^{14}C dates and the extrapolated ages, our interpretations are as follow. First, unlike the MIS 3 paleosols (24,500, 28,900, 30,700, 34,400 ^{14}C years BP) that are characteristically high in magnetic susceptibility and were interpreted to have formed under oxidizing-dominated conditions (Feng et al., 1998), the MIS 2 paleosols (15,090, 13,030, 8300 ^{14}C years BP) are characteristically low in magnetic susceptibility and were interpreted to have formed under reducing-dominated conditions (Feng, 2001). Second, less windy and better vegetation conditions generally dominated the late period of the LGM (15,090–8300 ^{14}C years BP), during which three paleosols (incipient histosols) were formed (15,090, 13,030, 8300 ^{14}C years BP). Third, windy and poorer vegetation conditions dominated the early part of the LGM (~24,000–16,000 ^{14}C years BP). Fourth, ~1400 years cycles during the deglacial period (7000 years from ~8000 to ~15,000 ^{14}C years BP) are indicated by five gleyed and non-gleyed couplets.

The positive correlation between the magnetic susceptibility and sand percentage in Alaska (Beget et al., 1990) and in Siberia (Chlachula et al., 1998) was interpreted to indicate the strength of wind during cold times. The data from the Northern Mongolian Plateau also suggests a positive correlation between magnetic susceptibility and sand percentage (Feng, 2001). Based on the negative correlation of the susceptibility with silt percentage and organic matter content, we proposed a different interpretation that may be applicable to all high-latitude eolian situations (Feng, 1999, 2001). That is, reducing conditions of incipient histosol development contributes to the alteration of magnetic minerals from strongly magnetic forms to weakly magnetic forms (Fassbinder et al., 1990; Feng, 1996, 1997, 1998, 1999, 2001; Feng and Johnson, 1995; Feng and Chen, 1999; Feng et al., 1994a,b,c, 1998; Mullins, 1977; Williams, 1992) with an assumption that the post-burial alteration might

have been minimal under this eolian-pro condition, in which previously formed incipient histosols were quickly "isolated" by later-deposited eolian deposits. Therefore, the magnetic susceptibility is basically an indicator of redox cycles. This interpretation is in complete agreement with the results of examination of the Alaskan loess by Liu et al. (1999). They concluded that lower magnetic susceptibility in finer loess units was resulted from reduction processes during warmer periods in this permafrost dominant area.

3. Proxy data from the Southern Margin of the North American Icesheet

Climatic conditions in the central Great Plains during the Last Glacial Maximum have been the focus of the Quaternary studies for the past century. However, disagreement remains regarding the environmental interpretation. Some researchers suggest that the conditions were semi-desert (e.g., Lugn, 1968), while others argue that the conditions were closed coniferous forest (e.g., Wright, 1970). More importantly, the dynamic relationship between the North American Laurentide Icesheet and eolian activity along the southern margin of the icesheet is not adequately addressed yet, although the icesheet has been acknowledged as the trigger of global abrupt climate events (Broecker, 1995). The massive loess deposition in the mid-continental United States (Fig. 3) has been attributed to the existence of the North American Icesheet during the Last Glacial Maximum (Ruhe, 1983). It seems that the eolian events in the Great Plains along the southern margin of the North American Icesheet were associated with the glacial dynamics in the Great Lakes area (Feng et al., 1994a). Were the glacial dynamics in the Hudson Bay area that were proposed to have influenced the sea-surface temperature in the North Atlantic controlled by the same mechanism as the one that controlled the glacial dynamics in the Great Lakes area? If so, the large initial perturbations or forcing factors are likely fast and cumulative responses of the North American Icesheet to external atmospheric changes (Clarke and Marshall, 1999). It is then reasonable to propose that

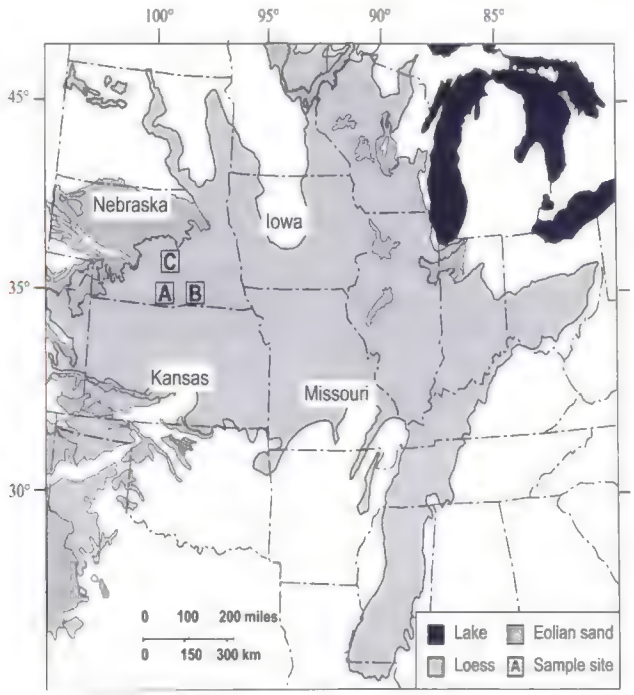

Fig. 3. Distribution of the Peoria Loess in the mid-continent of the United States showing the three sites discussed in the text: (A) Eustis; (B) Buzzard's; (C) Bignell Hill.

the external atmospheric changes were most likely initiated from tropical waters that have been historically proven to be the major sources of precipitation in North America. Thus, the North American Icesheet might have functioned as a linkage between the Tropical Pacific and North Atlantic. Here, we attempt to use detailed information from the loess sequence in the Great Plains to elucidate the linkage between the Tropical Pacific and North Atlántic.

3.1. Stratigraphy and chronology

The eolian deposits corresponding to the last glacial, namely the Peoria Loess, are bracketed by two soil units: the underlying Gilman Canyon pedocomplex and the overlying Brady Soil (Feng et al., 1994a,b,c). The Gilman Canyon pedocomplex formed when the North American Icesheet was advancing and the Brady Soil developed when the icesheet was rapidly retreating. The Peoria Loess, 20–40 m thick in south central Nebraska, might have preserved a detailed record of icesheet dynamics during the last glacial. The ^{14}C dates (bulk samples) of the overlying Brady Soil range from ~11,000 to ~8000 ^{14}C years BP with a date cluster around 10,000 ^{14}C years BP. With consideration of the technical uncertainties and many possibilities of contamination, we can only statistically place the end of the Peoria Loess deposition at ~10,000 ^{14}C years BP. As for the underlying Gilman Canyon Pedocomplex, the dates (organic humate of bulk sample) vary widely from 37,000 to 19,000 ^{14}C years BP with three clusters around 32,000, 25,000 and 21,000 ^{14}C years BP (see Feng et al., 1994a for the details). Again, we can only statistically place the start of the Peoria Loess at ~21,000 years BP. The Peoria Loess itself can be divided into three zones: lower and upper zones, separated by a dark-blue zone in the middle. The dark-blue zone was a waterlogged zone at the Eustis (40.82 N, 100.45 E; A in Fig. 3) and Buzzard's sections (40.82 N, 100.35 E; B in Fig. 3) of central Nebraska where the Peoria Loess is about 20 m thick. The dark-blue zone turns into a less-dark but heavily gleyed zone at the Bignell Hill section (40.87 N, 100.45 E; C in Fig. 3). The dark-blue zone has been dated at 14,500–14,800 ^{14}C years BP (charcoal) at several localities in central Kansas and central Nebraska (Wells, 1983; Wells and Steward, 1987).

Here, we focus on the thickest section at Bignell Hill in the south central Nebraska. The lower Peoria Loess (23–44 m below the land surface) is massive and relatively homogeneous. The heavily gleyed zone (equivalent to the dark-blue zone) occurs at 21–23 m (Fig. 4). The upper Peoria Loess, 4–21 m below the land surface, has rhythmic patterns of two orders: strongly gleyed and weakly gleyed couplets that are 3–5 m thick and coarse-grained and fine-grained laminae (second order) that are about 4 mm thick. The first-order rhythmic pattern is thinner (about 2 m) and more visible and the second-order laminae are also thinner (about 2 mm) in the Eustis and Buzzard's sections. If the statistically placed terminal age of the upper Peoria Loess (~10,000 ^{14}C years BP) is accepted and the widely distributed dark-blue zone in north-central Kansas and south-central Nebraska dated at 14,500–14,800 ^{14}C years BP is taken as a marker stratum, the second-order laminae in the upper Peoria Loess (4 mm at Bignell Hill sections and 2 mm at Eustis and Buzzard's sections) represent the annual dustfall layers. The annual-layer concept was further tested using two charcoal-based dates: one from 7 m below the land surface at the Bignell Hill section and another from 6.3 m below the land surface at the Eustis section. The Bignell Hill date (at a depth of 7 m) is 11,880 ^{14}C years BP and annual-layer counts produce an age of 10,800 years BP. This nearly 1000-year difference is likely caused by vertical intrusion of a tree trunk (dating target). The Eustis date (at a depth of 6.3 m) is 12,330 ^{14}C years BP and annual-layer counting age gives 12,500, supporting the annual-layer concept.

3.2. Magnetic susceptibility

The magnetic susceptibility was measured at 50–80-cm intervals in the Bignell Hill section, at 10-cm intervals in the Eustis section, and at 30-cm intervals in the Buzzard's section (the upper portion is not exposed here). The susceptibility in the Bignell Hill section records the first-order rhythmic pattern. In the upper Peoria Loess, susceptibility is higher in the weakly gleyed layers than in the strongly gleyed layers. The heavily gleyed zone in the middle (equivalent to the dark blue zone dated at 14,500–14,800 ^{14}C years BP) marks a transitional zone, where a drastic decrease of susceptibility occurs upward. The

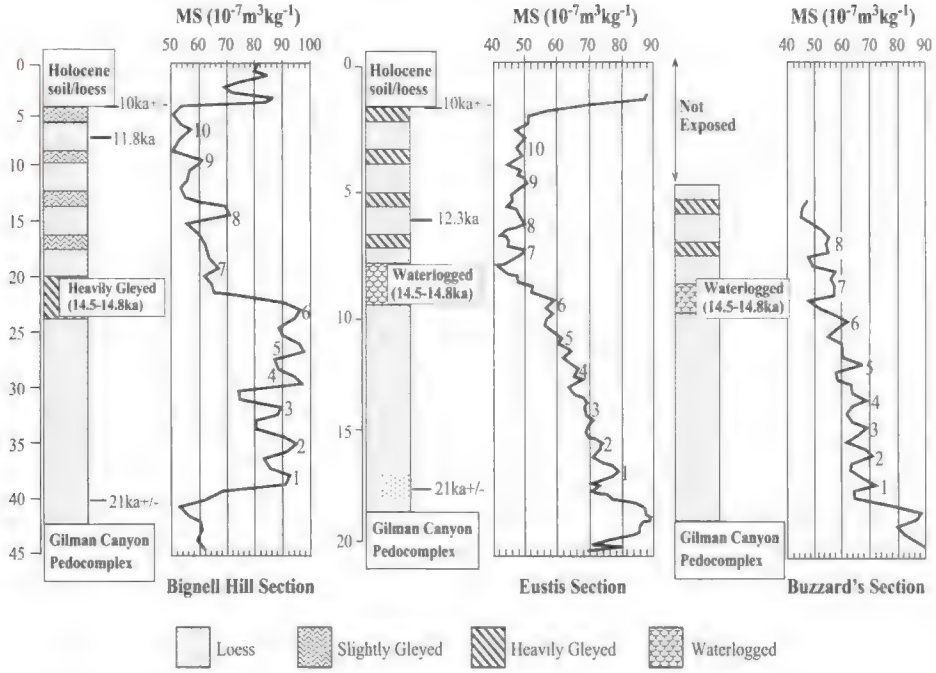

Fig. 4. Stratigraphy and variations in magnetic susceptibility (MS) of the Peoria Loess at the three sections. The waterlogged layer dated at 14,500–14,800 ^{14}C years. BP is the stratigraphic marker of the Peoria Loess in the central Great Plains. Numbers 1–10: 10 susceptibility-indicated gleyed/non-gleyed couplets.

susceptibility indicates the possible existence of the first-order rhythmic pattern in the lower Peoria Loess as well. The susceptibility-indicated first-order cycles observed at the Bignell Hill section are further corroborated by the data from the Eustis and Buzzard's sections (Fig. 4). These 10 susceptibility peaks are significant statistically (at the 95% confidence level) and well supported by regional stratigraphic correlations (see Feng et al., 1994a).

3.3. Discussion

The dark-blue zone dated at 14,500–14,800 ^{14}C years BP (charcoal), separating the upper Peoria Loess from the lower Peoria Loess, is interpreted to have resulted from large-scale climate ameliorations, as documented by pollen and insect assemblages in the Midwest of the United States (Schwert and Ashworth, 1988), and also the time interval of C-4 (cool-moist type) plant domination in the central Great Plains (Feng, 1998). The second-order laminae (2–4-mm-thick fine-coarse couplets) seem to be annual layers of dustfalls. The first-order rhythmic pattern, strongly/weakly gleyed couplets, suggests cyclic environmental changes with a periodicity of approximately 1000 years. These 10 cycles spanning from 21,000 to 10,000 ^{14}C years BP recorded in the Peoria Loess might be causally and chronologically associated with ice advances of the North American Icesheet in the Great Lakes area, although an exact chronological comparison cannot be made because of large age errors inherited from bulk soil samples. The icesheet advances occurred around: 21.0, 20.0, 19.0, 18.1, 17.2, 16.7, 15.5, 14.8, 12.9, 12.3, 11.7, 9.9 ka (Mickleson et al., 1983).

The strongly gleyed layers in the upper Peoria Loess, which contain abundant and well-preserved fossil plant debris and have lower magnetic susceptibility values, were formed under wet and probably well-vegetated conditions. Our interpretation of the variations in the susceptibility of the Peoria Loess along the southern margin of the North American Icesheet is similar to that of the eolian deposit along the southern margin of Siberia in the Northern Mongolian Plateau. That is, the wet (waterlogged?) and well-vegetated (tundra?) condi-

tions altered magnetic minerals from strongly magnetic forms of oxidized iron to weakly magnetic forms, and consequently the magnetic susceptibility was lowered.

4. Final discussions

The stratigraphic (sand/silt) and magnetic susceptibility (high/low) transition dated about 15,000 ^{14}C years BP along the southern margin of Siberia (Fig. 2) may be synchronous with the stratigraphic (massive/laminated) and susceptibility (high/low) transition marked by the dark-blue zone dated at 14,500–14,800 ^{14}C years BP along the southern margin of the North American Icesheet (Fig. 4). This transition, corresponding to a pollen- and insect-indicated climate amelioration in the Midwest of the United States (Schwert and Ashworth, 1988) and to a period of C-4 plant domination in the central Great Plains (Feng, 1998), may well be causally related to the drastic changes in ventilation of the Deep North Atlantic Water (Adkins et al., 1998), and probably to an extreme aridification in Africa around 15,000 ^{14}C years BP (Sirocko et al., 1999).

The 10 susceptibility-indicated cycles spanning from ~21,000 to ~10,000 ^{14}C years BP recorded in the Peoria Loess along the southern margin of the North American Icesheet were most likely causally and chronologically related to these nearly 1000-year cycles of ice advances of the North American Icesheet in the Great Lakes area (Mickleson et al., 1983). These 1000-year cycles may be also related to those cycles expressed as the East Asia Monsoon (EAM) strength variations in the South China Sea that occurred around: 17.0, 15.9, 15.5, 14.7, 13.5, 13.3, 12.1, 11.5, 10.7 ka (Wang and Samthein, 1999). These cycles may also be the same as the dominating cycles (1070-year) recorded in the Santa Barbara basin of the northeastern Pacific (Heusser, 1998; Sirocko et al., 1999) and also the same as the second dominating cycles (i.e., 1100-year) recorded in the GISP2 ice core in Greenland (Grootes and Stuiver, 1997).

We propose here that the possible millennial–centennial variations in ENSO (Cane and Clement, 1999), which were demonstrated to be active during the late Pleistocene (Rittenour et al., 2000), might be the controlling mechanism to link the Tropical Pacific (e.g., records from the South China Sea) to the North Atlantic (e.g., records from Greenland) through North America (e.g., records from the central Great Plains). The North American linkage between the Tropical Pacific and the North Atlantic were already implied by other works (e.g., Behl and Kennett, 1996; Benson et al., 1997; Feng, 2000; Rittenour et al., 2000; Sirocko et al., 1999).

The ~1400-year cycles during the period from ~8000 to ~15,000 years BP documented in the southern margin of Siberia may be causally and chronologically related to the dominant periodicity (1470 years) of climatic changes in the North Atlantic area (Bond et al., 1997, 2001; Clarke and Marshall, 1999; Grootes and Stuiver, 1997). That is, the southern Siberian eolian sequence might have recorded ~1400-year cycles in the thermal variations of the Arctic Ocean that was directly linked with the thermal variations in the North Atlantic Ocean (Darby et al., 2001). Or, the ~1400-year cycles recorded in the southern Siberian eolian sequence were directly linked with the North Atlantic via the westerlies (Broecker, 1995; Porter and An, 1995; Visbeck, 2002).

To conclude, the ~1000-year cycles recorded in North American eolian sequences seem responding to a low-latitude forcing (e.g., the Tropical Pacific) and the ~1400-year cycles recorded in the southern Siberian eolian sequences appear responding to a high-latitude forcing (e.g., the North Atlantic). However, our data do not allow us propose plausible mechanisms controlling these two different cycles.

Acknowledgments

This paper is a result of projects supported by three U.S. National Science Foundation grants (EAR-9630142; INT-9806430; and BCS-0078557), a National Geographic Society research grant (NGS-6938-00), a postdoctoral fellowship at Lamont-Doherty Earth Observatory of Columbia University (1992–1994), a graduate research grant at University of Kansas (1990–1991) and two Separately Budgeted Research Grants (1997 and 1998) from Montclair State University.

References

Adkins, J.F., Cheng, H., Royle, E.A., Druffel, E.R.M., Edwards, R.W., 1998. Deep-sea coral evidence for rapid change in ventilation of the deep North Atlantic 15,400 years ago. Science 280, 725–727.

Beget, J.E., Stone, D.B., Hawkins, D.B., 1990. Paleoclimatic forcing of magnetic susceptibility variation in Alaskan loess during the late Quaternary. Geology 18, 40–43.

Behl, R.J., Kennett, J.P., 1996. Brief interstadial events in the Santa Barbara basin, NE Pacific, during the past 60 kyr. Nature 379, 243–246.

Benson, L., Burdett, J., Lund, S., Kashgarian, M., Mensing, S., 1997. Nearly synchronous climate change in the Northern Hemisphere during the Last termination. Nature 388, 263–265.

Bond, G.C., Lotti, R., 1995. Iceberg discharge into the North Atlantic on millennial timescales during the last glaciation. Science 267, 1005–1249.

Bond, G., Showers, W., Cheseby, M., Lotti, R., Almasi, P., deMenocal, P., Priore, P., Cullen, H., Hajdas, I., Bonani, G., 1997. A pervasive millennial-scale cycle in north Atlantic Holocene and glacial climates. Science 278, 1257–1285.

Bond, G., Kromer, B., Beer, J., Muscheler, R., Evans, M.N., Showers, W., Hoffmann, S., Lotti-Bond, R., Hajdas, I., Bonani, G., 2001. Persistent solar influence on north Atlantic climate during the Holocene. Science 294, 2130–2136.

Broecker, W.S., 1995. Massive iceberg discharge as triggers for global climate change. Nature 372, 421–424.

Cane, M., 1998. A role for the Tropical Pacific. Nature 282, 59–60.

Cane, M., Clement, A.C., 1999. A role for the Tropical Pacific coupled ocean–atmosphere system on Milankovitch and millennial timescales. In: Clarke, P.U., Webb, R.S., Keigwin, L.D. (Eds.), Mechanisms of Global Climate Variability at Millennial Timescales, AGU Monograph, vol. 112, pp. 363–372.

Chlachula, J., Evans, M.E., Rutter, N.W., 1998. A magnetic investigation of a Late Quaternary loess/paleosol record in Siberia. Geophysics International 132, 128–132.

Clarke, P.U., Marshall, S.J., 1999. A glaciological perspective on Heinrich Events. In: Clarke, P.U., Webb, R.S., Keigwin, L.D. (Eds.), Mechanisms of Global Climate Variability at Millennial Timescales, AGU Monograph, vol. 112, pp. 243–262.

Darby, D., Bischof, J., Cutter, G., de Vernal, A., Hillaire-Marcel, C., Dwyer, G., McManus, J., Osterman, L., Polyak, L., Poore, R., 2001. New record shows pronounced changes in Arctic Ocean circulation and climate. EOS (December 4), 606–607.

Fassbinder, J.W.E., Stanjek, H., Vali, H., 1990. Occurrence of magnetic bacteria in soil. Nature 343, 161–163.

Feng, Z.-D., 1996. Climatic implication of magnetic susceptibility and Be-10 in Chinese loess. Catena 25, 211–216.

Feng, Z.-D., 1997. Geochemical characteristics of a loess–soil sequence in central Kansas, USA. Soil Science Society of America Journal 61, 534–541.

Feng, Z.-D., 1998. Eolian environments in Nebraska during the Marine Isotope Stage 2. International Symposium on Aerosol, Loess, and Global Change. Washington State University, pp. 107–110. MISC0190.

Feng, Z.-D., 1999. Gobi Dynamics in the northern Mongolian Plateau during the past 50,000 years. In: Derbyshire, E. (Ed.), International Symposium on LoessFest, pp. 69–71. May 21–24, Bonn, Germany.

Feng, Z.D., 2000. Abrupt climate events and icesheet dynamics during the last glacial. In: Zhou, S.Z. (Ed.), International Symposium on Quaternary Glaciation in Monsoon Asia, pp. 25–26. June 15–18, Chengdu, China.

Feng, Z.-D., 2001. Gobi dynamics in the northern Mongolian Plateau during the past 20000+ years: preliminary results. Quaternary International 76/77, 77–83.

Feng, Z.-D., Chen, F.H., 1999. Problems of magnetic susceptibility signature as the summer monsoon proxy in Chinese loess sequences. International Symposium on Paleosols and Climate Change, Chinese Science Bulletin, vol. 44 (suppl. 1), pp. 97–104.

Feng, Z.-D., Johnson, W.C., 1995. Factors affecting the magnetic susceptibility of a loess–soil sequence, Barton County, Kansas, USA. Catena 24, 25–37.

Feng, Z.D., Johnson, W.C., Diffendal, R.F., 1994a. Environment of eolian deposition in south-central Nebraska during the Last Glacial Maximum. Physical Geography 15 (3), 250–258.

Feng, Z.-D., Johnson, W.C., Sprowl, D.R., Lu, Y.-C., Ward, P.A., 1994b. Climatic signals from loess–soil sequences in the central Great Plains, USA. Palaeogeography, Palaeoclimatology, Palaeoecology 110, 345–358.

Feng, Z.-D., Johnson, W.C., Sprowl, D.R., Lu, Y.C., 1994. Loess accumulation and soil formation in central Kansas during the past 400,000 year. Earth Surface Processes and Landforms 19, 55–67.

Feng, Z.D., Chen, F.H., Tang, L.Y., Kang, J.C., 1998. East Asian Monsoon variations and Gobi dynamics in Stages 3 and 4. Catena 33, 29–46.

Grootes, P.M., Stuiver, M., 1997. Oxygen 18/16 variability in Greenland snow and ice with 103- to -105 yr time resolution. Journal of Geophysical Research 102, 26455–26470.

Heusser, L., 1998. Direct correlation of millennial-scale changes in western Northern American vegetation and climate with changes in the California current system over the past 60,000 years. Paleoceanograpgy 13, 252–262.

Khosbayar, P., 1989. Map of Geological Complexes of Mongolia, 1:500,000. Moscow.

Leuschner, D.C., Sirocko, F., 2000. The low-latitude monsoon climate during Dansgaad–Oeschger cycles and Heinrich Events. Quaternary International 67/68, 243–254.

Liu, X.M., Hess, P., Rolph, T., Beget, E., 1999. Properties of magnetic mineralogy of Alaskan loess: evidence for pedogenesis. Quaternary International 62, 93–102.

Lugn, L.A., 1968. The origin of loess and the relation to the Great Plains in North America. In: Schultz, C.B., Frye, J.C. (Eds.), Loess and Related Eolian Deposits of the World. University of Nebraska Press, Lincoln, NE, pp. 139–182.

MacAyeal, D.R., 1993. Binge/Purge oscillations of the Laurentide Icesheet as a cause of the North Atlantic's Heinrich Events. Paleoceanography 8 (6), 775–784.

Mickleson, D.M., Clayton, L., Fullerton, D.S., Borns, H.W., 1983. The Late Wisconsin glacial record of the Laurentide icesheet in

the United States. In: Porter, S.C. (Ed.), Later Quaternary Environments of the western United States. University of Minnesota Press, Minneapolis, pp. 3–37.

Mullins, G.E., 1977. Magnetic susceptibility of the soil and its significance in soil science: a review. Journal of Soil Science 28, 223–246.

Porter, S.C., An, Z.S., 1995. Correlation between climate events in the North Atlantic and China during the last glaciation. Nature 375, 305–308.

Rittenour, T.M., Brigham-Grette, J., Mann, M.E., 2000. El Nino-like climate teleconnections in New England during the late Pleistocene. Science 288, 1039–1042.

Ruhe, R.V., 1983. Depositional environment of late Wisconsin loess in the midcontinental United States. In: Porter, S.C. (Ed.), Late Quaternary Environments of the United States. University of Minnesota Press, Minneapolis, pp. 130–137.

Schwert, D.P., Ashworth, A.C., 1988. Late Quaternary history of the northern beetle fauna of North America: a synthesis of fossil and distributional evidence. Memoirs of the Entomological Society of Canada 144, 93–107.

Sirocko, F., Leuschner, D., Staubwasser, M., Maley, J., Heusser, L., 1999. High-frequency oscillations of the last 70,000 years in the Tropical/Subtropical and Polar Climates. In: Clarke, P.U., Webb, R.S., Keigwin, L.D. (Eds.), Mechanisms of Global Climate Variability at Millennial Timescales, AGU Monograph, vol. 112, pp. 113–125.

Stocker, T., 1998. The seesaw effect. Science 282, 61–62.

Thompson, R., Oldfield, F., 1986. Environmental Magnetism. Allen and Oldwin, London.

Visbeck, M., 2002. The ocean's role in Atlantic climate variability. Science 297, 2223–2224.

Wang, L., Sarnthein, M., 1999. Millennial reoccurrence of century-scale abrupt events of East Asian monsoon: a possible heat conveyor for the global deglaciation. Paleoceanography 14 (6), 725–731.

Weaver, A.J., 1999. Millennial timescale variability in ocean/climate models. In: Clarke, P.U., Webb, R.S., Keigwin, L.D. (Eds.), Mechanisms of Global Climate Variability at Millennial Timescales, AGU Monograph, vol. 112, pp. 285–300.

Wells, P.V., 1983. Late Quaternary vegetation of the Great Plains. Nebraska Academy of Sciences, Transactions 11, 83–89.

Wells, P.V., Steward, J.D., 1987. Spruce charcoal, coniferous macrofossils, land snails and land vertebrate fauna in Wisconsian sediments on the High Plains of Kansas. In: Johnson, W.C. (Ed.), Kansas Geological Survey Guidebook on Quaternary Environments of Kansas. Kansas Geological Survey, pp. 129–140.

Williams, M., 1992. Evidence for the dissolution of magnetite in recent Scottish peats. Quaternary Research 37, 171–182.

Wright, H.E., 1970. Vegetation history of the central Great Plains. In: Dort, W., Jones, J.K. (Eds.), Pleistocene and Recent Environments of the Central Great Plains. University of Kansas Press, Lawrence, Kansas, pp. 157–172.

附录二

The Holocene
23(12) 1721–1730
© The Author(s) 2013
Reprints and permissions:
sagepub.co.uk/journalsPermissions.nav
DOI: 10.1177/0959683613505337
hol.sagepub.com
SAGE

Holocene climate variations retrieved from Gun Nuur lake-sediment core in the northern Mongolian Plateau

Z-D Feng,[1] YZ Ma,[2] HC Zhang,[3] Ts Narantsetsega[4] and XS Zhang[5]

Abstract

Our pollen-based climate reconstruction shows that both temperature and moisture were low during the early Holocene from ~10,000 to ~8000 cal. a BP and gradually climbed from ~8000 to ~6000 cal. a BP. The last ~6000 years have been generally warm and wet with high-amplitude fluctuations. The high-moisture conditions for the past ~6000 years are not only corroborated by high arboreal pollen/non-arboreal (AP/NAP; trees and shrubs over herbs) pollen ratio and high pollen concentration but also by high organic matter content and diatom data. We suggest that lower winter insolation and remaining ice covers in the early Holocene might have slowed down temperature rise in the continental interiors and that the resulted low temperature might have suppressed regional evaporation that was a major water vapor source for precipitation. At the same time, icemelt-water injection into the North Atlantic Ocean might have also suppressed water vapor supplies to the downwind areas, including the northern Mongolian Plateau. The increase in winter insolation and the final melting of ice sheets, together with the increased atmospheric CO_2 concentration and the associated increase in atmospheric water vapor, could be responsible for the higher temperature during the past ~6000 years. The icemelting and the associated rise of sea level during the past ~6000 years might be responsible for the weakening of the winter monsoon in the interior of Asian continent, thus alluring farther eastward penetration of the relatively warm and wet Atlantic air masses and consequently bringing more precipitation to the northern Mongolian Plateau.

Keywords

climate change, Holocene, Mongolian Plateau, pollen analysis

Received 31 October 2012; revised manuscript accepted 12 August 2013

Introduction

Future environmental changes, including the changes in water resources and ecological systems, in response to future global warming in the northern Mongolian Plateau may be assessed if the driving forces of climate change at present and in the past are identified. The Holocene is of particular relevance because similar natural boundary conditions might exist in the future (Wanner et al., 2008). Generally speaking, the Holocene climate change should have been driven by four major forcing factors: (1) winter insolation, (2) summer insolation, (3) atmospheric CO_2 concentration, and (4) ice cover extent. In addition, the combined effect of lower winter insolation and larger ice cover (including larger and longer snow covers and larger permafrost extents) in the early Holocene may have acted as a strong high-latitude force influencing the northern Mongolian Plateau, while after ~7000 yr BP, the combined effect of increased atmospheric CO_2 concentration (Bush, 2005) and moderate summer insolation under warmed ocean surface and lessened ice cover conditions, when 'modern' level of atmospheric CO_2 concentration and 'modern' ice extent were approaching (Ruddiman, 2008), may have acted as a strong low-latitude force influencing the northern Mongolian Plateau. Furthermore, a climatic feedback mechanism of combined effect of CO_2 and water vapor was proposed by Bush (2005) and corroborated by Prokopenko et al. (2007) to explain the mid- and late Holocene warming observed in southern Siberia.

The Holocene climate in the northern Mongolian Plateau, where our study site (i.e. Gun Nuur) is situated, was earlier proposed to have been associated with the East Asian monsoon (Harrison et al., 1996; Tarasov et al., 2000). The Westerlies system was recently advocated as a dominating climatic system controlling the entire Asian arid–semi-arid belt, including the northern Mongolian Plateau during the entire Holocene (Chen et al., 2008). A third proposition stated that the Holocene moisture variations in the arid and hyper-arid east-central Asia, including the northern Mongolian Plateau, have been primarily modulated by the temperature (Wang et al., 2011; Wang and Feng, 2013). These disagreements call for more high-resolution paleoclimatic reconstructions from the northern Mongolian Plateau.

This paper is the fourth report on Gun Nuur to fully explore the climatic history based on 49 radiocarbon dates and 372 fossil pollen samples of GN-02 core collected in 2002 (i.e. core-A in Figure 1). The first one was by Dorofeyuk and Tarasov (1998) who provided a useful Holocene climatic framework based on limited dates and relatively low-resolution proxy data (i.e. core-C in Figure 1). The second one was by Feng et al. (2005) who reported their non-pollen data of GN-02 core drilled in 2002. The third one was by Zhang et al. (2012) who explored the Holocene histories of the lake-level and salinity changes based on proxies

[1]Chinese Academy of Sciences, China
[2]Beijing Normal University, China
[3]Yunnan Normal University, China
[4]Mongolian Academy of Sciences, Mongolia
[5]Lanzhou University, China

Corresponding author:
Z-D Feng, Xinjiang Institute of Ecology and Geography, Chinese Academy of Sciences, Urumqi 830011, China.
Email: fengzd@lzu.edu.cn; fengzd@ms.xjb.ac.cn

from carbonate materials (e.g. mineralogical and isotopic compositions) of GN-04 core drilled in 2004 (i.e. core-B in Figure 1).

The objective of this paper was to explore the climatic history based on pollen data. First, we argued that Scots pine (*Pinus sylvestris*), an overwhelmingly predominant pollen type in the Gun Nuur record, reflects high-moisture conditions in our record in particular (i.e. Gun Nuur) and also reflects higher temperature conditions in all cases from the Ulaanbaatar-Baikal corridor in general (see details in section 'Reconstructions of temperature and moisture indices'). Second, we devised a new set of temperature index (T) and moisture index (M) in which Scots pine (*P. sylvestris*) is a warm and wet component (Table 1). The logic to devise the new indices is the same as that used by Demske et al. (2005). That is, the relative changes in major vegetation types can be expressed by assigning recorded pollen taxa to groups corresponding to the modern distribution of plant communities.

Physiographic setting and methods

Gun Nuur (latitude 50°15′N, longitude 106°37′E, elevation 600 m a.s.l.), presently a closed lake in the middle portion of Buryn River, which is the eastern tributary of the Orkhon River, is situated within the forest-steppe zone in the middle of the Ulaanbaatar-Baikal corridor (48–56°N and 104–108°E) of the northern Mongolian Plateau (Figure 1). The maximum water depth is ~5 m, and the lake covers an area of 2.5 km^2. The lower reach of the eastern tributary of the Orkhon River is covered by steppe vegetation, while the upper reach is covered by forest-steppe vegetation dominated by Scots pine (*P. sylvestris*) trees on the sunny edges of montane forests (Dulamsuren et al., 2009). The alluvial plain around the lake is covered by low-lying sand dunes where *P. sylvestris* trees dominate the landscape (Dorofeyuk and Tarasov, 1998). The modern climate of the study area is temperate continental with cold and dry winters and warm and humid summers. The mean annual temperature is about −2°C with the mean annual precipitation of about 350 mm occurring mostly from July to September (Zhang et al., 2012).

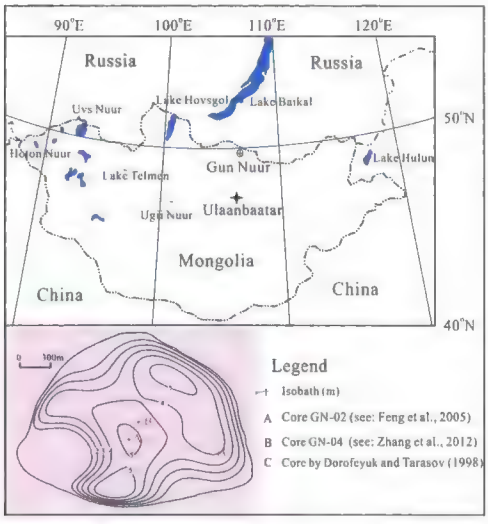

Figure 1. Location and isobath map of Gun Nuur.
Source: Adopted from Zhang et al. (2012).

A 745-cm-long lake core (i.e. core GN-02) was collected with a Livingstone-type piston corer in 2002 at the central part of the Gun Nuur, where the water depth was about 5 m. The core was cut longitudinally into two halves and subsampled by slicing of 2-cm-thick sediment sections immediately after core retrieval in the field. For pollen analysis of 372 samples, exotic *Lycopodium* tablets were first added for calculation of pollen concentration, and the samples were then treated with HCl (10%) and HF (39%). More than 300 pollen grains (excluding spores) were counted and identified for each sample. Pollen identification was aided by the published references (e.g. Moore et al., 1991; Wang et al., 1995) and also with our own reference collections of more than 500 plant species from northern China. Pollen counting was carried out using a Leica light microscope under 400× magnification. Raw pollen data were expressed as percentages of the sum of terrestrial pollen.

Results

Stratigraphy and chronology

The core can be stratigraphically divided into four major units (Figure 2). Sediment Unit A (745–720 cm) is dark fine-grained sand with extremely low total organic carbon (TOC) and $CaCO_3$ contents. Sediment Unit B (720–570 cm) is a silty and light-brown carbonate-enriched varve-like layer. Sediment Unit C (570–240 cm) is a sand–silt alternating unit containing three couplets. The silty subunits are characterized by relatively high TOC and $CaCO_3$ contents. Sediment Unit D (240–0 cm) is a sandy silt unit with a mollusks-rich layer at the depth of 205–234 cm. This unit has the highest TOC content of the entire sequence and also a relatively high $CaCO_3$ content.

A total of 49 AMS ^{14}C dates were obtained from core GN-02. A total of 48 AMS samples were bulk sediments, and one sample was wood. The dating reliability and possible problems were fully discussed in Chang et al. (2011), and the dates were presented in Zhang et al. (2012; see supplementary Table 1). The chronology was established through the following procedures. All 48 dates of

Table 1. Pollen-group subsums used for the calculation of vegetation-based temperature and moisture indices that are newly devised (in this paper).

Group	Type	Pollen taxa
S1	Xeromorphic desert	Chenopodiaceae, *Nitraria*, Zygophyllaceae, and *Ephedra*
S2	Meso-xeromorphic steppe	*Artemisia* and Aster
S3	Birch forest/shrubs	*Betula*, *Alnus*, Rosaceae, *Salix*, *Ulmus*, and *Taraxacum*
S4	Light-needled forest	*Pinus sylvestris* and *Juniperus*
S5	Cold-moist needled forest	*Picea*, *Abies*, *Pinus sibirica*, Ranunculaceae, Caryophyllaceae, *Scabiosa*, and Papaveraceae
S6	Moderate hydroperiod steppe	Cyperaceae and Polygonaceae
T	Temperature index	T =(S1 + S2 + S4)/(S3 + S5 + S6)
M	Moisture index	M = (S4 + S5 + S6)/(S1 + S2 + S3)

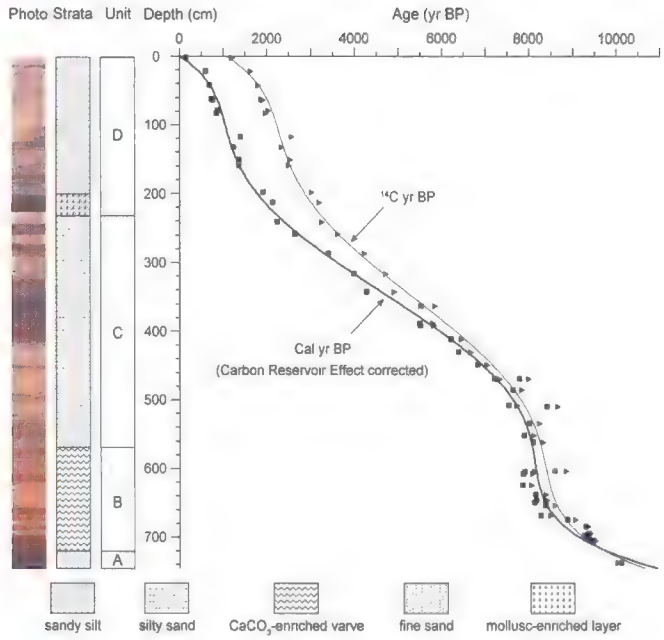

Figure 2. Age–depth model of GN-02 core.

bulk sediment samples were used to establish the age–depth model after reservoir corrections following the procedure below. A fifth-order polynomial regression was used to establish the age–depth relationship (Figure 2). The intercept of the regression curve at 0-cm core depth of 1060 a BP was regarded as present-day lake-reservoir effect. The uppermost dating sample from 5 to 0 cm core depth yielded an age of 1200 ± 40 a BP. Considering that this sample integrates the uppermost 5 cm of the core sediment, the obtained radiocarbon date (1200 ± 40 a BP) corresponds reasonably well with the model-determined age for the core top (1060 a BP). Furthermore, the 1000-year difference between the wood-derived radiocarbon age from the core base (744–743 cm) and the age-model inferred age at the same stratigraphic level indicates that the lake-reservoir effect for the lowermost sediments was similar to that for the uppermost sediments. Assuming that the lake-reservoir effect varied insignificantly between the base and top of core GN-02, 1060 years were subtracted from the bulk sediment dates to account for the lake-reservoir effect. The resulting lake-reservoir corrected radiocarbon years were then calibrated using 2σ probability ranges in CALIB 6.0 and IntCal 09 (Reimer et al., 2009).

Pollen assemblages

The cluster analysis yielded four major pollen zones that are approximately correspondent with the aforementioned sediment units (Figure 3).

Pollen Zone GN-A (745–720 cm; ~10,800–9800 cal. a BP) is characterized by the dominance of herbaceous pollen (~65%) with a relatively high percentage of summer-green tree pollen (~15%). The major herbaceous pollen types include Chenopodiaceae (~30%), *Artemisia* (~20%), and Gramineae (~10%) with some amounts of *Ephedra, Aster*, and Caryophyllaceae. The summer-green tree component mainly consists of *Betula* and *Ulmus*. The rest (~20%) is coniferous tree pollen (*Larix, Picea, Abies, Pinus sibirica*, and *P. sylvestris*). It is also noticeable that percentages of Cyperaceae and fern are quite high in this zone.

Pollen Zone GN-B (720–570 cm; 9800–8100 cal. a BP) is distinctive from GN-A by an increased *Betula* percentage and decreased Chenopodiaceae and *Ephedra* percentages. But the commonalities between Zone GN-A and Zone GN-B are more pronounced than their differences, and the major commonalities include rather visible appearance of *Larix, P. sibirica, Picea*, and *Abies* and constantly high percentages of *Artemisia* and Gramineae.

Pollen Zone GN-C (570–240 cm; 8100–2400 cal. a BP) is typified by a persistently high percentage of *P. sylvestris* accompanied with significant reduction in herbaceous components (mainly including Chenopodiaceae, *Artemisia*, Gramineae, and Cyperaceae). Other noticeable features of GN-C include nearly complete disappearance of *Larix, P. sibirica, Picea*, and *Abies* and dramatic increases in arboreal pollen/non-arboreal pollen (AP/NAP) ratio and in pollen concentration. The fluctuations in the percentages of arboreal components and herbaceous components further divide the Zone GN-C into three subzones.

Pollen Zone GN-D (240–0 cm; 2400–0 cal. a BP) is also dominated by *P. sibirica* pollen. But the most pronounced features are as follows: (1) reappearance of some coniferous tress (e.g. *Larix, P. sibirica, Picea*, and *Abies*), (2) reappearance of some summer-green trees (e.g. *Corylus, Betula*, and *Ulmus*), (3) appearance of *Tsuga* and Cupressaceae, and (4) recovery of some major herbaceous components (e.g. Chenopodiaceae, *Artemisia, Aster*, Gramineae, and Cyperaceae). Variations in *P. sibirica* and *Artemisia* percentages further divide this zone into five subzones.

Discussion and conclusion

Reconstructions of temperature and moisture indices

We first tested two different sets of already-published pollen-based climatic indices to explore their applicability to our record. The first set of temperature (T) and moisture (M) indices (see supplementary Table 2) was constructed by Demske et al. (2005) based on the observed relationships between modern plant distribution

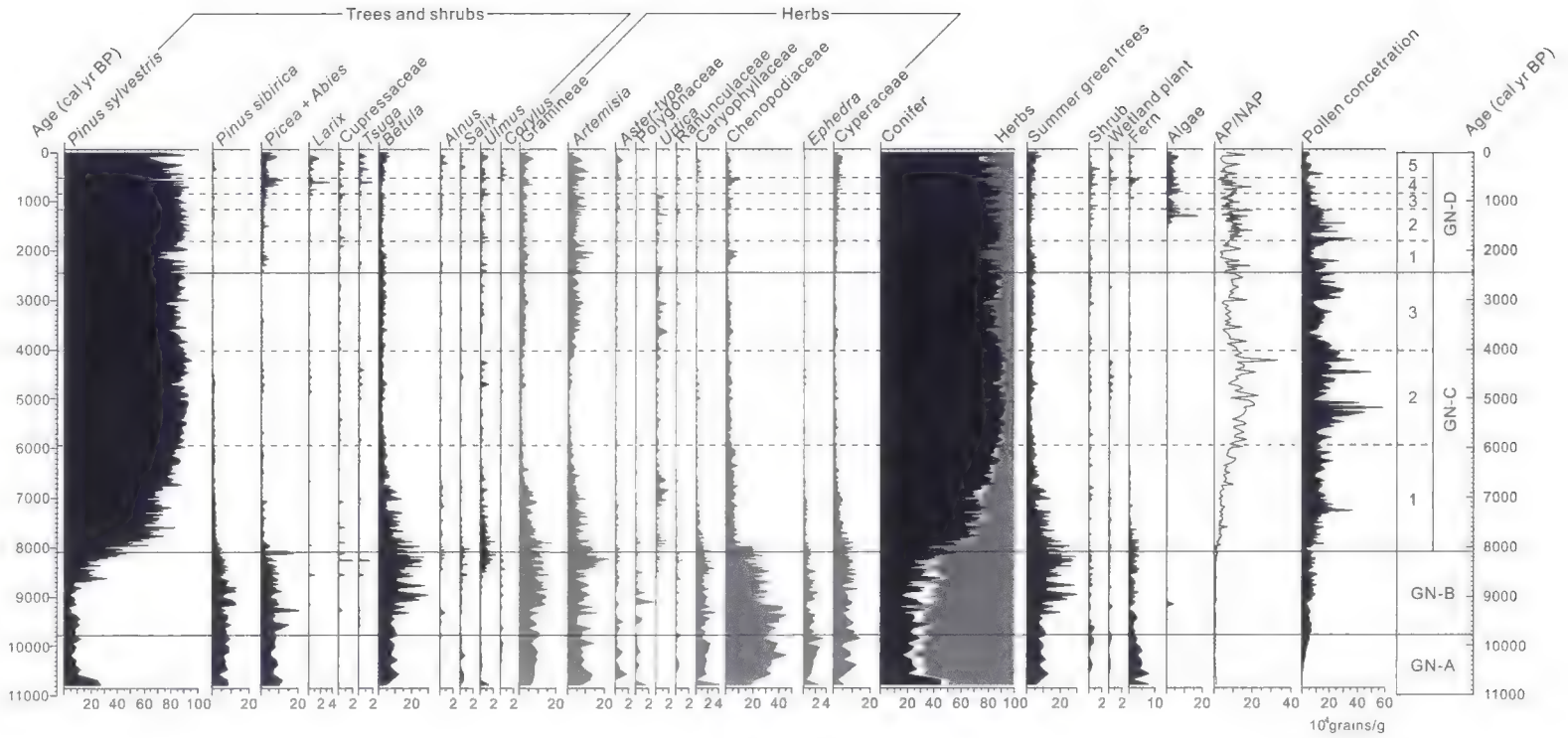

Figure 3. Pollen spectrum of GN-02 core.
AP: arboreal pollen; NAP: non-arboreal pollen.

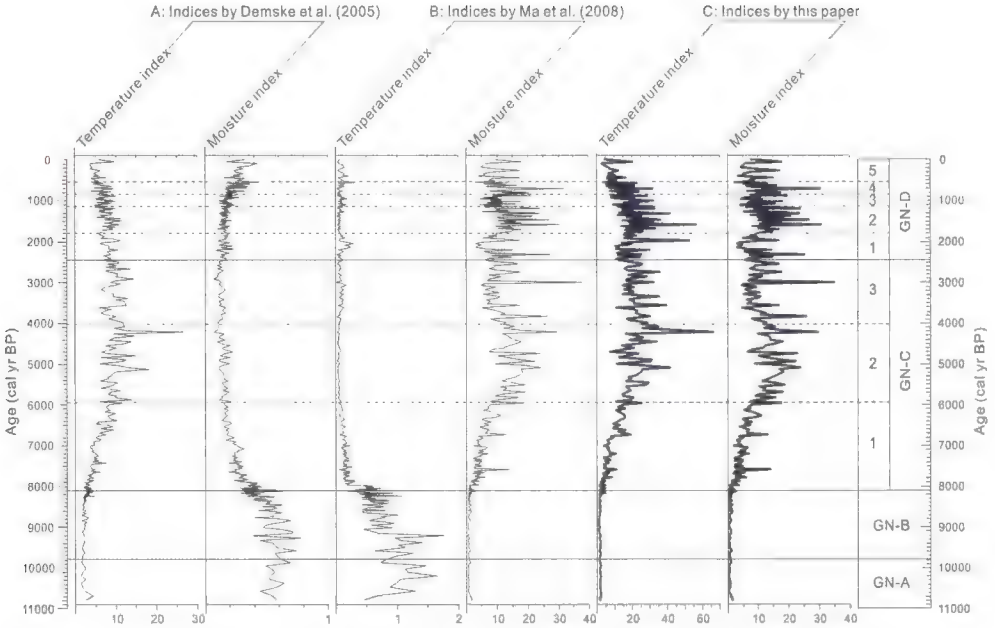

Figure 4. Reconstructions of pollen-based temperature in indices (T) and moisture indices (M) for Gun Nuur lake core (A by Demske et al. (2005), B by Ma et al. (2008), and C from this paper).

and associated climate in southern Siberia. The second set of T and M indices (see supplementary Table 3) was constructed by Ma et al. (2008) based on a surface-soil pollen data base generated along an S-N transect in the Mongolian Plateau. The reconstructed T using the index defined by Demske et al. (2005) shows that the temperature was rather low from ~11,000 to ~7000 cal. a BP and has been variably warm during the past ~7000 years (Figure 4A). The reconstructed M suggests that the wettest period lasted from ~11,000 to ~8000 cal. a BP that was followed by a drying trend lasting from ~8000 to ~6000 cal. a BP. After a persistent dry period between ~6000 and ~2500 cal. a BP, the moisture has been recovering for the past ~2500 years. The reconstructed T using the index defined by Ma et al. (2008) shows that the temperature was rather high from ~11,000 to ~8000 cal. a BP and has been constantly low during the past ~8000 years (Figure 4B). The reconstructed M suggests that the moisture was rather low from ~11,000 to ~8000 cal. a BP and has been relatively and variably high during the past ~6000 years after a 2000-year transition (from 8000 to 6000 cal. a BP). It is rather apparent that the reconstructed T and M curves using indices by Demske et al. (2005) are completely opposite to those using indices by Ma et al. (2008).

The opposite trends between these two sets of reconstructions resulted from two absolutely opposite angles from which the predominant pollen species, Scots pine (*P. sylvestris*), was bioclimatologically categorized. Specifically, Demske et al. (2005) developed their T and M indices in southern Siberia where the southward increasing trend of Scots pine abundance represents warming and drying trends along the modern bioclimatic N→S transect. In contrast, Ma et al. (2008) developed their T and M indices based on their own data set from the entire Mongolian Plateau where climate becomes cooler and wetter along the modern bioclimatic S→N transect. The observed gradual increase in Scots pine trees and the associated northward increase in Scots pine pollen percentage in the northern portion (i.e. cooler and wetter portion) of the Mongolian Plateau defined the Scots pine as a cooler and wetter component in the indices by Ma et al. (2008).

Scots pine (*P. sylvestris*) is a eurythermic species native to Europe and Asia, which also adapts to a wide range of precipitation conditions. Longitudinally, its distribution ranges from Ireland in the west to eastern Siberia in the east. Latitudinally, its distribution ranges from Inner Mongolia of China to Arctic Circle in Asia (Zhang, 2007). In the mountain ridges within Lake Baikal region, Scots pine (*P. sylvestris*) and larch (*Larix*) taiga prevails on drier/warmer south- and east-facing slopes and at drier/warmer lower elevations, while Siberian pine (*P. sibirica*), fir (*Abies*), and spruce (*Picea obovata*) taiga are widespread on wetter/cooler north- and west-facing slopes and at wetter/cooler higher elevations. Consequently, Scots pine has been regarded as a dry and warm component for reconstructing Holocene climate change in Lake Baikal area (i.e. Bezrukova et al., 2009, 2011; Demske et al., 2005; Tarasov et al., 2005, 2007, 2009). Our focal site (i.e. Gun Nuur) is situated in the middle portion of Buryn River basin, an eastern tributary of the Orkhon River, the latter (i.e. Orkhon) being a branch of the Selenga River that directly flows into Lake Baikal. Within the Selenga River basin, Scots pine trees absolutely dominate the sunny edges of montane forests (Dulamsuren et al., 2009). The alluvial plain around Gun Nuur is covered by low-lying sand dunes where Scots pine trees also dominate the landscape (Dorofeyuk and Tarasov, 1998). The domination of Scots pine at the sunny edges of montane forests in the northern Mongolian Plateau gives rise to the assumption that it is a rather drought-tolerant species, and the assumption was field confirmed within the forest-steppe ecotone in the northern Mongolian Plateau (Dulamsuren et al., 2009).

It is true that Scots pine is a rather drought-tolerant species compared with many other tree species in the Ulaanbaatar-Baikal corridor. But the situation is completely different between the Lake Baikal area in the center of the Siberian Taiga forest in the north and the Gun Nuur area in the middle of a forest-steppe zone in the south. Scots pine will definitely take over the place of dark coniferous trees (e.g. Siberian pine, fir, and spruce) in the Lake Baikal area if the soil moisture is sufficiently lowered. However,

Scots pine will definitely give way to herbaceous species in the Gun Nuur area if the soil moisture is sufficiently lowered. In other words, its growth does have a minimal requirement for soil moisture and thus actually is a wet-indicative species in comparison with major herbaceous species in steppes and forests-steppe (Dulamsuren et al., 2009; Zhang, 2007). Assuming that the Gun Nuur area has been primarily within forest-steppe zone during the entire Holocene, the limiting factor for Scots pine to expand should be the soil effective moisture. This assumption is in fact supported by the pollen data showing that the Scots pine–dominated vegetation (rather than dark coniferous trees-dominated) has been dominating the landscape during the past ~7000 years (see Figure 3). Therefore, we argue here that Scots pine should be a higher moisture component in our case (i.e. Gun Nuur).

Scots pine has been regarded as a higher temperature component in paleoclimate reconstructions of southern Siberia, including the Lake Baikal area (e.g. Bezrukova et al., 2009; Demske et al., 2005; Prokopenko et al., 2007; Tarasov et al., 1997, 2007, 2009), and the logic is simply derived from modern bioclimatic background of Scots pine growth in southern Siberia in general and in the Lake Baikal area in particular. Here, we present three sets of arguments supporting the proposition. Temporally, nearly all of Lateglacial and Holocene pollen sequences obtained from the southern boundary of the Siberian taiga forests ubiquitously show that Lateglacial steppe vegetation was gradually replaced by Scots pine–dominated forests during the early Holocene, suggesting that the expansion of Scots pine trees most likely resulted from postglacial warming (e.g. Blyakharchuk et al., 2004, 2007; Kremenetski et al., 1997; Rudaya et al., 2009; Tarasov et al., 1997, 2000). Latitudinally, two pieces of evidence support the notion that Scots pine is associated with high temperature. First, the pollen-indicated progressive and northward Holocene expansion of Scots pine trees from the northern Mongolian Plateau, through the Lake Baikal area, to central Siberia during the early Holocene implies that northward retreating of permafrost and the associated northward soil warming along the S→N transect were most likely the reasons behind the northward expansion of Scots pine trees (e.g. Bezrukova et al., 2009, 2011; Demske et al., 2005; MacDonald et al., 2000; Prokopenko et al., 2007; Tarasov et al., 2000). Second, the present abundance of Scots pine trees is definitely increasing along the N→S warming transect from central Siberia, through the Lake Baikal area, to the northern Mongolian Plateau. Topographically and attitudinally, Scots pine (*P. sylvestris*), together with larch (*Larix*), prevails on warmer south- and east-facing slopes and at warmer lower elevations in Lake Baikal area (Demske et al., 2005; Prokopenko et al., 2007; Tarasov et al., 2000). We also want to add that the low-temperature notion of Scots pine by Ma et al. (2008) is not statistically robust simply because only 10 sampling points of total 108 samples were from the Scots pine–present landscapes (forests and forests-steppe), and the 10 sampling points were from a relatively small area around the Lake Hovsgol at the northern tip of the Mongolian Plateau.

As argued above, Scots pine is a higher moisture component in Gun Nuur area in particular and a higher temperature component in all cases from the Ulaanbaatar-Baikal corridor in general. We have thus devised a new set of temperature index (T) and moisture index (M) to accommodate above arguments. The reconstructions based on the newly devised indices (Table 1) show that both T and M were low during the early Holocene between ~10,000 and ~8000 cal. a BP and gradually climbing in the following period between ~8000 and ~6000 cal. a BP. The last ~6000 years have been generally warm and wet with the recent millennium being slightly cooling (Figure 4C).

It is rather notable that the pollen-based reconstruction of high moisture for the past ~6000 years is well corroborated by AP/NAP ratio and also by pollen concentration (Figure 5). The organic matter content, an indicator of primary productivity in the watershed and in the lake (Shen et al., 2010), also lends a strong support to the reconstruction. Another set of supportive evidence comes from diatom abundance (Figure 5). Specifically, higher abundance of planktonic diatom from GN-02 core, as an indicator of a deeper lake (Dorofeyuk and Tarasov, 1998; Shen et al., 2010), corresponds with higher moisture index for the period between ~6500 and ~1500 cal. a BP. Higher abundance of benthic diatom, as an indicator of a shallower lake, approximately corresponds with lower moisture index for the period between ~9000 and ~7000 cal. a BP and also for the period between ~1500 and ~500 cal. a BP. It is notable that two samples within the unit of dark fine-grained sand (i.e. GN-A) have a very high abundance of planktonic diatom, and the eolian or fluvial nature of the sand (see Dorofeyuk and Tarasov, 1998; Zhang et al., 2012) suggests that the diatom may be of exotic origin. Furthermore, the well-expressed coexistence of Cyperaceae with Chenopodiaceae and Ephedra in the early Holocene between ~11,000 and ~8000 cal. a BP suggests that the lake was rather shallow and wetland components (e.g. Cyperaceae) were abundant around the lake (see Figure 3). And, the lack of Cyperaceae between ~6500 and ~2000 cal. a BP may also indicate that the lake was indeed deeper compared with that during the preceding ~11,000 and ~6500 cal. a BP) and the succeeding periods (~2000 and ~0 cal. a BP). It should be added that increased abundance of Cyperaceae in semi-arid and subhumid conditions, especially when highland contribution of Cyperaceae is negligible, was widely reported to be associated with lake shoaling and the associated increase in wetland areal extent (Shen et al., 2010; Wang et al., 2011). It should be noted that a grain-size peak at 3900–3500 cal. a BP was interpreted to represent shallower lake conditions (Zhang et al., 2012) and this interpretation is corroborated by a lower organic matter content and also by a slightly lowered moisture index. Overall, the reconstructed moisture index (newly devised) seems to be supported by other data and the reconstruction is thus trustworthy. It should be particularly mentioned that the extremely low pyrite content between 280 and 450 cm of GN-04 core was interpreted to have documented a dry mid-Holocene between ~6000 and ~2500 cal. a BP (see Zhang et al., 2012). However, pyrite as a proxy for marine organic matter decomposition (Berner, 1984, 1985) needs further investigations into its climatic and hydrological meanings in lake settings.

Regional comparison

In order to look into our record of Gun Nuur from a larger geographic perspective, we will review some recently published Holocene records from surrounding areas. The first area to be reviewed is the Altai Mountains in the western margin of the northern Mongolian Plateau where many lakes (including Uvs Nuur and Hoton Nuur labeled in Figure 1) have been intensively studied. According to their recent reconstruction from Hoton Nuur and also to their reviews of other's works (including Blyakharchuk et al., 2004, 2007; Dorofeyuk and Tarasov, 1998; Grunert et al., 2000; Tarasov et al., 2000), Rudaya et al. (2009) concluded that in the eastern Altai area within Mongolia, the first half of the Holocene (from ~11,000 to ~5000 cal. a BP) was warm and wet and the second half (from ~5000 to ~0 cal. a BP) was cool and dry, being consistent with the East Asian monsoon-dominated climate pattern. In the western Altai area within Kazakhstan, the first half of the Holocene was warm and dry and the second half was cool and wet, being consistent with the Westerlies-dominated climate pattern. In the northern Altai area within Russia, the first half of the Holocene was warm and wet and the second half was cool and wet.

In the eastern margin of the northern Mongolian Plateau, a recently reported Holocene climatic reconstruction from Lake

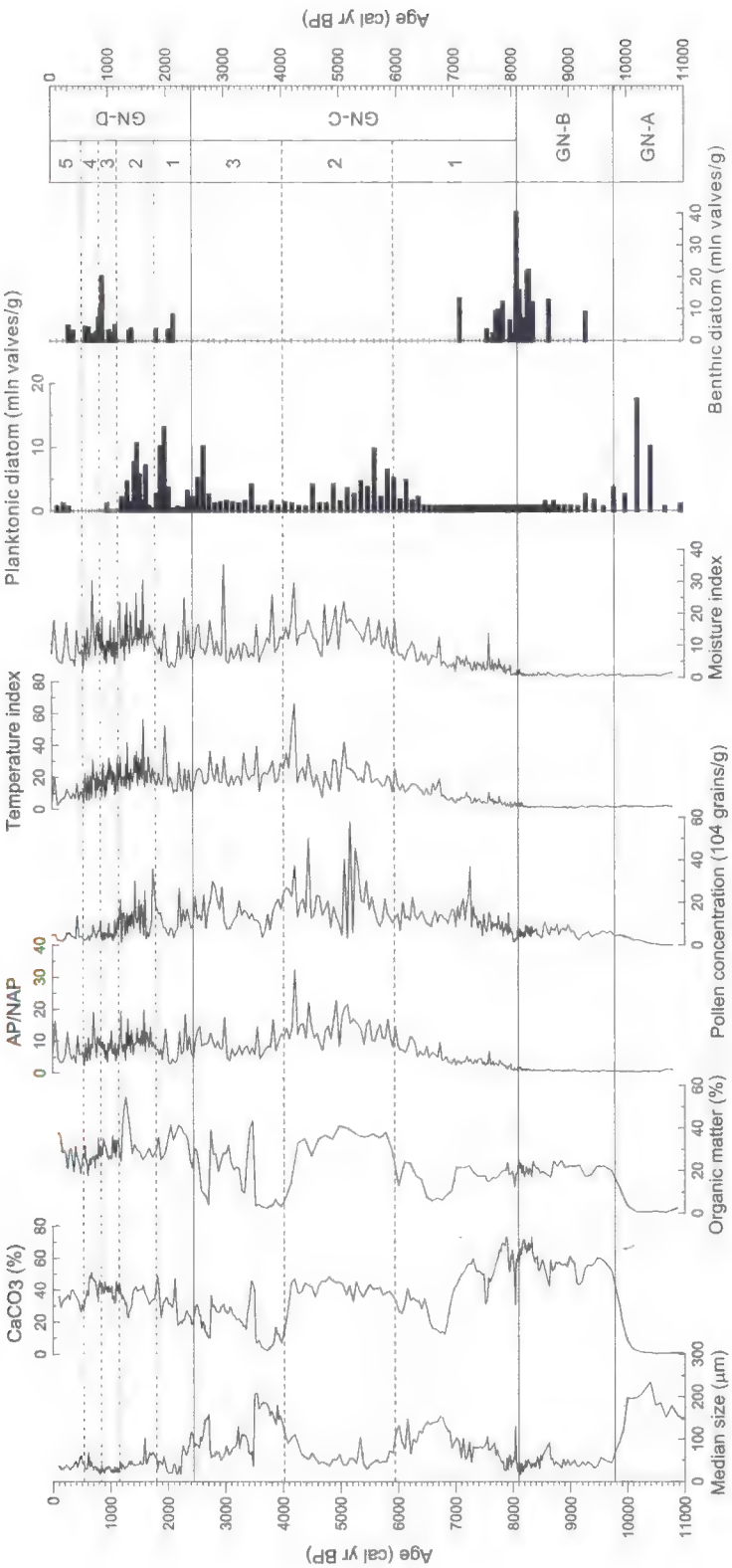

Figure 5. The reconstructions of newly devised T and M indices are supported by organic matter content, pollen AP/NAP ratio, pollen concentration, abundance of planktonic diatom, and abundance of benthic diatom (note: following data are from GN-04 core: grain-size, carbonate and organic matter contents; see Zhang et al. (2012)).

Hulun within Northeast China (Wen et al., 2010a, 2010b; see Figure 1 for location) shows that the early Holocene before ~8000 cal. a BP was warm and dry and the mid-Holocene between ~8000 and ~4500 cal. a BP was the wettest period of the entire Holocene under a slightly cooling condition. After a pronounced dry and relatively cool interval between ~4500 and ~3500 cal. a BP, the climate was generally warm and wet between ~3500 and ~1000 cal. a BP. The first half of the last millennium was cool and dry and the second half warm and wet. The Holocene reconstruction from Lake Hulun is corroborated by the peat $\delta^{13}C$ record from nearby Hani Peat (Hong et al., 2005).

To the south of Gun Nuur are Ugii Nuur and Lake Telmen (see Figure 1 for locations) where a mid-Holocene dry phase was reported to have lasted from ~6500 to ~3500 cal. a BP (Fowell et al., 2003; Peck et al., 2002; Wang et al., 2009, 2011). The preceding period before ~6500 cal. a BP and the succeeding period after ~3500 cal. a BP were relatively wet. This mid-Holocene dry phase was approximately corresponding with the warm mid-Holocene in southern Siberia to the north (Demske et al., 2005) and with the warm mid-Holocene in northern China to the south (Shi et al., 1993), implying that the mid-Holocene dry phase in the arid and semi-arid portions of the Mongolian Plateau was most likely the result of mid-Holocene high temperature (Wang et al., 2011; Wang and Feng, 2013).

To the north of Gun Nuur is Lake Baikal basin where lake cores and peatland sections have been intensively studied (e.g. Bezrukova et al., 2009, 2011; Demske et al., 2005; Fukumoto et al., 2012; Horiuchi et al., 2000; Prokopenko et al., 1999, 2007; Prokopenko and Williams, 2004; Shichi et al., 2009; Tarasov et al., 2005, 2007, 2009). The reconstructions show that birch and spruce-mixed forests and shrubs replaced wormwood steppe during the early Holocene and Scots pine open forests became dominant vegetation since ~7000 cal. a BP (Demske et al., 2005). However, inconsistencies among the reconstructions are readily visible. For example, three semi-quantitative reconstructions display approximately the same trends of temperature and moisture variations (Demske et al., 2005). That is, an increasing trend of the temperature index and a decreasing trend of the moisture index characterize the early Holocene (before ~6000 cal. a BP). The moisture index had a slight increasing trend, and the temperature index had a relatively steep declining trend after ~6000 cal. a BP. However, a quantitative reconstruction seems to tell a different story (Tarasov et al., 2007). The reconstructed annual precipitation and winter temperature have parallel trends, and both exhibit three stages of variations. The first stage was warming and wetting from ~11,000 to ~8000 cal. a BP, the second stage cooling and drying from ~8000 to ~6000 cal. a BP, and the third stage again warming and wetting during the past ~6000 years.

As stated earlier, the reconstructions of pollen-based temperature and moisture histories using the newly devised indices (see Table 1) show that both temperature and moisture were low during the early Holocene between ~10,000 and ~8000 cal. a BP and gradually climbed in the following period between ~8000 and ~6000 cal. a BP. The last ~6000 years have been generally warm and wet with high-amplitude fluctuations. The reconstructed moisture history is not only supported by AP/NAP ratio and pollen concentration but also by organic matter content and diatom data. Our moisture reconstruction is generally in agreement with the moisture reconstructions from Baikal records, that is, a drying early Holocene from ~11,500 to ~6000 cal. a BP and a wetting late Holocene since ~6000 cal. a BP (Demske et al., 2005; Tarasov et al., 2007). Our moisture reconstruction is also broadly in agreement with the moisture reconstructions from the Westerlies-dominated western Altai records, that is, a drying early Holocene from ~11,500 to ~5000 cal. a BP and a wetting late Holocene since ~5000 cal. a BP (Rudaya et al., 2009). The well-expressed second wet period lasting from ~3500 to ~1000 cal. a BP at Lake Hulun (Wen et al., 2010b) may also be a compressed correspondence to the late Holocene wetting retrieved from Gun Nuur.

Nevertheless, a cold early Holocene before ~6000 cal. a BP and a warm late Holocene after ~6000 cal. a BP retrieved from Gun Nuur are not geographically coherent with the above-reviewed reconstructions (Demske et al., 2005; Rudaya et al., 2009; Tarasov et al., 2007, 2009). The reviewed reconstructions nearly unanimously exhibit a warming early Holocene and a cooling late Holocene. However, the Holocene Thermal Maximum in the records from Lake Baikal was earlier noted to have occurred between ~6500 and 2500 cal. a BP (Demske et al., 2005), supporting our reconstruction at Gun Nuur. It should also be noted that a quantitative reconstruction from Lake Baikal (Tarasov et al., 2007) does show that the past ~6000 years have been gradually warming and slightly wetting after a cooling and drying stage from ~8000 to ~6000 cal. a BP. Furthermore, a synthetic study, through constraining the carbon reservoir corrections in Baikal chronologies and re-debating the climatic meanings of proxy data, shows an increase in both winter and summer temperatures after ~7000 cal. a BP (Prokopenko et al., 2007), being consistent with our temperature reconstruction from Gun Nuur.

Underlying mechanisms of regional climate change

If our reconstruction from Gun Nuur and the synthetic study from Lake Baikal (Prokopenko et al., 2007) can stand for further tests, the reconstructed cold and dry early Holocene from ~11,000 to ~6000 cal. a BP and warm and wet late Holocene (i.e. past ~6000 years) may be attributable to two factors: (1) combined effect of lower winter insolation and larger ice covers in the early Holocene (*Climate: Long-range Investigation, Mapping, and Prediction (*CLIMAP) Members, 1981; Ruddiman, 2008; Tarasov et al., 1997, 2007) and (2) combined effect of increased atmospheric CO_2 concentration and moderate summer insolation under warmed ocean surface and lessened ice cover conditions after ~7000 cal. a BP (Bush, 2005; Cooperative Holocene Mapping Project (COHMAP) Members, 1988; Peltier and Fairbanks, 2006; Prokopenko et al., 2007; Ruddiman, 2008). That is, lower winter insolation and remaining ice covers (and larger and longer snow-covers and larger permafrost extents) in the early Holocene might have retarded temperature rise in the continental interiors and the resulted low temperature might have efficiently suppressed regional evaporation that has been a major water vapor sources for precipitation in southern Siberia (Lydolph, 1977) and probably also in northern Mongolian Plateau. At the same time, ice-melt-water injection into the North Atlantic Ocean might have also suppressed water vapor supplies to the downwind areas, including the northern Mongolian Plateau in the early Holocene. It is not a surprise that the levels of some lakes were actually higher under early Holocene warming and dry conditions if the lakes were supplied by glacier-melting waters (Grunert et al., 2000; Zhang et al., 2012).

The increase in winter insolation and the final melting of ice covers, together with increased atmospheric CO_2 concentration and the associated increase in atmospheric water vapor (Bush, 2005), could be responsible for the higher temperature during the past ~7000 years. The melting of ice covers and the associated rise of global sea level might be responsible for the weakening of the winter monsoon in the interior of Asian continent, thus alluring farther eastward penetration of the relatively warm and wet Atlantic air masses (Moros et al., 2004; Peltier and Fairbanks, 2006; Rudaya et al., 2009) and consequently bringing in more water vapor to the east-central Asia, including the northern Mongolian Plateau (Bai et al., 2010).

Concluding remark

Although we have presented three sets of arguments supporting the proposition that Scots pine represents higher temperature conditions (see section 'Reconstructions of temperature and moisture indices'), but we do have trouble in untangling temperature signal from moisture signal. For example, the distribution of Scots pine in sunny slopes and at lower elevations in the Lake Baikal area suggests that Scots pine prefers higher temperature and lower moisture in comparison with other coniferous trees, but lower moisture primarily results from higher temperature via enhanced evaporation. Furthermore, unlike the reconstructed moisture index that is well corroborated by other proxies, the reconstructed temperature index is lack of corroboration from other proxies. Simply put, our confidence on the temperature reconstruction needs a boost from in-depth investigations of pollen–climate relationships and also from further bioclimatic understanding of Scots pine.

Funding

This paper is a result of projects supported by NSFC grants (No. 40930102, No: 40331012, and No: U1203821L08) and NSF grants (NSF-ESH-04-02509 and NSF-BCS06-52304).

References

Bai QM, Tian WS, Feng Z-D et al. (2010) Correlation between the precipitation in arid and semiarid Asian regions and the ocean warm pool climate. *Journal of Glaciology and Geocryology* 32(2): 295–307 (in Chinese).

Berner RA (1984) Sedimentary pyrite formation: An update. *Geochimica et Cosmochimica Acta* 48: 605–615.

Berner RA (1985) Sulphate reduction, organic matter decomposition and pyrite formation. *Philosophical Transactions of the Royal Society of London Series A: Mathematical and Physical Sciences* 315: 25–38.

Bezrukova EV, Abzaeva AA, Letunova PP et al. (2009) Evidence of environmental instability of the Lake Baikal after the last glaciations (based on pollen records from peatlands). *Archaeology, Ethnology and Anthropology of Eurasia* 37(3): 17–24.

Bezrukova EV, Belov AV and Orlova LA (2011) Holocene vegetation and climate variability in North Pre-Baikal region, East Siberia, Russia. *Quaternary International* 237: 74–82.

Blyakharchuk TA, Wright HE, Borodavko PS et al. (2004) Late glacial and Holocene vegetation changes on the Ulagan high-mountains plateau, Altai Mountains, southern Siberia. *Palaeogeography, Palaeoclimatology, Palaeoecology* 209: 259–279.

Blyakharchuk TA, Wright HE, Borodavko PS et al. (2007) Late glacial and Holocene vegetation history of the Altai Mountains (southwestern Tuva Republic, Siberia). *Palaeogeography, Palaeoclimatology, Palaeoecology* 245: 518–534.

Bush ABG (2005) CO_2/H_2O and orbitally driven climate variability over central Asia through the Holocene. *Quaternary International* 136: 15–23.

Chang FQ, Zhang HC, Ming QZ et al. (2011) AMS radiocarbon dating problems between 10 and 8 ka BP in lacustrine deposits from Lake Gun Nur, Northern Mongolia. *Radiocarbon* 53: 501–509.

Chen FH, Yu ZC, Yang ML et al. (2008) Holocene moisture evolution in arid central Asia and its out-of-phase relationship with Asian monsoon history. *Quaternary Science Reviews* 27: 351–364.

CLIMAP Members (1981) *Seasonal Reconstruction of the Earth's Surface at the Last Glacial Maximum* (GSA Map and Chart Series, MC-36). Boulder, CO: The Geological Society of America.

COHMAP Members (1988) Climatic changes of the last 18,000 years: Observation and modeling. *Science* 241: 1043–1052.

Demske D, Heumann G, Granoszewski W et al. (2005) Late glacial and Holocene vegetation and regional climate variability evidenced in high-resolution pollen records from Lake Baikal. *Global and Planetary Change* 46: 255–279.

Dorofeyuk NI and Tarasov PE (1998) Vegetation and lake levels in northern Mongolia in the last 12,500 years as indicated by data of pollen and diatom analyses. *Stratigraphy and Geological Correlation* 6: 70–83.

Dulamsuren C, Hauck M, Bader M et al. (2009) The different strategies of *Pinus sylvestris* and *Larix sibirica* to deal with summer drought in a northern Mongolian forest-steppe ecotone suggest a future superiority of pine in a warming climate. *Canadian Journal of Forest Research* 39: 2520–2528.

Feng Z-D, Wang WG, Guo LL et al. (2005) Lacustrine and eolian records of Holocene climate changes in the Mongolian Plateau: Preliminary results. *Quaternary International* 136: 25–32.

Fowell SJ, Hansen BCS, Peck JA et al. (2003) Mid to late Holocene climate evolution of the Lake Telmen Basin, North Central Mongolia, based on palynological data. *Quaternary Research* 59: 353–363.

Fukumoto Y, Kashima K, Orkhonselenge O et al. (2012) Holocene environmental changes in northern Mongolia inferred from diatom and pollen records of peat sediment. *Quaternary International* 254: 83–91.

Grunert J, Lehmkuhl F and Walther M (2000) Paleoclimatic evolution of the Uvs Nuur basin and adjacent areas (Western Mongolia). *Quaternary International* 65/66: 171–192.

Harrison SP, Yu G and Tarasov PE (1996) Late Quaternary lake-level record from Northern Eurasia. *Quaternary Research* 45: 138–159.

Hong YT, Hong B, Lin QH et al. (2005) Inverse phase oscillations between the East Asian and Indian Ocean summer monsoons during the last 12000 years and paleo-El Nino. *Earth and Planetary Science Letters* 231: 337–346.

Horiuchi K, Minoura K, Hoshino K et al. (2000) Palaeoenvironmental history of Lake Baikal during the last 23000 years. *Palaeogeography, Palaeoclimatology, Palaeoecology* 157: 95–108.

Kremenetski CV, Tarasov PE and Cherkinsky AE (1997) The latest pleistocene in southwestern Siberia and Kazakhstan. *Quaternary International* 41/42: 125–137.

Lydolph PE (1977) *Climates of the Soviet Union*. New York: Elsevier Scientific Publishing Co.

Ma YZ, Liu K-B, Feng Z-D et al. (2008) A survey of modern pollen and vegetation along a south-north transect in Mongolia. *Journal of Biogeography* 35: 1512 1532.

MacDonald GM, Velichko AA, Kremenetski CV et al. (2000) Holocene treeline history and climate change across Northern Eurasia. *Quaternary Research* 53: 302–311.

Moore PD, Webb JA and Collinson ME (1991) *Pollen Analysis*. Oxford: Blackwell Scientific Publications.

Moros M, Emeis K, Risebrobakken B et al. (2004) Sea surface temperature and ice rafting in the Holocene North Atlantic: Climate influences on northern Europe and Greenland. *Quaternary Science Reviews* 23: 2113–2160.

Peck JA, Khosbayar P, Fowell SJ et al. (2002) Mid to Late Holocene climate change in north central Mongolia as recorded in the sediments of Lake Telmen. *Palaeogeography, Palaeoclimatology, Palaeoecology* 183: 135–153.

Peltier WR and Fairbanks RG (2006) Global glacial ice volume and Last Glacial Maximum duration from an extended Barbados sea level record. *Quaternary Science Reviews* 25: 3322–3337.

Prokopenko AA and Williams DF (2004) Deglacial methane emission signals in the carbon isotopic record of Lake Baikal. *Earth and Planetary Science Letters* 218: 135–147.

Prokopenko AA, Khursevich GK, Bezrukova EV et al. (2007) Paleoenvironmental proxy records from Lake Hovsgol, Mongolia, and a synthesis of Holocene climate change in the Lake Baikal watershed. *Quaternary Research* 28: 2–17.

Prokopenko AA, Williams DF, Karabanov EB et al. (1999) Response of Lake Baikal ecosystem to climate forcing and pCO_2 change over the last glacial/interglacial transition. *Earth and Planetary Science Letters* 172: 239–253.

Reimer PJ, Baillie MGL, Bard E et al. (2009) IntCal09 and Marine09 radiocarbon age calibration curves, 0–50,000 years cal BP. *Radiocarbon* 51: 1111–1150.

Rudaya N, Tarasov P, Dorofeyuk N et al. (2009) Holocene environments and climate in the Mongolian Altai reconstructed from the Hoton-Nur pollen and diatom records: A step towards better understanding climate dynamics in Central Asia. *Quaternary Science Reviews* 28: 540–554.

Ruddiman WF (2008) *Earth's Climate: Past and Future*. 3rd Edition. New York: W. H. Freeman and Company.

Shen J, Xue B, Wu JL et al. (eds) (2010) *Lacustrine Deposits and Environmental Evolution*. Beijing: Science Press (in Chinese).

Shi YF, Kong ZC, Wang SM et al. (1993) Mid-Holocene climates and environments in China. *Global and Planetary Change* 7(1–3): 219–233.

Shichi K, Takahara H, Krivonogov SK et al. (2009) Late Pleistocene and Holocene vegetation and climate records from Lake Kotokel, central Baikal region. *Quaternary International* 205: 98–110.

Tarasov P, Bezrukova E, Karabanov E et al. (2007) Vegetation and climate dynamics during the Holocene and Eemian interglacials derived from Lake Baikal pollen records. *Palaeogeography, Palaeoclimatology, Palaeoecology* 252: 440–457.

Tarasov P, Dorofeyuk N and Meteltseva E (2000) Holocene vegetation and climate changes in Hoton-Nur basin, northwest Mongolia. *Boreas* 9: 117–126.

Tarasov P, Granoszewski W, Bezrukova E et al. (2005) Quantitative reconstruction of the last interglacial vegetation and climate based on the pollen record from Lake Baikal, Russia. *Climate Dynamics* 25: 625–637.

Tarasov PE, Bezrukova EV and Krivonogov SK (2009) Late Glacial and Holocene changes in vegetation cover and climate in southern Siberia derived from a 15 kyr long pollen record from Lake Kotokel. *Climate of the Past* 5: 1–11.

Tarasov PE, Jolly D and Kaplan JO (1997) A continuous Late Glacial and Holocene record of vegetation changes in Kazakhstan. *Palaeogeography, Palaeoclimatology, Palaeoecology* 136: 281–292.

Wang FS, Chien NF, Zhang YL et al. (1995) *Pollen Flora of China*. Beijing: Science Press (in Chinese).

Wang W and Feng Z-D (2013) Holocene moisture evolution across the Mongolian Plateau and its surrounding areas: A synthesis of climatic records. *Earth-Science Reviews* 122: 38–57.

Wang W, Ma YZ and Feng Z-D (2009) A high-resolution-Holocene climate reconstruction based on pollen and diatom data from central Mongolia. *Chinese Science Bulletin* 543: 1579–1589

Wang W, Ma YZ, Feng Z-D et al. (2011) A prolonged dry mid-Holocene climate revealed by pollen and diatom records from Lake Ugii Nuur in central Mongolia. *Quaternary International* 229: 74–83.

Wanner H, Beer J, Bütikofer J et al. (2008) Mid- to Late Holocene climate change: An overview. *Quaternary Science Reviews* 267: 1791–1828.

Wen RL, Xiao JL, Chang ZG et al. (2010a) Holocene climate changes in the mid-high-latitude-monsoon margin reflected by the pollen record from Hulun Lake, northeastern Inner Mongolia. *Quaternary Research* 73: 293–303.

Wen RL, Xiao JL, Chang ZG et al. (2010b) Holocene precipitation and temperature variations in the East Asian monsoonal margin from pollen data from Hulun Lake in northeastern Inner Mongolia, China. *Boreas* 39: 262–272.

Zhang CJ, Zhang WY, Feng Z-D et al. (2012) Holocene hydrological and climatic change on the northern Mongolian Plateau based on multi-proxy records from Lake Gun Nuur. *Palaeogeography, Palaeoclimatology, Palaeoecology* 323/325: 75–86.

Zhang XS (2007) *Chinese Vegetation and Distribution Patterns*. Beijing: Geological Press (in Chinese).

附录三

Available online at www.sciencedirect.com
ScienceDirect
ELSEVIER
Palaeogeography, Palaeoclimatology, Palaeoecology 257 (2008) 335–343
PALAEO
www.elsevier.com/locate/palaeo

Climatic dependency of soil organic carbon isotopic composition along the S–N Transect from 34°N to 52°N in central-east Asia

Z.-D. Feng [a,b,*], L.X. Wang [c], Y.H. Ji [d], L.L. Guo [e], X.Q. Lee [f], S.I. Dworkin [a]

[a] Department of Geology, Baylor University, Waco, TX 76798, USA
[b] MOE Key Laboratory of Western China's Environmental Systems, Lanzhou University, Lanzhou 730000, Gansu, China
[c] Provincial Environmental Quality Monitoring Administration, Shenyang 110031, Liaoning, China
[d] Institute of Botany, Chinese Academy of Sciences, Beijing 100093, China
[e] College of Resource Science and Technology, Beijing Normal University, Beijing 100875, China
[f] Institute of Geochemistry, Chinese Academy of Sciences, Guiyang 550002, Guizhou, China

Received 17 October 2006; received in revised form 5 October 2007; accepted 11 October 2007

Abstract

We explored the relationships between surface-soil (1–20 cm) organic carbon isotopic signatures and associated climatic factors in central-east Asia in an attempt to develop transfer functions that can be used to retrieve the paleoclimatic information stored in the thick eolian–paleosol sequences within the area. Our analysis shows that the negative correlation between the surface-soil organic $\delta^{13}C$ values and the mean annual precipitation is robust ($R^2=0.453$; $n=196$; $p<0.05$) and the negative correlation with the growing-season (April–September) precipitation is more significant ($R^2=0.4966$; $n=196$; $p<0.05$). Our study further shows that the positive correlation between the surface-soil organic $\delta^{13}C$ values and mean growing-season aridity is most significant ($R^2=0.5805$; $n=196$; $p<0.05$). We have smoothed both the organic $\delta^{13}C$ values and the mean growing-season aridity values using a 3-point moving-window average-filter method in an attempt to remove some of random errors and found that the positive correlation between the two is further increased ($R^2=0.7784$; $n=192$; $p<0.05$). These robust linear relationships demonstrate their value in reconstructing paleoclimate changes in the study area. The documented climatic dependency of the surface-soil carbon isotopic composition in the study area might have resulted both from the humidity-related isotopic enrichment processes of the dominant C_3 plants (stomatal conductance and photosynthetic discrimination) and from the aridity-related abundance of C_4 plants (mainly Chenopodiaceae species) along the S–N bioclimatic gradient.
© 2007 Elsevier B.V. All rights reserved.

Keywords: Soil carbon isotope; Mongolian Plateau; Chinese Loess Plateau; Bioclimatic dependency; Biogeochemistry

1. Introduction

Possible human-induced global climate change and accompanying human adverse impacts on the environments alert us the need to assess future climatic stability and environmental sustainability. However, our knowledge is still constraining us from making such assessments. Due to the fact that the earth's climatic systems have changed on different time scales and that the instrument-observed data are insufficient for establishing temporal patterns of climatic and environmental changes, we have to rely on various proxies for recons-

* Corresponding author. Department of Geology, Baylor University, Waco, TX 76798, USA.
E-mail address: zhaodong_feng@baylor.edu (Z.-D. Feng).

0031-0182/$ - see front matter © 2007 Elsevier B.V. All rights reserved.
doi:10.1016/j.palaeo.2007.10.026

tructing the temporal patterns. Unfortunately, some of the established proxies have been based only on very limited experimental data and some others are for specific bioclimates. The vast arid and semiarid central-east Asia region is ideal for testing those widely used proxies and even to establish new proxies specific for the unique nature of the bioclimatic regime. If climatic proxies can be reliably defined, the invaluable paleoclimatic information stored in the thick eolian–paleosol sequences of this region can be quantitatively retrieved in the study area and in other bioclimatically similar areas.

The organic carbon isotopic composition of soils has been intensively investigated and inherited similarities between soil organic carbon isotopic composition and associated plant carbon isotopic compositions have been well documented (e.g., Nadelhoffer and Fry, 1988; Balesdent et al., 1993; Wedin et al., 1995; Bird and Pousai, 1997). These relationships have been particularly well documented in arid and semiarid North China where aquatic plants are negligible in contributing to the soil organic carbon isotopic signatures (Wei et al., 1997; Liu et al., 2002). It has been documented that temperature is highly correlated with plant isotopic signatures in some cases (Teeri et al., 1980; Sage et al., 1999; Llorens et al., 2004) and precipitation is highly correlated with plant isotopic signatures in other cases (Stewart et al., 1995; Bowling et al., 2002; Fessenden and Ehleringer, 2003; Lu et al., 2004). In C_3 ($\delta^{13}C = -22‰ \sim -32‰$) and C_4 ($\delta^{13}C = -9‰ \sim -17‰$) mixed ecosystems, the C_4 percentage increases as the temperature increases and the precipitation decreases (Pyankov et al., 2000; Still et al., 2003; Llorens et al., 2004), implying that temperature- and precipitation-modulated effective soil moisture and associated vapor pressure deficit are the key factors in controlling $\delta^{13}C$ signatures in C_3 and C_4 mixed ecosystems. The inherited similarities between soil organic carbon isotopic composition and associated plant carbon isotopic composition and the documented statistical relationships between plant carbon isotopic composition and the controlling climatic factors have then been utilized by paleoclimate researchers to reconstruct paleovegetation and associated paleoclimate changes through analyzing soil organic carbon isotopic composition in terrestrial sediment sequences (e.g., Krishnamurthy et al., 1982; Schwartz et al., 1986; Guillet et al., 1988; Krishnamurthy and Bhattacharya, 1989; Cerling et al., 1989; McPherson et al., 1993; Giresse et al., 1994; Boutton et al., 1998; Kelly et al., 1998; Goodfriend, 1999; Gouveia et al., 2002; Pack et al., 2003). This study is particularly designed to quantitatively determine bioclimate-dependency along a chosen S–N transect from 34°N to 52°N in central-east Asia (around 105°E) that spans several major bioclimatic zones in hope that the relationships between the soil carbon isotopic compositions and the controlling climatic factors can be used to reconstruct the paleoclimatic changes in the study area and in other bioclimatically similar areas.

2. Physiographic settings of the study area

Located in the interior of the Asian continent, the study area (i.e., the Chinese Loess Plateau and the Mongolian Plateau) has a symmetric distribution pattern of precipitation with the lowest amount of precipitation in the middle (i.e., Gobi deserts), and the mean annual temperature is primarily latitude-dependent and increases southward. The air pressure difference between the Eurasian landmass and Pacific and Indian Oceans induces the Asian Summer Monsoon systems that bring moisture from the oceans to North China (i.e., the Chiese Loess Plateau and the southern part of the Mongolian Plateau), forming a northward decreasing precipitation gradient (Chen et al., 1991). The thermally induced low pressure cell centered on central-west Asia also induces moisture from the Atlantic and Arctic Oceans and brings moderate precipitation to the northern part of the Mongolian Plateau, forming a southward decreasing precipitation gradient (Compilation Commission of Chinese Physical Geography, 1984; Worden and Savada, 1989; Zhang and Lin, 1992).

Consequently, the vegetation distribution reflects well these temperature–moisture combinations (Fig. 1). From the Gobi northward to Siberia, the vegetation zones are: (1) desert steppe in southern Mongolia, (2) cold steppe in central Mongolia, (3) forest steppe in northern Mongolia, and (4) coniferous forest in the northernmost tip of Mongolia. From the Gobi southward to the southern Chinese Loess Plateau, the vegetation zones are: (1) desert steppe in Inner Mongolia, (2) warm steppe on the northern Chinese Loess Plateau, (3) forest steppe on the southern Chinese Loess Plateau, and (4) deciduous forest in the Qinling Mountains. The soil characteristics closely follow the vegetation patterns. For example, leached ash-like soils (spodosols) occur in coniferous forests, soft and organic-enriched soils (mollisols) in steppes, salt-enriched soils (aridsols) in deserts, and Fe/Al-enriched soils (alfisols) in deciduous forests. It should be particularly noted that the study area is dominated by a C_3 (mainly *Artemisia scoparia* and *Ajania achilleides*) and C_4 (predominantly Chenapodiaceae species) mixed ecosystem and the abundance of C_4 plants gradually decreases from the middle of the Gobi

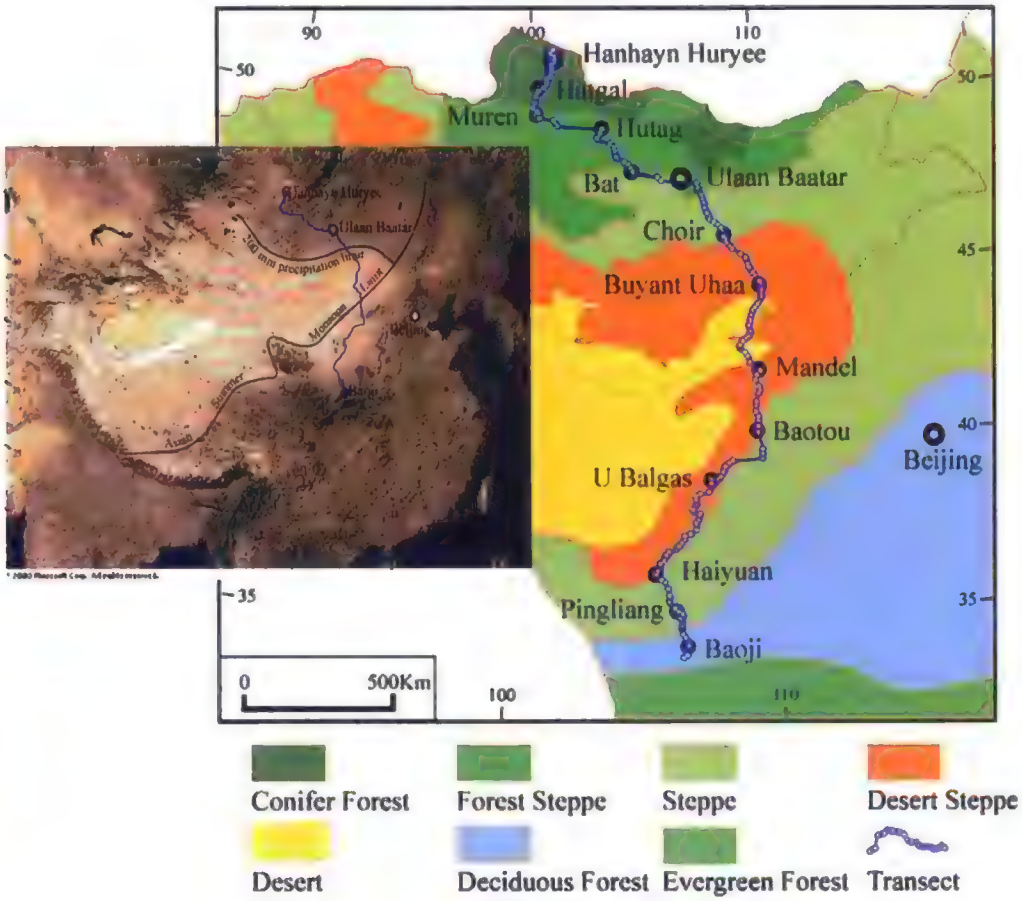

Fig. 1. Sketch map showing the S–N sampling transect (blue-circled line) and its relative position to the bioclimatic zones in the study area (i.e., the Chinese Loess Plateau and the Mongolian Plateau). *Insert map* is a remotely-sensed data-produced greenness map of central-east Asia and the SW NE oriented black line is the widely-accepted interior limit of the East Asian Summer Monsoon.

both towards south and north (see Pyankov et al., 2000; Wu, 1995).

3. Sampling and analytical procedures

Our sampling transect starts at 34°14′24″N and 106°55′30″E on the northern slope of the Qinling Mountain near Baoji (China) and ends at 51°35′08″N and 100°45′49″E at Hanhayn Huryee near the Mongolia–Russian border, spanning over 17 degrees of latitude. Soil samples were collected in the summer of 2002 approximately every 5 latitudinal minutes (5′) along the transect, and undisturbed sites were selected for sampling. The criterion of being undisturbed can be readily met in Mongolia (approximately 52°N to 42°N) and reasonably well met in Inner Mongolia of China (approximately 42°N to 38°N). In the case of the Chinese Loess Plateau (approximately 38°N to 34°N) where native vegetation is hardly preserved, sampling sites were selected along the fringes of the Qinling–Liupan–Quwu mountain chain where native vegetation still exists. Soil samples were taken from organic-enriched A horizons within the top 20 cm of the surface.

For laboratory analyses, dried and powdered soil samples were first sieved through meshes of 0.105 mm to remove large grains and un-decomposed roots. Each sieved fine portion was de-carbonated for 24 h by adding 10% HCl and by repeatedly rinsing with distilled water (till pH ≈ 7). The soil samples were finally dried at 50 °C for isotopic analyses. The prepared soil samples were combusted to produce CO_2 in a combustion system. The combustion-produced CO_2 was trapped in a cold finger of liquid N_2 and then bathed in a trap at −75 °C to gather pure CO_2. Carbon isotope of the CO_2 was measured by a MAT252 Mass

Spectrometer in the MOE Key Laboratory of Western China's Environmental Systems (Lanzhou University) and some of the measurements were randomly cross-checked in the State Key Laboratory of Environmental Geochemistry (Chinese Academy of Sciences) to assure the consistency of the measurements. The results are reported in the standard δ-notation. That is, $\delta^{13}C = [(^{13}C/^{12}C)_{sample} - (^{13}C/^{12}C)_{standard}]/^{13}C/^{12}C_{standard} \times 1000‰$, where $(^{13}C/^{12}C)_{sample}$ and $(^{13}C/^{12}C)_{standard}$ are $^{13}C/^{12}C$ ratios of sample measured and the Pee Dee Belemnite (PDB) standard, respectively. To minimize the standard deviation and assure the consistency of the measurements, calibration using the standard reference (standard GBW04407) was systematically made every five measurements (see Ehleringer and Cook, 1998 for details) and the calculated standard deviation is within 0.2‰.

To search for climatic dependency of the soil carbon isotopic composition, we first collected mean annual temperature and precipitation data at the meteorological stations that fall within a 2-degree belt (longitude) centered along the S–N sampling transect. The temperature and precipitation data from the 26 stations that fall within the 2-degree belt were then linearly interpolated and spatially distributed, and the mean annual temperature and precipitation data for each one of the 196 soil sampling sites were obtained from the linear interpolation-produced datasets based on the geographic locations. The growing-season aridity (April–September), the ratio of the growing-season potential evapotranspiration over the growing-season precipitation, was also spatially interpolated for each one of the 196 sampling sites in the same manner. Finally, the 196 sets of the spatially interpolated mean annual temperature and precipitation data at the sampling sites, as well as the growing-season precipitation and aridity, were used for statistically analyzing the relationships between the surface-soil carbon isotopic composition and the climatic factors. The spatial interpolations were accomplished using ArcGIS package and the statistical tools in the package were used to calculate the coefficients. To eliminate some of the random errors, we smoothed the surface-soil $\delta^{13}C$ values and the growing-season aridity values using a 3-point moving-window average-filter method available in the ArcGIS package.

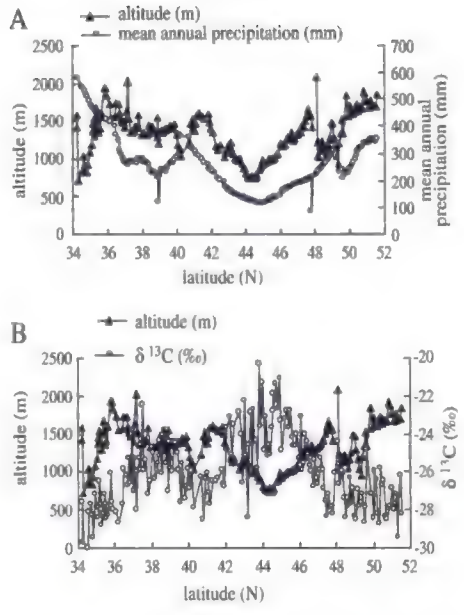

Fig. 3. Diagrams showing the positive correlation between altitude and mean annual precipitation along the sampling transect (*A*: *upper panel*) and the negative correlation between altitude and surface-soil organic $\delta^{13}C$ values along the sampling transect (*B*: *lower panel*).

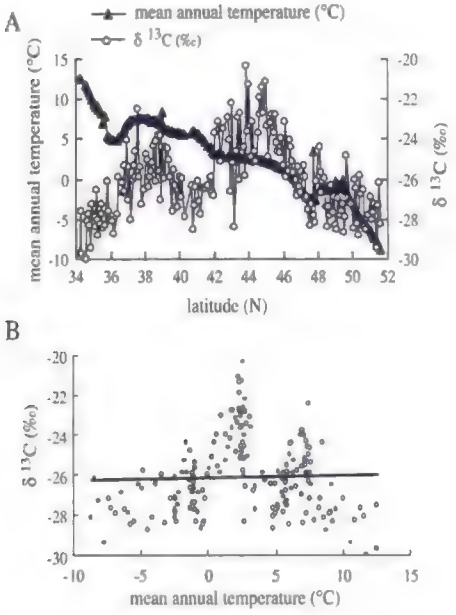

Fig. 2. Diagrams showing the relationship between the mean annual temperature and the surface-soil organic $\delta^{13}C$ values. *A* (*upper panel*): latitudinal variations of the mean annual temperature and the surface-soil organic $\delta^{13}C$ values. *B* (*lower panel*): the scatter plot showing the relationship between the mean annual temperature and the surface-soil organic $\delta^{13}C$ values ($R^2 = 0.0011$; $n = 196$).

4. Analytical results

The mean annual temperature and the surface-soil organic $\delta^{13}C$ values vary independently with latitude (Fig. 2A) and no linear correlation was observed ($R^2 =$

0.001; n=196) between the two (Fig. 2B). It is notable in Fig. 2B that the organic $\delta^{13}C$ values decrease (more negative) in response to both increasing temperature and decreasing temperature. This pattern is most likely the result of the precipitation that increases both towards south (temperature increasing direction) and north (temperature decreasing direction). It should be particularly noted that although the precipitation in the study area is basically latitude-dependent, the altitude seems to significantly affect the precipitation (Fig. 3A). The positive correlation (R^2=0.42; n=196; p<0.05) between the GPS-surveyed altitudes of the 196 sampling sites and the interpolated mean annual precipitation implies that the altitude's effect on precipitation is embodied in the original climatic dataset of the 26 meteorological stations (see Table 1) although the elevations (altitudes) of the 26 meteorological stations were not considered as a valid variable in spatially interpolating the climatic information of the 196 sampling sites. The altitude's effect on the latitude-dependent precipitation patterns was also supported by the ground observations that orographic precipitation is a common phenomenon in the study area (Chen et al., 1991; Worden and Savada, 1989; Zhang and Lin, 1992; Compilation Commission of Chinese Physical Geography, 1984). Since altitude is an important modifier of the latitude-dependency of the mean annual precipitation, we also examined the correlation coefficient between the surface-soil organic $\delta^{13}C$ values and altitude (R^2=0.36; n=196; p<0.05). Fig. 3B shows that higher elevations around 36°N, around 42°N, around 48°N and around 51°N effectively lowered the surface-soil organic $\delta^{13}C$ values, and lower elevations in the middle of Gobi (around 44°N) effectively elevated the organic $\delta^{13}C$ values. Fig. 4A shows the anti-phase relationship between the organic $\delta^{13}C$ values and the mean annual precipitation with a relatively high correlation coefficient (R^2=0.453; n=196; p<0.05) (Fig. 4B). This negative correlation suggests that every 100-mm increase in the mean annual precipitation results in a 1.16‰ decrease in the surface-soil $\delta^{13}C$ value (i.e., towards more negative). The empirical equation that can be used to retrieve past mean annual precipitation is: $P_{annual}=-35.958x-752.46$ (where P_{annual}=mean annual precipitation in mm and x=soil organic matter isotopic value in ‰). Our test further shows that the statistical correlation (negative) of the organic $\delta^{13}C$ values with the mean growing-season (April–September) precipitation is more robust

Table 1
Climatic data of 26 meteorological stations that were used to spatially interpolate the climatic information of the 196 sampling sites along the S–N sampling transect

Station name	Latitude (°N)	Longitude (°E)	Altitude (m)	Mean temperature (annual, °C)	Mean precipitation (annual, mm)	Growing-season PET (mm)	Growing-season aridity
Baoji	34°21′	107°08′	613	12.96	632.3	772.4	1.05
Dongsheng	39°50′	109°59′	1459	5.91	363.3	586.2	1.61
Taoile	38°48′	106°42′	1099	8.41	159.6	673.1	4.21
Zhongwei	37°32′	105°11′	1183	8.81	164.4	658.2	4.00
Zhongning	37°29′	105°40′	1184	9.35	192.6	678.8	3.52
Haiyuan	36°34′	105°39′	1697	7.03	340.4	583.0	1.71
Tongxin	36°59′	105°54′	1111	8.99	262.8	668.2	2.54
Guyuan	36°00′	106°16′	1752	6.15	438.9	557.3	1.27
Baotao	40°40′	109°51′	1069	6.86	620.6	638.1	2.33
Xiji	35°58′	105°43′	1916	5.23	408.8	531.0	1.29
Yinxhuan	38°29′	106°23′	1112	8.98	155.2	475.0	3.06
Yanchi	37°47′	107°24′	1348	8.31	227.9	462.6	2.93
Pinglian	35°33′	106°40′	1348	8.83	401.9	454.1	1.13
Hailiutu	41°34′	108°31′	1289	5.27	166.5	469.5	2.82
Bailinmiao	41°42′	110°26′	1377	4.23	217.7	640.1	2.94
Etuokeqi	39°06′	107°59′	1381	7.07	220.4	672.5	3.05
Rinchinl	51°07′	99°40′	1583	−6.04	199.7	391.4	1.96
Haigal	50°26′	100°09′	1687	−3.32	303.5	379.9	1.25
Tarialan	49°37′	102°00′	1236	0.61	316.7	492.0	1.55
Muren	49°38′	100°10′	1288	0.67	235.5	500.3	2.12
Hutag	49°23′	102°42′	933	0.84	278.0	518.3	1.86
Bulgan	48°48′	103°33′	1210	−0.28	307.0	467.9	1.52
Ulaanbator	47°56′	106°59′	1338	−0.30	243.7	482.0	1.97
Maanti	47°18′	107°29′	1430	−0.70	197.6	468.5	2.37
Choir	46°27′	108°13′	1286	1.38	185.0	538.0	2.91
Zamyn-uud	43°44′	111°54′	964	4.41	124.2	611.7	4.93

(R^2=0.4966; n=196; p<0.05) than with mean annual precipitation (Fig. 5). The empirical equation that can beused to retrieve past growing-season precipitation is: $P_{growing\text{-}season}$=−29.444$x$−546.01 (where $P_{growing\text{-}season}$= growing-season precipitation in mm and x=soil organic matter isotopic value in ‰).

Finally, we calculated the correlation coefficient between the surface-soil organic $\delta^{13}C$ values and the growing-season aridity (i.e., the ratio of potential evapotranspiration over precipitation during the growing season from April 1 to September 30). Fig. 6A shows that the organic $\delta^{13}C$ values closely follow the values of the growing-season aridity along the S–N transect. This positive correlation (R^2=0.5805; n=196; p<0.05) suggests that every 1-unit increase in the growing-season aridity results in 1.30‰ increase in the $\delta^{13}C$ value (Fig. 6B). The empirical equation that can be used to retrieve past mean annual aridity is: A_{mean}=0.4441x−14.137 (where A_{mean}=mean annual aridity and x=soil organic matter isotopic value in ‰). We have also smoothed the surface-soil $\delta^{13}C$ values and the growing-season aridity using a 3-point moving-window average-filter method to eliminate some of the random errors.

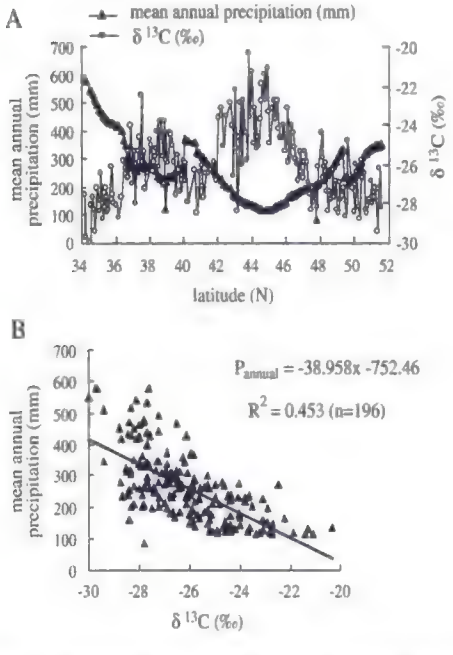

Fig. 4. Diagrams showing the relationship between the mean annual precipitation and the surface-soil organic $\delta^{13}C$ values. *A* (*upper panel*): latitudinal variations of the mean annual precipitation and the surface-soil organic $\delta^{13}C$ values along the S–N sampling transect. *B* (*lower panel*): scatter plot showing the linear relationship between the surface-soil organic $\delta^{13}C$ values and the mean annual precipitation (R^2=0.4530; n=196; p<0.05).

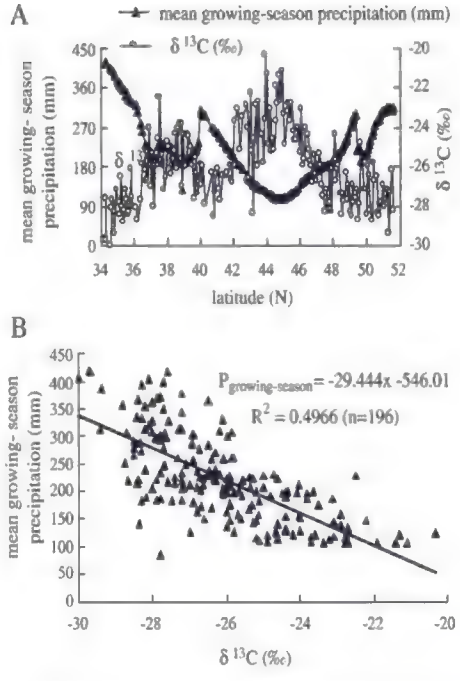

Fig. 5. Diagrams showing the relationship between the growing-season precipitation and the surface-soil organic $\delta^{13}C$ values. A (upper panel): latitudinal variations of the growing-season precipitation and the surface-soil organic $\delta^{13}C$ values along the sampling transect. B (lower panel): scatter plot showing the linear relationship between the surface-soil organic $\delta^{13}C$ values and the growing-season precipitation (R^2 = 0.4966; n = 196; p < 0.05).

The smoothed $\delta^{13}C$ curve follows the growing-season aridity curve more closely (Fig. 7A). Fig. 7B shows that the statistical correlation coefficient between the smoothed $\delta^{13}C$ values (192 data points) and the corresponding growing-season aridity (192 data points) is significantly improved (R^2=0.7784; n=192; p<0.05). The empirical equation that can be used to retrieve past growing-season aridity is: $A_{smoothed}$= 0.5872x+17.869 (where $A_{smoothed}$=3-point smoothed growing-season aridity and x=3-point smoothed soil organic matter isotopic values in ‰).

To sum up, the surface-soil $\delta^{13}C$ signatures in the study area are primarily dependent on the mean annual precipitation (R^2=0.453) and the dependency becomes a little stronger when only the growing-season precipitation is considered (R^2=0.4966). The mean growing-season aridity (the ratio of evapotranspiration over precipitation), which takes the evapotranspiration into account, appears to be a stronger controller (R^2=0.5805) than the growing-season precipitation over the surface-soil $\delta^{13}C$ signatures. When some of the random errors of the surface-soil $\delta^{13}C$ signatures and the mean

growing-season aridity were eliminated, using a 3-point moving-window average-filter method, the correlation coefficient between the surface-soil $\delta^{13}C$ values and the growing-season aridity is significantly improved (R^2=0.7784).

5. Discussions

A number of plant carbon isotopic experiments conducted in other areas (see Bowling et al., 2002; Liu et al., 2002; Fessenden and Ehleringer, 2003; Llorens et al., 2004) suggest that stomatal conductance and photosynthetic discrimination are directly affected by changes in the atmospheric humidity and that the photosynthate produced during water-stressed conditions is normally ^{13}C enriched in both C_3 and C_4 plant species compared to non-water-stressed conditions. Our study on C_3 plants (*A. scoparia* and *A. achilleides*) shows that water-stress indeed enriches ^{13}C in our study area (see Lee et al., 2005). A recent study on the Mongolian Plateau (Pyankov et al., 2000) demonstrated that the abundance of C_4 Chenopodiaceae species that have higher (or less negative) $\delta^{13}C$ values is closely correlated with climatic aridity. These studies lend support to our interpretation that the documented climatic dependency of the surface-soil

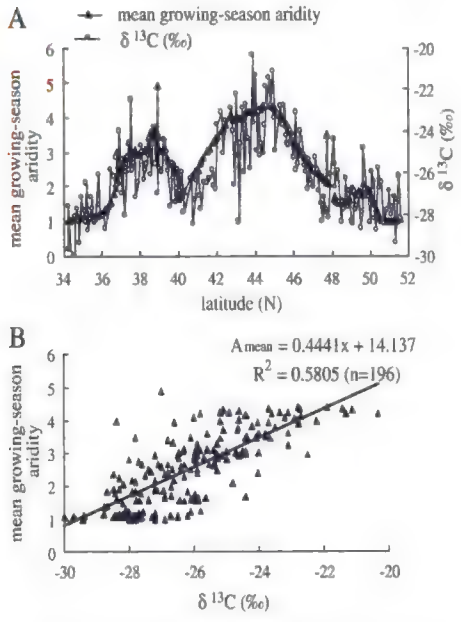

Fig. 6. Diagrams showing the relationship between the growing-season aridity and the surface-soil organic $\delta^{13}C$ values. A (upper panel): latitudinal variations of the growing-season aridity and the surface-soil organic $\delta^{13}C$ values along the sampling transect. B (lower panel): scatter plot showing the linear relationship between the surface-soil organic $\delta^{13}C$ values and the growing-season aridity (R^2 = 0.5805; n = 196; p < 0.05).

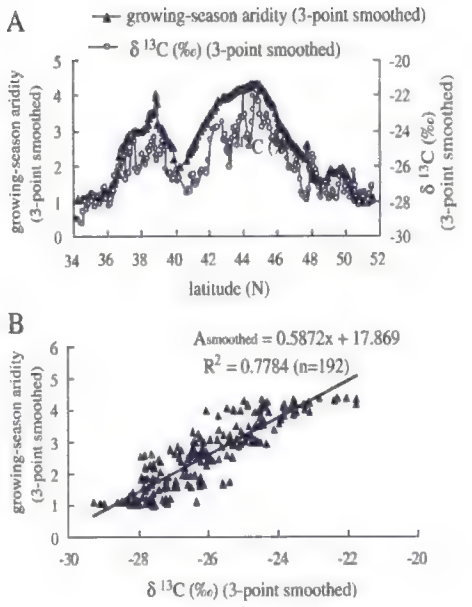

Fig. 7. Diagrams showing the relationship between the growing-season aridity and the surface-soil organic $\delta^{13}C$ values (3-point moving-window smoothed). A (upper panel): latitudinal variations of the growing-season aridity and the surface-soil organic $\delta^{13}C$ values (3-point moving-window smoothed) along the sampling transect. B (lower panel): scatter plot showing the linear relationship between the surface-soil organic $\delta^{13}C$ values and the growing-season aridity (R^2 = 0.7784; n = 192; p < 0.05).

carbon isotopic composition in this study might have resulted both from the humidity-related isotopic enrichment processes of the dominating C_3 plants (stomatal conductance and photosynthetic discrimination) and from the aridity-related abundance of C_4 Chenopodiaceae species along the S–N sampling transect. Specifically, the shrubs and herbs that favor warm growing seasons in the Erdos Plateau (37–39°N) and in the middle of Gobi (42–46°N) contribute to the documented higher (less negative) $\delta^{13}C$ values and the plants in the Qinling Mountains (34–36°N) at the southern tip and in the Khanglas Range (48–52°N) at the northern tip of the sampling transect contribute to the documented lower (more negative) $\delta^{13}C$ values. The lower $\delta^{13}C$ values around 40°N may be related to the Yellow River Bend wetland hydrogeomorphic regime.

The following empirical equations expressing the relationships between the surface-soil organic $\delta^{13}C$ signatures (x in the equations: soil organic matter isotopic values in ‰) and the climatic factors can be used to reconstruct paleoclimate changes in the study area and in other bioclimatically similar areas with varying confidence levels as indicated by their R^2 values, assuming that the relationships between bio-

climatic zones and their corresponding C_3 and C_4 composition in the past were more or less the same as those at the present. They are (1) Mean Annual Precipitation: $P_{annual}=-35.958x-752.46$ ($R^2=0.453$; $n=196$; $p<0.05$); (2) Mean Growing-Season Precipitation: $P_{growing\text{-}season}=-29.444x-546.01$ ($R^2=0.4966$; $n=196$; $p<0.05$); (3) Mean Growing-Season Aridity: $A_{mean}=0.4441x-14.137$ ($R^2=0.5805$; $n=196$; $p<0.05$); and (4) Smoothed (3-point smoothed) Growing-Season Aridity: $A_{smoothed}=0.578x+17.869$ ($R^2=0.7784$; $n=192$; $p<0.05$).

Finally, it should be particularly emphasized that atmospheric CO_2 concentration is another important factor that significantly modulates plant carbon isotopic composition and thus associated soil organic carbon isotopic composition (Pearman et al., 1976; Francey and Farquhar, 1982; Leavitt, 1994). It was demonstrated that every 100 ppm increase in atmospheric CO_2 concentration results in about 2.0‰ decrease (more negative) in the plant $\delta^{13}C$ values (Feng and Epstein, 1995). If this relationship by Feng and Epstein (1995) can be further validated, the empirical equations developed in this study can be confidently applied to reconstructing paleo-precipitation or/and paleo-aridity in the study area and other bioclimatically similar areas for the past 400,000 years during which the atmospheric CO_2 concentrations are known from ice cores.

Acknowledgements

This paper is resulted from three Chinese National Science Foundation projects (No. 40025105, No. 40331 102 and No. 40421101) and two U.S. National Science Foundation projects (NSF-ESH04-02509 and NSF-BCS 06-23478). We also want to express our sincere appreciation to Dr. Peter Kershaw and two anonymous reviewers whose suggestions greatly improved the manuscript.

References

Balesdent, J., Girardin, C., Mariotti, A., 1993. Site-related $\delta^{13}C$ of tree leaves and soil organic matter in a temperate forest. Ecology 74, 1713–1721.

Bird, M.I., Pousai, P., 1997. Variation of $\delta^{13}C$ in the surface soil organic carbon pool. Global Biogeochemical Cycles 11, 313–322.

Boutton, T.W., Archer, S.R., Midwood, A.J., Zitzer, S.F., Bol, R., 1998. $\delta^{13}C$ values of soil organic carbon and their use in documenting vegetation change in a subtropical savanna ecosystem. Geoderma 82, 5–41.

Bowling, D.R., McDowell, N.G., Bond, J.R., Law, B.E., Ehleringer, J.R., 2002. $\delta^{13}C$ content of ecosystem respiration is linked to precipitation and vapor pressure deficit. Oecologia 131, 113–124.

Cerling, T.E., Quade, J., Wang, Y., Bowman, J.R., 1989. Carbon isotopes in soils and paleosols as ecology and paleoecology indicators. Nature 341, 138–139.

Chen, L.X., Zhu, Q.G., Luo, H.B., He, J.H., Dong, M., Feng, Z.Q., 1991. The East Asian Monsoon. Meteorological Press, Beijing. (in Chinese).

Compilation Commission of Chinese Physical Geography (Chinese Academy of Sciences), 1984. Physical Geography of China: Climate. Science Press, Beijing. (in Chinese).

Ehleringer, G.R., Cook, C.S., 1998. Carbon and oxygen isotope ratios of ecosystem respiration along an Oregon conifer transect: preliminary observations based on small flask sampling. Tree Physiology 18, 513–519.

Feng, X., Epstein, S., 1995. Carbon isotopoes of trees from arid environments and implications for reconstructing atmospheric CO2 concentration. Geochimica et Cosmochimica Acta 59, 2599–2608.

Francey, R.J., Farquhar, G.D., 1982. An explanation of $^{13}C/^{12}C$ variations in tree rings. Nature 297, 28–31.

Fessenden, J.E., Ehleringer, J.R., 2003. Temporal variation in $\delta^{13}C$ of ecosystem respiration in the Pacific Northwest: link to moisture stress. Oecologia 136, 129–136.

Giresse, P., Maley, J., Brenac, P., 1994. Late Quaternary paleoenvironments in the Lake Barombi Mbo (West Cameroon) deduced from pollen and carbon isotopes of organic matter. Palaeogeography, Palaeoclimatology, Palaeoecology 107, 65–78.

Goodfriend, G.A., 1999. Terrestrial stable isotope records of Late Quaternary paleoclimates in the eastern Mediterranean region. Quaternary Science Reviews 18, 501–513.

Gouveia, S.E.M., Pessenda, L.C.R., Aravena, R., Boulet, R., Scheel-Ybert, R., Bendassoli, J.A., Ribeiro, A.S., Freitas, H.A., 2002. Carbon isotopes in charcoal and soils in studies of paleovegetation and climate changes during the late Pleistocene and the Holocene in the southeast and center-west regions of Brazil. Global and Planetary Change 33, 95–106.

Guillet, B., Faivre, P., Mariotti, A., Khobzi, J., 1988. The ^{14}C dates and $^{13}C/^{12}C$ ratios of soil organic matter as a means of studying the past vegetation in intertropical regions: examples from Columbia (South American). Palaeogeography Palaeoclimatology Palaeoecology 65, 51–58.

Kelly, E.F., Blecker, S.W., Yonker, C.M., Olson, C.G., Wohl, E.E., Todd, L.C., 1998. Stable isotope composition of soil organic matter and phytoliths as paleoenvironmental indicators. Geoderma 82, 59–81.

Krishnamurthy, R.V., Bhattacharya, S.K., 1989. Paleovegetational history in the Kashmir basin, India, derived from $^{13}C/^{12}C$ ratio in paleosols. Earth and Planetary Science Letters 95, 291–296.

Krishnamurthy, R.V., DeNiro, M.J., Pant, R.K., 1982. Isotope evidence for Pleistocene climatic changes in Kashmir, India. Nature 298, 640–641.

Leavitt, S.W., 1994. South American tree rings show declining $\delta^{13}C$ trend. Tellus 46 (B), 152–157.

Lee, X.W., Feng, Z.-D., Guo, L.L., Wang, L.X., Jin, L.Y., 2005. Soil- and plant- $\delta^{13}C$ variations along a N–S (32–55°N) transect in east-central Asia. Global Biogeochemical Cycles 19, 1–8. doi:10.1029/2004GB2303 GB4010.

Liu, W.G., Ning, Y.F., An, Z.S., 2002. Organic carbon isotopes and their responses to the vegetation in modern soils and paleosols in the Chinese Loess Plateau. Sciences in China (D) 32 (10), 832–836 (in Chinese).

Llorens, L., Penuelas, J., Beier, C., Emmett, B., Estiarte, M., Tietema, A., 2004. Effects of an experimental increase of temperature and drought on the photosynthetic performance of two Ericaceous shrub species along a N–S European gradient. Ecosystems 7, 613–624.

Lu, H.Y., Wu, N.Q., Gu, Z.Y., Guo, Z.T., Luo, W., Wu, H.B., Wang, G.A., Zhou, L.P., Han, J.M., Liu, T.S., 2004. Distribution of carbon isotope composition of modern soils in the Qinghai–Tibetan Plateau. Biogeochemistry 70, 273–297.

McPherson, G.R., Boutton, T.W., Midwood, A.J., 1993. Stable carbon isotope analysis of soil organic matter illustrates vegetation change at the grassland/woodland boundary in southeastern Arizona, USA. Oecologia 93, 95–101.

Nadelhoffer, K.J., Fry, B., 1988. Controls on natural nitrogen-15 and carbon-13 abundances in forest soil organic matter. Soil Science Society of American Journal 52, 1633–1640.

Pack, S.M., Miller, G.H., Fogel, M.L., Spooner, N.A., 2003. Carbon isotopic evidence for increased aridity in northwestern Australia through the Quaternary. Quaternary Science Reviews 22, 629–643.

Pearman, G.I., Francey, R.J., Fraser, P.J., 1976. Climatic implications of stable carbon isotopes in tree rings. Nature 260, 771–773.

Pyankov, V.I., Gunin, P.D., Tsoog, S., Black, C.C., 2000. C_4 plants in the vegetation of Mongolia: their natural occurrence and geographical distribution in relation to climate. Oecologia 123, 15–31.

Sage, R.F., Wedin, D.A., Li, M., 1999. The biogeography of C_4 photosynthesis: patterns and controlling factors (pp. 313–373.). In: Sage, R.F., Monson, R.K. (Eds.), C_4 Plant Biology. Academic Press, San Diego, California.

Schwartz, D., Mariotti, A., Lanfranchi, R., Guillet, B., 1986. $^{13}C/^{12}C$ ratios of soil organic matter as indicators of vegetation changes in the Congo. Geoderma 39, 97–103.

Stewart, G.R., Turnbull, M.H., Schmidt, S., Reskine, P.D., 1995. $\delta^{13}C$ natural abundance in plant communities along a rainfall gradient: a biological integrator of water availability. Australian Journal of Plant Physiology 22, 51–55.

Still, C.J., Berry, J.A., Ribas-Carbo, M., Helliker, B.R., 2003. The contribution of C_3 and C_4 plants to the carbon cycle of a tallgrass prairie: an isotopic approach. Oecologia 136, 347–359.

Teeri, J.A., Stowe, L.G., Livingston, D.A., 1980. The distribution of C_4 species of the Cyperaceae in North America in relation to climate. Oecologia 47, 307–310.

Wedin, D.A., Tieszen, L.L., Dewey, B., Pastor, J., 1995. Carbon isotope dynamics during grass decomposition and soil organic matter formation. Ecology 76, 1383–1392.

Wei, J.M., Dong, J.S., Zhang, J., 1997. Isotopic characteristics of modern pollen grains in the Chinese Loess Plateau. Bulletin of Chinese Sciences 42 (725–727) (in Chinese).

Worden, R.L., Savada, A.M., 1989. Mongolia: A Country Study. Federal Research Division, Library of Congress, Washington DC.

Wu, Z.Y. (Ed.), 1995. The Vegetation of China. Science Press, Beijing (in Chinese).

Zhang, J.C., Lin, Z.G., 1992. Climate of China. Wiley, New York.

附录四

Available online at www.sciencedirect.com
ScienceDirect
ELSEVIER
Palaeogeography, Palaeoclimatology, Palaeoecology 245 (2007) 505–517
PALAEO
www.elsevier.com/locate/palaeo

Eolian environmental changes in the Northern Mongolian Plateau during the past ~35,000 yr

Z.-D. Feng [a,b,*], X.W. Zhai [a], Y.Z. Ma [a], C.Q. Huang [a], W.G. Wang [c], H.C. Zhang [d], P. Khosbayar [e], T. Narantsetseg [e], K.-B. Liu [f], N.W. Rutter [g]

[a] MOE Key Laboratory of Western China's Environmental System, Lanzhou University, Lanzhou 730000, China
[b] Department of Geology, Baylor University, Waco, Texas 76798, USA
[c] Third Institute of Oceanography, State Ocean Administration, Xiamen 361005, China
[d] Institute of Geography and Lake Studies, Chinese Academy of Sciences, Nanjing 210008, China
[e] Institute of Geology and Mineral Resources, Mongolian Academy of Sciences, Ulaanbaatar 210620, Mongolia
[f] Department of Geography and Anthropology, Louisiana State University, Baton Rouge, LA 70803, USA
[g] Department of Earth and Atmospheric Sciences, University of Alberta, Edmond, Canada T6G2E3

Received 22 February 2006; received in revised form 16 July 2006; accepted 20 September 2006

Abstract

This study focuses on an eolian section (Shaamar section) in the Northern Mongolian Plateau and compares the eolian sequences in the Northern Mongolian Plateau with those along the southern boundary of the Gobi Deserts to better understand the dynamics of the Gobi deserts during the past ~35,000 ^{14}C yr BP. Only a weak Entisol-like paleosol was formed around 29,000 ^{14}C yr BP in the exposed MIS 3 portion at the Shaamar section, whereas an eolian–colluvium–paleosol sequence at nearby Bureghkanga section exhibits three paleosols formed around 29,000 ^{14}C yr BP, 31,000 ^{14}C yr BP, 34,000 ^{14}C yr BP. Loess–paleosol sequences in the western Siberian Lowland exhibit four paleosols formed from >40,000 to 25,000 ^{14}C yr BP (i.e., MIS 3). During MIS 2 two Mollisol-like paleosols were formed from ~25,000 to ~21,000 ^{14}C yr BP and from ~16,000 to ~13,000 ^{14}C yr BP and one Entisol-like paleosol was formed around 9500 ^{14}C yr BP at the Shaamar section. The MIS 2 was characterized primarily by silt deposition, except for the interval between ~21,000 and ~16,000 ^{14}C yr BP that was dominated by sand deposition. The Holocene began with the Mollisol-like paleosol formation (from ~8600 to ~7000 ^{14}C yr BP). The mid-Holocene (~7000 to ~3000 ^{14}C yr BP) was marked by a relatively poor vegetation cover and the late Holocene (since ~3000 ^{14}C yr BP) by the densest vegetation cover of the entire Holocene. In summary, the maximal extent of hyperarid and arid areas (Gobi deserts and Gobi-like) occurred twice: (1) from ~21,000 to ~16,000 ^{14}C yr BP and from ~13,000 to ~8600 ^{14}C yr BP when the dominant eolian deposition conditions extended from 56° N to 33° N or even larger. The extent of hyperarid and arid areas retreated to the area between 38° N and 48° N or even much smaller several times during MIS 3 and during the early Holocene. Considering the uncertainties of dates, it seems that the Holocene bioclimatic conditions might have changed more or less synchronously between the north and the south and that the bioclimatic conditions varied more frequently in the north than in the south during MIS 3. Two Mollisol-like paleosols (IIc: ~13,000 to ~16,000 ^{14}C yr BP; and IIIa: ~21,000 to ~25,000 ^{14}C yr BP) were well developed during MIS 2 in the north, but no corresponding major paleosols were discovered in the south, suggesting that the climate did not change synchronously during MIS 2. The climates during the stadial–interstadial MIS 3/2 transition (~25,000 to ~21,000 ^{14}C yr

* Corresponding author. Department of Geology, Baylor University, Waco, Texas 76798, USA. Tel.: +1 254 710 2194; fax: +1 254 710 2673.
E-mail address: Zhaodong_Feng@baylor.edu (Z.-D. Feng).

0031-0182/$ - see front matter © 2006 Elsevier B.V. All rights reserved.
doi:10.1016/j.palaeo.2006.09.009

BP) and during the last glacial maximum-deglacial transition (~16,000 to ~13,000 ^{14}C yr BP) were much more humid in the north than in the south.
© 2006 Elsevier B.V. All rights reserved.

Keywords: Paleoclimate changes; Loess; Gobi dynamics; Mongolian Plateau; Last glacial

1. Introduction

The strengths of the winter and summer monsoons in East Asia were proposed to have changed inversely (Li et al., 1988; An et al., 1991; Feng et al., 1993). Accordingly, dry conditions (times of weak summer monsoon) were proposed to have occurred in cold climates (times of strong winter monsoon). However, new evidence shows that this has not always been the case (Gasse et al., 1991; Porter and An, 1995; Feng et al., 1998, 2004, 2005, 2006). This observation has led to the unsettling question of whether the cold/dry and warm/wet conditions can be taken to characterize the last glacial and the Holocene, respectively, in the arid and semiarid areas of East Asia. This question can be answered only by understanding how the winter and summer monsoon systems have interacted. Have the winter monsoon system and summer monsoon system operated independently or has one forced the other? This study focuses on the Northern Mongolian Plateau, the core area of the Siberian–Mongolian High (Fig. 1A; see Lydolph, 1977; Zhang and Lin, 1992), in order to comprehend the dynamic history of the Gobi deserts along the northern boundary. A detailed investigation was first made of an eolian section (i.e., Shaamar section, Site A in Fig 1A) to establish a relatively reliable chronosequence of the eolian climate changes in the Northern Mongolian Plateau. A geographic comparison of the eolian sequences in the Northern Mongolian Plateau and the adjacent southern Siberia with those in the Southern Mongolian Plateau and the adjacent Chinese Loess Plateau was then made to depict the synchronism of the Gobi dynamics between the southern boundary and northern boundary. The depiction of the Gobi dynamics along the southern and northern boundaries is expected to assist us to understand how the winter and summer monsoon systems have interacted and will also help us to refine CLIMAP's (1981) portrayals of the Earth's Last Glacial boundary conditions and COHMAP's (1988) portrayals of the Earth's Holocene boundary conditions.

1.1. Physiographic settings

Located in the interior of the Asian continent, the Mongolian Plateau has a symmetric distribution pattern of precipitation with the lowest amount of precipitation in the middle of the Gobi deserts, and the mean annual temperature is primarily latitude-dependent and increases southward. The air pressure difference between the landmass and oceans induces the Asian Summer Monsoon systems that bring moisture from the Pacific and Indian Oceans to North China (i.e., Southern Mongolian Plateau), forming a northward decreasing precipitation gradient (Chen et al., 1991). The thermally induced low pressure cell centering in the central-west Asia also induces moisture from the Atlantic and Arctic Oceans and brings moderate precipitation to the Mongolia (i.e., the Northern Mongolian Plateau), forming a southward decreasing precipitation gradient (Compilation Commission of Chinese Physical Geography, 1984; Worden and Savada, 1989; Zhang and Lin, 1992). Consequently, the aridity index (i.e., the ratio of potential evaporation and precipitation) is as high as 7 in the middle of the Gobi deserts and gradually decreases both northward and southward (Worden and Savada, 1989). Correspondingly, the vegetation distributions well reflect these heat-water combinations (Fig. 1B). From the Gobi northward to the Siberia, the vegetation zones are: (1) desert in the southern Mongolia, (2) steppe in the central Mongolia, (3) forest steppe in northern Mongolia, and (4) coniferous forest in the northernmost tip of the Mongolia. From the Gobi southward to the northern Chinese Loess Plateau, the vegetation zones are: (1) desert in the northern Inner Mongolia and (2) steppe in southern Inner Mongolia and in the northern Chinese Loess Plateau. Further southward in the southern Chinese Loess Plateau, steppe forests and deciduous forests dominate the landscape.

The focal area of this study is the loess-covered Baikal-Ulaanbaatar Corridor (48–53° N, 104–108° E) where numerous eolian sections were reported (Khosbayar, 1989). This steppe forest-dominated corridor is flanked by the Kentel Mountains in the east and by the Hangayn Mountains in the west, and the eolian deposits were primarily derived from the floodplains in the lower reaches of the Selenge River and Orhon River (Feng, 2001). It should be reiterated that the focal area is situated within the core of the Siberian–Mongolian High (i.e, the source area of the East Asian winter monsoon) and receives negligible influence from the

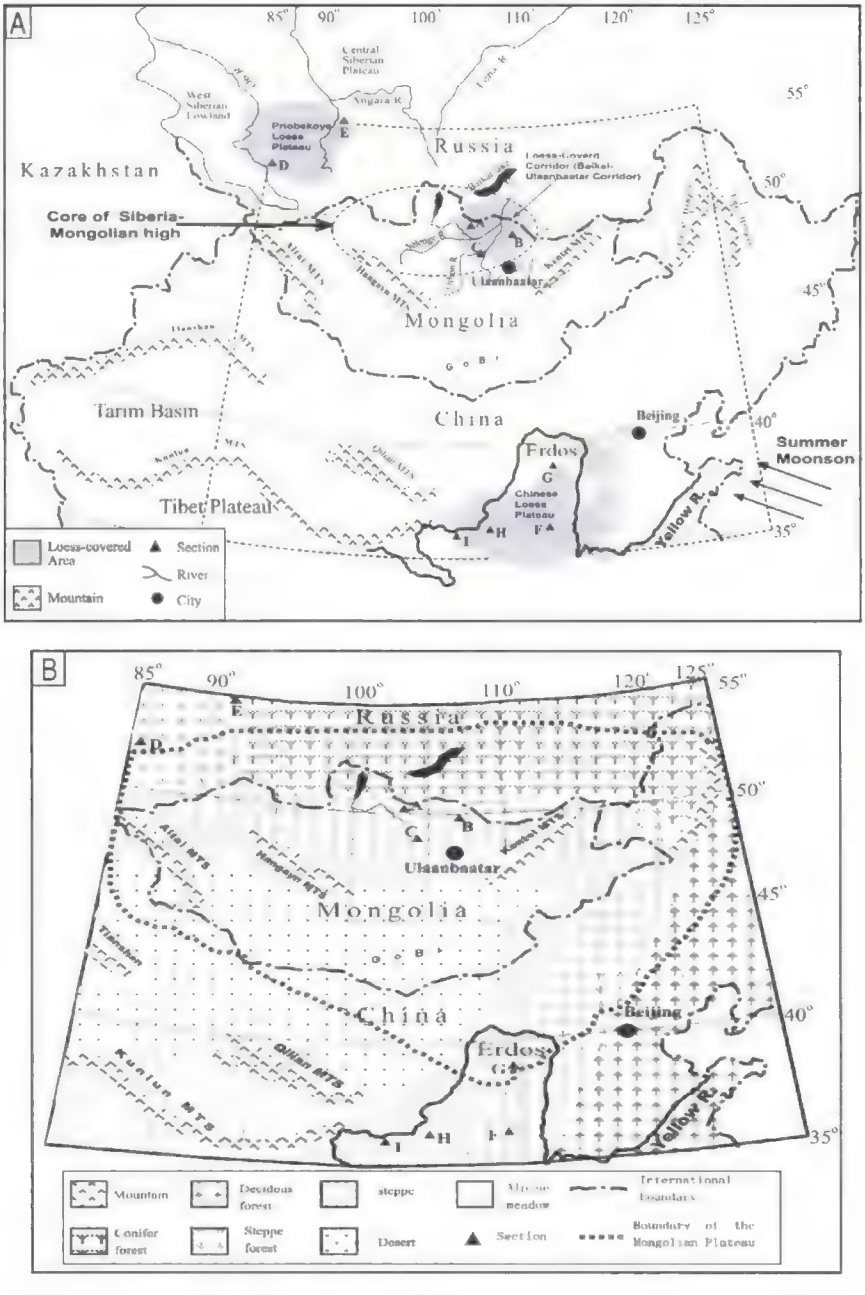

Fig. 1. Maps showing the physiographic settings of the central-east Asia (1A) and vegetation zones of the Mongolian Plateau (1B). A: the relative position of the focal area (Baikal-Ulaanbaatar Corridor) to the core of the Siberian-Mongolian High and the locations of all sections discussed in the text. The loess distributional extents are based on Chlachula (2003), Feng (2001) and An et al. (1991). Sites A (Shaamar), B (Khyaraany), C (Buregkhanga), D (Biysk) and E (Kurtak) are in the northern Mongolian Plateau and its adjacent Loess Plateau of Western Siberian Lowlands. Sites F (Luochuan), G (Yulin), H (Huining) and I (Beiyuan) are in the Chinese Loess Plateau. B: vegetation zones in the Mongolian Plateau and the zones extend to the Chinese Loess Plateau.

East Asian summer monsoon. Unlike the Chinese loess paleosol sequences that contain tangled mixture of both the winter and summer monsoons-related information, the loess paleosol sequence in the Northern Mongolian Plateau is expected to contain only the winter monsoon-related information. In brief,

establishing an independent winter-monsoon chronosequence is critical to understanding the interactions between the East Asian winter and summer monsoon systems.

1.2. Current knowledge

The temporal sequences of the Gobi areal extent along the southern boundary (within China) have been relatively well established, thanks to the sand/paleosol sequences in the Southern Mongolian Plateau and the loess/paleosol sequences in the adjacent Chinese Loess Plateau. We acknowledge two groups who made tireless efforts in reconstructing the late Quaternary environmental changes along the desert-loess transition zone within China: one led by Professor Zhou Weijian (see Zhou et al., 1996, 1999, 2001a,b, 2002; Li et al., 2003) and another led by Professor Sun Jimin (see Sun et al., 1995a,b, 1996; Sun and Liu, 2000).

However, our knowledge is rather limited regarding the Quaternary history of Gobi deserts along the northern boundary where the East Asian summer monsoon has negligible influence. Several studies were conducted in the 1970s and earlier 1980s by Russian scientists, which were summarized by Logatchov (1989). These studies did reveal that the late-Quaternary vegetation in the corridor from Ulaanbaatar to Lake Baikal alternated between forest–steppe and desert, but the chronologies of these studies, based on the four-fold glaciation concepts, were rather speculative. Our recent studies show that this forest steppe-covered topographic corridor was occupied by active sand dunes many times during the late Pleistocene and the Holocene (Feng et al., 1998; Feng, 2001; Feng and Khosbayar, 2004; Feng et al., 2005). Here, we report the results of our detailed field and laboratory investigations of the Shaamar section, the most complete and thickest eolian sequence discovered so far in the Northern Mongolian Plateau.

2. Laboratory methods

The magnetic susceptibility was measured by the procedure of Thompson and Oldfield (1986) using a Bartington MS 2B susceptibility meter. The particle size of bulk samples was measured using a Malvern Co. Ltd. Mastersizer 2000 laser diffraction particle size analyzer and pretreatments of the samples for particle size analysis include adding (1) H_2O_2 to remove organic and soluble salts, (2) diluted 6NHCl to remove carbonate, and (3) Na-hexametaphosphate to disperse the aggregates (see Singer and Janitzky, 1987). The carbonate content was measured using a Bascomb Calcimeter (Machette, 1986) and the organic matter with the titration method (see Singer and Janitzky, 1987). For pollen analysis, the sediments were treated with HCl (10%), NaOH (10%) and HF (36%). Exotic *Lycopodium* tablets were added for calculation of pollen concentration (Moore et al., 1991). Over 100 pollen grains were identified in all of the samples. The analytical intervals are 10 cm for magnetic susceptibility, particle size, carbonate concentration and organic matter content measurements. For pollen identification, the intervals are 25 cm in the three major paleosols and 50 cm in other units.

3. Analytical results and discussions

3.1. Chronostratigraphy

The Shaamar section (50.2° N and 105.2° E, 650 m above sea level and 33 m above the river bed) is found in Shaamar Gully, a small branch of Selenge River (site A with a triangular mark in Fig. 1A). The section can be divided into three units (see strata of Shaamar-1 in Fig. 2). Unit I (0–550 cm): a light-yellowish sand-dominated unit with only 1–2% clay and 10–15% silt. Unit II (550–1850 cm): a light-bluish (gleyed layers) silt–sand (30–60% silt vs. 40–75% sand) unit with an increased clay content (2–4%). Unit III (1850–3020 cm) contains two parts: the upper part (1850–2400 cm) is a grayish sand layer and the lower part (2400–3020 cm) is a light-bluish (gleyed) sand layer. These chronostratigraphic divisions are well supported by the divisions at the Khyaraany section (site B in Fig. 1A; see Feng, 2001). There are three well developed (major) paleosols (IIa, IIc, and IIIa) and six weakly developed (minor) paleosols (Ia, Ib, Ic, Id, IIb, and IIIb in Fig. 2). The three major paleosols are organic matter- and carbonate-enriched Mollisol-like loessial soils and the six minor paleosols are organic matter-enriched Entisol-like sandy soils. The major paleosol IIa (550–760 cm) is dated at 8672 ^{14}C yr BP at its bottom (760 cm). The major paleosol IIc (1610–1890 cm) is bracketed by two dates: 13,398 and 15,770 ^{14}C yr BP (see Fig. 2 and Table 1). The major paleosol IIIa (2170–2400 cm) is dated at 21,010 ^{14}C yr BP at its top (2170 cm). The minor paleosol (Id) at the depth of 400–500 cm is dated in the middle (450 cm) at 4780±80 ^{14}C yr BP. A clinosol-amplified "top" soil (Ia) was found at the base of the Shaamar Gully and four sub-paleosols within the topmost soil (Ia) were AMS dated on charcoals at post-bomb (the surface soil), 620±35, 1423±35 and 1681±37 ^{14}C yr BP, respectively (Shaamar-2 in Fig. 1).

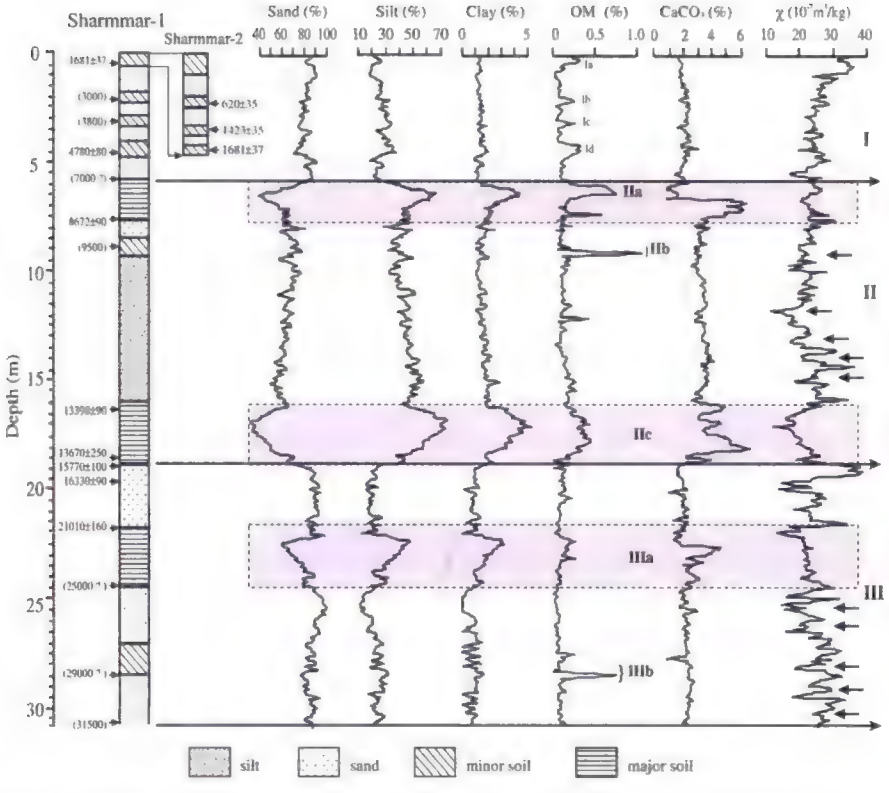

Fig. 2 Litho- and pedo-stratigraphy and chronology of the Shaamar section. The proxy data include particle size distributions (sand, silt and clay), organic matter content (OM), carbonate concentration ($CaCO_3$) and the magnetic susceptibility (χ). Arrows denote gleyed layers.

The ages of paleosols Ib and Ic can be inferred from two dates: 4780 ^{14}C yr BP in the middle of the minor paleosol (Id) and 1681 ^{14}C yr BP at the bottom of the topmost soil (Ia) assuming that the depositional rate was relatively constant, as suggested by the fact that the grain size does not vary from the top of the minor paleosol (Id) to the bottom of the top soil (Ia). The inferred age for the minor paleosol Ib is about 3000 ^{14}C yr BP and the age for the minor paleosol Ic is about 3800 ^{14}C yr BP. The top age (at 550 cm deep) of the carbonate-enriched major paleosol IIa is inferred to be about 7000 ^{14}C yr BP based on the top age (7070 ^{14}C yr BP) of the carbonate-rich layer in nearby Gun Nuur lake core. This inference is based on the environmental interpretation that the high carbonate concentrations both in the paleosol IIa of the Shaamar eolian section and in the carbonate-rich layer of the Gun Nuur lake core were resulted from a high evaporation rate during the early Holocene (Wang et al., 2004; Feng et al., 2005). The minor paleosol IIb (850–940 cm) is interpolated to have formed around 9500 ^{14}C yr BP based on the depositional rate (i.e., 1 cm=5 yr) of unit II (550–1850 cm). The bottom age (at a depth of 2400 cm) of the major paleosol IIIa is inferred to be about 25,000 ^{14}C yr BP based on a date (24,600 ^{14}C yr BP) of a stratigraphically similar paleosol at nearby Bureghhanga section (site C in Fig. 1A; Feng, 2001). The minor paleosol IIIb (2700–2850 cm) is inferred to be about 29,000 ^{14}C yr BP based on a date (28,900 ^{14}C yr BP) of a stratigraphically similar paleosol at nearby Bureghhanga section (site B in Fig. 1A; Feng et al., 1998). The base (at 3020 cm deep) of the section is extrapolated to be approximately 31,500 ^{14}C yr BP based on the calculated depositional rate (i.e., 1 cm=18 yr) of the sand unit between the paleosol IIc (15,770 ^{14}C yr BP at 1890 cm) and paleosol IIIa (21,010 ^{14}C yr BP at 2170 cm). The extrapolation is in turn based on the similarity of particle-size distribution between the sand unit (1890–2170 cm) bracketed by the paleosols IIc and IIIa and the sand unit (2400-3020 cm) beneath paleosol IIIa.

3.2. Pedogenic history

The horizontally interbedded and well-sorted eolian deposits were primarily derived from the floodplains in

Table 1
^{14}C dates of the Shaamar section (AMS dates were measured at NSF AMS Facility at University of Arizona, USA; two conventional dates were measured at ^{14}C Dating Laboratory of Lanzhou University, China)

Sample no.	Lab no.	Depth (cm)	Material	Method	$^{13}C/^{12}C$(‰)	^{14}C age (yr. BP)
SH02-C14-08	AA51938	SH02-60	Charcoal	AMS	−27.6	Post-bomb
SH02-C14-06	AA51936	SH02-140	Charcoal	AMS	−24.8	620±35
SH02-C14-04	AA51936	SH02-195	Charcoal	AMS	−24.5	1423±35
SH02-C14-02	AA51935	SH02-245	Charcoal	AMS	−23.1	1681±37
MN-C14-19	AA519333	0	Sediment	AMS	−26.7	Post-bomb
MN-C14-18	AA519332	70	Sediment	AMS	−27	Post-bomb
4th Paleosol	CG-3465	450	Sediment	Conventional	N/A	4780+/−80
MN-C14-14	AA519328	760	Sediment	AMS	−25.9	8672+/−90
MN-C14-11	AA519325	1680	Sediment	AMS	−24.4	13998+/−99
6th Paleosol	CG-3466	1850	Sediment	Conventional	N/A	13670+/−80
MN-C14-9	AA519323	1890	Sediment	AMS	−22.8	15770+/−90
MN-C14-8	AA519322	1960	Sediment	AMS	−22.3	16330+/−100
MN-C14-7	AA519321	2040	Sediment	AMS	−23.2	13360+/−100
MN-C14-6	AA519320	2170	Sediment	AMS	−14.3	21010+/−160
MN-C14-13*	AA519327	840	Snail	AMS	−9.6	17660+/−120
MN-C14-12*	AA519326	1290	Snail	AMS	−12.8	17660+/−110
MN-C14-17**	AA519331	190	Sediment	AMS	−26.6	Post-bomb
MN-C14-2**	AA519316	2850	Sediment	AMS	−24.5	11083+/−80
MN-C14-1**	AA519315	3020	Sediment	AMS	−24.7	9424+/−85

*Denotes too-old dates (snail ages); **denotes too-young dates (later root penetrations along then-valley slopes).

the lower reaches of the Selenge River and Orhon River. These horizontally-interbedded paleosol and eolian layers indicate that previously-deposited eolian sedimentary sheets (not dunes) might have been relatively well preserved by subsequently-formed soils, suggesting that major environmental events might have been more or less completely recorded in these sequences. We also observed that the eolian deflation and transport of the present floodplain sediments re-sort and re-deposit the sediments, i.e., sand is transported by saltation to lower elevations adjacent to rivers and silt is transported primarily in suspension to higher elevations and long distances.

There are three lithostratigraphic divisions in the Shaamar section. Unit I (0–550 cm), a sand-dominated unit, has been deposited in the past ~7000 ^{14}C yr BP during which four minor Entisol-like paleosols formed around 4800, around 3800, around 3000 ^{14}C yr BP, and during the past 1600 yr, respectively. Unit 2 (550–1850 cm; from ~7000 to ~16,000 ^{14}C yr BP), a gleyed silt–sand unit, is characterized by high percentages of silt and clay and also by a high concentration of $CaCO_3$. This unit (II) contains two major Mollisol-like paleosols with thick organic-enriched A horizons and well-developed Bk horizons. It means that organic matter accumulated in the soil A horizons with the carbonate being leached downward to form thick Bk horizons (Feng et al., 1994a,b,c) during these two major soil-forming periods (paleosol IIa: ~7000 to ~8600 ^{14}C yr BP; paleosol IIc: ~13,000 to ~16,000 ^{14}C yr BP). Unit 3 (1850–3020 cm) is the coarsest and the least leached portion of the entire section. The major Mollisol-like paleosol IIIa (from ~21,000 to ~25,000 ^{14}C yr BP) is well marked by relatively high silt and clay contents and also by relatively high percentages of organic matter and carbonate. The organic matter-enriched Entisol-like paleosols IIb (~9500 ^{14}C yr BP) and IIIb (~29,000 ^{14}C yr BP) may suggest that climates were significantly ameliorated around 9500 ^{14}C yr BP and around 29,000 ^{14}C yr BP.

The sand–silt unit (II) including the major paleosols IIa and IIc is consistently finer and more $CaCO_3$-enriched than the overlying sandy unit I and the underlying sandy unit III, suggesting that the climatic or/and environmental conditions during the late glacial and earlier Holocene (from ~16,000 to ~7000 ^{14}C yr BP) were different from those before (from ~31,500 to ~16,000 ^{14}C yr BP) and after (since ~7000 ^{14}C yr BP). Gleyed horizons were observed in the field in unit II (550–1850 cm; from ~7000 to ~16,000 ^{14}C yr BP) and in the lower part of the unit III (2400–3020 cm: from ~25,000 to ~31,500 ^{14}C yr BP). Those gleyed horizons are well marked by magnetic-susceptibility troughs (arrow-indicated in Fig. 2), suggesting that the gleying-related reduction might have effectively lowered the magnetic susceptibility (see Feng, 2001; Feng and Khosbayar, 2004, for details). It implies that the periodic waterlogging conditions were quite common between

~8600 and ~13,000 ^{14}C yr BP) and between ~25,000 and ~31,000 ^{14}C yr BP). It is also noted that the upper parts of the major paleosols (IIa, IIc and IIIa) are marked by lower magnetic susceptibility probably due to organic acid-induced reduction effect in these soil A horizons (Chlachula et al., 1998; Chlachula, 2003; Feng and Chen, 1999; Feng, 2001).

3.3. Vegetation history

The results of the pollen study are summarized in an abbreviated pollen percentage diagram (Fig. 3). First, pollen assemblages do not distinguish the three lithostratigraphic divisions, although the paleosols (major and minor) seem to have somewhat different pollen characteristics. Specifically, all of the paleosols (major and minor) have relatively high pollen concentrations except for paleosol IIb that is only expressed by a relatively high percentage of Gramineae pollen. Second, the overall pollen concentration is relatively low, ranging from 10 to 160 grains/g. Third, coniferous tree pollen (including *Pinus*, *Picea*, *Abies*, *Larix* and Cupressaceae) dominates the pollen spectrum, varying from 30% to 80%. Fourth, the relatively low percentages of *Pinus* and *Picea* tree pollen from 2 m to 25 m (from ~3000 to ~25,000 ^{14}C yr BP) is compensated by relatively high percentages of Cupressaceae, broad-leaved trees (consisting of *Ulmus*, *Betula*, *Salix*, *Populus*, *Juglans* and *Quercus*), Gramineae and xeric herb taxa (including Chenopodiaceae, *Nitraria*, *Ephedra*, Zygophyllaceae, *Tribulus*, and *Peganum*). Fifth, the percentages of mesic herb pollen (including *Artemisia*, *Aster*-type, *Taraxacum*-type, Gramineae, Polygonaceae, Ranunculaceae, *Urtica* and *Dipsacus*) steadily increase from 3020 cm (~31,500 ^{14}C yr BP) to 850 cm (~9500 ^{14}C yr BP) and decrease from the middle of paleosol IIa (600 cm deep) to the top of the section with a dramatic drop (i.e., a trough) at a depth of around 760 cm (dated at 8672 ^{14}C yr BP). Finally, the Holocene portion beginning at the bottom of major paleosol IIa (~8600 ^{14}C yr BP) is characterized by an increasingly high pollen concentration and also by a persistent appearance of wetland herb pollen (e.g., Cyperaceae, *Sparganium* and Alismataceae).

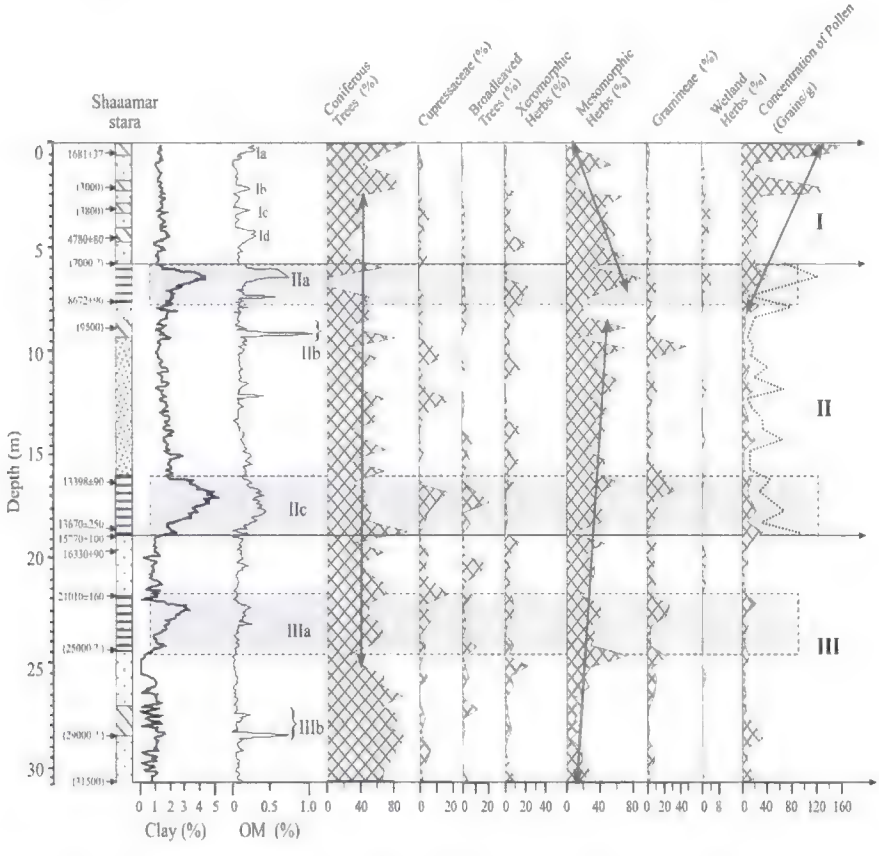

Fig. 3. Pollen assemblage variations with reference to chrono-stratigraphy and clay and organic matter contents at the Shaamar section.

Our interpretation of the vegetation history is that the present forest–steppe landscape, characterized by steadily high pollen concentrations and relatively high percentages of coniferous trees and herbs (xeric, mesic, and wetland), was established during the Holocene (since ~8600 ^{14}C BP). The last glacial maximum and deglacial (from ~8600 to ~25,000 ^{14}C BP) were probably typified by a desert steppe landscape with relatively sparse vegetation covers, as suggested by low pollen concentration values. In spite of the relatively high arboreal pollen percentages (especially coniferous trees), trees were probably absent in the study area, although very small populations of Cupressaceae and some broadleaved trees could have survived in favorable habitats. Most of the coniferous tree pollen was most likely wind-transported from long-distances. The three Mollisol-like paleosols (IIa, IIc, and IIIa) were most likely formed under steppe conditions. The minor Entisol-like paleosols (Ia, Ib, Ic, Id, IIb and IIIb) were probably formed under increased vegetation cover and improved soil-moisture conditions during dominant sand deposition periods. The vegetation before ~25,000 ^{14}C BP was probably also a desert–steppe but with closer proximity to *Pinus* tree patches.

4. Gobi dynamics

4.1. A depiction of the northern boundary changes

Based on the research results presented in this paper with reference to our earlier work on late Quaternary eolian records in the Northern Mongolian Plateau (Feng et al., 1998; Feng, 2001; Feng and Khosbayar, 2004; Wang et al., 2004; Feng et al., 2005) and to Chlachula's works in the Western Siberian Lowland (Chlachula et al., 1998; Chlachula, 2001, 2003) and others' works (Melinikova, 1991; Kremenetski et al., 1997; Tarasov et al., 1997; Velichko et al., 2002; Blyakharchuk et al., 2004), we are now able to present a general history of the late Pleistocene eolian environments in the Northern Mongolian Plateau.

MIS 3 (~57,000 to ~25,000 ^{14}C BP): The loess–paleosol sequences in the Priobskoye Loess Plateau of the Western Siberian Lowland (52–55° N and 85–90° E, see Fig. 1A for the locations of sites D and E) contain four paleosols (Fig. 4) formed during the period from >40,000 to ~25,000 ^{14}C BP (Chlachula, 2003). An eolian–colluvium–paleosol sequence at the Bureghkanga section (site C in Fig. 1A) exhibits three paleosols formed during the period from ~35,000 to ~25,000 ^{14}C BP: around 34,000, around 31,000, and around 29,000 ^{14}C yr BP (Feng et al., 1998). A weakly developed (minor) Entisol-like paleosol formed around 29,000 ^{14}C BP was observed in the exposed MIS 3 portion of the Shaamar section. It appears that the bioclimatic conditions ameliorated at least four times during the entire MIS 3 in the Northern Mongolian Plateau and the adjacent southern Siberia.

MIS 2 (~25,000 to ~8600 ^{14}C BP): A podzolic pedocomplex was dated to have formed at 26,000–22,000 ^{14}C BP in the Altai area along the southern boundary of the west-central Siberia (Melinikova, 1991; Kremenetski et al., 1997; Tarasov et al., 1997; Velichko et al., 2002; Blyakharchuk et al., 2004). The chrono-sequence of litho- and pedo-stratigraphy at the Shaamar section shows that two Mollisol-like major paleosols (IIc and IIIa) were formed from ~25,000 to ~21,000 ^{14}C BP and from ~16,000 to ~13,000 ^{14}C BP and one Entisol-like paleosol (IIb) was formed around 9500 ^{14}C BP. This time period (MIS 2) was characterized primarily by silt deposition, interrupted by sand deposition between ~21,000 and ~16,000 ^{14}C BP. The pollen concentration in the silt-dominated unit II (550–1850 cm) is not substantially higher than that in the sand-dominated unit III (see Fig. 3), but the pollen flux is three times higher in unit II than in unit III (see dashed line following the pollen concentration curve within unit II in Fig. 3) if the deposition rate is taken into account. Specifically, the depositional rate is 20 cm/century for the silt-dominated unit II and only 7 cm/century for the sand-dominated unit III. The lower depositional rate for the sand-dominated unit III, as well as the sand-dominated unit I (rate=8 cm/century), is interpreted to be caused by post-depositional deflation under sparse vegetation covers. In other words, the vegetation covers during the late glacial and the early Holocene (~16,000 to ~7000 ^{14}C BP) and probably also during the major paleosol IIIa formation (~25,000 to ~21,000 ^{14}C BP) were much denser than what is indicated in Fig. 3.

MIS 1 (~8600–0 ^{14}C BP): The Holocene Mollisol-like paleosol IIa (~8600 to ~7000 ^{14}C BP) was formed under leaching conditions as indicated by the depth of the carbonate layer (see Fig. 2). A period of drought during the transition from the late glacial to the Holocene (approximately 690–650 cm deep) is indicated by a low percentage of coniferous tree pollen and by a high percentage of xeric herb pollen (see Fig. 3). Four Entisol-like paleosols (including the topmost soil Ia) were formed around 4800, around 3800, around 3000 ^{14}C yr BP, and during the past 1600 yr, respectively (see Fig. 4). Two peaks of pollen concentration corresponding to the minor paleosols Ia and Ib suggest that the climates were favorable for forest–steppe development when these two paleosols formed (around 3000 ^{14}C BP, and since ~1600 ^{14}C BP). It is

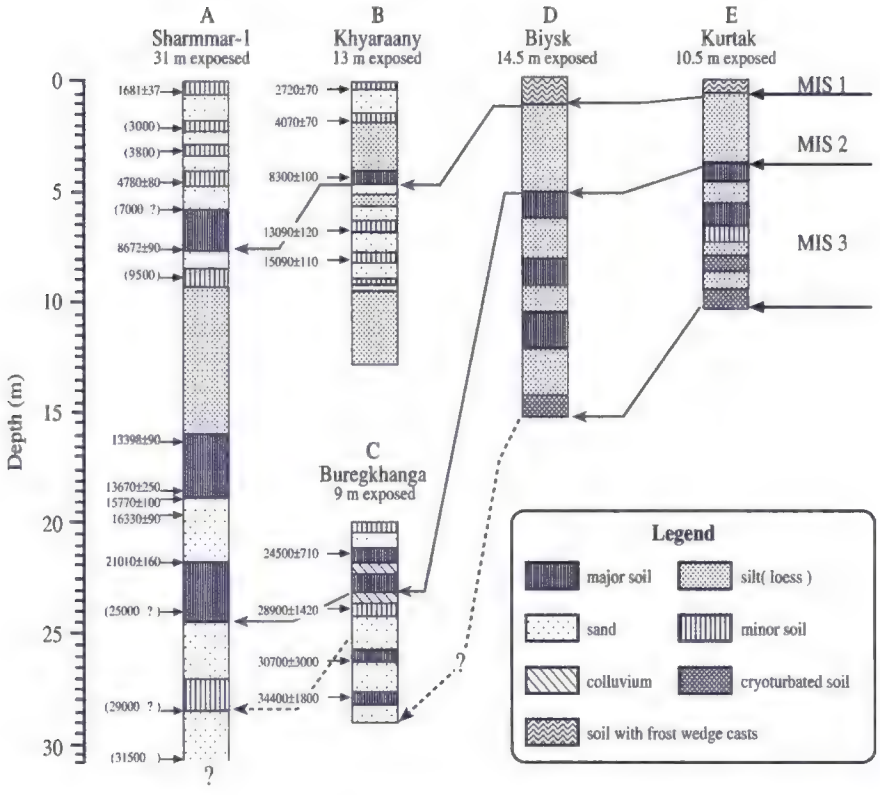

Fig. 4. Litho- and pedo-stratigraphies and chronologies of late Pleistocene eolian sequences in the topographic corridor from Baikal Lake to Ulaanbaatar (Feng et al., 1998; Feng, 2001; Feng and Khosbayar, 2004; and this study) and in the western Siberian Lowland (Chlachula, 2003). The site locations are marked in Fig. 1A.

also evident that wetland herbs appeared during the formation of the major paleosol IIa (~8600 to ~7000 ^{14}C BP) and persisted throughout the Holocene. Wetland herbs were perhaps derived from the Selenge River floodplains, probably implying that the Selenge River's floodplains were less flooded during the last glacial (~35,000 to ~8600 ^{14}C yr BP).

One more point we want to make is that during the floodplain deflation periods, sand was deflated from the floodplains to nearby uplands under sparse vegetation covers and some of the deposited sand in the uplands underwent repeated deflations, resulting in a relatively low rate of net deposition during the sand deposition period (~7 cm/century). In contrast, during the silt deposition periods, long-distance suspension-transported silt was effectively trapped by denser vegetation covers in the uplands, resulting in a relatively high rate of net deposition (~20 cm/century). The final point we want to make is that field-observed and susceptibility-marked gleyed layers in unit II (550–1850 cm; from ~7000 to ~16,000 ^{14}C yr BP) and in the lower part of unit III (2400–3020 cm: from ~25,000 to ~31,500 ^{14}C yr BP) suggest that periodic waterlogging occurred, perhaps under permafrost-related conditions.

4.2. A brief review of the southern boundary changes

Fig. 5 reveals that the MIS 3 pedo-stratigraphy varies from the east (e.g., site F: Luochuan section in Fig. 1A) to the west in the Chinese Loess Plateau (e.g., site G: Huining section and site I: Beiyuan section in Fig. 1A). Specifically, MIS 3 is expressed as a single pedocomplex of accretionary A horizons (3 m thick) in the eastern part and as multiple (2–3) paleosols of accretionary A horizons interbedded with loess units (totally 5–8 m thick) in the western part of the Chinese Loess Plateau. The MIS 3 pedocomplex is bracketed by two TL dates at the Luochuan section: 48,000 and 28,000 yr BP (Guo et al., 1996; Nie et al., 1996). Three TL dates (30,100 yr BP, 35,900 yr BP, 43,890 yr BP) at Yulin section (Su and Dong, 1994) and two TL dates (40,180 yr BP and 61,080 yr BP) at Huining section

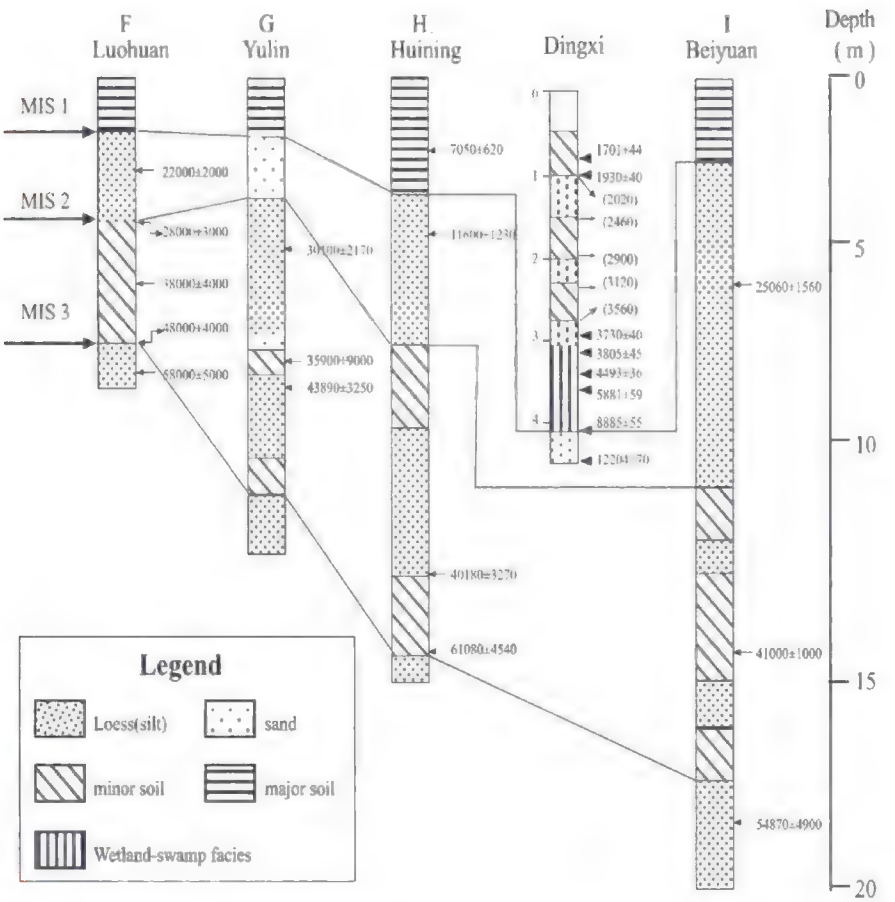

Fig. 5. Litho- and pedo-stratigraphy and chronologies of late Pleistocene eolian sequences in the southern Mongolian Plateau (e.g., Erdos Plateau) and in the Chinese Loess Plateau (Su and Dong, 1994; Nie et al., 1996; Guo et al., 1996; Feng et al., 1998; Wang et al., 2000). The site locations are marked in Fig. 1A.

(Wang et al., 2000) were obtained from the MIS 3 pedocomplexes. The interpolated ages at the Beiyuan section suggest that the three MIS paleosols were formed at 50,000–40,000 TL yr BP (i.e., Sm_1), 37,000–32,000 ^{14}C yr BP (i.e., Sm_2), and 29,000–23,000 ^{14}C yr BP (i.e., Sm_3) (Feng et al., 1998). Minor MIS 2 paleosols are reported along the loess-desert transitional zone in the Erdos Plateau (Zhou et al., 2001a,b, 2002), but the MIS 2 in the entire Chinese Loess Plateau is expressed as "pure" loess without any pedogenic imprints. The MIS 1 (Holocene) is expressed as a thick Mollosol (~2 m thick) in the eastern part of the Loess Plateau. It is also classified as a Holocene soil in the western part although it can actually be divided into two parts: an upper Entisol-loess complex and a lower Mollisol or wetland-swamp facies, as well expressed in the Dingxi section (Fig. 5) near Huining site (site H in Fig. 1A). The Holocene sequence at the Dingxi section shows that the early-middle Holocene (~9000 to ~4000 ^{14}C yr BP) was a period of major paleosol formation in the uplands and a wetland-swamp facies formation in the floodplains that were then ubiquitous in this presently semiarid western part of the Chinese Loess Plateau. The late Holocene at the Dingxi section consists of three paleosol-loess couplets and the three weakly developed paleosols (i.e., Entisols) were inferred to have been formed from ~3500 to ~3100 ^{14}C yr BP, from ~2900 to ~2400 ^{14}C yr BP, and from ~2000 to ~1000 ^{14}C yr BP, respectively (Feng et al., 2004, 2005, 2006).

4.3. Final discussion

The eolian sequences in the Mongolian Plateau suggest that the northern boundary of the Gobi deserts and its adjacent arid-semiarid areas dramatically retreated (southward) 5–7 times during MIS 2 and MIS

3 (between 10,000 and 57,000 ^{14}C yr BP): (1) from ~13,000 to ~16,000 ^{14}C yr BP, (2) from ~21,000 to ~25,000 ^{14}C yr BP, (3) around 29,000 ^{14}C yr BP, (4) around 31,000 ^{14}C yr BP, and (5) around 34,000 ^{14}C yr BP. One or two more retreats might have occurred during the earlier part of MIS 3 (between 35,000 and 57,000 ^{14}C yr BP), as exhibited in the Western Siberian Lowland (Chlachula, 2003). In comparison, the southern boundary of the Gobi deserts and its-adjacent arid–semiarid areas retreated northward only three times during MIS 2 and MIS 3: (1) from 23,000 to 29,000 ^{14}C yr BP, (2) from 32,000–37,000 ^{14}C yr BP, and (3) from 40,000 to 50,000 TL yr BP, as expressed in the Chinese Loess Plateau. The maximal extent of hyperarid and arid areas (Gobi and Gobi-like) occurred twice: (1) from ~21,000 to ~16,000 ^{14}C yr BP and from ~13,000 to ~8,600 ^{14}C yr BP when the eolian deposition conditions extended at least from 55° N (as recorded in loess–paleosol sequences in Priobskoye Loess Plateau of the West Siberian Lowland; see Chlachula, 2001, 2003) to 33° N (as recorded in loess–paleosol sequence in the southern margin of the Chinese Loess Plateau, see Liu, 1985, 1987; Sun et al., 1997) along the N–S transct around 110° E. The extent of hyperarid and arid areas retreated to somewhere between 48° N (as recorded in eolian and fluvial sequences in Ulaanbaatar area and adjacent areas, see Logatchov, 1989; Feng et al., 1998) and 38° N (as recorded in sand-paleosol sequence in Yulin area, see Zhou et al., 1996, 1999) several times during MIS 3 (again along the N–S transct around 110° E). During the Holocene, the northern boundary retreated most dramatically from ~8600 to 7000 ^{14}C yr BP when a well-developed Mollisol (~2 m thick) covered a large area in the Northern Mongolian Plateau. Minor soils (Entisols) and associated pollen assemblages indicate that the northern boundary retreated four times during mid-late Holocene: (1) around 4800 ^{4}C yr BP, (2) around 3800 ^{14}C yr BP, (3) around 3000 ^{14}C yr BP, and (4) during the past 1600 ^{14}C yr BP, as recorded in the Shaamar section. The southern boundary retreated most dramatically from ~9000 to ~4000 ^{14}C yr BP and much less dramatically during the following periods: (1) from ~3500 to ~3100 ^{14}C yr BP, (2) from ~2900 to ~2400 ^{14}C yr BP, and (3) from ~2000 to ~1000 ^{14}C yr BP, as recorded at the Dingxi section in the western part of the Chinese Loess Plateau (Feng et al., 2006).

To sum up, considering the uncertainties of dates, it appears that the bioclimatic conditions varied more frequently in the north than in the south during MIS 3. The climates during MIS 3 alternated three times between loess deposition-indicated dry conditions and paleosol formation-indicated wet conditions in the south (Sun et al., 1997; Feng et al., 1998). In the north, the climates during MIS 3 alternated between permafrost activity-indicated cold conditions and paleosol formation-indicated warm conditions (Feng et al., 1998; Chlachula, 2001, 2003). It should be noted that the major Mollisol-like paleosol IIc (~16,000 to ~13,000 ^{14}C yr BP) has no corresponding paleosol development in the south and that the Mollisol-like paleosol IIIa (~25,000 to ~21,000 ^{14}C yr) may be chronologically correspond to the weakly-developed Sm_3 (29,000–23,000 ^{14}C yr BP) in the south, suggesting that the climate did not change synchronously between the north and the south during MIS 2.

Acknowledgements

This paper is directly or indirectly resulted from several projects. They include three Chinese National Science Foundation projects (No. 40025105, No. 40331102 and No. 40421101) and three U.S. National Science Foundation projects (NSF-ESH-04-02509, NSF-BCS-06-23478, NSF-BCS00-78557). Dr. Paul Hesse and two anonymous reviewers are sincerely appreciated for their comments that helped the authors greatly in revising the paper. We dedicate this paper to Dr. Khosbayar, our friend and co-author, who passed away in February of 2005.

References

An, Z.S., Kukla, G.J., Porter, S.C., Xiao, J.L., 1991. Late Quaternary dust flux on the Chinese Loess Plateau. Catena 18, 125–132.

Blyakharchuk, T.A., Wright, H.E., Borodavko, P.S., van der Knaap, W.O., Ammann, B., 2004. Later Glacial and Holocene vegetation changes on the Ulagan high-mountain plateau, Altai Mountains, southern Siberia. Palaeogeography, Palaeoclimatology, Palaeoecology 259, 259–279.

Chen, L.X., Zhu, Q.G., Luo, H.B., He, J.H., Dong, M., Feng, Z.Q., 1991. The East Asian Monsoon. Meteorological Press, Beijing (in Chinese).

Chlachula, J., 2001. Pleistocene climate change, natural environmental and Palaeolithic occupation of the Altai area, west-central Siberia. Quaternary International 80/81, 131–167.

Chlachula, J., 2003. The Siberian loess records and its significance for reconstruction of Paleistocene climate change in north-central Asia. Quaternary Science Reviews 22, 1876–1906.

Chlachula, J., Evans, M.E., Rutter, N.W., 1998. A magnetic investigation of a Latea Quaternary loess/paleosol record in Siberia. Geophysics International 132, 128–132.

CLIMAP Members, 1981. Seasonal reconstruction of the Earth's surface at the Last Glacial Maximum. GSA Map and Chart Series, MC-36. Geological Society of America.

COHMAP Members, 1988. Climatic changes of the last 18,000 years: observation and modeling. Science 241, 1043–1052.

Compilation Commission of Chinese Physical Geography (Chinese Academy of Sciences), 1984. Physical Geography of China: Climate. Science Press, Beijing (in Chinese).

Feng, Z.-D., 2001. Gobi dynamics in the Northern Mongolian Plateau during the past 20,000+ yr: preliminary results. Quaternary International 76/77, 77–83.

Feng, Z.-D., Chen, F.H., 1999. Problems of magnetic susceptibility signature as the proxy of the summer monsoon intensity in Chinese Loess Plateau. Chinese Science Bulletin 44 (suppl. 1), 97–104.

Feng, Z.-D., Khosbayar, P., 2004. Paleo-subarctic eolian environments along the southern margin of the North American Icesheet and the southern margin of Siberia during the Last Glacial Maxim. Palaeogeography, Palaeoclimatology, Palaeoecology 212, 265–275.

Feng, Z.-D., Thompson, L.G., Mosley-Thompson, E., Yao, T.D., 1993. Temporal variations of Climate in China during the past 10,000 years. The Holocene 3, 174–180.

Feng, Z.-D., Johnson, W.C., Lu, Y.C., Ward, P.A., 1994a. Climatic signals from loess-soil sequences in the central Great Plains. Palaeogeography, Palaeoclimatology, Palaeoecology 110, 345–358.

Feng, Z.-D., Johnson, W.C., Sprowl, D.R., Lu, Y.C., 1994b. Loess accumulation and soil formation in central Kansas during the past 400,000 year. Earth Surface Processes and Landforms 19, 55–67.

Feng, Z.-D., Johnson, W.C., Diffendal, R.F., 1994c. Environments of eolian deposition in Nebraska during the Last Glacial Maximum. Physical Geography 15, 251–261.

Feng, Z.-D., Chen, F.H., Tang, L.Y., Kang, J.C., 1998. East Asian Monsoon Variations and Gobi Dynamics in Stages 3 and 4. Catena 33, 29–46.

Feng, Z.-D., An, C.B., Tang, L.Y., Jull, A.J.T., 2004. Stratigraphic evidence of megahumid mid-Holocene climate in the western part of the Chinese Loess Plateau. Global and Planetary Change 43, 145–155.

Feng, Z.-D., Wang, W.G., Guo, L.L., Li, X.Q., Ma, Y.Z., Zhang, H.C., An, C.B., 2005. Holocene climate changes in the Mongolian Plateau: preliminary results. Quaternary International 136, 25–32.

Feng, Z.-D., An, C.B., Wang, H.B., 2006. Holocene Climatic and Environmental Changes in the Arid and Semiarid Regions of China: A Review. The Holocene 16, 119–130.

Gasse, F., Arnold, M., Jontes, J.C., Fort, M., Gibert, E., Huc, A., Li, B.Y., Li, Y.F., Liu, Q., Melieres, F., Van Campo, E., Wang, F.B., Zhang, Q.S., 1991. A 13000-year climate record from western Tibet. Nature 353, 742–745.

Guo, Z.T., Liu, T.S., Wu, N.Q., Lu, H.Y., Han, J.M., 1996. Heinrich events recorded in Chinese Loess sequence during the last two glacial cycles. Quaternary Sciences 1, 21–30 (in Chinese).

Khosbayar, P. 1989. Map of Geological Complexes of Mongolia (1:500,000). Moscow (in Russian).

Kremenetski, C.V., Tarasov, P.E., Cherkinsky, A.E., 1997. The latest Pleistocene in southwestern Siberia and Kazakhstan. Quaternary International 41/42, 125–134.

Li, J.J., Feng, Z.-D., Tang, L.Y., 1988. Late Quaternary monsoon patterns on the Loess Plateau of China. Earth Surface Processes and Landforms 13, 125–135.

Li, X.Q., Zhou, W.J., An, Z.S., Dodson, J., 2003. The vegetation and monsoon variations at the desert-loess transition belt at Midwan in northern China for the last 13 ka. The Holocene 13 (5), 779–784.

Liu, T.S. (Ed.), 1985. Loess and Environments. Ocean Press, Beijing.

Liu, T.S. (Ed.), 1987. New Aspects of Loess Research. Ocean Press, Beijing.

Logatchov, N.A., 1989. Late Cenozoic of Mongolia (Stratigraphy and Paleogeography). The Joint Soviet–Mongolia Scientific Research Transcation, vol. 47. Moscow Publishing House, Moscow (in Russian).

Lydolph, P.E., 1977. Climates of the Soviet Union. Elsevier Scientific Publishing Co., New York.

Machette, M., 1986. Calcium and magnesium carbonates. In: Singer, M.J., Janitzky, P. (Eds.), Field and Laboratory Procedures used in a Soil Chronosequence study. U.S. Geological Survey Bulletin, vol. 1648. U.S. Government Printing Office, Washington, DC, pp. 30–33.

Melinikova, A.P., 1991. Glacial retreats in Tianshan Mountain during the Holocene. Glaciology and Cryopedology 13, 291–298 (in Chinese).

Moore, P.H., Webb, J.A., Collinson, M.E., 1991. Pollen Analysis, 2nd edition. Blackwell Scientific Publications, London.

Nie, G.Z., Liu, J.Q., Guo, Z.T., 1996. Major climatic events recorded in Weinan loess paleosol sequence: chronological evidence. Quaternary Sciences 13, 221–232 (in Chinese).

Porter, S.C., An, Z.S., 1995. Correlation between climate events in the North Atlantic and China during the last glaciation. Nature 375, 305–308.

Singer, M., Janitzky, P., 1987. Field and laboratory procedures used in soil chronosequence study. U.S. Geological Survey Bulletin 1648.

Su, Z.Z., Dong, G.R., 1994. Environmental changes in the northern Shaanxi Province during the past 130,000 years. Journal of Desert Research 14, 45–52 (in Chinese).

Sun, J.M., Liu, T., 2000. Multiple origins and interpretations of the magnetic susceptibility signal in Chinese wind-blown sediments. Earth and Planetary Science Letters 180, 287–296.

Sun, J.M., Ding, Z.L., Liu, T.S., 1995a. Environmental change of the desert-loess transitional zone over the last glacial–interglacial cycle. Scientia Geologica Sinica (Suppl. 1), 1–8 (in Chinese).

Sun, J.M., Ding, Z.L., Liu, T.S., 1995b. Environmental change along the boundary between Loess Plateau and Deserts since the last interglacial. Quaternary Sciences 2, 117–122 (in Chinese).

Sun, J.M., Ding, Z.L., Liu, T.S., 1996. Re-discussion on the stratigraphic divisions of the Salawusu Group and its depositional environments. Marine Geology & Quaternary Geology 16 (1), 23–31 (in Chinese).

Sun, X.J., Song, C.Q., Wang, F.Y., Sun, M.R., 1997. Vegetation history of Loess Plateau during the last 100,000 years based on pollen data. Quaternary International 37, 25–36.

Tarasov, P.E., Jolly, D., Kaplan, J.O., 1997. A continuous Later Glacial and Holocene record of vegetation changes in Kazakhstan. Palaeogeography, Palaeoclimatology, Palaeoecology 136, 281–292.

Thompson, R., Oldfield, F., 1986. Environmental Magnetism. Allen and Oldwin, London.

Velichko, A.A., Catto, N., Drenova, A.N., Klimanov, A.V., Kremenetski, K.V., Nechaev, V.P., 2002. Climate changes in East Europe and Siberia at the late glacial–Holocene transition. Quaternary International 91, 75–99.

Wang, W.Y., Liu, J.Q., Pan, M., Liu, T.S., 2000. TL dating of Last interglacial–glacial loess–paleosol sequence at Huining section. Marine Geology & Quaternary Geology 20 (3), 67–72 (in Chinese).

Wang, W.G., Feng, Z.-D., Li, X.Q., Zhang, H.C., Ma, Y.Z., An, C.B., Guo, L.L., 2004. The Holocene abrupt climate shifts recorded in Gun Nuur lake core, Northern Mongolia. Chinese Science Bulletin 49 (5), 520–526.

Worden, R.L., Savada, A.M., 1989. Mongolia: A Country Study. Federal Research Division Library of Congress, Washington, DC.

Zhang, J.C., Lin, Z.G., 1992. Climate of China. Wiley, New York.

Zhou, W.J., Donahue, D.J., Porter, S.C., Jule, T.A., Li, Xi.Q., Stuiver, M., AN, Z.S., Eiji, M., Dong, G.R., 1996. Variability of monsoon climate in East Asia at the end of the Last Glaciation. Quaternary Research 46, 219–229.

Zhou, W.J., Head, M.J., Lu, X.F., 1999. Teleconnection of climate events between East Asia and polar high latitude areas during the

last deglaciation. Palaeogeography, Palaeoclimatology, Palaeoecology 152, 163–172.

Zhou, W.J., Head, M.J., Deng, L., 2001a. Climate changes in northern China since the late Pleistocene and its response to global change. Quaternary International 83/85, 285–292.

Zhou, W.J., Wu, Z.K., Jull, A.J.T., Burr, G., Donahue, D.D., Li, B.S., 2001b. Environmental and climatic changes as recorded in geological sediments from the arid and semiarid zone of China. Radiocarbon 43 (2), 585–593.

Zhou, W.J., Dodson, J., Head, M.J., Li, B.S., Hou, Y.J., Lu, X.F., Donahue, D.J., Jull, A.J.T., 2002. Environmental variability within Chinese desert-loess transition zone over the last 20,000 years. The Holocene 12 (1), 117–122.

附录五

Contents lists available at SciVerse ScienceDirect

Quaternary International

journal homepage: www.elsevier.com/locate/quaint

Bioclimatic change of the past 2500 years within the Balkhash Basin, eastern Kazakhstan, Central Asia

Z.-D. Feng [a,*], H.N. Wu [b], C.J. Zhang [c], M. Ran [d], A.Z. Sun [e]

[a] Xinjiang Institute of Ecology and Geography, Chinese Academy of Sciences, Urumqi 830011, China
[b] Peili College of Petroleum Engineering, Lanzhou City University, Lanzhou 730070, China
[c] College of Geological Sciences and Mineral Resources, Lanzhou University, Lanzhou 730000, China
[d] MOE Key Laboratory of Oasis Ecology, Xinjiang University, Urumqi 830046, China
[e] Key Laboratory of Cenozoic Geology and Environment, Institute of Geology and Geophysics, Chinese Academy of Sciences, Beijing 100029, China

ARTICLE INFO

Article history:
Available online 22 July 2013

ABSTRACT

On the bases of analytical data of an 850-cm-long sediment core collected from Balkhash Lake with a chronological control of seventeen AMS dates, this research reconstructed the lake salinity using carbonate content and the oxygen isotopic composition as proxies and reconstructed the basin-wide moisture using A/C ratio and pollen concentration as proxies. Basin-wide mean annual temperature (MAT) and mean annual precipitation (MAP) were reconstructed using climate-pollen response surface method. The reconstruction appears to be supportive to the early proposition that the climate in the westerlies-dominated areas has been generally characterized by cool-wet and warm-dry modes. Balkhash Basin has experienced three stages of climate change during the past ~2500 years: cool-wet from ~2500 to ~1800 cal. BP, moderate from ~1800 to 650 cal. BP, and cooling and wetting during the past ~650 years with the past ~100 showing warming and drying. The moisture evolution has closely followed the MAP variation and the MAT must have modulated the moisture evolution through controlling the evaporation. The first-order variation in lake salinity has been controlled by basin-wide temperature, i.e., low temperature raises the salinity level in the lake through reducing the ice-melt water supply to the lake. The second-order variation in the lake salinity seems to be modulated by pronounced variations in basin-wide moisture. Those low-amplitude variations in basin-wide moisture levels left no detectable imprints in lake salinity proxy records.

© 2013 Elsevier Ltd and INQUA. All rights reserved.

1. Introduction

Climate change during the past 2500 years (i.e., the time span this paper deals with) has basically been paced by solar activities that are superimposed on orbital forcing factors (Ruddiman, 2008; Mann et al., 2009). Land-air interactions in smaller spatial scales (Anderson et al., 2002; Bridgman and Oliver, 2006) and human and volcanic disturbances in shorter temporal scales (Bauer et al., 2003; Maasch et al., 2005) are documented as "perturbation factors" affecting climate change.

The Balkhash Basin is situated in the eastern part of the Central Asian Arid Zone (CAAZ) that stretches from the Caspian Sea in the west to the Altai Mountains in the east (Fig. 1). The W–E striking Tianshan Mountains approximately along the 40th parallel block the climatic influence of the Arabian Sea from the south and allow the climatic dominance of the westerlies from the west (Gong et al., 2001; Heorling et al., 2001; Staubwasse and Weiss, 2006). The warm-season precipitation in the CAAZ is primarily from the North Atlantic via the northward-shifted westerlies, whereas the cold-season precipitation is primarily from the Mediterranean Sea via the southward-shifted westerlies (Aizen et al., 2001; Bridgman and Oliver, 2006; Bothe et al., 2011). Frequent southward invasions of the polar front are the most important precipitation-promoting mechanism (Lydolph, 1977; Aizen et al., 2001). The cold-season climate in the study area is modulated by the interactions between the westerlies and the North Atlantic Oscillation (NAO) and that the warm-season climate is controlled by the interactions between the Asian Low occupying the interiors of Asia and the Azores High reaching CAAZ (Aizen et al., 2001; Meeker and Mayewski, 2002) (Fig. 2). The westerlies-domination over the CAAZ during the Holocene (i.e., past 11,500 years) has also been demonstrated by the temporal consistency between the records from the West Europe and the records

* Corresponding author.
E-mail addresses: fengzd@lzu.edu.cn, fengzd@ms.xjb.ac.cn, fengzd@xju.edu.cn (Z.-D. Feng), wuhn510@163.com (H.N. Wu), cjzhang@lzu.edu.cn (C.J. Zhang), ranm07@lzu.cn (M. Ran), sunaizhi@mail.iggcas.ac.cn (A.Z. Sun).

1040-6182/$ – see front matter © 2013 Elsevier Ltd and INQUA. All rights reserved.
http://dx.doi.org/10.1016/j.quaint.2013.06.032

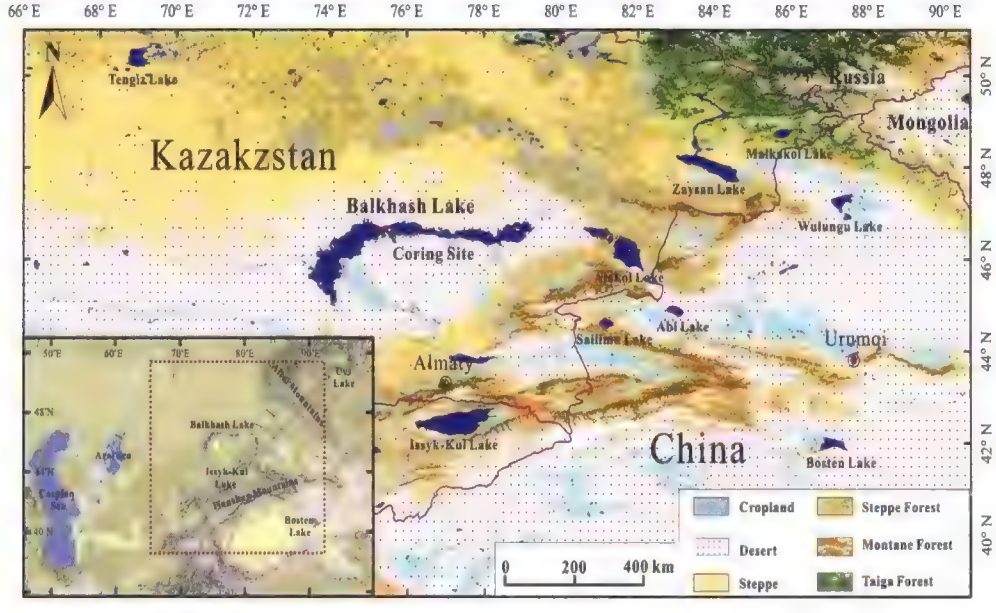

Fig. 1. Land-cover map showing the distribution of vegetation and the location of Balkhash Lake. The inset map in the lower-left corner shows the location relation of the Balkhash Lake to the Caspian Sea and the Aral Sea.

from the CAAZ. That is, unlike the Asian monsoon-dominated areas where the Holocene climate change has been characterized by either warm-wet mode or cool-dry mode (Shi et al., 1993; Holme et al., 2009), the Holocene climate change in the westerlies-dominated areas has been typified by either a warm-dry mode or cool-wet mode (see: Geel et al., 2004; Yang et al., 2002, 2009; Kroonenberg et al., 2007; Boomer et al., 2009).

Nevertheless, neither data nor interpretations are unequivocally supportive to the "warm-dry" and "cool-wet" generalization. For example, the chronological correspondence between the last two major highstands (i.e., wet events) in the Caspian Sea occurred around 2600 cal. BP and around 1600 AD (i.e., cool times) and the global cooling events associated with minima in solar activities (Kroonenberg et al., 2007) do lend strong supports to the "warm-dry" and "cool-wet" generalization (Boomer et al., 2000, 2009). More supports came from the Aral Sea where the major high-salinity events (i.e., dry times), documented by dinoflagellate cysts, of the past 2000 years occurred during warm intervals (e.g., AD 0–400, AD 900–1350 and since AD 1800). However, another high-salinity event in the Aral Sea occurred during a cool interval between AD 1500 and AD 1650 surely undermined the acceptability of the generalization. The reconstructed temporal variations in the dust deposition in the Aral Sea also fundamentally undermined the acceptability (Huang et al., 2011), being completely consistent with "warm-wet" and "cool-dry" modes generalized for the Asian monsoon-dominated areas. More eolian sediments were supplied to the Aral Sea during cold intervals under stronger Siberian High Pressure conditions. The broad similarity between the eolian record in the Aral Sea (Huang et al., 2011) and the lacustrine $\delta^{18}O$ record in Turkey (Jones et al., 2006) implies that there was less moisture entering western Central Asia from the Mediterranean during cool intervals. The pollen-indicated climate change in the Aral Sea has followed neither the generalized "warm-dry" and "cool-wet" modes nor the solar activity-dictated temperature trend of large scale. Specifically, pollen data show that cold and arid conditions prevailed between ca. AD 0 and 400, AD 900 and 1150, and AD 1500 and 1650 with the expansion of desert vegetation and that warm and wet climate conditions prevailed between ca. AD 400 and 900, and AD 1150 and 1450 with the expansion of steppe vegetation (Sorrel et al., 2006).

However, the aforementioned discrepancies among different datasets (e.g., salinity, vegetation, and dust) may be reconcilable if different processes are involved. For example, lake salinity may be controlled by temperature-dictated amount of ice-melting and may have little to do with the amount of precipitation if the lake is mainly supplied by ice-melt water (Sorrel et al., 2007). Dust input to the lake may be controlled by large-scale atmospheric circulation and may have little to do with basin-wide vegetation coverage if availability of eolian particles in the basin is not a limiting factor (Huang et al., 2011). We intend to accept the proposition that basin-wide vegetation may be a real expression of basin-wide climate and that pollen record from a closed lake can be used to retrieve past climate (Blyakharchuk et al., 2007; Tarasov et al., 2007; Rudaya et al., 2009). This paper attempts to reconstruct the bioclimatic change of the past 2500 years within the Balkhash Basin in the eastern part of Kazakhstan in hope that some of the aforementioned discrepancies can be reconciled.

2. Regional setting

Lake Balkhash (Fig. 1) is one of the largest lakes in Asia (approximately 73–80 °N and 44–47 °E; 330 m a.s.l.). The basin drains into the lake via seven rivers. The Ili River is the most significant one originating from the Tianshan Mountains and supplying most of the inflowing water to the lake. The lake currently covers an area of 16,400 km^2 and it is hydrographically divided into two very different parts: the western fresh part and the eastern salty part. During recent time, the area of the lake expanded to >18,000 km^2 during wet years and shrank to <16,000 km^2 during dry years (Petr, 1992). The climate of the lake area is continental with average July temperature of +30 °C and average January temperature of −14 °C. The annual mean temperature (MAT) is ~6 °C and mean annual

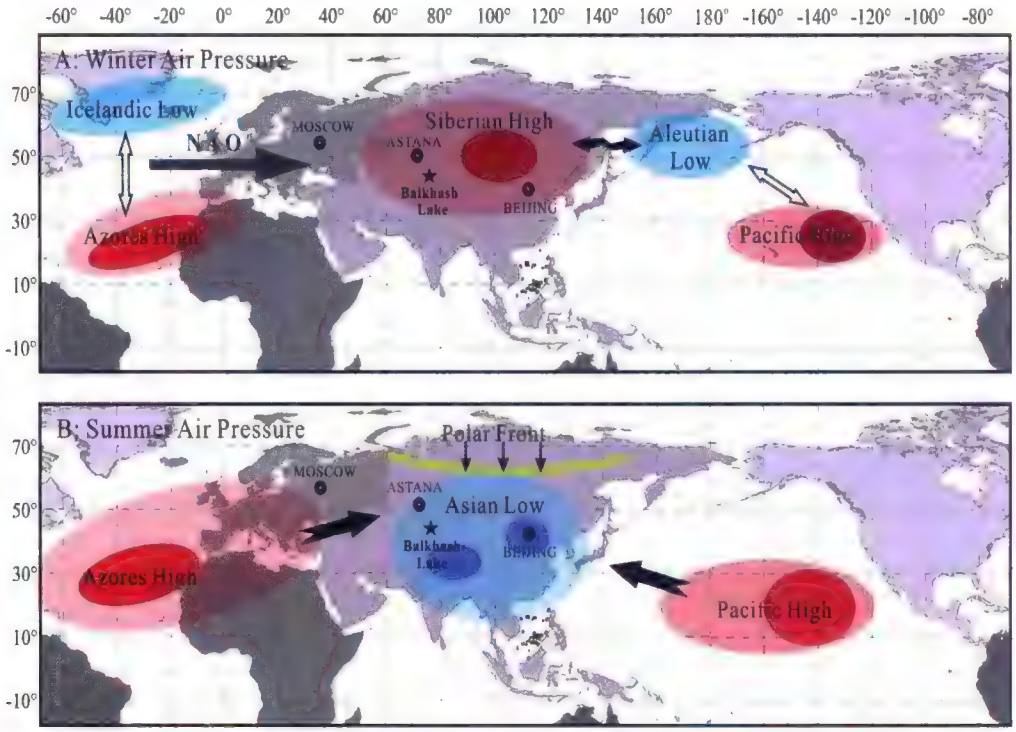

Fig. 2. Winter air pressure systems (A): the strength of Siberia High depends not only on the pressure contrast between the Asian interior and the Pacific, but also on the pressure contrasting relationships of Siberian High with Aleutian Low to the east and with Icelandic Low to the west. Summer air pressure systems (B): the Asian low not only allures the Pacific High to the Asian interior to form the East Asian Monsoon but also to induce the Azores High to penetrate into the Central Asian Arid Zone (i.e., CAAZ). Note 1: the dark-red circles within the light-red circles are the cores of high pressure cells. Note 2: the dark-blue circles within the light-blue circles are the cores of low pressure cells.

precipitation (MAP) is ~ 150 mm with an evaporation of ~ 1000 mm (Propastin, 2011). The basin-wide MAP ranges from 3 to 10 °C and the basin-wide MAP ranges from 130 to 450 mm (Gou et al., 2008). The shores of the lake are occupied by *Populus*-dominated riparian forests and also by wetland plants including common reed (*Phragmites australis*) and Lesser Indian Reed Mace (*Typha angustata*). The basin-wide vegetation includes taiga forests in the northeast (i.e., Altai Mountains), Montane forests in the southeast (i.e., Tianshan Mountains), steppe-forests in the north and desert in the west (ESA and UCLouvain, 2010). The vertical zones of vegetation in mountains from higher to lower elevations include: tundra, alpine meadows, coniferous forests, mixture of deciduous trees and shrubs with steppes, steppes, and deserts.

3. Materials and methods

3.1. Coring and composition analysis

An 850-cm-long sediment core (75.6 °N, 46.4 °E) was collected with a Livingstone-type piston corer in the summer of 2007 at the eastern end of the western fresh-water part. Seventeen (17) samples of bulk sediment were radiocarbon dated using accelerator mass spectrometry at the NSF-AMS Facility at the University of Arizona (Table 1). Total organic matter content (TOC) was determined at 2-cm intervals (389 samples) using the anti-titration method with concentrated sulfuric acid (H_2SO_4) and potassium dichromate ($K_2Cr_2O_7$). The carbonate content was determined at 2-cm intervals (389 samples) by treating bulk sediment samples with dilute 1N HCl and measuring the generated CO_2 volume. For isotopic analysis (389 samples), phosphoric acid was added to finer portion (<40 mm) of the samples and the acid-produced CO_2 gas was purified and transferred into a Finnigan Delta plus mass spectrometer to analyze the oxygen isotopic composition. The grain size of 190 samples was measured using a Malvern Mastersizer 2000 laser diffraction particle size analyzer (note: after other analyses no samples left for grain size analysis for the depths from 400 to 250 cm). Sample pretreatment for grain-size analysis included: (1) using H_2O_2 to remove organic matter and soluble salts, (2) using diluted 1 N HCl to remove carbonate and (3) using Na-hexametaphosphate to disperse aggregates. All of the aforementioned analyses were conducted in the MOE Key Laboratory of Western China's Environmental Systems at Lanzhou University.

3.2. Pollen analysis

For pollen analysis of 207 pollen samples obtained at 4-cm intervals, a tablet of *Lycopodium* was added for calculation of pollen concentration (Moore et al., 1991). The procedure for fossil pollen analysis includes treating 5–10 g of sediment sample with 10% HCl, 10% KOH, 36% hydrofluoric acid (HF) to eliminate carbonate, humid acid, and silicate, respectively. The pollen in the residue was then concentrated with a 7-μm mesh sieve in conjunction with ultrasonic vibration. Finally, water-free glycerol was used for mounting pollen samples on microscopic slides. The treated samples were then examined with a transmitted light microscope at 400×–1000× magnification. More than 300 pollen grains were counted for each sample. Pollen types were identified using pollen references including pollen books and photographs (Wang et al., 1995)

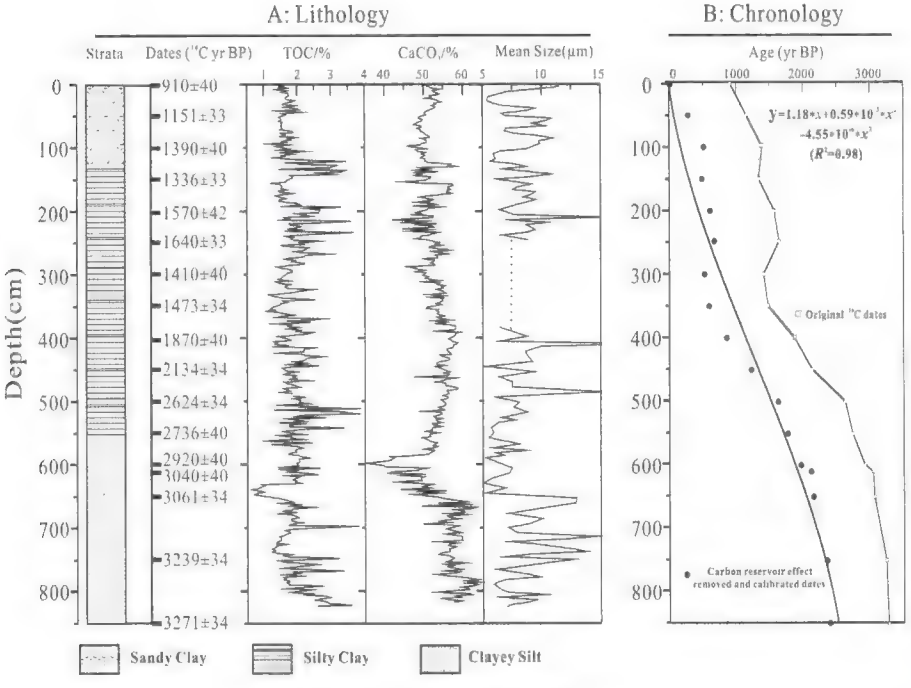

Fig. 3. Lithology and chronology of the Balkhash Lake core.

and our own reference slide collection of more than 200 plant species from northern China. Pollen concentrations were calculated on the basis of exotic *Lycopodium* spore counts and were expressed as the number of grains per gram (grains/g). Pollen diagrams were plotted using Tilia (Grimm, 1990). CONISS cluster analysis was conducted for providing reference for pollen zoning.

We first calculated the A/C ratio (*Artemisia*/Chenopodiaceae) and the ratio is a widely-used index to semi-quantitatively assess the moisture (aridity) variations in the arid and semi-arid Asia (El-Mosilimany, 1990; Liu et al., 2008; Van Campo et al., 1996; Zhao et al., 2009, 2012). We then tried three pollen-based quantitative methods to reconstruct the mean annual temperature (MAT) and the mean annual precipitation (MAP) variations: (1) climate-pollen response surface (CPRS); (2) climate-pollen transfer function (CPTF), and (3) plant functional type - modern analogue technique (PFT-MAT). CPRS method was developed on the bases of 215 surface pollen spectra from northern China including Xinjiang near our study site, Balkhash Lake (Song et al., 1997) and CPTF method was developed on the bases of 646 surface pollen spectra from Mongolia and the eastern part of northern China (Wen et al., 2013). PFT-based reconstruction searches for affinity between the fossil pollen assemblage and the modern pollen dataset and the modern pollen dataset used includes 211 surface pollen spectra from China (Jiang et al., 2009) and 1855 surface pollen spectra from Europe (Guiot et al., 1993) and from former Soviet Union (Tarasov et al., 1998).

4. Results

4.1. Stratigraphy and chronology

The core can be stratigraphically divided into three units (Fig. 3). Sediment Unit 1 (850–650 cm) is a clayey silt layer with the organic matter and carbonate contents being higher than the averages. Sediment Unit 2 (650–120 cm) is a silty clay layer with moderate contents of the organic matter (~2%) and carbonate (~55%). Sediment Unit 3 (120–0 cm) is a sandy clay layer with organic matter and carbonate contents being lower than the averages. The uppermost date of 910 ^{14}C BP (0–2 cm) is here regarded as the carbon reservoir effect and the effect was subtracted from all dates assuming that the reservoir effect does not vary significantly throughout the core. All dates (reservoir effect-free) were then calibrated to calendar years before present (BP = 1950 AD) with the program CALIB 6.0 using INTCAL 09 (Reimer et al., 2009). Finally, a linear age-depth model was established using a best-fitting method (Fig. 3).

4.2. Pollen data

The core can be palynologically divided into four pollen assemblage zones based on percentages of the major pollen taxa using the constrained incremental sum of squares (CONISS) method (Fig. 4). Overall, herb component dominates the pollen spectrum, and tree pollen is a minor component throughout the core. The following discussion will only focus on the major pollen zones (iZones 1, 2, 3, and 4), because the differences among the CONISS-divided sub-zones within each of the major pollen zones are generally insignificant.

Pollen Zone 1 (850–588 cm; ~2500–~1830 cal. BP) is characterized by following features in comparison with the overlying Pollen Zone 2: (1) higher pollen percentages of some mesic species (e.g., Rosaceae, *Tamarix*, *Artemisia*, Crucifeae, and Poaceae), (2) lower pollen percentages of xeric species (e.g., Zygophyllaceae, Chenopodiaceae and *Ephedra*), and (3) considerably higher pollen concentration.

Pollen Zone 2 (588–288 cm; ~1830–~725 cal. BP) is typified by decreased pollen percentages of some mesic species (e.g., Rosaceae, *Tamarix*, *Artemisia*, Crucifeae, and Poaceae) with accompanied increases in xeric species (e.g., Zygophyllaceae, Chenopodiaceae and *Ephedra*). The pollen concentration is considerably lower than that in the underlying Pollen Zone 1.

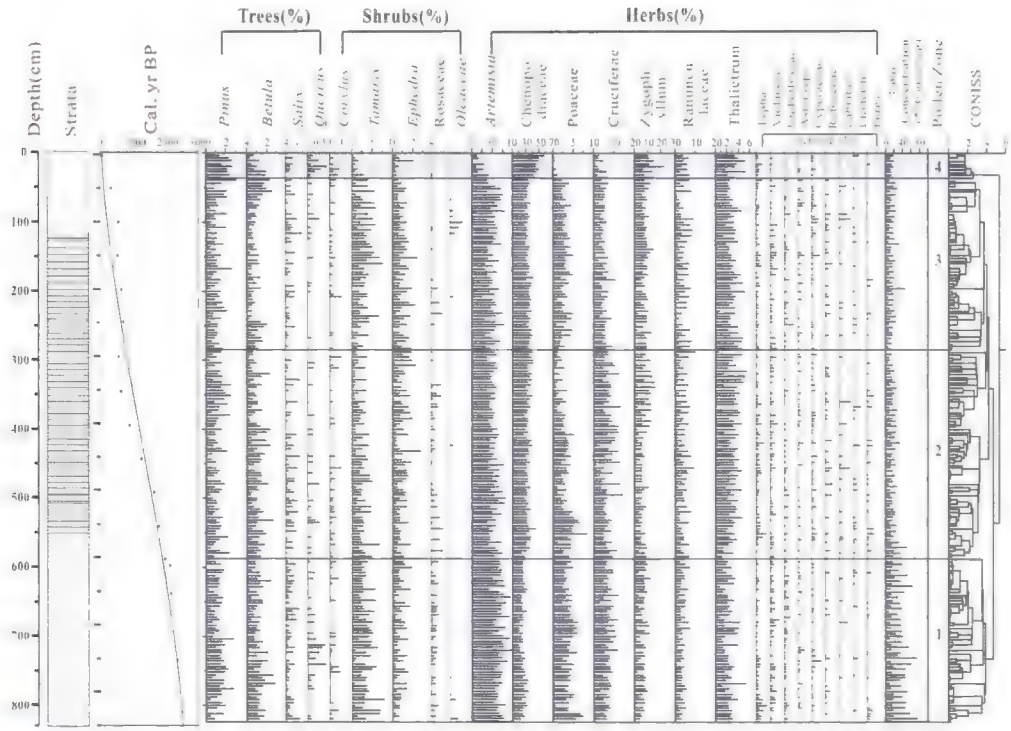

Fig. 4. Pollen spectrum of the Balkhash Lake core.

Pollen Zone 3 (288–40 cm; ~725–~60 cal. BP) is marked by continuation of the increasing trend of xeric species (e.g., Zygophyllaceae, Chenopodiaceae and *Ephedra*) and also by continuation of the decreasing trend of pollen concentration. Accompanied are the pollen percentage decreases of some mesic species (e.g., Rosaceae, Crucifeae, and Poaceae).

Pollen Zone 4 (40–0 cm: ~60–~0 cal. BP) is typified by a dramatic increase in Chenopodiaceae and a slight increase in Zygophyllum with accompanied decreases in *Artemisia* and Poaceae. It is likely that these changes were caused by an increase of aridity resulted from the observed rapid warming of the past ~60 years (Lioubimtseva and Cole, 2006; Gou et al., 2008). It should be particularly noted that the dates were calibrated to 1950 and the past ~60 seems meaningless. But, the inherent large errors in radiocarbon dates and the undoubted continuation of the lake deposition after 1950 justify the assumption that the topmost 40-cm sediment was most likely deposited during the past ~60 years.

4.3. Reconstructions of lake salinity and basin climate

We tried three pollen-based quantitative methods to reconstruct temperature and precipitation variations: (1) climate-pollen response surface (CPRS); (2) climate-pollen transfer function (CPTF), and (3) plant functional type– modern analogue technique (PFT-MAT). Apparently, the three reconstructions completely lack consistency (Fig. 5). Here, we prefer the CPRS-based reconstruction over the other two for four reasons. First, the CPRS method was developed on the basis of surface pollen spectra from northern China including Xinjiang near our study site, Balkhash Lake (Song et al., 1997). Second, the observed warming of the past ~100 years (Lioubimtseva and Cole, 2006; Gou et al., 2008) seems to be well captured by the CPRS-based reconstruction. Third, the CPRS-based MAT reconstruction (i.e., temporally ranging from 4.6 to 5.2 °C) appears to be more reasonable in comparison with the present basin-wide MAT (spatially ranging from 3 to 10 °C) than the other two reconstructions (temporally ranging from 1.4 to 4.8 °C). Fourth, the high-degree resemblance between the CPRS-based MAP curve and the A/C ratio-indicated moisture curve (Fig. 6) implies that the CPRS-based MAP reconstruction is more or less reasonable.

The CPRS-based reconstruction shows that Balkhash Basin experienced three stages of climate change (Fig. 6). Climate Stage 1 was a low-temperature and high-precipitation period lasting from ~2500 to ~1800 cal. BP, with a brief interval around ~2150 cal. BP being lower in precipitation. Climate Stage 2, spanning from ~1800 to ~650 cal. BP, started with a dramatic decline in MAP that reached the minimum around ~1700 cal. BP and was generally characterized by increased MAT and also by decreased MAP compared with the previous stage (i.e., Climate Stage 1). Climate Stage 3 (i.e., the past ~650 years) was a cooling and wetting period with the past ~100 years having an opposite trend (i.e., warming and drying). The interval between ~250 and ~100 cal. BP (i.e., approximately from the middle of 17th to the end of 19th centuries) was significantly cooler with increased precipitation.

The A/C ratio, as a moisture (or aridity) proxy, shows that the basin also experienced three stages of moisture evolution (Fig. 6). Moisture Stage 1 spanned from ~2500 to ~1800 cal. BP and was characterized by a considerably high moisture level with a peak moisture interval lasting from ~2200 to ~2100 cal. BP. During Moisture Stage 2, covering the period between ~1800 and ~650 cal. BP, the moisture level dropped significantly in comparison with the previous stage. Moisture Stage 3 (the past ~650 years) exhibits an increasing trend of moisture closely following the increasing trend of MAP. The three stages of A/C ratio-based moisture evolution are well corroborated by the total pollen concentration. The A/C ratio values of these three stages are all within the reported A/C ratio range of desert-steppe (i.e., 0.5–2.0) (Zhao et al., 2012).

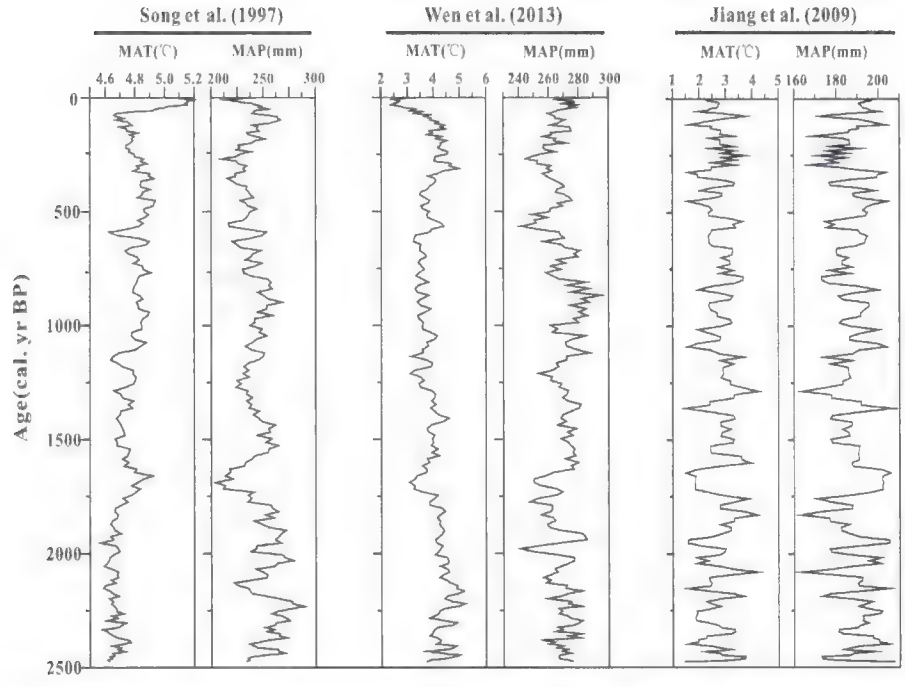

Fig. 5. Pollen-based quantitative reconstructions (5-point moving average) of mean annual temperature (MAT) and mean annual precipitation (MAP) using Pollen Response Surface method (Song et al., 1997), Transfer Function method (Wen et al., 2013) and the improved PAT-MAT method (Jiang et al., 2009).

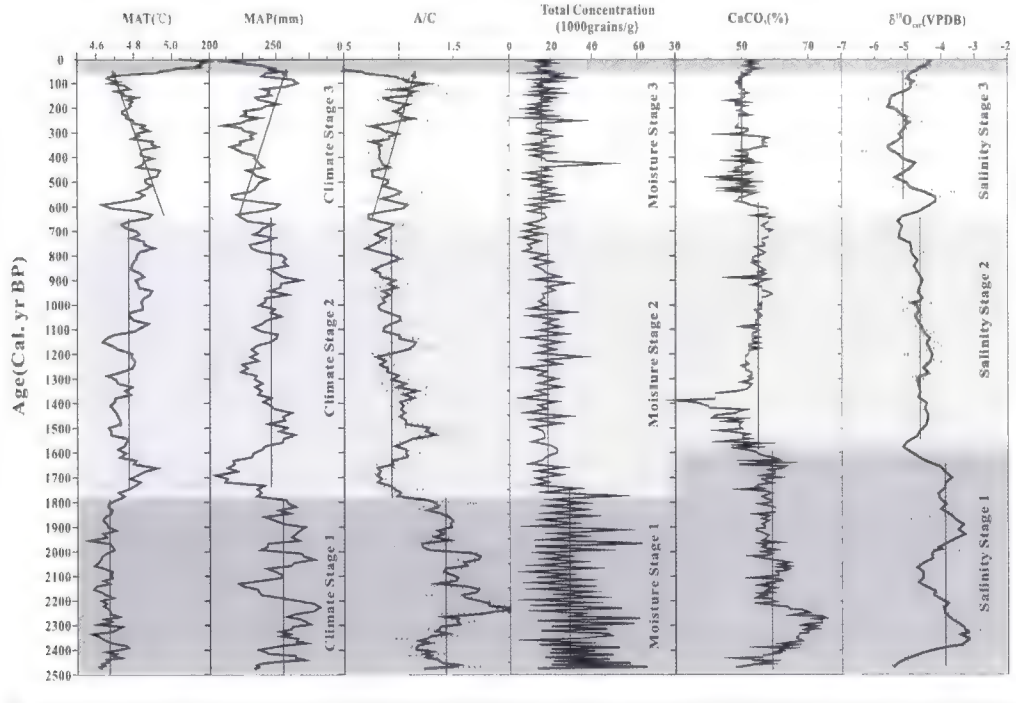

Fig. 6. Three sets of proxies. (1) MAT and MAP (five-point moving averages) reconstructed using Pollen Response Surface method (Song et al., 1997); (2) salinity: carbonate concentration (%) and $\delta^{18}O_{car}$ (five-point moving average); and (3) moisture: A/C ratio (five-point moving average) and total pollen concentration (1000 grains per gram).

We measured the carbonate content of the lacustrine deposits and the carbonate oxygen isotopic composition (i.e., $\delta^{18}O_{car}$). The precipitation of carbonate in lakes is primarily controlled by the temperature and the biological productivity. Carbonate solubility decreases with a temperature-driven increase in evaporation. Biological productivity refers to the fact that aquatic plants can absorb CO_2 from lake water through photosynthesis, leading to increases in the pH values of the lake water and thus to increases in carbonate precipitation. Carbonate precipitation in closed lakes of arid areas has a close relationship with the lake salinity as indicated by the Mg/Ca ratio (Gasse et al., 1987; Aravena et al., 1992; Zhang et al., 2010), thus rendering the carbonate content a salinity proxy. The oxygen isotopic composition of lacustrine carbonate in closed lakes of arid-semiarid areas is largely dependent on the ratio of evaporation over precipitation (Gasse et al., 1987; Li and Ku, 1997; Zhang et al., 2010). Strong evaporation leads to the enrichment of heavier oxygen isotope, thus also rendering the $\delta^{18}O_{car}$ as a salinity proxy.

As lake water salinity proxies, both the carbonate content (%) and the oxygen isotopic composition ($\delta^{18}O_{car}$) show that the lake experienced three stages of salinity variations (Fig. 6). Salinity Stage 1 spanned from ~2500 to ~1600 cal. BP and was characterized by considerably high values in $CaCO_3$ (%) and in $\delta^{18}O_{car}$. A relatively low-salinity interval occurred approximately between 2200 and 2000 cal. BP within Salinity Stage 1. Salinity Stage 2, covering the period between ~1600 and ~650 cal. BP, started with a deep trough of the salinity proxy values (from ~1600 to ~1400 cal. BP) and was generally marked by lowered values of salinity proxies. Salinity Stage 3 (the past ~650 years) experienced a further lowering of the salinity.

5. Discussion

The data appear to be supportive to the early proposition that the climate in the westerlies-dominated areas has been generally characterized by cool-wet (i.e., lower MAT and higher MAP) and warm-dry (i.e., higher MAP and lower MAP) modes. The reconstruction shows that Balkhash Basin experienced three stages of climate change: cool-wet from ~2500 to ~1800 cal. BP, moderate from ~1800 to 650 cal. BP, and cooling and wetting during the past ~650 years, with the past ~100 seeing warming and drying.

The moisture evolution has closely followed the MAP variation, and the MAT must have understandably modulated the moisture evolution through controlling the evaporation in the basin. For example, Climate Stage 1 (cool-wet) chronologically corresponded with Moisture Stage 1 (highest moisture stage), and the increasing moisture from ~650 to ~100 cal. BP was most likely the result of rising MAP (wetting) combined with declining MAT (cooling). The detailed variations in MAP during the Climate Stage 2 were well reflected by the moisture variations (A/C ratio).

The high salinity level during Salinity Stage 1 (between ~2500 and ~1600 cal. BP) mainly occurred during a high-moisture period (Moisture Stage 1) under a high-precipitation condition (Climate Stage 1), implying that lake salinity was controlled neither by basin-wide moisture level nor by basin-wide precipitation. Instead, basin-wide low temperature during Climate Stage 1 (~2500–~1800 cal. BP) was most likely the contributing factor to the high salinity during Salinity Stage 1 (~2500–~1600 cal. BP). Low temperature during Climate Stage 1 might have significantly reduced the amount of ice-melt water inflowing to the lake, and the 200-year difference between low temperature and high salinity was most likely the delayed response time of lake salinity to temperature change.

The secondary salinity low from ~2200 to ~2000 cal. BP, as suggested by a trough in $\delta^{18}O_{car}$ values, superimposed on the generally high salinity level of Salinity Stage 1, was likely the delayed response of lake salinity to the considerably lowered moisture level (i.e., low A/C ratio) between ~2500 and ~2300 cal. BP. The salinity trough from ~1600 to ~1400 cal. BP, as suggested by a trough in carbonate concentration and somewhat corroborated by $\delta^{18}O_{car}$ values, was likely the delayed response of lake salinity to the considerably lowered moisture level (low A/C ratio) between ~1800 and ~1600 cal. BP. Generally speaking, the lake salinity is relatively insensitive to those relatively low-amplitude variations in moisture levels.

To sum up, the pollen-based reconstruction exhibits three stages of climate change in Balkhash Basin: cool-wet from ~2500 to ~1800 cal. BP, moderate from ~1800 to 650 cal. BP, and cooling and wetting during the past ~650 years, with the past ~100 being warm and dry. The first-order variation in lake salinity has been likely controlled by basin-wide temperature, with ~200 years of delayed response of lake salinity to basin-wide temperature. Low temperature within the basin raises the salinity level in the lake through reducing the ice-melt water supply to the lake. The second-order variation in the lake salinity seems to be modulated by pronounced variations in basin-wide moisture, with ~200 years of delayed response of lake salinity to basin-wide moisture variations. Those low-amplitude variations in basin-wide moisture levels left no detectable imprints in lake salinity proxy records.

Table 1
Radiocarbon dating results of Balkhash Lake core.

Sample ID	Depth (cm)	Dated material	$\delta^{13}C$ (‰)	^{14}C age (yr BP)	Carbon reservoir effect removed and calibrated age (2δ) (cal. yr BP)
BK-A-1	0–2	Bulk sediment	−24.1	910 ± 40	0
BK-A-2	50–52	Bulk sediment	−24.7	1151 ± 33	265–331
BK-A-3	100–102	Bulk sediment	−23.6	1390 ± 40	475–556
BK-A-4	150–152	Bulk sediment	−25.6	1336 ± 33	434–529
BK-A-5	200–202	Bulk sediment	−23.7	1570 ± 40	553–612
BK-A-6	248–250	Bulk sediment	−24.2	1640 ± 33	652–728
BK-A-7	300–302	Bulk sediment	−23.9	1410 ± 40	496–559
BK-A-8	350–352	Bulk sediment	−25.5	1473 ± 34	585–646
BK-A-9	400–402	Bulk sediment	−23.6	1870 ± 40	784–938
BK-A-10	450–452	Bulk sediment	−24.7	2134 ± 34	1168–1291
BK-A-11	500–502	Bulk sediment	−23.9	2624 ± 34	1545–1703
BK-A-12	550–552	Bulk sediment	−25.4	2736 ± 40	1692–1869
BK-A-13	600–602	Bulk sediment	−23.6	2920 ± 40	1876–2061
BK-A-14	610–612	Bulk sediment	−23.6	3040 ± 40	1995–2180
BK-A-15	650–652	Bulk sediment	−25.4	3061 ± 40	2038–2184
BK-A-16	750–752	Bulk sediment	−24.7	3239 ± 35	2307–2460
BK-A-17	850–852	Bulk sediment	−11.7	3271 ± 34	2330–2488

Acknowledgements

This paper is a result of research projects supported by four Chinese Nature Science Foundation grants (No.U1203821L08, No.40930102, No.40331102 and No. 0671190) and two U.S. National Science Foundation grants (NSF-BCS-06-23478 and NSF-ESH-04-02509). Thanks also go to two anonymous reviewers who provided extremely valuable comments on an earlier version of this paper.

References

Aizen, E.M., Aizen, V.B., Melack, J.M., Nakamura, T., Ohta, T., 2001. Precipitation and atmospheric circulation patterns at mid-latitudes of Asia. International Journal of Climatology 21, 535–556.

Anderson, D.M., Overpeck, J.T., Gupta, A.K., 2002. Increase in the Asian Southwest Monsoon during the past four centuries. Science 297, 596–599.

Aravena, R., Warner, B.G., MacDonald, G.M., Han, K.I., 1992. Carbonate isotope composition of lake sediments in relation to lake productivity and radiocarbon dating. Quaternary Research 37, 333–345.

Bauer, E., Claussen, M., Brovkin, V., 2003. Assessing climate forcing of the Earth system for the past millennium. Geophysical Research Letters 30 (6), 1276,. http://dx.doi.org/10.1029/2002GL016639.

Blyakharchuk, T.A., Wright, H.E., Borodavko, P.S., van der Knaap, W.O., Ammann, B., 2007. Late Glacial and Holocene vegetational history of the Altai Mountains (southwestern Tuva Republic, Siberia). Palaeogeography Palaeoclimatology Palaeoecology 245 (3–4), 518–534.

Boomer, I., Aladin, N., Plotnikov, I., Whatley, R., 2000. The palaeolimnology of the Aral Sea: a review. Quaternary Science Reviews 19, 1259–1278.

Boomer, I., Wunnemann, B., Mackay, A.W., Austin, P., Sorrel, P., Reinhardt, C., Keyser, D., Guichard, F., Fontugne, M., 2009. Advances in understanding the late Holocene history of the Aral Sea region. Quaternary International 194, 79–90.

Bothe, O., Fraedrich, K., Zhu, X., 2011. Precipitation climate of Central Asia and the large-scale atmospheric circulation. Theoretical Applied Climatology. http://dx.doi.org/10.1007/s00704-011-0537-2.

Bridgman, B.H., Oliver, J.E., 2006. The Global Climate System: Patterns, Processes, and Teleconnections. Cambridge University Press, New York, p. 243.

El-Mosilimany, A.P., 1990. Ecological significance of common non-arboreal pollen: examples from drylands of the Middle East. Review of Palaeobotany and Palynology 64, 343–350.

ESA and UCLouvain, 2010. The Globe Coverage 2009 Project. http://dup.esrin.esa.it/globcover.

Gasse, F., Fontes, J.C., Plaziat, P., Carbonel, P., Kaczmarska, I., De Deckker, P., Soulie-Marsche, I., Callot, Y., Dupeuble, P.A., 1987. Biological remains, geochemistry and stable isotope for the reconstruction of environmental and hydrological changes in the Holocene lakes from north Sahara. Palaeogeography Palaeoclimatology Palaeoecology 60, 1–46.

Geel, B.V., Bokovenko, N.A., Burova, N.D., Chugunov, K.V., Dergachev, V.A., Dirksen, V.G., Kulkova, M., Nagler, A., Parzinger, H., van der Plicht, J., Vasiliev, S.S., Zaitseva, G.I., 2004. Climate changes and the expansion of the Scythian culture after 850 BC: a hypothesis. Journal of Archaeological Sciences 31, 1735–1742.

Gong, D.Y., Wang, S.W., Zhu, J.H., 2001. East Asian winter monsoon and Arctic Oscillation. Geophysical Research Letters 28 (10), 2073–2076.

Gou, L.D., Xia, Z.Q., Li, J., Tang, Z.J., 2008. Climatic characteristics within Balkhash Basin. Journal of Hohai University 36 (3), 316–321.

Grimm, E.C., 1990. Tilia and Tilia graph PC spreadsheet and graphics software for pollen data. INQUA Working Methods Newsletter 4, 5–7.

Guiot, J., Harrison, S.P., Prentice, T.C., 1993. Reconstruction of Holocene patterns of moisture in Europe using pollen and lake-level data. Quaternary Research 40, 139–149.

Heorling, M.P., Hurrell, J.W., Xu, T., 2001. Tropical origins for recent North Atlantic climate change. Science 292, 90–92.

Holme, J.A., Cook, E.R., Yang, B., 2009. Climate change over the past 2000 years in Western China. Quaternary International 194, 91–107.

Huang, X.T., Oberhänsli, H., von Suchodoletz, H., Sorrel, P., 2011. Dust deposition in the Aral Sea: implications for changes in atmospheric circulation in central Asia during the past 2000 years. Quaternary Science Reviews 30, 3661–3674.

Jiang, W.Y., Guiot, J., Chu, G.Q., 2009. An improved methodology of the modern analogues technique for palaeoclimate reconstruction in arid and semi-arid regions. Boreas 39, 145–153.

Jones, M.D., Roberts, C.N., Leng, M.J., Turkes, M., 2006. A high-resolution late Holocene lake isotope record from Turkey and links to North Atlantic and monsoon climate. Geology, 34,361–34,364.

Kroonenberg, S.B., Abdurakhmanov, G.M., Badyukova, E.N., van der Borg, K., Kalashnikov, A., Kasimov, N.S., Rychagov, G.I., Svitoch, A.A., Vonhof, H.B., Wesselingh, F.P., 2007. Solar-forced 2600 BP and Little Ice Age highstands of the Caspian Sea. Quaternary International 173/174, 137–143.

Li, H.C., Ku, T.L., 1997. $\delta^{13}C$ and $\delta^{18}O$ covariance as a paleohydrological indicator for closed-basin lakes. Palaeogeography Palaeoclimatology Palaeoecology 133, 69–80.

Liu, X.Q., Herzschuh, U., Shen, J., Jiang, Q.F., Xiao, Y.X., 2008. Holocene environmental and climatic changes inferred from Wulungu Lake in northern Xinjiang, China. Quaternary Research 70, 412–425.

Lioubimtseva, E., Cole, A., 2006. Uncertainties of climate change in arid environments of Central Asia. Reviews of Fisheries Science 14, 14–29.

Lydolph, P.E., 1977. Climates of the Soviet Union. Elsevier Scientific Publishing Co, New York, p. 115.

Maasch, K.A., Mayewski, P.A., Rohling, E.J., Stager, J.C., Karlen, W., Meeker, L.D., Meyerson, E.A., 2005. A 2000-year context for modern climate change. Geografiska Annaler 87 (A), 1–15.

Mann, M.E., Zhang, Z.H., Rutherford, S., 2009. Global signature and dynamical origins of the Little Ice Age and Medieval Climate Anomaly. Science 326, 1256–1260.

Meeker, L.D., Mayewski, P.A., 2002. A 1400-year high-resolution record of atmospheric circulation over the North Atlantic and Asia. The Holocene 12 (3), 257 -266.

Moore, P.D., Webb, J.A., Collinson, M.E., 1991. Pollen Analysis. Blackwell Science, Oxford.

Petr, T., 1992. Lake Balkhash, Kazakhstan. International Journal of Salt Lake Research 1 (1), 21–46.

Propastin, P., 2011. Patterns of Lake Balkhash water level changes and their climatic correlation during the period of 1992–2010. Lakes and Reservoirs Research and Management 17, 161–169.

Reimer, P.J., Baillie, M.G.L., Bard, E., 2009. IntCal09 and Marine09 radiocarbon age calibration curves, 0–50,000 years cal BP. Radiocarbon 51, 1111–1150.

Rudaya, N., Tarasov, P., Dorofeyuk, N., Solovieva, N., Kalugin, I., Andrew, A., Dryin, A., Diekmann, B., Riedel, F., Tserendash, N., Wagnere, M., 2009. Holocene environments and climate in the Mongolian Altai reconstructed from the Hoton-Nur pollen and diatom records: a step towards better understanding climate dynamics in central Asia. Quaternary Science Reviews 28, 540–554.

Ruddiman, W.F., 2008. Earth's Climate, Past and Future, third ed. Freeman and Company, New York, p. 420.

Shi, Y.F., Kong, Z.C., Wang, S.M., 1993. Mid-Holocene climates and environments in China. Global and Planetary Change 7, 219–233.

Song, C.Q., Lu, H.Y., Sun, X.J., 1997. modern pollen-climate quantitative relationships in North China and their applications. Chinese Science Bulletin 42 (20), 2182–2186.

Sorrel, P., Popescu, S.M., Head, M.J., Suc, J.P., Klotz, S., Oberhänsli, H., 2006. Hydrographic development of the Aral Sea during the last 2000 years based on quantitative analyses of dinoflagellate cysts. Palaeogeography Palaeoclimatology Palaeoecology 234, 304–327.

Sorrel, P., Popescu, S.M., Klotz, S., Suc, J.P., Oberhänsli, H., 2007. Climate variability in the Aral Sea basin (Central Asia) during the late Holocene based on vegetation changes. Quaternary Research 67, 357–370.

Staubwasse, M., Weiss, M., 2006. Holocene climate and cultural evolution in late prehistoric-early historic West Asia. Quaternary Research 66, 372–387.

Tarasov, P.E., Webb, I.I.I.T., Andreev, A.A., 1998. Present-day and mid-Holocene biomes reconstructed from pollen and plant macrofossil data from the former Soviet Union and Mongolia. Journal of Biogeography 25, 1029–1053.

Tarasov, P., Bezrukova, E., Karabanov, E., Nakagawa, T., Wagner, M., Kulagina, N., Letunova, P., Abzaeva, A., Granoszewski, W., Riedel, F., 2007. Vegetation and climate dynamics during the Holocene and Eemian interglacials derived from Lake Baikal pollen records. Palaeogeography Palaeoclimatology Palaeoecology 252 (3–4), 440–457.

Van Campo, E., Cour, P., Sixuan, H., 1996. Holocene environmental changes in Bangong Co. Basin (western Tibet): part 2, the pollen record. Palaeogeography Palaeoclimatology Palaeoecology 120, 49–63.

Wang, F.X., Qian, N.F., Zhang, Y.L., 1995. Pollen Flora of China, second ed. Science Press, Beijing, p. 180 (in Chinese).

Wen, R.L., Xiao, J.L., Ma, Y.Z., Feng, Z.-D., Li, Y.C., Xu, Q.H., 2013. Pollen–climate transfer functions intended for temperate eastern Asia. Quaternary International (in this volume).

Yang, B., Brauning, A., Johnson, K.R., Shi, Y., 2002. General characteristics of temperature variation in China during the last two millennia. Geophysical Research Letters 29 (9). http://dx.doi.org/10.1029/2001GL014485.

Yang, B., Wang, J.S., Brauning, A., Dong, Z.B., Esper, J., 2009. Late Holocene climatic and environmental changes in arid central Asia. Quaternary International 194, 68–78.

Zhang, C.J., Feng, Z.-D., Yang, Q.L., Gou, X.H., 2010. Carbon- and carbonate-related proxies-recorded Holocene climatic variations in Bosten Lake of the Tarim Basin. The Holocene 20 (3), 263–273.

Zhao, Y., Yu, Z.C., Chen, F.H., Zhang, J.W., Yang, B., 2009. Vegetation response to Holocene climate change in monsoon-influenced region of China. Earth-Science Reviews 97, 242–256.

Zhao, Y., Liu, H.Y., Li, F.R., Huang, X.Z., Sun, J.H., Zhao, W.W., Herzschuh, U., Tang, Y., 2012. Application and limitations of the *Artemisia*/Chenopodiaceae pollen ratio in arid and semi-arid China. The Holocene 22, 1385–1392.

附录六

Contents lists available at ScienceDirect

Quaternary International

journal homepage: www.elsevier.com/locate/quaint

Vegetation changes and associated climate variations during the past ~38,000 years reconstructed from the Shaamar eolian-paleosol section, northern Mongolia

Yuzhen Ma [a,b,*], Kam-biu Liu [c], Zhaodong Feng [d], Hongwei Meng [a], Yanli Sang [d], Wei Wang [e], Hucai Zhang [f]

[a] Key Laboratory of Environmental Change and Natural Disaster, Ministry of Education of China, Beijing Normal University, Beijing 100875, China
[b] State Key Laboratory of Earth Surface Processes and Resource Ecology, Beijing Normal University, Beijing 100875, China
[c] Department of Oceanography and Coastal Sciences, School of the Coast and Environment, Louisiana State University, Baton Rouge, LA 70803, USA
[d] Laboratory of Climatic and Environmental Changes in Arid Lands, Xinjiang Institute of Ecology and Geography, Urumqi 830011, China
[e] College of Resources and Environment Sciences, Inner Mongolia University, Huhhot 010021, China
[f] Research Laboratory of Plateau Lake Ecology and Global Change, Yunnan Normal University, Kunming 650500, China

ARTICLE INFO

Article history:
Available online 12 September 2013

ABSTRACT

This study presents a pollen-based reconstruction of the vegetation changes and associated climate variations at the Shaamar eolian-paleosol section in the northern Mongolian Plateau. The semi-quantitative reconstructions of paleovegetation types and temperature and moisture indices show that the vegetation in the Shaamar area was a taiga forest dominated by *Picea*, *Abies*, and *Pinus sibirica*-type between ~38,000 and ~30,000 cal. BP when the reconstructed moisture level was the highest of the past ~38,000 years. The vegetation during the ensuing period from ~30,000 to ~23,000 cal. BP was mainly a steppe dominated by *Artemisia* and Poaceae under low temperature and relatively low moisture conditions. The vegetation during the period from ~23,000 to ~10,000 cal. BP varied from a taiga forest, through steppe (dominated by Poaceae), taiga forest and forest steppe, to a taiga forest. The climate was cold and relatively dry in the early phase (~23,000 to ~20,000 cal. BP) and warmer and somewhat drier in the later phase (~19,000 to ~11,000 cal. BP). The pollen assemblages and the vegetation zonal indices suggest that the vegetation was a forest-steppe during the period from ~10,000 to ~3000 cal. BP under rising temperature and low moisture conditions. A taiga forest has dominated the landscape during the past ~3000 years under cooling and wetting conditions. Comparison of our pollen record with other paleoclimatic records suggests that the climate changes in the northern Mongolian Plateau have been controlled or modulated by ocean-atmospheric coupling dynamics in the North Atlantic region.

© 2013 Elsevier Ltd and INQUA. All rights reserved.

1. Introduction

1.1. Significance of climatic change in the northern Mongolian Plateau

The Earth's climatic systems of the past ~40,000 years have experienced dramatic variations on orbital and suborbital timescales, and this time frame includes the later part of Glacial Interstadial MIS 3 (~57,000 to ~25,000 cal. BP), Glacial Stadial MIS 2 (~25,000 to ~11,500 cal. BP), and Recent Interglacial MIS 1 or the Holocene (~11,500 cal. BP to present) (Berger and Loutre, 1991; Clemens et al., 1996; Bradley, 1999; Ruddiman, 2008). The systems have also experienced more dramatic variations on millennial and centennial timescales, as exemplified by the widely-reported Heinrich events with a quasi-periodicity of ~6000 years and the Dansgaard-Oeschger (D-O) oscillations with a quasi-periodicity of ~1500 years (Dansgaard et al., 1993; Bond et al., 1997, 2001; Bard et al., 2000; Wang et al., 2001; Alley et al., 2002; Yuan et al., 2004).

Although our knowledge regarding those orbital-scale and suborbital-scale climatic variations has been accumulated in an accelerated rate during the past half century, these events are still geographically unevenly documented and thus inadequate in depicting a reasonable global portrait. The northern Mongolian Plateau within Mongolia is one of the areas where our knowledge

* Corresponding author. Key Laboratory of Environmental Change and Natural Disaster, Ministry of Education of China, Beijing Normal University, No.19, XinjieKouWai St., HaiDian District, Beijing 100875, China.
E-mail addresses: mayzh@bnu.edu.cn (Y. Ma), kliu1@lsu.edu (K.-b. Liu), fengzd@lzu.edu.cn (Z. Feng), lzwangwei@sina.com (W. Wang), hucaizhang@yahoo.com (H. Zhang).

1040-6182/$ – see front matter © 2013 Elsevier Ltd and INQUA. All rights reserved.
http://dx.doi.org/10.1016/j.quaint.2013.08.037

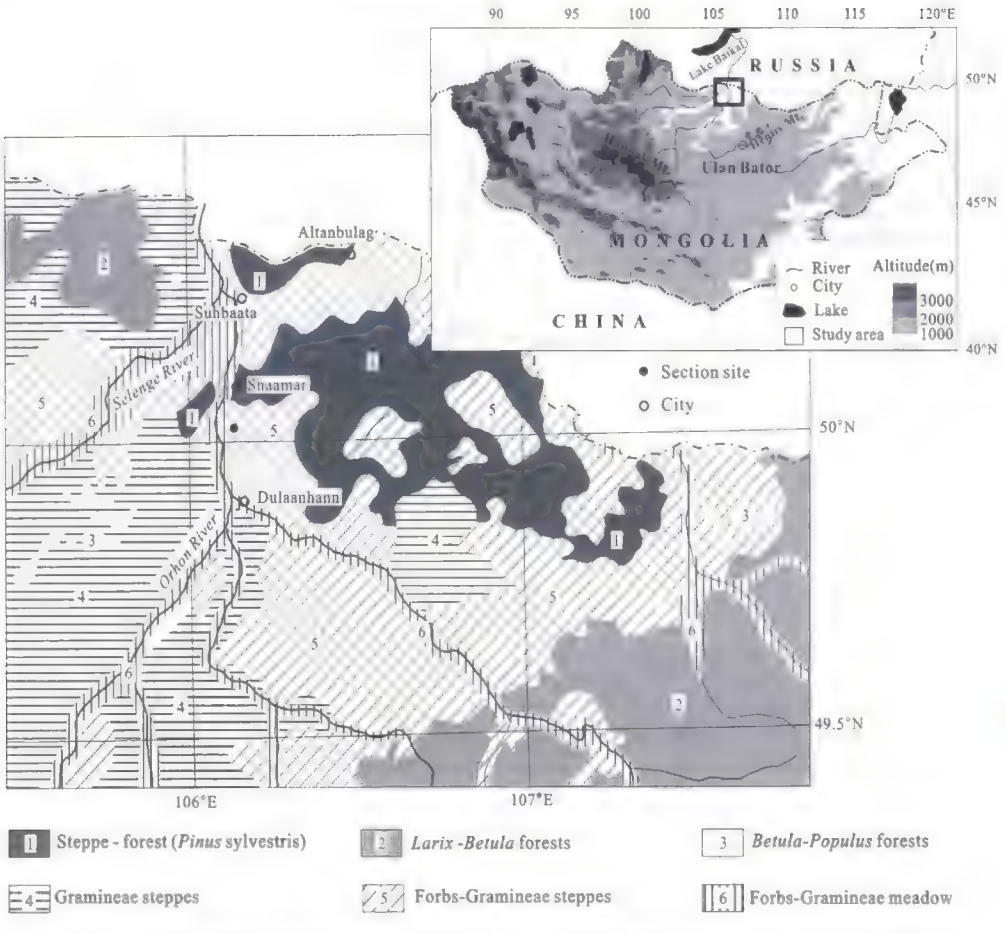

Fig. 1. Map showing the studied section site (i.e., Shaamar eolian-paleosol section) and regional vegetation (based on Lavrenko et al., 1979; Hilbig, 1995).

regarding these orbital-scale and suborbital-scale climatic variations is inadequate. Specifically, there are no high-resolution and well-dated sequences covering the late Pleistocene at all. Although the Holocene climatic variations have been recently investigated intensively by several teams (e.g., Tarasov et al., 2000; Peck et al., 2002; Fowell et al., 2003; Feng et al., 2005; Prokopenko et al., 2007; Rudaya et al., 2009; Wang et al., 2009, 2011; Zhang et al., 2012), the temporal-spatial patterns of the Holocene climatic variations in the northern Mongolian Plateau are still topics of heated debate. For example, Rudaya et al. (2009) lent support to an earlier argument by Harrison et al. (1996) and Tarasov et al. (2000) that the East Asian monsoon must have had a strong influence on most parts of the northern Mongolian Plateau during the Holocene. On the other hand, Chen et al. (2008) argued that the entire Central Asian Arid Zone (CAAZ) including the northern Mongolian Plateau has been controlled by the westerlies during the Holocene.

This study focuses on the pollen-based reconstruction of vegetation changes and associated climate variations at the Shaamar eolian-paleosol section (~30 m thick) in the northern Mongolian Plateau and also on its comparison with monsoon-related records from China and with westerlies-related records from the North Atlantic region. It is hoped that earlier depictions of global climate changes (e.g., CLIMAP Members, 1981; COHMAP Members, 1988) can be refined and that our understanding of the climate dynamics affecting the northern Mongolian Plateau during the past ~40,000 years can be improved.

1.2. Study area

Eolian deposits (48–53° N, 104–108° E) almost completely cover the topographical corridor stretching from Ulan Bator in the south to Lake Baikal in the north situated in the interior of the Asian continent (Khosbayar, 1989; Logatchov, 1989), and the topographical corridor is flanked by the Hentiy Mountains in the east and by the Hangay Mountains in the west (Fig. 1). Twelve eolian sections were reconnoitered, and four of them were investigated intensively by Feng's team (Feng et al., 1998, 2005, 2007a; Feng, 2001; Feng and Khosbayar, 2004). The results show that the eolian deposits have more or less continuously documented the bioclimatic history of the Late Pleistocene (i.e., past ~50,000 years).

At the present, the annual precipitation ranges from 250 mm in the south to 400 mm in the north and the mean annual

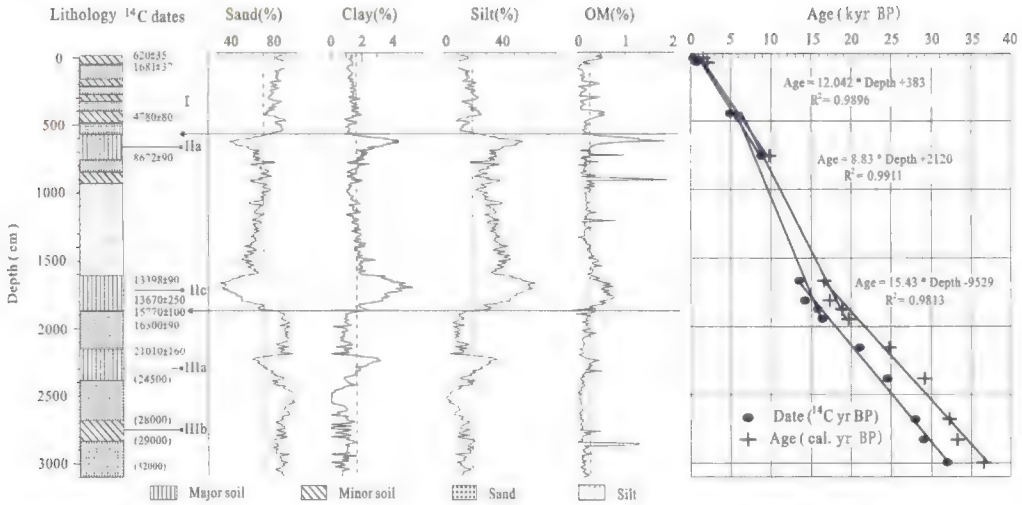

Fig. 2. Stratigraphy and depth-age model for Shaamar eolian-paleosol section (including sand%, Clay%, Silt% and OM%, from Feng et al., 2007a).

temperature ranges from 0 to −2 °C within the corridor. The January temperature varies between −20 and −24 °C and July temperature between 12 and 17 °C. The corridor is mainly covered with forest-steppes (Fig. 1), although coniferous forests occur on north-facing slopes and at higher elevations, and steppes and meadow steppes are present on south-facing slopes and lower elevations. The steppe vegetation is dominated by bunchgrasses (e.g., *Festuca lenensis, Koeleria macrantha, K. gracilis, Poa attenuate, Agropyrum cristatum and Stipa krylovii*) and *Artemisia* species (e.g., *Artmisia frigida, A. argyrophylla, A. borealis*). Other common herbaceous species include, *Aster alpinus, Saussurea salicifalre, Thalictrum foetidum, Astragalus brevifolius, Oxytropis pumila, Potentilla sericea, Stellera chamaejasme*, and *Polemonium coeruleum* (Lavrenko et al., 1979; Hilbig, 1995). The forest is dominated by *Larix sibirica* with some companion tree species including *Pinus sibirica, Pinus sylvestris, Betula rotundifolia, Rosa acicularis, Juniperus sibirica, Picea*, and *Populus*. Hygrophilous grasses and perennial forbs are quite common along the waterways and in the topographic depressions, including *Calamagrostis obtusata, Polygonum viviparum*, Caryophyllaceae, Cyperaceae, Ranunculaceae, Saxifragaceae, and Umbelliferae. It should be particularly noted that the sandy soil-mantled terraces along the Selenga and Orhon rivers are covered by steppe-forest type of vegetation. The forest component is dominated by *Pinus sylvestris* trees, often accompanied by *Pinus sibirica, Ulmus pumila*, and *R. acicularis* shrubberies, and the steppe component is dominated by meadow steppe species (e.g., *Poa nemoralis, Artemisia laciniata, Carex korshinskyi*, Ranunculaceae, and *Polygonum angustifolium*).

2. Material and methods

2.1. Stratigraphy and chronology

The Shaamar eolian-palaeosol section (50.2°N, 105.2°E, 650 m a.s.l.) is a natural outcrop of ~30 m in thickness above the riverbed on the southern bank of the Selenga River (Fig. 1). The section was lithostratigraphically divided into three units (see Feng et al., 2007a for details). Unit I (0–550 cm) is a sand-dominated layer, Unit II (550–1850 cm) a silt-sand layer, and Unit III (1850–3090 cm) a sand layer (Fig. 2). Pedostratigraphically, there are three major paleosols (IIa, IIc and IIIa) marked by high silt and clay contents and also by high percentages of organic matter and carbonate and six minor paleosols characterized by increased organic carbon contents (see Feng et al., 2007a for details).

Totally, 11 AMS and conventional ^{14}C dates were obtained and they were measured at the NSF-AMS Facility at the University of Arizona and Radiocarbon Dating Laboratory of Lanzhou University (Table 1). The age of sand unit from 2400 cm to the bottom of the section (3090 cm) can be extrapolated from two dates: 15771 ^{14}C BP at the bottom of major paleosol IIc (1890 cm) and 21010 ^{14}C BP at the top of major paleosol IIIa (2170 cm), assuming that the depositional rate was relatively constant throughout the sand unit (i.e., Unit 3: 1850–3090 cm). This assumption seems to be supported by the fact that the grain size of the sand unit (i.e., Unit 3: 1850–3090 cm) varies insignificantly. The age of IIIa and IIIc can be inferred based on the calculated depositional rate (i.e., 1 cm = 11 yr) of the major paleosol IIc unit (13,398 ^{14}C BP at 1680 and 15,770 ^{14}C BP at 1890 cm) and the date of the stratigraphically correlative paleosol at nearby Bureghhanga section (Feng et al., 2007a). The major paleosol IIIa (2170–2400 cm) is dated at 21,010 ^{14}C BP at its top (2170 cm). The bottom of the major paleosol IIIa is extrapolated to be approximately 24,500 ^{14}C BP based on the calculated depositional rate (i.e., 1 cm = 11 yr) of the major paleosol IIc and a date (24,500 ^{14}C BP) of a stratigraphically correlative paleosol at nearby Bureghhanga section (Feng et al., 2007a). The minor paleosol (2700–2850 cm) is extrapolated to be approximately 28,000 ^{14}C BP at its top (2700 cm) based on the calculated depositional rate (i.e., 1 cm = 18 yr) of the sand unit between the paleosol IIc (15,770 ^{14}C BP at 1890 cm) and paleosol IIIa (21,010 ^{14}C BP at 2170 cm). And its bottom of the minor paleosol (2700–2850 cm) is inferred to be about 29,000 ^{14}C BP based on the calculated depositional rate (i.e., 1 cm = 11 yr) and a date (28,900 ^{14}C BP) of a stratigraphically correlative minor paleosol at nearby Bureghhanga section (Feng et al., 2007a). Also the base (at 3020 cm deep) of the section is extrapolated to be approximately 32,000 ^{14}C BP based on the calculated depositional rate (i.e., 1 cm = 18 yr) of the sand unit. The Holocene portion of the Shaamar section is actually an eolian-paleosol complex containing one major paleosl (IIa) and four minor paleosols (Ia, Ib, Ic, Id). The major paleosol IIa (550–760 cm) is dated at 8672 ^{14}C BP at its bottom (760 cm). The minor paleosol (Id) at the depth of 400–500 cm is dated at 4780 ± 80 ^{14}C BP in the middle (450 cm). A clinosol-amplified "top" soil (Ia) was found at

the foothill of the Shaamar gully and three sub-paleosols within the top soil (1a) were AMS dated (on charcoals) at 620 ± 35, 1423 ± 35 and 1681 ± 37 ^{14}C BP, respectively (Feng et al., 2007a).

pollen assemblages (Liu and Lam, 1985; MacDonald and Ritchie, 1986; Sugden and Meadows, 1989). It is used here to validate the reconstructed vegetation history by fossil pollen assemblages

Table 1
^{14}C dates of Shaamar eolian section (AMS dates were measured at NSF AMS Facility at University of Arizona, USA; conventional dates were measured at ^{14}C Dating Laboratory of Lanzhou University, China) (adopted from Feng et al., 2007a).

Sample no.	Lab No.	Depth (cm)	Material	Method	$\delta^{13}C$(‰)	Date (^{14}C yr BP)	Age (cal yr BP)
SH02-C14-06	AA51936	50	Charcoal	AMS	−24.8	620 ± 35	620
SH02-C14-02	AA51935	60	Charcoal	AMS	−23.1	1681 ± 37	1608
4th Paleosol	CG-3465	450	Sediment	Conventional	N/A	4780 ± −80	5542
MN-C14-14	AA519328	760	Sediment	AMS	−25.9	8672 ± −90	9706
MN-C14-11	AA519325	1680	Sediment	AMS	−24.4	13,398 ± −99	15,780
6th Paleosol	CG-3466	1850	Sediment	Conventional	N/A	13,670 ± 80	16,200
MN-C14-9	AA519323	1890	Sediment	AMS	−22.8	15,770 ± 90	18,900
MN-C-14-8	AA519322	1960	Sediment	AMS	−22.3	16,330 ± −100	19,000
MN-C14-6	AA519320	2170	Sediment	AMS	−14.3	21,010 ± −160	24,610
7th Paleosol	CG9811	2400	Sediment	Conventional	N/A	24,500 ± 710	29,290
8th Paleosol	CG9812	2800	Sediment	Conventional	N/A	28,900 ± 1420	33,290

Chronostratigaphically, the section can be divided into three segments approximately corresponding with the three lithostratigraphic units. The first segment spans from the surface (0 cm) to 760 cm with bracketing ages of ~0 and ~8700 ^{14}C BP.; the second segment from 450 to 1850 cm with bracketing ages of ~4800 and ~15,800 ^{14}C BP; and the third segment from 1680 to 3090 cm with bracketing ages of ~13,400 and ~32,000 ^{14}C BP. The three-segment-based depth-age models (Fig. 2) were used to "date" each one of the 65 samples and the model-resulted dates of 65 pollen samples were then calibrated using 2σ probability ranges in CALIB 6.0 and INTCAL 09 (Reimer et al., 2009). A note should be added here regarding the sedimentation rate. As shown in Fig. 2, the first and third segments (i.e., sand-dominated layers) have lower sedimentation rates than the second segment (a silt-dominated layer). The lower sedimentation rates for sand units suggest that some deflation might have occurred in sand-dominated layers.

2.2. Pollen analysis

Sixty-five (65) samples were obtained from the Shaamar section and the analytical intervals were 25 cm in the three major paleosols and 50 cm in other units for pollen analysis. One *Lycopodium* marker spore (University of Lund, batch 938934) tablet was added to each sample for calculating total pollen and spore concentrations prior to processing. The samples were processed using HCl (10%) and HF (36%). Furthermore, the pollen in the residue was concentrated with a 7 um mesh sieve in conjunction with ultrasonic vibration. Finally, water-free glycerol was used for storage and preparation of microscopic slides.

Pollen identification and counting was carried out using a Leica light-microscope under 400 × magnifications. A minimum of 100 pollen grains were counted for each of the samples. Pollen identification was achieved with the help of published pollen books and papers (Moore et al., 1991; Wang et al., 1995; Ma et al., 2009) and also with reference to an extensive modern pollen collection of more than 500 plant species from Mongolia and northern China. Pollen percentages are calculated from a total pollen sum. Graph and CorelDraw software are used for map plotting pollen diagrams (Fig. 3).

2.3. Data analyses

2.3.1. Statistical analyses

Discriminant analysis is a mathematical technique used to measure the degree of similarity between modern and fossil (Fig. 3) and to identify modern analogues from the fossil pollen spectra (Figs. 4 and 5). SPSS software was used for discriminant analysis of pollen spectra.

The vegetation types, the probability of modern analogue, and the vegetation zonal index (Liu and Lam, 1985) are calculated (Figs. 4 and 5) for both the fossil pollen samples from the Shaamar section (data of this study) and the modern pollen samples from the N–S transect across Mongolia (data from Ma et al., 2008). It should be particularly mentioned that two assumptions are made in discriminant analysis: (1) relatively high Poaceae percentage (>10%) in the pollen spectra indicates the existence of steppe vegetation and (2) considerably high percentages of *Picea* + *Abies* (>30%) indicate taiga vegetation. The assumptions are based on following two observations. First, a modern pollen rain study has documented that Poaceae pollen is extremely under-represented (<5–10%) in the surface pollen assemblages from the overgrazed steppes and forest-steppes of Mongolia due to human disturbance (Ma et al., 2008). Second, the fossil pollen percentages of *Picea* + *Abies* within some pollen zones in the Shammar section seem to be much higher than the pollen percentages of *Picea* + *Abies* typically found in the modern pollen transect across Mongolia (Ma et al., 2008).

2.3.2. Pollen-based temperature and moisture indices

Ma et al. (2008) proposed a set of temperature index (*T*) and moisture index (*M*) based on a surface pollen data generated along a S–N transect (42.5–51.5 °N) in the northern Mongolian Plateau. These two indices (T and M) are calculated based on the ratios between groups of pollen taxa that represent different moisture and temperature conditions in the northern Mongolian Plateau. These groups of climate-sensitive pollen taxa are classified based on the results of hierarchical cluster analysis (HCA) and non-metric multidimensional scaling (NMS) methods and six vegetation groups were identified (Ma et al., 2008). The calculated S–N trends of modern pollen-based T and M indices are generally in good agreement with the S–N trends of the present-day temperature and precipitation in the northern Mongolian Plateau, thereby confirming the suitability of these pollen-based indices for assessing the histories of temperature and moisture variations in the Shaamar area. Following the same methodology, a semi-quantitative set of Temperature and Moisture indices (Table 2 and Fig. 5) was used in this paper to reconstruct the climatic history in Shaarmar area. It should be noted that minor modifications were made to accommodate differences in recorded pollen taxonomic diversity and geobotanical characteristics between the two regions.

Table 2
Six pollen taxon groups (S1–S6) used for calculation of temperature index (T) and moisture index (M) (after Ma et al., 2008).

Group	Type	Main pollen taxa
S1	Xeromorphic desert	Chenopodiaceae, *Nitraria*, Zygophyllaceae (*Tribulus*, Zygophyllum, *Peganum*)
S2	Desert-steppe	Polemoniaceae, *Anthemis* –type, *Ephedra*, *Convolvulus*
S3	Meso-xeromorphic steppe	*Artemisia*, *Aster*-type, *Stellera*, Campanulaceae,
S4	Birch forest/shrube	*Betula*, *Ainus*, Rosaceae, *Salix*/*Ulmus*, *Taraxacum*-type
S5	Cold - moist needled forest	*Picea* + *Abies*, *Juniperus*, *Pinus sibirica*-type, *Pinus sylvestris*-type Ranunculaceae, Caryophyllaceae,
S6	Moderate hydroperiod steppe	Cyperaceae, Polygonaceae
	Pollen-climate indices	**Calculation**
T	Temperature index	$T-(P_{S1}+P_{S2}+P_{S3})/(P_{S4}+P_{S5}+P_{S6})$
M	Moisture index	$M-(P_{S5}+P_{S6})/(P_{S1}+P_{S2}+P_{S3}+P_{S4})$

3. Results and interpretation

3.1. Pollen spectra

The pollen record from the Shaamar section can be divided into seven zones based on the fossil pollen spectra (Fig. 3).

Zone 1 (3100–2540 cm, ~38,000–~29,600 cal. BP) is notable for its highest percentages of taiga forest components including *Picea* + *Abies* (mostly 11.36–60.66%) and *Pinus sibirica*-type (mostly 8.89–40.71%) with relatively high pollen concentrations. Other coniferous forest components (e.g., *Pinus sylvestris*-type, *Larix*, and Cupressaceae) are also well represented. The percentages of herb and summer-green tree components are extremely low.

Zone 2 (2540–2150 cm, ~29,600–~23,400 cal. BP) is marked by an increases in the pollen percentages of herb components including *Artemisia* (3.77–43.01%), Poaceae (4.72–27.27%), and Chenopodiaceae (3.03–22.73%), at the expense of taiga forest components such as *Pinus sibirica*-type (1.85–11.61%) and *Picea* + *Abies* (4.84–35.53%). Chenopodiaceae reaches the highest percentages of the entire section accompanied by low pollen concentrations and a negligible amount of summer-green tree pollen.

Zone 3 (2150–1850 cm, ~23,400–~18,700 cal. BP) is depicted by notable increases in the percentages of *Picea* + *Abies* pollen (9.93–85.60%), accompanied by decreased percentages of Poaceae (0.79–15.79%) and *Artemisia* (5.60–17.88%). The summer-green tree pollen is barely detectable and the pollen concentrations are relatively low.

Zone 4 (1850–1610 cm, ~18,700–~16,200 cal. BP) contains the highest percentages of Poaceae pollen (5.91–44.50%) of the entire section with relatively high pollen concentrations. *Aster*-type and *Artemisia* pollen are consistently present. The percentages of xeromorphic plant pollen (including Chenopodiaceae, *Nitraria*, Zygophyllaceae, and *Tamarix*) are noticeably low with barely detectable amounts of summer-green tree pollen.

Zone 5 (1610–800 cm–16,200–~9700 cal. BP) is dominated by high-frequency and high-amplitude variations in percentages of *Picea* + *Abies* (4.48–59.65%), *Aster*-type (4.54–37.61%), Poaceae (0.96–49.44%) and *Taraxacum*-type (1.75–52.99%) with low pollen concentration. Commonly appeared herbs include *Artemisia*and and Chenopodiaceae. This Zone can be divided into three subzones.

The upper subzone (1610–1450 cm, ~16,200–~15,000 cal. BP) and the lower subzone (1010–800 cm, ~11,700–~9700 cal. BP) are characterized by higher percentages of *Picea* + *Abies* (4.48–59.65%) and *Pinus* (<30.00%) with extremely low pollen concentrations. The middle zone (1450–1010 cm, ~15,000–~11,700 cal. BP) is distinguishable by a dramatic rising in the percentages of *Aster*-type (6.94–37.61%) with relatively high pollen concentrations. Furthermore, desert pollen taxa such as Zygophyllaceae and *Tamarix* are found in trace amounts and the percentages of *Pinus sibirica*-type pollen and *Pinus sylvestris*-type pollen decline in the middle subzone.

Zone 6 (800–240 cm, ~9700–~3200 cal. BP) is characterized by four features: (1) relatively low percentages of *Picea* + *Abies*, (2) abrupt appearance of several mesophytic herbs (including *Stellera*, Campanulaceae, Papaveraceae, Ranunculaceae and Polemoniaceae), (3) a dramatic increase in pollen concentration, and (4) absence of summer-green tree pollen.

Zone 7 (240–0 cm, ~3200–~0 cal. BP) is marked by increases in pollen percentages of *Picea* + *Abies* (10.21–31.47%), *Pinus sibirica*-type (14.15–44.23%), and *Pinus sylvestris*-type (14.47–45.41%) with relatively high pollen concentrations. Both xeromorphic herbs (e.g., Chenopodiaceae, Zygophyllaceae, and *Tamarix*) and mesophytic herbs (e.g., Campanulaceae, Papaveraceae and Ranunculaceae) decrease drastically, whereas *Aster*-type increases slightly. Pollen of all summer-green trees almost completely disappears.

3.2. Result of statistical analyses

In order to substantiate that the modern pollen–vegetation relationship can be applied to aid interpretation of the fossil pollen data, the discriminant scores for the fossil pollen spectra were plotted along the first two discriminant functions and compared with those of the surface samples from five vegetation regions along the S–N transect across Mongolia (Ma et al., 2008) (Fig. 4).

All five group centroids of surface samples (i.e., taiga, forest-steppe, steppe, desert-steppe, and desert) are distinguishable from each other on the first two discriminant function axes, although some overlap exists between the taiga and the forest-steppe groups, and the desert group is more distinctly separate from the other groups (Fig. 4). Among the fossil pollen spectra, most samples from the fossil pollen zones 1, 2, 3, 4 and 7 of the Shaamar section fall within or are close to the ranges of four of the modern vegetation groups (except desert) developed along the S–N transect across Mongolia, suggesting that in some degrees the fossil pollen groups are analogous to the modern pollen rain representative of these vegetation types. It should be noted that the most of fossil samples from zone 5 are close to both steppe group and steppe-forest group. It should also be noted that the fossil samples from zone 6 is close to the modern range of the forest-steppe group, but nearly all of the samples fall outside of the range.

The probability of modern analogue and the vegetation zonal index were calculated and plotted for each fossil pollen samples. Fig. 5 shows that most of pollen samples have high values of probability of modern analogue (>0.5), suggesting that they are typical for the major vegetation types that they are assigned. The misclassified samples generally have very low values (<0.2) of probability of modern analogue, indicating that they are far away from their group centroids and thereby atypical of their assigned vegetation types (Liu and Lam, 1985; Reese and Liu, 2005). The results of discriminant analysis therefore suggest that modern analogues can be identified for the fossil pollen spectra from the Shaamar section based on a comparison with the modern pollen samples derived from the S–N transect across Mongolia.

3.3. Interpretations

Based on the pollen assemblages, the semiquantitatively-inferred paleovegetation types and the pollen-based temperature and moisture indices (Figs. 3 and 5), it is possible to reconstruct the history of vegetation changes and associated climate variations during the past ~38,000 years.

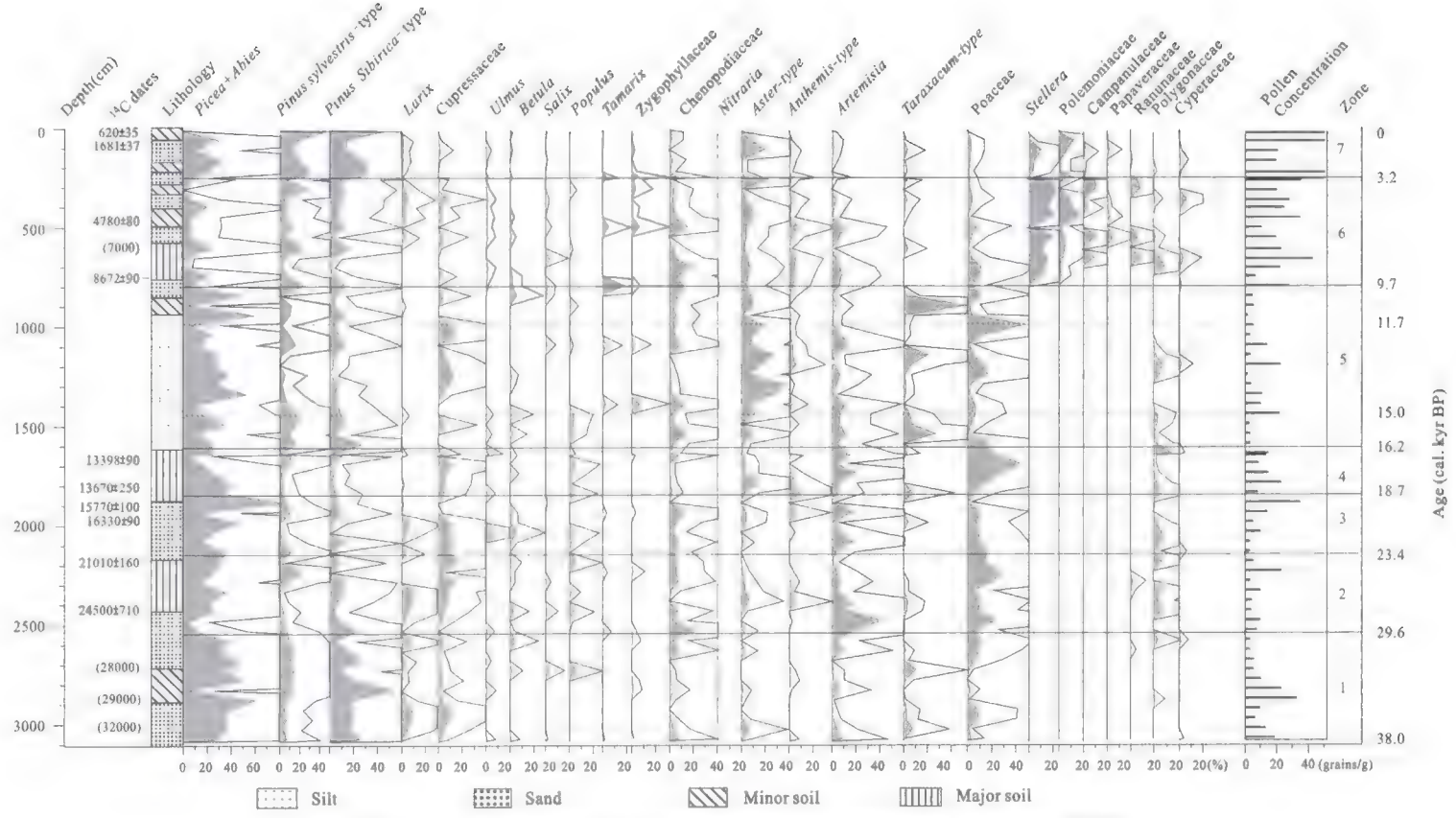

Fig. 3. Main pollen taxa percentage diagrams for Shaamar eolian-paleosl section (solid line: percentages with 5 × exaggeration).

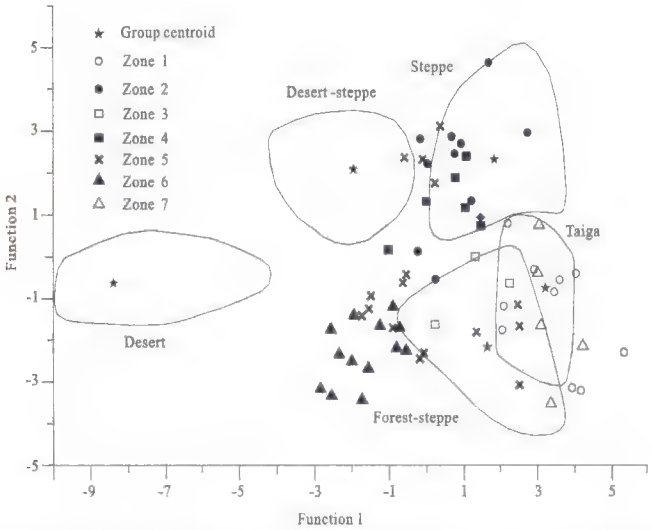

Fig. 4. Ordination of the fossil pollen samples from the Shaamar eolian-paleosol section along discriminant functions 1 and 2. Samples from different fossil pollen assemblage zones are designated by different symbols. The ranges of the surface samples (polygons) along the N–S transect across Mongolia from the five vegetation regions (Ma et al., 2008) are delineated for comparison.

Between ~38,000 and ~30,000 cal. BP the pollen assemblages, marked by highest percentages of *Picea* + *Abies* (mostly 11.36–60.66%) and *Pinus sibirica*-type (mostly 8.89–40.71%) with relatively high pollen concentrations, likely reflect a taiga forest. This interpretation is based on following two observations. First, *Pinus* pollen is well-dispersed and is documented to be over-represented in the modern pollen spectrum, whereas *Picea* and *Abies* have relatively poor dispersal ability (Liu et al., 1999; Lu et al., 2008; Ma et al., 2008). For example, the percentage of *Pinus* pollen may exceed 50% at sites where pine trees are not locally present. But, the pollen percentages of *Abies* and *Picea* normally range from 20% to 50% within fir and spruce forests and the percentages drop dramatically outside the forests. However, less than 10% of *Abies* and *Picea* pollen may been observed in some desert samples where pollen concentration is normally very low (Liu et al., 1999; Lu et al., 2008; Ma et al., 2008). Second, the association between the interpreted taiga forest and the sand layer between ~38,000 and ~30,000 cal. BP at the Shaamar section is well collaborated by the fact that the forest patches (dominated by *Pinus sylvestris* trees and *Pinus sibirica* trees) within the steppe-forests in the topographical corridor stretching from Ulan Bator to Lake Baikal are distributed on the sand-covered terraces of the Selenge River and the branch rivers (Feng et al., 2007a). Furthermore, the high probability values of modern analogue and the vegetation zonal index (i.e., taiga) lend further supports to the interpretation that is further elaborated by reconstructed low values of temperature index and high values of moisture index.

From ~30,000 to ~23,000 cal. BP, the pollen assemblages dominated by *Artemisia* and Poaceae with relatively low pollen concentrations suggest a steppe landscape that probably developed under relatively cold and dry climates. The vegetation zonal indices remain at or near steppe levels, accompanied by high probabilities of modern analogue, suggesting that the interpreted steppe for the period between ~30,000 and ~23,000 cal. BP is similar to the modern one in the northern Mongolian Plateau. A pronounced spike of temperature at ~29,000 cal. BP corresponding with a lowered moisture is quite remarkable.

The period from ~23,000 to ~19,000 cal. BP was another taiga-occupation interval when reconstructed temperature index was slightly increased and the reconstructed moisture index was increased over the preceding period (i.e., from ~30,000 to ~23,000 cal. BP). The subsequent period from ~19,000 to ~16,500 cal. BP was marked by a dramatic rising of Poaceae pollen and also by a notable increasing of pollen concentration, indicating an expansion of Poaceae-dominated steppes in response to warming climate. The vegetation zonal index also shows that the vegetation was steppe. But, the probability of modern analogue was low from ~19,000 to ~17,500 cal. BP, suggesting that the vegetation communities became increasingly dissimilar to their modern counterparts during that time interval.

The pollen assemblages is characterized by higher percentages of *Picea* + *Abies* (mostly >15.00%) and *Pinus* (mostly <30.00%) with lowest pollen concentrations during ~16,500–~15,000 and ~12,000–~10,000 cal. BP. *Pinus* was most likely wind-transported from long-distances. *Picea* and *Abies* pollen grains were mostly transported from nearby Mountains in view of the relatively low pollen concentrations and the relatively poor dispersal ability of *Picea* and *Abies* (Liu et al., 1999; Lu et al., 2008; Ma et al., 2008). The vegetation zonal index and the probability of modern analogue values also show that the vegetation was taiga forest and the reconstructed temperature level is very low in the two periods. Between ~15,000 and ~12,000 cal. BP., some samples have the very low values (<0.2) of probability of modern analogue indicating that they are atypical for the vegetation types. The pollen assemblages marked by higher percentage of *Aster*-type and *Picea* + *Abies* with relatively high pollen concentrations maybe indicate that steppe and forest-steppe vegetation were developed under rising temperature and low moisture conditions in this period.

The pollen assemblages and the vegetation zonal indices suggest that the vegetation was a forest-steppe during the period from ~10,000 to ~3000 cal. BP under rising temperature and low moisture conditions. A taiga forest has dominated the landscape during the past ~3000 years under cooling and wetting conditions. The probabilities of modern analogue are high for the entire

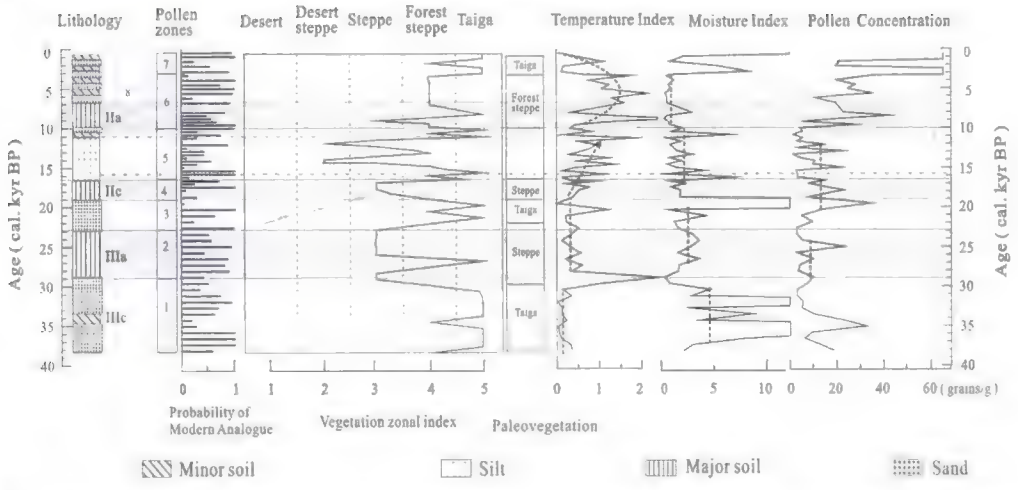

Fig. 5. Climate and vegetation reconstructions from the Shaamar eolian-paleosol section. Left Panel: Results of discriminant analysis for the pollen data presented as values of vegetation zonal index and probability of modern analogue. Right Panel: Pollen-based temperature and moisture indices and total pollen concentrations.

Holocene, lending a strong support to the Holocene vegetation reconstruction. It is quite noticeable that the reconstructed temperature curve has a bow-shaped change during the past ~10,000 years: climbing (i.e., warming) from ~10,000 to a maximum at ~6000 cal. BP, and declining (i.e., cooling) since ~6000 cal. BP. The reconstructed moisture was low from ~10,000 to ~3000 cal. BP and dramatically increased during the past ~3000 years.

4. Discussion

4.1. Regional comparison

The generally wet climate reconstructed for the later part of MIS 3 (i.e., from ~38,000 to ~30,000 cal. BP) in the northern Mongolian Plateau has its corroborative evidence in northern China. An extremely wet climate during the later period of MIS 3 (~40,000 to ~30,000 cal. BP) was evidenced by a dramatic expansion of coniferous forests in the Chinese Loess Plateau (Feng et al., 2007b) and by the high lake level and large lake areas in the southern Mongolian Plateau (Pachur et al., 1995; Ma et al., 2003; Zhang et al., 2004), and by the expansion of temperate conifer at western Japan (Hayashi et al., 2010).

MIS 2 (~30,000 to ~10,000 cal. BP) experienced a colder climate in the earlier part (~30,000 to ~20,000 cal. BP) than in the later part. The taiga vegetation during ~23,000 to ~19,000 cal. BP in the northern Mongolian Plateau and the cool-tolerant conifers in western Japan (Gotanda and Yasuda, 2008; Hayashi et al., 2010) appears to be chronologically correlative with the last glacial maximum documented in the North Atlantic region (Dansgaard et al., 1993; Bond et al., 1997; Alley et al., 2002).

The reconstructed temperature from the Shaamar section has a bow-shaped change during the past ~10,000 years: climbing (i.e., warming) from ~10,000 to ~6000 cal. BP and declining (i.e., cooling) since ~6000 cal. BP. The reconstructed moisture was low from ~10,000 to ~3000 cal. BP and bounced during the past ~3000 years. The reconstructions from the Shaamar section are generally consistent with three semi-quantitative reconstructions from Lake Baikal. The three reconstructions from Lake Baikal display approximately the same trends of temperature and moisture indices (Demske et al., 2005), i.e., increasing (i.e., warming) trends of the temperature index and decreasing (i.e., drying) trends of the moisture index for the early Holocene (before ~6000 cal. BP), and increasing (i.e., wetting) trends of moisture index and declining (i.e., cooling) trends of temperature index for the late Holocene (after ~6000 cal. BP). It appears that the middle Holocene was the warmest and driest period of the entire Holocene and bracketed by a cool-wet early Holocene and a cool-wet late Holocene in the topographical corridor stretching from Ulan Bator to Lake Baikal.

It should be noted that the reconstructed moisture from the northern Mongolian Plateau seems to be anti-phased with that from northern China where the middle Holocene was warm and wet and the late Holocene was cool and dry (Feng and Khosbayar, 2004; Feng et al., 2006a, 2006b, 2011; Ma et al., 2004; Xiao et al., 2004; Cao et al., 2010; Xu et al., 2010). This anti-phased relationship can be primarily attributed to the insolation-driven temperature variations in East Asia. That is, high temperature strengthened the East Asian monsoon and thus brought more precipitation to northern China during the middle Holocene, thus resulting in a warm and wet climate. In contrast, high temperature during the middle Holocene effectively enhanced evaporation in the northern Mongolian Plateau, which lies too far north to be reached by the East Asian summer monsoon, thereby resulting in a warm and dry climate (Wang et al., 2009, 2011; Wang and Feng, 2013). As for the late Holocene, considerably lowered temperature effectively reduced the evaporation in the northern Mongolian Plateau, thus resulting in a wet climate.

4.2. Global teleconnections

This section attempts to explore the mechanisms controlling or modulating the climate change of the past ~38,000 years in the northern Mongolian Plateau by comparing our pollen record from the Shaamar section with cave-stalagmite record from China and with ice-core record from Greenland. The $\delta^{18}O$ data from Hulu Cave (Wang et al., 2001) and Dongge Cave Stalagmites (Yuan et al., 2004) and Greenland ice core (Dansgaard et al., 1993) were downloaded from NOAA site (www.ngdc.noaa.gov/paleo/icecore/greenland/summit/index.html) and the solar insolation curves were from Laskar et al. (2004) (Fig. 6). The taiga forest-dominated and extremely wet period spanning from ~38,000 to ~30,000 cal. BP at the Shaamar section chronologically corresponds with a

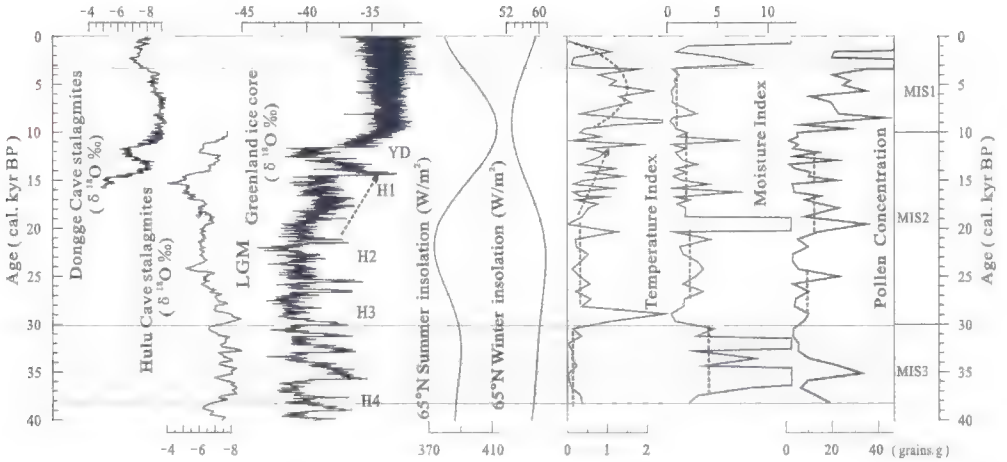

Fig. 6. Comparison of the reconstructed temperature and moisture indices from Shaamar eolian-paleosol section with monsoon records from Asian (Wang et al., 2001; Yuan et al., 2004), ice-core record from Greenland (Dansgaard et al., 1993) and solar insolation (Laskar et al., 2004).

moderate warm period in the Greenland record and a moderate strength period of the summer East Asian Monsoon in China (Wang et al., 2001). We hypothesize that the relatively high winter insolation during the middle portion of MIS 3 (~48,000 to ~34,000 cal. BP) may be the reason for the moderate warmth in the North Atlantic region that promoted the supply of water vapor via the westerlies to the northern Mongolian Plateau. The relatively low summer insolation and growth of the ice sheets during the later part of the MIS 3 (Clark et al., 2009) may have lowered the temperature in the northern Mongolian Plateau, and the lowered temperature may have further enhanced the moisture by suppressing the evaporation.

The following period from ~30,000 to ~20,000 cal. BP was the time when the summer insolation was declining and the corresponding low temperature the North Atlantic region including Greenland may have resulted in low temperatures and low moistures in the northern Mongolian Plateau. The climbing trend of the reconstructed temperature from ~19,000 to ~11,000 cal. BP at the Shaamar section seems to be a delayed response to the climbing trend of the $\delta^{18}O$ data-suggested temperature climbing from ~21,000 to ~13,000 cal. BP in the North Atlantic region (Dansgaard et al., 1993; Bond et al., 1997; Dahl-Jensen et al., 1998; Bard et al., 2000; Alley et al., 2002), again lending support to the hypothesized linkage between the North Atlantic region and the northern Mongolian Plateau. Furthermore, the warming trend since ~19,000 cal. BP in the northern Mongolian Plateau corresponds with the timing of the retreat of Northern Hemisphere mountain glaciers and ice sheets (Rinterknecht et al., 2006; Clark et al., 2009), with the sea level rising and warming of the tropical Atlantic and tropical Pacific oceans (Clark et al., 2004), and also with the ending of the Last Glacial Maximum in the mid-latitudes (Schaefer et al., 2006).

4.3. Two notes

First, two (i.e., IIIa and IIc in Fig. 2) of the three major paleosols (i.e., IIIa, IIc, and IIa) deserve special mentioning here. The paleosol IIIa at the Shaamar section was formed primarily under a steppe vegetation (not under forest-steppe or taiga) during the very early part of MIS 2 (~30,000 to ~23,000 cal. BP), being consistent with the biogeographic definition of Mollisol formation (Bhattacharyya et al., 2006; Feng et al., 2007a, 2011). The IIIa chronologically well corresponds with the podzolic pedocomplex formed from ~26,000 to ~22,000 ^{14}C BP in southwestern Siberia (Melinikova, 1991; Tarasov et al., 1997; Chlachula, 2001; Velichko et al., 2002; Blyakharchuk et al., 2004). Being quite similar to the major paleosol IIIa, the major paleosol IIc was also formed under a steppe vegetation (not under forest steppe or taiga) during the period from ~19,000 to 16,500 cal. BP and has its chronological counterparts in the records from southwestern Siberia (Melinikova, 1991; Tarasov et al., 1997; Velichko et al., 2002) and also from eastern Kazakhstan (Feng et al., 2011). However, there are no chronologically corresponding major paleosols reported from northern China. It should also be noted that the high percentage of Poaceae, characterized by low pollen productivity and poor dispersal ability, and the higher pollen concentration than sand layer adjacent to paleosol (Fig. 5) suggest that the plants are flourished and the vegetation cover is high during the two periods when the major paleosol IIIa and IIC were formed.

Second, a Bolling/Allerod (B/A)-like interstadial event lasting from ~15,000 to ~13,000 cal. BP was reported to be widespread in southern Siberia (Horiuchi et al., 2000; Blyakharchuk et al., 2004, 2007, 2008; Demske et al., 2005; Tarasov et al., 2007; Rudaya et al., 2008, 2009; Bezrukova et al., 2009). But, our record offers only muted and inconclusive evidence in support of the existence of the B/A-like event. A Younger Dryas-like stadial event lasting from ~13,000 to ~10,000 cal. BP (Blyakharchuk et al., 2004, 2007, 2008; Demske et al., 2005; Tarasov et al., 2007; Rudaya et al., 2008, 2009; Bezrukova et al., 2009) was also reported to be widespread in southern Siberia. The temperature trough spanning from ~12,000 to ~10,000 cal. BP in the Shaamar record is most likely the expression of the Younger-Dryas-like cold event. It should be stressed that both the Bolling/Allerod (B/A)-like interstadial event and the Younger Dryas-like stadial event are well documented both in Greenland ice-core record and in Chinese cave-stalagmite records (see Fig. 6).

Acknowledgement

This paper is a result of projects supported by several Chinese NSF grants (No. 41271207, No. 40871092, No. 40331012, No. 40671190, No. 40930102) and two U.S. NSF grants (ATM-0402475, ATM-0402509).

References

Alley, R.B., Brook, E.J., Anandakrishnan, S., 2002. A northern lead in the orbital band: north–south phasing of Ice-Age events. Quaternary Science Reviews 21, 431–441.

Bard, E., Rostek, F., Turon, J.L., Gendreau, S., 2000. Hydrological impact of Heinrich events in the subtropical Northeast Atlantic. Science, 1321–1324.

Berger, A., Loutre, M.F., 1991. Insolation values for the climate of the last 10 million years. Quaternary Science Reviews 10, 297–317.

Bezrukova, E.V., Abzaeva, A.A., Letunova, P.P., Kulagina, N.V., Orlova, L.A., 2009. Evidence of environmental instability of the Lake Baikal area after the last glaciations. Archaeology Ethnology & Anthropology of Eurasia 37 (3), 17–25.

Bhattacharyya, T., Pal, D.K., Lal, S., Chandran, P., Ray, S.K., 2006. Formation and persistence of Mollisols on zeolitic Deccan basalt of humid tropical India. Geoderma 136, 609–620.

Blyakharchuk, T.A., Wright, H.E., Borodavko, P.S., van der Knaap, W.O., Ammann, B., 2004. Late Glacial and Holocene vegetational changes on the Ulagan high-mountain plateau, Altai Mountains, southern Siberia. Palaeogeography, Palaeoclimatology, Palaeoecology 209, 259–279.

Blyakharchuk, T.A., Wright, H.E., Borodavko, P.S., van der Knaap, W.O., Ammann, B., 2007. Late glacial and Holocene vegetational history of the Altai mountains (southwestern Tuva Republic, Siberia). Palaeogeography, Palaeoclimatology, Palaeoecology 245, 518–534.

Blyakharchuk, T.A., Wright, H.E., Borodavko, P.S., van der Knaap, W.O., Ammann, B., 2008. The role of pingos in the development of the Dzhangyskol lake–pingo complex, central Altai Mountains, southern Siberia. Palaeogeography, Palaeoclimatology, Palaeoecology 257, 404–420.

Bond, G., Showers, W., Cheseby, M., Lotti, R., Almasi, P., de Menocal, P., Priore, P., Cullen, H., Hajdas, I., Bonani, G., 1997. A pervasive millennial-scale cycle in north Atlantic Holocene and glacial climates. Science 278, 1257–1266.

Bond, G., Kromer, B., Beer, J., Muscheler, R., Evans, M., Showers, W., Hoffmann, S., Lotti-Bond, R., Hajdas, I., Bonani, G., 2001. Persistent solar influence on north Atlantic climate during the Holocene. Science 294, 2130–2136.

Bradley, R.S., 1999. Paleoclimatology: Reconstructing Climates of the Quaternary. second ed. Harcourt Academic Press, New York.

Cao, X.Y., Xua, Q.H., Jing, Z.C., Tang, J.G., Li, Y.C., Tian, F., 2010. Holocene climate change and human impacts implied from the pollen records in Anyang, central China. Quaternary International 227, 3–9.

Chen, F.H., Yu, Z.C., Yang, M.L., Ito, E., Wang, S.M., Madsen, D.B., Huang, X.Z., Zhao, Y., Sato, T., John, B., Birks, H., Boomer, I., Chen, J.H., An, C.B., Wünnemann, B., 2008. Holocene moisture evolution in arid central Asia and its out-of-phase relationship with Asian monsoon history. Quaternary Science Reviews 27, 351–364.

Chlachula, J., 2001. Pleistocene climate change, natural environments and palaeolithic occupation of the upper Yenisei area, south-central Siberia. Quaternary International 80–81, 101–130.

Clark, P.U., Dyke, A.S., Shakun, J.D., Carlson, A.E., Clark, J., Wohlfarth, B., Mitrovica, J.X., Hostetler, S.W., McCabe, A.M., 2009. The last glacial maximum. Science 325, 710–714.

Clark, P.U., McCabe, A.M., Mix, A.C., Weaver, A.J., 2004. Rapid rise of sea level 19,000 years ago and its global implications. Science 304, 1141–1144.

CLIMAP Members, 1981. Seasonal Reconstruction of the Earth's Surface at the Last Glacial Maximum. In: GSA Map and Chart Series, MC-36. Geological Society of America.

Clemens, S.C., Murray, D.W., Prell, W.L., 1996. Nonstationary phase of the Plio-Pleistocene Asian monsoon. Science 274, 943–948.

COHMAP Members, 1988. Climatic changes of the last 18000 years: observations and model simulations. Science 241, 1043–1052.

Dahl-Jensen, D., Mosegaard, K., Gundestrup, N., Clow, G.D., Johnsen, S.J., Hansen, A.W., Balling, N., 1998. Past temperatures directly from the Greenland Ice Sheet. Science 282, 268–271.

Dansgaard, w., Johnsen, S.J., Clausen, H.B., Dahl-Jensen, D., Gundestrup, N.S., Hammer, C.U., Hvidberg, C.S., Steffensen, J.P., Sveinbjörnsdottir, A.E., Jouzel, J., Bond, G., 1993. Evidence for generalinstability of past climate from a 250-kyr-ice-core record. Nature 364, 218–220.

Demske, D., Heumann, G., Granoszewski, W., Nita, M., Mamakowa, K., Tarasov, P.E., Oberhänsli, H., 2005. Late glacial and Holocene vegetation and regional climate variability evidenced in high-resolution pollen records from Lake Baikal. Global and Planetary Change 46, 255–279.

Feng, Z.D., Chen, F.H., Tang, L.Y., Kang, J.C., 1998. East Asian monsoon climates and Gobi dynamics in marine isotope stages 4 and 3. Catena 33, 29–46.

Feng, Z.D., 2001. Gobi dynamics in the Northern Mongolian Plateau during the past 20000– yr preliminary results. Quaternary International 76/77, 77–83.

Feng, Z.D., Khosbayar, P., 2004. Paleosubarctic Eolian environments along the southern margin of the North American ice sheet and the southern margin of Siberia during the Last Glacial Maximum. Palaeogeography, Palaeoclimatology, Palaeoecology 212, 265–275.

Feng, Z.D., Wang, W.G., Guo, L.L., Khosbayar, P., Narantsetseg, T., Jull, A., An, C.B., Li, X.Q., Zhang, H.C., Ma, Y.Z., 2005. Lacustrine and eolian records of Holocene climate changes in the Mongolian Plateau: preliminary results. Quaternary International 136, 25–32.

Feng, Z.D., An, C.B., Wang, H.B., 2006a. Holocene climatic and environmental changes in the arid and semi-arid areas of China: a review. The Holocene 16, 119–130.

Feng, Z.D., Tang, L.Y., Wang, H.B., Ma, Y.Z., Liu, K.B., 2006b. Holocene vegetation variations and the associated environmental changes in the western part of the Chinese Loess Plateau. Palaeogeography, Palaeoclimatology, Palaeoecology 241, 440–456.

Feng, Z.D., Zhai, X.W., Ma, Y.Z., Huang, C.Q., Wang, W.G., Zhang, H.C., Khosbayar, P., Narantsetseg, T., Liu, K.B., Rutter, N.W., 2007a. Eolian environmental changes in the Northern Mongolian Plateau during the past ~35,000 yr. Palaeogeography, Palaeoclimatology, Palaeoecology 245, 505–517.

Feng, Z.D., Tang, L.Y., Ma, Y.Z., Zhai, Z.X., Wu, H.N., Li, F., Zou, S.B., Yang, Q.L., Wang, W.G., Derbyshire, E., Liu, K.B., 2007b. Vegetation variations and associated environmental changes during marine isotope stage 3 in the western part of the Chinese Loess Plateau. Palaeogeography, Palaeoclimatology, Palaeoecology 246, 278–291.

Feng, Z.D., Ran, M., Yang, Q.L., Zhai, X.W., Wang, W., Zhang, X.S., Huang, C.Q., 2011. Stratigraphies and chronologies of late Quaternary loess–paleosol sequences in the core area of the central Asian arid zone. Quaternary International 240, 156–166.

Fowell, S.J., Hansen, B.C.S., Peck, J.A., Khosbayar, P., Ganbold, E., 2003. Mid- to late-Holocene climate evolution of the Lake Telmen Basin, north-central Mongolia, based on palynological data. Quaternary Research 59, 353–363.

Gotanda, K., Yasuda, Y., 2008. Spatial biome changes in southwestern Japan since the Last Glacial Maximum. Quaternary International 184, 84–93.

Harrison, S.P., Yu, G., Tarasov, P.E., 1996. Late Quaternary lake-level record from northern Eurasia. Quaternary Research 45, 138–159.

Hayashi, R., Takahara, H., Hayashida, A., Takemura, K., 2010. Millennial-scale vegetation changes during the last 40,000 yr based on a pollen record from Lake Biwa, Japan. Quaternary Research 74, 91–99.

Hilbig, W., 1995. The Vegetation of Mongolia. SPB Academic Publishing, Amsterdam.

Horiuchi, K., Minoura, K., Hoshino, K., Oda, T., Nakamura, T., Kawai, T., 2000. Palaeoenvironmental history of Lake Baikal during the last 23000 years. Palaeogeography, Palaeoclimatology, Palaeoecology 157, 95–108.

Khosbayar, P., 1989. Map of Geological Complexes of Mongolia (1:500,000). Moscow Publishing House, Moscow (in Russian).

Laskar, J., Robutel, P., Joutel, F., Gastineau, M., Correia, A.C.M., Levrard, B., 2004. A long-term numerical solution for the insolation quantities of the Earth. Astronomy & Astrophysics 428 (1), 261–285.

Lavrenko, E.M., Iunatov, A.A., Aleksandr, A., Dashniam, B., 1979. Vegetation Map of Mongolian People's Republic (Scale 1: 1,500,000). Moscow Publishing House, Moscow (in Russian).

Liu, K.B., Lam, N.S.N., 1985. Paleovegetational reconstruction based on modern and fossil pollen data: an application of discriminant analysis. Annals of the Association of American Geographers 75, 115–130.

Liu, H.Y., Cui, T., Pott, R., Speier, M., 1999. The surface pollen of the woodland-steppe ecotone in southeastern Inner Mongolia, China. Review of Palaeobotany and Palynology 105 (3–4), 237–250.

Lu, H.Y., Wu, N.Q., Yang, X.D., Shen, C.M., Zhu, L.P., Wang, L., Li, Q., Xu, D.K., Tong, G.B., Sun, X.J., 2008. Spatial pattern of *Abies* and *Picea* pollen distribution along the elevation gradient in the Qinghai–Tibetan Plateau and Xinjiang, China. Boreas 37, 254–262.

Logatchov, N.A., 1989. Late Cenozoic of Mongolia (Stratigraphy and Paleogeography). The Joint Soviet-mongolia Scientific Research Transaction 47. Moscow Publishing House, Moscow (in Russian).

Ma, Y.Z., Zhang, H.C., Pachur, H.J., Wünnemann, B., Li, J.J., Feng, Z.D., 2003. Late Glacial and Holocene vegetation history and paleoclimate of the Tengger Desert, northwestern China. Chinese Science Bulletin 48 (14), 1457–1463.

Ma, Y.Z., Zhang, H.C., Pachur, H.J., Wunnemann, B., Li, J.J., Feng, Z.D., 2004. Modern pollen-based interpretations of mid-Holocene palaeoclimate (8500 to 3000 cal., BP) at the southern margin of the Tengger Desert, northwestern China. The Holocene 14 (6), 841–850.

Ma, Y.Z., Liu, K.B., Feng, Z.D., Sang, Y.L., Wang, W., Sun, A.Z., 2008. A survey of modern pollen and vegetation along a south-north transect in Mongolia. Journal of Biogeography 35, 1512–1532.

Ma, Y.Z., Meng, H.W., Sang, Y.L., Sun, A.Z., Wu, J., Wang, W., 2009. Pollen keys for identification of Coniferopsida and compositae classes under light microscopy and their ecological significance. Acta Palaeontologica Sinica 48 (2), 240–253 (in Chinese).

MacDonald, G.M., Ritchie, J.C., 1986. Modern pollen spectra from the western interior of Canada and the interpretation of Late Quaternary vegetation development. New Phytologist 103, 245–268.

Melnikova, A.P., 1991. Glacial retreats in Tianshan Mountain during the Holocene. Glaciology and Cryopedology 13, 291–298 (in Chinese).

Moore, P.D., Webb, J.A., Collinson, M.E., 1991. Pollen Analysis. Blackwell Scientific Publications, Oxford.

Pachur, H.J., Wünemann, B., Zhang, H.C., 1995. Lake evolution in the Tengger desert, northwestern China, during the last 40,000 years. Quaternary Research 44, 171–180.

Peck, J.A., Khosbayar, P., Fowell, S.J., Pearce, R.B., Ariunbileg, S., Hansen, B.C., Soninkhishig, N., 2002. Mid to Late Holocene climate change in north central Mongolia as recorded in the sediments of Lake Telmen. Palaeogeography, Palaeoclimatology, Palaeoecology 183, 135–153.

Prokopenko, A.A., Khursevich, G.K., Bezrukova, E.V., Kuzmin, M.I., Boes, X., Williams, D.F., Fedenya, S.A., Kulagina, N.V., Letunova, P.P., Abzaeva, A.A., 2007. Paleoenvironmental proxy records from Lake Hovsgol, Mongolia, and a synthesis of Holocene climate change in the Lake Baikal watershed. Quaternary Research 68, 2–17.

Reese, C.A., Liu, K-b, 2005. A modern pollen rain study from the central Anders region of South America. Journal of Biogeography 32, 709–718.

Reimer, P.J., Baillie, M.G.L., Bard, E., Bayliss, A., Beck, J.W., Blackwell, P.G., Ramsey, C.B., Buck, C.E., 2009. Intcal09 and marine09 radiocarbon age calibration curves 0–50,000 years Cal BP. Radiocarbon 51, 1111–1150.

Rinterknecht, V.R., Clark, P.U., Raisbeck, G.M., Yiou, F., Bitinas, A., Brook, E.J., Marks, L., Zelcs, V., Lunkka, J.P., Pavlovskaya, I.E., Piotrowski, J.A., Raukas, A., 2006. The last deglaciation of the southeastern sector of the Scandinavian Ice Sheet. Science 311, 1449–1452.

Rudaya, N.A., Tarasov, P.E., Dorofeyuk, N.I., Kalugin, I.A., Andreev, A.A., Diekmann, B., Daryin, A.V., 2008. Environmental changes in the Mongolian Altai during the Holocene. Archaeology, Ethnology and Anthropology of Eurasia 36 (4), 2–14.

Rudaya, N., Tarasov, P., Dorofeyuk, N., Solovieva, N., Kalugin, I., Andreev, A., Daryin, A., Diekmann, B., Riedel, F., Tserendash, N., Wagner, M., 2009. Holocene environments and climate in the Mongolian Altai reconstructed from the Hoton-Nur pollen and diatom records: a step towards better understanding climate dynamics in Central Asia. Quaternary Science Reviews 28, 540–554.

Ruddiman, W.F., 2008. Earth's Climate: Past and Future. Freeman W. H., New York.

Schaefer, M.J., Denton, G.H., Barrell, J.A., Ivy-Ochs, S., Kubik, P., Andersen, B.G., Phillips, M.K., Lowell, T.V., Schluchter, C., 2006. Near-synchronous interhemispheric termination of the last glacial maximum in mid-latitudes. Science 312, 1510–1513.

Sugden, J.M., Meadows, M.E., 1989. The use of multiple discriminant analysis in reconstructing recent vegetation changes on the Nuwelveldverg, South Africa. Review of Palaeobotany and Palynology 60 (1–2), 131–147.

Tarasov, P.E., Jolly, D., Kaplan, J.O., 1997. A continuous Late Glacial and Holocene record of vegetation changes in Kazakhstan. Plaeogeography, Palaeoclimatology. Palaeoecology 136, 281–292.

Tarasov, P., Dorofeyuk, N., Metel'Tseva, E., 2000. Holocene vegetation and climate changes in Hoton Nuur Basin, northwest Mongolia. Boreas 29, 117–126.

Tarasov, P., Bezrukova, E., Karabanov, E., Nakagawa, T., Wagner, M., Kulagina, N., Letunova, P., Abzaeva, A., Granoszewski, W., Riedel, F., 2007. Vegetation and climate dynamics during the Holocene and Eemian interglacials derived from Lake Baikal pollen records. Palaeogeography, Palaeoclimatology, Palaeoecology 252, 440–457.

Velichko, A.A., Catto, N., Drenova, A.N., Klimanov, A.V., Kremenetski, K.V., Nechaev, V.P., 2002. Climate changes in East Europe and Siberia at the late glacial–Holocene transition. Quaternary International 91, 75–99.

Wang, W., Ma, Y.Z., Feng, Z.D., Meng, H.W., Sang, Y.L., Zhai, X.W., 2009. Vegetation and climate changes during the last 8660 cal. a BP in central Mongolia, based on a high-resolution pollen record from Lake Ugii Nuur. Chinese Science Bulletin 54 (9), 1579–1589.

Wang, W., Ma, Y.Z., Feng, Z.D., Narantsetseg, T., Liu, K.B., Zhai, X.W., 2011. A prolonged dry mid-Holocene climate revealed by pollen and diatom records from Lake Ugii Nuur in central Mongolia. Quaternary International 229, 74–83.

Wang, W., Feng, Z.D., 2013. Holocene moisture evolution across the Mongolia Plateau and its surrounding areas: a synthesis of climatic records. Earth-science Reviews 122, 38–57.

Wang, Y.J., Cheng, H., Edwards, R.L., An, Z.S., Wu, J.Y., Shen, C.C., Dorale, J.A., 2001. A high-resolution absolute-dated late Pleistocene Monsoon record from Hulu Cave, China. Science 294, 2345–2348.

Wang, F.X., Qian, N.F., Zhang, Y.L., Yang, H.Q., 1995. Pollen Flora of China, second ed. Science Press, Beijing. (in Chinese).

Xiao, J.L., Xu, Q.H., Nakamura, T., Yang, X.L., Liang, W.D., Inouchi, Y., 2004. Holocene vegetation variation in the Daihai Lake region of north-central China: a direct indication of the Asian monsoon climatic history. Quaternary Science Reviews 23, 1669–1679.

Xu, Q.H., Xiao, J.L., Li, Y.C., Tian, F., Nakagawa, T., 2010. Pollen-based quantitative reconstruction of Holocene climate changes in the Daihai lake area, Inner Mongolia, China. Journal of Climate 23, 2856–2868.

Yuan, D., Cheng, H., Edwards, R.L., Dykoski, C.A., Kelly, M.J., Zhang, M., Qing, J., Lin, Y., Wang, Y., Wu, J., Dorale, J.A., An, Z., Cai, Y., 2004. Timing, duration, and transitions of the last interglacial Asian monsoon. Science 304, 575–578.

Zhang, C.J., Zhang, W.Y., Feng, Z.D., Mischke, S., Gao, X., Gao, D., Sun, F.F., 2012. Holocene hydrological and climatic change on the northern Mongolian Plateau based on multi-proxy records from Lake Gun Nuur. Palaeogeography, Palaeoclimatology, Palaeoecology 323–325, 75–86.

Zhang, H.C., Peng, J.L., Ma, Y.Z., Chen, G.J., Feng, Z.D., Li, B., Fan, H.F., Chang, F.Q., Lei, G.L., Wünnemann, B., 2004. Late Quaternary palaeolake levels in Tengger desert, NW China. Palaeogeography, Palaeoclimatology, Palaeoecology 211, 45–58.

附录七

ORIGINAL ARTICLE

A survey of modern pollen and vegetation along a south–north transect in Mongolia

Yuzhen Ma[1], Kam-biu Liu[2]*, Zhaodong Feng[3]†, Yanli Sang[3], Wei Wang[3] and Aizhi Sun[3]

[1]State Key Laboratory of Earth Surface Processes and Resource Ecology, Academy of Disaster Reduction and Emergency Management, Beijing Normal University, Beijing, China, [2]Department of Oceanography and Coastal Sciences, School of the Coast and Environment, Louisiana State University, Baton Rouge, LA, USA and [3]MOE Key Laboratory of Western Environmental Systems, Lanzhou University, Lanzhou, Gansu, China

ABSTRACT

Aim This modern pollen-rain study documents the spatial and quantitative relationships between modern pollen and vegetation in Mongolia, and explores the potential for using this relationship in palaeoclimatic reconstructions.

Location East-central Mongolia.

Methods We collected 104 pollen surface samples along a south–north transect across five vegetation zones in Mongolia. Discriminant analysis was used to classify the modern pollen spectra into five pollen assemblages corresponding to the five vegetation zones. Hierarchical cluster analysis was used to divide the main pollen taxa into two major groups and seven subgroups representing the dry and moist vegetation types and the main vegetation communities within them.

Results Each vegetation zone along the transect can be characterized by a distinctive modern pollen assemblage as follows: (1) desert zone: Chenopodiaceae–Zygophyllaceae–*Nitraria*–Poaceae pollen assemblage; (2) desert-steppe zone: Poaceae–Chenopodiaceae pollen assemblage; (3) steppe zone: *Artemisia*–*Aster*-type–Poaceae–*Pinus* Haploxylon-type pollen assemblage; (4) forest-steppe zone: *Pinus* Haploxylon-type–*Picea*–*Artemisia*–*Betula*, montane forb/shrub and pteridophyte pollen assemblage; and (5) mountain taiga zone: *Pinus* Haploxylon-type–*Picea*–Poaceae–Cyperaceae, montane forb/shrub and Pteridophyte pollen assemblage.

Main conclusions Based on the ratio between the major pollen taxon groups and subgroups, we propose two pollen–climate indices that represent the precipitation and temperature conditions in the study region. When plotted along our south–north transect, the moisture indices (M) and temperature indices (T) mimic the regional gradients of precipitation and temperature across Mongolia very closely. These pollen–climate indices can be used for palaeoclimatic reconstruction based on fossil pollen data.

Keywords

Cluster analysis, discriminant analysis, environmental gradient, modern pollen rain, Mongolia, ordination, palynology, pollen surface samples, pollen–climate indices, vegetation.

*Correspondence: Kam-biu Liu, Department of Oceanography and Coastal Sciences, School of the Coast and Environment, Louisiana State University, 1002Y Energy, Coast, and Environment Building, Baton Rouge, LA 70803, USA.
E-mail: kliu1@lsu.edu
†Present address: Zhaodong Feng, Department of Geology, Baylor University, Waco, TX 76798, USA.

INTRODUCTION

In order for palynologists to reconstruct past environments accurately with fossil pollen evidence, it is first necessary to understand how the current vegetation is represented in the modern pollen rain of the study area (Webb, 1987; Webb *et al.*, 1993). In Mongolia, however, no comprehensive study of the relationship between modern pollen and vegetation exists. With few exceptions (e.g. Tarasov *et al.*, 2000a), the Holocene pollen records from Mongolia are poorly dated (Dorofeyuk & Tarasov, 1998; Gunin *et al.*, 1999), and few studies have incorporated a modern pollen-rain analysis into their work.

Important generalizations and reconstructions of modern and mid-Holocene biomes have been produced by Tarasov

et al. (1998, 1999a) for the territory of the former Soviet Union and Mongolia based on pollen and plant macrofossil data. Based on the scores of the plant functional types (PFTs) calculated for 1245 surface pollen spectra (644 of which were from the Former Soviet Union and Mongolia, but few from the latter) covering northern Eurasia and western North America, the climate at 6 kyr BP and the Last Glacial Maximum has been reconstructed for this region (Tarasov *et al.*, 1999a,b, 2000b). At the same time, a parallel study based on a set of 102 modern pollen spectra from Mongolia concluded that the spatial patterns in modern pollen data reflect the current vegetation, and that *Larix* has low pollen productivity and poor pollen dispersal, which results in low pollen representation (Gunin *et al.*, 1999). Tarasov *et al.* (2000a) interpreted the pollen record from the Hoton-Nur basin in north-western Mongolia based on this conclusion and the quantitative method of pollen-based biome reconstruction. However, despite all the works cited above that utilize a modern pollen data set from northern Eurasia, including Mongolia, no data set or intensive study focusing on the modern pollen rain in Mongolia has been published to date, and the detailed relationships (both quantitative and qualitative) between pollen and vegetation and/or climate remain poorly known. The paucity of such knowledge is even more acute for the desert and desert-steppe regions of southern Mongolia, where pollen surface samples are completely lacking in the existing data network (Tarasov *et al.*, 1999b, 2000b).

To establish the spatial and statistical relationships between modern pollen and vegetation, we collected modern pollen samples from 104 sites along a transect from south to north in Mongolia in July and August of 2002. This study is a systematic analysis of the modern pollen rain along this transect. These data will help to broaden our understanding of the modern relationships between pollen and vegetation in the region, and fill a large gap in the pollen data network for Mongolia.

STUDY AREA

The study area, encompassing 104 surface soil samples, lies roughly between 42°45′55″ and 51°35′08″ N latitude, and between 99°57′56″ and 110°07′35″ E longitude. It includes the Hovsgol nuur area, the Hangay–Hentiy mountain area, the drainage area of the Selenge and Orhon rivers, and the Tov and East Gobi area in east-central Mongolia. It is situated in the northern part of Central Asia, far from the ocean (Fig. 1).

The climate of the study area is distinctly continental (Tuvdendorzh & Myagmarzhav, 1985; Orshikh *et al.*, 1990) (Fig. 2). The mean annual precipitation decreases steadily from north-west to south-east, which is an important factor in the distribution of vegetation formations. The highest precipitation values, exceeding 600 mm, occur locally in the mountains of the Hovsgol region. The East Gobi has the lowest values, roughly 50 mm, and has periods without any precipitation lasting several years.

The winter (November to March) is very cold. The lowest temperatures are recorded in January, with monthly averages below −16°C and minimum temperatures as low as −24°C. The winter is also dry, with less than 5% to 10% of the annual precipitation. Snow may fall in the north and in the mountains. There are long periods with clear skies and without wind.

The summer (June–August) is the wettest season, with about 70% of the annual precipitation. The highest rainfall is usually in July, which is also the warmest month, with mean temperatures between 12°C in the north and in the mountains and 24°C in the East Gobi. From the north-west to the south-east the climate becomes drier and warmer.

The spring (April, May) is characterized by a combination of strong winds, low relative air humidity, and very low precipitation. Fierce dust and sand storms develop in the early afternoon hours (Tuvdendorzh & Myagmarzhav, 1985; Orshikh *et al.*, 1990).

VEGETATION AND CLIMATE

Figure 1 gives the distribution of the main vegetation zones in Mongolia (Lavrenko *et al.*, 1979; Lavrenko & Karamisheva, 1990). Biogeographically, Mongolia is a transitional zone from Siberian taiga to dry steppe, steppe-desert, and desert in Central Asia, and the major portion of its territory is in the steppe and forest-steppe zones. From south to north our transect traverses five vegetation zones. Botanical nomenclature follows Hilbig (1995).

Desert vegetation

The vegetation in the East Gobi occurs in an elevation belt between 1200 and 750 m, with a mean annual temperature of 4–6°C, a July temperature > 24°C, and a January temperature < −16°C. Precipitation occurs almost exclusively in the summer. It amounts to 50–150 mm annually, but less than 40 mm $year^{-1}$ is not uncommon (Fig. 2). Winters are cold and cloudless. Important vegetation components of the desert include low shrubs and semi-shrubs, most of them belonging to the families Chenopodiaceae (*Anabasis*, *Haloxylon*, *Kalidium*, *Kochia*, *Iljinia*, *Salsola*, *Sympegma*, *Nanophyton*); Asteraceae (*Ajania*, *Artemisia*, *Asterothamnus*, *Brachanthemum*); Polygonaceae (*Atraphaxis*, *Calligonum*); Zygophyllaceae (*Nitraria*, *Zygophyllum*); Tamaricaceae (*Reaumuria*, *Tamarix*); Fabaceae (*Caragana*, *Oxytropis*); Rosaceae (*Potaninia*); and Convolvulaceae (*Convolvulus*).

Two major desert communities can be recognized based on their characteristic vegetation composition (Hilbig, 1995). The Chenopodiaceae community (Fig. 1; type 1) is a very important and widespread community in the desert zone. Characteristic dominants include *Anabasis brevifolia*, *Salsola passerina*, *Nanophyton erinaceum*, *Haloxylon ammodendron*, *Kalidium gracile*, *Kochia prostrata*, *Nitraria sibirica*, *Nitraria sphaerocarpa*, *Zygophyllum xanthoxylon*, *Peganum nigellastrum*, *Reaumuria soogorica*, and *Ephedra przewalskii*. Accompanying components include *Stipa gobica*, *Cleistogenes sinensis*, *Aristida adscenesionis*, *Caragana leucaphloea*, *Artemisia scoparia*,

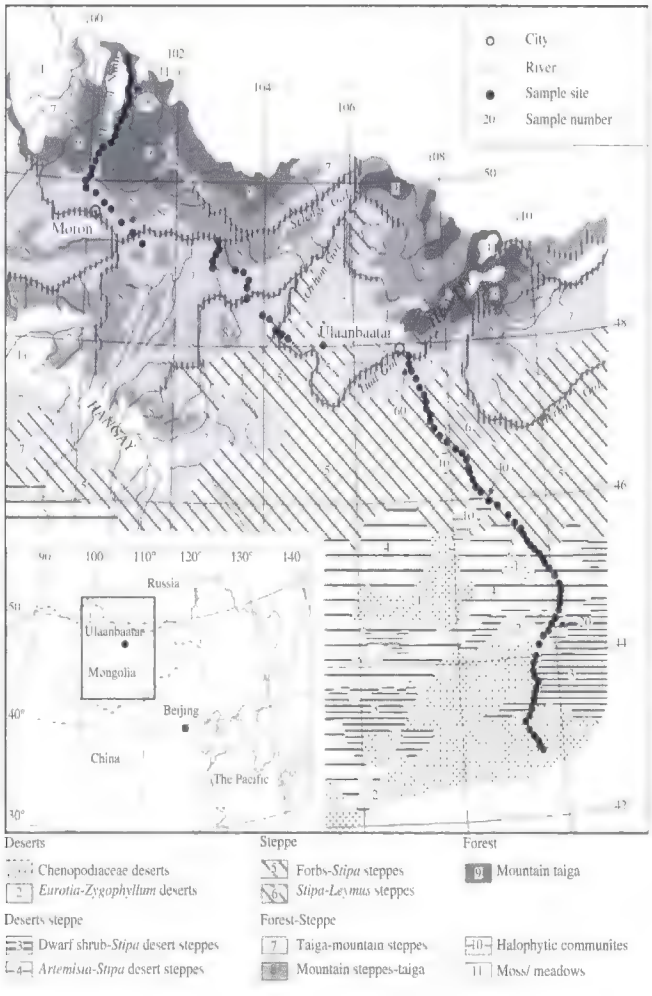

Figure 1 Vegetation map of Mongolia (based on Lavrenko *et al.*, 1979; Lavrenko & Karamisheva, 1990) and the locations of the 104 sample sites.

Tanacetum achillaeoides, *Ajania* spp., *Oxytropis aciphylla*, *Calligonum mongolicum*, *Asterothamnus*, *Allium* spp., *Brachanthemum gobicum*, *Halimodendron*, *Dodartia*, *Convolvulus*, *Scorzonera capito*, and *Potaninia mongolica* (Hilbig, 1995).

The *Eurotia–Zygophyllum* community (Fig. 1; type 2) is present in the desert zone, where the climate becomes slightly more humid, and there is a vegetation cover of 10–20%. The shrub layer is dominated by *Eurotia ceratoides*, *Zygophyllum xanthoxylon*, *Caragana leucophloea*, *Artemisia xerophytica*, *Atraphaxis frutescens*, *Calligonum mongolicum*, and *Ephedra* sp. The herb layer is composed mainly of *Stipa glareosa*, *Allium mongolicum*, *Convolvulus ammanii*, *Echinops gmelinii*, *Scorzonera pseudodivaricata*, *Lagochilus ilicifolius*, *Ptilotrichum canescens*, *Asparagus gobicus*, *Ajania achilleoides*, *Cleistogenes songorica*, *Anabasis brevifolia*, and *Iris tenuifolia*.

Desert-steppe vegetation

The *Artemisia–Stipa* desert-steppe (Fig. 1; type 4) is found in the northern part of the East Gobi between 750 and 1000 m elevation, where there is a mean annual temperature of 3–4°C, a July temperature of 22–24°C, and a January temperature of −16 to −18°C. The mean annual precipitation is 100–150 mm (Fig. 2). The vegetation is dominated by species of Poaceae (such as *Stipa krylovii*, *S. gobica*, and *Cleistogenes soongorica*) mixed with subshrubs of *Artemisia frigida*, *A. xerophytica*, *A. caespition*, *Tanacetum sibiricum*, *T. achillaeoides*, and *T. trifidum*. Other common species include *Agropyrum sibiricum*, *Allium mongolium*, *Caragana pyhmaea*, *C. leucophloea*, *Convolvulus ammannii*, *Heteropappuss hispidus*, *Scorzonera divaricata*, *Anabasis brevifolia*, *Salsola passerine*, *Kochia prostrata*, *Eurotia cerataide Reaumuria soongorica*, *Oxytropis aciphylla*, *Peganum nigellastrum*, *Brachanthemum gobicum*, *Potaninia mongolica*, and *Zygophyllum xanthoxylon*.

The dwarf shrub–*Stipa glareosa* desert-steppe (Fig. 1; type 3), consisting mainly of *Convolvulus*, *Reaumuria*, *Zygophyllum*, *Tribulus*, *Artemisia*, *Peganum*, *Stipa*, *Eragrostis*, *Aristida*, *Eurotia*, *Calligonum*, *Caragana* and *Bassia*, is distributed mainly in the East Gobi (Hilbig, 1995).

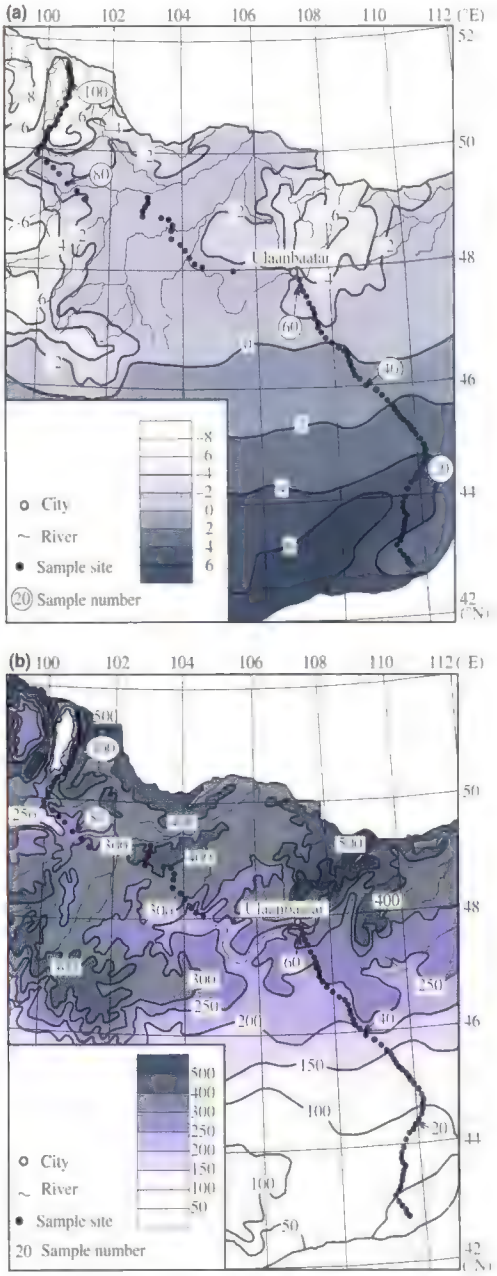

Figure 2 (a) Mean annual temperature (°C) and (b) mean annual precipitation (mm) for Mongolia (from Orshikh *et al.*, 1990).

Steppe vegetation

This vegetation type, consisting mainly of *Artemisia–Stipa* grass steppe and *Stipa–Leymus* steppe communities, occupies a vast region of central and eastern Mongolia, at elevations between 950 and 1400 m.

The forbs–*Stipa* grass steppe vegetation (Fig. 1; type 5; Hilbig, 1995), which is also known as the *Cymbario dahuricae–Stipetum krylovii* association (Hilbig, 1987), is the characteristic steppe community. This grass steppe is referred to as the dry steppe to distinguish it from the moister mountain steppe. It occurs in the hills east of the Hangay, and west, south, and south-east of the Hentiy. Geographically, these areas belong to the central Halha and the southern Mongolian–Daurian region. The mean annual temperature in this area varies from 3 to −2°C (Fig. 2), with a coldest temperature of −17 to −20°C and a warmest temperature of 16 to 22°C. The annual precipitation in these regions ranges from 150 to 300 mm (Fig. 2). Grass steppe contains a significant portion of tall and medium-sized grasses, particularly tussock grasses. Dominant species are *Stipa capillata* (*Stipa krylovii*), *Cleistogenes squarrosa*, and *Artemisia frigida*. Second dominant species are *Agropyrum cristatum*, *Elymus chinensis*, *Carex durinscula*, *Artemisia adamsii*, *A. scoparia*, *A. plusfria*, *A. peatinata* and *Achnatherum splendens*. Mixed in with these are forbs such as *Cymbaria dahurica*, *Goniolimion speciosum*, *Parmelia camtschadalis*, *Kochina prostrate*, *Saussurea salicifolia*, and *Peganum harmile*, as well as the subshrub *Caragana pygmaes* (Yunatov, 1959; Hilbig, 1995). In addition, where *Stipa* steppe is close to settlements of cattle farmers the land is degraded and dominated by other grasses and forbs (*Elymus chinensis*, *Cleistogenes squarrosa*, and *Artemisia frigida*).

The *Stipa–Leymus* steppe vegetation (Fig. 1; type 6) can be found in the moister areas. It is composed mainly of *Stipa krylovii* and *Leymus chinensis* (Hilbig, 1995).

Forest-steppe vegetation

This vegetation is widespread to the north and north-east of the Hangay, and to the north-west, west, and south of the Hentiy, generally between the Selenge and Orhon rivers. The forest-steppe vegetation borders the mountain taiga zone to the north and the steppe and desert-steppe zones to the south. Within the zone, patches of forest among steppe are well differentiated. Particularly in the lower mountain belt the north-facing slopes and higher elevations are often covered with needle-leaved forest, whereas steppe is nowadays concentrated on south-facing slopes and in and around valleys. In the east–west-oriented mountain ranges, the crest often marks the transition between forest and steppe (Yunatov, 1959; Hilbig, 1995). Furthermore, the steppe vegetation seems to have been expanding at the expense of forest (Hilbig, 1995).

The taiga mountain steppe vegetation (Fig. 1, type 7) is composed mainly of mountain and high-mountain herb–bunchgrass steppes locally mixed with *Larix sibirica* forests. This vegetation type typically occurs between 1000 and 1600 m elevation. The annual precipitation varies between 250 and 400 mm. The mean annual temperature is 0 to −2°C (Fig. 2), with a January mean temperature of −20 to −24°C and a July mean temperature of 12–17°C. A few companion species such as *Betula* and *Populus* grow in the higher mountain region.

Mountain steppe vegetation is fairly sparse, covering 60–70% of the ground surface, and is dominated by bunchgrasses such as *Festuca lenensis*, *Koeleria macrantha*, *K. gracilis*, *Poa attenuate*, *Agropyrum cristatum*, and *Stipa krylovii*. Several *Artemisia* species may be present: *Artemisia frigida*, *A. argyrophylla*, and *A. borealis*. Other common herbaceous species include *Aster alpinus*, *Saussurea salicifalre*, *Thalictrum foetidum*, *Astragalus brevifolius*, *Oxytropis pumila*, *Pulsatilla*, *Thymus serpyllum*, *Allium bidentatum*, *Arenaria capillaris*, *Bupleurum bicaule*, *Hedysarum pumilum*, *Iris potaninii*, *Pedicularis flava*, *Ptilotrichum canescens*, *Potentilla sericea*, *P. acaulis*, *Stellaria petraea*, *Stellaria chamaejasme*, and *Sibbaldianthe adpressa* (Yunatov, 1959; Hilbig, 1995).

On severely overgrazed spots the mountain steppe has degraded into a kind of short-turf mat dominated by *Carex duriuscula*. Such impoverished steppes also contain *Artemisia frigida*, and grasses become less important, with the exception of *Agropyron cristatum*. With an increase in elevation, the type changes to the mountain steppe-taiga vegetation (Fig. 1, type 8), consisting mainly of *Larix sibirica* forests, *Pinus sylvestris* forests, and mixed *Betula–Larix sibirica* forests combined with mountain steppe (Yunatov, 1959; Hilbig, 1995).

Mountain taiga vegetation

The mountain taiga vegetation (Fig. 1, type 9) is distributed mainly in the Hovsgol Nuur area at elevations of 1700–1950 m, with an annual mean temperature of −2 to −6°C, a January mean temperature of −24°C, and a July mean temperature of 12°C. The annual precipitation varies between 300 mm and 500 mm (Fig. 2). Mountain taiga is dominated by *Larix sibirica* and *Pinus sibirica*. Characteristic species of the shrub layer are *Rosa acicularis*, *Betula rotundifolia*, and, at higher altitudes, *Spiraea alpina*, *Lonicera altaica*, *Juniperus sibirica*, *Ledum palustre*, and *Rhododendron* spp. Hygrophilous grasses and perennial forbs occur here as well: *Calamagrostis obtusata*, *C. purpurea*, *Aegopodium alpestre*, *Polygonum viviparum*, *Trisetum*, *Elymus*, and members of the Caryophyllaceae, Cyperaceae, Ranunculaceae, Saxifragaceae, and Apiaceae (Yunatov, 1959; Hilbig, 1995).

FIELD AND LABORATORY METHODS

Field methods

Our sampling transect starts from south-eastern Mongolia, heads northwards, and then cuts across northern Mongolia in an east-to-west direction. We collected 104 samples from lowland desert to mountain taiga at an interval of 4 min (4′) latitude per sample (Fig. 1). Among these samples, numbers 1–25 and 90–104 were collected from nature reserves. Each sample was a composite of 10–20 subsamples of surface soil that were obtained randomly from an area of 20 m^2 to ensure even representation (Fig. 1; Table. 1). Some samples contained a small amount of moss and litter material at the top (1 cm).

Laboratory methods

Individual surface samples were homogenized before processing for pollen. One *Lycopodium* spore tablet (containing 12,542 ± 3.3% exotic *Lycopodium* spores, manufactured by Lund University, Batch No. 124961) was added to each sample prior to processing in order to allow total pollen and spore concentrations to be calculated. The samples were processed using 10–15% HCl (2 h), 5% KOH (boiling 3–5 min), and acetolysis solution consisting of a 9 : 1 mixture of acetic anhydride and sulphuric acid (Moore *et al.*, 1991). Furthermore, the pollen in the residue was concentrated with a 7-μm mesh sieve in conjunction with ultrasonic vibration. Finally, water-free glycerol was used for storage and preparation of microscopic slides.

Pollen identification was aided by the use of published pollen books and papers (Moore *et al.*, 1991; Wang *et al.*, 1995; Wan & Wei, 1999). We also consulted an extensive pollen reference-slide collection of more than 500 taxa from this and other regions.

A Leica light-microscope (Wetzler, Germany) was used to identify and count pollen. Routine counting was carried out at 400× magnification, and critical identifications were made under oil immersion at 1000×. A minimum of 500 pollen grains were counted from each sample. Pollen percentages were calculated using a total pollen sum excluding spores, and presented as curves in a pollen percentage diagram (Fig. 3). Pollen and spore concentrations were calculated on the basis of exotic *Lycopodium* spore counts and were expressed as the number of grains per gram of sediment (Fig. 4). Taxa with pollen percentages consistently below 2% or pollen concentration values consistently below 100 grains g^{-1} were excluded from the pollen diagrams. GRAPH and COREL DRAW software were used to plot the pollen diagrams.

Numerical analyses

Twenty-four pollen taxa were selected for the numerical analyses. These included *Pinus* Haploxylon-type, *Pinus* Diploxylon-type, *Picea*, *Abies*, *Larix*, *Betula*, *Alnus*, Rosaceae, *Artemisia*, *Aster*-type, *Anthemis*-type, *Taraxacum*-type, Poaceae, Ranunculaceae, Polemoniaceae, Liliaceae, Caryophyllaceae, *Convolvulus*, Polygonaceae, Chenopodiaceae, Zygophyllaceae, *Nitraria*, *Ephedra* and Cyperaceae. The selection of these pollen taxa was based on their importance in characterizing the major vegetation regions in Mongolia and the pollen assemblages as presented above. All samples (104) were used in the numerical analyses.

Discriminant analysis

Understanding the quantitative relationships between modern pollen rain and contemporary vegetation is vital for the interpretation of vegetation history based on fossil data. Discriminant analysis has been used in palynological research for deriving a predictive model of group membership based on

Table 1 Site information for the 104 modern pollen surface samples from Mongolia.

No.	Lat. (N)	Long. (E)	Alt. (m)	Material	Vegetation type	Main taxa
1	42°45′55″	109°37′04″	1031	Sand + litter	Chenopodiaceae desert	Chenopodiaceae, *Nitraria*, *Ephedra* and Zygophyllaceae
2	42°50′21″	109°36′02″	1104	Sand + litter		
3	42°54′49″	109°31′11″	1147	Sand + litter		
4	43°00′05″	109°24′49″	1195	Sand + litter		
5	43°06′11″	109°12′41″	1217	Sand + soil		
6	43°10′15″	109°08′51″	1100	Sand + litter		
7	43°15′12″	109°13′05″	1070	Sand + soil		
8	43°19′57″	109°20′50″	1014	Sand + soil		
9	43°25′13″	109°29′20″	1000	Sand + soil	*Stipa* desert steppe	Poaceae
10	43°30′22″	109°35′57″	979	Sand + soil	Chenopodiaceae desert	Chenopodiaceae, *Nitraria Ephedra* and Zygophyllaceae
11	43°35′03″	109°38′01″	950	Sand + soil		
12	43°40′10″	109°37′43″	1011	Sand + soil	*Stipa* desert steppe	Poaceae
13	43°45′06″	109°36′43″	937	Sand + soil	Chenopodiaceae desert	Chenopodiaceae, *Nitraria*, *Ephedra* Zygophyllaceae and Poaceae
14	43°49′34″	109°35′51″	887	Sand + soil		
15	43°54′55″	109°36′59″	884	Sand + soil		
16	44°00′13″	109°38′22″	803	Soil + litter	*Eurota* – *Zygophyllum* desert	Chenopodiaceae, *Zygophyllum*, Poaceae, *Allium*, *Artemisia*, *Caragana*, *Calligonum* and *Ephedra*
17	44°06′11″	109°40′40″	773	Sand + soil		
18	44°12′13″	109°43′22″	754	Soil + litter		
19	44°16′39″	109°46′08″	751	Soil + litter		
20	44°20′19″	109°51′42″	782	Sand + soil		
21	44°25′03″	109°57′27″	810	Sand + soil	*Artemisia* – Poaceae desert steppe	Poaceae, *Artemisia*, *Ajania*, *Convolvulus*, Chenopodiaceae, *Zygophyllum* and *Caragana*
22	44°31′25″	110°03′46″	748	Sand + soil		
23	44°35′22″	110°05′47″	774	Soil + litter		
24	44°39′51″	110°07′20″	791	Sand + soil		
25	44°45′10″	110°07′35″	848	Soil + litter		
26	44°49′52″	110°07′34″	889	Soil		
27	44°55′50″	110°06′32″	985	Soil		
28	45°00′05″	110°02′41″	931	Sand + soil		
29	45°05′00″	109°58′54″	917	Soil + litter		
30	45°10′07″	109°54′50″	925	Sand + soil		
31	45°15′13″	109°48′18″	964	Soil + litter	Forb + *Stipa* steppe	Poaceae (*Stipa*, *Cleistogenes*, *Elymus*, *Agropyrum*), *Artemisia*, *Caragana*, *Cymbaria* and *Convolvulus*
32	45°20′05″	109°42′00″	991	Soil + litter		
33	45°25′22″	109°36′29″	988	Soil + litter		
34	45°30′06″	109°32′45″	988	Soil + litter		
35	45°35′27″	109°29′14″	1011	Soil + litter		
36	45°40′20″	109°26′13″	1012	Soil + litter		
37	45°45′26″	109°21′13″	1051	Soil + litter		
38	45°50′09″	109°09′57″	1066	Soil + litter		
39	45°55′05″	109°03′00″	1071	Soil + litter	Forb + *Stipa* steppe	Poaceae (*Stipa*, *Cleistogenes*, *Elymus*, *Agropyrum*), *Artemisia*, *Caragana* and *Cymbaria*
40	46°00′01″	108°46′48″	1218	Soil + litter		
41	46°05′19″	108°38′07″	1154	Soil		
42	46°10′06″	108°33′49″	1178	Soil		
43	46°15′03″	108°29′16″	1191	Soil		
44	46°19′49″	108°24′22″	1277	Soil		
45	46°21′10″	108°21′01″	1288	Soil		
46	46°30′26″	108°19′12″	1292	Soil	*Stipa* – *Elymus* steppe	*Elymus*, *Stipa*, *Heteropappus hispidus*, *Artemisia*, *Caragana* and *Allium*
47	46°34′50″	108°16′49″	1266	Soil		
48	46°40′02″	108°06′51″	1332	Soil + litter		
49	46°45′01″	107°56′13″	1240	Soil + litter	Forb + *Stipa* steppe	Poaceae (*Stipa*, *Cleistogenes*, *Elymus*, *Agropyrum*), *Artemisia*, *Caragana* and *Cymbaria*
50	46°50′08″	107°46′19″	1266	Soil		
51	46°55′07″	107°43′54″	1322	Soil + litter		
52	47°00′15″	107°38′20″	1312	Soil + litter		
53	47°05′09″	107°35′49″	1314	Soil + litter		
54	47°09′48″	107°34′09″	1358	Soil + litter		
55	47°15′07″	107°31′06″	1415	Soil + litter		

Table 1 Continued

No.	Lat. (N)	Long. (E)	Alt. (m)	Material	Vegetation type	Main taxa
56	47°24′58″	107°25′50″	1415	Soil		
57	47°30′03″	107°22′50″	1504	Soil		
58	47°35′40″	107°16′29″	1581	Soil	Taiga forests – mountain forb/ bunchgrass steppes	*Artemisia*, *Aster*-type, Poaceae, *Potentilla*, *Stellera*, *Oxytropis*, *Pinus*, *Larix*, *Picea* and *Betula*
59	47°40′37″	107°14′18″	1678	Soil		
60	47°45′12″	107°14′33″	1568	Soil		
61	47°50′24″	107°09′20″	1570	Soil		
62	47°59′32″	105°26′06″	1231	Soil	*Stipa* steppe	Poaceae, *Artemisia*, *Caragana* and *Cymbaria*
63	48°05′54″	104°24′00″	1080	Soil + litter	*Stipa* steppe	Poaceae (*Stipa*, *Cleistogenes*, *Agropyrum*, *Elymus*,), *Artemisia*, *Caragana* and *Cymbaria*
64	48°09′41″	104°20′43″	1042	Soil + litter		
65	48°14′49″	104°13′32″	1022	Soil + litter		
66	48°20′18″	104°06′49″	1120	Soil + litter	Mountain steppes	Poaceae, *Artemisia* and *Betula*
67	48°24′57″	103°59′22″	1222	Soil	Forb + *Stipa* steppe	Poaceae, *Artemisia*, *Potentilla* and *Stellera*
68	48°29′42″	103°39′47″	1172	Soil + litter	*Stipa* steppe	Poaceae, *Artemisia*, *Caragana* and *Cymbaria*
69	48°34′00″	103°35′47″	1095	Soil + litter		
70	48°44′57″	103°34′29″	1170	Soil + litter	Taiga forest – mountain forb/ bunchgrass steppes	Poaceae, *Artemisia*, *Aster*-type, *Potentilla*, *Stellera*, *Carex*, *Larix*, *Pinus*, *Picea* and *Betula*
71	48°49′47″	103°30′30″	1255	Soil		
72	48°55′00″	103°20′39″	1477	Soil + litter		
73	49°00′35″	102°47′59″	1422	Soil + litter		
74	49°05′09″	102°47′23″	1289	Soil + litter		
75	49°10′09″	102°51′27″	1161	Soil + litter	Mountain steppes	Poaceae, *Artemisia*, *Caragana* and *Cymbaria*
76	49°15′02″	102°57′16″	1035	Soil + litter		
77	49°19′57″	102°58′08″	944	Soil + litter	Forb + *Stipa* steppe	Poaceae, *Artemisia*, *Aster*-type, *Potentilla* and *Stellera*
78	49°24′57″	100°59′28″	1197	Soil + litter	Mountain steppe	Poaceae, *Artemisia*, *Caragana* and *Cymbaria*
79	49°30′28″	100°53′04″	1333	Soil		
80	49°34′49″	100°49′14″	1516	Soil	Mountain steppe – Taiga	*Larix*, *Pinus*, *Betula*, *Picea*, *Rosa*, Poaceae, *Artemisia*, *Aster*-type, *Potentilla*, *Stellera*, *Carex* and *Oxytropis*
81	49°38′03″	100°13′10″	1338	Soil		
82	49°45′02″	100°08′18″	1566	Soil + litter		
83	49°49′50″	100°06′22″	1840	Soil + litter		
84	49°56′56″	99°57′56″	1560	Soil	Grass mountain steppe	Poaceae, *Artemisia*, *Aster*-type, *Potentilla*, *Polygonum*, Caryophyllaceae and Ranunculaceae
85	50°00′55″	99°58′15″	1677	Soil		
86	50°05′02″	100°00′10″	1614	Soil + litter	Mountain steppe – Taiga	*Larix*, *Pinus*, *Picea*, *Rosa*, *Betula*, *Polygonum*, *Calamagrostis*, *Aegopodium*, *Trisetum*, *Elymus*, Caryophyllaceae, Cypercaceae and Ranunculaceae
87	50°10′06″	100°01′19″	1588	Soil + litter		
88	50°14′33″	100°03′10″	1599	Soil + litter		
89	50°20′03″	100°06′25″	1646	Soil + litter		
90	50°25′08″	100°09′56″	1711	Soil + moss	Taiga forest	*Larix*, *Pinus* and *Picea*
91	50°30′00″	100°24′28″	1672	Soil + moss		
92	50°35′01″	100°30′47″	1685	Soil + moss		
93	50°40′01″	100°31′38″	1687	Soil + moss	Mountain steppe – Taiga	*Larix*, *Pinus*, *Picea*, *Rosa*, *Betula* and Poaceae
94	50°44′59″	100°31′51″	1669	Soil + moss		
95	50°50′04″	100°39′41″	1914	Soil + moss	Taiga forest	*Larix*, *Pinus* and *Picea*
96	50°54′40″	100°44′00″	1873	Soil + moss		
97	50°59′56″	100°43′04″	1766	Soil + moss		
98	51°05′41″	100°44′09″	1681	Soil + moss		
99	51°10′13″	100°44′02″	1670	Soil + moss		
100	51°15′13″	100°50′39″	1758	Soil + moss	Mountain steppe – Taiga	*Larix*, *Pinus*, *Picea*, *Rosa*, *Betula* and Poaceae
101	51°20′24″	100°50′21″	1758	Soil + moss		
102	51°25′06″	100°47′24″	1689	Soil + moss	Taiga forest	*Larix*, *Pinus* and *Picea*
103	51°30′23″	100°41′09″	1696	Soil + moss	Mountain steppe – Taiga	*Larix*, *Pinus*, *Picea*, *Rosa*, *Betula* and Poaceae
104	51°35′08″	100°45′49″	1842	Soil + moss		

the observed characteristics of each pollen sample. The procedure generates a discriminant function based on linear combinations of the predictor variables that provide the best discrimination between the groups (SPSS Inc., 2001; McCune & Grace, 2002). Liu & Lam (1985) used discriminant analysis as an inferential statistical technique to measure the degree of

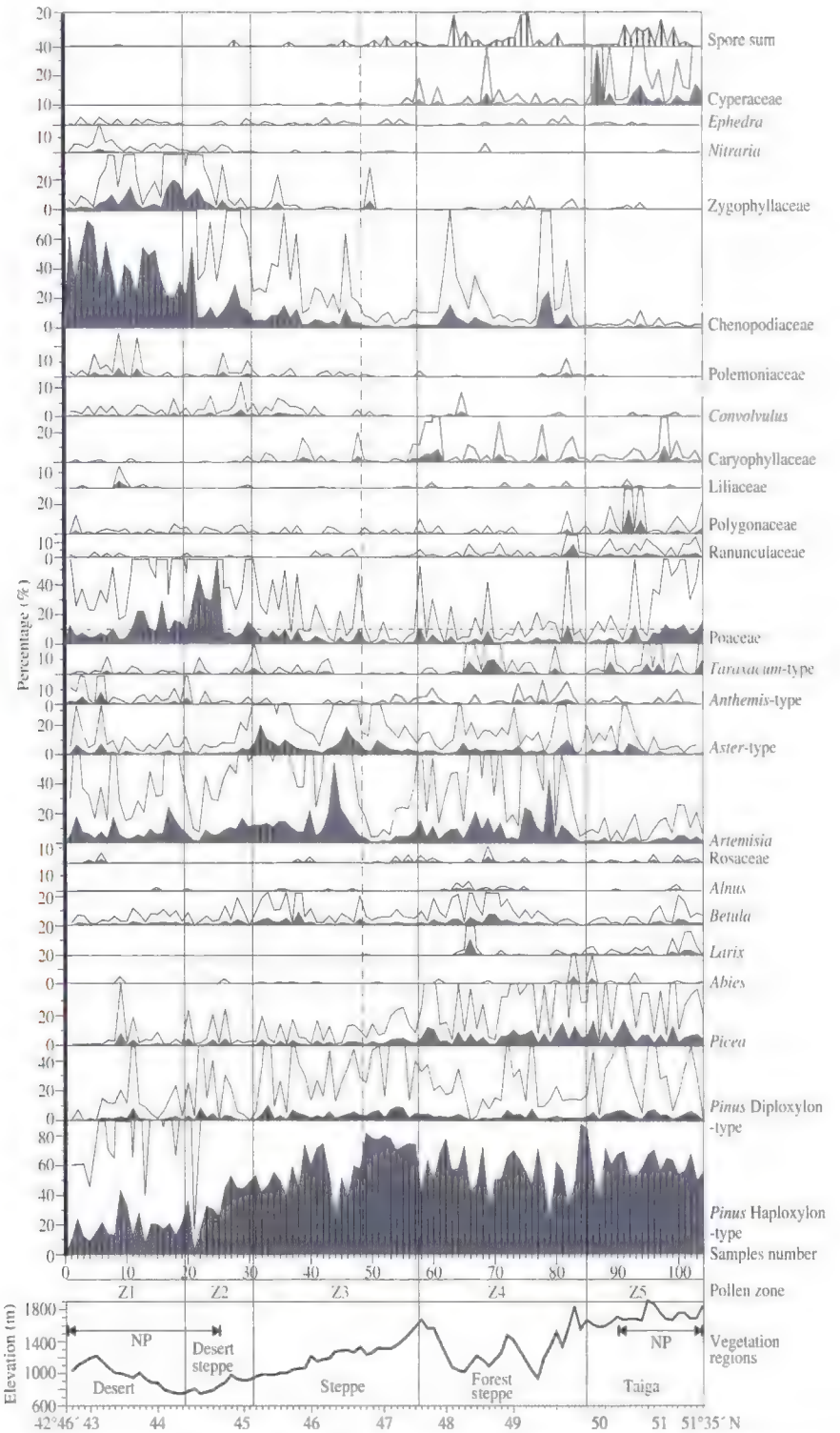

Figure 3 Pollen percentage diagram of the 104 surface samples along the south–north transect in Mongolia (black line: 5× exaggeration). Vegetation zones and elevations along the transect are shown at the bottom. NP, nature reserve area.

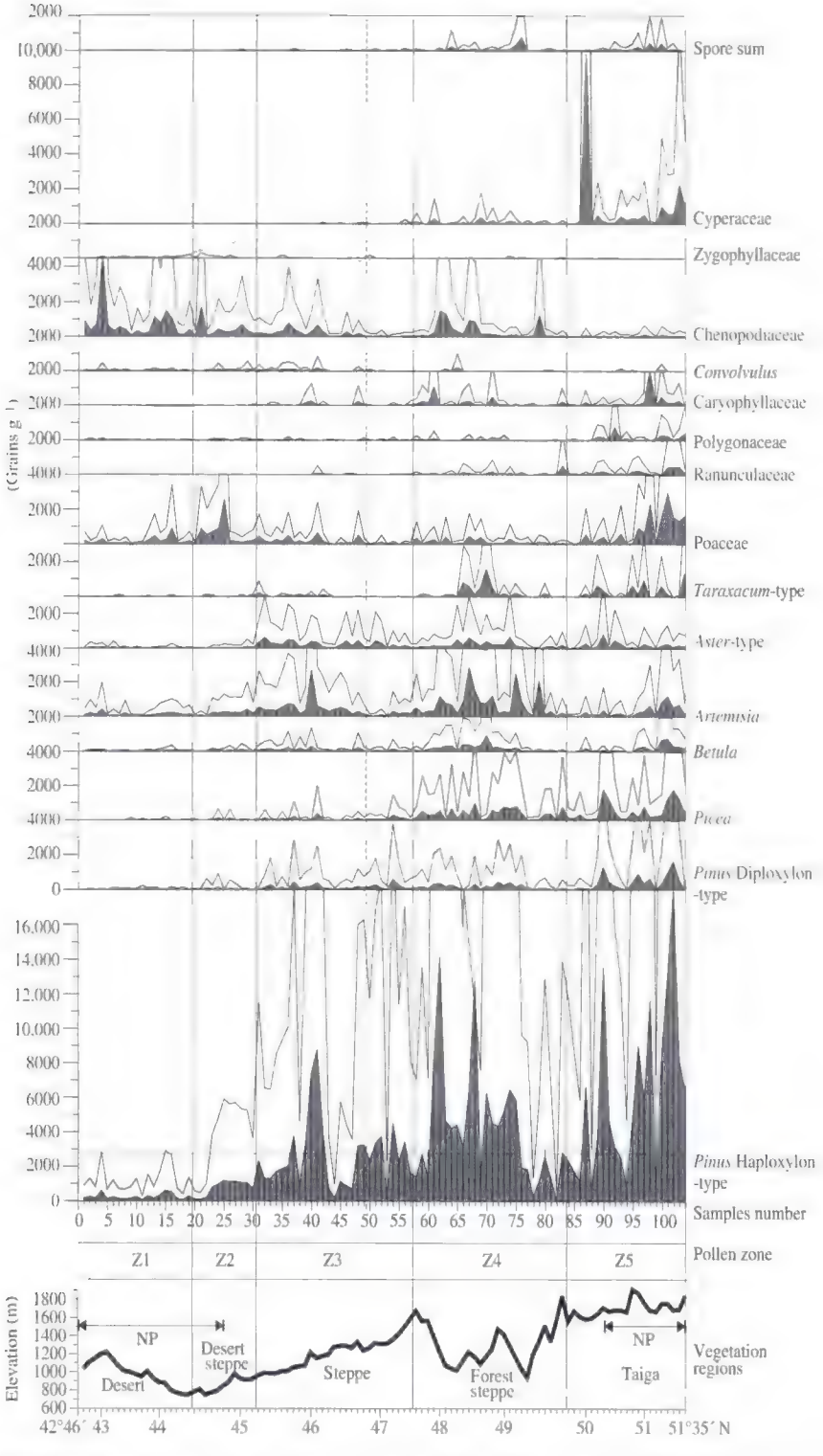

Figure 4 Pollen concentration diagram of the 104 surface samples along the south–north transect in Mongolia (black line: 5× exaggeration). Vegetation zones and elevations along the transect are shown at the bottom. NP, nature reserve area.

similarity between modern and fossil pollen assemblages. Since then, discriminant analysis has proved to be an effective tool with which to evaluate objectively the *a prior* classification of surface pollen samples into groups based on their vegetation regions (Sugden & Meadows, 1989; Liu, 1990; Lynch, 1996; Reese & Liu, 2005; Graf & Chmura, 2006). In this paper, we use discriminant analysis to determine how well the modern pollen assemblages can provide modern analogues for certain vegetation types, and to build the discriminant functions for identifying modern analogues from fossil pollen spectra obtained from this region.

Discriminant analysis requires an *a priori* classification of pollen surface samples into groups based on their vegetation regions (Liu & Lam, 1985; Liu, 1990; Lynch, 1996). Here we assigned the 104 modern pollen spectra to five major *a priori* groups based on their regional vegetation and local plant communities (Fig. 1). These five modern pollen sample groups, namely Z1, Z2, Z3, Z4, and Z5, are interpreted to correspond to five vegetation types, i.e. desert, desert-steppe, steppe, forest-steppe, and taiga, respectively.

The subprogram DISCRIMINANT in SPSS 11.0 (SPSS Inc., 2001) was used to perform the discriminant analysis. Two useful parameters can be computed with discriminant analysis (Liu & Lam, 1985). First, the *vegetation zone index* is based on the distance between a sample and the centroid of each *a priori* group in multidimensional space. Then, in palynological terms, *the probability of modern analogue* compares a pollen assemblage with the 'palynological signature' of its assigned vegetation region (as represented by its group centroid). A low probability for a sample suggests that the sample, although geographically derived from or statistically assigned to a vegetation region, in fact contains a pollen assemblage distinct from the palynological signature of this vegetation region (Liu & Lam, 1985).

Cluster analysis

Cluster analysis is a numerical technique that classifies samples (cases) or taxa (variables) into groups according to the dissimilarity between them. It has been widely used to analyse modern pollen data (Birks, 1973; Markgraf *et al.*, 1981). Hierarchical cluster analysis (HCA) is an exploratory tool designed to reveal natural groupings (or clusters) within multivariate ecological data, provided that they can be represented by a distance matrix. It has a long history of use in ecology (McCune & Grace, 2002). It is most useful for clustering a small number (less than a few hundred) of objects. Here we used the hierarchical cluster analysis procedure in the R-mode to study the relationships among the principal pollen taxa.

Non-metric multidimensional scaling

Non-metric multidimensional scaling (NMS), an ordination technique, was performed to determine how taxa distributions in all samples may be influenced by environment gradients (such as moisture, temperature, and elevation). NMS was chosen as opposed to other ordination techniques (e.g. detrended correspondence analysis, principal components analysis) primarily because it does not assume that variables are linearly related. Furthermore, the use of ranked distances improves the linearity of the relationship between distances measured in the pollen taxa and environmental space (Clarke, 1993; McCune & Grace, 2002). For this reason, NMS has been a popular choice in ecology in recent years (Taylor *et al.*, 2001; Enright *et al.*, 2005; Boucher & Mead, 2006; Soh *et al.*, 2006).

We used average-linkage clustering (between-groups linkage) with the Pearson product-moment correlation coefficient in SPSS 11.0 (SPSS Inc., 2001) for the hierarchical cluster analysis. The non-metric multidimensional scaling procedure was conducted using the 'autopilot (slow and thorough)' mode in PC-ORD 4.14 (McCune & Grace, 2002). The Sørensen (Bray-Curtis) method was used to calculate the distance matrix for ordination.

All the results were plotted using the program CORELDRAW 11.0.

RESULTS

Pollen spectra

The 104 surface samples (Table 1) were divided into five pollen zones (Figs 3 & 4), based on their location and local plant community, corresponding to five major vegetation types: (1) desert, (2) desert-steppe; (3) steppe; (4) forest-steppe; and (5) taiga. The main features of the pollen spectra in each vegetation type are described below.

Zone 1 (Desert vegetation, sites 1–19) Chenopodiaceae–Zygophyllaceae–*Nitraria*– Poaceae pollen assemblage

The desert pollen assemblage is dominated by Chenopodiaceae (20.35–68.44%), Zygophyllaceae (1.36–17.22%), Poaceae (3.29–22.22%), and *Artemisia* (3.07–18.18%). Minor pollen types include *Nitraria* (1–3%), *Ephedra*, *Anthemis*-type, Polemoniaceae, and *Convolvulus*. The abundance of tree pollen (e.g. *Pinus*, *Picea*, *Betula*, Ranunculaceae and Caryophyllaceae) is low.

Zone 2 (Desert-steppe vegetation, sites 20–30) Poaceae–Chenopodiaceae pollen assemblage

The desert-steppe pollen assemblage is characterized by maximum percentages of Poaceae (7.03–57.04%), together with Chenopodiaceae (6.3–22.18%), *Artemisia* (1.98–10.61%), Zygophyllaceae (1.33–10.07%), and fair amounts of *Convolvulus*, *Nitraria*, *Aster*-type, *Betula* (< 2.5%) and *Picea* (< 5%). The pollen concentration of Poaceae is relatively high, whereas those of other taxa are low. Furthermore the percentages of Chenopodiaceae and Zygophyllaceae seem to increase towards the ecotone with the desert.

Zone 3 (Steppe vegetation, sites 31–57) *Pinus* Haploxylon-type–*Artemisia*–*Aster*-type–Poaceae pollen assemblage

The steppe pollen assemblage is marked by high percentages of *Pinus* Haploxylon-type (39.14–78.44%), *Artemisia* (7.59–23.57%) and *Aster*-type (0.91–22.19%), and by low percentages of Poaceae (1.08–9.91%), Chenopodiaceae, and *Convolvulus*, with trace amounts of *Betula* and *Picea*. The concentrations of *Artemisia*, *Aster*-type, and *Convolvulus* are relatively high. However, some samples (i.e. sites 49–57) contain very high percentages (71.70–78.44%) but very low concentrations of *Pinus* Haploxylon-type, and very low concentrations of *Artemisia* and Poaceae.

Zone 4 (Forest-steppe, sites 58–83) *Pinus* Haploxylon-type–*Picea*–*Artemisia*–*Betula* pollen assemblage

The forest-steppe pollen assemblage (Figs 3 & 4) is distinctive in its variability because of biogeographical differences within the forest-steppe vegetation. In areas near *Larix* forest stands (sites 58–61, 70–74, 80–83) the pollen assemblage is dominated by *Pinus* Haploxylon-type (32.77–70.16%), together with moderate percentages of *Picea* (2.64–15.32%), *Artemisia* (2.64–15.53%), Poaceae (0.82–12.26%), Caryophyllaceae (0.78–8.16%), *Betula* (0.16–7.32%), *Taraxacum*-type, and *Aster*-type. In the mountain steppe zone (sites 66, 67, 69, 75, 76, 78 and 79), where taiga is 1–3 km away, the pollen assemblage is composed of *Pinus* Haploxylon-type (24.16–56.31%), *Artemisia* (7.02–23.92%), *Picea* (1.07–7.55%), and Chenopodiaceae (0.53–18.98%), together with *Betula* (0.61–7.21%), Poaceae (0.96–8.41%), and *Aster*-type. In the river valley or near ecotones (sites 62–65, 68 and 77), the pollen assemblage consists mainly of *Pinus* Haploxylon-type (56.98–78.13%), *Artemisia* (2.82–10.39%), *Picea* (0.57–8.90%), Poaceae (0.52–5.13%), *Aster*-type (0.64–8.53%), Chenopodiaceae (1.30–8.16%), and *Betula* (0.47–4.19%), along with *Taraxacum*-type, *Aster*-type, Ranunculaceae, Caryophyllaceae and Cyperaceae.

All in all, the forest-steppe pollen assemblages are composed mainly of *Pinus* Haploxylon type, *Picea*, *Artemisia*, and *Betula*, with varying contributions from montane forb/shrub and wetland elements (such as Ranunculaceae, Caryophyllaceae, Polygonaceae and Cyperaceae). Pteridophyte spores are typically common, and pollen concentrations of the main taxa are generally high.

Zone 5 (taiga, sites 84–104) *Pinus* Haploxylon-type–*Picea*–Poaceae–Cyperaceae pollen assemblage

The taiga pollen assemblage consists of *Pinus* Haploxylon-type (50.00–84.72%), *Picea* (2.21–16.67%), and Poaceae (1.10–12.97%), with *Artemisia*, *Aster*-type, *Taraxacum*-type, Ranunculaceae, Polygonaceae, Caryophyllaceae, *Betula*, and Rosaceae. The concentrations of the main taxa are also very high. Pollen from montane forbs/shrubs (e.g. Ranunculaceae and Caryophyllaceae), wetland plants (such as Cyperaceae (0.70–14.03%) and Polygonaceae), and fern spores are abundant, as expected from the high effective moisture in this zone. Remarkably, the pollen of *Larix*, the dominant tree in this forest community, occurs only rarely (< 3%).

Numerical analyses

Discriminant analysis

The results of discriminant analysis show that discriminant functions 1 and 2 explain 83.9% and 10.0%, respectively, of the total variance within the data set (Table 2). The five group centroids on the first two discriminant functions (Fig. 5) are clearly separated from each other. The samples of desert, desert-steppe and steppe are most distinct from those of the other major vegetation types. However, some overlap occurs between forest-steppe and taiga. Some of the overlapping samples are from the ecotonal area between forest-steppe and taiga, reflecting the transitional character of the vegetation and the palynological signatures. This transitional character is also indicated by the classification results of discriminant analysis

Table 2 Standardized discriminant function coefficients of the 24 pollen taxa used in the discriminant analysis.

Pollen taxa	Function 1	Function 2	Function 3	Function 4
Pinus Haploxylon	1.460	4.683	0.452	2.094
Pinus Diploxylon	0.324	1.242	0.199	0.575
Picea	0.486	0.286	0.355	0.371
Abies	−0.057	0.664	0.008	0.174
Larix	0.023	0.443	0.220	0.431
Betula	0.366	0.847	−0.154	0.77
Alnus	0.038	−0.070	−0.156	−0.280
Rosaceae	0.185	−0.387	−0.096	0.068
Polygonum	0.392	0.451	0.551	0.424
Convolvulus	−0.024	0.601	0.266	−0.131
Poaceae	0.566	2.801	0.862	0.774
Caryophyllaceae	0.243	0.102	−0.107	0.181
Ranunculaceae	0.334	0.072	0.112	0.217
Polemoniaceae	0.347	0.692	0.504	−0.418
Anthemis-type	0.230	0.389	0.139	−0.140
Aster-type	0.425	1.353	−0.383	0.662
Taraxacum-type	0.321	0.609	0.182	0.424
Artemisia	0.950	2.387	0.132	0.780
Chenopodiaceae	−0.225	2.683	0.121	1.555
Zygophyllaceae	−0.427	0.880	−0.086	0.480
Nitraria	−0.756	0.131	0.177	0.358
Ephedra	−0.104	0.119	−0.274	0.071
Liliaceae	−0.711	−0.148	−0.331	0.337
Cyperaceae	0.667	1.657	0.553	1.157
Percentage of variance	75.40	15.40	5.70	3.50
Cumulative percentage of variance	75.40	90.80	96.50	100.00

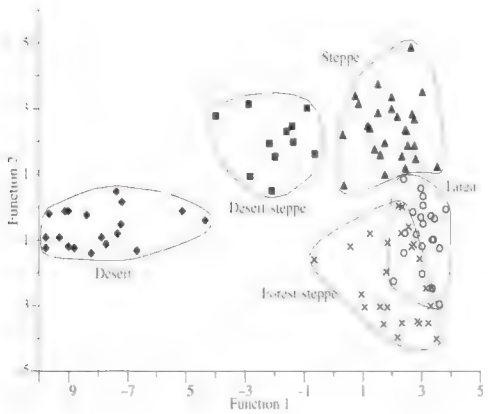

Figure 5 Ordination of the 104 surface samples along discriminant functions 1 and 2.

(Table 3), the probability of modern analogue, and the vegetation zonal index (Fig. 6).

A comparison of the predicted group (pollen zone) memberships with the *a priori* groups shows that 97.1% of the samples are correctly classified (Table 3). The misclassified samples generally have very low values (< 0.1) of probability of modern analogue, indicating that they are transitional in character or that they are unique among members of their own groups (Liu & Lam, 1985; Reese & Liu, 2005). For example, sites 82 and 83 are located near the ecotone between forest-steppe and taiga, and site 12 is unique among samples in pollen zone 1. The boundaries between vegetation regions generally correspond to abrupt changes in the vegetation zonal indices (Fig. 6).

In summary, the results of the discriminant analysis confirm that the five vegetation regions have distinctive palynological signatures as represented by the five pollen assemblages, and most of the pollen samples are typical of these major vegetation types (Fig. 6), except that some overlap occurs between the forest-steppe and taiga groups. The statistical analysis can also reflect the small azonal vegetation communities existing within a broad vegetation region and the transitional communities near the ecotone. The numerical techniques are useful in identifying the dominant pollen types representing each major vegetation type and in depicting the transitional or unique samples.

Hierarchical cluster analysis

The HCA results are presented in a dendrogram (Fig. 7). Pollen taxa are listed along the left vertical axis. The horizontal axis shows the distance between clusters when they are joined (SPSS Inc., 2001).

Two major groupings (A and B) are indicated by HCA (Fig. 7). Group A is composed mainly of montane trees and forbs/shrubs, and B is composed of herbs and shrubs. Within Group A, montane conifers and montane forbs/shrubs requiring lower temperature and moderate humidity (*Pinus* Haploxylon-type, *Pinus* Diploxylon-type, *Abies*, *Picea*, Caryophyllaceae, and Ranunculaceae) cluster together (A1), as do deciduous tree/shrubs and heliophytic taxa (*Betula*, *Alnus*, Rosaceae, *Taraxacum*-type and *Larix*) (A2), and those characteristic of moderate hydroperiod wetlands (Cyperaceae and Polygonaceae) (A3). Group B can be divided into four subgroups. Steppe forbs/shrubs (*Artemisia* and *Aster*-type) constitute B1. B2 is composed of Polemoniaceae, Liliaceae, and *Ephedra*. Xerophilous desert forbs/shrubs (Chenopodiaceae, *Nitraria*, Zygophyllaceae, and *Anthemis*-type) constitute B3. B4 includes *Convolvulus* and Poaceae.

Within the Asteraceae family, the *Anthemis*-type, the *Taraxacum*-type, and the *Artemisia* and *Aster*-type are separated into three distinct subgroups (Fig. 7). The *Anthemis*-type clusters with xeric taxa in subgroup B3, the *Taraxacum*-type clusters with moderate-humidity taxa in subgroup A2, and the *Artemisia* and *Aster*-type are combined into subgroup B1. The separation seems consistent with their distributions within these sub-environments. The palynological identification of these subgroups may provide a useful basis for palaeoenvironmental reconstruction from fossil-pollen assemblages.

Non-metric multidimensional scaling

The NMS procedure suggests two dimensions for the final solution. The variance explained by the first and the second axes was 74.2% and 20.8%, respectively (Fig. 8). The model stress value was 12.7979, and the final instability was

Table 3 Classification results of the surface samples by discriminant analysis. 97.1% of the original grouped cases were correctly classified.

Grouped	Vegetation type	No. of samples	Predicted group membership				
			Desert	Desert-steppe	Steppe	Forest-steppe	Taiga
Original grouped	Desert	19	19* (100.0†)	0 (0.0)	0 (0.0)	0 (0.0)	0 (0.0)
	Desert steppe	11	0 (0.0)	11 (100.0)	0 (0.0)	0 (0.0)	0 (0.0)
	steppe	27	0 (0.0)	0 (0.0)	27 (100.0)	0 (0.0)	0 (0.0)
	Steppe forest	26	0 (0.0)	0 (0.0)	0 (0.0)	25 (96.2)	1 (3.80)
	Taiga	21	0 (0.0)	0 (0.0)	0 (0.0)	2 (9.5)	19 (90.5)

*Number of samples classified as that group.

†Percentage of samples classified as that group.

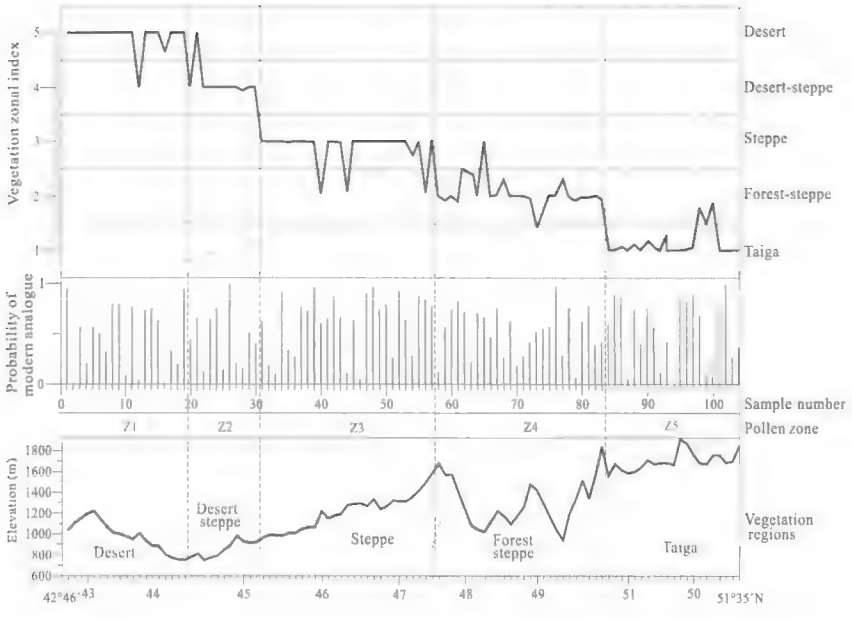

Figure 6 Results of the discriminant analysis for the 104 surface samples, presented as values of vegetation zonal index and probability of modern analogue.

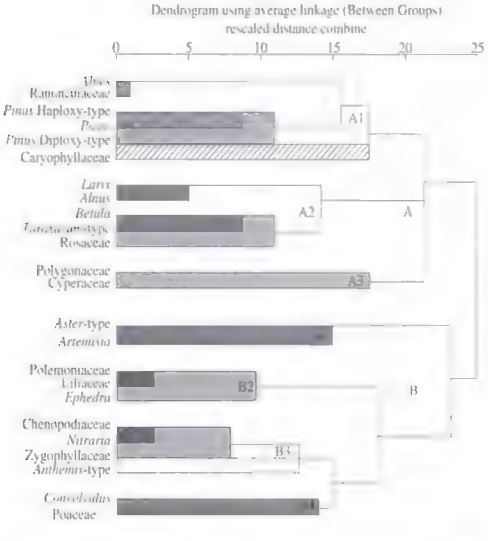

Figure 7 Dendrogram of pollen taxon groups classified by hierarchical cluster analysis.

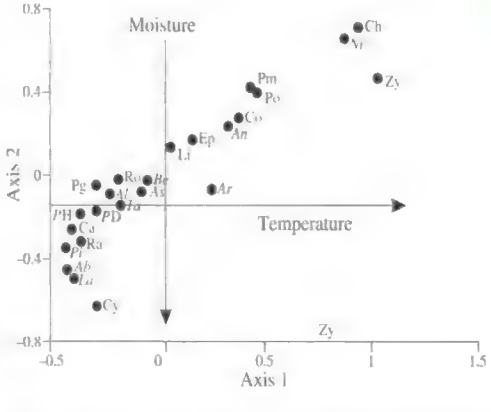

Figure 8 Non-metric multidimensional scaling plot of pollen taxa in two-dimensional ordinal space. Ch, Chenopodiaceae; *Ni*, *Nitraria*; Zy, Zygophyllaceae; Pm, Polemoniaceae; Po, Poaceae; *Co*, *Convolvulus*; *An*, *Anthemis*-type; *Ep*, *Ephedra*; Li, Liliaceae; *Ar*, *Artemisia*; *As*, *Aster*-type; *Be*, *Betula*; Ro, Rosaceae; *Al*, *Alnus*; *Ta*, *Taraxacum*-type; Pg, Polygonaceae; *Pi*, *Picea*; *Ab*, *Abies*; Ra, Ranunculaceae; PD, *Pinus* Diploxylon-type; PH, *Pinus* Haploxylon-type; Ca, Caryophyllaceae; *La*, *Larix*; Cy, Cyperaceae.

0.00000887 (< 0.00001). The axes extracted were stronger than those expected by chance ($P = 0.0196$) based on the Monte Carlo test. The NMS ordination and the positions of the 24 pollen types on the first two NMS axes are shown in Fig. 8.

The first axis, on which Zygophyllaceae and Chenopodiaceae have the highest positive values and *Picea* and *Abies* have the highest negative values, probably reflects the temperature gradient. Montane forest trees, montane forbs/shrubs and moderate hydroperiod wetland plants, such as *Picea*, *Abies*, *Pinus*, *Larix*, *Betula*, *Alnus*, Rosaceae, Ranunculaceae, Caryophyllaceae, *Taraxacum*-type, Cyperaceae and Polygonaceae, have negative values on the first axis. Xerophytic desert forbs/shrubs and steppe forbs/shrubs, such as Chenopodiaceae, *Nitraria*, Zygophyllaceae, Polemoniaceae, Poaceae, *Convolvulus*, *Anthemis*-type *Ephedra*, Liliaceae and *Artemisia*, have

positive values on the first axis. There is good agreement between NMS and HCA results except for the *Aster*-type.

The second axis, on which the xerophytic plants (Chenopodiaceae and *Nitraria*) have the highest positive value and the hydroperiod wetland plants (Cyperaceae) have the highest negative value, probably reflects the moisture gradient. Figure 8 also shows a clear separation between birch forest/shrubs and the cold-moist needle-leaved forest component. It seems that birch forest/shrubs occur in drier places than cold-moist needle-leaved forest, as indicated by their modern geographic distribution.

In addition, a gradient of increasing elevation can be traced diagonally from the top right to the low left corner, as represented by the ordination of lower-elevation desert shrubs (Chenopodiaceae, *Nitraria*) and alpine conifers (*Larix*, *Abies*, *Picea*) in the plot, respectively.

DISCUSSION

The relationship between surface pollen and vegetation can be affected by various factors, including pollen production and dispersion mechanism. In Mongolia, as well as in other regions, the complex relationship between pollen and vegetation should be understood in the light of these factors and processes.

Pollen assemblages and vegetation

The most remarkable characteristic of pollen zone 1 is the highest percentages of Chenopodiaceae and lowest of *Pinus* Haploxylon-type. The highest frequencies of xerophytic desert forb/shrub taxa (Chenopodiaceae, Zygophyllaceae and *Nitraria*) suggest that these pollen taxa are derived from the local vegetation, i.e. desert. The presence of *Pinus* Haploxylon-type at relatively low percentages, despite the absence of pine trees in the desert, is the result of long-distance transport of this pollen.

Samples in pollen zone 2 are dominated by Poaceae and *Pinus* Haploxylon-type, along with Chenopodiaceae, *Artemisia*, and Zygophyllaceae. These samples are derived from the desert-steppe. The rather high percentages of Poaceae (up to 60%) in our samples contrast with results from some other studies. The latter studies from the Chinese desert-steppe show dominance by Chenopodiaceae and *Artemisia* pollen even though grasses are very common in the vegetation (Li *et al.*, 2005; Liu *et al.*, 2006). The high abundance of Poaceae pollen in our samples (sites 21–25) is probably explained by the fact that these samples are derived from a nature reserve, where the natural vegetation is protected. By contrast, Poaceae pollen percentages are relatively low in samples collected outside the nature reserve, where the vegetation has been disturbed by human activities. Most of the samples used in previous studies on the Chinese desert-steppe were derived from anthropogenically disturbed areas.

The samples in pollen zone 3 come from the *Artemisia–Stipa* grass steppe, where the natural vegetation is not protected and has been heavily disturbed by grazing. This zone is characterized by high percentages and concentrations of *Pinus* Haploxylon-type, *Artemisia*, and *Aster*-type, but Poaceae occurs only in low percentages. Another interesting observation is that percentages of *Pinus* Haploxylon-type are very high in some samples (sites 49–57). It is notable that these samples were collected near the capital of Mongolia (Ulaanbaatar), where much of the steppe has been converted into pasture. Some researchers have suggested that the pollen frequency of *Artemisia* is higher than that of Poaceae in the grass-dominated steppe owing to the lower representation of Poaceae pollen, meaning that *Artemisia* dominates the palynological signature from steppe (Liu *et al.*, 1999). However, Liu *et al.*'s surface samples were collected from over-grazed steppes where grasses were selectively eaten by grazing animals before flowering, and therefore the over-representation of *Artemisia* in these steppe samples is probably an artefact of human disturbance. Based on our data from both inside and outside the nature reserve we argue that Poaceae abundance tends to be suppressed in the modern pollen rain from steppes where the human impact is pervasive. As a corollary, the very high pollen percentages of *Pinus* Haploxylon-type in zone 3 may also be an artefact of human disturbance (overgrazing).

The variable pollen assemblages of pollen zone 4, the forest-steppe group, contain three subtypes reflecting the mosaic character of this vegetation region (see Figs 3, 4 & 6). This pollen zone is characterized mainly by high percentages of *Pinus* Haploxylon-type, *Picea*, *Artemisia* and *Betula*, the sporadic but occasionally abundant presence of montane forbs/shrubs and pteridophyte spores, and high pollen concentrations of the main taxa.

In pollen zone 5, it is noteworthy that the frequency of *Larix* pollen is very low (maximum 3.23% in site 102), even in the *Larix*-dominated taiga. Here the pollen assemblage is dominated by *Pinus* Haploxylon-type, *Picea*, Poaceae, and Cyperaceae, together with taxa from montane forbs/shrubs, wetland plants, and pteridophyte spores.

In summary, the different vegetation zones in Mongolia contain different pollen assemblages that can be distinguished qualitatively and quantitatively. Pollen from xeric desert taxa (Chenopodiaceae, Zygophyllaceae, and *Nitraria*) is most abundant in the desert region, whereas abundant Poaceae pollen characterizes the desert-steppe region. High percentages of *Artemisia* and *Aster*-type characterize the steppes, where grasses are depleted as a result of overgrazing (Hilbig, 1995). Both forest-steppe and taiga contain high pollen percentages of *Pinus* Haploxylon-type and *Picea*, but these two vegetation types can be distinguished by the abundance of steppe forbs (*Artemisia*, *Aster*-type) and temperate summer-green tree taxa (*Betula* and *Alnus*) in the forest-steppe sites, and the abundance of montane forbs/shrubs and graminoid taxa (Poaceae and Cyperaceae) in taiga sites.

Pollen dispersal and representation

Pollen dispersal is an important factor affecting the representation of the various taxa in the modern pollen rain. Here we

select 10 important taxa to discuss their patterns of pollen dispersal and representation.

Pinus

Three species of pine are present in Mongolia: *Pinus pumila*, *P. sibirica* and *P. sylvestris*. Of these, *P. sylvestris* produces Diploxylon-type pollen and the other two species (*P. pumila*, *P. sibirica*) produce Haploxylon-type pollen. *Pinus pumila* and *P. sibirica* grow in the Hangay and Hentiy mountains and in the Hovsgol Nuur area. *Pinus sylvestris* is widespread along the sandy river terraces of the Orhon, Selenge, and Onon (Hilbig, 1995).

Pinus is dominant in the modern pollen rain in all the vegetation zones in the study area except the desert. *Pinus* percentages are lowest in the desert vegetation and highest in the overgrazed area, where the steppe has been converted to pasture. The high percentages of pine pollen in pasture areas can be explained by the effective long-distance transport of pine pollen from the forest-steppe and the suppression of local pollen production as a result of overgrazing. However, *Pinus* pollen concentrations are low in the steppe, rise to moderate values in forest-steppe, and are highest in taiga. The highest percentages and concentrations of *Pinus* pollen occur in the taiga, probably reflecting the local presence or even abundance of pine tree in the taiga. The lowest *Pinus* pollen percentages and concentrations occur in the desert and desert-steppe, but even here, where pine trees are absent, *Pinus* pollen may still occur with values in the order of 10–50% as the result of long-distance transport by wind. *Pinus* percentages and concentrations are moderate in the forest-steppe because pine pollen can be derived locally from pine trees growing on the north-facing slopes and at higher elevations (Figs 3 & 4).

In general, pine trees may not be locally present at sites where *Pinus* pollen occurs at values < 50%. Our conclusion is supported by previous studies indicating that *Pinus* pollen is well dispersed and is greatly over-represented in the pollen rain (e.g. Li, 1993; Li *et al.*, 1993). The concentration of *Pinus* pollen must be considered in palaeovegetational reconstructions from fossil pollen data.

Picea

Picea pollen occurs at < 5% and only discontinuously in the desert, desert-steppe and steppe zones. The pollen concentration of *Picea* begins to increase from the forest-steppe (site 58) northwards. The highest *Picea* percentages correspond closely to the distribution of spruce trees in the forest-steppe and taiga zones. Indeed, the dispersal distance of *Picea* is shorter than that of *Pinus*.

Larix

Although *Larix* is the most common tree in the modern forest-steppe and taiga, the pollen abundance of *Larix* is very low. Many previous studies have shown that *Larix* pollen is usually greatly under-represented and that its percentages fluctuate greatly (Igarashi, 1996; Noshiro *et al.*, 1997; Minckley & Whitlock, 2000; Andreev *et al.*, 2001). *Larix* has low pollen productivity and poor pollen dispersal. *Larix* pollen attained slightly higher percentages (5–10%) only within *Larix* stands, whereas outside *Larix* stands the pollen usually decreased dramatically (almost to zero) (Noshiro *et al.*, 1997; Minckley & Whitlock, 2000). Gunin *et al.* (1999) suggested that the pollen dispersal distance from the *Larix* tree is usually less than 200–350 m, and that the pollen is easily destroyed by water. Andreev *et al.* (2001) pointed out that *Larix* pollen is relatively rare, even in surface samples from larch forests, and that its low frequency in pollen spectra does not reflect its true regional abundance, as evidenced by surface samples from larch forests in many areas of East Siberia. They further suggested that a low but consistent presence of *Larix* in fossil pollen spectra indicates the presence of larch trees growing close to the site (Noshiro *et al.*, 1997; Gunin *et al.*, 1999; Minckley & Whitlock, 2000; Andreev *et al.*, 2001). Kataoka *et al.* (2003) also reported that *Larix* is generally under-represented in pollen surface samples from the Lake Baikal region.

Poaceae

In our study area, Poaceae pollen percentages have higher values in the desert, desert-steppe and taiga than in the steppe and forest-steppe zones, where grasses are supposed to be prevalent. This phenomenon can probably be explained by the fact that the desert, desert-steppe, and taiga areas investigated are situated in nature reserves, where the true abundance of grasses in the natural vegetation is maintained (a fact confirmed by the high total pollen concentration values). By contrast, the steppe and forest-steppe areas sampled are disturbed by livestock, which feed on grasses selectively over steppe forbs.

Many researchers have found that, owing to its low representation, Poaceae pollen values are usually below 5% in most samples, and the presence of Poaceae pollen even at low percentages (3–10%) probably indicates the existence of grassland/steppe vegetation dominated by grasses (Huang *et al.*, 1993; Wang *et al.*, 1996; Li, 1998; Liu *et al.*, 1999; Li *et al.*, 2005). However, our data show that, although Poaceae is under-represented as a result of its low pollen productivity, higher percentages (about 10–40%) may be found in areas where the natural vegetation is better preserved.

Betula, Chenopodiaceae, *Artemisia*, and *Aster*-type

Betula pollen occurs in all the vegetation zones, especially in the forest-steppe, with values of 1–8%. The broad distribution indicates that it is well dispersed. Chenopodiaceae pollen is present in all sites but is particularly abundant in desert, desert-steppe, steppe, and forest-steppe. Therefore Chenopodiaceae pollen may be somewhat over-represented. *Artemisia* pollen not only is present at all sites but is abundant in most samples. Likewise, *Aster*-type is present at

all sites. Both *Artemisia* and *Aster*-type pollen seem to be over-represented relative to the abundance of their plants in the vegetation.

Cyperaceae and Zygophyllaceae

Cyperaceae pollen occurs only in the forest-steppe and taiga, whereas Zygophyllaceae pollen is present only in the desert and desert-steppe. The occurrence of these pollen types is consistent with the distributions of their plant populations.

Pollen–climate indices

Several methods have been developed and tested for the quantitative reconstruction of climate variables, for example the response surface analysis and transfer function methods. However, these methods cannot be effectively applied to this region because modern climatic data are sparse in Mongolia. The ratios of various pollen types have been used effectively as environmental indicators and can often help to identify trends that are difficult to see from the percentages and concentrations alone. For example, Liu *et al.* (2005, 2007) used the Poaceae/Asteraceae (P/A) pollen ratio as an index of moisture availability in the Altiplano of South America. Similarly, the A/C (*Artemisia*/Chenopodiaceae) ratio has been used as a moisture indicator in the Middle East (El-Moslimany, 1990) and Central Asia (e.g. Van Campo *et al.*, 1996; Liu *et al.*, 1998; Demske & Mischke, 2003; Herzschuh *et al.*, 2004). Yu *et al.* (1998) and Cour *et al.* (1999) reported that Chinese desert areas yield A/C values below 0.5. Fowell *et al.* (2003) suggested a semi-quantitative 'aridity pollen index' expressed as a ratio of desert-steppe (*Artemisia*–Chenopodiaceae) to steppe (Poaceae) taxa to distinguish dry steppe from moist meadow steppe and forest-steppe vegetation in north-central Mongolia. Accordingly, higher values of the index are indicative of decreasing moisture availability.

As discussed above, however, Poaceae species in desert, desert-steppe, steppe, forest-steppe and taiga could be abundant locally in the azonal vegetation communities, except in some areas that are disturbed by overgrazing. Owing to the possible distortion of Poaceae pollen abundance by human activities in these arid and semi-arid environments, the 'aridity pollen index' expressed as a ratio of desert-steppe (*Artemisia*–Chenopodiaceae) to steppe (Poaceae) taxa may not be an appropriate indicator to use for palaeoclimatic reconstruction. Our reservation about this pollen index is supported by recent vegetation analyses from the Alashan Plateau (Herzschuh *et al.*, 2004).

In this paper, we propose two new pollen–climate indices for Mongolia that are based on the extensive modern pollen data base generated in this study – a moisture index (M) and a temperature index (T) (Table 4). The two indices are calculated based on the ratios between groups of pollen taxa that represent different moisture or temperature conditions in the study region. These groups of climate-sensitive pollen taxa are classified largely based on the results of the HCA (Fig. 7) and NMS (Fig. 8), but some memberships in each group are modified based on knowledge of ecological conditions acquired from the field or on considerations pertaining to the pollen representation of specific taxa (e.g. Poaceae, discussed above).

We divided the main pollen taxa into six groups based on their relationships to six major vegetation communities (Table 4). Group S1, including Chenopodiaceae, *Nitraria*, and Zygophyllaceae, is the main component of the xeromorphic desert. Group S2, containing Polemoniaceae, *Convolvulus*, *Anthemis*-type, *Ephedra*, and Liliaceae, occurs commonly in desert-steppe. Group S3, including *Artemisia* and *Aster*-type, is representative of the meso-xeromorphic steppe. These three groups are basically composed of the members of groups B1 to B4 delineated by HCA and NMS (Figs 7 & 8), with the exception of Poaceae. Poaceae is excluded from this and all other groups because its abundance could be distorted by human disturbance, as discussed above. Groups S4 to S6 represent the cold-moist needle-leaved forest and montane forbs, birch forest/shrubland, and moderate hydroperiod steppe vegetation types, respectively. The 13 pollen taxa included in these three groups are the same as those in groups A1, A2, and A3 classified by HCA and arranged by NMS (Figs 7 & 8).

Table 4 Main pollen taxa in the six pollen taxon groups (S1–S6) used in the calculation of the pollen ratios, which were used in the derivation of the two pollen–climate indices – the temperature index (T) and moisture index (M).

Group	Type	Main pollen taxa
S1	Xeromorphic desert	Chenopodiaceae, *Nitraria*, Zygophyllaceae
S2	Desert-steppe	Polemoniaceae, *Anthemis*-type, Liliaceae, *Ephedra*, *Convolvulus*
S3	Meso-xeromorphic steppe	*Artemisia*, *Aster*-type
S4	Birch forest/shrubs	*Betula*, *Alnus*, Rosaceae, *Taraxacum*-type
S5	Cold-moist needled forest	*Picea*, *Abies*, *Larix*, *Pinus* Haploxylon-type *Pinus* Diploxylon-type Ranunculaceae, Caryophyllaceae
S6	Moderate hydroperiod steppe	Cyperaceae, Polygonaceae
	Pollen–climate indices	**Calculation**
T	Temperature index	$T = (P_{S1} + P_{S2} + P_{S3})/(P_{S4} + P_{S5} + P_{S6})$
M	Moisture index	$M = (P_{S5} + P_{S6})/(P_{S1} + P_{S2} + P_{S3} + P_{S4})$

Temperature index. The temperature index (T) is calculated as follows:

$$T = (P_{S1} + P_{S2} + P_{S3})/(P_{S4} + P_{S5} + P_{S6}).$$

The rationale for this is based on the results of HCA and NMS, which clearly divide the pollen taxa into two main groups. As mentioned above, the pollen groups S4–S6 used in the above equation are equivalent to A1–A3 delineated by HCA, whereas S1–S3 are derived from B1–B4. Accordingly, the ratio of pollen percentages (P) between these two groups could be used as a temperature index – the higher the ratio, the higher the temperature.

Moisture index. The moisture index (M) is calculated as the ratio of pollen percentages (P) between groups S1, S2, S3, S4, and groups S5, S6:

$$M = (P_{S5} + P_{S6})/(P_{S1} + P_{S2} + P_{S3} + P_{S4}).$$

The rationale for this is based on the results of HCA and NMS, modern biogeographical patterns, and field observations of vegetation distributions. The xeromorphic desert, desert-steppe and meso-xeromorphic steppe vegetation types (S1, S2 and S3) occur mainly in the lowlands and in the warmer, southern part of the study region. The birch forest/shrubland (S4) occurs mainly on sunny (south-facing) slopes of mountains and needs lower moisture to grow than the coniferous forests (S5) and moderate hydroperiod steppes (S6) in Mongolia.

To test the validity of these new indices we calculated the pollen percentage of each pollen group (S1 to S6) for each surface sample and plotted these values for all the samples along our transect to examine their spatial variation (Fig. 9a–f). We also plotted the curves for the moisture index and the temperature index along the same transect. It is clear that the moisture index is highest in the taiga, moderate in the forest-steppe and steppe, and lowest in the desert-steppe and desert (Fig. 9i), whereas the temperature index is highest in the desert and desert-steppe, decreases in the steppe and forest-steppe, and is lowest in the taiga (Fig. 9h). As a complement to the moisture index we also plotted the A/C (*Artemisia*/Chenopodiaceae) pollen ratio along the transect, which basically parallels our moisture index curve (Fig. 9g). In order to compare our pollen–climate indices directly with actual climate data we extracted the mean annual precipitation (MAP) and mean annual temperature (MAT) data from the climatic maps of Mongolia (Orshikh *et al.*, 1990) and plotted these values along our transect (Fig 9j,k). The trends of our moisture and temperature indices mimic the spatial gradients of precipitation and temperature in Mongolia very closely. For example, the steady rise in precipitation from desert-steppe to steppe, the precipitation peak within the forest-steppe (sites 72–75), and the precipitation maxima in the taiga are captured by the moisture index curve (see arrows in Fig. 9i,k). Similarly, the gradual decline in temperature northwards across the steppe, as well as the abrupt temperature drop across the ecotone from the forest-steppe to taiga are also well represented by the temperature index curve (Fig 9h,j).

SUMMARY AND CONCLUSIONS

This paper presents modern pollen spectra from 104 surface samples collected along a generally south–north transect across Mongolia. The transect traverses five major vegetation zones, namely desert, desert-steppe, steppe, forest-steppe, and taiga, following a broad climatic gradient of decreasing temperature and increasing precipitation with increasing elevation. The 104 modern pollen spectra suggest that each vegetation zone is characterized by a distinctive pollen assemblage, as follows: (1) desert zone: Chenopodiaceae–Zygophyllaceae–*Nitraria*–Poaceae pollen assemblage; (2) desert-steppe zone: Poaceae–*Pinus* Haploxylon-type–Chenopodiaceae pollen assemblage; (3) steppe zone: *Pinus*-Haploxylon-type–*Artemisia*–*Aster*-type–Poaceae pollen assemblage; (4) forest-steppe zone: *Pinus* Haploxylon-type–*Picea*–*Artemisia*–*Betula*, montane forb/shrub–pteridophyte pollen assemblage; and (5) mountain taiga zone: *Pinus* Haploxylon-type–*Picea*–Poaceae–Cyperaceae, montane forb/shrub–pteridophyte pollen assemblage. HCA classifies the 22 main pollen taxa into two major groups and seven subgroups. The two main groups basically contain xerophytic plants characteristic of desert and steppe vegetation types in one, and mesophytic trees, shrubs and herbs characteristic of montane environments in the other. Discriminant analysis, which correctly classifies 95.2% of the surface samples into their respective *a priori* groups, confirms that each major vegetation zone can be quantitatively represented by a distinctive palynological signature, which can provide a basis for the reconstruction of palaeovegetational and palaeoclimatic reconstructions based on fossil pollen assemblages from the study region.

This study sheds light on several important issues in pollen dispersal and representation in the arid and semi-arid regions of Central Asia. As expected, *Pinus* is greatly over-represented in the modern pollen rain, in that pine trees may not be locally present in areas where *Pinus* pollen occurs at < 50% in a pollen sample, especially if the pollen concentration of *Pinus* is low. *Picea* is also slightly over-represented in areas outside the distribution range of spruce trees, apparently as a result of the long-distance dispersal ability of its saccate pollen. By contrast, *Larix* is grossly under-represented, as its pollen rarely exists at > 3% even within the taiga where larch trees are common. Another interesting finding of this study is that Poaceae pollen percentages are higher in samples collected within nature reserves, where the natural vegetation is better preserved than outside. This raises the possibility that the under-representation of Poaceae in the modern pollen rain from semi-arid steppe or grassland environments, a phenomenon previously reported in the palynological literature, is actually an artefact of human disturbance. Overgrazing by livestock can significantly reduce the flowering populations of grasses and suppress its pollen production, resulting in an increase in the pollen representation of steppe forbs such as *Artemisia*.

Based on the quantitative pollen–vegetation relationships derived from our regional modern pollen data set, we have

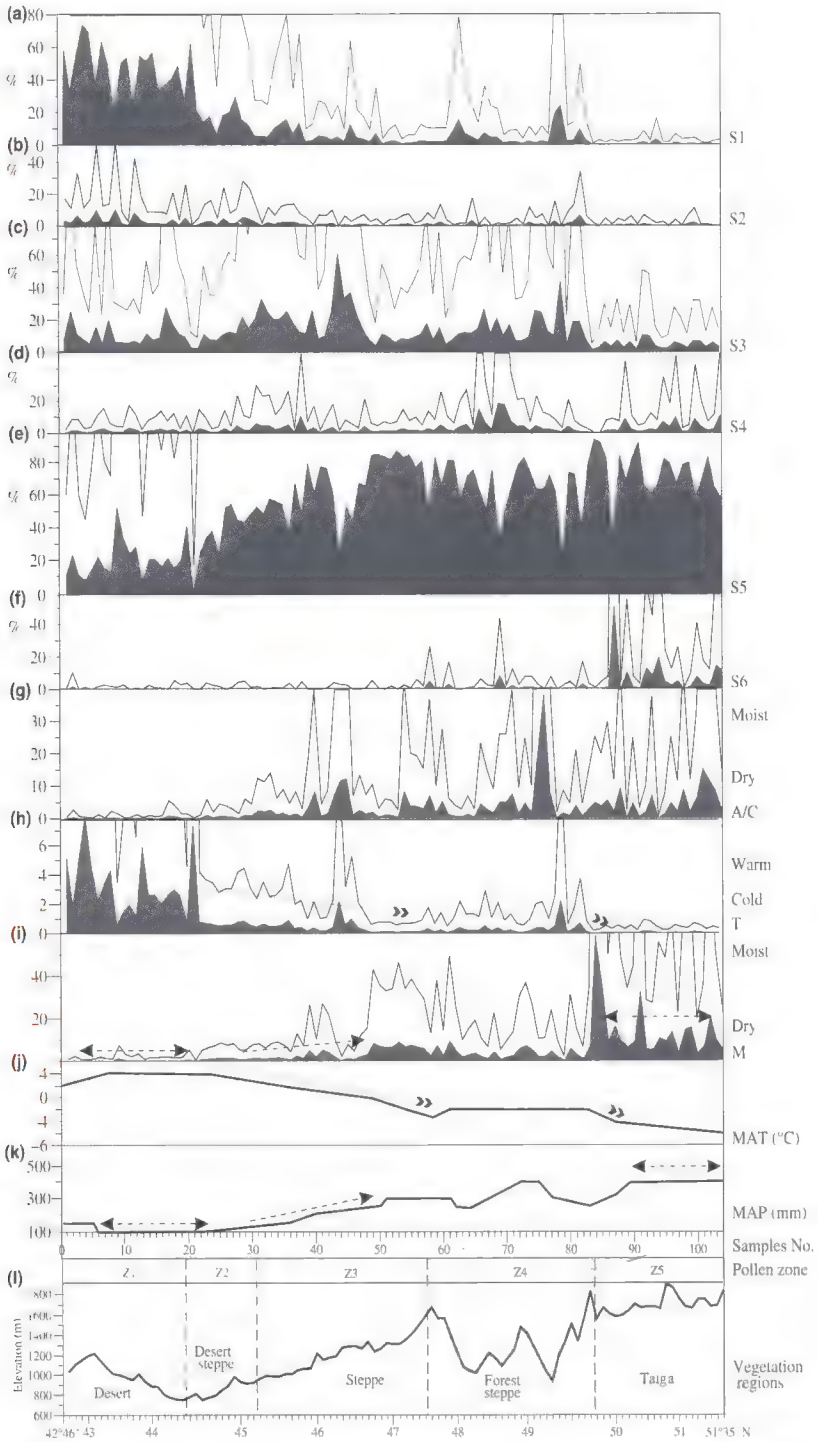

Figure 9 Grouped pollen percentages of the six pollen groups (S1–S6) used in the calculation of pollen–climate indices (panels a–f); the A/C ratio (g); the temperature index, T (h); the moisture index, M (i); the mean annual temperature, MAT (j); the mean annual precipitation, MAP (k); and elevations (l) of the 104 surface samples along the south–north transect across Mongolia. Black line: 5× exaggeration. Single or double arrows with dotted lines in (h), (i), (j), (k) denote parallel trends between the pollen index curves (T, M) and the corresponding climatic gradients (MAT, MAP). The data for MAP (mm) and MAT (°C) are derived from Orshikh *et al.*, (1990).

developed two pollen indices to represent the principal climatic gradients in Mongolia. The temperature index is based on the ratio between the pollen percentages of 13 pollen taxa characteristic of montane forests and steppes and 10 pollen taxa characteristic of xeromorphic deserts and meso-xeromorphic steppes; and the moisture index is based on the ratio between 14 pollen taxa characteristic of lowland, warmer, or sunny environments and nine pollen taxa from alpine conifers and herbs from moderate hydroperiod steppes. A comparison between these pollen–climate indices and trends derived from the climatic map of Mongolia suggests that they mimic the regional gradients of precipitation and temperature very closely.

Pollen records of late-Quaternary climatic and vegetational changes from Mongolia and even the whole of Central Asia are still relatively rare. One of the major challenges facing palynologists working in these semi-arid and arid regions is the inadequate coverage of modern pollen-rain studies in such a vast territory, resulting in a poor understanding of the relationships between modern pollen and the corresponding patterns of vegetation and climate. Our data set of 104 pollen surface samples from a pivotal region along a distinct climatic and vegetational gradient from desert to taiga across Mongolia fills a major gap in the regional data network for Central Asia. The pollen–vegetation–climate relationships established in this study, including the two new pollen–climate indices, provide a quantitative basis for palaeoclimatic reconstruction based on fossil pollen data from this region.

ACKNOWLEDGEMENTS

This paper was supported by grants from the Chinese National Science Foundation (NSFC) (Nos 40025105, 40331102, and 40421101) and the US National Science Foundation (NSF) (ATM-0402475, ATM-0402509, BCS-0623514, BCS-0623478, BCS-0078557). We thank our Mongolian colleagues for their assistance in fieldwork and logistics.

REFERENCES

Andreev, A.A., Klimanov, V.A. & Sulerzhitsky, L.D. (2001) Vegetation and climate history of the Yana River lowland, Russia, during the last 6400 yr. *Quaternary Science Reviews*, **20,** 259–266.

Birks, H.J.B. (1973) Modern pollen rain studies in some Arctic and Alpine environments. *Quaternary plant ecology* (ed. by H.J.B. Birks and R.G. West), pp. 143–168. Blackwell, Oxford.

Boucher, T.V. & Mead, B.R. (2006) Vegetation change and forest regeneration on the Kenai Peninsula, Alaska following a spruce beetle outbreak, 1987–2000. *Forest Ecology and Management*, **227,** 233–246.

Clarke, K.R. (1993) Non-parametric multivariate analyses of changes in community structure. *Australian Journal of Ecology*, **18,** 117–143.

Cour, P., Zheng, Z., Duzer, D., Calleja, M. & Yao, Z. (1999) Vegetational and climatic significance of modern pollen rain in northwestern Tibet. *Review of Palaeobotany and Palynology*, **104,** 183–204.

Demske, D. & Mischke, S. (2003) Palynological investigation of a Holocene profile section from the Palaeo- Gaxun- Nur-Basin. *Chinese Science Bulletin*, **48,** 1418–1422.

Dorofeyuk, N.I. & Tarasov, P.E. (1998) Vegetation and lake levels of northern Mongolia since 12,500 yr B.P. based on the pollen and diatom records. *Stratigraphy. Geological Correlation*, **6,** 70–83.

El-Moslimany, A.P. (1990) Ecological significance of common nonarboreal pollen: examples from drylands of the Middle East. *Review of Palaeobotany and Palynology*, **64,** 343–350.

Enright, N.J., Miller, B.P. & Akhter, R. (2005) Desert vegetation and vegetation-environment relationships in Kirthar National Park, Sindh, Pakistan. *Journal of Arid Environments*, **61,** 397–418.

Fowell, S.J.B., Hansen, C.S., Peck, J.A., Khosbayar, P. & Ganbold, E. (2003) Mid to late Holocene climate evolution of the Lake Telmen Basin, North Central Mongolia, based on palynological data. *Quaternary Research*, **59,** 353–363.

Graf, M.T. & Chmura, G.L. (2006) Development of modern analogues for natural, mowed and grazed grasslands using pollen assemblages and coprophilous fungi. *Review of Palaeobotany and Palynology*, **141,** 139–149.

Gunin, P.D., Vostokova, E.A., Dorofeyuk, N.I., Tarasov, P.E. & Black, C.C. (1999) *Vegetation dynamics of Mongolia*. Geobotany 26, pp. 233–238. Kluwer Academic, Boston, MA.

Herzschuh, U., Tarasov, P., Wunnemann, B. & Hartmann, K. (2004) Holocene vegetation and climate of the Alashan Plateau, NW China, reconstructed from pollen data. *Palaeogeography, Palaeoclimatology, Palaeoecology*, **211,** 1–17.

Hilbig, W. (1987) Changes in segetal vegetation under conditions of industrialized agriculture. *Archiv für Naturschutz und Landschaftsforschung*, **27,** 229–249.

Hilbig, W. (1995) *The vegetation of Mongolia*. SPB Academic Publishing, Amsterdam.

Huang, C.X., Van Campo, E. & Doublemei, F. (1993) Studies on Tibetan surface pollen. *Arid Land Geography*, **16,** 75–83 (in Chinese).

Igarashi, Y. (1996) A Lateglacial climatic reversion in Hokkaido, Northeast Asia, inferred from the *Larix* pollen record. *Quaternary Science Reviews*, **15,** 989–995.

Kataoka, H., Takahara, H., Krivonogov, S.K., Bezrukova, E.V., Orlova, L., Kropivina, S., Miyoshi, N. & Kawamuro, K. (2003) Pollen record from the Chivyrkui Bay Outcrop on the Eastern Shore of Lake Baikal since the Late Glacial. *Long continental record from Lake Baikal* (ed. by K. Kashiwaya), pp. 207–218. Springer-Verlag, Tokyo.

Lavrenko, E.M. & Karamisheva, Z.V. (eds) (1990) Vegetation map of Mongolian People's Republic. 1:3,000,000. *National atlas of the Mongolian People's Republic* (ed. by N. Orshikh, N.A. Morgunova and M.N. Rodionov), pp. 72–73. Ulanbator, Moscow (in Russian).

Lavrenko, E.M., Iunatov, A.A., Aleksandr, A. & Dashniam, B. (1979) *Vegetation map of Mongolian People's Republic (scale 1: 1,500,000)*. GUGK, Moscow (in Russian).

Li, W. (1993) Some problems of Holocene pollen analysis. *Research of the historical change of the environment for human survival in China* (ed. by L. Zhang), pp. 4–10. Ocean Press, Beijing (in Chinese).

Li, W. (1998) *Quaternary vegetation and environment of China*, pp. 48–72. Science Press, Beijing (in Chinese).

Li, W., Yao, Z. & Liu, G. (1993) *Research of the Quaternary vegetation and environment in the northern and middle subtropical zone in China*. Ocean Press, Beijing (in Chinese).

Li, Y.C., Xu, Q.H., Yang, X.L. & Zheng, Z.H. (2005) Pollen assemblages of major steppe communities in China. *Acta Ecologica Sinica*, **125,** 555–564 (in Chinese).

Liu, H.Y., Cui, H., Pott, R. & Speier, M. (1999) Surface pollen of the woodland-steppe ecotone in southeastern Inner Mongolia, China. *Review of Palaeobotany and Palynology*, **105,** 237–250.

Liu, H.Y., Wang, Y., Tian, Y.H., Zhu, J.L. & Wang, H.Y. (2006) Climatic and anthropogenic control of surface pollen assemblages in East Asian steppes. *Review of Palaeobotany and Palynology*, **138,** 281–289.

Liu, K.-b. (1990) Holocene paleoecology of the boreal forest and Great Lakes–St. Lawrence forest on northern Ontario. *Ecological Monographs*, **60,** 179–212.

Liu, K.-b. & Lam, S.-N.N. (1985) Paleovegetational reconstruction based on modern and fossil pollen data: an application of discriminant analysis. *Annals of the Association of American Geographers*, **17,** 115–130.

Liu, K.-b., Yao, Z. & Thompson, L.G. (1998) A pollen record of Holocene climatic changes from the Dunde ice cap, Qinghai-Tibetan Plateau. *Geology*, **26,** 135–138.

Liu, K.-b., Reese, C.A. & Thompson, L.G. (2005) Ice-core pollen record of climatic changes in the central Andes during the last 400 years. *Quaternary Research*, **64,** 272–278.

Liu, K.-b., Reese, C.A. & Thompson, L.G. (2007) A potential pollen proxy for ENSO derived from the Sajama ice core. *Geophysical Research Letters*, **34,** L09504, doi:10.1029/2006GL029018.

Lynch, E.A. (1996) The ability of pollen from small lakes and ponds to sense fine-scale vegetation patterns in the Central Rocky Mountains, USA. *Review of Palaeobotany and Palynology*, **94,** 197–210.

Markgraf, V., D'Antoni, H.L. & Ager, T.A. (1981) Modern pollen dispersal in Argentina. *Palynology*, **5,** 43–63.

McCune, B. & Grace, J.G. (2002) *Analysis of ecological communities*. MjM Software Design, Gleneden Beach, OR.

Minckley, T. & Whitlock, C. (2000) Spatial variation of modern pollen in Oregon and southern Washington, USA. *Review of Palaeobotany and Palynology*, **112,** 97–123.

Moore, P.D., Webb, J.A. & Collinson, M.E. (1991) *Pollen analysis*. Blackwell Scientific Publications, Oxford.

Noshiro, S., Terada, K., Tsuji, S. & Suzuki, M. (1997) *Larix–Picea* forests of the Last Glacial Age on the eastern slope of Towada Volcano in northern Japan. *Review of Palaeobotany and Palynology*, **98,** 207–222.

Orshikh, N., Morgunova, N.A. & Rodionov, M.N. (eds) (1990) *The national atlas of the Mongolian People's Republic*. Ulanbator–Moscow, Moscow (in Russian).

Reese, C.A. & Liu, K.-b. (2005) A modern pollen rain study from the central Anders region of South America. *Journal of Biogeography*, **32,** 709–718.

Soh, M.C.K., Sodhi, N.S. & Lim, S.L.H. (2006) High sensitivity of montane bird communities to habitat disturbance in peninsular Malaysia. *Biological conservation*, **129,** 149–166.

SPSS Inc. (2001) *SPSS base 11.0 for Windows user's guide*. SPSS Inc, Chicago.

Sugden, J.M. & Meadows, M.E. (1989) The use of multiple discriminant analysis in reconstructing recent vegetation changes on the Nuweveldberg, South Africa. *Review of Palaeobotany and Palynology*, **60,** 131–147.

Tarasov, P.E., Webb, T., III, Andreev, A.A., Afanas'eva, N.B., Berezina, N.A., Bezusko, L.G., Blyakharchuk, T.A., Bolikhovskaya, N.S., Cheddadi, R., Chernavskaya, M.M., Chernova, G.M., Dorofeyuk, N.I., Dirksen, V.G., Elina, G.A., Filimonova, L.V., Glebov, F.Z., Guiot, J., Gunova, V.S., Harrison, S.P., Jolly, D., Khomutova, V.I., Kvavadze, E.V., Osipova, I.M., Panova, N.K., Prentice, I.C., Saarse, L., Sevastyanov, D.V., Volkova, V.S. & Zernitskaya, V.P. (1998) Present-day and mid-Holocene biomes reconstructed from pollen and plant macrofossil data from the former Soviet Union and Mongolia. *Journal of Biogeography*, **25,** 1029–1053.

Tarasov, P.E., Peyron, O., Guio, J., Brewer, S., Volkova, V.S., Bezusko, L.G., Dorofeyuk, N.I., Kvavadze, E.V., Osipova, I.M. & Panova, N.K. (1999a) Last Glacial Maximum climate of the former Soviet Union and Mongolia reconstructed from pollen and plant macrofossil data. *Climate Dynamics*, **14,** 227–240.

Tarasov, P.E., Guiot, J., Cheddadi, R., Andreev, A.A., Bezusko, L.G., Blyakharchuk, T.A., Dorofeyuk, N.I., Filimonova, L.V., Volkova, V.S. & Zernitskaya, V.P. (1999b) Climate in northern Eurasia 6000 years ago reconstructed from pollen data. *Earth and Planetary Science Letters*, **171,** 635–645.

Tarasov, P., Dorofeyuk, N. & Metel'tseva, E. (2000a) Holocene vegetation and climate changes in Hoton-Nur basin, northwest Mongolia. *Boreas*, **29,** 117–126.

Tarasov, P.E., Volkova, V.S., Webb, T., III, Guiot, J., Andreev, A.A., Bezusko, L.G., Bezusko, T.V., Bykova, G.V., Dorofeyuk, N.I., Kvavadze, E.V., Osipova, I.M., Panova, N.K. & Sevastyanov, D.V. (2000b) Last Glacial Maximum biomes reconstructed from pollen and plant macrofossil data from Northern Eurasia. *Journal of Biogeography*, **27,** 609–620.

Taylor, F., Whitehead, J. & Domack, E. (2001) Holocene paleoclimate change in the Antarctic Peninsula: evidence from the diatom, sedimentary and geochemical record. *Marine Micropaleontology*, **41,** 25–43.

Tuvdendorzh, D. & Myagmarzhav, B. (eds) (1985) *Atlas of the climate and ground water resources in the Mongolian People's Republic*. GUGMS, Ulaan Bator.

Van Campo, E., Cour, P. & Huang, C.X. (1996) Holocene environmental changes in Bangong Co basin (Western Tibet). Part 2: the pollen record. *Palaeogeography, Palaeoclimatology, Palaeoecology*, **120,** 49–63.

Wan, T. & Wei, Z.J. (1999) *Pollen morphology of modern plants in the grasslands of Inner Mongolia*. Chinese Agricultural Press, Beijing (in Chinese).

Wang, F.S., Chien, N.F., Zhang, Y.L. & Yang, H.Q. (1995) *Pollen flora of China*. Science Press, Beijing (in Chinese).

Wang, B.Y., Song, C.Q. & Sun, X.J. (1996) Study on surface pollen in middle Inner Mongolia, China. *Acta Botanica Sinica*, **38,** 902–909 (in Chinese).

Webb, T., III (1987) The appearance and disappearance of major vegetational assemblages: long term vegetational dynamics in eastern North America. *Vegetatio*, **69,** 177–188.

Webb, T., III, Bartlein, P.J., Harrison, S. & Anderson, K.H. (1993) Vegetation, lake levels and climate in eastern United States since 18,000 yr B.P. *Global climates since the Last Glacial Maximum* (ed. by H.E. Wright, T. Webb III and J.E. Kutzbach), pp. 415–467. University of Minnesota Press, Minneapolis, MN.

Yu, G., Prentice, I.C., Harrison, S.P. & Sun, X. (1998) Pollen-based biome reconstruction for China at 0 and 6000 years. *Journal of Biogeography*, **25,** 1055–1069.

Yunatov, A.A. (1959) *Main features of the vegetation cover of Mongolia*. Science Press, Beijing (in Chinese).

BIOSKETCHES

Yuzhen Ma is a professor at Beijing Normal University, China. She is a palynologist with special interest in Quaternary environmental changes in the arid and semi-arid regions of China and Central Asia.

Kam-biu Liu is the George William Barineau III Professor in Oceanography and Coastal Sciences at Louisiana State University, USA. His research interests are in Quaternary palaeoecology and palaeoclimatology, palaeotempestology, and global environmental changes using multiple proxies and archives, especially pollen, lake sediments, and ice cores.

Zhaodong (Jordan) Feng is an associate professor at Baylor University, USA. His research interests are in palaeopedology, geomorphology, and climatic change, especially in the loess-covered regions of China, Central Asia, and the USA.

Editor: Glen MacDonald

附录八

Contents lists available at ScienceDirect

Quaternary International

journal homepage: www.elsevier.com/locate/quaint

Climatic and hydrological variations during the past 8000 years in northern Xinjiang of China and the associated mechanisms

Min Ran [a], Chengjun Zhang [b], Zhaodong Feng [c, *]

[a] School of Geographical Sciences, Southwest University, 2 Tiansheng Road, Beibei District, Chongqing 400715, China
[b] College of Geological Sciences and Mineral Resources, Lanzhou University, 222 Tianshui Road South, Lanzhou 730000, China
[c] Xinjiang Institute of Ecology and Geography, Chinese Academy of Sciences, 818 Beijing Road South, Urumqi 830011, China

ARTICLE INFO

Article history:
Available online xxx

Keywords:
Northern Xinjiang
A/C ratio
$\delta^{18}O$ data
Holocene moisture change
Holocene salinity change

ABSTRACT

This paper reviews the published literature regarding the climatic and hydrological variations of the past 8000 years in the northern Xinjiang of China in hope that some of the controversies surrounding the Holocene climate history can be reconciled. Based on the well-tested premise that the overall relationship between the A/C ratios and the bioclimates in arid and semi-arid areas of China still holds, we compared the A/C ratio-based SMI (Standardized Moisture Index) of five selected lacustrine sequences. Our comparison shows that the regional average SMI had a general rising trend, and the rising trend was reasonably corroborated by other pollen proxies. The rising trend can be explained by invoking its climatic linkage with the North Atlantic Ocean, and a possible linkage with ENSO is an additional or an alternative mechanism for explaining the rising trend. The nearly parallel rising trends of seven $\delta^{18}O$-indicated SSI curves (Standardized Salinity Index) mean that the lake-water salinity has been rising since ~8.0 cal. ka BP. The rising trend can be explained by invoking the Holocene variations in the areal extent of ice covers in the Tianshan Mountains and the Altay Mountains. That is, the persistent shrinking of the ice extent in the mountains generated less and less melting water supplies to the lakes and thus resulted in saltier and saltier waters in the lakes. The contradiction between the increasing trend of the basin-wide moisture and the increasing trend of the lake-water salinity can be reconciled as follows: the increasing trend of the precipitation accompanied by the lowering tend of the temperature might have increasingly enhanced the effective soil moisture in northern Xinjiang, but the increase in the basin-wide moisture was not enough to compensate for the decrease in the lake inflowing water resulted from the shrinkage of ice-covered areas in the mountains.

© 2014 Elsevier Ltd and INQUA. All rights reserved.

1. Introduction

The Central Asian Arid Zone (CAAZ) refers to the arid-semiarid belt that stretches from the Caspian Sea in the west to the Hinggan Mountains in the east (approximately 35–55°N and 50–120°E). The warm-season precipitation in the CAAZ is primarily from the North Atlantic Ocean via the northward-shifted westerlies, whereas the cold-season precipitation is primarily from the Mediterranean Sea via the southward-shifted westerlies (Aizen et al., 2001; Bothe et al., 2012). The cold-season climate in the study area is modulated by the interactions between the westerlies and the North Atlantic Oscillation (NAO) and that the warm-season climate is controlled by the interactions between the Asian Low occupying the eastern half of CAAZ and the Azores High reaching the western half of CAAZ (Aizen et al., 2001; Meeker and Mayewski, 2002).

The Central Asian Arid Zone (CAAZ) is divided by the Altay Mountains into the eastern half and the western half, and our study area (i.e., northern Xinjiang) is the easternmost part of the western half. The low-lying topography between the Altay Mountains and the Tianshan Mountains in northern Xinjiang allows for moisture influx from the prevailing westerlies (Fig. 1a), and the W–E striking Tianshan Mountains block the climatic influence of the Arabian Sea from the south (Staubwasse and Weiss, 2006). The westerlies-domination over the western half of CAAZ during the Holocene has also been demonstrated by the temporal consistency between the records from the West Europe and the records from the western half of CAAZ (Chen et al., 2008; Ran and Feng, 2013; Wang and Feng, 2013). However, Asian monsoon domination was speculated to

* Corresponding author.
E-mail addresses: fengzd@lzu.edu.cn, fengzd@xju.edu.cn (Z. Feng).

http://dx.doi.org/10.1016/j.quaint.2014.07.056
1040-6182/© 2014 Elsevier Ltd and INQUA. All rights reserved.

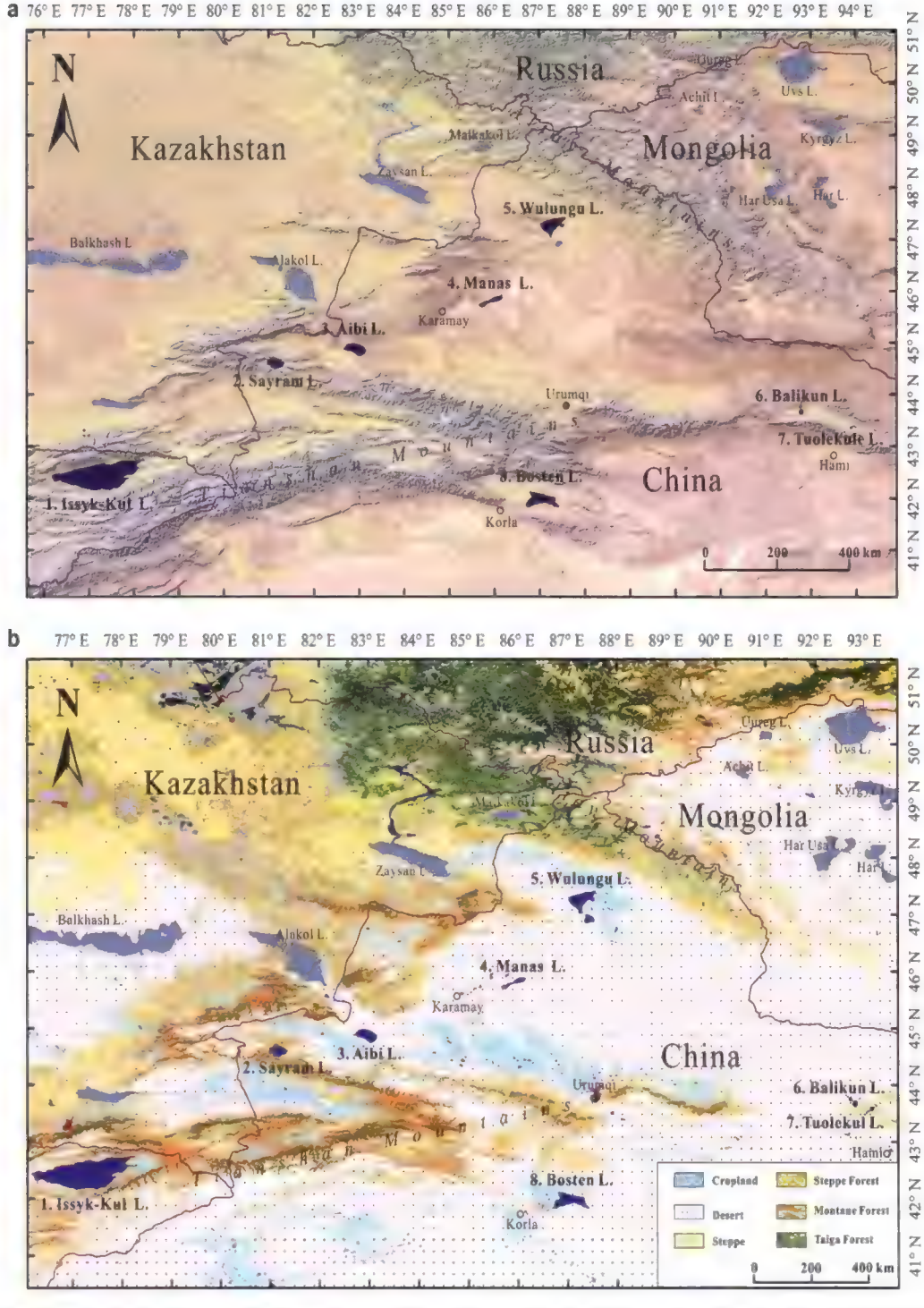

Fig. 1. a (upper panel) Locations of the reviewed eight lakes and the topographic context of the lakes. b (lower panel) Distributions of vegetation and the relations with the reviewed eight lakes.

have extended to our study area during Holocene warm periods (Winkler and Wang, 1993). This speculation was first supported by the data from Manas Lake (Sun et al., 1994; Lin et al., 1996; Rhodes et al., 1996) and recently by the data from Yili Valley (Li et al., 2011; Cheng et al., 2012).

However, the aforementioned discrepancies among different datasets may be reconcilable if different processes are invoked. For example, lake salinity may have little to do with the amount of precipitation if the lake is mainly supplied by ice meltwater (Sorrel et al., 2007). Instead, it may be controlled first by temperature-dictated amount of ice melting and then by the areal extent of remaining ice covers (Zhang et al., 2010; Feng et al., 2013). We intend to accept the proposition that basin-wide vegetation may be a real expression of basin-wide climate and that pollen record from a closed lake or a semi-closed lake can be used to retrieve past climate (Demske et al., 2005; Tarasov et al., 2006; Blyakharchuk et al., 2007; Ma et al., 2008; Rudaya et al., 2009; Zhao et al., 2012). This paper reviews the published literature regarding the climatic and hydrological variations of the past 8000 years in the northern Xinjiang of China in hope that some of the aforementioned discrepancies can be reconciled.

2. Physiographic settings

Northern Xinjiang includes the Junggar Basin, the northern slope of the Tianshan Mountains, and the southwestern slope of the Altay Mountains (Fig. 1a). The climate is continental with fairly large annual and diurnal ranges of temperature variations. The vertical differentiation of climates from the basin to the mountains is well expressed. For instance, the annual mean temperature (MAT) is above 8 °C and the mean annual precipitation (MAP) is below 100 mm at 200-m elevation in the basin. MAT is below −15 °C and MAP is above 600 mm at 4000-m elevation in central Tianshan Mountains (Hu, 2004; Chen, 2010). The basin-wide vegetation includes taiga forests in the northern tip (i.e., Altai Mountains), montane forests at high elevations of mountains, steppe-forests in the medium elevations and steppe at the foothills. Deserts dominate the landscapes of northern Xinjiang (Fig. 1b).

This paper reviews eight lacustrine sequences (Fig. 1a and b) including one from Issyk-Kul Lake in neighboring Kyrgyzstan. The physiographic characteristics of those eight lakes are listed in Table 1. We chose the past 8000 years as our study period because this is the time period shared by all of reviewed eight sequences. One more point should be noted regarding the chronologies of all participating sequences. If the age–depth model was not given or/and if the ^{14}C dates were not calibrated in the referred papers, we first calibrated the dates to calendar year before present (BP = 1950 AD) with the program CALIB 6.0 using the INTCAL 09 calibration data set (Reimer et al., 2009). The age–depth model was then established by linear interpolation between two neighboring dates.

3. Premises of proxies

3.1. A/C ratio as a basin-wide moisture proxy

Pollen-based proxies have been preferred for paleoclimate reconstructions because they have been intensively and extensively tested in modern bioclimatic settings, and the *Artemisia*/Chenopodiaceae ratio (i.e., A/C ratio), a focal proxy of this study, is one of such proxies. *Artemisia* and Chenopodiaceae, the most common plant taxa in arid and semi-arid regions, are characteristics of a highly continental climate with cold winters and dry summers (El-Moslimany, 1990). Because *Artemisia* (A) requires more water than Chenopodiaceae (C), the A/C ratio has thus been widely used as a proxy to reconstruct the past moisture variations from fossil pollen assemblages in arid and semi-arid regions. To reconcile recent controversies surrounding the reliability of the A/C ratio as a moisture proxy, Zhao et al. (2012) further tested the validity of the A/C ratio based on 608 pollen assemblages across northern China. The results show that median and mean values of A/C ratio decrease from 3.05 (median) and 6.03 (mean) in steppes, to 1.54 and 3.26 in steppe deserts, and to 0.47 and 0.62 in deserts, respectively. They concluded that the overall relationship between the A/C ratios and the bioclimates in arid and semi-arid areas of China still holds when data from various sources are pooled. However, two precautions were noted in that paper (Zhao et al., 2012): (1) A/C ratio from lake cores may underestimate the degree of basin-wide dryness because of the input of *Artemisia* by water from surrounding mountains; and (2) overwhelming domination of the salt- and drought-tolerant Chenopodiaceae in saline conditions may undermine the validity of the A/C ratio as a moisture proxy.

In order to have an intercomparable A/C ratio-based moisture index among all of participating sequences, we converted the A/C ratio of an individual sequence into a standardized moisture index (i.e., SMI). Specifically, we assigned an ordinal value to each 200-year time slice. The ordinal value that ranges from 0 (the lowest) to 4 (the highest) is resulted by the ratio between the average value of the 200-year time slice considered and the highest 200-year average of the record-covering period. Specifically, the A/C ratio may be related to *in situ* "absolute" moisture conditions at an individual site and the ratios from different sequences in a region may be used to compare the spatial variations of moisture levels. In contrast, the SMI (Standardized Moisture Index) is a "relative" moisture indicator and can be used to semi-quantitatively depict a regional history of moisture variations if there is a geographic coherency or consistency among the SMIs of all participating sequences in a region (Davis et al., 2003; Herzschuh, 2006; Zhao et al., 2009; Ran and Feng, 2013; Wang and Feng, 2013).

3.2. $\delta^{18}O$ as a lake-water salinity proxy

The oxygen isotopic signature ($\delta^{18}O$) in lacustrine carbonates (either minerals or ostracod shells) is controlled by many factors.

Table 1
Physiographic characteristics of the reviewed eight lakes in northern Xinjiang (also including Issy-Kul Lake from the neighboring Kyrgyzstan).

No.	Lake name	Longitude (°)	Latitude (°)	Elevation (m)	Temperature (°C)	Precipitation (mm)	Evaporation (mm)
1	Issky-Kul	42.5	76.5	1600	10.0	250	820
2	Sayram	44.6	81.2	2072	0.5	350	550
3	Aibi	44.9	82.6	200	7.8	95	1315
4	Manas	45.8	85.9	257	6.1	100	2100
5	Wulungu	47.2	87.4	479	3.4	117	1844
6	Balikun	43.7	92.8	1575	1.0	210	1638
7	Tuolekule	43.6	92.9	1575	1.3	211	1603
8	Bosten	42.1	86.9	1048	8.3	141	2039

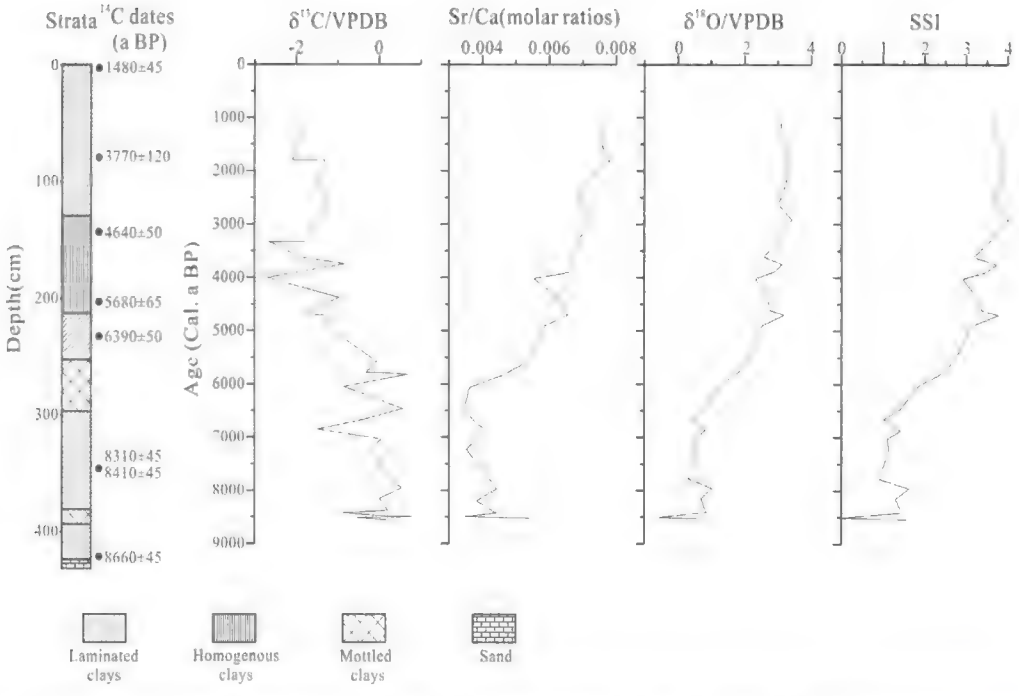

Fig. 2. Data from Issyk-Kul Lake in the neighboring Kyrgyzstan (Ricketts et al., 2001). The data include carbonate $\delta^{13}C$, Sr/Ca, $\delta^{18}O$ and the $\delta^{18}O$-based SSI (Standardized Salinity Index).

Among them, the salinity and temperature of the lake water are the leading ones. Generally, the isotopic signature is influenced by the isotopic composition of the dissolved CO_2 that is directly related to the salinity of the lake water (Fontes et al., 1996). The salinity is in turn controlled by the ratio of the evaporation (salt concentration) over the precipitation (salt dilution) (Mischke and Wunnemann, 2006; Zhang et al., 2010), suggesting that the carbonate isotopic signature ($\delta^{18}O$) in closed or semi-closed lakes in arid and semi-arid

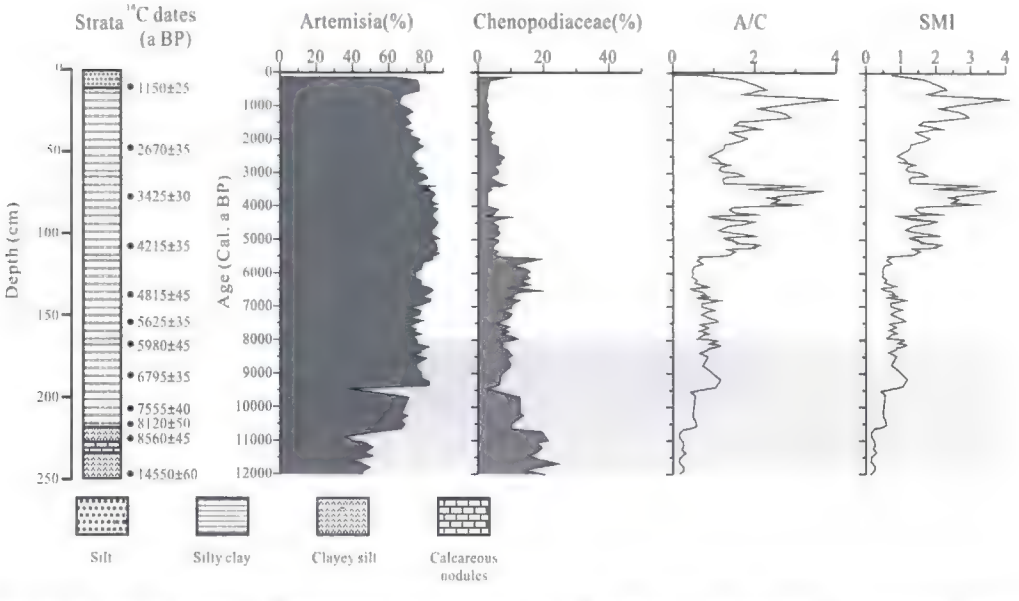

Fig. 3. Data from Sayram Lake (Jiang et al., 2013). The data include pollen percentage of *Artemisia* (A), pollen percentage of Chenopoidiaceae (C), A/C ratio and the A/C ratio-based SMI (Standardized Moisture Index).

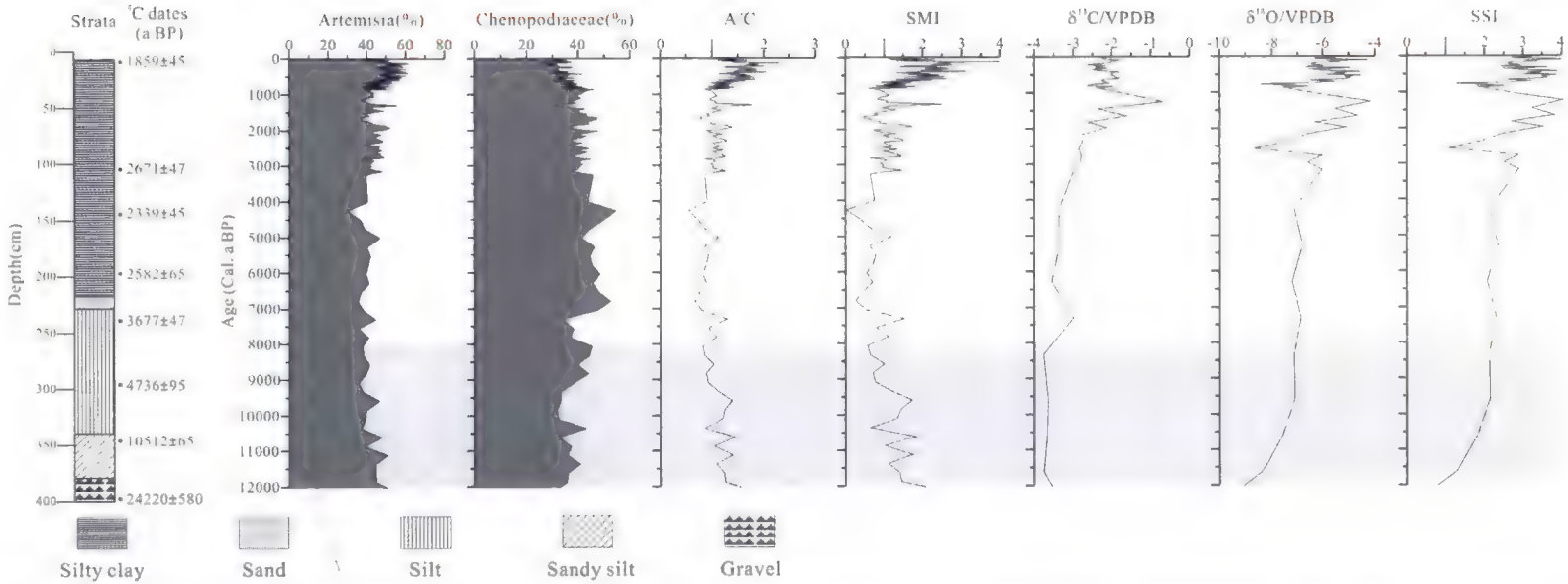

Fig. 4. Pollen data (Wang et al., 2013) and stable isotopic data (Zhang, 2014, unpublished data) from Aibi Lake. Pollen data include pollen percentage of *Artemisia* (A), pollen percentage of Chenopoidiaceae (C), A/C ratio and the A/C ratio-based SMI (Standardized Moisture Index). Stable isotopic data include carbonate $\delta^{13}C$, $\delta^{18}O$ and the $\delta^{18}O$-based SSI (Standardized Salinity Index).

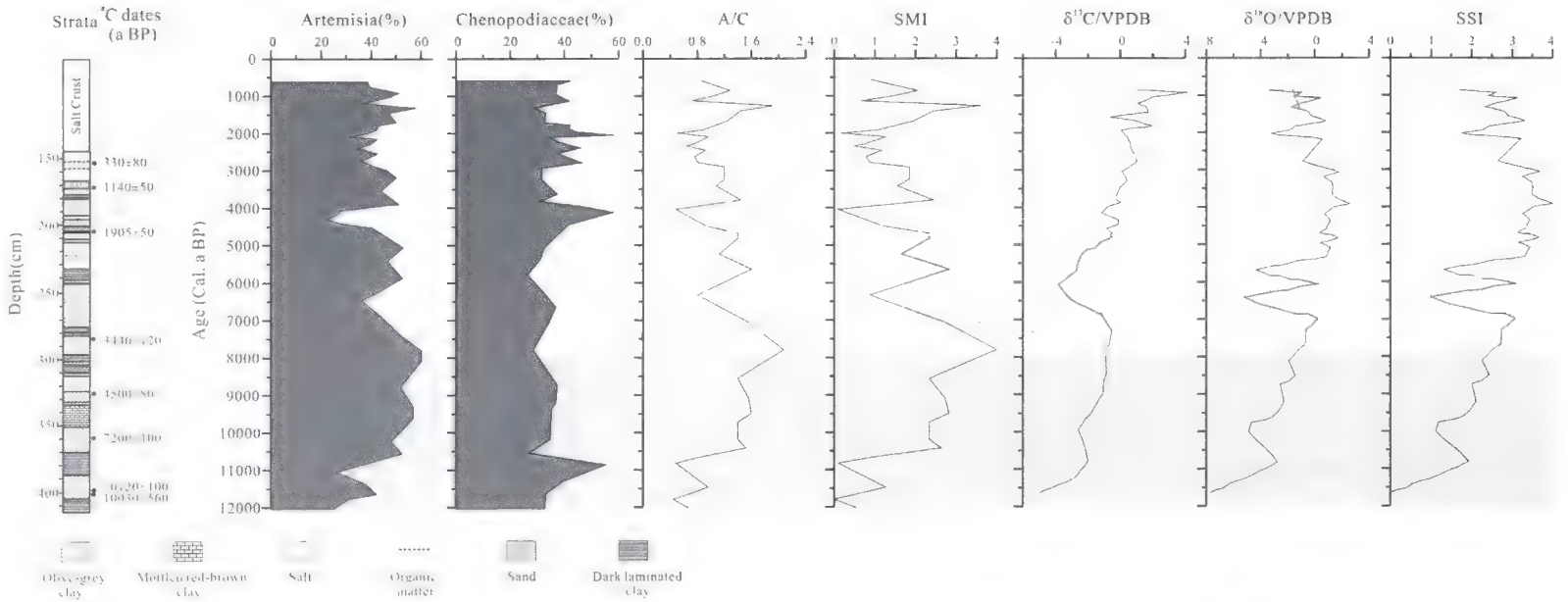

Fig. 5. Pollen data (Sun et al., 1994) and stable isotopic data (Rhodes et al., 1996) from Manas Lake. Pollen data include pollen percentage of *Artemisia* (A), pollen percentage of Chenopoidiaceae (C), A/C ratio and the A/C ratio-based SMI (Standardized Moisture Index). Stable isotopic data include carbonate $\delta^{13}C$, $\delta^{18}O$ and the $\delta^{18}O$-based SSI (Standardized Salinity Index).

areas is mainly controlled by the ratio of the evaporation over the precipitation. The isotopic composition is further complicated in northern Xinjiang where the amount of ice melting water in surrounding mountains, rather than precipitation within the basin, controls the water balance and thus the lake-water salinity in those closed and semi-closed lakes. Normally, the $\delta^{13}C$ and $\delta^{18}O$ of lacustrine carbonates change synchronously and both are controlled by the ratio of the evaporation over the precipitation (Leng and Marshall, 2004; Shen et al., 2010) when the lake is a closed or semi-closed one. However, the two may change in opposite directions, suggesting that the temperature has stronger control over the $\delta^{18}O$ than over the $\delta^{13}C$ (Wu and Wang, 1997). It was also reported that the $\delta^{13}C$ of lacustrine carbonates was controlled by the lake productivity whereas the $\delta^{18}O$ is still a valid lake-water salinity proxy in Issyk-Kul Lake, two being unrelated (Ricketts et al., 2001).

In order to have an intercomparable $\delta^{18}O$-based lake-water salinity index among all of participating sequences, we converted the measured $\delta^{18}O$ values of an individual sequence into a standardized salinity index (i.e., SSI). Using the same approach as used for developing the Standardized Moisture Index (SMI), we assigned an ordinal value to each 200-year time slice. The ordinal value that ranges from 0 (the lowest) to 4 (the highest) is resulted by the ratio between the average $\delta^{18}O$ value of the 200-year time slice considered and the highest 200-year average $\delta^{18}O$ value of the record-covering period. Specifically, the measured $\delta^{18}O$ values may be related to *in situ* "absolute" lake-water salinity at an individual site and the measured $\delta^{18}O$ values from different sequences in a region may be used to compare the spatial variations of lake-water salinity. In contrast, the SSI (Standardized Salinity Index) is a "relative" lake-water salinity indicator and can be used to semi-quantitatively depict a regional history of lake salinity if there is a geographic coherency or consistency among the SSIs of all participating sequences.

4. Record reviews

4.1. Issyk-Kul Lake

The lake (location in Fig. 1a and b) is situated at an elevation of 1600 m within the western Tianshan Mountain in the territory of Kyrgyzstan. The mean annual temperature (MAT) is 10.0 °C and the mean annual precipitation (MAP) is 250 mm with a potential evaporation of 820 mm (Table 1). There is no pollen data published yet from this lake and this review thus focuses on the $\delta^{18}O$ data of lacustrine ostracod shells (Ricketts et al., 2001). The $\delta^{18}O$ data (Fig. 2), together with trace element data, were interpreted to indicate the regional aridity. The interpretation stated that the Issyk-Kul basin went from a moist climate in the early Holocene to a more arid climate in the late Holocene. The data show that the lake water was fresh from ~8.7 to ~6.9 cal. ka BP under an open lake condition and became less fresh after ~6.9 cal. ka BP under a closed lake condition. The upward decreasing trend of the $\delta^{13}C$ of lacustrine ostracod shells was interpreted to be controlled by the upward increasing trend of the lake productivity that was in turn corroborated by the upward increasing trends of the content of organic matter and the abundance of diatom frustules.

4.2. Sayram Lake

The MAT is 0.5 °C and the MAP is 350 mm with a potential evaporation of 550 mm (Table 1) at the lake site (2072 m a.s.l.). There is no carbonate $\delta^{18}O$ data published yet from this lake and this review thus focuses on pollen data (Jiang et al., 2013). *Artemisia*/Chenopodiaceae (A/C) ratios, together with the principal component

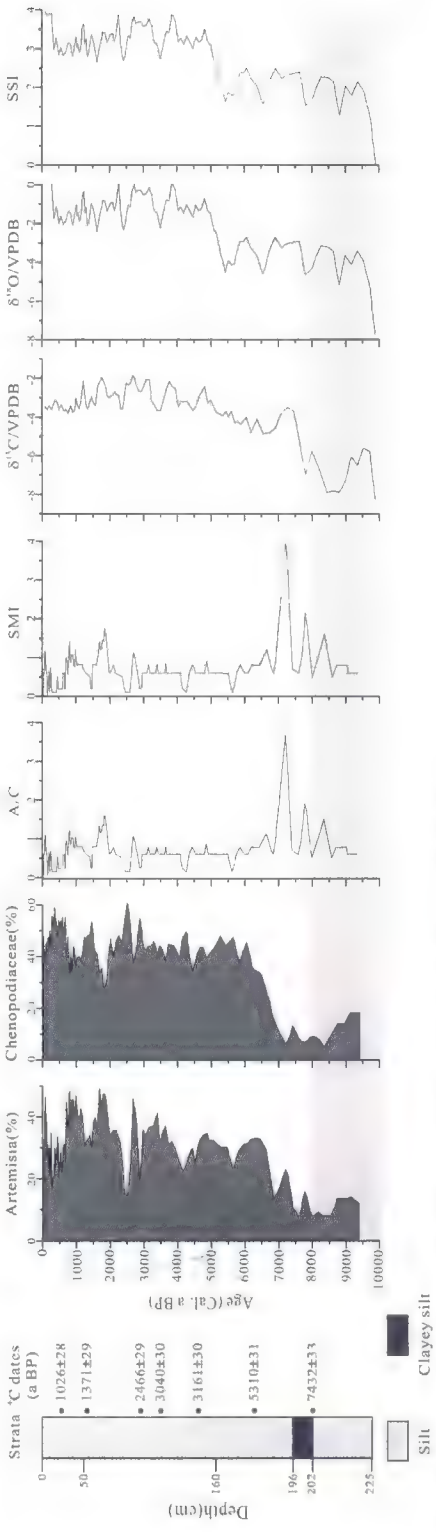

Fig. 6. Pollen data (Jiang et al., 2008) and stable isotopic data (Jiang et al., 2007) from Wulungu Lake. Pollen data include pollen percentage of *Artemisia* (A), pollen percentage of Chenopodiaceae (C), A/C ratio and the A/C ratio-based SMI (Standardized Moisture Index). Stable isotopic data include carbonate $\delta^{13}C$, $\delta^{18}O$ and the $\delta^{18}O$-based SSI (Standardized Salinity Index).

analysis of pollen data, were used to infer the basin-wide moisture variations. The results show that the lake basin was dominated by desert vegetation before ~9.6 cal. ka BP under dry conditions and by desert steppe vegetation between ~9.6 and ~5.5 cal. ka BP under improved moisture conditions (Fig. 3). The meadow steppe vegetation occupied the landscape between ~5.5 and ~3.5 cal. ka BP under greatly improved moisture conditions and the desert steppe vegetation resumed between ~3.5 and ~2.5 cal. ka BP under drastically deteriorated moisture conditions. The following period between ~2.5 and ~0.2 cal. ka BP was dominated by meadow steppe vegetation again under greatly improved moisture conditions. The uppermost portion of the record may reflect a drying of the past ~200 years or simply recent human disturbances.

4.3. Aibi Lake

The MAT is 7.8 °C and the MAP is 95 mm with a potential evaporation of 1315 mm (Table 1) at the lake site (200 m a.s.l.). The pollen data used were from Wang et al. (2013) and the carbonate $\delta^{18}O$ data from Zhang (Chengjun Zhang, 2014, unpublished data). The pollen and stratigraphic data show that a swamp or wetland environment (i.e., not lake) dominated the basin between ~13.9 and ~7.4 cal. ka BP and the following period between ~7.4 and ~3.6 cal. ka BP witnessed an increase in moisture conditions. The moisture conditions were greatly ameliorated from ~3.6 cal. ka BP onward, leading to further basin-wide vegetation amelioration. The A/C ratio, and the SMI as well, unequivocally supports the notion that the moisture has been rising during the past ~3600 years. The $\delta^{18}O$ data, as well as the $\delta^{13}C$ data, suggest that the lake-water salinity has been generally rising during the past ~8000 years with two refreshing episodes: one at ~2.5 cal. ka BP and another at ~1.0 cal. ka BP (Fig. 4).

4.4. Manas Lake

The MAT is 6.1 °C and the MAP is 100 mm with a potential evaporation of 2100 mm (Table 1) at the lake site (257 m a.s.l.). The pollen data used were from Sun et al. (1994) and the carbonate $\delta^{18}O$ data from Rhodes et al. (1996). The geochemistry- and stratigraphy-based interpretation stated that the lake transgressed from ~10.0 to ~6.0 ^{14}C ka BP (Rhodes et al., 1996). A dramatic lake regression from ~6.0 to ~4.5 ^{14}C ka BP coincided with a drastic decrease in moisture. A second lake transgression occurred between ~4.5 and ~2.5 ^{14}C ka BP and was followed by a stepwise establishment of hyper-saline conditions of the past ~2500 years. The pollen data were interpreted as following: a desert condition from ~11.0 to ~9.0 ^{14}C ka BP, a steppe condition from ~9.0 to ~4.0 ^{14}C ka BP, and again a desert condition after ~4.0 ^{14}C ka BP (Sun et al., 1994). The A/C ratio shows that the basin-wide moisture was rising from ~12.0 to ~7.6 cal. ka BP and then declined to a low value at ~6.0 cal. ka BP. It had fluctuated along a low mean value between ~6.0 and ~0.6 cal. ka BP (Fig. 5). The $\delta^{18}O$ data, as well as the $\delta^{13}C$ data, show that the lake-water salinity has been constantly rising during the past ~12,000 years with a trough lasting from ~6.5 to ~5.0 cal. ka BP. The isotopic trough chronologically corresponded with the lake regression lasting from ~6.0 to ~4.5 ^{14}C ka BP when fluvial deposition occurred, implying that the isotopic trough (low salinity) was not resulted from lake-water refreshing, rather from lake desiccation (Rhodes et al., 1996).

4.5. Wulungu Lake

Wulungu Lake is situated in the northern margin of the Zunggar Basin and receives its inflowing water primarily from the Altay Mountains. The MAT is 3.4 °C and the MAP is 117 mm with a

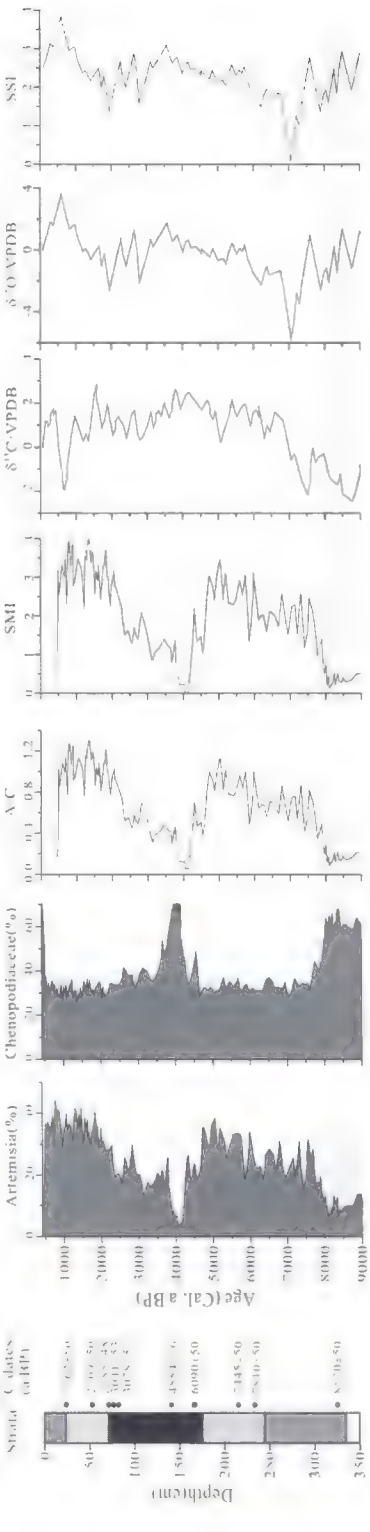

Fig. 7. Pollen data (An et al., 2011) and stable isotopic data (Xiao and Zhang, 2011) from Balikun Lake. Pollen data include pollen percentage of *Artemisia* (A), pollen percentage of Chenopodiaceae (C), A/C ratio and the A/C ratio-based SMI (Standardized Moisture Index). Stable isotopic data include carbonate $\delta^{13}C$, $\delta^{18}O$ and the $\delta^{18}O$-based SSI (Standardized Salinity Index).

potential evaporation of 1844 mm (Table 1) at the lake site (479 m a.s.l.). The pollen data used are from Liu et al. (2008) and the $\delta^{18}O$ data of ostracod shells from Jiang et al. (2007). The original interpretation by Liu et al. (2008) stated that the pollen assemblage before ~6.7 cal. ka BP might be only of local significance because of the strong contribution of wetland pollen types that may have blurred climatic signatures of pollen assemblages. A general wetting trend since ~6.7 cal. ka BP is suggested by a decreasing trend of pollen-based desert biome scores. A comprehensive interpretation of multi-proxy records (including pollen assemblages, geochemical measurements, and ostracod assemblages) by Jiang et al. (2007) stated that a dry and moderately cool climate characterized the early Holocene (from ~10.0 to ~7.6 cal. ka BP) and a wet and warm climate the middle Holocene (from ~7.6 to ~5.3 cal. ka BP). The late Holocene was divided into four subdivisions: a dry and warm climate from ~5.3 to ~3.6 cal. ka BP, a dry and moderately cool climate from ~3.6 to ~2.1 cal. ka BP, a wet and moderately cool climate from ~2.1 to ~1.3 cal. ka BP, and a dry and moderately cool climate since 1.3 cal. ka BP.

If the interpretation by Liu et al. (2008) is justifiable that the pollen assemblage before ~6.7 cal. ka BP might be only of local significance, the high A/C ratios before ~6.7 cal. ka BP (Fig. 6) might also be only of local significance because wetland normally elevates *Artemisia* and suppresses Chenopodiaceae (Liu et al., 2008). The A/C ratio, and the SMI as well, has not varied significantly since ~6.7 cal. ka BP although a weak peak was expressed for the period spanning from ~2.5 to 1.5 cal. ka BP. The $\delta^{18}O$ data of ostracod shells, as well as $\delta^{13}C$ data, displayed a two-step rising trend (Jiang et al., 2007): the first step from ~10.0 to ~6.0 cal. ka BP and the second step from ~6.0 to ~0 cal. ka BP (Fig. 6), suggesting that the lake-water salinity has been more or less constantly rising during the past ~10,000 years.

4.6. *Balikun Lake*

Balikun Lake is situated in the eastern margin of the Junggar Basin (see Fig. 1a). The MAT is 1.0 °C and the MAP is 210 mm with a potential evaporation of 1638 mm (Table 1) at the lake site (1575 m a.s.l.). The pollen data used are from An et al. (2011) and the carbonate $\delta^{18}O$ data from Xue and Zhong (2011). The A/C ratio, and the SMI as well, exhibits a general increasing trend since ~10.0 cal. ka BP with its plateaus spanning from ~2.5 to ~0.8 cal. ka BP and with a trough spanning from ~4.5 to ~3.0 cal. ka BP (Fig. 7). The A/C ratio-indicated increasing trend of moisture during the past ~10,000 years and the lower moisture interval from ~4.5 to ~3.0 cal. ka BP were also corroborated by other pollen proxies (An et al., 2011). The carbonate $\delta^{18}O$ curve unequivocally expresses a rising trend since ~7.5 cal. ka BP and the carbonate $\delta^{13}C$ curve lends a support to the rising trend with a minor exception around ~1.0 cal. ka BP when the two ($\delta^{18}O$ and $\delta^{13}C$) had opposite trends. The minor exception of $\delta^{13}C$ curve was explained to be a result of the change in CO_2 exchange rate between the atmosphere and the lake water (Xue and Zhong, 2011).

4.7. *Tuolekule Lake*

Tuolekule Lake is about 150 km from the Balikun Lake (see Fig. 1a). The MAT is 1.3 °C and the MAP is 211 mm with a potential evaporation of 1603 mm (Table 1) at the lake site (1575 m a.s.l.). There is no carbonate $\delta^{18}O$ data published yet from this lake and this study thus focuses on pollen data (Tao, 2011). The A/C ratio at Tuolekula Lake well corroborates the A/C ratio at Balikun Lake in showing a dramatic rising trend since ~4.0 cal. ka BP (Fig. 8), but it fails to show the early rise from ~8.0 to ~5.0 cal. ka BP at Balikun Lake (Xue and Zhong, 2011).

4.8. *Bosten Lake*

Bosten Lake is situated in the southern slope of the Tianshan Mountains (see Fig. 1a). The MAT is 8.4 °C and the MAP is 141 mm with a potential evaporation of 2039 mm (Table 1) at the lake site (1048 m a.s.l.). This lake has been intensively studied since 1990s for reconstructing its Holocene history and the earlier works were

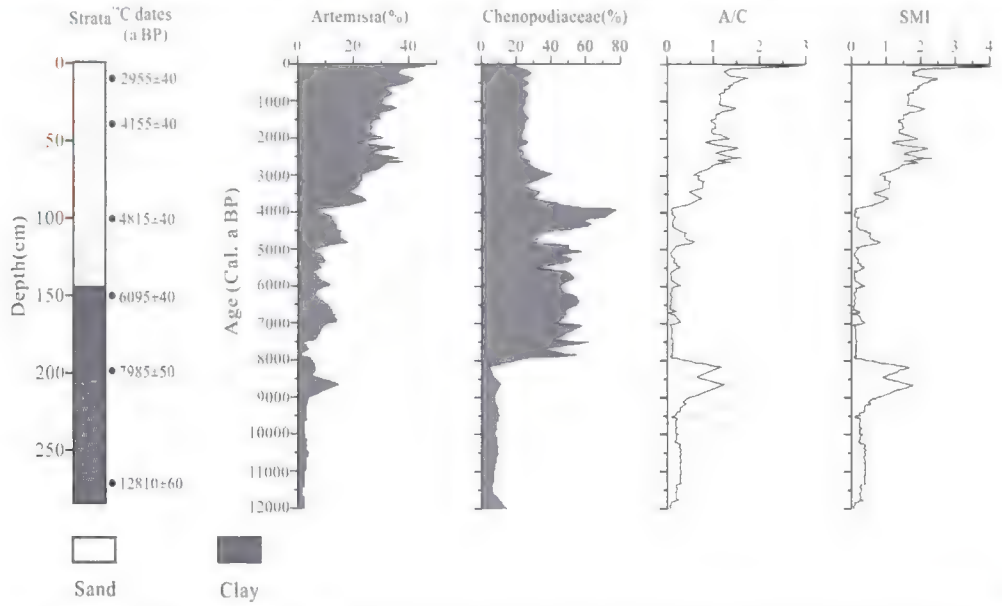

Fig. 8. Data from Tuolekule Lake (Tao, 2011). The data include pollen percentage of *Artemisia* (A), pollen percentage of Chenopoidiaceae (C), A/C ratio and the A/C ratio-based SMI (Standardized Moisture Index).

reviewed by Feng et al. (2006). A series of papers on its Holocene history have been recently published (e.g., Chen et al., 2006; Mischke and Wünnemann, 2006; Wünnemann et al., 2006; Huang et al., 2009) and these works were reviewed by Zhang et al. (2010).

The A/C ratio data used are from Huang (2006) and the $\delta^{18}O$ data of ostracod shells from Mischke and Wünnemann (2006). The A/C ratios were generally low from ~8.0 to ~6.0 cal. ka BP and generally high from ~6.0 to ~0.5 cal. ka BP (Fig. 9). And, it recovered after a trough at ~0.5 cal. ka BP. The A/C ratio-based interpretation of Holocene moisture variations is also corroborated by other pollen proxies (Huang, 2006). The $\delta^{18}O$ data of ostracod shells, as well as the $\delta^{13}C$ data, display dramatic fluctuations along a rising trend, and this rising trend was well corroborated by carbonate mineralogical data (Zhang et al., 2010).

5. Regional comparison and discussion

5.1. A/C ratio-suggested basin-wide moisture variations

It should be reiterated that the overall relationship between the A/C ratios and the bioclimates in arid and semi-arid areas of China still holds (Zhao et al., 2012). However, Zhao and her colleagues offered two precautionary notes: (1) lake-core A/C ratio may underestimate the degree of basin-wide dryness because of the input of *Artemisia* by water from surrounding mountains; and (2) overwhelming domination of salt- and drought-tolerant Chenopodiaceas in saline conditions may undermine the validity of the A/C ratio as a moisture proxy. In addition, areal expansion or shrinkage of wetlands around a lake may also undermine the validity of the A/C ratio as a moisture proxy (Liu et al., 2008). It should be further cautioned that the expansion (or shrinkage) of wetlands does not have a fixed relation with lake-level falling (or rising). For example, lake-level rising may result in an expansion of wetlands by lengthening the lake shorelines, whereas lake-level falling may also result in an expansion of wetlands by shoaling the lake margins (Charman, 2002).

Our comparison of the seven SMI curves (Fig. 10) refuses to offer a geographically-coherent picture of Holocene moisture variation. The most troubling sites are Manas Lake and Wulungu Lake where the highest A/C ratio values appeared in the early Holocene and where no A/C decreasing trend of the past ~6000 years was expressed. At Manas Lake, the first Holocene lake transgression that lasted from ~10.0 to ~6.0 ^{14}C ka BP (Rhodes et al., 1996) and the high A/C ratio interval that spanned from 10.5 to 6.5 cal. ka BP (Sun et al., 1994) led the authors to propose that northern Xinjiang was mainly controlled or modulated by the East Asian monsoon climate, rather than by the westerlies climate, during the Holocene. At Wulungu Lake, a general wetting trend since ~6.7 cal. ka BP is suggested by a decreasing trend of pollen-based desert biome scores, but the A/C ratio failed to show such a trend. The A/C ratio does not seem to work well at Wulungu Lake and the large areal extent of saline surface soils may be responsible. Presently, saline surface soils are dominant in the basin bottom where the groundwater table is quite shallow and the bottom has a fairly large areal extent (see Fig. 1a). The saline condition may have dominated the basin bottom for past ~7000 years in Wulungu basin, thus somewhat undermining the validity of the A/C ratio as a moisture proxy. Admittedly, we have no *in situ* data from Manas Lake to argue against the validity of A/C ratio as a moisture proxy, but the saline condition is presently more predominant in Manas basin than in Wulungu basin, implying that the large areal extent of saline surface soils may also be the blame for the "unexpected" A/C ratios at Manas Lake.

We calculated the average SMI of all seven SMI curves (including Manas and Wulungu curves) and the average shows that the A/C

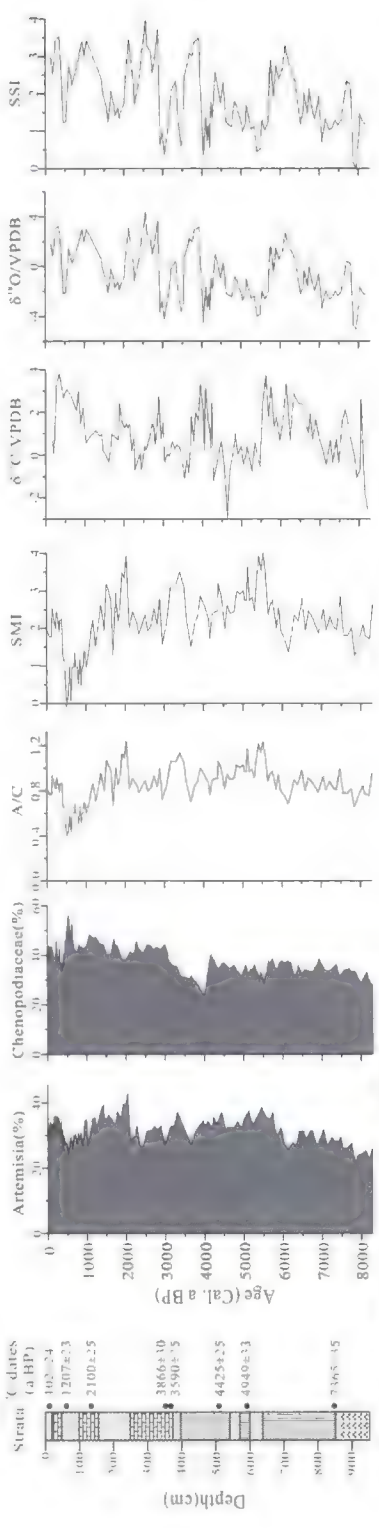

Fig. 9. Pollen data (Huang, 2006) and stable isotopic data (Mischke and Wünnemann, 2006) from Bosten Lake. Pollen data include pollen percentage of *Artemisia* (A), pollen percentage of Chenopodiaceae (C), A/C ratio and the A/C ratio-based SMI (Standardized Moisture Index). Stable isotopic data include carbonate $\delta^{13}C$, $\delta^{18}O$ and the $\delta^{18}O$-based SSI (Standardized Salinity Index).

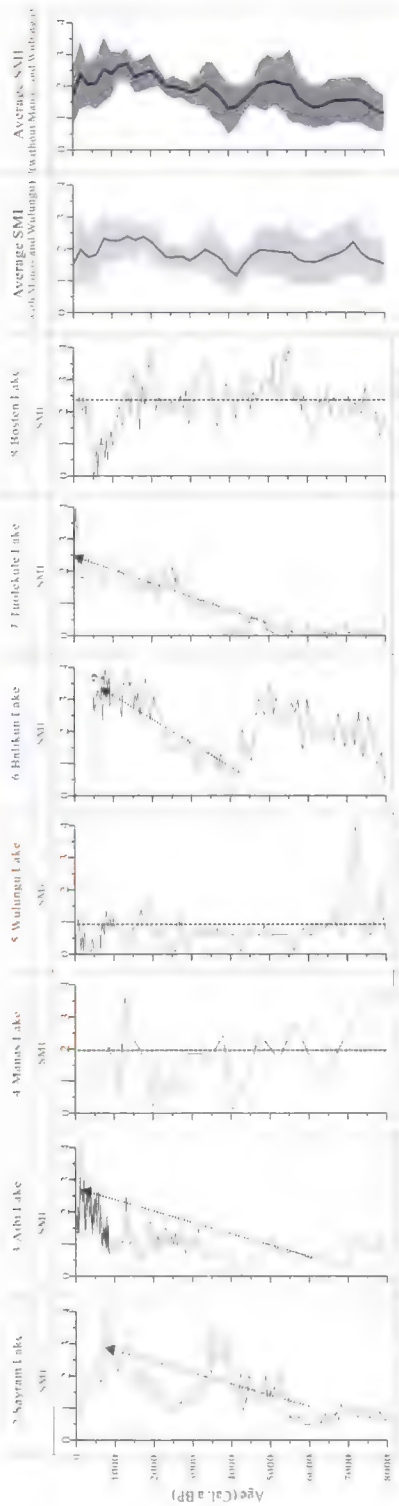

Fig. 10. Regional comparison of the A/C ratio-based SMI (Standardized Moisture Index). Also included are the average SMI with consideration of Manas Lake and Wulungu Lake and the average SMI without consideration of Manas Lake and Wulungu Lake.

ratio-suggested moisture levels were higher during both the early interval (~8.0–~5.0 cal. ka BP) and the late interval (~2.0–~0 ca; ka BP) with the middle interval (~5.0–~2.0 cal. ka BP) being lower. Apparently, the higher A/C ratio for the early interval (~8.0–~5.0 cal. ka BP) was contributed by those "unexpectedly" high A/C ratios from Manas Lake and Wulungu Lake. We then calculated the average of the five SMI curves by excluding Manas and Wulungu curves and an increasing trend of the average A/C ratio emerges (last curve in Fig. 10 and first curve in Fig. 11). Although the relatively large discrepancies among those five selected A/C ratio curves (excluding Manas and Wulungu curves) somewhat undermine our confidence, those A/C ratio-suggested moisture histories from those five lakes were reasonably corroborated by other pollen proxies, and our confidence is thus resumed.

The general rising trend of the average moisture in northern Xinjiang can be explained by invoking its climatic linkage with the North Atlantic Ocean (Fig. 11). That is, the rising trend of winter insolation in the Northern Hemisphere during the past ~8000 years may be the forcing factor (Berger and Loutre, 1991) for the rising trend of the winter temperature in northern Europe (Davis et al., 2003). The latter (i.e., winter temperature) may be the reason for the rising trend of the winter precipitation in Norway (Bakke et al., 2008). The winter wetting trend in northern Europe could be the reason for the A/C ratio-suggested wetting trend in northern Xinjiang, since the latter might have been influenced by the prevailing westerlies that presently bring water vapor from the North Atlantic Ocean to northern Xinjiang.

However, an alternative explanation can be offered by invoking the NAO (North Atlantic Oscillations) and the ENSO (El Niño and Southern Oscillations). First, the positively-phased NAO was reportedly responsible for bringing more water vapor from the North Atlantic Ocean to the Central Asia including northern Xinjiang (Aizen et al., 2001; Bothe et al., 2012) and the increasingly more positively-phased NAO (Olsen et al., 2012) could be the driving force for the moisture increasing trend in northern Xinjiang (see Fig. 11). Second, a recently observed linkage between the ENSO activities and the precipitation in western Central Asia (including Caspian Sea and the downwind areas) may also offer a clue to explain the rising trend of moisture in northern Xinjiang. Specifically, a pronounced high pressure cell is formed over the western Tropical Pacific Ocean and the northern Indian Ocean during the ENSO events and the anticyclone system associated with the high pressure cell, together with the Subtropical Jet, effectively brings water vapor from the northern Indian Ocean to the western Central Asia including Caspian Sea and the downwind areas (Mariotti, 2007). The southward-shifted westerlies during winters are perfectly routed to bring the water vapor from the western Central Asia to northern Xinjiang. The reconstructed increasing trend of ENSO activities (Rein et al., 2005) can thus be an equally possible mechanism to explain the increasing trend of moisture in northern Xinjiang. To sum up, either one of the two (NAO and ENSO) or combination of the two can be an alternative mechanism.

5.2. $\delta^{18}O$-suggested lake-water salinity variations

Generally, carbonate isotopic signature ($\delta^{18}O$) in closed or semi-closed lakes in arid and semi-arid areas is controlled by the ratio of the evaporation over the precipitation. The isotopic composition is further complicated in northern Xinjiang where the amount of ice melting water in surrounding mountains, rather than precipitation within the basin, controls the water balance and thus the lake-water salinity in those closed and semi-closed lakes. The carbonate $\delta^{18}O$ variations from Manas Lake were interpreted to have been modulated by the precipitation associated with the East Asian monsoon (Lin and Wei, 1998). The carbonate $\delta^{18}O$ variations from

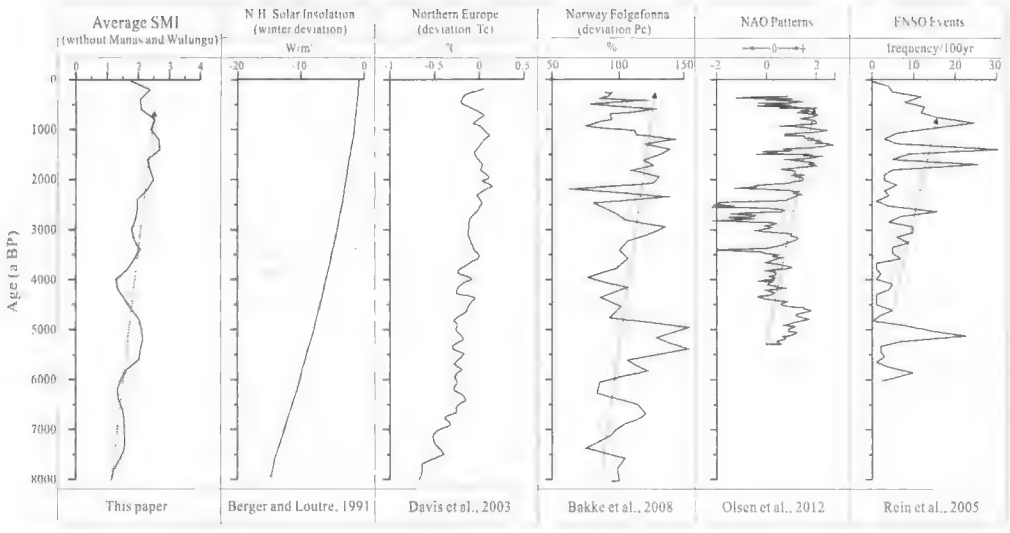

Fig. 11. Possible mechanisms that may explain the average SMI variation of the past ~8000 years in northern Xinjiang: winter insolation of Northern hemisphere (Berger and Loutre, 1991), winter temperature in northern Europe (Davis et al., 2003), winter precipitation in Norway (Bakke et al., 2008), variation in North Atlantic Oscillations (NAO) during the past ~5000 years (Olsen et al., 2012), and variation in El Nino and Southern Oscillation (ENSO) during the past ~6000 years (Rein et al., 2005).

Balikun Lake and several other lakes were interpreted to have responded to the switches of the precipitation-promoting systems between the Southwest Asian monsoon and the prevailing westerlies (Zhong et al., 2010). It means that the carbonate $\delta^{18}O$ variations were mainly controlled either by the sources of the precipitation or by the temperature of the precipitation. However, in closed and semi-closed lakes in arid and semiarid areas, the carbonate $\delta^{18}O$ variations are more relevant to the lake-water salinity than to anything else (Fontes et al., 1996; Leng and Marshall, 2004; Zhang et al., 2010). The nearly parallel rising trends of all of the seven carbonate $\delta^{18}O$ data-resulted SSI curves (i.e., Standardized Salinity Index) mean that the lake-water salinity in the entire northern Xinjiang has been generally rising since ~8.0 cal. ka BP (Fig. 12).

Now a contradiction is confronting us: the A/C ratios seem to suggest a regional wetting trend and the $\delta^{18}O$ data do demonstrate a regional lake-salinity increasing trend during the past ~8000 years. In other words, the lakes in northern Xinjiang have become saltier and saltier over the course of the past ~8000 years during which northern Xinjiang appears to have experienced increasingly more humid climate. This contradiction cannot be reconciled by simply juggling the temperature and the precipitation: lowering the temperature or increasing the precipitation or doing both cannot reconcile the contradiction. Nevertheless, this contradiction may be reconciled by invoking the Holocene variations in the areal extent of ice covers in the surrounding mountains (i.e., the Tianshan Mountains and the Altay Mountains). Specifically, the Holocene variations in the areal extent of the ice covers in the mountains might have controlled the salinity variations of those lakes. Here, we use the Holocene ice-extent shrinking history (last curve in Fig. 12) of the Canadian Arctic (Koerner and Fisher, 1990) as an approximate parallel of the ice-extent shrinking history in northern Xinjiang, as no such data exist for northern Xinjiang. We consider this parallel acceptable because both the ice extent in northern Xinjiang and the ice extent in Canadian Arctic are controlled by the northern hemispheric insolation (Ruddiman, 2008). If this parallel is indeed acceptable, the Holocene persistent shrinking of the ice extent in the mountains means that the fresh water supply has become less and less, resulting in saltier and saltier lake water as indicated by the upward increasing trends of carbonate $\delta^{18}O$ signatures. The A/C ratio-suggested wetting of the past ~8000 years may well be the result of increasing precipitation under a general cooling condition (Wanner et al., 2008). To conclude, the increasing trend of the precipitation (most likely winter precipitation) accompanied by the lowering tend of the temperature conditions might have increasingly enhanced the effective soil moisture in northern Xinjiang, but the increase in the basin-wide moisture was not enough to compensate for the decrease in the lake inflowing water resulted from the shrinkage of ice-covered areas in the mountains.

Finally, two precautionary notes should be made, about Wulungu Lake and Manas Lake. The general increasing trends of the lake-water salinities during the past ~8000 years mean that the lake levels in northern Xinjiang should have been declining. However, the level of Wulungu Lake was argued to have a rising trend (Liu et al., 2008). We think that their argument, based on pollen and particle-size data, is not well-grounded for two reasons. First, pollen proxies may be indicative of basin-wide moisture level and the moisture level may be disassociated with lake level if the lake was mainly supplied by ice meltwater (Zhang et al., 2010; Feng et al., 2013). Second, particle-size data can be interpreted either as an indication of lake shoaling (i.e., less inflowing water) or as an indication of strengthened water dynamics (i.e., more inflowing water) (Shen et al., 2010). We suggest that the Holocene stratigraphy of the Wulungu Lake shore should be traced to validate or invalidate their argument. The record from Manas Lake was argued to lend a support to the proposition that the Asian monsoon domination has extended to northern Xinjiang during the Holocene. Nearly all of the recently-published lake records from northern Xinjiang favors the proposition that the westerlies have dominated northern Xinjiang during the Holocene (e.g., Chen et al., 2008; Ran and Feng, 2013; Wang and Feng, 2013, and the references thereafter). However, the recently-reported data from Yili Valley (Li et al., 2011; Cheng et al., 2012) lend strong support to the proposition of Asian monsoon domination, and admittedly we are not in the position to dismiss those data.

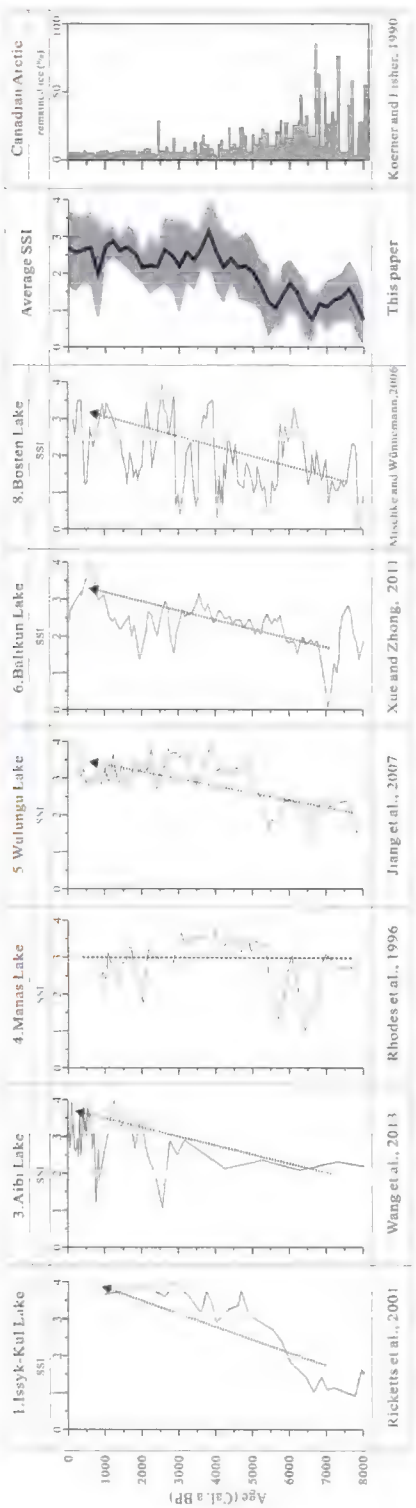

Fig. 12. Regional comparison of the $\delta^{18}O$-based SSIs (Standardized Salinity Index). Also included are the regional average of SSI (this paper) and the areal extent of remaining ice covers in Arctic Canada (Koerner and Fisher, 1990) as an approximate parallel of the areal extent of remaining ice covers in northern Xinjiang.

6. Concluding remarks

(1) Based on the well-tested premise that the overall relationship between the A/C ratios and the bioclimates in arid and semi-arid areas of China still holds, we compared the A/C ratio-based SMI (Standardized Moisture Index) of five selected lacustrine sequences (Sayram, Aibi, Balikun, Tuolekule, and Bosten). Our comparison shows that the regional SMI had a general rising trend and the rising trend was reasonably corroborated by other pollen proxies. The rising trend can be explained by invoking its climatic linkage with the North Atlantic Ocean and a possible linkage with ENSO is an additional or an alternative mechanism for explaining the rising trend.

(2) The nearly parallel rising trends of the reviewed seven carbonate $\delta^{18}O$ data-resulted SSI curves (i.e., Standardized Salinity Index) mean that the lake-water salinity in the entire northern Xinjiang has been generally rising since ~8.0 cal. ka BP. The rising trend can be explained by invoking the Holocene variations in the areal extent of ice covers in the Tianshan Mountains and the Altay Mountains. That is, the Holocene persistent shrinking of the ice extent in the mountains generated less and less melting water supplies to the lakes and thus resulted in saltier and saltier waters in the lakes.

(3) A contradiction is confronting us: the lakes in northern Xinjiang have become saltier and saltier over the course of the past ~8000 years during which northern Xinjiang appears to have experienced increasingly more humid climates. A reconcilable explanation is that the increasing trend of the precipitation (most likely winter precipitation) accompanied by the lowering tend of the temperature conditions might have increasingly enhanced the effective soil moisture in northern Xinjiang, but the increase in the basin-wide moisture was not enough to compensate for the decrease in the lake inflowing water resulted from the shrinkage of ice-covered areas in the mountains.

Acknowledgements

This paper is a result of research projects supported by two Chinese Nature Science Foundation grant (No. U1203821L08 and No. 40671190) and one U.S. National Science Foundation grant (NSF-BCS-06-52304).

References

Aizen, E.M., Aizen, V.B., Melack, J.M., Nakamura, T., Ohta, T., 2001. Precipitation and atmospheric circulation patterns at mid-latitudes of Asia. International Journal of Climatology 21, 535–556.

An, C.B., Lu, Y.B., Zhao, J.J., Tao, S.C., Dong, W.M., Li, H., Jin, M., Wang, Z.L., 2011. A high-resolution record of Holocene environmental and climatic changes from Lake Balikun (Xinjiang, China): implications for central Asia. The Holocene 22, 43–52.

Bakke, J., Lie, O., Dahl, S., Nesje, A., Bjune, A.E., 2008. Strength and spatial patterns of the Holocene wintertime westerlies in the NE Atlantic region. Global and Planetary Change 60, 28–41.

Berger, A., Loutre, M.F., 1991. Insolation values for the climate of the last 10 million years. Quaternary Science Reviews 10, 297–317.

Blyakharchuk, T.A., Wright, H.E., Borodavko, P.S., van der Knaap, W.O., Ammann, B., 2007. Late Glacial and Holocene vegetational history of the Altai Mountains (southwestern Tuva Republic, Siberia). Palaeogeography Palaeoclimatology Palaeoecology 245 (3–4), 518–534.

Bothe, O., Fraedrich, K., Zhu, X., 2012. Precipitation climate of Central Asia and the large-scale atmospheric circulation. Theoretical and Applied Climatology 108, 345–354.

Charman, D.J., 2002. Peatland Systems and Environmental Change. John Wiley & Sons, Chichester, p. 301.

Chen, F.H., Huang, X.Z., Yang, M.L., Yang, X.L., Fan, X., Zhao, H., 2006. Westerly dominated Holocene climate model in and central Asia-case study on Bosten

Lake, Xinjiang, China. Quaternary Sciences 26, 881–887 (in Chinese with English Abstract).
Chen, F.H., Yu, Z.C., Yang, M.L., Ito, E., Wang, S.M., Madsen, D.B., Huang, X.Z., Zhao, Y., Sato, T., Birks, H.J.B., Boomer, I., Chen, J.H., An, C.B., Wunnemann, B., 2008. Holocene moisture evolution in arid central Asia and its out-of-phase relationship with Asian monsoon history. Quaternary Science Reviews 27, 351–364.
Chen, X., 2010. Physical Geography of Chinese Arid Zone. Science Press, Beijing, China, p. 802.
Cheng, H., Zhang, P.Z., Spotl, C., Edwards, R.L., Cai, Y.J., Zhang, D.Z., Sang, W.C., Tan, M., An, Z.S., 2012. The climatic cyclicity in semiarid-arid central Asia over the past 500,000 years. Geophysical Research Letters 39, L01705.
Davis, B.A.S., Brewer, S., Stevenson, A.C., Guiot, J., Contributors, D., 2003. The temperature of Europe during the Holocene reconstructed from pollen data. Quaternary Science Reviews 22, 1701–1706.
Demske, D., Heumann, G., Granoszewski, W., Nita, M., Mamakowa, K., Tarasov, P.E., Oberhänsli, H., 2005. Late glacial and Holocene vegetation and regional climate variability evidenced in high-resolution pollen records from Lake Baikal. Global Planetary Change 46, 255–279.
El-Moslimany, A.P., 1990. Ecological significance of common non-arboreal pollen: examples from drylands of the Middle East. Review of Palaeobotany and Palynology 64, 343–350.
Feng, Z.D., An, C.B., Wang, H.B., Zhai, X.W., 2006. Holocene climatic and environmental changes in the arid and semiarid regions of China: a review. The Holocene 16, 1–12.
Feng, Z.D., Wu, H.N., Zhang, C.J., Ran, M., Sun, A.Z., 2013. Bioclimatic change of the past 2500 years within Balkhash Basin in the eastern Kazakhstan of Central Asia. Quaternary International 311, 63–70.
Fontes, J.C., Gasse, F., Gibert, E., 1996. Holocene environmental changes in Lake Bangong basin (Western Tibet). Part 1: chronology and stable isotopes of carbonates of a Holocene lacustrine core. Palaeogeography, Palaeoclimatology, Palaeoecology 120, 25–47.
Herzschuh, U., 2006. Palaeo-moisture evolution in monsoonal Central Asia during the last 50,000 years. Quaternary Science Reviews 25, 163–178.
Huang, X.Z., 2006. Holocene Climate Variability of Arid Central Asia Documented by Bosten Lake, Xinjiang, China (Ph.D. dissertation). Lanzhou University (in Chinese with English Abstract).
Huang, X.Z., Chen, F.H., Fan, Y.X., Yang, M.L., 2009. Dry late-glacial and early Holocene climate in arid central Asia indicated by lithological and palynological evidence from Bosten Lake, China. Quaternary International 194, 19–27.
Hu, R.J., 2004. Physical Geography of Chinese Tianshan. Chinese Environmental Science Press, Beijing, China, p. 443.
Jiang, Q.F., Shen, J., Liu, X.Q., Zhang, E.L., Xiao, X.Y., 2007. A high-resolution climatic change since Holocene inferred from multi-proxy of lake sediment in westerly area of China. Chinese Science Bulletin 52 (14), 1970–1979.
Jiang, Q.F., Ji, J.F., Shen, J., Matsumoto, R.Y.O., Tong, G.B., Qian, P., Ren, X.M., Yan, D.Z., 2013. Holocene vegetational and climatic variation in westerly-dominated areas of Central Asia inferred from the Sayram Lake in northern Xinjiang, China. Science China: Earth Sciences 56, 339–353.
Koerner, R.M., Fisher, D.A., 1990. A record of Holocene summer climate from a Canadian high-Arctic ice core. Nature 343, 630–631.
Leng, M.J., Marshall, J.D., 2004. Palaeoclimate interpretation of stable isotope data from lake sediment archives. Quaternary Science Reviews 23, 811–831.
Li, X.Q., Zhao, K.L., Dodson, J., Zhou, X.Y., 2011. Moisture dynamics in central Asia for the last 15 kyr: new evidence from Yili Valley, Xinjiang, NW China. Quaternary Science Reviews 30, 3457–3466.
Lin, R.F., Wei, K.Q., Cheng, Z.Y., Wang, Z.X., Gasse, F., Fontes, J.C., Gibert, E., Tucholka, P., 1996. A palaeoclimatic study on lacustrine cores from Manas Lake, Xinjiang, western China. Geochimica 25, 63–72 (in Chinese with English Abstract).
Lin, R.F., Wei, K.Q., 1998. Palaeoclimate implications of oxygen isotope record from lacustrine sediments of Manas lake, Xinjiang, a comparison with those from Qinhai lake and Siling lake. Quaternary Science 4, 308–318 (in Chinese with English Abstract).
Liu, X.Q., Herzschuh, U., Shen, J., Jiang, Q., Xiao, X., 2008. Holocene environmental and climatic changes inferred from Wulungu Lake in northern Xinjiang, China. Quaternary Research 70, 412–425.
Ma, Y.Z., Liu, K.B., Feng, Z.D., Sang, Y.L., Wang, W., Sun, A.Z., 2008. A survey of modern pollen and vegetation along a south–north transect in Mongolia. Journal of Biogeography 35, 1512–1532.
Mariotti, A., 2007. How ENSO impacts precipitation in southwest central Asia. Geophysical Research Letters 34, L16706.
Meeker, L.D., Mayewski, P.A., 2002. A 1400-year high-resolution record of atmospheric circulation over the North Atlantic and Asia. The Holocene 12, 257–266.
Mischke, S., Wünnemann, B., 2006. The Holocene salinity history of Bosten Lake (Xinjiang, China) inferred from ostracod species assemblages and shell chemistry: possible palaeoclimatic implications. Quaternary International 154–155, 100–112.
Olsen, J., Anderson, N.J., Knudsen, M.F., 2012. Variability of the North Atlantic Oscillation over the past 5,200 years. Nature Geoscience 5, 808–812.
Ran, M., Feng, Z.D., 2013. Holocene moisture variations across China and driving mechanisms: a synthesis of climatic records. Quaternary International 313–314, 179–193.
Reimer, P.J., Baillie, M.G.L., Bard, E., 2009. IntCal09 and Marine09 radiocarbon age calibration curves, 0–50,000 years cal BP. Radiocarbon 51, 1111–1150.
Rein, B., Luckge, A., Reinhardt, L., Sirocko, F., Wolf, A., Dullo, W.C., 2005. El Nino variability off Peru during the last 20,000 years. Paleoceanography 20, 400?.
Ricketts, R.D., Johnson, T.C., Brown, E.T., Rasmussen, K.A., Romanovsky, V.V., 2001. The Holocene paleolimnology of Lake Issyk-Kul, Kyrgyzstan: trace element and stable isotope composition of ostracods. Palaeogeography, Palaeoclimatology, Palaeoecology 176, 207–227.
Rhodes, T.E., Gasse, F., Lin, R.F., Fontes, J.C., Wei, K.Q., Bertrand, P., Gibert, E., Melieres, F., Tucholka, P., Wang, Z.X., Cheng, Z.Y., 1996. A late Pleistocene–Holocene lacustrine record from Lake Manas, Zunggar (northern Xinjiang, western China). Palaeogeography, Palaeoclimatology, Palaeoecology 120, 105–121.
Rudaya, N., Tarasov, P., Dorofeyuk, N., Solovieva, N., Kalugin, I., Andreev, A., Daryin, A., Diekmann, B., Riedel, F., Tserendash, N., Wagner, M., 2009. Holocene environments and climate in the Mongolian Altai reconstructed from the Hoton-Nur pollen and diatom records: a step towards better understanding climate dynamics in central Asia. Quaternary Science Reviews 28, 540–554.
Ruddiman, W.F., 2008. Earth's Climate: Past and Future. Freemand and Company, New York, p. 388.
Shen, J., Xue, B., Wu, J.L., Wu, Y.H., Liu, X.Q., Yang, X.D., Liu, J., Wang, S.M., 2010. Lake Sediment and Environmental Evolution. Science Press, Beijing, China, p. 473.
Staubwasse, M., Weiss, M., 2006. Holocene climate and cultural evolution in late prehistoric-early historic West Asia. Quaternary Research 66, 372–387.
Sorrel, P., Popescu, S.M., Klotz, S., Suc, J.P., Oberhansli, H., 2007. Climate variability in the Aral Sea basin (Central Asia) during the late Holocene based on vegetation changes. Quaternary Research 67, 357–370.
Sun, X.J., Du, N.Q., Weng, C.Y., Lin, R.F., Wei, K.Q., 1994. Paleovegetation and Paleoenvironment of Manasi Lake, Xinjiang, N.W. China during the last 14000 years. Quaternary Sciences 3, 239–248 (in Chinese with English Abstract).
Tao, S.C., 2011. Pollen Record of Vegetation and Environmental Changes from Lakes Sediment in Eastern Xinjiang, China, during the Holocene (Ph.D. dissertation). Lanzhou University (in Chinese with English Abstract).
Tarasov, P., Jin, G.Y., Wagner, M., 2006. Mid-Holocene environmental and human dynamics in northeastern China reconstructed from pollen and archaeological data. Palaeogeography, Palaeoclimatology, Palaeoecology 241, 284–300.
Wang, W., Feng, Z.D., 2013. Holocene moisture evolution across the Mongolian Plateau and its surrounding areas: a synthesis of climatic records. Earth-Science Reviews 122, 38–57.
Wang, W., Feng, Z.D., Ran, M., Zhang, C.J., 2013. Holocene climate and vegetation changes inferred by pollen records from Lake Aibi of northern Xinjiang, China. Quaternary International 311, 54–62.
Wanner, H., Beer, J., Butikofer, J., Crowley, T.J., Cubasch, U., Fluckiger, J., Goosse, H., Grosjean, M., Joos, F., Kaplan, J.O., Kuttel, M., Müller, S.A., Prentice, I.C., Solomina, O., Stocker, T.F., Tarasov, P., Wagner, M., Widmann, M., 2008. Mid- to Late Holocene climate change: an overview. Quaternary Science Reviews 27, 1791–1828.
Winkler, M.G., Wang, P.K., 1993. The late-Quaternary vegetation and climate of China. In: Wright Jr., H.E., Kutzbach, J.E., Webb III, T., Ruddiman, W.F., Street Perrott, F.A., Bartlein, P.J. (Eds.), Global Climates Since the Last Glacial Maximum. University of Minnesota Press, Minneapolis, pp. 2210–2261.
Wu, J.L., Wang, S.M., 1997. Carbonate ^{18}O- and ^{13}C-recorded environmental changes in RM lake core in Zoige of the eastern Tibetan Plateau. Marine Geology and Quaternary Geology 17, 63–71.
Wunnemann, B., Mischke, S., Chen, F., 2006. A Holocene sedimentary record from Bosten lake, China. Palaeogeography, Palaeoclimatology, Palaeoecology 234, 223–238.
Xue, J.B., Zhong, W., 2011. Holocene climate variation denoted by Barkol Lake sediments in northeastern Xinjiang and its possible linkage to the high and low latitude climates. Science China Earth Science 54, 603–614.
Zhang, C.J., Feng, Z.D., Yang, Q.L., Guo, X.H., Sun, F.F., 2010. Holocene environmental variations recorded by organic-related and carbonate-related proxies of the lacustrine sediments from Bosten Lake, northwestern China. The Holocene 20, 363–373.
Zhao, Y., Yu, Z.C., Chen, F.H., Zhang, J.W., Yang, B., 2009. Vegetation response to Holocene climate change in monsoon-influenced region of China. Earth-Science Reviews 97, 242–256.
Zhao, Y., Liu, H.Y., Li, F.R., Huang, X.Z., Sun, J.H., Zhao, W.W., Herzschuh, U., Tang, Y., 2012. Application and limitations of the *Artemisia*/Chenopodiaceae pollen ratio in arid and semi-arid China. The Holocene 22, 1385–1392.
Zhong, W., Xue, J.B., Li, X.D., Xu, H.J., Jun, O., 2010. A holocene climatic record denoted by geochemical indicators from Barkol Lake in the Northeastern Xinjiang, NW China. Geochemistry International 48, 792–800.

附录九

Holocene climatic reconstructions from the fossil pollen record at Qigai Nuur in the southern Mongolian Plateau

The Holocene
23(10) 1391–1402
© The Author(s) 2013
Reprints and permissions:
sagepub.co.uk/journalsPermissions.nav
DOI: 10.1177/0959683613489581
hol.sagepub.com
SAGE

Aizhi Sun[1] and Zhaodong Feng[2]

Abstract

This study focuses on the reconstructions of vegetation and climate changes during the past ~11,000 years on the basis of 222 fossil pollen samples from Qigai Nuur (core QGN-2004) in the southern part of the Mongolian Plateau. Plant Functional Type – Modern Analogue Technique was used for quantitative climatic reconstructions from fossil pollen data. Our results showed that regional vegetation experienced dramatic shifts between steppe forest and dry steppe before 9200 cal. yr BP in the Qigai Nuur region. The reconstructed mean annual temperature and especially mean annual precipitation also showed fluctuations at that time. From ~9200 to ~2800 cal. yr BP, the vegetation was dominated by steppe forests, and the reconstructed climate was generally warm and wet, but with two cold and dry intervals at ~7400 to ~6000 cal. yr BP and at ~4000 to ~2800 cal. yr BP. From ~2800 to ~850 cal. yr BP, dry steppe vegetation dominated the landscape under slightly cooler and much drier climate conditions. During the past ~850 years, the vegetation was characterized by abundant herbs and the climate showed rising temperature and fluctuating precipitation. The comparison of the reconstructed precipitation from the Qigai Nuur core with monsoon-strength records from southern China shows that the first-order variation in the precipitation was most likely controlled by the summer insolation-dictated Inter-Tropical Convergence Zone movements (i.e. N–S shifts). The comparison of the reconstructed precipitation from Qigai Nuur core with surface sea temperature in the Western Tropical Pacific Ocean suggests that the second-order variation in the precipitation was most likely modulated by the El Niño-Southern Oscillation dynamics (i.e. E–W shifts).

Keywords

East Asian summer monsoon, Holocene, Mongolian Plateau, palaeoclimate, pollen, vegetation

Received 16 July 2012; revised manuscript accepted 19 March 2013

Introduction

The southern part of the Mongolian Plateau is important in context of ongoing global climate change for two reasons. First, as a part of the Central Asian Arid Zone (CAAZ), the climate has been very sensitive to natural and anthropogenic forcing factors (Intergovernmental Panel on Climate Change (IPCC), 2007) and the warming-induced drying trend in CAAZ during the past 100 years is a warning sign for severe water shortage and ecological degradation under projected future warming conditions. Second, the present summer monsoonal margin is primarily situated within the southern part of the Mongolian Plateau (Gao, 1962) and the sensitivity of the monsoonal margin to climate change has been a research focus in climate and palaeoclimate communities because the sensitivity is of a serious concern for future regional socio-economic development (Huang et al., 2004; Xu, 1997). To understand the significance of current global change, it is necessary to establish the temporal background of the climate changes during the most recent geological era, i.e. the Holocene (i.e. the past 11,500 years), because the projected global changes will occur under similar natural boundary conditions.

This research places a particular focus on the reconstruction of Holocene climate change based on pollen fossil data retrieved from Qigai Nuur (39.5°N and 109.5°E) that is situated just within the aforementioned monsoonal margin (Figure 1a). We hope that our reconstruction can facilitate the reconciliation of the existing controversies surrounding the Holocene climatic changes in the East Asian monsoonal margin. These controversies include very different points of views on: (1) synchronous or asynchronous association of temperature and precipitation (e.g. Chen FH et al., 2006; Feng et al., 2006; Shi et al., 1993; Xiao et al., 2004), (2) the timing of the Holocene Thermal Maximum (e.g. An et al., 2000; Feng et al., 2006; Xiao et al., 2004; Zhou et al., 2001), and (3) the dynamics of the monsoon northern limit (e.g. An, 2000; Hartmann and Wünemann, 2009; Herzschuh et al., 2004; Zhao et al., 2008).

Study region and site

Qigai Nuur is situated in the middle part of Mu Us Sandy Land, which lies between the steppe-dominated margin of the Loess Plateau to the southeast and the Tengger Desert to the northwest (Figure 1b). The mean annual temperature (MAT) is ~7°C and the mean annual precipitation (MAP) is ~300 mm with the evaporation exceeding 1000 mm at Wushen County Meteorological Station that is only 20 km from Qigai Nuur. Qigai Nuur is the sixth of seven catenulated lakes forming along an abandoned river channel that were later modified by sand-dune activities. At present, it is a closed basin lake with a surface area of about 5 km^2 and a maximum water depth of about 3 m. The modern natural vegetation in the Qigai Nuur region is dominated by steppes (Figure 1b), mainly consisting of *Salsola* spp., *Caragana*,

[1]Key Laboratory of Cenozoic Geology and Environment, Institute of Geology and Geophysics, Chinese Academy of Sciences, China
[2]Xinjiang Institute of Ecology and Geography, Chinese Academy of Sciences, China

Corresponding author:
Zhaodong Feng, Xinjiang Institute of Ecology and Geography, Chinese Academy of Sciences, 818 South Beijing Road, Urumqi 830011, China.
Email: fengzd@lzu.edu.cn

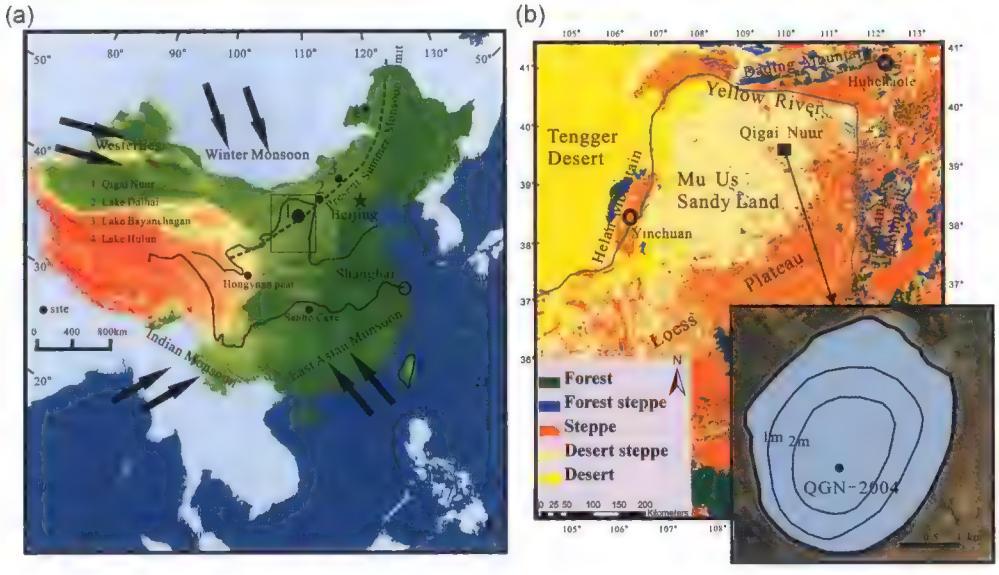

Figure 1. Location of Qigai Nuur and other lakes mentioned in the text. (a) Present summer monsoon limit (Gao, 1962); (b) vegetation distribution in study region, inset showing lake bathymetry and coring location (e.g. Qigai Nuur basin and surrounding area) (Zhang, 2007).

Artemisia arenaria, Chenopodiaceae, *Agriophyllum squarrosum*, and *Corispermum* spp. Meadow steppes and wetland marshes are also found in topographic depressions, lake shores and river valleys (Zhang, 2007).

Material and methods

Core collection and sediment composition analysis

An 8.2 m long sediment core (QGN-2004) was collected with a UWITEC piston corer in the summer of 2004 in the central part of Qigai Nuur where the water depth is 2.9 m. The core was cut longitudinally into two halves and visually described immediately after core retrieval in the field. The grain size was measured at 2 cm intervals using a Malvern Mastersizer 2000 laser diffraction particle size analyzer (size range 0.02–2000 μm). Sample pretreatment for grain-size analysis included: (1) using H_2O_2 to remove organic matter and soluble salts, (2) using diluted 1 N HCl to remove carbonate and (3) using Na-hexametaphosphate to disperse aggregates. Total organic matter content (TOC) was determined at 2 cm intervals using the titration method with concentrated sulfuric acid (H_2SO_4) and potassium dichromate ($K_2Cr_2O_7$). All of the aforementioned analyses were conducted in the MOE Key Laboratory of Western China's Environmental Systems at Lanzhou University.

Dating analysis

Seventeen samples of bulk sediment were radiocarbon dated using accelerator mass spectrometry (AMS) at the NSF-AMS Facility at the University of Arizona (Table 1). To assess the carbon reservoir effect, we obtained an age of 1947 ^{14}C yr BP on the bulk sediment sampled at 0–2 cm. We also constructed a linear relationship between the depths and the nine dates for the upper 300 cm of the core without including the top date (i.e. 1947 ^{14}C yr BP) and the intercepted age for the top (i.e. 0 cm) is 2020 years, being reasonably consistent with the measured reservoir effect of ~1950 years. To account for the reservoir effect for the entire core, 1950 years were subtracted from the bulk sediment radiocarbon dates assuming that the reservoir effect is the same throughout the core. Then, all dates were calibrated to calendar years before present (BP–AD 1950) with the program CALIB 6.0 using INTCAL 09 calibration data set (Reimer et al., 2009). Four linear age–depth models were established for four core segments based on the relationships between the depths and dates: between 0 cm and 302 cm, between 302 cm and 382 cm, between 382 cm and 572 cm, and between 572 and 820 cm. It should be noted that the ages older than 9000 cal. yr BP were extrapolated from the age–depth model between 572 cm and 632 cm. Calibrated radiocarbon ages are used throughout the paper.

Pollen analysis

A total of 222 pollen samples were obtained at 2–4 cm intervals from the sediment core. For pollen analysis, a tablet of *Lycopodium* (containing 27,637±563 spores) was first added for calculation of pollen concentration (Moore et al., 1991). The procedure for fossil pollen analysis includes treating 5–10 g of sediment sample with 10% HCl, 10% KOH, 36% hydrofluoric acid (HF) to eliminate carbonate, humid acid, and silicate, respectively. Furthermore, the pollen in the residue was concentrated with a 7 μm mesh sieve in conjunction with ultrasonic vibration. Finally, water-free glycerol was used for mounting pollen samples on microscopic slides. The treated samples were then examined with a transmitted light microscope (Olympus BX 51) at 400× to 1000× magnification. More than 300 pollen grains (not including spores) were counted for each sample. Pollen types were identified using pollen references including pollen books and photographs (Erdtman, 1978; Moore and Webb, 1987; Wang et al., 1995) and our own reference slide collection of more than 200 plant species from northern China. The percentage of each pollen type was calculated based on the sum of all counted pollen grains excluding spores. Pollen concentrations were calculated on the basis of exotic

Table 1. Radiocarbon dates and calibrated ages of Qigai Nuur core.

Laboratory no.	Depth (cm)	Dated material	$\delta^{13}C$ (‰)	^{14}C dates (yr BP, ± error)	Corrected ^{14}C dates (yr BP)	Calibrated ages (cal. yr BP)
AA64196	0–2	Bulk sediment	−11.2	1950±50	0±50	0
AA64201	84–85	Bulk sediment	−9.0	2700±70	750±70	557–893
AA64202	94–95	Bulk sediment	−8.9	2780±60	830±60	671–906
AA64204	124–125	Bulk sediment	−7.7	2480±60	530±60	508–636
AA64205	154–155	Bulk sediment	−4.2	2490±40	540±40	505–652
AA64206	174–175	Bulk sediment	−5.2	3120±60	1170±60	962–1257
AA64208	209–210	Bulk sediment	−3.8	3280±40	1340±40	1178–1309
AA64209	231–232	Bulk sediment	−6.0	3490±60	1540±60	1318–1536
AA64210	261–262	Bulk sediment	−6.3	3540±60	1590±60	1349–1680
AA64211	301–302	Bulk sediment	−3.1	3760±40	1820±40	1624–1865
AA64214	381–382	Bulk sediment	−9.6	6120±70	4170±70	4455–4853
AA64216	450–451	Bulk sediment	−10.6	7340±60	5390±60	6000–6293
AA64217	501–502	Bulk sediment	−8.1	8340±110	6390±110	7019–7553
AA64218	541–542	Bulk sediment	−10.4	9320±60	7370±60	8036–8327
AA64219	571–572	Bulk sediment	−9.0	9670±90	7720±90	8349–8749
AA64220	601–602	Bulk sediment	−7.4	9650±50	7700±50	8406–8586
AA64221	631–632	Bulk sediment	−6.0	10,170±60	8230±60	9024–9401

Lycopodium spore counts and were expressed as the number of grains per gram (grains/g). Pollen diagrams were plotted using Tilia (version 1.7.16) (Grimm, 1990). CONISS cluster analysis was conducted for providing reference for pollen zoning.

Several pollen indices have been designed to capture climate-related information for arid and semi-arid regions. For example, the C/A ratio (Chenopodiaceae/*Artemisia*) has been shown to be a useful aridity index in arid and semi-arid Asia (El-Moslimany, 1990; Liu et al., 1998; Van Campo et al., 1996; Zhao et al., 2009a). But, this index was found to be problematic in the northern part of the Mongolian Plateau when Chenopodiaceae pollen overwhelmingly dominates the pollen spectrum in the arid conditions (Wang et al., 2011) or when Poaceae pollen is adequately represented in the pollen spectrum in semi-arid conditions (Fowell et al., 2003). Another pollen percentage ratio ((C+A)/P) of the combined Chenopodiaceae and *Artemisia* (C+A) to Poaceae (P) was designed to retrieve the Holocene aridity history in central Mongolia (Fowell et al., 2003). However, Poaceae has been sufficiently demonstrated to be under-represented in pollen spectrum in the entire Mongolian Plateau (Gunin, 1999; Ma et al., 2008) and this index is thus also questionable (Wang et al., 2011). Here, we design another index (A/(E+N)) for capturing the Holocene humidity variations in the Qigai Nuur area (where A is *Artemisia* pollen percentage, E is *Ephedra* pollen percentage, N is *Nitraria* pollen percentage). It is well documented that the abundance of *Ephedra* and *Nitraria* increases with increasing aridity in arid environments (Li et al., 2005; Sun et al., 1994; Xu et al., 2009; Zhao et al., 2008). In contrast, the abundance of *Artemisia* increases with increasing humidity in arid environments (Ma et al., 2008; Wang et al., 2011; Wen et al., 2010a, 2010b). Therefore, a pollen percentage ratio of *Artemisia* (A) to the combined *Ephedra* and *Nitraria* (E+N) is used here as a humidity index. Furthermore, we also design another index (Br/Co) for capturing the Holocene temperature variations in the Qigai Nuur area (Br is broadleaved tree pollen percentage, Co is coniferous tree pollen percentage). The rationale for designing this index is based on global plant function types in general (Prentice et al., 1996) and on the Mongolian Plateau's plant geography in particular (Demske et al., 2005; Ma et al., 2008; Tarasov et al., 2007; Xu et al., 2010). That is, coniferous trees grow in cool environments, while broadleaved trees in warm environments.

Quantitative climatic reconstructions using fossil pollen data

Three different pollen-based methods have been adopted to quantitatively reconstruct the Holocene temperature and precipitation along the East Asian summer monsoonal margin: (1) pollen response surface (PRS) at Lake Daihai (Xu et al., 2003); (2) transfer function (TF) at Lake Hulun (Wen et al., 2010b), and (3) Plant functional type – modern analogue technique (PFT–MAT) at Lake Bayanchagan (Jiang et al., 2006, 2009). PRS method was developed on the basis of 215 surface pollen spectra from northern China (Sun et al., 1996) and TF method was developed on the basis of 646 surface pollen spectra across a S–N transect from northern China to northern Mongolia (Wen et al., 2010b). PFT-based quantitative reconstruction searches for the affinity between the fossil pollen assemblage considered and the modern pollen data set compared (Prentice et al., 1992, 1996; Tarasov et al., 2000) and the modern pollen data set used by Jiang et al. (2006, 2009) includes 211 surface pollen spectra from northern China (Members of China Quaternary Pollen Data Base, 2001) and 1855 surface pollen spectra from the former Soviet Union and Europe (Guiot et al., 1993; Tarasov et al., 1998). We applied the aforementioned three methods to the modern pollen spectra (i.e. the surface pollen data) of Qigai Nuur core to test their adaptability to the pollen data of Qigai Nuur core. The results show that the PFT–MAT method performs the best, the difference between the reconstructed MAP and the recorded MAP being only ~20 mm and the difference between the reconstructed MAT and the recorded MAT being only ~1°C (Table 2). Therefore, the PFT–MAT method is adopted in this study to reconstruct the Holocene climate in the Qigai Nuur area.

Based on broad classes of plants defined by life form, leaf form, phenology and climatic thresholds, pollen taxa were assigned into the plant functional type (PFT) (Prentice et al., 1996). The PFT assignments of each pollen taxon were carried out mainly using the PFT classification scheme of Jiang et al. (2006). PFT scores are defined as the sums of the square root of the pollen percentage values above 0.5% (Prentice et al., 1996). After each pollen taxon within each sample had been given a PFT assignment, we reconstructed the changes in vegetation, based on the affinity scores for biome types. In this study, we are restricted to 50 taxa that are represented in the modern pollen data base.

Table 2. Comparison of the reconstructed MAP and MAT using three different pollen-based methods (note: MAT is ~7°C and MAP is ~300 mm at nearby Wushen County Meteorological Station, only 20 km from Qigai Nuur).

	MAP (mm)			MAT (°C)		
	PRS	TF	PFT–MAT	PRS	TF	PFT–MAT
Surface pollen-based reconstruction	250	171	279	9.32	5.28	7.95
Difference between reconstructed values and instrumental climate data	−50	−130	−21	+2.32	−1.72	+0.95

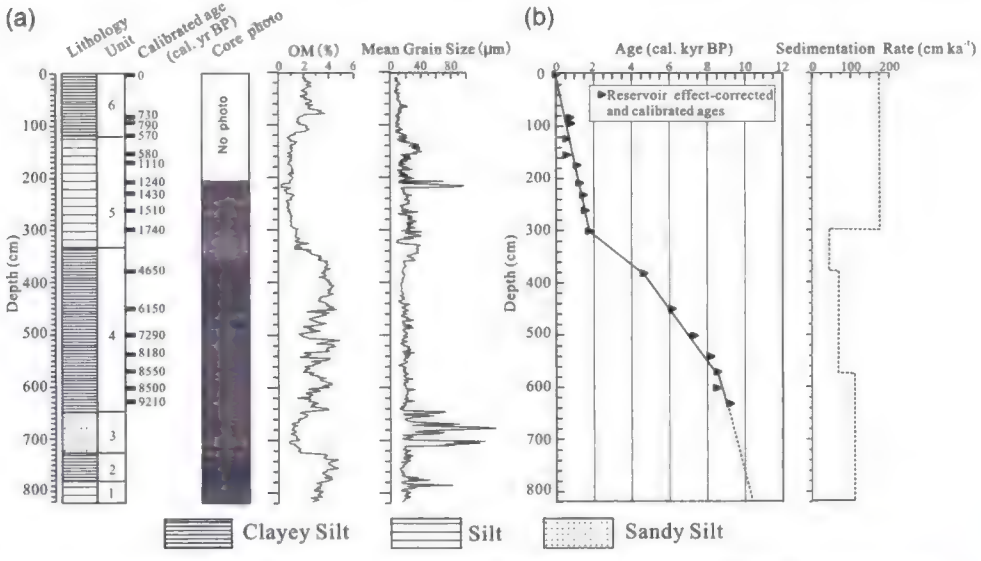

Figure 2. Lithology, core photo, OM (%), mean grain size (μm), age–depth model, and estimated sedimentation rate of Qigai Nuur core.

The PFT-MAT method calculates a chord distance between the pollen taxa considered and the modern analogues compared to determine the dissimilarity between the fossil and modern pollen spectra (Davis et al., 2003; Nakagawa et al., 2002). For each fossil spectrum, we selected eight modern analogues with the smallest chord distance that represents the 'best modern analogues'. The mean climate parameters of each fossil pollen assemblage are then calculated using the method described by Guiot et al. (1993) and Magny et al. (2001). All calculations were carried out using the PPPBASE software package (Guiot and Goeury, 1996). The climate data of a specific surface pollen sample site are obtained by a weighted average of observed data from its adjacent weather stations within an area of 5°×5° (Guiot and Goeury, 1996).

Results

Chronology

The 8.2 m lacustrine sediments core covers the last 10,700 years (Figure 2b). The estimated depositional rates for the four core segments are: ~175 cm/kyr between 0 cm and 302 cm, ~35 cm/kyr between 302 cm and 382 cm, ~50 cm/kyr between 382 cm and 572 cm, and ~90 cm/kyr between 572 cm and 820 cm (Figure 2b). Again, it should be particularly noted that the ages between 632 cm and 820 cm were extrapolated based on the linear relationship between the three dates and the corresponding depths between 570 and 632 cm (Figure 2b). This age extrapolation for the depths between 632 cm and 820 cm is admittedly not statistically robust, but the considerably coarser strata between 630 and 820 cm are reasonably collaborated by the steeper line of the age–depth model.

Sediment lithology and composition

The core can be stratigraphically divided into six units primarily according to the mean grain size and the organic matter content (OM) (Figure 2a). Sediment Unit 1 (820–780 cm) is a brown-gray silt layer with the mean grain size of ~15 μm and the average organic matter content (OM) of ~3%. Sediment Unit 2 (780–720 cm) is a dark-colored clayey silt layer with the mean grain size of ~10 μm. This layer is also distinctively characterized by an elevated OM content (up to ~4%). Sediment Unit 3 (720–650 cm) is a light-colored sandy silt layer with the mean grain size of ~60 μm. Considerably lowered OM content (down to ~1%) and variably coarse grain size (from ~20 to 80 μm) are unique features of this unit. Sediment Unit 4 (650–340 cm) is a laminated and dark-colored clayey silt layer. The lamination is marked by relatively dramatic variations in OM contents, ranging from ~1% to ~5%. Sediment Unit 5 (340–120 cm) is a brown-gray clayey silt layer with mean grain size of ~20 μm and the mean OM content of ~1%. Sediment Unit 6 (120–0 cm) is a brown-gray clayey silt layer with the mean grain size of ~15 μm and the mean OM content of ~2%.

Fossil pollen data

In total, 56 different types of terrestrial fossil pollen were identified from all samples analyzed in this study and they include 16

tree taxa and 40 herbaceous and shrubs taxa. In addition, *Pediastrum* also was identified. The core can be palynologically divided into six pollen assemblage zones based on percentages of the major pollen taxa using the constrained incremental sum of squares (CONISS) method and the six pollen zones are reasonably corresponding with the aforementioned sediment units with more sub-units within the pollen zones 4, 5 and 6 (Figure 3).

Pollen Zone 1 (820–780 cm; ~10,700–10,300 cal. yr BP) corresponds with Sediment Unit 1 and the pollen assemblage is dominated by herbs, mainly including Chenopodiaceae (30–50%), *Artemisia* (7–20%) and *Ephedra* (5–12%). The coniferous tree component including *Pinus* (10–30%), Cupressaceae (1–6%) and *Picea* (1–5%) contributes to ~20% of the total pollen sum. The percentage of broadleaved tree pollen and the pollen concentration are quite low.

Pollen Zone 2 (780–720 cm; ~10,300–9800 cal. yr BP) corresponds with Sediment Unit 2. The assemblage is marked by an increase in broadleaved tree pollen (up to 20%) at the expense of herb pollen. The broadleaved trees are *Quercus* (5–10%), *Betula* (0.3–1.6%), *Alnus* (0–1%), *Ulmus* (0–2%) and *Juglans* (0–1.3%), and *Quercus* is the major contributor to the increase of broadleaved tree pollen. It is also notable that the percentages of 'wet' terrestrial herbs (i.e. Cyperaceae and Ranunculaceae) and aquatic *Typha* and the concentrations of *Pediastrum* increased significantly compared with the underlying Pollen Zone 1.

Pollen Zone 3 (720–650 cm; ~9800–~9200 cal. yr BP), corresponding with Sediment Unit 3, is distinctively characterized by dramatic increases in drought-tolerant shrubs (*Ephedra, Nitraria* and *Aster*-type) and also by dramatic decreases in pollen concentration and in percentages of Cyperaceae and *Quercus* pollen.

Pollen Zone 4 (650–330 cm: ~9200–~2800 cal. yr BP), corresponding with Sediment Unit 4, is uniquely typified by a variably high pollen concentration and by a relatively high percentage of broadleaved tree pollen (e.g. *Quercus, Betula* and *Ulmus*). The pollen percentages of some herb and shrub pollen (e.g. *Artemisia*, Cyperaceae, Chenopodiaceae, Rosaceae, *Corylus* and *Tamarix*) are also higher than the underling Pollen Zone 3. Pollen Zone 4 can be divided into three subzones (i.e. 4-1, 4-2 and 4-3).

Subzone 4-1 (650–580 cm; ~9200–~8500 cal. yr BP) is marked by increases in herb and in broadleaved pollen at the expense of the coniferous tree pollen. The increase in broadleaved tree pollen is primarily attributable to the increases in *Quercus* (up to 6%) and *Ulmus* (7%). It is also noticeable that mesophytic-types (e.g. *Artemisia*, Rosaceae and *Hippophae*) increase, while xero-types (e.g. *Ephedra* and *Nitraria*) decrease in this subzone.

Subzone 4-2 (580–430 cm; ~8500–~5800 cal. yr BP) is characterized by an upward-decreasing trend of herbs (especially *Artemisia*) and also by an upward-increasing trend of coniferous tree (especially *Pinus*). The most remarkable feature of this subzone is considerable increases in Chenopodiaceae and *Ephedra* pollen percentages. Subzone 4-3 (430–330 cm; ~5800–~2800 cal. yr BP) is quite distinguishable from the underlying subzone 4-2 in four aspects: (1) a higher pollen concentration, (2) a dramatic increase in *Quercus* pollen, (3) a considerable increase in Ranunculaceae pollen, and (4) a dramatic increase in the *Pediastrum* concentration.

Pollen Zone 5 (330–140 cm; ~2800–~850 cal. yr BP) approximately corresponds with Sediment Unit 5 (340–120 cm). The pollen assemblage is marked by high coniferous tree pollen (40–95%) at the expense of some herbs (especially Chenopodiaceae and *Artemisia*) and broadleaved trees (especially *Quercus*) with a drastically lowered pollen concentration. Another noticeable feature is drastically lowered percentages of wet-indicative species including Cyperaceae and *Typha*, and lowered concentration of *Pediastrum*. This zone can be further divided into two subzones (i.e. 5-1 and 5-2).

Subzone 5-1 (330–220 cm: ~2800–~1300 cal. yr BP) has the highest coniferous tree pollen and the lowest Chenopodiaceae and *Artemisia* pollen percentages of the entire core. It should be reiterated that coniferous tree pollen (especially *Pinus*) dominated this interval (~2800–~1300 cal. yr BP). Subzone 5-2 (220–140 cm; ~1300–~850 cal. yr BP) has increased herbs and decreased coniferous trees. The increase of herbs in subzone 5-2 is mainly contributed by increases in Poaceae (5–17%), Cyperaceae (3–15%), Chenopodiaceae (10–50%) and *Taraxacum*-type (5–18%).

Pollen Zone 6 (140–0 cm; ~850–~0 cal. yr BP) approximately corresponds with Sediment Unit 6 (120–0 cm) and is dominated by herbs. This zone can be divided into two subzones (i.e. 6-1 and 6-2).

Subzone 6-1 (140–80 cm; ~850–~450 cal. yr BP) is distinguished by high percentages of Chenopodiaceae and Cyperaceae pollen and also by a low pollen concentration.

Subzone 6-2 (80–0 cm; ~450–~0 cal. yr BP) is typified by a high percentage of *Artemisia* pollen (up to 70%) and also by a relatively high percentage of Cupressaceae (up to 12%) with a significantly elevated pollen concentration.

Quantitative climatic reconstructions

Our PFT–MAT-based reconstructions of the mean annual temperature (MAT) and the mean annual precipitation (MAP) show that the regional climate experienced three different phases from ~10,700 to ~9200 cal. yr BP, that is, cold and dry (i.e. Pollen Zone 1 in Figure 4), warm and wet (i.e. Pollen Zone 2), and cold and dry (i.e. Pollen Zone 3). The climate in the Qigai Nuur area was a generally warm and wet from ~9200 to ~2800 cal. yr BP (i.e. Pollen Zone 4) with obvious fluctuations in the reconstructed MAP. From ~2800 to ~1400 cal. yr BP the regional climate was considerably cooling and slightly drying and the past ~1400 years was characterized by rising MAT and fluctuating MAP.

From ~9200 to ~2800 cal. yr BP, after a brief mild and relatively humid interval between ~9200 and ~8500 cal. yr BP, the first pronounced warm and wet period persisted from ~8500 to ~7400 cal. yr BP and this warm and wet climate was succeeded by a rather pronounced cool and dry interval lasting from ~7400 to ~6000 cal. yr BP. The following period from ~6000 to ~2800 cal. yr BP was characterized by three distinctive features: (1) a generally warm and wet early period (i.e. from ~6000 to ~4000 cal. yr BP), (2) a generally cool and dry late period (i.e. from ~4000 to ~2800 cal. yr BP), and (3) declining trends of both MAT and MAP from ~6000 to ~2800 cal. yr BP.

Our PFT–MAT-based reconstructions of MAT and MAP are relatively well corroborated by other proxy data from the core. For example, the organic matter content (i.e. OM content in Figure 4) nearly parallels the reconstructed MAP curve. The pollen concentration appears to reflect the first-order variations in MAP. That is, the major climatic stages corresponding with pollen zones are reasonably replicated by the pollen concentration. Our temperature index, Br/Co (where Br is broadleaved tree pollen percentage, Co is coniferous tree pollen percentage), seems to have captured the first-order variations in MAT and our humidity index, A/(E+N) (where A is *Artemisia* pollen percentage, E is *Ephedra* pollen percentage, N is *Nitraria* pollen percentage), seems to have captured the first-order variations in MAP. In other words, the major variations of MAT are reasonably replicated by the Br/Co ratio and the major variations of MAP are reasonably replicated by the A/(E+N) ratio.

To sum up, the Qigai Nuur area experienced three major cool and dry stages corresponding with Pollen Zones 1, 3 and 5 and two major warm and wet stages corresponding with Pollen Zones 2 and 4 during the Holocene. The final stage (i.e. Pollen Zone 6; past ~850 years) has been characterized by rising MAT and fluctuating MAP. The generally warm and wet climate from ~9200 to

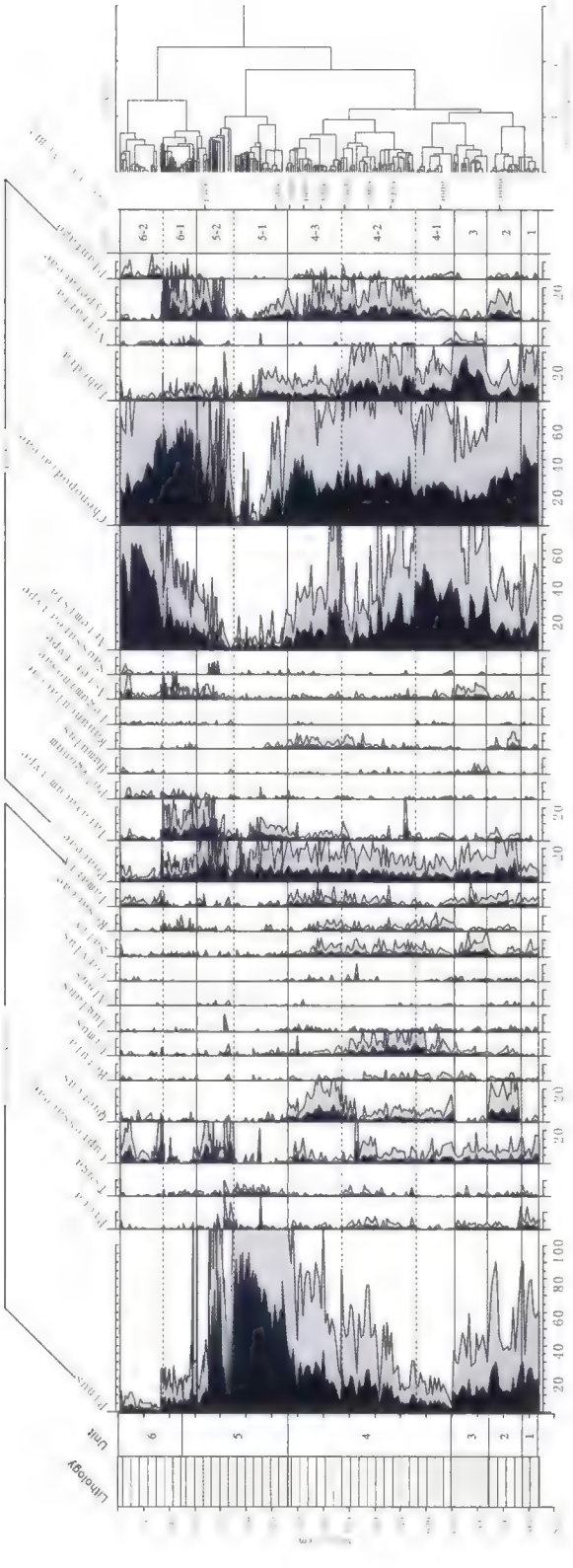

Figure 3. Pollen spectra and taxa percentages of Qigai Nuur core.

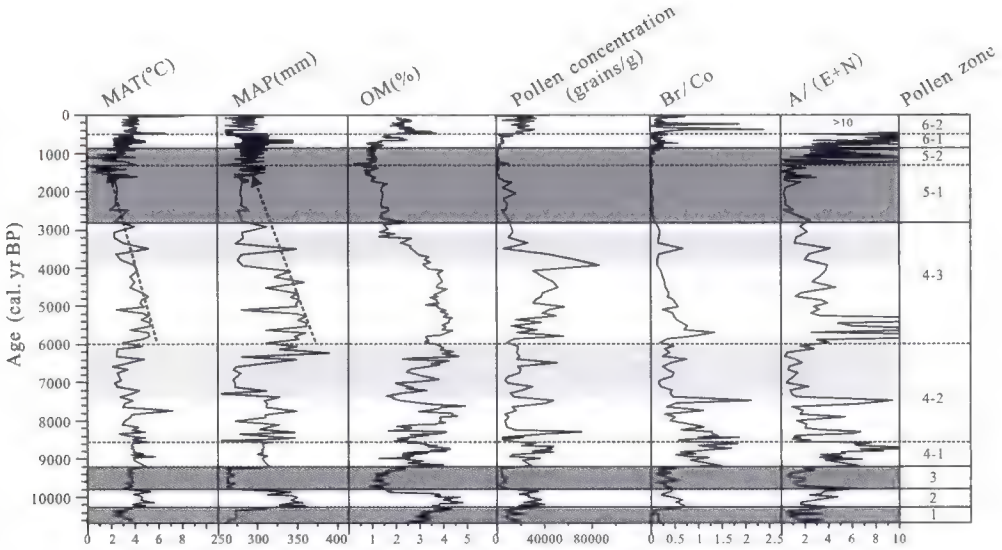

Figure 4. Comparison of reconstructed mean annual temperature (MAT) and mean annual precipitation (MAP) with other proxy data including OM (%) and pollen concentration (grains/g). Two pollen ratios are also presented for comparison and they are Br/Co (where Br is broadleaved tree pollen percentage, Co is Coniferous tree pollen percentage) and (E+N)/A (where E is *Ephedra* pollen percentage, N is *Nitraria* pollen percentage, A is *Artemisia* pollen percentage). The dark-shaded strips mark the Holocene cool and dry stages (i.e. Pollen Zones 1, 3 and 5) and the light-shaded strips mark the mid-Holocene cool and dry epochs. The dashed lines mark the trends of MAT and MAP changes.

~2800 cal. yr BP (i.e. Pollen Zone 4) was interrupted twice by cool and dry epochs, the first occurring from ~7400 to ~6000 cal. yr BP and the second occurring from ~4000 to ~3000 cal. yr BP. Two more observations can be made from Figure 4. First, the reconstructed MAT and MAP have changed more or less synchronously throughout the entire Holocene. Second, both of the reconstructed MAT and MAP exhibit declining trends from ~6000 to ~1400 cal. yr BP.

Discussion

Vegetation and climate changes in the Qigai Nuur area

Our data show that both lake sedimentation and regional vegetation of the Qigai Nuur area experienced pronounced shifts from ~10,700 to ~9200 cal. yr BP. Specifically, the lake first received silt deposits under a Chenopodiaceae-dominated regional vegetation condition (probably a steppe) between ~10,700 and ~10,300 cal. yr BP (i.e. Pollen Zone 1) and then clayey silt deposits under a greatly ameliorated regional vegetation condition (likely a steppe-forest) between ~10,300 and ~9800 cal. yr BP (i.e. Pollen Zone 2). A sandy silt layer was deposited in the lake between ~9800 and ~9200 cal. yr BP (i.e. Pollen Zone 3) when drought-tolerant shrubs (*Ephedra* and *Nitraria*) dominated the regional vegetation (probably a dry steppe or even a desert).

The lake level from ~9200 to ~2800 cal. yr BP (i.e. Pollen Zone 4) was generally high as indicated by uniformly fine clayey silt deposits, and the vegetation was dominated by relatively densely covered steppe-forests as suggested by high pollen concentrations and high percentage of broadleaved tree pollen. However, the vegetation types and coverage had also changed during this warm and wet period (Figure 3). Specifically, the vegetation probably started with a woodland landscape with scattered *Quercus* under a mild and relatively humid climate from ~9200 to ~8500 cal. yr BP (i.e. Pollen Subzone 4-1). The subsequent landscape was probably a *Ulmus*-marked woodland under a generally warm and wet climate from ~8500 to ~6000 cal. yr BP (i.e. Pollen Subzone 4-2) and the vegetation in the later part of this interval (i.e. from ~7400 to ~6000 cal. yr BP) was deteriorated probably to a steppe under a cool and dry condition. The vegetation between ~6000 and ~2800 cal. yr BP (i.e. Pollen Subzone 4-3) was characterized by increases in the percentages of *Quercus* and Ranunculaceae pollen and also in *Pediastrum* concentration and also by high pollen concentrations, suggesting that the climate was relatively warm and rather wet. It is also notable that the vegetation in the later part of this interval (i.e. from ~4000 to ~2800 cal. yr BP) was deteriorated probably to a steppe under a cool and dry condition. It should be noted that this cool and dry climate started at ~4000 cal. yr BP in Qigai Nuur area may well correspond with the widely reported '4000 cal. yr BP Event' by Perry and Hsu (2000) or the 'Holocene Event 3' by Bond et al. (2001) or '4.2 ka Event' by others that was reported to have played an important role in the collapse of Neolithic cultures in northern China (Liu and Feng, 2012; Wu and Liu, 2004).

The period from ~2800 to ~850 cal. yr BP (i.e. Pollen Zone 5) is marked by high *Pinus* pollen percentage (40–95%) at the expense of broadleaved trees and some herbs with low pollen concentration. *Pinus*, the dominated pollen taxon in Pollen Zone 5, was widely reported to be by far over-represented in surface pollen spectrum (Li, 1998; Ma et al., 2004), thereby causing difficulty in its climatic interpretation. More specifically, in northern China and in Mongolia *Pinus* pollen percentage of surface samples can reach up to 55% with an average of 30% in the areas where no *Pinus* forest exists at all (Ma et al., 2004, 2008). We have investigated the over-representation issues of *Pinus* in the Qigai Nuur area where no *Pinus* forest exist. Our data from 30 surface samples show that *Pinus* pollen can reach up to 70% with an average of 35% (AZ Sun, unpublished data, 2004) and the *Pinus* pollen grains are basically airborne from the mountains that are ~200 km away from the lake (e.g. Daqing Mountains to the north, Helan Mountains to the west, and Luliang Mountains to the east; see Figure 1). It implies that

Pinus-dominated coniferous forests in those mountains might have expanded considerably during the period from ~2800 to ~850 cal. yr BP under a significantly cooler climate and the *Pinus* pollen gains were then transported to the Qigai Nuur area. At the same time (i.e. from ~2800 to ~850 cal. yr BP), the Qigai Nuur area was poorly vegetated under a dry climate, as indicated by low pollen concentration and also by very low percentages of broadleaved trees and herbs. The pollen assemblages of late stage of the late Holocene (i.e. Pollen Zone 5; past ~850 years) were characterized by high percentages of Poaceae, *Taraxacum*-type, Cyperaceae and Chenopodiaceae pollen in the lower portion (i.e. Pollen Subzone 6-1; ~850–~450 cal. yr BP) and by high percentages of *Artemisia, Plantago* and Cupressaceae in the upper portion (i.e. Pollen Subzone 6-2; ~450–~0 cal. yr BP). The reconstructed MAT has a slight rising trend throughout Pollen Zone 6 (Figure 4) and the reconstructed MAP was slightly higher in the lower portion (i.e. ~850–~450 cal. yr BP) than in the upper portion (i.e. ~450–~0 cal. yr BP).

Comparison with regional palaeoclimate records

Shi et al. (1993) reported that the Holocene Megathermal (i.e. maximum temperature) Period occurred from ~9500 to ~3300 cal. yr BP in China and its climax (i.e. warmest period) was inferred to have occurred from ~8000 to ~6850 cal. yr BP. An et al (2000) reported the onset of the Megathermal Period was variously placed at 10,000–7500 ^{14}C yr BP and its end at 5000–2000 ^{14}C yr BP. Later, Feng et al. (2004) argued that the Holocene Megathermal Period was actually expressed as the Holocene Megahumid Period (i.e. maximum precipitation) in northern China and it spanned from ~10,000 to ~4000 cal. yr BP, with its climax (i.e. the wettest period) occurring from ~8400 to ~6000 cal. yr BP. The Holocene Megathermal Period or/and the Holocene Megahumid Period was later translated into the Holocene Maximum Strength Period of the East Asian Summer Monsoon (Herzschuh, 2006; Zhao et al., 2009b). The maximum strength period was inferred to have lasted from ~10,000 to ~3500 cal. yr BP by Herzschuh (2006), from ~11,000 to ~4000 cal. yr BP by Zhao et al. (2009b), and from ~7000 to ~4500 cal. yr BP by Wang et al., (2010).

Here, our attention will be directed to the timings of the Holocene Megahumid Period (i.e. maximum precipitation) along the summer monsoon margin in northern China by focusing on recently published pollen-based quantitative reconstructions (Figure 5). The Holocene Megahumid Period seems to be bracketed by ~6000 and ~4000 cal. yr BP with a secondary 'Megahumid' interval lasting from ~9200 to ~7400 cal. yr BP at Qigai Nuur (site 1 in Figure 1). At Lake Daihai (site 2 in Figure 1) to the northeast of Qigai Nuur, the quantitative reconstruction by Xu et al. (2010) was achieved by applying a transfer function to the data of 277 fossil pollen samples. The reconstruction shows that the Holocene Megahumid Period lasted from ~7500 to ~3500 cal. yr BP. At Lake Bayanchagan (site 3 in Figure 1) to the northeast of Lake Daihai, the quantitative reconstruction by Jiang et al. (2009) was achieved by PFT–MAT (i.e. PFT Modern Analogue Technique) to the data of 90 fossil pollen samples. The reconstructed MAT maximum (i.e. the Holocene Megathermal Period) occurred between ~10,500 and ~8000 cal. yr BP and the reconstructed MAP maximum (i.e. the Holocene Megahumid Period) occurred between ~10,500 and ~5500 cal. yr BP. At Lake Hulun (site 4 in Figure 1) to the northeast of Lake Bayanchagan, the quantitative reconstruction was achieved through applying their own transfer functions (Wen et al., 2010b) to the data of 170 fossil pollen samples. The Holocene Megahumid Period at Lake Hulun is bracketed by ~7500 and ~5000 cal. yr BP with a secondary 'Megahumid' interval lasting from ~3400 to ~1500 cal. yr BP.

Apparently, these four quantitative reconstructions failed to reach an agreement either on the compatibility between MAT and MAP (i.e. first group of controversies) or on the timing of the Holocene Megahumid Period (i.e. second group of controversies) or on the competitive relationship between precipitation and evaporation (i.e. third group of controversies). These large discrepancies or inconsistencies may be a result of chronology-related issues (e.g. dating targets, number of dates, methods for age–depth models, etc.) or/and methodology-related issues (e.g. three different methods used). Or, they may be 'real' expressions in different regions. But, our reconstruction is generally consistent with those widely accepted reconstructions of the East Asian summer monsoon strength from cave (e.g. Sanbo Cave in Figure 1a) stalagmites (e.g. Dong et al., 2010; Hu et al., 2008) and peat sequences (e.g. Hongyuan peat in Figure 1a) (Hong et al., 2003) in southern China. The consistency and the observed modern linkage between the monsoon strength in southern China and the climate in the monsoonal margin (Liu et al., 2008; Wang et al., 1981; Zhang and Li, 1994) are somewhat boosting our confidence on our reconstruction. In addition, the reconstructed MAP at the Qigai Nuur bears a great resemblance to the reconstructed sea surface temperature (SST) in the Western Tropical Pacific Ocean (see Stott et al., 2004) and the resemblance offers a reasonable explanation for the reconstructed MAP at Qigai Nuur (see section 'Underlying mechanisms'). That is, our reconstruction from Qigai Nuur demonstrates that: (1) MAT and MAP have changed more or less synchronously, (2) the Holocene Megahumid Period occurred during the early and middle Holocene, that is, the wettest period occurred between ~6000 and ~4000 cal. yr BP and the secondary 'Megahumid' interval lasting from ~9200 to ~7400 cal. yr BP, and (3) strengthened monsoon under higher temperature may have brought more precipitation to the monsoonal margin, thus resulting in wetter climates. Of course, the discrepancies demand further studies.

Underlying mechanisms

Summer insolation in the Northern Hemisphere, as a major driver of the global temperature change, started to increase at ~20,000 cal. yr BP, reached a maximum at ~10,000 cal. yr BP and has been gradually declining since ~10,000 cal. yr BP (Figure 6; Kutzbach and Gallimore, 1988). The summer insolation trend has been closely followed by the reconstructed trend of the East Asian summer monsoon strength retrieved from Sanbao Cave in Hubei Province of southern China (Figure 6) and the causal linkage between the summer insolation and the East Asian monsoon strength have been extensively and intensively explored (see An et al., 2000; Feng et al., 2006; Koutavas et al., 2002; Kutzbach and Gallimore, 1988; Kutzbach and Liu, 1997; Shi et al., 1993). The reconstructed MAT at Qigai Nuur situated at the East Asian summer monsoonal margin should have been controlled or modulated by the East Asian summer monsoon strength during the Holocene and it is thus not surprising to see the similar trends between the MAT at Qigai Nuur and the monsoon strength at Sanbo Cave. The well-expressed broad similarities imply that the first-order Holocene variations in MAP of Qigai Nuur area should have been responding to the summer insolation with some time lags resulting from the 'oceanic buffering effect'. The oceanic buffering effect means that low-latitude oceans were gradually and sufficiently warmed from the peak insolation period (~10,000–~9000 cal. yr BP) to the Holocene Climatic Optimum (approximately from 9000 to 6000 cal. yr BP) so that the enhanced evaporation effectively injected more water vapor into the East Asian Monsoon system (see Feng et al., 2006). The first-order variations in reconstructed MAP were most likely resulted from the summer insolation-dictated Inter-Tropical Convergence Zone (ITCZ) positioning. That is, northward shift (i.e. wetting) or southward shift (i.e. drying) determined

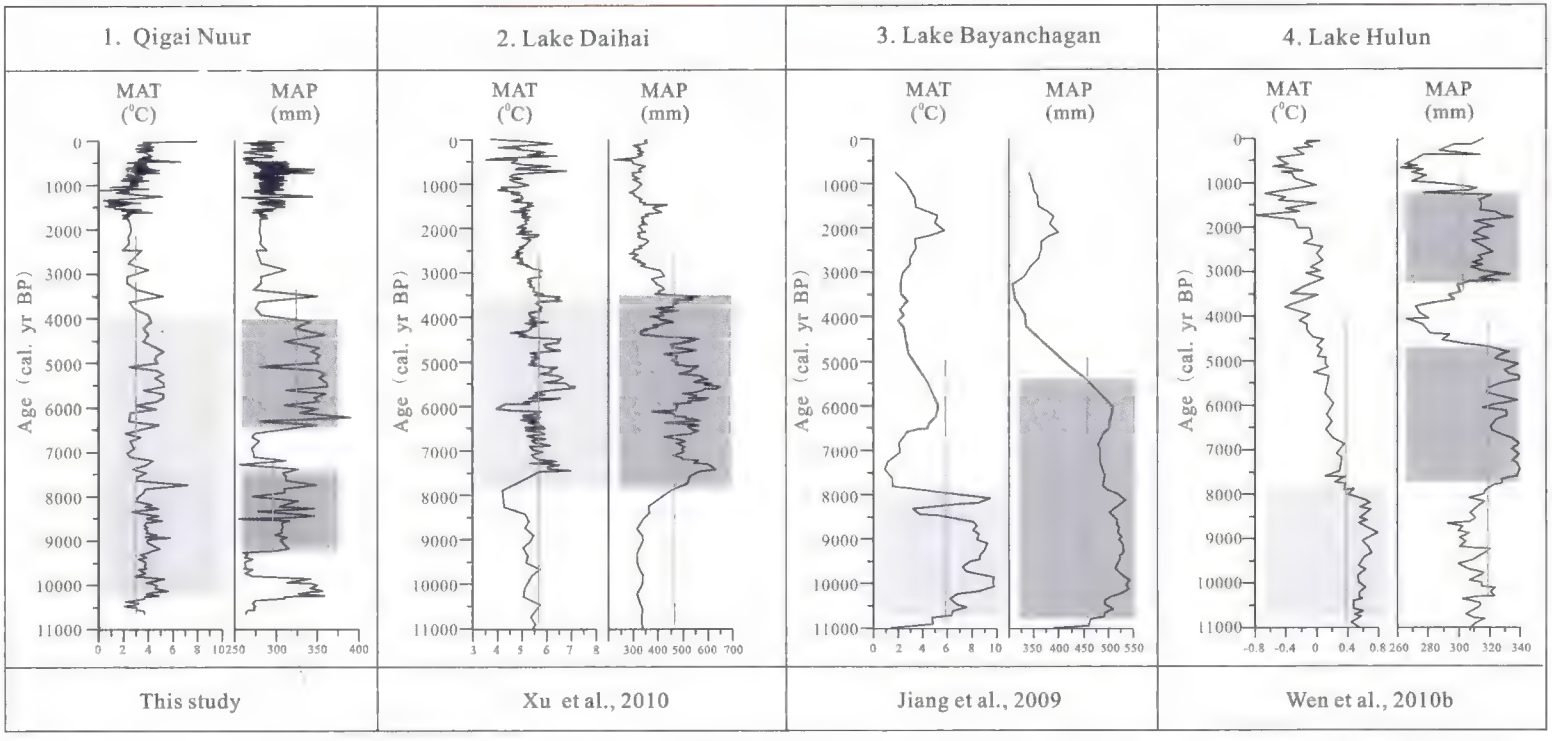

Figure 5. Comparison of the reconstructed MAT and MAP variations from Qigai Nuur core with those from Lake Daihai, Lake Bayanchagan and Lake Hulun. The light-shaded areas mark the time intervals of the Holocene Megathermal Period (i.e. high temperature). The dark-shaded areas indicate the time intervals of the Holocene Megahumid Period (i.e. high precipitation). The gray lines indicate the mean values of different stages.

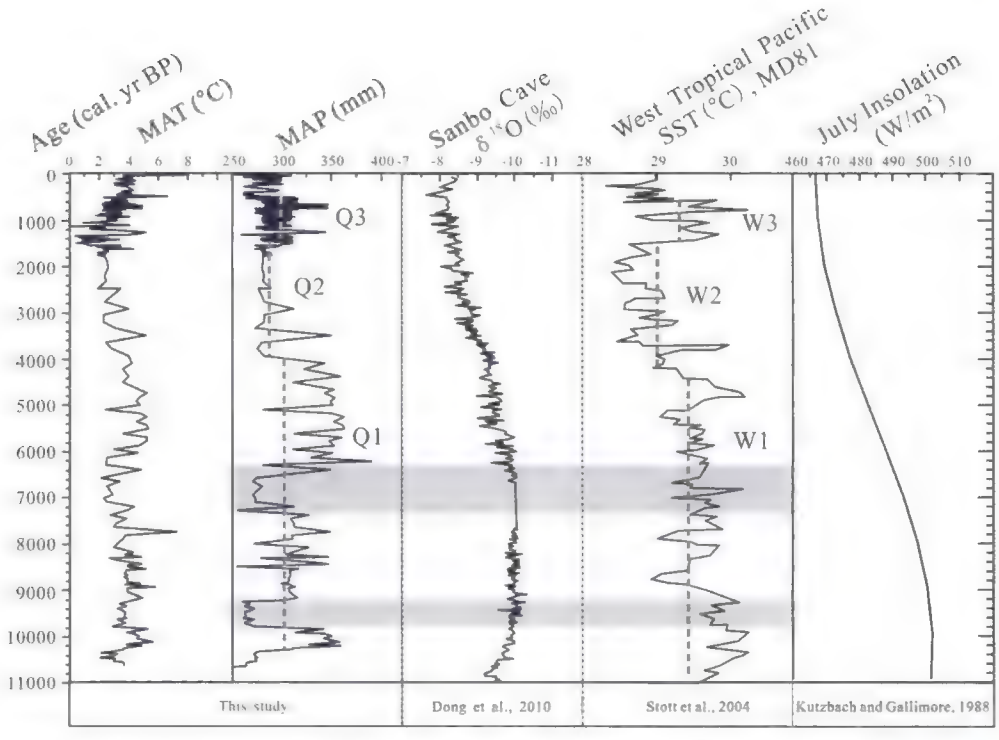

Figure 6. Comparison of the reconstructed MAT and MAP variations from Qigai Nuur with $\delta^{18}O$ of Sanbo Cave stalagmite, sea surface temperature (SST) of the Western Tropical Pacific Ocean (site MD81, 5°N, 127°E), and July insolation at 25°N. The dashed lines show the mean values of different stages. The light-shaded areas mark the time intervals of two major dry intervals during the early and middle Holocene.

the general strength of the East Asian monsoon (An et al., 2000; Chiang and Kushnir, 2000). However, more detailed or second-order variations in the reconstructed MAP at Qigai Nuur resemble those in the reconstructed sea surface temperature (SST) in the Western Tropical Pacific Ocean (site MD81, 5°N, 127°E, see Figure 1a) and the resemblance implies that the MAP variations in Qigai Nuur area might have been tightly modulated by the SST in the Western Tropical Pacific during the Holocene (Stott et al., 2004). Specifically, the Q1-labeled segment in the reconstructed MAP at Qigai Nuur covering the period from ~10,300 to ~4000 cal. yr BP corresponds with W1-labeled segment in the reconstructed Western Tropical Pacific SST from ~11,000 to ~4400 cal. yr BP with some time lags; the Q2-labeled segment of MAP with W2-labeled segment of SST; and the Q3-labeled segment of MAP with W3-labeled segment of SST. That is, higher MAP in the East Asian monsoonal margin has most likely resulted from higher SST in the Western Tropical Pacific. The causal linkage between the MAP and the SST might have been established via the SST influence on the East Asian summer monsoon strength and the variations in the SST in the Western Tropical Pacific was most likely modulated by the El Niño-Southern Oscillation (ENSO) dynamics (Higginson et al., 2004; Ju and Slingo, 2006). That is, more frequent ENSO activities brought more warm water to the Eastern Tropical Pacific (i.e. American side) and thus resulted in lower SST in the Western Tropical Pacific, leading to less water vapor transported to the East Asian monsoon margin where Qigai Nuur is situated.

Finally, we are encountering difficulties in explaining two major dramatically dry intervals that are well defined by pollen data and other proxy data (e.g. organic matter content and grain size). The first such interval occurred between ~9800 and ~9200 cal. yr BP and the second one occurred between ~7400 and ~6000 cal. yr BP. These two dry intervals chronologically correspond with relatively high SST intervals in the Western Tropical Pacific (Figure 6). Admittedly, we are not yet able to offer a reasonable explanation for these two 'oddly' dry events.

Conclusions

Fossil pollen data at Qigai Nuur in the southern Mongolian Plateau show that regional vegetation changed dramatically between steppe forest and dry steppe during the period from ~10,700 to 9200 cal. yr BP. The vegetation was then dominated by steppe-forest from ~9200 to ~2800 cal. yr BP and then deteriorated to dry steppe vegetation between ~2800 and ~850 cal. yr BP. During the past ~850 years, the vegetation was characterized by high percentages of various herbs. PFT–MAT quantitative reconstruction revealed that the climate changed in three steps before ~9200 cal. yr BP: (1) cold and dry from ~10,700 to ~10,300 cal. yr BP, (2) considerably warm and significantly wet from ~10,300 to ~9800 cal. yr BP, and (3) slightly cool and dramatically dry between ~9800 and ~9200 cal. yr BP. From ~9200 to ~2800 cal. yr BP, the climate was generally warm and wet with two cold and dry intervals at ~7400–~6000 cal. yr BP and at ~4000–~2800 cal. yr BP. The climate was cooler and slightly drier from ~2800 to ~1400 cal. yr BP and has been characterized by rising temperature and fluctuating precipitation during the last ~1400 years. Our reconstructions demonstrate that: (1) temperature and precipitation have changed more or less synchronously, (2) the Holocene Megathermal Period occurred during the early and middle Holocene, (3) the first-order variations in the reconstructed

MAP were most likely a result of summer insolation-dictated ITCZ positioning (i.e. N–S shifts), and (4) the second-order variation in the reconstructed MAP was most likely modulated by the ENSO dynamics (i.e. E–W shifts).

Finally, we want to add that two indices we defined in this paper appear to work reasonably. The curve of pollen percentage ratio between broadleaved tree and coniferous tree (Br/Co ratio) parallels the general trend of the reconstructed MAT and the curve of pollen percentage ratio of *Artemisia* (A) to the combined *Ephedra* and *Nitraria* (E+N) (A/(E+N)) shows a similar trend with the reconstructed MAP, suggesting that these two pollen indices are useful for estimating MAT and MAP.

Acknowledgements

We are indebted to Professor Yuzhen Ma, Professor Chengjun Zhang, Dr Xinwei Zhai, Dr Huining Wu, Dr Wei Wang, Dr Qili Yang and Ms Yixin Hu for their help during coring in the field and for core slicing (sampling) in the laboratory of Lanzhou University. Thanks also go to Professor ZC Yu and two anonymous reviewers for their valuable comments and suggestions on paper structure and some minor modifications.

Funding

This study was financially supported by several NSFC grants (No. 40930120, No. 41002058, No. 41172332, No. 40331012, No. 40421101) and two US NSF grants (NSF-ESH-04-02509, NSF-BSC-06-52304).

References

An ZS (2000) The history and variability of the East Asian paleomonsoon climate. *Quaternary Science Reviews* 19: 171–187.

An ZS, Porter SC, Kutzbach JE et al. (2000) Asynchronous Holocene optimum of the East Asian monsoon. *Quaternary Science Reviews* 19(8): 743–762.

Bond G, Kromer B, Beer J et al. (2001) Persistent solar influence on north Atlantic climate during the Holocene. *Science* 294: 2130–2136.

Chen FH, Cheng B, Zhao Y et al. (2006) Holocene environmental change inferred from a high-resolution pollen record, Lake Zhuyeze, arid China. *The Holocene* 16: 675–684.

Chiang J and Kushnir Y (2000) Interdecadal changes in eastern Pacific ITCZ variability and its influence on the Atlantic ITCZ. *Geophysical Research Letters* 27: 3687–3690.

Davis BAS, Brewer S, Stevenson AC et al. (2003) The temperature of Europe during the Holocene reconstructed from pollen data. *Quaternary Science Reviews* 22: 1701–1716.

Demske D, Heumann G, Granoszewski W et al. (2005) Late glacial and Holocene vegetation and regional climate variability evidenced in high-resolution pollen records from Lake Baikal. *Global and Planetary Change* 46: 255–279.

Dong J, Wang Y, Cheng H et al. (2010) A high-resolution stalagmite record of the Holocene East Asian monsoon from Mt Shennongjia, central China. *The Holocene* 20(2): 257–264.

El-Moslimany AP (1990) Ecological significance of common non-arboreal pollen: Examples from drylands of the Middle East. *Review of Palaeobotany and Palynology* 64: 343–350.

Erdtman G (1978) *Handbook of Palynology*. (In Chinese) (Translated by the Institute of Botany, the Chinese Academy of Sciences). Beijing: Science Press.

Feng ZD, An CB, Tang LY et al. (2004) Stratigraphic evidence of a Megahumid climate between 10,000 and 4000 years B.P. in the western part of the Chinese Loess Plateau. *Global and Planetary Change* 43(3–4): 145–155.

Feng ZD, An CB and Wang HB (2006) Holocene climatic and environmental changes in the arid and semi-arid areas of China: A review. *The Holocene* 16(1): 119–130.

Fowell SJ, Hansen B, Peck JA et al. (2003) Mid to late Holocene climate evolution of the Lake Telmen Basin, North Central Mongolia, based on palynological data. *Quaternary Research* 59(3): 353–363.

Gao YX (1962) *Some Problems on East Asia Monsoon*. Beijing: Science Press, pp. 49–63 (in Chinese).

Grimm EC (1990) Tilia and Tilia graph PC spreadsheet and graphics software for pollen data. *INQUA, Working Methods, Newsletter* 4: 5–7.

Guiot J, Harrison SP and Prentice TC (1993) Reconstruction of Holocene patterns of moisture in Europe using pollen and lake-level data. *Quaternary Research* 40: 139–149.

Guiot J and Goeury C (1996) PPPBASE, a software for statistical analysis of paleoecological and paleoclimatological data. *Dendrochronologia* 14: 295–300.

Gunin PD (1999) *Vegetation Dynamics of Mongolia*. Copenhagen: Kluwer Academic, 238 pp.

Hartmann K and Wünemann B (2009) Hydrological changes and Holocene climate variations in NW China, inferred from lake sediments of Juyanze palaeolake by factor analyses. *Quaternary International* 194: 28–44.

Herzschuh U (2006) Palaeo-moisture evolution in monsoonal Central Asia during the last 50,000 years. *Quaternary Science Reviews* 25(1–2): 163–178.

Herzschuh U, Tarasov P, Wünemann B et al. (2004) Holocene vegetation and climate of the Alashan Plateau, NW China, reconstructed from pollen data. *Palaeogeography, Palaeoclimatology, Palaeoecology* 211(1–2): 1–17.

Higginson MJ, Altabet MA, Wincze L et al. (2004) A solar (irradiance) trigger for millennial-scale abrupt changes in the southwest monsoon. *Paleoceanography* 19: PA3015, doi:10.1029/2004PA001031.

Hong YT, Hong B, Lin QH et al. (2003) Correlation between Indian Ocean summer monsoon and North Atlantic climate change during the Holocene. *Earth and Planetary Science Letters* 211: 371–380.

Hu CY, Henderson GM, Huang JH et al. (2008) Quantification of Holocene Asian monsoon rainfall from spatially separated cave records. *Earth and Planetary Science Letters* 266: 221–232.

Huang F, Lisa K, Xiong SF et al. (2004) Vegetation, environment and human activity since Holocene in east Inner Mongolia. *Science in China (Series D)* 34(11): 1029–1040.

Intergovernmental Panel on Climate Change (2007) *Climate Change 2007: The Physical Science Basis*. Contribution of Working Group I to the Fourth Assessment Report of the Intergovernmental Panel on Climate Change, Solomon S, Qin D, Manning M et al. (eds). Cambridge: Cambridge University Press.

Jiang WY, Guiot J, Chu GQ et al. (2009) An improved methodology of the modern analogues technique for palaeoclimate reconstruction in arid and semi-arid regions. *Boreas* 39: 145–153.

Jiang WY, Guo ZT, Sun XJ et al. (2006) Reconstruction of climate and vegetation changes of Lake Bayanchagan (Inner Mongolia): Holocene variability of the East Asian monsoon. *Quaternary Research* 65(3): 411–420.

Ju J and Slingo J (2006) The Asian summer monsoon and ENSO. *Quarterly Journal of the Royal Meteorological Society* 121: 1133–1168.

Koutavas A, Lynch-Stieglitz J, Marchitto TW et al. (2002) El Nino-like pattern in ice age Tropical Pacific sea surface temperature. *Science* 297: 226–229.

Kutzbach JE and Gallimore RG (1988) Sensitivity of a coupled atmosphere mixed layer ocean model to changes in orbital forcing at 9000 years BP. *Journal of Geophysical Research* 93: 803–821.

Kutzbach JE and Liu Z (1997) Response of the African monsoon to orbital forcing and ocean feedbacks in the middle Holocene. *Science* 278: 440–443.

Li WY (1998) *Quaternary Vegetation and Environment of China*. Beijing: Science Press (in Chinese).

Li YC, Xu QH, Yang XL et al. (2005) Pollen indication to vegetation in the eastern part of desert China. *Chinese Science Bulletin* 50(13): 1356–1364.

Liu FG and Feng ZD (2012) A dramatic climatic transition at ~4000 cal. yr BP and its cultural responses in Chinese cultural domains. *The Holocene* 22(10): 1181–1197.

Liu JH, Zhang PZ, Cheng H et al. (2008) Asian summer monsoon precipitation recorded by stalagmite oxygen isotopic composition in the western Loess Plateau during AD 1875–2003 and its linkage with ocean–atmosphere system. *Chinese Science Bulletin* 53(13): 2041–2049.

Liu KB, Yao ZJ and Thompson LG (1998) A pollen record of Holocene climatic changes from the Dunde ice cap, Qinghai–Tibetan Plateau. *Geology* 26: 135–138.

Ma YZ, Liu KB, Feng ZD et al. (2008) A survey of modern pollen and vegetation along a south–north transect in Mongolia. *Journal of Biogeography* 35: 1512–1532.

Ma YZ, Zhang HC, Pachur HJ et al. (2004) Modern pollen-based interpretations of mid-Holocene palaeoclimate (8500 to 3000 cal. BP) at the southern margin of the Tengger Desert, northwestern China. *The Holocene* 14(6): 841–850.

Magny M, Guiot J and Schoellammer P (2001) Quantitative reconstruction of Younger Dryas to mid-Holocene paleoclimates at Le Locle, Swiss Jura, using pollen and lake-level data. *Quaternary Research* 56: 170–180.

Members of China Quaternary Pollen Data Base (2001) Simulation of China biome reconstruction based on pollen data from surface sediment samples. *Acta Botanica Sinica* 43: 201–209.

More PD and Webb JA (1987) *Palynology Analytical Manual*. (In Chinese) (Translated by Li WY, Xiao XM, Liu GX). Nanning: Guangxi People's Publishing House.

Moore PD, Web JA and Collinson ME (1991) *Pollen Analysis, 2nd Edition*. Oxford: Blackwell Scientific Publication.

Nakagawa T, Tarasov PE, Nishida K et al. (2002) Quaternary pollen-based climate reconstruction in central Japan: Application to surface and late Quaternary spectra. *Quaternary Science Reviews* 21: 2099–2113.

Perry CA and Hsu KJ (2000) Geophysical, archaeological, and historical evidence support a solar-output model for climate change. *Proceedings of the National Academy of Sciences* 97: 12,433–12,438.

Prentice IC, Cramer W, Harrison SP et al. (1992) A global biome model based on plant physiology and dominance, soil properties and climate. *Journal of Biogeography* 19: 117–134.

Prentice IC, Guiot J, Huntley B et al. (1996) Reconstructing biomes from palaeoecological data: A general method and its application to European pollen data at 0 and 6 ka. *Climate Dynamics* 12: 185–194.

Reimer PJ, Baillie MGL, Bard E et al. (2009) IntCal09 and Marine09 radiocarbon age calibration curves, 0–50,000 years cal BP. *Radiocarbon* 51: 1111–1150.

Shi YF, Kong ZC, Wang SM et al. (1993) Mid-Holocene climates and environments in China. *Global and Planetary Change* 7: 219–233.

Stott L, Cannariato K, Thunell R et al. (2004) Decline of surface temperature and salinity in the western tropical Pacific Ocean in the Holocene epoch. *Nature* 431: 56–59.

Sun XJ, Du NQ, Weng CY et al. (1994) Paleovegetation and paleoenvironment of Manasi Lake, Xinjiang, N.W. China during the last 14,000 years. *Quaternary Sciences* 3: 239–248 (in Chinese with English Abstract).

Sun XJ, Wang BY and Song CQ (1996) Pollen–climate response surfaces of selected taxa from Northern China. *Science in China (Series D)* 26(5): 431–436.

Tarasov P, Bezrukova E, Karabanov E et al. (2007) Vegetation and climate dynamics during the Holocene and Eemian interglacials derived from Lake Baikal pollen records. *Palaeogeography Palaeoclimatology Palaeoecology* 252(3–4): 440–457.

Tarasov PE, Volkova VS, Webb T III et al. (2000) Last glacial maximum biomes reconstructed from pollen and plant macrofossil data from northern Eurasia. *Journal of Biogeography* 27: 609–620.

Tarasov PE, Webb T, III, Andreev AA et al. (1998) Present-day and mid-Holocene biomes reconstructed from pollen and plant macrofossil data from the former Soviet Union and Mongolia. *Journal of Biogeography* 25: 1029–1053.

Van Campo E, Cour P and Sixuan H (1996) Holocene environmental changes in Bangong Co. Basin (western Tibet): Part 2, the pollen record. *Palaeogeography Palaeoclimatology, Palaeoecology* 120: 49–63.

Wang FX, Qian NF, Zhang YL et al (1995) *Pollen Flora of China*. 2nd Edition. Beijing: Science Press (in Chinese).

Wang SW, Zhao ZC and Chen ZH (1981) Reconstruction of the summer regime for the last 500 years in China. *Geojournal* 5: 117–122.

Wang W, Ma YZ, Feng ZD et al. (2011) A prolonged dry mid-Holocene climate revealed by pollen and diatom records from Lake Ugii Nuur in central Mongolia. *Quaternary International* 229(1–2): 74–83.

Wang YB, Liu XQ and Herzschuh U (2010) Asynchronous evolution of the Indian and East Asian Summer Monsoon indicated by Holocene moisture patterns in monsoonal central Asia. *Earth-Science Reviews* 103: 135–153.

Wen RL, Xiao JL, Chang ZG et al. (2010a) Holocene climate changes in the mid–high-latitude-monsoon margin reflected by the pollen record from Hulun Lake, northeastern Inner Mongolia. *Quaternary Research* 73: 293–303.

Wen RL, Xiao JL, Chang ZG et al. (2010b) Holocene precipitation and temperature variations in the East Asian monsoonal margin from pollen data from Hulun Lake in northeastern Inner Mongolia, China. *Boreas* 39: 262–272.

Wu WX and Liu TS (2004) Possible role of the 'Holocene Event 3' on the collapse of Neolithic Cultures around the Central Plain of China. *Quaternary International* 117: 153–166.

Xiao JL, Xu QH, Nakamura T et al. (2004) Holocene vegetation variation in the Daihai Lake region of north-central China: A direct indication of the Asian monsoon climatic history. *Quaternary Science Reviews* 23:1669–1679.

Xu GC (1997) *Arid-Semi Arid Climate Change in China*. Beijing: China Meteorological Press (in Chinese).

Xu QH, Tian F, Li YC et al. (2009) Pollen assemblages of Tauber traps and surface soil samples in steppe area of northern China and their relationship with vegetation and climate. *Journal of Palaeogeography* 11(1): 81–90 (in Chinese with English abstract).

Xu QH, Xiao JL, Li YC et al. (2010) Pollen-based quantitative reconstruction of Holocene climate changes in the Daihai Lake Area, Inner Mongolia, China. *Journal of Climate* 23(11): 2856–2868.

Xu QH, Xiao JL, Toshio N et al. (2003) Quantitative reconstructed climatic changes of Daihai basin by pollen data. *Marine Geology & Quaternary Geology* 23(4): 99–108 (in Chinese with English abstract).

Zhang SQ and Li SQ (1994) The influence of fluctuation of global temperature on precipitation in China. *Quarterly Journal of Applied Meteorology* 5: 333–339 (in Chinese with English abstract).

Zhang XS (2007) *Vegetation Map of the People's Republic of China (1: 100 000)*. Beijing: Geological Publishing House.

Zhao Y, Xu QH, Huang XZ et al. (2009a) Differences of modern pollen assemblages from lake sediments and surface soils in arid and semi-arid China and their significance for pollen-based quantitative climate reconstruction. *Review of Palaeobotany and Palynology* 159: 519–524.

Zhao Y, Yu ZC, Chen FH et al. (2008) Holocene vegetation and climate change from a lake sediment record in the Tengger sandy desert, northwest China. *Journal of Arid Environments* 72: 2054–2064.

Zhao Y, Yu ZC, Chen FH et al. (2009b) Vegetation response to Holocene climate change in monsoon-influenced region of China. *Earth-Science Reviews* 97(1–4): 242–256.

Zhou WJ, Head MJ and Lin D (2001) Climate changes in northern China since the late Pleistocene and its response to global change. *Quaternary International* 83–85: 285–292.

附录十

Contents lists available at SciVerse ScienceDirect

Quaternary International

journal homepage: www.elsevier.com/locate/quaint

Pollen-recorded bioclimatic variations of the last ~22,600 years retrieved from Achit Nuur core in the western Mongolian Plateau

Aizhi Sun [a,*], Zhaodong Feng [b], Min Ran [c], Chengjun Zhang [d]

[a] Key Laboratory of Cenozoic Geology and Environment, Institute of Geology and Geophysics, Chinese Academy of Sciences, Beitucheng Western Road, Chaoyang District, Beijing 100029, China
[b] Xinjiang Institute of Ecology and Geography, Chinese Academy of Sciences, Urumqi 830011, China
[c] MOE Key Laboratory of Oasis Ecology, College of Resources and Environmental Sciences, Xinjiang University, Urumqi 830046, China
[d] College of Resources and Environmental Sciences, Lanzhou University, Lanzhou 730000, China

ARTICLE INFO

Article history:
Available online 23 July 2013

ABSTRACT

This research focuses on the reconstructions of vegetation variations and the associated climate changes over the past ~22,600 years based on pollen data of 91 samples obtained from Achit Nuur in the western part of the Mongolian Plateau. The vegetation in the Achit Nuur area was forests in higher elevations and steppes in lower elevations from ~22,600 to ~13,200 cal BP. The subsequent period from ~13200 to ~6400 cal BP was characterized by steppes in higher elevations and deserts in lower elevations, followed by taiga expansion in high elevations in the following period from ~6400 to ~1600 cal BP. The last ~1600 years were characterized by high herb percentages. Pollen-based reconstruction of the temperature showed that the Achit area experienced cold conditions between ~22,600 and ~13,200 cal BP and mild conditions from ~13,200–~6400 cal BP with the past ~5000 years being relatively warm. The reconstructed precipitation suggests two wet periods: (1) from ~22,600 to ~13,200 cal BP and (2) from ~6400 to ~1600 cal BP. The two intervening dry periods are (1) from ~13,200–~6400 cal BP and (2) from ~1600 to 0 cal BP.

© 2013 Elsevier Ltd and INQUA. All rights reserved.

1. Introduction

The western Mongolian Plateau where the study site (i.e., Achit Nuur) is situated is an important climatic conjunction between the Pacific-influenced climates and the Atlantic-influenced climates. Many palaeoenvironmental studies, mostly on the basis of radiocarbon-dated sedimentary records from lakes, were conducted in this region and surrounding regions (e.g., Altai Mountains, northern and central Mongolian Plateau, northern China Xinjiang region) and have been published during the past twenty years (e.g., Harrison et al., 1996; Tarasov et al., 1998, 2000; Gunin, 1999; Grunert et al., 2000; Rudaya et al., 2009). However, discrepancies are more pronounced than consistencies regarding the Holocene climate change sequences in this region and three controversies are relevant to this study focusing on a Holocene record from Achit Nuur in the western Mongolian Plateau. Group one claims that the western Mongolian Plateau has been primarily influenced by the East Asian Monsoon during the Holocene and that influence was at its maximum during the mid-Holocene Climatic Optimum (Harrison et al., 1996; Tarasov et al., 2000). Group two states that the entire Central Asian Arid Zone (CAAZ) that stretches from the Caspian Sea in the west to the Hinggan Mountains in the east and that includes the western Mongolian Plateau has been climatically controlled by the North Atlantic Ocean and experienced the Holocene moisture changes that was out-phased with that in monsoon-dominated China (Chen et al., 2008). Group three proposes that the Holocene moisture variations in the arid and hyper-arid Mongolian Plateau including the western Mongolian Plateau has been primarily modulated by the temperature and that the mid-Holocene was the driest interval under warmest climate (Wang et al., 2009, 2011; Wang and Feng, 2013). These palaeoclimatological controversies call for more high-resolution palaeoclimatic reconstructions from the entire Mongolian Plateau.

This paper presents a record of environmental variations and the associated vegetation changes based on 91 pollen samples and 10 ^{14}C dates from a 200 cm lake core at Achit Nuur (49°25′N, 90°31′E) (Fig. 1) in hope the preliminary reconstruction by Gunin (1999) that was based on only four radiocarbon dates and only twenty pollen samples can be significantly improved for furthering our understanding of regional climatic variations.

* Corresponding author.
E-mail addresses: sunaizhi@mail.iggcas.ac.cn (A. Sun), fengzd@xju.edu.cn (Z. Feng).

1040-6182/$ – see front matter © 2013 Elsevier Ltd and INQUA. All rights reserved.
http://dx.doi.org/10.1016/j.quaint.2013.07.002

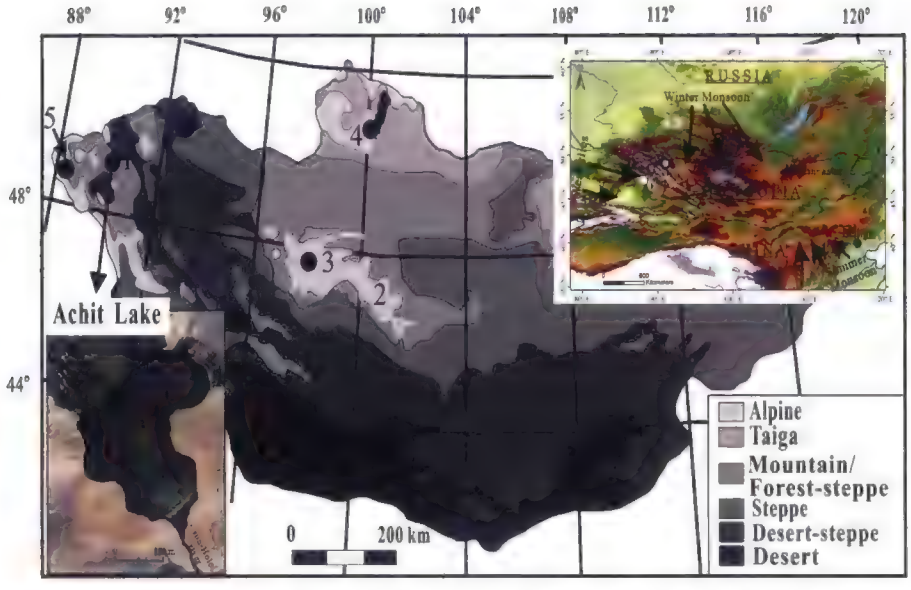

Fig. 1. Location and settings. A. Location of Achit Nuur (site 1) and other sections mentioned in the text (2: Ugii Nuur; 3: Telman Lake; 4: Hovsgol Lake; 5: Hoton Nuur; 6: Wulungu Lake). B. Vegetation map of the Mongolia region (Hilbig, 1995). C. Map of Achit Nuur showing the location of sediment core (from http://maps.google.com).

2. Regional setting

Achit Nuur (49°25′N, 90°31′E, 1444 ± 5 m), a large fresh-water lake, is located in the intermountain basin surrounded by Mongolian Altai Mountains in the west, Mungen Taiga Mountain in the north and Kaharkhiraa–Turgen Mountain in the east (Fig. 1B). The lake has an area of 297 km^2. The maximum length is 24 km and the maximum width is 18 km, and the average depth is ca. 2 m and the maximum depth is ca 5 m. This freshwater lake has inflows from the Huv-Usny-Gol River and the Mogen-Buren River and has an outflow through the Usun-Holoi into the Kobdo River, the Kobdo River flowing into the closed Hara-Us-Nuur Lake.

The climate around Achit Nuur is characterized by long, cold, dry winters and short, cool, relatively wet summers. Mean temperatures vary between −16 and −21 °C in January and between 15 and 20 °C in July. Mean annual precipitation (MAP) ranges between 200 and 300 mm in the lake area. The Achit Nuur basin has low-lying swampy northern and southern shores covered with salt-marsh vegetation and high-ground eastern and western shores covered with desert steppe vegetation. The regional vegetation is dominated by species of *Stipa krylovii*, *Stipa gobica*, and *Cleistogenes soongorica*, mixed with subshrubs of *Artemisia frigida*, *Artemisia xerophytica*, *Artemisia caespition*, *Tanacetum sibiricum*, *Tanacetum achillaeoides*, and *Tanacetum trifidum*. Macrophyte vegetation (*Chara* and *Potamogeton*) is widespread in the shallow zone (Hilbig, 1995). It should be mentioned that mountain taiga vegetation, dominated by *Larix sibirica* and *Pinus sibirica*, is distributed mainly in the Mongolian Altai Mountain and that the associated shrub layer includes *Rosa acicularis* and *Betula rotundifolia*. The forest-steppe vegetation borders the mountain taiga zone to the north and the steppe and desert-steppe zones to the south.

3. Materials and methods

3.1. Core collection and non-pollen proxy measurements

A 2.0-m-long sediment core was collected with a Livingstone-type gravitational piston corer in August of 2010 in the central part of Achit Nuur where the water depth is 3.8 m. The core was cut longitudinally into two halves and visually described immediately after core retrieval in the field.

The grain size was measured at 2-cm intervals using a Malvern Co. Ltd. Mastersizer 2000 laser diffraction particle size analyzer (size range 0.02–2000 μm). Sample pretreatment included: (1) adding H_2O_2 to remove organic matter and soluble salts, (2) using diluted 1 N HCl to remove carbonate and (3) using Na-hexametaphosphate to disperse aggregates. Total organic matter content (TOC) was determined at 2 cm intervals using the anti-titration method with concentrated sulfuric acid (H_2SO_4) and potassium dichromate ($K_2Cr_2O_7$). All of the aforementioned analyses were conducted in the MOE Key Laboratory of Western China's Environmental Systems at Lanzhou University.

The core can be stratigraphically divided into five units primarily according to the organic matter content (OM) and the mean grain size (Fig. 2A). Sediment Unit 1 (200–165 cm) is a light-grey clay layer with a mean grain size of ~5 μm and an average organic matter content (OM) of ~2.5%. Sediment Unit 2 (165–150 cm) is a dark-colored silt or fine sand layer with a mean grain size of ~120 μm and an average organic matter content of ~5%. Sediment Unit 3 (150–130 cm) is a light-grey silt layer with a mean grain size of ~18 μm and an average organic matter content (OM) of ~7.5%. Sediment Unit 4 (130–112 cm) is a brownish-grey layer with a mean grain size of ~90 μm and an average organic matter content of ~5%. Sediment Unit 5 (112–0 cm) is a laminated and dark-colored silt with two interbedded sandy silt layers (i.e., 112–105 cm and 62–52 cm). Compared with the underlying Sediment Unit 4, Sediment Unit 5 has a higher OM (~10%) and a lower mean grain size (~22 μm).

3.2. Dating and age-depth model

Ten samples of bulk sediment were radiocarbon dated using accelerator mass spectrometry (AMS) at the NSF-AMS Facility at the University of Arizona (Table 1). To assess the carbon reservoir effect, we obtained an age of 2099 ^{14}C BP on the bulk sediment

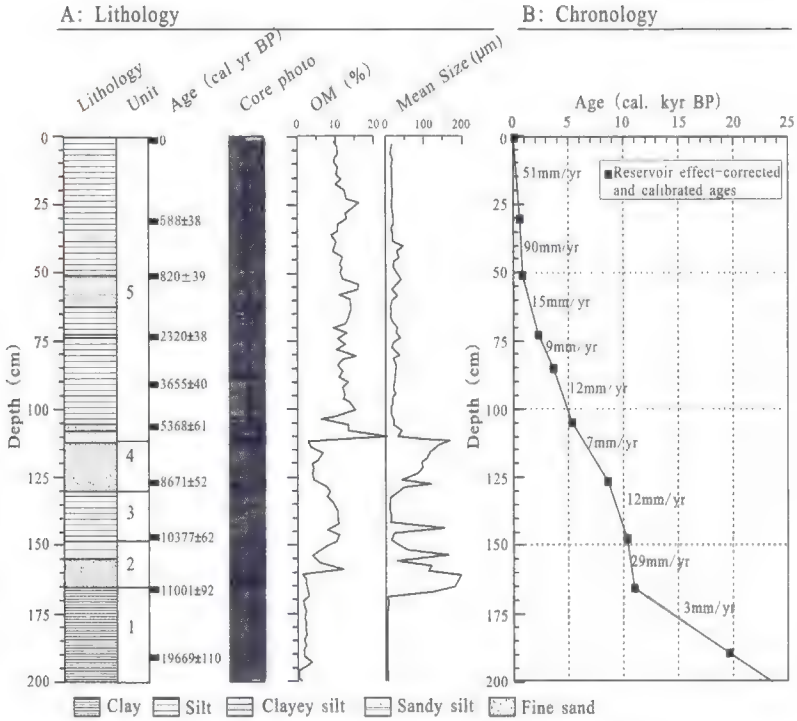

Fig. 2. Lithology, core photo, OM (%),Mean Grain Size (μm), and age-depth model of Achit Nuur core.

sampled at 0–2 cm (see Table 1). To account for the reservoir effect for the entire core, 2100 years were subtracted from all original ^{14}C ages assuming that it is constant through the core, and then all dates were calibrated to calendar years before present (BP = 1950 AD) with the program CALIB 6.0 using the INTCAL 09 calibration dataset (Reimer et al., 2009). The age-depth model was established based on a linear relationship between the depths and dates. Ages older than 19500 cal BP were extrapolated from the age-depth model between 165 cm and 190 cm in depth (Fig. 2). The age-depth model indicates that the upper 200 cm of the Achit Nuur core sediment covers the last ca. 22,600 years. The estimated depositional rates are ranged from 3 mm/y to 90 mm/y at whole core sediment. Calibrated radiocarbon ages are used throughout the paper.

Table 1
Dating results of Achit Nuur core.

LAB code	Depth/ cm	Dated material	$\delta^{13}C$ (‰)	^{14}C age (yr BP)	Calibrated age after subtracting the reservoir effect (2δ) (cal BP)
AA94349	0–2	Bulk sediment	−13.3	2099 ± 35	0
AA94350	30–31	Bulk sediment	−13.0	2673 ± 38	524–652
AA94351	51–52	Bulk sediment	−11.7	2981 ± 39	725–926
AA94352	73–74	Mollusc	−8.3	4421 ± 38	2180–2460
AA94353	85–86	Bulk sediment	−9.0	5497 ± 40	3488–3823
AA94354	105–106	Bulk sediment	−7.9	6717 ± 61	5258–5478
AA94355	127–128	Root	−7.9	9971 ± 52	8547–8795
AA94356	148–149	Bulk sediment	−7.6	11300 ± 62	10235–10519
AA94357	165–167	Bulk sediment	−6.9	11796 ± 92	10755–11247
AA94358	190–191	Bulk sediment	−3.7	18600 ± 110	19463–19875

3.3. *Pollen analysis and pollen indices*

Totally, 91 pollen samples were obtained at 2–4 cm intervals from the sediment core. For pollen analysis, a tablet of *Lycopodium* (containing 27,637 ± 563 spores) was first added for calculation of pollen concentration (Moore et al., 1991). The fossil pollen samples were first treated with HCl (5–10%) and HF (36%) and sieved in ultrasonic bath. Pollen types were identified using pollen references including pollen books and photographs (Erdtman, 1978; Moore and Web, 1987; Wang et al., 1995) and our own type-slide collection of more than 200 plant species from northern China. The treated samples then were mounted and examined with a transmitted light microscope (Olympus BX 51) at 400× magnification. More than 300 pollen grains (not including spores) were counted for each one of the samples. The percentage of each pollen type was calculated based on the sum of all counted pollen grains and the pollen diagrams were plotted using Grapher (8.0) software.

Several pollen indices have been designed to capture climate-related information for arid and semi-arid regions. For example, the ratio of Non-arboreal pollen to Arboreal pollen (NAP/AP) has been demonstrated to be an effective moisture index especially in sub-humid and semi-arid areas (Moore et al., 1991), and has been used in the Russian Altai Mountains (Blyakharchuk et al., 2007), the northern Mongolia (Dorofeyuk and Tarasov, 1998), and the Chinese Loess Plateau (Feng et al., 2004, 2006). SFI index (steppe-forest index = [(*Artemisia* + Chenopodiaceae + *Ephedra* + Caryophillaceae)/Trees]) is the ratio of the main steppe pollen sum over the tree pollen sum and was used to reconstruct the areal extent of steppe expansion in Lake Hovsgol (Prokopenko et al., 2007). In additional, the [C + A]/P ratio ([(Chenopodiaceae + *Artemisia*)/Poaceae]) was also designed to retrieve the Holocene aridity history in the Lake Telmen region of

central Mongolia (Fowell et al., 2003), though Poaceae has been demonstrated to be extremely under-represented in the pollen spectrum of the entire Mongolian Plateau (Gunin, 1999; Ma et al., 2008).

3.4. Vegetation and environmental reconstructions

The qualitative interpretation of pollen spectra can be checked with a quantitative method of pollen-based biome reconstruction (named Biomization, Prentice et al., 1996). Based on contemporary knowledge of the biogeography and ecology of modern plants, the pollen taxa are assigned to plant functional types (PFTs) and to main vegetation types (biomes) (Table 2). An affinity score for each single biome is then calculated according to Prentice et al. (1996). The pollen taxa-PFTs matrix applied in the present study is based on the Biomization procedure presented in Yu et al. (2000), but it was thoroughly improved by the information provided in Herzschuh et al. (2004) and Tarasov et al. (1998) (Table 2).

Table 2
Assignment of pollen taxa to the plant functional types (PFTs) for northern China (after Tarasov et al., 1998; Yu et al., (2000).

Abbreviation	Plant functional type	Pollen taxa
bec	Boreal evergreen conifer	*Abies*, *Picea*
bs	Boreal summergreen tree/shrub	*Betula*, *Salix*
ctc	Cool-temperate conifer	*Abies*
df	Desert forb/shrub	Asteraceae, Brassicaceae, Caryphyllaceae, Chenopodiaceae, Elaeagnaceae, *Ephedra*, Liliaceae, Polygonaceae, *Polygonum*, *Potentilla*
ec	Eurythermic conifer	*Pinus*
es	Eurythermic summergreen tree/shrub	*Alnus*
g	Grass	Poaceae
s	Sedge	Cyperaceae
sf	Steppe forb/shrub	Apiaceae, *Artemisia*, Asteraceae, Brassicaceae Caryophyllaceae, Chenopodiaceae, Elaeagnaceae, Fabaceae, Labiatae, Liliaceae, Moraceae, *Humulus*, *Plantago*, Polygonaceae, *Polygonum*, Thalictrum, Rosaceae, *Potentilla*, *Sanguisorba*, *Galium*, *Rumex*, *Urtica*, Valerianaceae
ts	Temperate summergreen tree/shrub	*Acer*, *Betula*, *Fraxinus*, *Quercus*, *Rubia*, *Salix*
ts1	Cool-temperate summergreen trees/shrub	*Carpinus*, *Corylus*, *Tilia*, *Ulmus*
ts2	Intermediate-temperate summergreen tree/shrub	*Celtis*, *Juglans*, *Pterocarya*, Thymelaceae

To reconstruct changes in palaeoclimatic parameters, PFT modern analogue technique (PFT-MAT) was applied. PFT-MAT method calculates a chord distance between the pollen taxa considered and modern analogues compared to determine the dissimilarity between the fossil and modern pollen spectra (Nakagawa et al., 2002; Davis et al., 2003; Jiang et al., 2006, 2009; Sun and Feng, 2013), which is constrained using modern pollen datasets and corresponding climatological data. The modern pollen dataset used in this study includes 1855 surface pollen spectra covering Mongolia and Europe (Guiot et al., 1993; Tarasov et al., 1998) and 211 surface pollen spectra from northern China provided by Members of China Quaternary Pollen Data Base (2001). The climate data of a specific surface pollen sample site are obtained using a weighted average of observed data from its adjacent weather stations within an area of 5 × 5° (Guiot and Goeury, 1996). For each fossil spectrum, we selected eight modern analogues with the smallest chord distance that represents the "best modern analogues". The mean climate parameters of each fossil pollen assemblage are then calculated using the method described by Guiot et al. (1993) and Magny et al. (2001). All calculations were carried out using the PPPBASE software package (Guiot and Goeury, 1996). We calculated three individual climatic parameters: the mean annual temperature (MAT), and mean annual precipitation (MAP).

4. Results

4.1. Fossil pollen data

Totally, 47 different types of terrestrial fossil pollen were identified from all samples analyzed in this study and they include 14 tree taxa and 33 herbaceous and shrub taxa (e.g., *Pinus*, *Picea*, Cupressaceae, *Betula*, *Quercus*, *Ulmus*, *Salix*, *Alnus*, *Corylus*, Rosaceae, *Ephedra*, *Nitraria*, *Tamarix*, Poaceae, *Artemisia*, Chenopodiaceae, *Aster*-type, *Taraxacum*-type, *Anther*-type, *Humulus*, Ranunculaceae, *Polygonum*, Cyperaceae, etc.). In addition, three aquatic pollen and two algae (e.g., *Typha*, *Sparganium*, *Alisma*; *Pediastrum* and *Myriophyllum*) were also identified. The core can be divided into three pollen assemblage zones and five subzones based on percentages of the major pollen taxa, and the three pollen zones and five subzones correspond well with the aforementioned sediment units (Fig. 3).

Pollen Zone 1 (200–172 cm; ~22,600–~13,200 cal BP) corresponds with the Sediment Unit 1 and the pollen assemblage is dominated by herb component (65–80%), mainly including Cyperaceae (12–35%), Poaceae (7–20%), *Aster*-type (3–6%), *Taraxacum* (2–8%), and *Anther*-type (1–10%). The coniferous tree component, including *Pinus* (10–20%), *Picea* (2–7%), Cupressaceae (0–7%) and *Larix* (0–2%), comprises ~20% of the total pollen sum. The broadleaved tree pollen percentage and pollen concentration are quite low. It should be mentioned that wetland taxa (e.g., Cyperaceae and *Typha*) percentages have the highest values of the entire core.

Pollen Zone 2 (172–112 cm; ~13,200–~6400 cal BP) corresponds with the Sediment Unit 2, 3, and 4, and is marked by a higher percentage of herbs and a relatively high pollen concentration. This zone can be further divided into three subzones.

Pollen subzone 2–1 (172–150 cm; ~13,200–~10,500 cal BP) corresponds with the Sediment Unit 2 and the pollen assemblage is dominated by herb and shrub components, mainly including *Artemisia* (35–45%), Chenopodiaceae (20–30%), Poaceae (8–17%) and *Ephedra* (1–8%). The coniferous tree component abruptly decreased (<10%) and mainly includes *Pinus*, *Picea*, and Cupressaceae. Broadleaved tree pollen started to emerge and main pollen types are *Quercus*, *Betula*, *Populus*, and *Ulmus*. Pollen subzone 2–2 (150–130 cm; ~10,500–~8900 cal BP) corresponds with the Sediment Unit 3. Compared with Pollen subzone 2–1, Poaceae and *Betula* pollen percentages and pollen concentration increased while *Ephedra* pollen percentages decreased in pollen subzone 2–2. Pollen subzone 2–3 (130–112 cm; ~8900–~6400 cal BP), corresponding with the Sediment Unit 4, is distinctively characterized by dramatic increases in drought-tolerant shrubs (e.g., *Ephedra*) and also by dramatic decreases in pollen concentration. The *Pinus* pollen percentage gradually increased.

Pollen Zone 3 (112–0 cm; ~6400–~0 cal BP) corresponds with the Sediment Unit 5. The assemblage is marked by increased coniferous (up to 45%) and broadleaved tree pollen percentages (up to 10%) at the expense of the herb pollen percentage (50–70%). The coniferous trees are mainly *Pinus* (20–35%), *Picea* (1–5%), Cupressaceae (0–9%) and *Larix* (0–5%), and *Pinus* is the major contributor to the increase in the coniferous tree pollen percentage. The

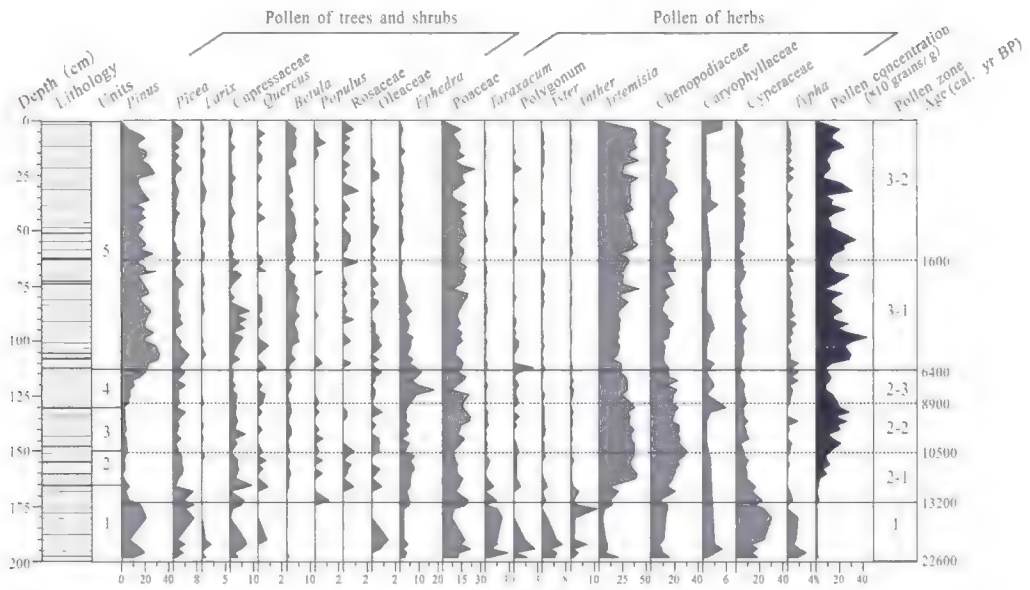

Fig. 3. Pollen spectra and taxa percentages of Achit Nuur core.

broadleaved trees are mainly *Betula* (2–6%), *Populus* (0–2%) and *Quercus* (0–1%). The pollen concentration increased significantly compared with the underlying Pollen subzone 2–3. This zone can also be divided into two subzones. Compared with pollen subzone 3–2 (62–0 cm; ~1600–~0 cal BP), pollen subzone 3–1 (112–62 cm; ~6400–~1600 cal BP) has higher tree pollen percentages (e.g., *Pinus*, *Picea*, Cupressaceae, *Betula*) and higher pollen concentration (the mean value is ~20 × 10^3 grains/g).

4.2. Vegetation and environmental reconstructions

The qualitative interpretation of the vegetation history of Achit Nuur is in concordance with that reconstructed by the quantitative method of biomization. Fig. 4 shows that biome types of the highest scores at each level are associated with a greater likelihood of that vegetation type being present near the site. The method of biomization and the taxa-biome matrix used here do not allow the

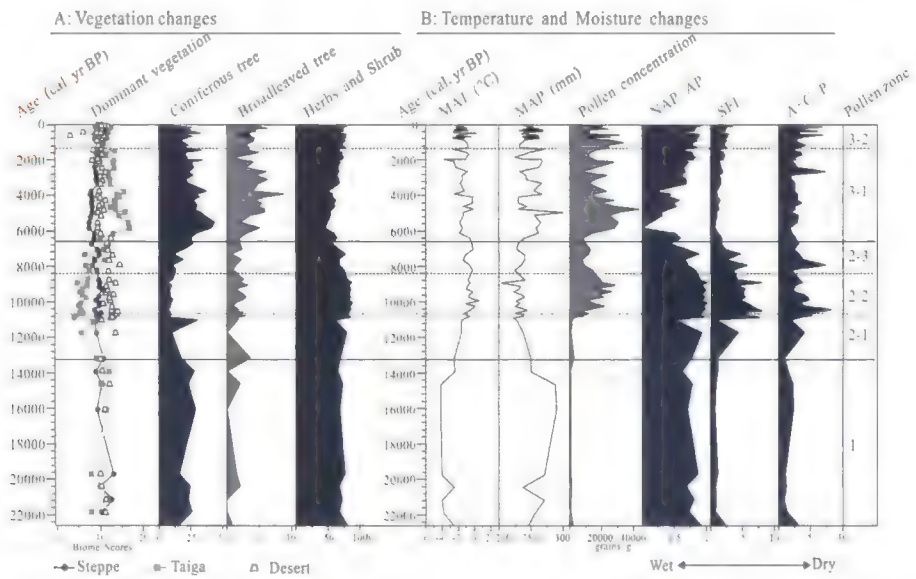

Fig. 4. Vegetation and environmental reconstructions. A: Vegetation changes, including dominant vegetation by biomization reconstructed, pollen percentages of coniferous tree, broadleaved tree, and herbs and shrub. B: Temperature and Moisture changes, including the reconstructed results of MAT, MAP, pollen concentration, NAP/AP ratio, SFI index, and [A + C]/P ratio. AP: Arboreal pollen, NAP: Non-arboreal pollen; SFI: steppe-forest index ((*Artemisia* + Chenopodiaceae + *Ephedra* + Caryophillaceae)/Trees; A: *Artemisia*; C: Chenopodiaceae; P: Poaceae.

reconstruction of transitional vegetation types (e.g., forest-steppe or desert-steppe). However, additional information can be obtained by examining the relative values of forest and non-forest biome scores. The scores for steppe are close to those for taiga in the bottom part (~22,600–~13,200 cal BP) and top part (~1600–~0 cal BP) of the Achit Nuur record, probably suggesting a forest-steppe transitional vegetation. The scores for desert are close to those for steppe during the period between ~13,200 and ~6400 cal BP, most likely indicating a desert-steppe transitional vegetation. The vegetation reconstructed for the period between ~6400 and ~1600 cal BP is a taiga. The reconstructed biome types are relatively well corroborated by main pollen assemblage (e.g., percentages of coniferous trees, broadleaved trees and Herbs) (Fig. 4).

Our reconstruction of MAT was well identified the cold climates during Last Glacial Maximum and the subsequent late glacial from ~22,600 to ~13,200 cal BP. A general warming between ~13,200 and ~10,500 cal BP was also well-displayed, being relatively consistent with the records from North Atlantic region (Davis et al., 2003; Moros et al., 2004). The highest values of the reconstructed MAT well marked the early-middle Holocene "hyperthermal period" lasting from ~10,500–~6400 cal BP (Harrison et al., 1996; Tarasov et al., 2000; Rudaya et al., 2009) and the fluctuating decline of the reconstructed MAT characterized the following period from ~6400 to ~2000 cal BP, being supportive to the cooling of large-scale (Wanner et al., 2008). It seems that the slight warming of the past ~1000 years reported from the Western Pacific Warm Pool (Stott et al., 2004) and also from the Arabian Sea of the Indian Ocean (Gupta et al., 2003) were also captured in our record from Achit Nuur (Fig. 4). The reconstructed MAP exhibits two wet periods: (1) from ~22,600 to ~13,200 cal BP and (2) from ~6400 to ~1600 cal BP. The two intervening dry periods are: (1) from ~13,200–~6400 cal BP and (2) from ~1600 to 0 cal BP.

5. Discussion and conclusions

5.1. Vegetation variations and associated climate changes

The pollen assemblage of Achit Nuur sediment core reveals a detailed history of changes in the vegetation and climate over the Achit Nuur area during the last ~22,600 y (Figs. 3 and 4). The highest values of wetland taxa (e.g., Cyperaceae, *Typha*) percentages showed that the lake basin was dominated by meadow-steppe between ~22,600 and ~13,200 cal BP, suggesting that the moisture was high. This reconstructed high moisture is corroborated by the lowest values of SFI scores and [A + C]/P ratios. A higher percentage of coniferous tree pollen suggested that the dark-coniferous forests expanded in the surrounding mountains compared with the subsequent stages. It can thus be inferred that the climate was cold and humid during the period from ~22,600 to ~13,200 cal BP.

The vegetation was desert-steppe dominated by *Artemisia*, Chenopodiaceae, Poaceae, and *Ephedra*, as shown by the high herb pollen sum, high SFI scores and high [A + C]/P ratios during the period from ~13,200–~6400 cal BP, meaning that the climate in this region is mild and dry and the lake level declined. All data (including MAT, MAP, NAP/AP ratio, [A + C]/P ratio, and SFI score) indicated that the moisture level was the lowest and the temperature was the highest between 10,500 and 6400 cal BP.

The biomization reconstruction shows that Taiga vegetation in high elevations and deciduous forest in medium elevations expanded in the surrounding mountains as indicated by increased pollen percentages of coniferous and broadleaved trees between ~6400 and ~1600 cal BP. The expansion of forests in the surrounding mountains and lowered values in the NAP/AP ratio and SFI score all suggested that the moisture level was increased under declined temperature conditions. Since ~1600 cal BP, steppe vegetation recovered in the lake basin and the climate became drier than the previous stage under increased temperature conditions, as indicated by increases in NAP/AP ratio, [A + C]/P ratio and SFI scores.

5.2. Regional comparison

To understand the Holocene vegetation and climate history of the western Mongolian Plateau in a large-scale geographic context, the following section will focus on the issues surrounding the Holocene pollen records. We chose five sections from three surrounding areas in hope that our understanding of the large-scale controlling mechanisms can be improved. These five sections are Ugii Nuur, Lake Telmen, and Lake Hovsgol in the northern Mongolian Plateau, Hoton Nuur in the northern part of the Altai Mountain, and Lake Wulungu in northern Xinjiang.

Ugii Nuur (site 2 in Fig. 1) (Wang et al., 2009, 2011), Lake Telmen (site 3 in Fig. 1) (Peck et al., 2002; Fowell et al., 2003), and Lake Hovsgol (site 4 in Fig. 1) (Prokopenko et al., 2007) are situated in the northern Mongolian Plateau. Multi-proxy reconstruction from Ugii Nuur shows that a mild climate with moderate moisture conditions supported a desert steppe landscape during ~9100–6700 cal BP, followed by a mid-Holocene dry phase lasting from ~6700 to 3300 cal BP. The changes in Chenopodiaceae percentage and pollen-based moisture index exhibit a wet period between ~2600 and 1000 cal BP that was followed by a relatively dry period (i.e., the past ~1000 years). The pollen-based aridity index (i.e., [A + C]/P) from Lake Telmen (Peck et al., 2002; Fowell et al., 2003) exhibits a mid-Holocene dry phase lasting from 7100 to 4600 cal BP, which is generally supportive to the mid-Holocene dry phase reconstructed at Ugii Nuur. The following period, from ~4600 to 0 cal BP, has been generally wet with two short dry intervals at ~3000 and at ~1800 cal BP. At Lake Hovsgol (Prokopenko et al., 2007), the pollen-based steppe-forest index (i.e., SFI index) indicated a wet condition from ~9500 to ~6000 cal BP, a mid-Holocene dry phase from ~6000 to ~3500 cal BP, and a relatively wet phase after ~3500 cal BP. On the whole, above three pollen records from the northern Mongolian Plateau suggest that the climate was mild and wet during the early Holocene (~9500–~7000 cal BP) and the late Holocene (after ~3500 cal BP), but dry during the middle Holocene (~7000–~3500 cal BP).

A newly recovered sequence from Hoton Nuur (site 5 in Fig. 1) (Rudaya et al., 2009) within the Mongolian Altai area significantly improved the sampling resolution over the old sequence reported by Tarasov et al. (2000). The pollen-based quantitative reconstruction of precipitation using the best modern analogue technique suggests that the regional climate was relatively dry prior to 10,500 cal BP and became substantially wetter during the following interval between 10,500 and 5000 cal BP. Pollen data and biome reconstruction demonstrate that a cool steppe predominated around Hoton Nuur before 10,500 cal BP, followed by the spread of boreal trees and open woodland vegetation between 10,500 and 6500 cal BP. From 6500 cal BP onward, steppe taxa in the pollen spectra increase significantly, indicating a strengthening of steppe communities and a weakening of taiga communities.

Wulungu Lake in northern Xinjiang (Xiao et al., 2006; Liu et al., 2008) (site 6 in Fig. 1) had experienced a shallow lake or wetland environment during the early Holocene (~10,000–6700 cal BP) as indicated by high pollen-based wetland biome scores (Xiao et al., 2006; Liu et al., 2008). A general wetting trend since 6700 cal BP is suggested by an increasing of A/C ratio and a decreasing of pollen-based desert biome scores, suggesting that the Holocene moisture optimum occurred between 4200 and 500 cal BP (Liu et al., 2008).

To sum up, in the arid areas of the northern Mongolian Plateau (e.g., Ugii Nuur, Lake Telmen, and Lake Hovsgol), a mid-Holocene dry phase can be established, and both the early Holocene and the late Holocene are characterized by relatively wet (and probably also cool) climates. In the Mongolian Altai area (e.g., Hoton Nuur), the regional climate was relatively dry prior to 10,500 cal BP and became substantially wetter during the following interval between 10,500 and 5000 cal BP. A drying trend over the past ~5000 years is well expressed by all pollen proxies. In the northern Xinjiang, a dry early Holocene and a progressively wetter middle and late Holocene pattern can be established for Lake Wulungu.

The record covering the past ~22,600 years from Achit Nuur in the western Mongolian Plateau seems in a good agreement with large-scale picture of climate change during the same period, somewhat boosting our confidence on our reconstructions. However, the Holocene part of the record from Achit Nuur does not correlate with the records from nearby Hoton Nuur and from Wulungu Lake. Instead, the Holocene part of the record from Achit Nuur is more or less consistent with the records from the northern Mongolian Plateau (including Ugii Nuur, Lake Telmen, and Lake Hovsgol), seemingly lending support to the proposition that the moisture levels in arid and hyper-arid areas of the Mongolian Plateau has been primarily controlled or modulated by temperature (Wang et al., 2009, 2011; Wang and Feng, 2013). The proposition states that the elevated temperature resulted in an increase in evaporation and thus led to a decrease in moisture level. This inference is generally supported by qualitative (e.g., pollen assemblages) and semi-quantitative (e.g., pollen ratios and biome scores) reconstructions reconstruction from Achit Nuur. The dilemma we have to face is that the reconstructed MAP goes along with the qualitatively and semi-quantitatively reconstructed moisture levels, severely undermining the proposition that temperature has controlled or modulated the moisture levels. However, if the reconstructions of MAT and MAP can stand for further tests, the climate change in Achit area seems to have followed cool-wet mode and warm-dry mode, a typical temperature-precipitation combination for the westerlies-dominated climate (Aizen et al., 2001; Bridgman and Oliver, 2006; Bothe et al., 2011).

5.3. A brief summary

During the period of ~22,600–~13,200 cal BP, the vegetation of the Achit Nuur region was forests and steppes. That is, steppes dominated the lake basin and cold-tolerant forests dominated the surrounding mountains, suggesting a cold and wet climate. Subsequently from ~13,200 to ~6400 cal BP, deserts in lower elevations and steppes in higher elevations developed under mild and dry conditions in the Achit area. Taiga vegetation expanded in the surrounding mountains under cooling and humid conditions from ~6400 to ~1600 cal BP and forests and steppes resumed over the past ~1600 years.

Pollen-based biomization and PFT-MAT quantitative reconstruction demonstrate that: (1) temperature and moisture have changed asynchronously during the last glacial, (2) the warmest period occurred between ~10,500 and ~7000 cal BP and the most humid period occurred between ~22,600 and ~13,200 cal BP, and (3) higher temperatures may have brought not only more precipitation, but also more evaporation, thereby resulting in dry climates between ~13,200 and ~6400 cal BP.

Acknowledgments

This study was financially supported by several NSFC grants (No. 40930120, No. 41002058, No. 41172332, No. 40331012, No. 40421101) and two U.S. NSF grants (NSF-ESH-04-02509, NSF-BSC-06-52304).

References

Aizen, E.,M., Aizen, V.B., Melack, J.M., Nakamura, T., Ohta, T., 2001. Precipitation and atmospheric circulation patterns at mid-latitudes of Asia. International Journal of Climatology 21, 535–556.

Blyakharchuk, T.A., Wright, H.E., Borodavko, P.S., van der Knaap, W.O., Ammann, B., 2007. Late Glacial and Holocene vegetational history of the Altai Mountains (southwestern Tuva Republic, Siberia). Palaeogeography, Palaeoclimatology, Palaeoecology 245, 518–534.

Bothe, O., Fraedrich, K., Zhu, X., 2011. Precipitation climate of Central Asia and the large-scale atmospheric circulation. Theoretical Applied Climatology. http://dx.doi.org/10.1007/s00704-011-0537-2.

Bridgman, B.H., Oliver, J.E., 2006. The Global Climate System: Patterns, Processes, and Teleconnections. Cambridge University Press, New York, p. 243.

Chen, F.H., Yu, Z.C., Yang, M.L., Ito, E., Wang, S.M., Madsen, D.B., Huang, X.Z., Zhao, Y., Sato, T., Birks, H.J.B., Boomer, I., Chen, J.H., An, C.B., Wünnemann, B., 2008. Holocene moisture evolution in arid central Asia and its out-of-phase relationship with Asian monsoon history. Quaternary Science Reviews 27 (3–4), 351–364.

Davis, B.A.S., Brewer, S., Stevenson, A.C., Guiot, J., Data, Contributors, 2003. The temperature of Europe during the Holocene reconstructed from pollen data. Quaternary Science Reviews 22, 1701–1716.

Dorofeyuk, N.I., Tarasov, P.E., 1998. Vegetation and lake levels in Northern Mongolia in the last 12,500 years as indicated by data of pollen and diatom analyses. Stratigraphy and Geological Correlation 6 (1), 70–83.

Erdtman, G., 1978. Handbook of Palynology (Translated by the Institute of Botany, the Chinese Academy of Sciences). Science Press, Beijing (in Chinese).

Feng, Z.D., An, C.B., Tang, L.Y., Jull, A.J.T., 2004. Stratigraphic evidence of a Mega-humid climate between 10,000 and 4000 years B.P. in the western part of the Chinese Loess Plateau. Global and Planetary Change 43 (3–4), 145–155.

Feng, Z.D., Tang, L.Y., Wang, H.B., Ma, Y.Z., Liu, K.B., 2006. Holocene vegetation variations and the associated environmental changes in the western part of the Chinese Loess Plateau. Palaeogeography, Palaeoclimatology, Palaeoecology 241, 440–456.

Fowell, S.J., Hansen, B., Peck, J.A., Khosbayar, P., Ganbold, E., 2003. Mid to late Holocene climate evolution of the Lake Telmen basin, north central Mongolia, based on palynological data. Quaternary Research 59 (3), 353–363.

Grunert, J., Lehmkuhl, F., Walther, M., 2000. Paleoclimatic evolution of the Uvs Nuur basin and adjacent areas (Western Mongolia). Quaternary International 65/66, 171–191.

Guiot, J., Harrison, S.P., Prentice, T.C., 1993. Reconstruction of Holocene patterns of moisture in Europe using pollen and lake-level data. Quaternary Research 40, 139–149.

Guiot, J., Goeury, C., 1996. PPPBASE, a software for statistical analysis of paleoecological and paleoclimatological data. Dendrochronologia 14, 295–300.

Gunin, P.D., 1999. Vegetation Dynamics of Mongolia. Kluwer Academic Publisher, Copenhagen, p. 238.

Gupta, A.K., Anderson, D.M., Overpeck, J.T., 2003. Abrupt changes in the Asian southwest monsoon during the Holocene and their links to the North Atlantic Ocean. Nature 421, 354–357.

Harrison, S.P., Yu, G., Tarasov, P.E., 1996. Late Quaternary lake-level record from Northern Eurasia. Quaternary Research 45 (2), 138–159.

Herzschuh, U., Tarasov, P., Wünemann, B., Hartmann, K., 2004. Holocene vegetation and climate of the Alashan Plateau, NW China, reconstructed from pollen data. Palaeogeography Palaeoclimatology Palaeoecology 211 (1–2), 1–17.

Hilbig, W., 1995. The Vegetation of Mongolia. SPB Academic Publishing, Amsterdam, p. 258.

Jiang, W.Y., Guo, Z.T., Sun, X.J., Wu, H.B., Chu, G.Q., Yuan, B.Y., Hatté, C., Guiot, J., 2006. Reconstruction of climate and vegetation changes of Lake Bayanchagan (Inner Mongolia): Holocene variability of the East Asian monsoon. Quaternary Research 65 (3), 411–420.

Jiang, W.Y., Guiot, J., Chu, G.Q., Wu, H.B., Yuan, B.Y., Hatté, C., Guo, Z.T., 2009. An improved methodology of the modern analogues technique for palaeoclimate reconstruction in arid and semi-arid regions. Boreas 39, 145–153.

Liu, X.Q., Herzschuh, U., Shen, J., Jiang, Q.F., Xiao, X.Y., 2008. Holocene environmental and climatic changes inferred from Wulungu Lake in northern Xinjiang, China. Quaternary Research 70 (3), 412–425.

Ma, Y.Z., Liu, K.-B., Feng, Z.D., Sang, Y.L., Wang, W., Sun, A.Z., 2008. A survey of modern pollen and vegetation along a south–north transect in Mongolia. Journal of Biogeography 35, 1512–1532.

Magny, M., Guiot, J., Schoellammer, P., 2001. Quantitative reconstruction of Younger Dryas to Mid-Holocene paleoclimates at Le Locle, Swiss Jura, using pollen and lake-level data. Quaternary Research 56, 170–180.

Members of China Quaternary Pollen Data Base, 2001. Simulation of China biome reconstruction based on pollen data from surface sediment samples. Acta Botanica Sinica 43, 201–209.

Moore, P.D., Web, J.A., 1987. Palynology Analytical Manual (Li WY, Xiao XM, Liu GX Trans.). Guangxi People's Publishing House, Nanning (in Chinese).

Moore, P.D., Webb, J.A., Collinson, M.E., 1991. Pollen Analysis, second ed. Blackwell Scientific Publication, Oxford, p. 216.

Moros, M., Emeis, K., Risebrobakken, B., Snowball, I., Kuijpers, A., Mcmanus, J., Jansen, E., 2004. Sea surface temperature and ice rafting in the Holocene North Atlantic: climate influences on northern Europe and Greenland. Quaternary Science Reviews 23, 2113–2160.

Nakagawa, T., Tarasov, P.E., Nishida, K., Gotanda, K., Yasuda, Y., 2002. Quaternary pollen-based climate reconstruction in central Japan: application to surface and Late Quaternary spectra. Quaternary Science Reviews 21, 2099–2113.

Peck, J.A., Khosbayar, P., Fowell, S.J., Pearce, R.B., Ariunbileg, S., Hansen, B., Soninkhishig, N., 2002. Mid to Late Holocene climate change in north central Mongolia as recorded in the sediments of Lake Telmen. Palaeogeography Palaeoclimatology Palaeoecology 183 (1–2), 135–153.

Prentice, I.C., Guiot, J., Huntley, B., Jolly, D., Cheddadi, R., 1996. Reconstructing biomes from palaeoecological data: a general method and its application to European pollen data at 0 and 6 ka. Climate Dynamics 12, 185–194.

Prokopenko, A.A., Alexander, A., Khursevich, G.K., Bezrukova, E.V., Kuzmin, M.I., Boes, X., Williams, D.F., Fedenya, S.A., Kulagina, N.V., Letunova, P.P., Abzaeva, A.A., 2007. Paleoenvironmental proxy records from Lake Hovsgol, Mongolia, and a synthesis of Holocene climate change in the Lake Baikal watershed. Quaternary Research 68 (1), 2–17.

Reimer, P.J., Baillie, M.G.L., Bard, E., Bayliss, A., Beck, J.W., Blackwell, P.G., Ramsey, C.B., Buck, C.E., Burr, G.S., Edwards, R.L., et al., 2009. IntCal09 and Marine09 radiocarbon age calibration curves, 0–50,000 years cal BP. Radiocarbon 51, 1111–1150.

Rudaya, N., Tarasov, P., Dorofeyuk, N., Solovieva, N., Kalugin, I., Andreev, A., Daryin, A., Diekmann, B., Riedel, F., Tserendash, N., Wagner, M., 2009. Holocene environments and climate in the Mongolian Altai reconstructed from the Hoton-Nur pollen and diatom records: a step towards better understanding climate dynamics in Central Asia. Quaternary Science Reviews 28 (5–6), 540–554.

Stott, L., Cannariato, K., Thunell, R., Haug, G.H., Koutavas, A., Lund, S., 2004. Decline of surface temperature and salinity in the western tropical Pacific Ocean in the Holocene epoch. Science 431, 56–59.

Sun, A.Z., Feng, Z.D., 2013. Holocene climatic reconstructions from the fossil pollen record at Qigai Nuur in the southern Mongolian Plateau. The Holocene. http://dx.doi.org/10.1177/0959683613489581.

Tarasov, P., Dorofeyuk, N., Metl'tseva, E., 2000. Holocene vegetation and climate changes in Hoton-Nur basin, northwest Mongolia. Boreas 29 (2), 117–126.

Tarasov, P.E., Webb III, I.T., Andreev, A.A., Afanas'eva, N.B., Berezina, N.A., Blyakharchuk, T.A., Bolikhovskaya, N.S., Cheddadi, R., Chernavskaya, M.M., Chernova, G.M., et al., 1998. Present-day and mid-Holocene biomes reconstructed from pollen and plant macrofossil data from the former Soviet Union and Mongolia. Journal of Biogeography 25, 1029–1053.

Wang, F.X., Qian, N.F., Zhang, Y.L., Yang, H.D., 1995. Pollen Flora of China, second ed. Science Press, Beijing. (in Chinese).

Wang, W., Feng, Z.-D., 2013. Holocene moisture evolution across the Mongolian Plateau and its surrounding areas: a synthesis of climatic records. Earth-Science Reviews 122, 38–57.

Wang, W., Ma, Y.Z., Feng, Z.D., Meng, H.W., Sang, Y.L., Zhai, X.W., 2009. Vegetation and climate changes during the last 8660 cal. a BP in central Mongolia, based on a high-resolution pollen record from Lake Ugii Nuur. Chinese Science Bulletin 54 (9), 1579–1589.

Wang, W., Ma, Y.Z., Feng, Z.D., Narantsetseg, Ts., Liu, K.B., Zhai, X.W., 2011. A prolonged dry mid-Holocene climate revealed by pollen and diatom records from Lake Ugii Nuur in central Mongolia. Quaternary International 229 (1–2), 74–83.

Wanner, H., Beer, J., Bütikofer, J., Crowley, T.J., Cubasch, U., Flückiger, J., Goosse, H., Grosjean, M., Joos, F., Kaplan, J.O., Küttel, M., Müller, S.A., Prentice, I.C., Solomina, O., Stocker, T.F., Tarasov, P., Wagner, M., Widmann, M., 2008. Mid- to Late-Holocene climate change: an overview. Quaternary Science Reviews 267, 1791–1828.

Xiao, X.Y., Jiang, Q.F., Liu, X.Q., Xiao, H.F., Shen, J., 2006. High resolution sporopollen record and environmental change since Holocene in the Wulungu Lake, Xinjiang. Acta Micropalaeontologica Sinica 23 (1), 77–86 (in Chinese with English Abstract).

Yu, G., Chen, X.D., Ni, J., Cheddadi, R., Guiot, J., Han, H., Harrison, S.P., Huang, C., Ke, M., Kong, Z., Li, S., Li, W., Liew, P., Liu, G., Liu, Q., Liu, K.-B., et al., 2000. Palaeovegetation of China: a pollen data-based synthesis for the mid-Holocene and last glacial maximum. Journal of Biogeography 27, 635–664.

附录十一

Contents lists available at ScienceDirect

Quaternary International

journal homepage: www.elsevier.com/locate/quaint

A prolonged dry mid-Holocene climate revealed by pollen and diatom records from Lake Ugii Nuur in central Mongolia

Wei Wang [a,b], Yuzhen Ma [c], Zhaodong Feng [b,d,*], Ts Narantsetseg [e], Kam-Biu Liu [f], Xinwei Zhai [b]

[a] College of Environment and Resources, Inner Mongolia University, Huhhot, Inner Mongolia, China
[b] MOE Key Laboratory of West China's Environmental System, Lanzhou University, Lanzhou, Gansu, China
[c] MOE, Key Laboratory of Environmental Change and Natural Disaster, Beijing Normal University, Beijing, China
[d] Department of Geology, Baylor University, Waco, TX, USA
[e] Institute of Geology and Mineral Resources, Mongolian Academy of Sciences, Ulan Batar, Mongolia
[f] Department of Oceanography and Coastal Sciences, School of the Coast and Environment, Louisiana State University, Baton Rouge, USA

ARTICLE INFO

Article history:
Available online 16 June 2010

ABSTRACT

A high-resolution pollen- and diatom-based bioclimatic reconstruction from Ugii Nuur lake core with a chronological support of 14 AMS dates revealed that a prolonged dry climate prevailed between 5830–3080 ^{14}C BP in central Mongolia, as indicated by a dramatic increase in Chenopodiaceae pollen percentages at the expense of *Pinus*, Poaceae, Cyperaceae and other mesophytic forbs pollen percentages. Higher values of pollen-based temperature index and lower values of pollen-based moisture index also support the notion that the mid-Holocene was persistently warm and dry relative to the preceding and following periods. This mid-Holocene drought is further confirmed by diatom and sedimentary variations, both the planktonic/benthic diatom ratio and the deposition rate being the lowest. Reviews of published regional palaeoclimate data suggest that a prolonged mid-Holocene drought might have prevailed extensively in the central-east Asian arid and hyper-arid areas. The prolonged and extensive drought might have been resulted from a well-documented large-scale temperature rise. The temperature rise-dictated enhancement of evaporation might have exceeded the precipitation increase (if any), resulting in the aridity increase.

© 2010 Elsevier Ltd and INQUA. All rights reserved.

1. Introduction

Holocene climate change has been highlighted to establish baselines for predicting and comprehending the future warming and associated regional ecological response because similar contexts might exist in the future (Wanner et al., 2008). The mid-Holocene (around 5000–6000 cal. BP) was particularly singled out as a period that underwent most profound Holocene climatic changes (Steig, 1999; Ruddiman, 2001; Broecher, 2003; Oppo et al., 2003) and the profound changes have been proposed to have resulted from a large-scale reorganization of ocean-atmospheric coupled systems. Understanding the reorganization is essential not only to comprehending the past of the earth's climate systems, but also to comprehending the future of a warming world. However, knowledge regarding the mid-Holocene climate changes is still rather limited, and more high-resolution data from climate sensitive regions is needed. The arid and semiarid Mongolia Plateau, located in the Asian continental interior, is such a highly climate sensitive area.

A warm and wet mid-Holocene climate was widely reported in the semiarid northern China (see Feng et al., 2006 and the references therein) and a wet (and probably warm) mid-Holocene climate is well-documented in the sub-humid northern Mongolian Plateau (Harrison et al., 1996; Tarásov et al., 2000) and the adjacent southern Siberia (Velichko et al., 1997; Demske et al., 2005). However, the published data suggest that a dry mid-Holocene climate might have prevailed in the arid and hyper-arid areas in northwestern China (including northern Xinjiang, western Inner Mongolia and Erdos Plateau) (Rhodes et al., 1996; Zhang et al., 2000; Chen et al., 2003a,b, 2006; Li et al., 2003; Hartmann and Wünnemann, 2009). This mid-Holocene drought might have extended to the semiarid central Mongolia. Tarasov et al. (1999) reported that the summer temperature around 6000 ^{14}C BP in the central Mongolia was ~2 °C higher and the available moisture was ~10% less than today. Recent pollen studies from Lake Telmen (48°50′N, 97°20′E, 1789 m a.s.l.) further confirmed a dry

* Corresponding author. Department of Geology, Baylor University, Waco, TX 76978, USA. Tel.: +1 254 710 2194; fax: +1 254 710 2673.
E-mail address: Zhaodong_feng@baylor.edu (Z.-D. Feng).

1040-6182/$ – see front matter © 2010 Elsevier Ltd and INQUA. All rights reserved.
doi:10.1016/j.quaint.2010.06.005

mid-Holocene climate in central Mongolia (Peck et al., 2002; Fowell et al., 2003) although the data resolution was rather low (~40 samples for a period of ~6100 ^{14}C years). This paper presents much higher resolution records of pollen (386 samples for the past ~8120 ^{14}C years), diatom (75 samples for ~8120–2010 ^{14}C BP) and sedimentary analyses (376 samples for ~8120–2010 ^{14}C BP) from Ugii Nuur (47°46′N, 102°46′E, 1330 m a.s.l.), which is situated in the northern foothills of Hangay Mountain in central Mongolia, in hope that more details of mid-Holocene climate changes can be revealed. The data (the present paper complements and refines data previously published by Wang et al., 2009) are also expected to add more information to more accurately delineate the areal extent of the dry mid-Holocene climate, thus furthering our understanding of the large-scale mechanism(s) controlling or modulating the mid-Holocene climate changes.

2. Physiographic setting

The climate in central Mongolia where the study site is located is characterized by an extreme continentality with cold and dry winters and relatively warm and wet summers. The mean annual temperature is about 0 °C and the mean annual precipitation is about 250 mm (Tuvdendorzh and Myagmarzhav, 1985). The Ugii Nuur (see Fig. 1), a freshwater lake, lies in the foothill piedmont at the northern flank of the Hangay Mountains with a lake surface area of ~12 km^2 and a maximum water depth of 17 m (field observed in 2004). A branch river originating from the eastern Hangay Mountains wanders its way across montane steppes into the Ugii Nuur and outflows northwestward into the Orhon River.

As shown in Fig. 1, the modern zonal vegetation around and to the southeast of the lake (i.e., Ugii Nuur) is *Stipa*-dominated steppes, and the vegetation to the north and northwest of the lake is dominated by montane steppes (e.g., montane *Festuca* steppes) and montane forest-steppes (e.g., montane *Larix/Pinus/Betula* forests-*Festuca* steppes) (Lavrenko et al., 1979; Tuvdendorzh and Myagmarzhav, 1985; Hilbig, 1995). The upper stream of the Ugii Nuur watershed is occupied by montane *Festuca* steppes and the lower stream by *Stipa*-dominated steppes that are co-dominated with *Cleistogenes Squarrosa* and *Artemisia frigida*. The lower stream *Stipa*-dominated steppes contain two other sub-settings: (1) dry *Stipa* steppes accompanied with more *Kochia prostrate* and *Salsola ruthenica* in sunnier and drier slopes, and (2) meadows consisting

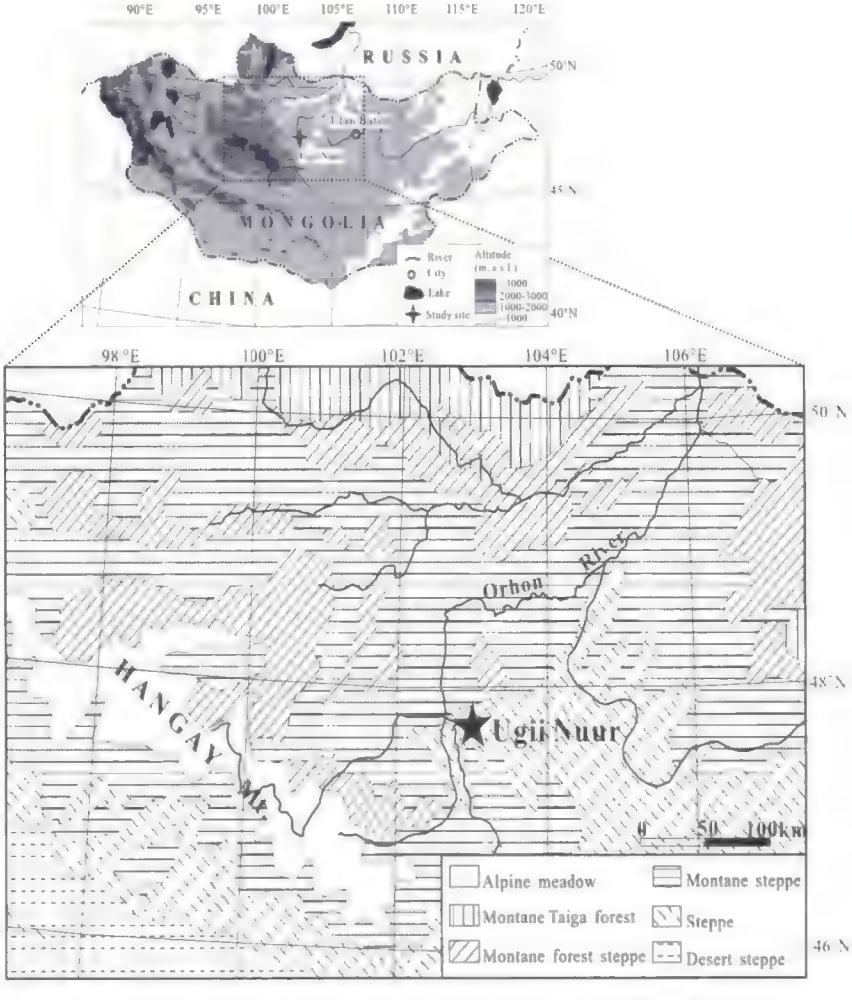

Fig. 1. Vegetation types around the studied lake (i.e., Ugii Nuur) and its relative location within Mongolia (upper panel).

of *Carex*, Poaceae and forbs in riverbank and lakeshore wetlands (Lavrenko et al., 1979; Tuvdendorzh and Myagmarzhav, 1985; Hilbig, 1995).

3. Methods

Modern pollen samples of inflowing river surface sediments (samples 1–4 in Fig. 2), uppermost sediment of the lake core (assumed to be modern deposits) (sample 5 in Fig. 2) and modern surface samples from piedmont steppes of lower elevations (samples 6 and 7 in Fig. 2) and montane steppes of higher elevations (samples 8 and 9 in Fig. 2) were collected for pollen analysis to provide modern references for interpreting fossil pollen spectrum on sources, transport processes and bioclimatic representation. An 854-cm long core was drilled with gravitational piston corer in 2004 at the east-central part of the Ugii Nuur where the water depth is 14.5 m. The drilling site was selected to avoid direct influences of lake inflow and outflow to assure continuous preservation of the lake sediments. Fossil pollen samples were collected at intervals of ~2 cm and total 386 samples were analyzed. Fossil diatom samples were collected at 10 cm intervals for the depths between 100 and 854 cm and total 75 samples were obtained. Sampling intervals for grain size measurements were ~2 cm (between 100 and 854 cm) and totally 376 samples were analyzed. The uppermost portion (0–100 cm) has no diatom and grain size data because core samples were used for other analyses.

Pollen extraction was carried out following standard palynological procedures (Faegri and Iversen, 1975). Pollen samples were treated with alkali, hydrochloric acid and hydrofluoric acid to remove organic matter, carbonate and silicate, and one *Lycopodium*

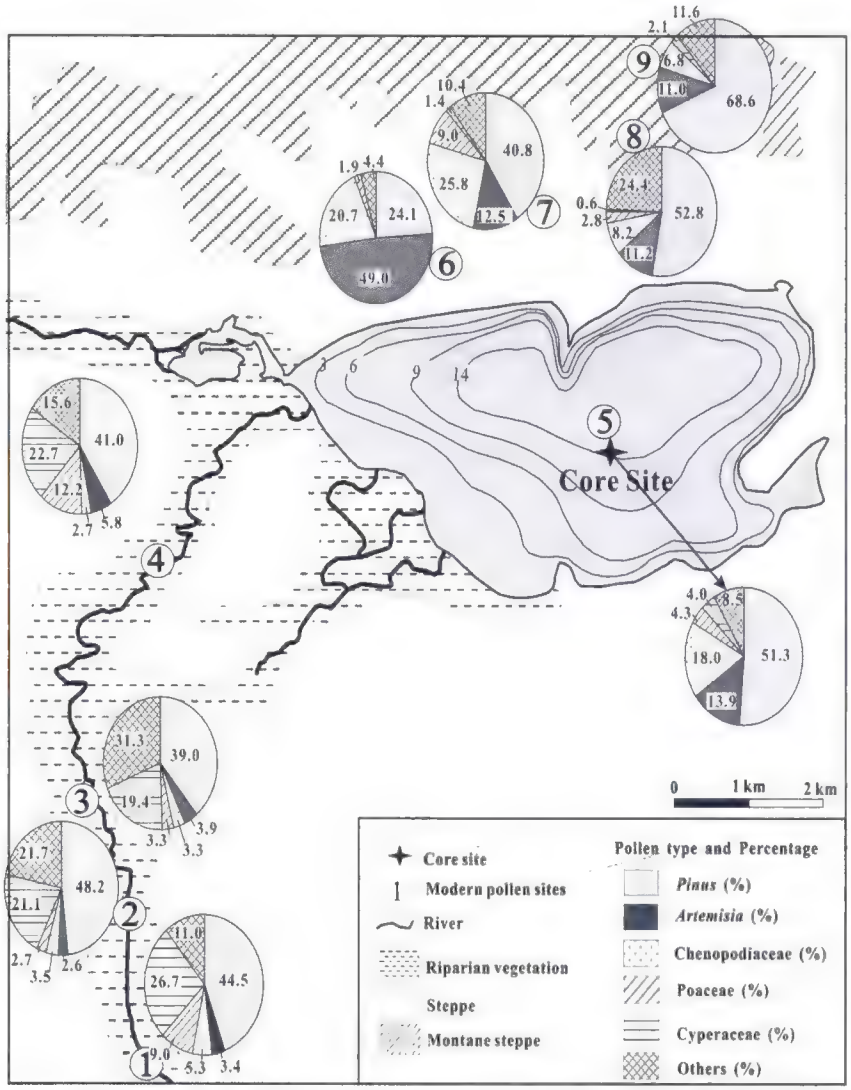

Fig. 2. Surface pollen sampling sites and associated pollen assemblages. Sampling sites 1–4: inflowing river surface sediments, sampling site 5: topmost sediment of lake core, sampling sites 6 and 7: top soil samples from *Stipa*-dominated steppes in foothill piedmont of lower elevations, sampling sites 8 and 9: top soil samples from montane steppes of higher elevations (from Wang et al., 2009).

tablet (Lund University, Batch No. 938934) was added before extraction for calculation of the pollen concentration (Stockmarr, 1971). Pollen types were identified with references of key books (Erdtman, 1969; Moore et al., 1991; Wang et al., 1995) and a total of 52 families or genera were identified. More than 350 pollen grains (not including spores) were counted for each sample and the percentage was calculated based on the sum of terrestrial pollen. Pollen percentage diagram and total pollen concentration were plotted against depth using Grapher 2.0. Cluster analysis (CONISS) was conducted to provide references for pollen zone divisions (Bennett, 1996). Diatom extraction procedures include boiling samples in 25% HCl, rinsing in distilled water and treating with 30% H_2O_2. Further decantation (settling for 5 seconds) was allowed to remove coarse particles for final suspension (Koc et al., 1993; Stoermer and Smol, 1999). Diatom valves were counted along ten random transects across the slide and counting continued until 300 valves were reached for diatom-poor samples (Schrader and Gersonde, 1978). Identification and ecological preferences of the diatom species were taken mainly from published literature (Gasse, 1986; Krammer and Lange-Bertalot, 1986–1991; Camburn and Charles, 2000). Particle size of bulk sample was measured using the Malvern Co. Ltd. Mastersizer 2000 laser diffraction particle size analyzer. Radiocarbon dating was conducted on bulk sediments at the NSF-Arizona AMS Facility, USA.

Pollen-based temperature (T) and moisture (M) indices, which was developed based on the survey of 104 modern surface pollen samples collected along a north-south transect in Mongolia (Ma et al., 2008), was employed to reconstruct temperature and moisture sequences. These two indices were calculated based on the ratios between groups of pollen taxa that represent different moisture or/and temperature conditions in the Mongolian Plateau. Specifically, the main pollen taxa of the surface samples were classified into six bioclimatic groups (S1, S2, S3, S4, S5 and S6) largely based on the numerical analysis (including hierarchical cluster analysis (HCA) and Non-metric multidimensional scaling (NMS)) and the ecological conditions of their parent plants (see Table 1), and T and M indices are then calculated using the following two equations:

$$T = (S1 + S2 + S3)/(S4 + S5 + S6) \quad \text{and}$$

$$M = (S5 + S6)/(S1 + S2 + S3 + S4)$$

4. Results

4.1. Modern pollen data

Fig. 2 shows that all modern pollen assemblages have relatively high percentages of *Pinus* pollen, ranging between ~30% and ~70%. As there are no pine forests or pine-associated forest-steppes developed around the lake and in the watershed, the *Pinus* pollen must have been transported by wind from the nearest pine-dominated forest-steppes ~80 km away to the north. *Pinus* pollen is thus over-represented in the pollen spectrum, further confirming the widely-reported over-representation problem of *Pinus* pollen (Wu and Xiao, 1995; Wang et al., 1996; Ma et al., 2008).

In contrast, the modern pollen survey indicates that the pollen percentages of Chenopodiaceae are higher in the piedmont steppes under relatively drier conditions (samples 6 and 7 in Fig. 2) than those of inflowing river surface sediment samples (samples 1–4 in Fig. 2) and montane steppes (samples 8 and 9 in Fig. 2). The data seem to be consistent with published data, in showing that Chenopodiaceae pollen percentage and its relative abundance can be considered as acceptable aridity proxies in arid and semiarid areas. For example, the Chenopodiaceae pollen percentage and Chenopodiaceae plant abundance were demonstrated to have increased from steppes to desert steppes in the Mongolian Plateau (Gunin et al., 1999; Pyankov et al., 2000; Ma et al., 2008). The *C/A* ratio (Chenopodiaceae/*Artemisia*) has been shown to be an acceptable aridity index in the arid and semiarid Middle East and northern Tibetan Plateau (El-Mosilimany, 1990; Van Campo et al., 1996; Liu et al., 1998). In addition, the pollen percentage ratio ($[C+A]/P$) of the combined Chenopodiaceae and *Artemisia* ($C+A$) to Poaceae (P) was also used to indicate aridity in the Lake Telmen study in central Mongolia (Fowell et al., 2003). However, extra caution should be observed in use of these pollen ratios in such situations, as in long-distance wind-blown pollen-dominated or mountain river-transported pollen-dominated situations (Sun et al., 1994; Ma et al., 2005).

Poaceae has been well demonstrated to be under-represented in pollen spectra in the southern Mongolian Plateau (Liu et al., 1999) and also in the northern Mongolian Plateau (Gunin et al., 1999). The modern pollen data also show that Poaceae pollen percentages are rather low, being below 10% in eight of the nine samples (sample 4 is an exception), although Poaceae plants dominate the zonal vegetation around the lake area. Cyperaceae is a typical component in montane meadows and wetland meadows (Hilbig, 1995; Gunin et al., 1999). An increase in Cyperaceae pollen percentage may thus suggest an expansion of wetland meadows or/and montane meadows, reflecting a cool or/and humid climate (Fowell et al., 2003). It seems that the pollen assemblage of the uppermost sediment of the lake core (sample 5) reasonably represents the pollen components from different processes: *Pinus* pollen from long-distance, Cyperaceae from riverbank and lakeshore wetland meadows (probably also from montane steppes), and Chenopodiaceae and *Artemisia* from steppes.

Table 1
Pollen groups (S1–S6) used for calculation of pollen-climate indices (Ma et al., 2008).

Group	Type	Main pollen taxa
S1	Xeromorphic desert	Chenopodicaceae, *Nitraria*, Zygophyllaceae
S2	Desert-steppe	*Polemoniaceae, Anthemis-type*, Liliaceae, *Ephedra, Convolvulus*
S3	Meso-xeromorphic steppe	*Artemisia, Aster*-type
S4	Birch forest/shrubs	*Betula, Alnus*, Rosaceae, *Taraxacum*-type
S5	Cold-moist needled forest	*Picea, Abies, Pinus-Haploxylon*-type, *Pinus-Diploxylon*-type, *Larix*, Ranunculaceae, Caryophyllaceae
S6	Moderate hydroperiod steppe	Cyperaceae, Polygonaceae

4.2. Lithology and chronology

The core can be divided into three sediment units based on visual observation and laboratory-analyzed grain size data (Fig. 3). Sediment Unit 1 (854–484 cm) consists of grey-brown clayey silt with median size (Md) ranging from 5 to 20 μm and sand content less than 2%. Sediment Unit 2 (484–242 cm) is a light-grey silt layer containing two carbonate-rich sub-units (at 450–492 cm and at 368–348 cm). The median size (Md) ranges from 15 to 50 μm with an average of ~30 μm, and sand percentage up to 16% (mean = ~8%). Sediment Unit 3 (242–0 cm) is a grey clayey silt layer with the median size (Md) ranging from 5 to 15 μm, and sand content below 1%.

Fourteen AMS ^{14}C dates were obtained (Table 2) and age-depth models established by statistically best-fitting methods for three sedimentary units according to the variations of grain size and lithology (see details in the captions of Fig. 3). Based on these age

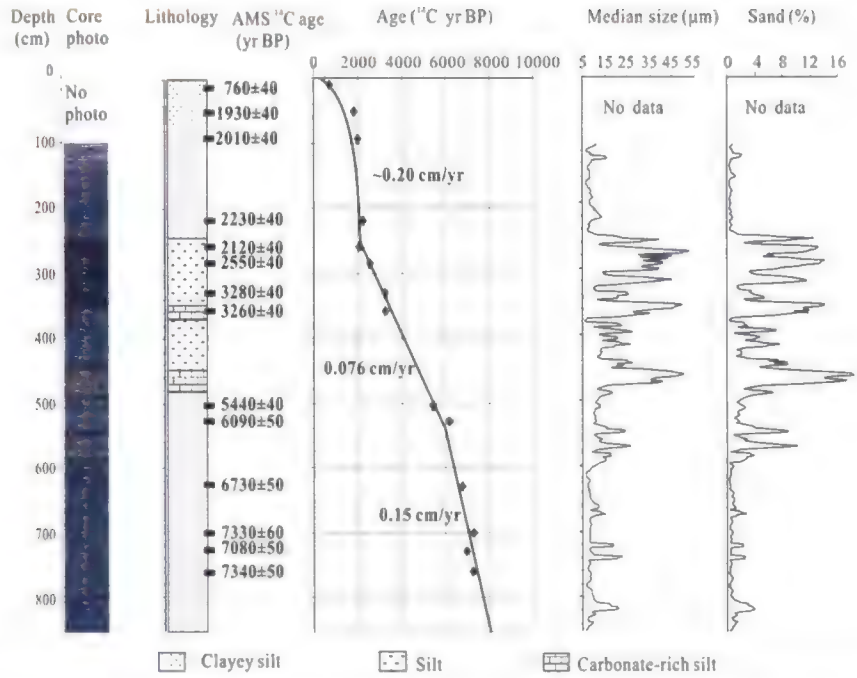

Fig. 3. Litho-stratigraphy (with photo), AMS dates and the corresponding grain size data (median size and sand percentage) of Ugii Nuur core (notes: six dates (i.e., 760, 1930, 2010, 2230, 2120, 2550 ^{14}C yr BP) were used to develop a best-fitting curvilinear (a log relation) model (R^2 = 0.9259) for the upper part (0–242 cm), and seven dates (i.e., 2230, 2120, 2550, 3280, 3260, 5440, 6090 ^{14}C yr BP) were used to generate a linear model (R^2 = 0.974) for the middle part (484–242 cm), and six dates (i.e., 5440, 6090, 6730, 7330, 7080, 7340 ^{14}C yr BP) were used to produce a linear model for the lower part (484–854 cm) (R^2 = 0.879)).

models, deposition rates were calculated for different sediment units. Specifically, the average deposition rates are ~0.20, 0.076 and 0.15 cm/y for the Sediment Unit 3 (0–242 cm), Unit 2 (242–484 cm) and Unit 1 (484–854 cm) respectively. The low deposition rate of the middle coarse portion (242–484 cm) was proposed to be related to a low-level inflow and shallow water under a persistent drought. The extrapolated age of the bottom (854 cm) is 8120 ^{14}C BP.

4.3. Fossil pollen and diatom data

Three pollen assemblage zones were recognized based on visual inspection and CONISS analysis (Fig. 4). Pollen Zone 1 (854–530 cm; 8120–5830 ^{14}C BP), which is approximately correspondent to the grey-brown clayey silt layer (Sediment Unit 1: 854–484 cm), is characterized by a moderate percentage of Chenopodiaceae pollen and high percentages of Poaceae and Cyperaceae pollen. Mesophytic forbs (e.g., Ranunculaceae, *Thalictrum*, *Sanguisorba*, *Taraxacum*-type, *Aster*-type, etc.) are well expressed although the percentages are rather low.

Pollen Zone 2 (530–320 cm; 5830–3080 ^{14}C BP) approximately corresponds with the light-grey silt layer (Sediment Unit 2: 484–242 cm) in which the calculated deposition rate is the lowest (0.076 cm/y) of the entire core. The pollen assemblage is characterized by the highest Chenopodiaceae pollen percentage and the lowest Cyperaceae and Poaceae pollen percentages with the highest pollen concentration of the entire core. The mesophytic forbs pollen percentages decrease and *Ephedra* pollen percentage increases relative to Pollen Zone 1.

Pollen Zone 3 (320–0 cm; 3080–0 ^{14}C BP) approximately corresponds with the grey clayey silt layer (Sediment Unit 3: 242–0 cm). The pollen percentages of *Pinus*, *Artemisia*, Cyperaceae and Poaceae increase remarkably at the expense of Chenopodiaceae, and the mesophytic forbs pollen increases both in percentages and types whereas *Ephedra* nearly completely disappeared.

Three diatom zones were recognized on the basis of the variations in the abundance of planktonic and benthic genera (Fig. 5). Diatom Zone 1 (854–575 cm; 8120–6200 ^{14}C BP), approximately corresponding with the Sediment Unit 1 (854–484 cm), is shared by planktonic and benthic genera. The planktonic genera include *Aulacoseira granulata* (Ehr.) Simonsen, *A. alpigena* (Grunow) Krammer, *Stephanodiscus spp.* and *Cyclotella ocellata*, and the benthic genera consist of *Ellerbeckia arenaria* (Moore) Crawford, *Cocconeis* (3 taxa) and *Epithemia* (3 taxa). The ratio of planktonic to

Table 2
AMS dates of the Ugii Nuur core (all dated at the Arizona NSF AMS Facility).

Laboratory no.	Sample no.	Depth (cm)	Dating material	Delta^{13}C	^{14}C age (yr BP)
AA81667	UG3–5	3–5	Sediment	−24.8	756 ± 36
AA81668	UG45–46	45–46	Sediment	−25.9	1929 ± 39
AA81669	UG86–87	86–87	Sediment	−26.1	2014 ± 38
AA64246	UG224	224–225	Sediment	−28.7	2228 ± 36
AA64247	UG260	260–261	Sediment	−20.9	2117 ± 38
AA64248	UG290	290–291	Sediment	−25	2549 ± 36
AA64249	UG330	330–331	Sediment	−26.7	3283 ± 43
AA64250	UG360	360–361	Sediment	−18.7	3260 ± 44
AA64255	UG504	504–505	Sediment	−28.2	5442 ± 39
AA64256	UG533	533–534	Sediment	−28.8	6091 ± 49
AA64260	UG630	630–631	Sediment	−26.5	6727 ± 45
AA64262	UG700	700–701	Sediment	−27.2	7325 ± 70
AA64263	UG730	730–731	Sediment	−27.9	7077 ± 53
AA64264	UG760	760–761	Sediment	−28	7341 ± 54

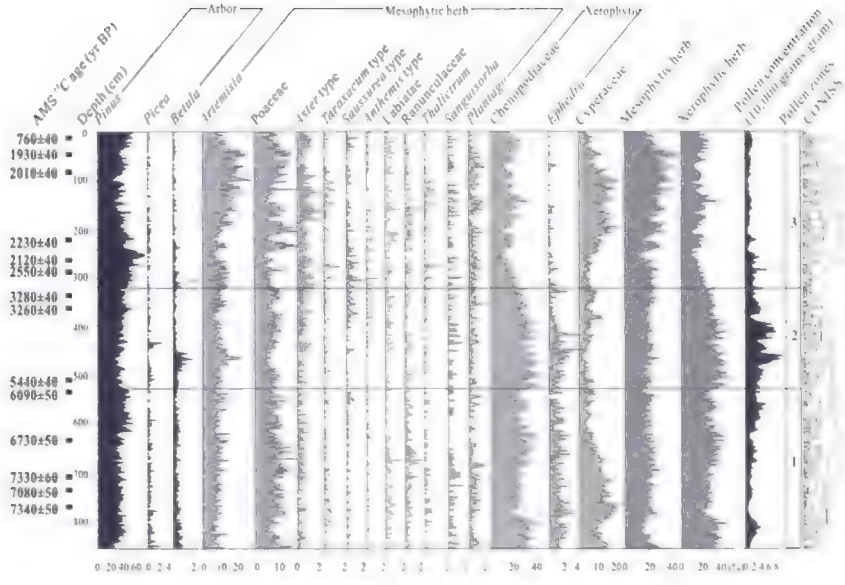

Fig. 4. Pollen percentage diagrams of Ugii Nuur core (adopted from Wang et al., 2009).

benthic diatoms is relatively high, ranging between 10 and 40 with an average value of ~20.

Diatom Zone 2 (575–250 cm; 6200–2340 ^{14}C BP), approximately corresponding with the Sediment Unit 2 (484–242 cm), is characterized by a drastic decrease in planktonic genera. Three (*Aulacoseira alpigena* (Grunow) Krammer, *Stephanodiscus spp.* and *Cyclotella ocellata*) of the four planktonic genera (Fig. 5) nearly completely disappeared and *Aulacoseira granulata* (Ehr.) Simonsen is reduced to merely detectable levels. Two benthic genera (*Cocconeis* and *Epithemia*) in the zone 2 exhibits an observable increase relative to the zone 1 and the ratio of planktonic to benthic diatoms declines to the lowest level of the entire core, the average being below 5.

Diatom Zone 3 (250–100 cm; 2340–2010 ^{14}C BP), corresponding with the Sediment Unit 3 (242–0 cm), shows planktonic abundance (mainly *Aulacoseira granulate* (Ehr.) Simonsen). The ratio of planktonic to benthic diatoms increase significantly with an average of ~40.

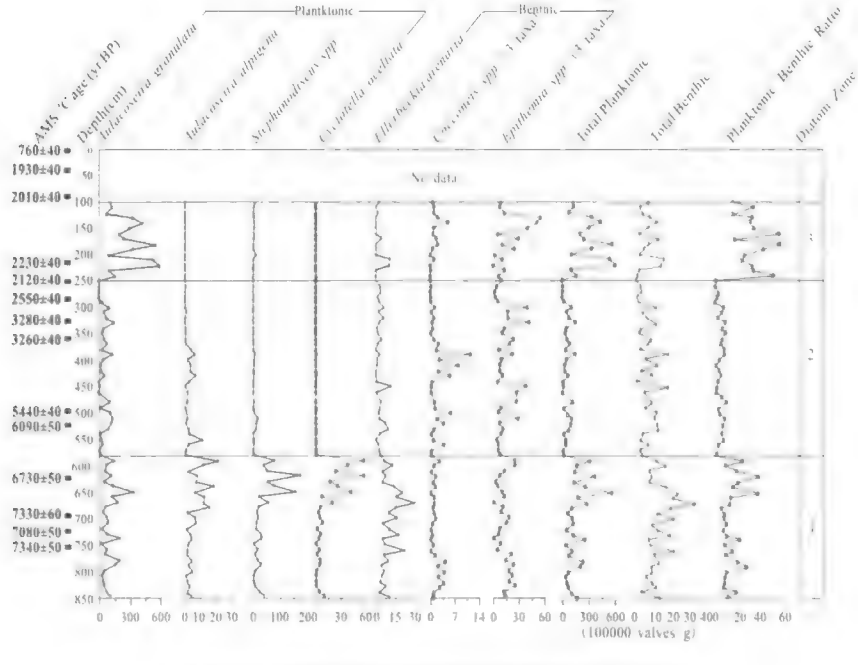

Fig. 5. Diatom abundance diagrams of planktonic and benthic genus in Ugii Nuur core.

5. Discussion and conclusions

5.1. Mid-Holocene prolonged drought in central Mongolia

Tarasov et al. (1999) documented a warmer-summer and drier mid-Holocene (around 6000 ^{14}C BP) in central Mongolia. Fowell et al. (2003) reported, primarily based on the data of 40 pollen samples from Lake Telmen, that a mid-Holocene drought occurred between ~6090 and ~4100 ^{14}C BP. In order to validate (or invalidate) the notion of the mid-Holocene being dry and further investigate the details of mid-Holocene climate in central Mongolia, three pollen-based aridity indices were calculated and then compared with diatom data and sedimentary data to ascertain the best effective aridity index for interpreting the Holocene bioclimatic changes from Ugii Nuur core.

First, the ratio ($[C+A]/P$) of the combined Chenopodiaceae and *Artemisia* ($C+A$) to the Poaceae (P) pollen percentage, which was used in the Lake Telmen study (Fowell et al., 2003), was calculated (diagram C in Fig. 6). A pronounced drought, as indicated by the peak $(C+A)/P$ ratio, appears to have occurred between ~5400 and ~4800 ^{14}C BP. Nevertheless, it should be cautioned that the $(C+A)/P$ ratio was developed in the Lake Telmen area where *Artemisia* pollen absolutely dominates the pollen spectrum under a wetter condition (i.e., in Telmen lake area) of montane steppes (Hilbig, 1995; Fowell et al., 2003) and that the sensitivity of the $(C+A)/P$ ratio as an aridity index may be reduced in drier conditions (e.g., in Ugii Nuur area of dry steppes) where Chenopodiaceae pollen dominates the pollen spectra. In other words, either increased *Artemisia* percentage (A) or/and increased Chenopodiaceae percentage (C) will elevate the $(C+A)/P$ ratio, implying that $(C+A)/P$ ratio is not useful to distinguish an *Artemisia*-dominated wetter steppe condition from a Chenopodiaceae-dominated drier steppe condition.

The $(C+A)/P$ ratio as an aridity index is contradicted by the C/A ratio as expected, the latter (C/A ratio) being widely regarded as an acceptable aridity index for arid and semiarid areas. The observed general anti-phase relationship between *Artemisia* (A) and Chenopodiaceae (C) throughout the entire Ugii Nuur core (see Fig. 4) seemingly suggests that the C/A ratio may be a more reasonable aridity index, and the index suggests a dry phrase between ~5920 and ~3400 ^{14}C BP (diagram D in Fig. 6). However, the C/A ratio might also be problematic especially for Pollen Zone 1 in which the *Artemisia* pollen percentages are normally lower than 10%. As a result, the C/A ratio-inferred aridity of Pollen Zone 1 seems to be considerably exaggerated. In order for the C/A ratio to work as an acceptable aridity index, *Artemisia* has to be a wet-indicative component. However, the observed anti-phase relationship of the *Artemisia* pollen percentage with the pollen percentages of undisputable wet components (including Poaceae, Cyperaceae and mesophytic forbs pollen percentages) in Pollen Zone 1 simply suggests that the *Artemisia* pollen represents a dry condition within Pollen Zone 1. Nevertheless, the C/A ratio as an aridity index seems to work properly for Pollen Zones 2 and 3, because the variations of *Artemisia* pollen percentage are in phase with those of the undisputable wet components (including Poaceae, Cyperaceae and mesophytic pollen percentages) and are in anti-phase with those of xerophytic pollen percentages (i.e. *Ephedra*) within these two zones.

Furthermore, the pollen-based moisture and temperature indices developed on the basis of 104 uppermost soils along the N–S transect throughout Mongolia (Ma et al., 2008) should be applicable to the Ugii Nuur core because the site is located at the middle of the uppermost soil transect of Ma et al. (2008). First, the moisture index was calculated to reconstruct the moisture sequence and then calculated temperature index to constrain our interpretation of moisture index. Two observations can be made from the calculated indices (diagrams E and F in Fig. 6). First, Pollen Zone 2 (530–320 cm; 5830–3080 ^{14}C BP) has a higher temperature index and lower moisture index than Pollen Zone 1 (854–530 cm; 8120–5830 ^{14}C BP) and Pollen Zone 3 (320–0 cm; 3080–0 ^{14}C BP).

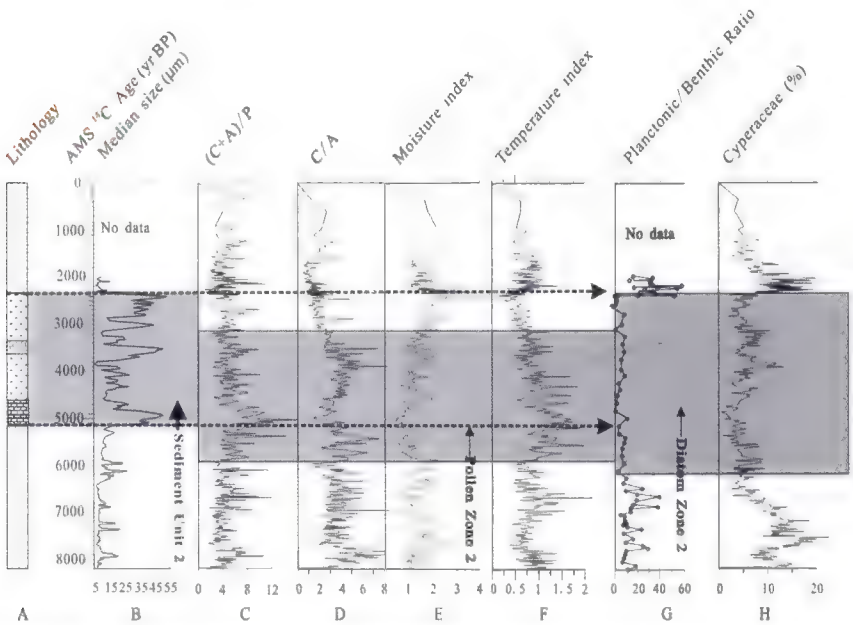

Fig. 6. Pollen-based bioclimatic indices (including $[C+A]/G$ ratio, C/A ratio, Moisture Index and Temperature Index) from Ugii Nuur core with reference to the lithology and chronology. Also included are the ratio of planktonic and benthic diatoms and the percentage of Cyperaceae.

Second, the overall trend of the moisture index is in anti-phase with the overall trend of the temperature index. The first observation convincingly demonstrates that a prolonged drought did occur between 5830 and 3080 ^{14}C BP in central Mongolia. The second observation may imply that the variation in the moisture might have been directly related to the variation in the temperature, meaning that the available moisture might have been primarily controlled by temperature-dictated evaporation.

To further understand the mid-Holocene prolonged drought in the Ugii Nuur area, special attention should be paid to the phase relationships among Sediment Unit 2 (484–242 cm; 5120–2330 ^{14}C BP), Pollen Zone 2 (530–320 cm; 5830–3080 ^{14}C BP), and Diatom Zone 2 (575–250 cm; 6200–2340 ^{14}C BP). Diatom Zone 2 (575–250 cm) with a low ratio of planktonic to benthic diatoms (diagram G in Fig. 6) suggests that the water depth of Ugii Nuur was rather low between ~6200 and ~2340 ^{14}C BP, lasting for ~3860 ^{14}C years. The long-lasting shallow-water period was further confirmed by a mirror record of Cyperaceae pollen percentage (diagram H in Fig. 6). The dramatic decrease in Cyperaceae pollen percentage between ~6200 and ~2340 ^{14}C BP most likely resulted from drought-related contraction of riverbank and lakeshore wetlands (probably also including contraction of montane steppes). It can be further concluded from Fig. 6 that the diatom-indicated drought started first at ~6200 ^{14}C BP, and that the pollen-indicated vegetation then started to deteriorate in response to the diatom-indicated drought at ~5830 ^{14}C BP, the latter (vegetation) being delayed for ~370 ^{14}C years. The sediment started to respond to the vegetation deterioration at ~5120 ^{14}C BP, the latter (sediment) being delayed for ~700 ^{14}C years. The sediment-indicated ending time of the prolonged mid-Holocene drought is ~2340 ^{14}C BP and the diatom-indicated ending time is ~2330 ^{14}C BP, the two being almost synchronous. The pollen-indicated ending time of the prolonged drought is ~3080 ^{14}C BP, suggesting that the post-drought vegetation amelioration started about ~750 ^{14}C years earlier than the diatom-indicated water-level rise and the associated sediment change did. To sum up, a general mid-Holocene drought seems to have spanned from ~6200 to ~2340 ^{14}C BP as indicated by diatom data, and the drought seems to have peaked between ~5830 and ~3080 ^{14}C BP as indicated by pollen records and pollen-based moisture index (i.e., Moisture index in Fig. 6). A conservatively estimated time span of the mid-Holocene drought is the period between ~5120 and ~3080 ^{14}C BP, as indicated by an overlap of all three sets of data (i.e., Sediment Unit 2, Pollen Zone 2, and Diatom Zone 2).

The pollen concentration data do not seem to support the aforementioned interpretation of mid-Holocene prolonged drought. The highest pollen concentration in the Pollen Zone 2 (530–320 cm, 5830–3080 ^{14}C BP) occurred in the inferred drought period when the deposition rate (0.076 cm/y) is lower and the grain size is coarser in relation to the preceding and following periods. This unexpected high pollen concentration within Sediment Unit 2 is at least partially attributable to the lower deposition rate and the drought-resultant lake contraction. Low deposition rates during the prolonged drought might have more effectively concentrated pollen grains in the contracted lake.

5.2. Regional comparison of mid-Holocene drought

The existing data show that a warm and wet climate characterized the mid-Holocene in semiarid northern China (see Feng et al., 2006 and the references therein) and a wet (and probably warm) climate characterized the mid-Holocene in the sub-humid northern Mongolian Plateau and adjacent southern Siberia (Harrison et al., 1996; Tarasov et al., 1999, 2000; Horiuchi et al., 2000; Demske et al., 2005). However, more recently-studied and relatively well-dated Holocene climatic sequences suggest that a prolonged drought might have prevailed extensively in the central-east Asian arid and hyper-arid areas during the mid-Holocene.

The following discussion will focus on four well-dated Holocene sequences from the northern margin and four well-dated Holocene sequences from the southern margin of the arid and hyper-arid areas (Fig. 7) to illustrate that the central-east Asian arid and hyper-arid areas were probably devastated by a prolonged drought during the mid-Holocene. The reconstructed lowest soil moisture and lowest lake level period occurred between 5830 and 3080 ^{14}C BP in Ugii Nuur area of central Mongolia (diagram A in Fig. 7) and this record confirmed the pollen-documented mid-Holocene drought occurred between ~6090 and ~4100 ^{14}C BP in the Lake Telmen area of central Mongolia (diagram B in Fig. 7, see Fowell et al., 2003 and Peck et al., 2002). Pollen and strata data from an aeolian sequence at Sharmmar also indicate a mid-Holocene drought in the Baikal–Ulan Bator corridor between ~7000 and ~3000 ^{14}C BP (diagram C in Fig. 7; see Feng et al., 2007). Pollen data from Lake Hovsgol suggest that a natural deforestation and accompanying steppe expansion occurred between ~6000 and ~3500 cal. BP (~5300–3300 ^{14}C BP) in the Lake Hovsgol watershed (diagram D in Fig. 7, see Prokopenko et al., 2007).

In the southern margin of the central-east Asian arid and hyper-arid areas, the mid-Holocene drought is also extensively documented. Pollen data from Lake Manas (northern Xinjiang, northwestern China) show that a pronounced drought, as indicated by depressed pollen *A/C* ratio, occurred between ~6000 and ~4500 ^{14}C BP (diagram E in Fig. 7, see Rhodes et al., 1996). Two recently-studied and well-dated Holocene lacustrine records from the Alashan Plateau indicate that the mid-Holocene was also characterized by dry climates. Specifically, a multi-proxy analysis of lake core from Lake Juyanze shows that the Holocene lake level and runoff factor reached the minimum between ~7600 and ~5400 cal. BP (~6700–~4700 ^{14}C BP), suggesting a dry mid-Holocene (diagram F in Fig. 7, see Hartmann and Wünnemann, 2009). Pollen data (pollen concentration and *Nitraria* pollen percentage) from Lake Zhuyeze suggest that a prolonged drought occurred between ~7100 and ~3800 cal. BP (~6200–~3500 ^{14}C BP) (diagram G in Fig. 7, see Chen et al., 2006). A dry mid-Holocene climate between ~8000 and ~4000 ^{14}C BP was also reported from the northern tip (i.e., Lake Yanhaizi) of the Erdos Plateau based on sedimentary and geochemical data (diagram H in Fig. 7; see Chen et al., 2003a).

Two preliminary conclusions can be drawn from the aforementioned review. First, a prolonged drought might have prevailed extensively in the central-east Asian arid and hyper-arid areas during the mid-Holocene (approximately between ~6000 and ~3000 ^{14}C BP). Second, the prolonged drought had extended to the semiarid areas of the northern Mongolian Plateau (i.e., central Mongolia), although it did not seem to have extended to the semiarid areas of northern China where a warm and wet climate prevailed during the mid-Holocene. The prolonged mid-Holocene drought in the central-east Asian arid and hype-arid areas might have been resulted from the well-documented large-scale temperature rise (see Shi et al., 1993 and the references thereafter). That is, the temperature rise-dictated increase in evaporation might have exceeded the precipitation increase (if any) in the arid and hyper-arid areas, resulting in the aridity increase. However, the large-scale mid-Holocene temperature rise might have been responsible for the dramatically decreased aridity that was resulted from precipitation increase in the semiarid northern China under strengthened monsoon influences (Feng et al., 2006, 2007). The mid-Holocene temperature rise might have also been responsible for the available moisture increase in the sub-humid northern

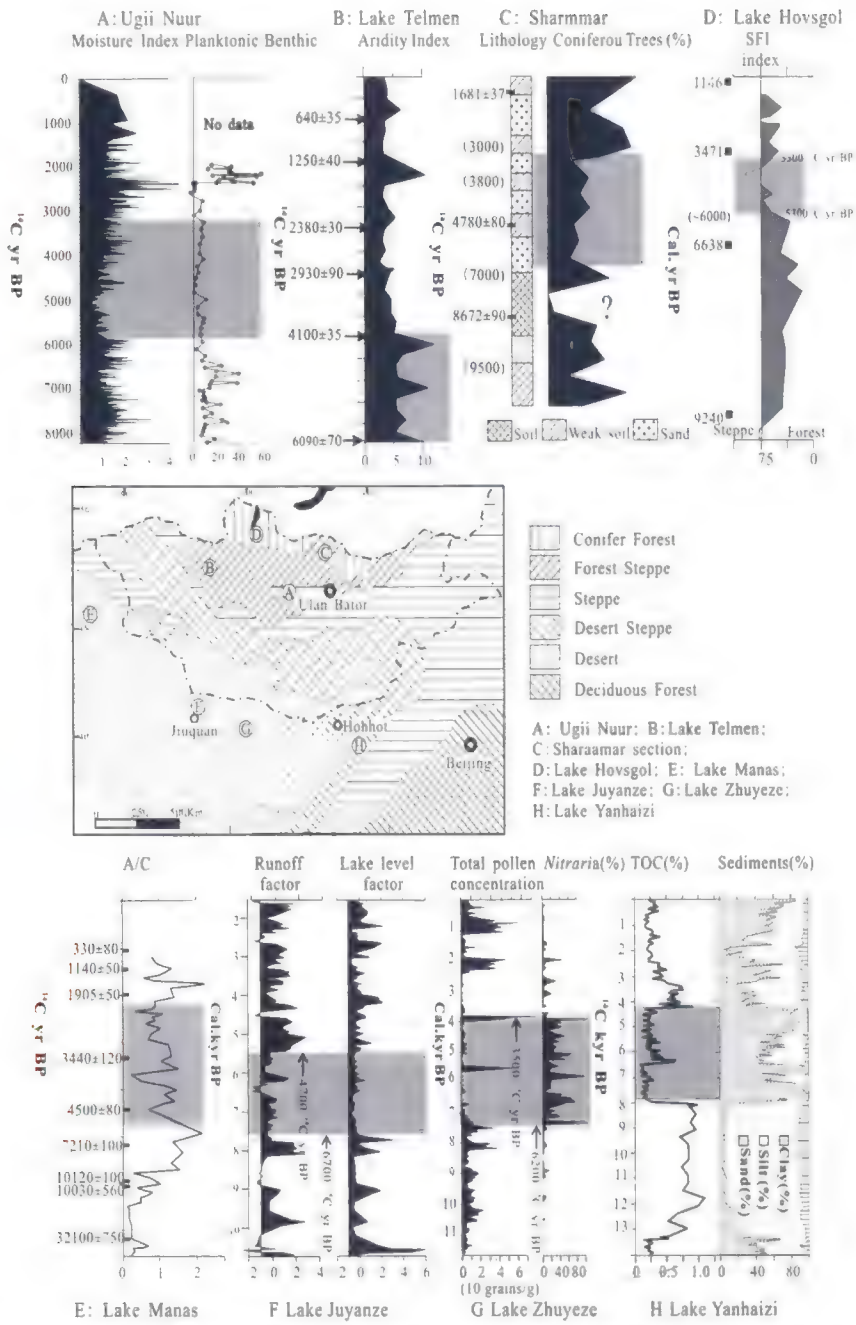

Fig. 7. A review of mid-Holocene climate records from Mongolia and northwestern China (upper panel: records from Mongolia; middle-panel: map showing bioclimatic boundaries and reviewed record sites; low-panel: records from northwestern China). Diagram A: pollen-based moisture index sequences and diatom records from Ugii Nuur (this paper); diagram B: pollen-based aridity index from Lake Telmen; diagram C: lithology and conifer pollen content from Sharmmar eolian section; and diagram D: steppe-forest index from Lake Hovsgol (diagrams A–D in upper panel). Diagram E: A/C ratio from Lake Manas; diagram F: water level and runoff factor from Lake Juyanze, diagram G. pollen concentration and *Nitraria* pollen percentage from Lake Zhuyeze; and diagram H: total organic matter content and sediment texture records from Lake Yanhaizi (diagrams E-H in lower panel).

Mongolian Plateau and the adjacent Siberia probably by enhancing the recycling processes of regionally evaporated water vapor (Lydolph, 1977) and the enhanced water-vapor recycling processes did not seem to have significantly influenced the semiarid central Mongolia. Finally, the aforementioned preliminary conclusion of "prolonged mid-Holocene drought of the central-east Asian arid and hyper-arid areas" is based on the data from the northern margin and the southern margin. More extensive investigations are thus needed from the core areas of the arid and hyper-arid areas to validate (or invalidate) this preliminary conclusion.

Acknowledgements

This paper is a result of projects supported by three Chinese NSF grants (No: 40331012, 40671190, 40701193) and three U.S. NSF grants (NSF-ESH-04-02509, NSF-BCS-06-23478, NSF-BCS00-78557). Thanks also were given to late Prof. Khosbayar for field help and data collection.

References

Bennett, K.D., 1996. Determination of the number of zones in a biostratigraphical sequence. New Phytologist 132, 155–170.

Broecher, W.S., 2003. Does the trigger for abrupt climate change reside in the ocean or in the atmosphere? Science 300, 1519–1922.

Camburn, K.E., Charles, D.F., 2000. Diatoms of Low-alkalinity Lakes in the Northeastern United States. The Academy of Natural Sciences of Philadelphia, Philadelphia.

Chen, C.-T.A., Lan, H.-C., Lou, J.-Y., Chen, Y.-C., 2003a. The dry Holocene Megathermal in Inner Mongolia. Palaeogeography, Palaeoclimatology, Palaeoecology 193, 181–200.

Chen, F.H., Wu, W., Holmes, J.A., Madsen, D.B., Zhu, Y., Jin, M., Oviatt, C.G., 2003b. A mid-Holocene drought interval as evidenced by lake desiccation in the Alashan Plateau, Inner Mongolia, China. Chinese Science Bulletin 48, 1401–1410.

Chen, F.H., Cheng, B., Zhao, Y., Zhu, Y., Madsen, D.B., 2006. Holocene environmental change inferred from a high-resolution pollen record, Lake Zhuyeze, arid China. The Holocene 16 (5), 675–684.

Demske, D., Heumann, G., Granoszewski, W., Nita, M., Mamakowa, K., Tarasov, P.E., Oberhänsli, H., 2005. Late glacial and Holocene vegetation and regional climate variability evidenced in high-resolution pollen records from Lake Baikal. Global and Planetary Change 46, 255–279.

El-Mosilimany, A.P., 1990. Ecological significance of common non-arboreal pollen: examples from drylands of the Middle East. Review of Palaeobotany and Palynology 64, 343–350.

Erdtman, G., 1969. Handbook of Palynology. Munksgaard, Copenhagen.

Faegri, K., Iversen, J., 1975. Textbook of Pollen Analysis. Munksgaard, Copenhagen.

Feng, Z.-D., An, C.B., Wang, H.B., 2006. Holocene climatic and environmental changes in the arid and semi-arid areas of China: a review. The Holocene 16 (1), 1–12.

Feng, Z.-D., Zhai, X.W., Ma, Y.Z., Huang, C.Q., Wang, W.G., Zhang, H.C., Khosbayar, P., Narantsetseg, T., Liu, K.-B., Rutter, N.W., 2007. Eolian environmental changes in the Northern Mongolian Plateau during the past ~35,000 yr. Palaeogeography, Palaeoclimatology, Palaeoecology 245, 505–517.

Fowell, S.J.B., Hansen, B.C.S., Peck, J.A., Khosbayar, P., Ganbold, E., 2003. Mid to late Holocene climate evolution of the Lake Telmen Basin, North Central Mongolia, based on palynological data. Quaternary Research 59, 353–363.

Gasse, F., 1986. East African diatoms: taxonomy, ecological distribution. In: Bibliothecta Diatomologica, Band 11. J. Cramer, Berlin.

Gunin, P.D., Vostokova, E.A., Dorofeyuk, N.I., Tarasov, P.E., Black, C.C., 1999. Vegetation dynamics of Mongolia. Geobotany 26. Kluwer Academic Publishers, Dordrecht. 238.

Harrison, S.P., Yu, G., Tarasov, P.E., 1996. Late Quaternary lake-level record from northern Eurasia. Quaternary Research 45, 138–159.

Hartmann, K., Wünnemann, B., 2009. Hydrological changes and Holocene climate variations in NW China, inferred from lake sediments of Juyanze palaeolake by factor analyses. Quaternary International 194, 28–44.

Hilbig, W., 1995. The Vegetation of Mongolia. SPB Academic Publishing, Amsterdam.

Horiuchi, K., Minoura, K., Hoshino, K., Oda, T., Nakamura, T., Kawai, T., 2000. Palaeoenvironmental history of Lake Baikal during the last 23000 years. Palaeogeography, Palaeoclimatology, Palaeoecology 157, 95–108.

Koc, N., Jansen, E., Haflidason, H., 1993. Paleoceanographic reconstructions of surface ocean conditions in the Greenland, Iceland and Norwegian seas through the last 14 ka based on diatoms. Quaternary Science Reviews 12, 115–140.

Krammer, K., Lange-Bertalot, H., 1986–1991. Bacillariophyceae. In: Ettl, H., Gerloff, J., Heynig, H., Mollenhauser, D. (Eds.), Süßwasserflora von Mitteleuropa, Band 2 (1–4). Gustav Fisher Verlag, Stuttgrat/Jena.

Lavrenko, E.M., Iunatov, A.A., Aleksandr, A., Dashniam, B., 1979. Vegetation map of Mongolian People's Republic (Scale 1: 1,500,000) Moscow (in Russian).

Li, X.Q., Zhou, W.J., An, Z.S., Dodson, J., 2003. The vegetation and monsoon variations at the desert loess transition belt at Midiwan in northern China for the last 13 ka. The Holocene 13 (5), 779–784.

Liu, H.Y., Cui, H.T., Pott, R., Speier, M., 1999. The surface pollen of the woodland-steppe ecotone in southeastern Inner Mongolia, China. Review of Palaeobotany and Palynology 105, 237–250.

Liu, K.-B., Reese, C.A., Thompson, L.G., 1998. A pollen record of Holocene climatic changes from the Dunde ice cap, Qinghai-Tibetan Plateau. Geology 26, 135–138.

Lydolph, P.E., 1977. Climates of the Soviet Union. In: Landsberg, H.E. (Ed.), World Survey of Climatology 7. Elsevier Publishing Company, Amsterdam, pp. 1–443.

Ma, Y.Z., Fang, X.M., Li, J.J., Wu, F.L., Zhang, J., 2005. The vegetation and climate change during Neocene and Early Quaternary in Jiuxi Basin, China. Science in China (Series D) 48 (5), 676–688.

Ma, Y.Z., Liu, K.-B., Feng, Z.D., Sang, Y.L., Wang, W., Sun, A.Z., 2008. A survey of modern pollen and vegetation along a south–north transect in Mongolia. Journal of Biogeography 35, 1512–1532.

Moore, P.D., Webb, J.A., Collinson, M.E., 1991. Pollen Analysis, second ed. Blackwell Scientific Publications, Oxford.

Oppo, D.W., McManus, J.F., Cullen, J.L., 2003. Deepwater variability in the Holocene epoch. Nature 422, 277–278.

Peck, J.A., Khosbayar, P., Fowell, S.J., Pearce, R.B., Ariunbileg, S., Hansen, B.C.S., Soninkhishig, N., 2002. Mid to Late Holocene climate change in north central Mongolia as recorded in the sediments of Lake Telmen. Palaeogeography, Palaeoclimatology, Palaeoecology 183, 135–153.

Prokopenko, A.A., Khursevich, G.K., Bezrukova, X.B., Kuzmin, M.I., Boes, X., Williams, D.F., Fedenya, S.A., Kulagina, N.V., Letunova, P.P., Abzaeva, A.A., 2007. Paleoenvironmental proxy records from Lake Hovsgol, Mongolia, and a synthesis of Holocene climate change in the Lake Baikal watershed. Quaternary Research 68, 2–17.

Pyankov, V.I., Gunin, P.D., Tsoog, S., Black, C.C., 2000. C_4 plants in the vegetation of Mongolia: their natural occurrence and geographical distribution in relation to climate. Oecologia 123, 15–31.

Rhodes, T.E., Gasse, F., Lin, R.F., Fontes, J.-C., Wei, K.Q., Bertrand, P., Gibert, E., Mélières, F., Tucholka, P., Wang, Z.X., 1996. A late Pleistocene-Holocene lacustrine record from Lake Manas, Zunggar (northern Xinjiang, western China). Paleogeography, Palaeoclimatology, Palaeoecology 120, 105–121.

Ruddiman, W.F., 2001. Earth's Climate: Past and Future. Freeman W H and Company, New York.

Schrader, H.J., Gersonde, R., 1978. Diatoms and silicoflagellates in the eight metres section of the lower Pliocene of Capo Rossello. Utrecht Micropaleontological Bulletin 17, 129–176.

Shi, Y.F., Kong, Z.C., Wang, S.M., 1993. Mid-Holocene climates and environments in China. Global and Planetary Change 7, 219–233.

Steig, E.J., 1999. Mid-Holocene climate change. Science 286, 1485–1487.

Stockmarr, J., 1971. Tablets with spores used in absolute pollen analysis. Pollen and Spores 13, 615–621.

Stoermer, E.F., Smol, J.P., 1999. The Diatoms: Applications for the Environmental and Earth Sciences. Cambridge University Press, Cambridge.

Sun, X.J., Du, N.Q., Weng, C.Y., 1994. Paleovegetation and paleoenvironment of Manasi Lake, Xinjiang, N.W. China during the last 14000 years. Quaternary Science 3, 239–248 (in Chinese).

Tarasov, P.E., Dorofeyuk, N., Metel'tseva, E., 2000. Holocene vegetation and climate changes in Hoton-Nur basin, northwest Mongolia. Boreas 29, 117–126.

Tarasov, P.E., Guinot, J., Cheddadi, R., Andreev, A., Bezusko, L.G., Blyakharchuk, T.A., Dorofeyuk, N.I., Filimonova, L.V., Volkova, V.S., Zernitskaya, V.P., 1999. Climate in northern Eurasia 6000 years ago reconstructed from pollen data. Earth and Planetary Science Letters 171, 635–645.

Tuvdendorzh, D., Myagmarzhav, B., 1985. Atlas of the Climate and Ground Water Resources in the Mongolian People's Republic. GUGMS of Mongolia, Ulan Bator.

Van Campo, E., Cour, P., Hang, S.X., 1996. Holocene environmental changes in Bangong Co basin (Western Tibet). Part 2: the pollen record. Palaeogeography, Palaeoclimatology, Palaeoecology 120, 49–63.

Velichko, A.A., Andreev, A.A., Klimanov, V.A., 1997. Climate and vegetation dynamics in the tundra and forest zone during the late glacial and Holocene. Quaternary International 41/42, 71–96.

Wang, B.Y., Song, C.Q., Sun, X.J., 1996. Study on surface pollen in middle Inner Mongolia, China. Acta Botanica Sinica 38, 902–909 (in Chinese).

Wang, F.X., Qian, N.F., Zhang, Y.L., Yang, H.Q., 1995. Pollen Flora of China, second ed. Science Press, Beijing (in Chinese).

Wang, W., Ma, Y.Z., Feng, Z.D., Meng, H.W., Sang, Y.L., Zhai, X.W., 2009. Vegetation and climate changes during the last 8660 cal. a BP in central Mongolia based on a high-resolution pollen record from Lake Ugii Nuur. Chinese Science Bulletin 54 (9), 1579–1589.

Wanner, H., Beer, J., Bütikofer, J., Crowley, T.J., Cubasch, U., Flückiger, J., Goosse, H., Grosjean, M., Joos, F., Kaplan, J.O., Küttel, M., Müller, S.A., Prentice, I.C., Solomina, O., Stocker, T.F., Tarasov, P., Wagner, M., Widmann, M., 2008. Mid- to Late Holocene climate change: an overview. Quaternary Science Reviews 27, 1791–1828.

Wu, Y.S., Xiao, J.Y., 1995. A preliminary study on modern pollen rain of Zarbuye salt lake area, Xizang. Acta Botanica Yunnanica 17, 72–78 (in Chinese).

Zhang, H.C., Ma, Y.Z., Wünnemann, B., Pachur, H.-J., 2000. A Holocene climatic record from arid northwestern China. Palaeogeography, Palaeoclimatology, Palaeoecology 162, 389–401.

附录十二

Contents lists available at SciVerse ScienceDirect

Earth-Science Reviews

journal homepage: www.elsevier.com/locate/earscirev

Holocene moisture evolution across the Mongolian Plateau and its surrounding areas: A synthesis of climatic records

Wei Wang [a], Zhaodong Feng [b,*]

[a] College of Environment and Resources, Inner Mongolia University, Huhhot 010021, China
[b] Xinjiang Institute of Ecology and Geography, Chinese Academy of Sciences, Urumqi 830011, China

ARTICLE INFO

Article history:
Received 22 February 2012
Accepted 22 March 2013
Available online 29 March 2013

Keywords:
Mongolian Plateau
Holocene climate change
Moisture evolution
Bioclimate reconstruction

ABSTRACT

Based on the review of 26 high-standard Holocene climatic reconstructions (mainly pollen-based) from the Mongolian Plateau and its surrounding areas, temporal and spatial patterns of the Holocene moisture evolution are synthesized. The regionally-averaged moisture history from the summer monsoon-influenced semi-arid belt in China (i.e., Region A) demonstrates that the moisture index curve is broadly in agreement with the synthesized East Asian Monsoon Strength curve, both following the general trend of the West Tropical Pacific SST that is in turn the delayed response to the northern hemispheric summer solar insolation. The regionally-averaged moisture indices from the winter monsoon-dominated southern Siberia including Lake Baikal area and the Altai Mountains (i.e., Region B) exhibit a general declining trends since 10.6–9.6 cal. kyr BP, being largely consistent with the trends of the annual precipitation and the warm-season temperature in the Russian Plain. The consistency might be attributable to the Holocene declining trend of the warm-season temperature in North Atlantic region. The predominant feature of the regionally-averaged moisture index from the westerlies-affected northern Xinjiang (i.e., Region C) is a persistent increasing trend since ~8 cal. kyr BP. The wetting trend of northern Xinjiang during the past 8000 years might be attributable to the increasing trend of winter insolation and to the associated increasing trend of cold-season temperature in northwestern Europe. The chronological correspondences between dry phases and warm intervals in the arid areas of the Mongolian Plateau (i.e., northern Mongolian Plateau within Mongolia and southern Mongolian Plateau within China, Region D) lend a support to the proposal that the mid-Holocene dry phase was most likely the result of mid-Holocene high warm-season temperature.

© 2013 Elsevier B.V. All rights reserved.

Contents

1. Introduction . . . 39
2. Methodology . . . 40
   2.1. A brief summary of proxy premises . . . 40
   2.2. Data quality evaluation . . . 41
   2.3. Development of regionally-averaged moisture indices . . . 41
3. Spatial patterns of the Holocene moisture evolution . . . 41
   3.1. Summer monsoon-influenced semiarid belt . . . 45
   3.2. Winter monsoon-dominated Southern Siberia . . . 46
      3.2.1. Lake Baikal area . . . 46
      3.2.2. Altai Mountains . . . 46
   3.3. Westerlies-affected Northern Xinjiang . . . 48
   3.4. Arid areas of the Mongolian Plateau . . . 49
      3.4.1. Northern Mongolian Plateau . . . 49
      3.4.2. Southern Mongolian Plateau . . . 51
4. Synthesis and discussion . . . 51
   4.1. Summer monsoon-influenced semiarid belt . . . 51
   4.2. Winter monsoon-dominated southern Siberia . . . 53

* Corresponding author. Tel.: +86 18009915202, fax: +86 991 7885300.
E-mail address: fengzd@lzu.edu.cn (Z.-D. Feng).

0012-8252/$ – see front matter © 2013 Elsevier B.V. All rights reserved.
http://dx.doi.org/10.1016/j.earscirev.2013.03.005

4.3. Westerlies-affected northern Xinjiang . . . 53
4.4. Arid areas of the Mongolian Plateau . . . 53
5. Concluding remarks . . . 54
Acknowledgment . . . 54
References . . . 55

1. Introduction

The Mongolian Plateau includes the entire country of Mongolia and the Inner Mongolian Autonomous Region of China with the Gobi in the center (Fig. 1). Its western boundary is demarcated by the Mongolian Altai Mountains and its eastern boundary by the Hinggan Mountains. The plateau touches the southern tip of the Lake Baikal basin in the north and borders the northern margin of the Chinese Loess Plateau in the south. Climatologically, the Mongolian Plateau is extremely important because it is on the pathway of southward invasion of the polar front that directly links the high-latitude climate systems with low-latitude climate systems (Aizen et al., 2001; Visbeck, 2002). The Mongolian High Pressure System, which developed over the northern part of the Mongolian Plateau and the adjacent southern Russian Siberia, is interacted with the Azores High Pressure System that dominates the summer climate of central Asia and with the East Asian Low Pressure System that controls the summer climate of eastern Asia (Lydolph, 1977; Bridgman and Oliver, 2006). Specifically, the temporal dynamics (i.e., growth and decay) of the Mongolian High Pressure System is highly dependent on the temporal dynamics (i.e., growth and decay) of the Azores High Pressure System to the west and also on the temporal dynamics (i.e., growth and decay) of the East Asian Summer Monsoon to the south (Gong et al., 2001; Bridgman and Oliver, 2006). In addition, the strength of the Mongolian High Pressure System not only depends on the pressure contrast between the Asian interiors and the subtropical Pacific Ocean, but also depends on the pressure contrasts of the Mongolian High Pressure System with the Aleutian Low Pressure System to the east and with the Icelandic Low Pressure System to the west (Lydolph, 1977; Meeker and Mayewski, 2002; Bridgman and Oliver, 2006). The Icelandic Low-associated North Atlantic Oscillation (NAO) is demonstrated to be in anti-phase with the Aleutian Low-associated North Pacific Oscillation (NPO). That is, the positive phase of the NPO in the North Pacific realm concurs with the negative phase of the NAO in the North Atlantic realm (Kim et al., 2004;

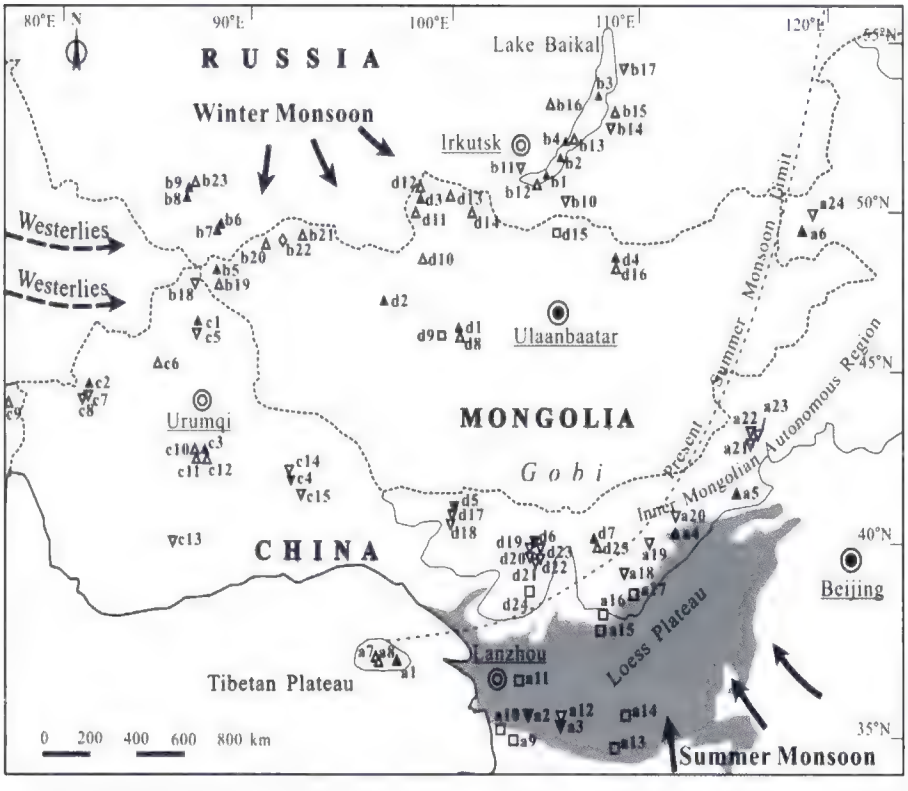

Fig. 1. Map showing the examined sites and their climatic contexts. Sites a1–a6, b1–b9, c1–c4 and d1–d7 were in-depth reviewed in this paper and the other sites were just examined for their data qualities (i.e., not in-depth reviewed). Note: ▲ Lake cores that passed quality scrutiny; ▼ exposed lacustrine section or peat section that passed quality scrutiny; △ lake core that did not pass quality scrutiny; ▽ exposed lacustrine section or peat section that did not pass quality scrutiny; □ eolian section or eolian–lacustrine complex or peat-eolian complex that did not pass quality scrutiny; and palaeolake terrace records that did not pass quality scrutiny.
The climate contexts are after Gao (1962), Lydolph (1977) and Visbeck (2002).

Bridgman and Oliver, 2006). This seesaw teleconnection between the NAO and the NPO may modulate the dynamics of the Mongolian High Pressure System or/and may be modulated by the dynamics of the Mongolian High Pressure System (Kutzbach and Liu, 1997; Gong et al., 2001).

Paleoclimatologically, the Mongolian Plateau should have witnessed the aforementioned competing interactions among different climate systems. As for the past 11,500 years (i.e., the Holocene), the time span that this review paper covers, those interactions should have been driven by four major forcing factors: (1) winter insolation, (2) summer insolation, (3) atmospheric CO_2 concentration, and (4) the extent of the Northern Hemisphere ice cover (Ruddiman, 2007). The combined effect of the lower winter insolation and the larger ice cover (including larger and longer snow cover and larger extent of permafrost) in the early Holocene may have acted as a strong high-latitude force. And the combined effect of the increased atmospheric CO_2 concentration (Bush, 2005) and the moderate summer insolation under warmed ocean surface, immediately after "modern" level of atmospheric CO_2 concentration and "modern" ice extent were reached at ~7000 yr BP (Ruddiman, 2007), may acted as a strong low-latitude force. In addition, a climatic feedback mechanism of combined CO_2 and water vapor was proposed by Bush (2005) and corroborated by Prokopenko et al. (2007) to explain the mid and late Holocene warming observed in Russian Siberia and central Asia. All of the three climate systems (Atlantic-related westerlies, high latitude-associated winter monsoon, and low latitude-associated summer monsoon) and the associated teleconnections, as well as the aforementioned feedback mechanism, may have operated with different strengths in different time intervals during the Holocene.

The spatial patterns of the Holocene moisture variations in the Mongolian Plateau and its surrounding areas have been the center of debate for the past two decades. For example, Harrison et al. (1996) and Tarasov et al. (2000) argued, primarily based on the chronological correspondence between high moisture interval in the northern Mongolian Plateau and southern Siberia and the Chinese Megathermal Optimum (wet and warm) spanning from 9.5 to 3.3 cal. kyr BP (Shi et al., 1993), that the maximum Asian monsoon must have reached as far westward as the Mongolian Altai Mountains. Based on the review of 75 sequences from central Asia, Herzschuh (2006) argued that the westerlies-dominated central Asia has experienced a similar moisture trend with that of monsoon-dominated China during the Holocene. However, a drastically different view was recently proposed by Chen and his colleagues (Chen et al., 2008). They argued, based on synthesis of 11 published records, that the entire Central Asian Arid Zone (CAAZ) including the northern Mongolian Plateau (see Fig. 1) has experienced synchronous moisture changes that are approximately opposite to those in monsoon-dominated China. Specifically, CAAZ experienced a dry early Holocene (12.0–8.0 cal. kyr BP) and a wet middle and late Holocene (since ca. 8.0 cal. kyr BP), and the moisture variations in CAAZ was argued to be out of the phase with that in Asian monsoonal area that was recently reported to have experienced a wet early Holocene (~10.5 to ~6.5 cal. kyr BP), a relatively wet mid Holocene (~6.5 to ~4.5 cal. kyr BP) and a dry late Holocene (since ca. 4.5 cal. kyr BP) (Herzschuh, 2006; Zhao et al., 2009; Wang et al., 2010; Zhang et al., 2011). Furthermore, neither the westerly-dominated pattern nor the monsoon-dominated pattern seems to be applicable to the arid and hyper-arid areas of the northwestern China and to the arid and semiarid areas of Mongolia where a prolonged dry mid-Holocene climate was reported to have prevailed (Feng, 2001; Feng et al., 2005; An et al., 2008; Wang et al., 2009, 2011).

The climatological complexity and the paleoclimatological controversies of the Mongolian Plateau call for reexamining the published data with higher standards and through different lenses and also for understanding those data in large-scale geographic contexts. This paper aims to review the published data not only from the Mongolian Plateau (including the entire country of Mongolia and Inner Mongolian Autonomous Region of China) but also from its surrounding areas including the summer monsoon-influenced semiarid belt (i.e., monsoonal margin of China) to the southeast of the Mongolian Plateau, the winter monsoon-dominated southern Siberia (mainly including Lake Baikal area and the Altai Mountains) to the north and the westerlies-affected northern Xinjiang of China to the west.

2. Methodology

2.1. A brief summary of proxy premises

Pollen-based proxies have been preferred for palaeoclimate reconstructions because they have been intensively and extensively tested in modern bioclimatic settings. The proxies are either semi-quantitative or quantitative indices for either thermal or moisture reconstructions. The semi-quantitative indices include *Artemisia*:Chenopodiaceae ratio (i.e., A/C ratio), arboreal pollen percentage or tree and shrub pollen percentage (i.e., AP percentage), and pollen grouping-based ratios for indicating thermal or/and moisture conditions (e.g., aridity index, moisture index, temperature index, steppe-forest index, and biome scores). A/C ratio has been extensively used as an index of moisture level in arid and semiarid areas based on the observation that the percentage of Chenopodiaceae increases with increasing aridity at the expense of the percentage of *Artemisia* (El-Mosilimany, 1990). The ratio was used as a semi-quantitative indicator of moisture level at several of our reviewed sites and the sites include Lake Aibi (our unpublished data), Lake Bosten (Huang, 2006; Huang et al., 2009), Lake Balikun (Tao et al., 2010) and Lake Juyanze (Herzschuh et al., 2004). Arbor pollen (i.e., AP) percentage was demonstrated to be an effective moisture index especially in sub-humid and semi-arid areas (Moore et al., 1991). This moisture index was used in several of the reviewed sequences including five from Russian and Mongolian Altai Mountains (Blyakharchuk et al., 2004, 2007), three from the summer monsoon influenced semi-arid belt (Liu et al., 2002a; Feng et al., 2004; Shen et al., 2005; Feng et al., 2006b), and one from the northern Mongolia (Dorofeyuk and Tarasov, 1998). The pollen grouping-based ratios applied in the reviewed papers include aridity indices, moisture indices, steppe-forest index, and biome scores. For example, an aridity index (i.e., (C + A)/P ratio, C for Chenopodiaceae, A for *Artemisia*, P for Poaceae) was designed by Fowell et al. (2003) to reconstruct the Holocene moisture evolution in Lake Telmen area of central Mongolia (Fowell et al., 2003). A modern climate–vegetation relationship-based moisture index was proposed and also used by Demske et al. (2005) to reconstruct the Holocene bioclimatic changes in Lake Baikal area. A modern climate–pollen relationship-based moisture index was developed by Ma et al. (2008) based on surface soil pollen data of the northern Mongolian Plateau and this index was applied in the Lake Ugii Nuur area in central Mongolia (Wang et al., 2009, 2011). SFI index is the ratio of the steppe pollen sum over the tree pollen sum and was used to reconstruct the areal extent of steppe expansion in Lake Hovsgol (Prokopenko et al., 2007). The biome score method assigns fossil pollen taxa to modern vegetation-based plant function types (PFT) and results in specific scores for major vegetation types such as tundra, taiga, steppe and desert (Prentice et al., 1996), and has been widely used as a semi-quantitative indicator of moisture level. Biome scores were calculated in the following reviewed sequences: Buguldeika of Lake Baikal (Tarasov et al., 2007), Hoton Nuur of the Mongolian Altai area (Rudaya et al., 2009) and Lake Bayanchagan of China (Jiang et al., 2006).

Quantitatively reconstructing key parameters of past climates has been a persistent pursuit of palaeoclimatologists. The quantitatively definable relationships between vegetation distributions and climates are the premises for the establishment of pollen-based quantitative indices. Consequently, pollen-based quantitative indices have been developed using such methods as regression (ter Braak and Juggins, 1993; Birks, 1995), best modern analog (Overpeck et

al., 1985; Guiot, 1990) and statistic information (Klimanov, 1984). In other words, Holocene variations in precipitation (annual or growing season) and temperature (annual or seasonal) can be quantitatively retrieved using these modern setting-based transfer functions. Transfer function-based quantitative reconstructions of annual precipitation were achieved at the following sites: Buguldeika of Lake Baikal (Tarasov et al., 2007), Lake Hoton Nuur of the Mongolian Altai area (Rudaya et al., 2009), Lake Bayanchagan (Jiang et al., 2006) and Lake Daihai (Xu et al., 2010) in northern China, and Lake Hulun of northeastern China (Wen et al., 2010a). In addition, some of non-pollen proxy sequences were discussed in this review to lend supports to the pollen-based climate interpretations, but those non-pollen sequences did not enter in our moisture estimation. The discussed non-pollen proxies include grain size (a proxy for water depth), diatom ratio between planktonic and benthic species (a proxy for water depth), percentages of warm-water and cold-water diatom species (a proxy for water temperature), organic matter content (a proxy for plant productivity), chemical and mineral compositions of lacustrine deposits (proxies for water balance and water salinity), and carbon isotope of organic matter from bulk sediment (a proxy for plant productivity and an indirect indicator for water balance).

2.2. Data quality evaluation

Our review paper focuses on recently-published works that pass our quality scrutiny based on five criteria: (1) reliability of chronologies, (2) validity of proxies used, (3) high-resolution (sampling resolution and preservation of high-resolution information), (4) stability of depositional environment, and (5) geographic representation (Morrill et al., 2003; Mayewski et al., 2004; Feng et al., 2006a; Wanner et al., 2008). To have an intercomparable standard of data quality, we designed a comprehensive scheme including nine variables that reflect the aforementioned five criteria. Admittedly, this scheme is somewhat subjective, but it well expresses the rationale behind sedimentation-based palaeoclimatic reconstructions. Specifically, each one of the nine variables for a particular archive (or sequence) is assigned a score according to its suitability for Holocene paleoclimatic reconstruction and the total of the nine scores (Table 1) gives an intercomparable index or quality index showing the overall suitability of a particular archive (or sequence) to be accepted for a high-quality depiction of the Holocene paleoclimatic history. The score for each variable is given in the column following the corresponding data or description in Table 1 and the suitability is classified into three levels, 1 being the lowest and 3 the highest. The following are the specific scoring scheme for each of the nine variables. (1) Type of archive: lacustrine and peat sequences are considered to be the best for their continuity and pollen preservation and are thus assigned a score of 3, and eolian–paleosol and lacustrine–eolian complex sequences are assigned a score of 2. (2) Geographic representation: the score of 3 was assigned to those sequences with large geographic representation of continental significance while isolated and medium-sized mountain basin with regional significance was given a score of 2, and the lowest score of 1 was given to those sequences with only local significance. (3) Present lake depth: this variable reflects the stability of the depositional environment. Water depth deeper than 5 m is scored as 3, 2–5 m as 2, and less than 2 m as 1, assuming that the deeper the present lake the less possibility the lake dried during the Holocene, and thus more chance to preserve continuously-deposited and least-disturbed sediments. (4) Dating material: the highest score (i.e., 3) is given to the preferred radiocarbon dating materials including pollen concentrates, humic acid, and terrestrial macro-fossil samples (e.g., charcoal, seeds, twigs, and leaves); a score of 2 is given to other radiocarbon materials including snail and organic matter from bulk sediments. (5) Number of dates (Holocene): the score is 3 for >8 dates, 2 for 5–8 dates, and 1 for <5 dates. (6) Dating method and radiocarbon reservoir effect: AMS dates with radiocarbon reservoir effect appraised are given a score of 3; AMS dates on pollen concentrates, humic acid, and terrestrial macro-fossil samples (e.g., charcoal, seeds, twigs, and leaves) are also given a score of 3 (no need for reservoir effect appraisal); and conventional ^{14}C and AMS ^{14}C dates without radiocarbon reservoir effect appraised are given a score of 2. (7) Sequence continuity: if a sequence is more or less continuous, the score is 3; and if stratigraphic hiatus was reported or/and confirmed by dates, the score is 1. (8) Resolution: 3 is assigned for <100-year resolution, 2 for 100 ~ 300-year resolution, and 1 for >300-year resolution. (9) Proxy quality: pollen proxies are the preferred ones and thus gain a score of 3; multi-proxy reconstruction also gains a score of 3; and others gain a score of 2.

Once again, considering the relatively well-defined climatic meanings of pollen proxies, pollen proxies are always preferred over other proxies (i.e., geochemical- or geophysical-proxies) even if other proxies from the same sequence also passed our quality scrutiny. It should also be noted here that the multi-proxy records from Lake Yanhaizi (Chen et al., 2003a), which passed our quality scrutiny but has no pollen record, was adopted for its indispensable geographic representation. And, the pollen record from Midiwan section (Li et al., 2003a) within the summer monsoon-influenced semi arid belt was excluded because its interpretation was mainly based on pollen concentration and the interpretation failed to consider the variation in sedimentation rate.

Totally, we examined 87 sequences, 73 being lacustrine or peat-related sequences, 12 being either eolian-dominated or peat-dominated complexes, and 2 being palaeolake terrace. The quality index of ≥ 22 is considered here to be the threshold to pass our data quality scrutiny and 26 of the examined 87 sequences passed our scrutiny.

2.3. Development of regionally-averaged moisture indices

In order to depict regional pictures of moisture variations, we averaged the individual moisture reconstructions using a region-averaging method. Specifically, we selected the most reliable moisture proxy (e.g., A/C ratio, arboreal pollen percentage, moisture index, aridity index and pollen-based annual precipitation) for each reconstruction and assign an ordinal value to each 200-year time slice. The ordinal value that ranges from 0 (the lowest) to 4 (the highest) is resulted by the ratio between the average value of the 200-year time slice considered and the highest 200-year average of the Holocene in that particular reconstruction. The average of the assigned ordinal values for each 200-year time slices from all qualified reconstructions within a particular region gives the regionally-averaged moisture index (i.e., RA-moisture index). In other words, the RA-moisture index is the average moisture of all in-depth reviewed reconstructions in a particular region. To show the consistency among the participating reconstructions, mean errors (i.e., error bars) are defined as the sum of differences between the RA-moisture index and each individual index divided by the number of the participating reconstructions. This region-averaging method does smooth out the details of individual sequences, but it produces a regionally representative picture if all of the sequences in a particular region demonstrate geographically coherent trends (Davis et al., 2003; Herzschuh, 2006; Zhao et al., 2009; Wang et al., 2010).

3. Spatial patterns of the Holocene moisture evolution

In order to understand the Holocene moisture history of the Mongolian Plateau in a large-scale geographic context, our review will first examine the Holocene moisture records from the surrounding areas (i.e., the summer monsoon-influenced semiarid belt, the winter monsoon-dominated southern Siberia and the westerlies-affected northern Xinjiang) and then look at the Mongolian Plateau itself in hope that our understanding of the large-scale controlling mechanisms can be improved.

Table 1
Holocene palaeoclimatic records and quality index from the Mongolian Plateau and its surrounding area.

No	Site name	Lat. (°)	Long. (°)	Eleva. (m a.s.l.)	Type of archive	S	Geographic representation	S	Present lake depth (m)	S	Dating material	S	Number of dates	S	Dating method and radiocarbon reservoir effect (yr)	S	Sequence continuity (kyr)	S	Resolution (yr)	S	Proxy	S	Quality index	References
A: Summer monsoon influenced semi-arid belt																								
a1	Qinghai Lake (QH-2000)	36.70	100.60	3194	▲	3	Continental	3	22.3	3	OM	2	7	2	AMS ^{14}C, 1039	3	0–15	3	~50	3	P, GC	3	25 [b]	Liu et al. (2002a) and Shen et al. (2005)
a2	Sujiawan	35.53	104.52	1700	▼	3	Regional	2	Dry	1	Ch, HM	3	7	2	AMS ^{14}C	3	0–14.8	3	~140	2	P,L,GC, GS	3	22	Feng et al. (2004, 2006b)
a3	Dadiwan	35.00	105.92	1400	▼	3	Regional	2	Dry	1	Ch, HM	3	9	3	AMS ^{14}C	3	0–13.7	3	~60	3	P,L,GC, GS	3	24	Feng et al. (2004, 2006b)
a4	Daihai Lake	40.58	112.68	1221	▲	3	Regional	2	13.1	3	OM	2	8	3	AMS ^{14}C, 360	3	0–10.2	3	~40	3	P, GC, GS	3	25	Xiao et al. (2004) and Xu et al. (2010)
a5	Banyanchagan Lake	41.65	115.21	1335	▼	3	Regional	2	Dry	1	OM,Pr	3	9	3	AMS ^{14}C, 570	3	0–12.5	3	~140	2	P	3	23	Jiang et al. (2006)
a6	Hulun Lake	49.13	117.50	545	▲	3	Continental	3	5.1	3	OM	2	14	3	AMS ^{14}C, 685	3	0–11	3	~60	3	P, GS	3	26	Wen et al. (2010a,b)
a7	Qinghai Lake (1F)	36.80	100.15	3194	△	3	Continental	3	26	3	OM, Pr	3	41	3	AMS ^{14}C, –	3	0–32	3	~20	3	GC, GS	2	26[a]	An et al. (2012)
a8	Qinghai Lake (14B)	~36.8	~100.1	3194	△	3	Continental	3	26	3	OM	2	3	1	AMS ^{14}C	2	0–12	3	~60	3	GC, GS	2	22[a]	Lister et al. (1991)
a9	Hezuo	~34.5	~103.2	2915	□	2	Continental	3	–	1	OM	2	1	1	^{14}C, –	3	0–80	3	~100	2	GC, M, GS	3	20	Fang et al. (2003)
a10	Yuanbo	~35.0	~103.0	n.d.	□	2	Continental	3	–	1	OM	2	2	1	^{14}C, –	3	3.2–75	1	~200	2	MS, GS, L	3	18	Chen et al. (1997)
a11	Shajnping	36.0	103.83	n.d.	□	2	Regional	2	–	1	OM	2	4	1	^{14}C, IRSL-	3	0–60	3	~150	2	MS, L	2	18	Fang et al. (1999)
a12	Dadiwan	35.77	105.82	1400	□	3	Regional	2	–	1	OM	2	4	1	^{14}C, –	3	0–11	3	~130	2	P	3	20	Xia et al. (1998)
a13	Yaoxian	34.93	108.83	n.d.	□	2	Local	1	–	1	Q&F	2	2	1	TL	3	0–12	3	~170	2	P	3	18	Li et al. (2003b)
a14	Heimugou	35.75	109.42	n.d.	□	2	Continental	3	–	1	Q&F	2	1	1	TL	3	0–50	3	~670	1	MS, L	2	18	An et al. (1991)
a15	Jinbian	37.50	108.33	1400	□	2	Continental	3	–	1	OM	2	11	3	AMS ^{14}C, –	3	0–10	3	~100	2	GS, MS	2	21	Xiao et al. (2002)
a16	Midiwan	37.65	108.62	1400	□	2	Local	1	–	1	Ch, OM	3	11	3	AMS ^{14}C, –	3	0–15.8	3	~100	2	P, GS, L	3	21	Li et al. (2003a)
a17	Yangtaomao	38.80	110.45	1400	□	2	Local	1	–	1	P, HM	3	5	2	AMS ^{14}C, –	3	7.8–13	1	~100	2	P, L, etc.	3	18	Zhou et al. (1996)
a18	Barhhar Nuur	39.32	109.27	1278	▽	3	Regional	2	Dry	1	OM	2	12	3	AMS ^{14}C, 1950	3	4–9	1	~50	3	GS, GC	3	21	Guo et al. (2007)
a19	Chasuqi	40.67	111.13	1000	▽	3	Local	1	–	1	OM	2	4	1	^{14}C, –	3	0–9.1	1	~70	3	P	3	18	Wang and Sun (1997)
a20	Diaojiaohaizi	41.30	112.35	1221	▽	3	Regional	2	Dry	1	OM	2	13	3	–	2	2–11.5	1	~70	3	P	3	20	Zhang et al. (1997)
a21	Haoluku	42.95	116.75	1295	▽	3	Regional	2	Dry	1	OM	2	4	1	AMS ^{14}C, –	2	0–11	3	~200	2	P, D, etc.	3	19	Liu et al. (2002b)
a22	Xiaonuchang	42.62	116.82	1460	▽	3	Regional	2	Dry	1	OM	2	3	1	AMS ^{14}C, –	2	3–11	1	~280	2	P, D	3	17	Liu et al. (2002b)
a23	Liuzhouwan	42.70	116.67	1365	▽	3	Regional	2	Dry	1	OM	2	2	1	AMS ^{14}C, –	2	0–14	3	~350	1	P, etc.	3	18	Wang et al. (2001)
a24	Zhalainor	49.33	117.53	n.d.	▽	3	Regional	2	Dry	1	OM	2	4	1	^{14}C, –	2	3.2–23.5	1	~160	2	P	3	17	Tong et al. (1997)
B: Winter monsoon dominated southern Siberia																								
b1	Vydrino Shoulder (Baikal Lake)	51.58	104.85	340	▲	3	Continental	3	665	3	P	3	12	3	AMS ^{14}C	3	1–16	3	~130	2	P	3	26	Demske et al. (2005)
b2	Posolskoe High (Baikal Lake)	52.08	105.87	340	▲	3	Continental	3	130	3	P	3	12	3	AMS ^{14}C	3	0.7–24.4	3	~90	3	P	3	27	Demske et al. (2005)
b3	Continent Ridge (Baikal Lake)	53.95	108.91	340	▲	3	Continental	3	386	3	P	3	10	3	AMS ^{14}C	3	0.9–14.4	3	~80	3	P	3	27	Demske et al. (2005)
b4	Buguldeika (Baikal Lake)	52.52	106.15	340	▲	3	Continental	3	355	3	OM	2	10	3	AMS ^{14}C, 1160	3	0.6–15	3	~250	2	P	3	25	Tarasov et al. (2007)
b5	Hoton Nuur-2	48.62	88.33	2083	▲	3	Regional	2	32	3	Pr	3	1[b]	2	AMS ^{14}C, –	2	0–11.5	3	~110	2	P	3	23	Rudaya et al. (2009)
b6	Akkol Lake	50.25	89.62	2204	▲	3	Regional	2	2.8	2	Pr, OM	3	12	3	AMS ^{14}C	3	0–10	3	~150	2	P	3	24	Blyakharchuk et al. (2007)
b7	Grusha Lake	50.38	89.42	2413	▲	3	Regional	2	3.5	2	OM	2	10	3	AMS ^{14}C, 0	3	0–12	3	~460	1	P	3	22	Blyakharchuk et al. (2007
b8	Uzunkol Lake	50.48	87.10	1985	▲	3	Regional	2	5.9	3	HA	3	5	2	AMS ^{14}C	3	0–16	3	~160	2	P	3	24	Blyakharchuk et al. (2004)

b9	Kendegelukol Lake	50.50	87.63	2050	▲	3	Regional	2	5.5	3	HA	3	6	2	AMS ^{14}C	3	0–15	3	~260	2	P	3	24	Blyakharchuk et al. (2004)
b10	Sphagnum (Baikal area)	49.65	107.80	1348	▽	3	Local	1	Dry	1	OM	2	4	1	AMS^{14}C, -	2	0–9	1	~100	3	P, D	3	17	Fukumoto et al. (2012)
b11	Dulikha (Baikal area)	51.08	104.97	524	▽	3	Local	1	Dry	1	Pr, OM	3	3	1	AMS ^{14}C	3	0–16	3	~130	2	P	3	17	Bezrukova et al. (2009)
b12	Vydrino Shoulder (Baikal Lake)	51.58	104.87	n.d.	△	3	Continental	3	675	3	P	3	10	3	AMS^{14}C	3	0–16	3	~120	2	D, GC	3	26[a]	Morley et al. (2005)
b13	BDP-93-2 (Baikal Lake)	n.d.	n.d.	n.d.	△	3	Continental	3	>300	3	OM	2	4	2	AMS^{14}C, -	2	0–18	3	~110	2	D	2	22	Karabanov et al. (2000)
b14	CHM-3 (Baikal area)	52.75	108.08	458	▽	3	Local	1	Dry	1	OM	2	2	1	AMS ^{14}C, -	2	0–12	3	~340	1	P	3	17	Shichi et al. (2009)
b15	Kotokel Lake	52.78	108.12	458	△	3	Regional	2	3.5	2	OM	2	3	1	AMS ^{14}C, -	2	0–15	3	~120	2	P	3	20	Tarasov et al. (2009)
b16	Tsagan_Tyrm Lake	52.87	106.58	n.d.	△	3	Regional	2	2.6	2	OM	2	4	1	AMS^{14}C, -	2	0–6.3	1	~140	2	P, D, M, GC	3	18	Sklyarov et al. (2010)
b17	Duguldzora (Baikal area)	54.35	109.55	478	▽	2	Local	1	Dry	1	Pr, OM	3	5	2	AMS ^{14}C, -	2	0–16	3	~160	2	P	3	19	Bezrukova et al. (2009)
b18	Daluoba	48.03	88.03	2082	▽	3	Regional	2	Dry	1	OM	2	1	1	^{14}C	2	0–7	1	~410	1	P	3	16	Yan and Xu (1992)
b19	Hoton Nuur-1	48.67	88.30	2083	△	3	Regional	2	4.8	2	OM	2	6	2	AMS ^{14}C, -	2	0–11	3	~600	1	P	3	20	Tarasov et al. (2000)
b20	Achit Nuur Lake	49.50	90.60	1435.	△	3	Regional	2	10	3	OM	2	4	1	^{14}C, -	2	0–14.6	3	~500	1	P	3	20	Gunin (1999)
b21	Bayan Nuur Lake	50.00	94.02	932.	△	3	Regional	2	>5	3	OM	2	4	1	^{14}C,	2	0–15.4	3	~150	2	P	3	21	Grunert et al. (2000)
b22	Uvs Nuur Lake	50.38	92.20	759		2	Regional	2	6	3	OM	2	3	1	AMS^{14}C, -	2	0–11.5	3	-	3	Terrace	2	20	Grunert et al. (2000)
b23	Tashkol Lake	50.45	87.67	2150	△	3	Regional	2	6.25	3	HA	3	6	2	AMS ^{14}C	3	4–16	1	~300	1	P	3	21	Blyakharchuk et al. (2004)
C: Westerlies affected northern Xinjiang																								
c1	Wulungu Lake (WLG2004)	47.17	87.22	478	▲	3	Regional	2	12	3	OM	2	6	2	AMS ^{14}C, 760	3	0–9.5	3	~80	3	P, GC, L	3	24	Jiang et al. (2007) and Liu et al. (2008)
c2	Aibi Lake (A2009)	45.03	82.91	200	▲	3	Regional	2	2.5	2	OM	2	7	2	AMS ^{14}C, 1800	3	0–15	3	~80	3	P	3	23	Unpublished
c3	Bosten Lake (BSTC04)	42.10	87.18	1048	▲	3	Regional	2	15	3	TOC, Pr	3	6	2	AMS ^{14}C, OSL, 1140	3	0–9	3	~140	2	P, D, GC	3	24	Huang (2006) and Huang et al. (2009)
c4	Balikun Lake (BLK06E)	43.67	92.80	1585	▼	3	Less regional	2	Dry	1	P,Pr, OM	3	13	3	790	3	0–16.7	3	~80	3	P	3	23	Tao et al. (2010)
c5	Wulungu Lake	n.d.	n.d.	478.6	▽	3	Regional	2	Dry	1	OM	2	2	1	^{14}C, -	2	0–12	3	~600	1	P	3	18	Yang and Wang (1994)
c6	Manasi Lake	45.75	86.00	251	△	3	Regional	2	Dry	1	Ca, OM	2	8	3	AMS ^{14}C, -	2	0–11	3	~250	2	P, GS, GC	3	21	Rhodes et al. (1996) and Sun et al. (1994)
c7	Aibi Lake (AZ section)	44.87	82.73	195	▽	3	Regional	2	Dry	1	OM	2	2	1	^{14}C	2	2.9–10	1	~350	1	P	3	16	Wu (1995) and Wu et al., 1996)
c8	Aibi Lake (ZkooB)	n.d.	n.d.	195	▽	3	Regional	2	Dry	1	OM	2	6	2	^{14}C	2	0–12	3	~600	1	GC	2	18	Li et al. (1993)
c9	Issyk-Kul Lake	42.50	77.17	1606	△	3	Regional	2	240	3	OM	2	8	3	AMS^{14}C	3	1–8.7	1	~190	2	GC	2	21	Ricketts et al. (2001)
c10	Bosten Lake (BSTC01)	41.93	86.75	1046	△	3	Regional	2	15	3	Pr	3	4	2	AMS^{14}C	3	0–8.5	1	~20	3	GC, GS, M	3	23[a]	Zhang et al. (2010)
c11	Bosten Lake (XBWu46)	41.93	86.75	1046	△	3	Regional	2	15	3	HA, Pr	3	6	2	AMS^{14}C	3	0–8.5	1	~20	3	GC, GS, M	3	23[a]	Wunnemann et al. (2006)
c12	Bosten Lake (XBWu46)	41.90	86.72	1046	△	3	Regional	2	15	3	Pr	3	6	2	AMS ^{14}C	3	0–8.4	1	~50	3	GC	2	22[a]	Wunnemann et al.(2003)
c13	Middle Tarim	39–41	82–84	~815	▽	3	Regional	2	Dry	1	Ch, Pr	3	4	1	AMS ^{14}C	3	0–12	3	~1000	1	P, GC, GS, MS	3	20	Feng and Liu (2005)
c14	Balikun Lake (BLK-1)	43.70	92.83	1580	▽	3	Regional	2	Dry	1	OM	2	7	2	^{14}C, 750	3	0–9.4	3	~40	3	GC, GS, MS	3	22[a]	Xue et al. (2008) and Zhong et al. (2010)
c15	Tuolekule Lake	43.33	94.22	1890	▽	3	Regional	2	Dry	1	OM	2	6	2	AMS ^{14}C, 200	3	0–15	3	~340	1	P, GS	3	20	An et al. (2011)

Table 1 (*continued*)

No	Site name	Lat. (°)	Long. (°)	Eleva. (m a.s.l.)	Type of archive	S	Geographic representation	S	Present lake depth (m)	S	Dating material	S	Number of dates	S	Dating method and radiocarbon reservoir effect (yr)	S	Sequence continuity (kyr)	S	Resolution (yr)	S	Proxy	S	Quality index	References
D: Arid areas of the Mongolian Plateau																								
d1	Ugii Nuur Lake	47.77	102.77	1330	▲	3	Regional	2	14.5	3	OM	2	14	3	AMS ^{14}C, 87	3	0–8.6	1	20–50	3	P, D, GS	3	23	Wang et al. (2009, 2011)
d2	Telmen Lake	48.83	97.33	1789	▲	3	Regional	2	24.5	3	P, HA	3	9	3	AMS ^{14}C	3	0–7.5	1	~200	2	P, GC, L	3	23	Fowell et al. (2003) and Peck et al. (2002)
d3	Hovsgol Lake	51.08	100.75	1641	▲	3	Regional	2	200	3	OM	2	5	2	AMS ^{14}C, 500	3	0–13.7	3	~300	1	P, D	3	22	Prokopenko et al. (2007)
d4	Gun Nuur Lake	50.25	106.60	600	▲	3	Regional	2	5.5	3	OM	2	7	2	AMS ^{14}C, –	2	0–11	3	~280	2	P, D	3	22	Dorofeyuk and Tarasov (1998)
d5	Juyanze Lake	41.88	101.85	907	▼	3	Regional	2	Dry	1	OM, HA	3	7	2	AMS ^{14}C, 1890	3	1.5–10.7	3	30–80	3	P	3	22	Herzschuh et al. (2004)
d6	Zhuyeze Lake	39.00	103.33	1320	▼	3	Regional	2	Dry	1	Ch, OM	3	9	3	AMS ^{14}C, 540	3	0–11.6	3	~50	3	P, L	3	24	Chen et al. (2003b, 2006)
d7	Yanhaizi Lake	40.10	108.43	1180	▲	3	Regional	2	0.5	1	OM, P	3	8	3	AMS ^{14}C	3	0–15	3	~100	2	GC, GS, M	3	23	Chen C.T.A. et al. (2003)
d8	Ugii Nuur Lake	47.73	102.77	1330	△	3	Regional	2	16	3	OM	2	3	1	AMS ^{14}C	2	1–11	3	~180	2	GC, M	3	21	Schwanghart et al. (2009)
d9	Karakourum S4	~47.0	~102.0	n.d.	□	2	Local	1	Dry	1	Q&F	3	8	3	OSL	3	1–11	3	~500	1	GC	2	19	Lehmkuhl et al. (2011)
d10	Daba Nuur	48.20	98.78	2465	△	3	Regional	2	4.5	2	OM	2	5	2	^{14}C, –	2	0–12	3	~500	1	P, D	3	20	Gunin (1999)
d11	Yamant-Nuur Lake	49.90	102.60	1000	△	3	Regional	2	>5	3	OM	2	0	1	AMS ^{14}C, –	2	0–16	3	~400	1	P	3	20	Gunin (1999)
d12	Hovsgol Lake	50.53	101.17	1645	△	3	Regional	2	>5	3	OM	2	2	1	AMS ^{14}C, –	2	0–7	2	~470	1	P, D	3	19	Dorofeyuk and Tarasov (1998)
d13	Hovsgol Lake	51.88	100.35	1641	△	3	Regional	2	236	3	OM	2	4	1	AMS ^{14}C, 500	3	0–27	3	~330	1	GC	2	20	Murakami et al. (2010)
d14	Dood Nuur Lake	51.33	99.38	1538	△	3	Regional	2	>5	3	OM	2	2	1	AMS ^{14}C, –	2	0–14.6	3	~660	1	P, D	3	20	Dorofeyuk and Tarasov (1998)
d15	Shaamar	50.20	105.20	650	..	2	Local	1	–	1	Ch, OM	3	8	3	AMS ^{14}C	3	0–11	3	~300	1	P, L, GC	3	20	Feng et al. (2007)
d16	Gun Nuur Lake	50.25	106.07	600	△	3	Regional	2	5	3	OM	2	9	3	AMS ^{14}C, 1200	3	0–9	1	~30	3	GC, GS	2	22[a]	Feng et al. (2005) and Zhang et al. (2012)
d17	Juyanze Lake	41.83	101.63	898	▽	3	Regional	2	Dry	1	Pr	3	4	1	AMS ^{14}C	3	2.7–5.5	1	30	3	GC, GS, MS	3	20	Mischke et al. (2002)
d18	Juyanze Lake	41.88	101.85	907	▽	3	Regional	2	Dry	1	OM, HA	3	7	2	AMS ^{14}C, 1890	3	1.5–10.7	1	30–80	3	GC, GS, M	3	21	Hartmann & Wünemann (2009)
d19	Zhuyeze Lake	39.07	103.60	1302	▽	3	Regional	2	Dry	1	OM	2	5	2	AMS ^{14}C, –	2	0–13.3	3	~140	2	P	3	20	Zhao et al. (2008)
d20	Zhuyeze Lake	39.05	103.67	1309	▽	3	Regional	2	Dry	1	OM, shell	2	11	3	AMS ^{14}C, –	2	0–1	3	~200	2	P, GS	3	21	Li et al. (2009)
d21	Zhuyeze Lake	39.05	103.67	1309	▽	3	Regional	2	Dry	1	OM	2	6	2	^{14}C, –	2	0–6.8	1	~160	2	GC, GS, MS	3	18	Shi et al. (2002)
d22	Baijian Lake	39.15	103.15	1280		2	Regional	2	Dry	1	Ca, shell	2	7	2	^{14}C, –	2	0–42.4	3	–	2	Terrace, t	3	19	Pachur et al. (1995)
d23	Yema Lake	39.10	103.67	1306	▽	3	Regional	2	Dry	1	OM	2	6	2	^{14}C, –	2	0–16	3	~40	3	GC, GS, MS	3	21	Chen et al. (1999) and Shi et al. (2002)
d24	Hongshui R.	38.17	102.75	1460	▽	2	Regional	2	Dry	1	Pr, OM	3	9	3	AMS ^{14}C, –	3	3–8	1	~40	3	P	3	21	Ma et al. (2004)
d25	Yanhaizi Lake	40.10	108.43	1180	△	3	Regional	2	0.5	1	OM	2	5	2	AMS ^{14}C	3	0–22	3	~100	2	GC	2	20	Qian et al. (2002)

Notes:

Quality index was calculated as the sum of specific quality scores showing the overall quality of a sequence.

Abbreviations: OM—organic matter; HM—Humate; HA—humic acid; Pr—plant residue; Ch—charcoal; Ca—carbonate; Q&F—Quartz and feldspar; P—pollen; D—diatom; GS—grain size; MS—magnetic susceptibility; M—mineral composition; GC—geochemical proxies; and L—lithology.

Symbol and its indications: ▲ Lake cores that passed quality scrutiny; ▼ exposed lacustrine section or peat section that passed quality scrutiny; □ lake core that did not pass quality scrutiny; ▽ exposed lacustrine section or peat section that did not pass quality scrutiny; △ eolian section or eolian–lacustrine complex or peat–eolian complex that did not pass quality scrutiny; and ○ palaeolake terrace records that did not pass quality scrutiny.

[a] Not included because pollen data from the same site was selected.

[b] Reliable chronology was acquired based on the comparison of primary pollen proxies with core Hoton Nuur-1 which based on 6 AMS dates.

3.1. Summer monsoon-influenced semiarid belt

The summer monsoon-influenced semiarid belt, namely monsoonal margin of China, refers to the strip along the present summer monsoon limit as marked in Fig. 1 (Gao, 1962). Based on the synthesis of earlier works, Shi and his colleagues (Shi et al., 1993) concluded that a warm and wet period of the Holocene (i.e., namely "Holocene Megathermal") occurred between ~8.5 and ~3.0 ^{14}C kyr BP (i.e., ~9.5 and ~3.3 cal. kyr BP) in the entire northern China, and the warmest and the wettest period (e.g., namely "mid-Holocene Climatic Optimum") occurred during ~7.2 to ~6.0 ^{14}C kyr BP (i.e., ~8.0 to ~6.8 cal. kyr BP). The periods before ~8.5 and after ~3.0 ^{14}C kyr BP were cold and dry. After this work (Shi et al., 1993), several comprehensive reviews regarding the Holocene climate changes in northern China have been published (e.g., An et al., 2000; He et al., 2004; An et al., 2006; Feng et al., 2006a; Zhao et al., 2009; Wang et al., 2010; Zhang et al., 2011).

The first site to be reviewed here is Lake Qinghai (Fig. 2; site a1 in Fig. 1 and Table 1) situated in the conjunction between the Tibetan Plateau and the Loess Plateau. Fig. 2 shows that the pollen percentage of trees and shrubs reached its Holocene maximum between ~7.2 ^{14}C kyr BP (i.e., ~8.0 cal. kyr BP) and ~6.0 ^{14}C kyr BP (i.e., ~6.8 cal. kyr BP). The percentage then constantly declined to a low value since ~3.8 ^{14}C kyr BP (i.e., ~4.2 cal. kyr BP) (Liu et al., 2002a; Shen et al., 2005). It should be noted that the pollen proxy-based interpretation is different from the recently-published geochemical proxy-based interpretation of the same lake (site a7 in Fig. 1; An et al., 2012). But, it should also be noted that this review preferred the pollen proxy-based interpretation over other proxy-based ones if pollen sequence passed our data quality scrutiny. The investigations from the western part of the Chinese Loess Plateau show that the Holocene sequences on valley terraces are ubiquitously composed of two complexes: the upper loess–paleosol complex and the lower wetland–swamp complex. The typical sequence at Sujiawan site (Fig. 2; site a2 in Fig. 1) was well dated (Feng et al., 2004, 2006b), and the wetland–swamp layer is bracketed by loess deposits at the beginning (8885 ± 55 ^{14}C yr BP or ~10.0 cal. kyr BP) and at the end (3805 ± 45 ^{14}C yr BP or ~4.2 cal. kyr BP). A wetland–swamp–fluvial complex at nearby Dadiwan section (Fig. 2; site a3 in Fig. 1) is a stratigraphically traceable equivalent to the wetland–swamp complex at Sujiawan section (Feng et al., 2004, 2006b). These two sections (Sujiawan and Dadiwan) complement each other to provide a sufficient resolution for the entire Holocene. That is, the Sujiawan section provides details for the late Holocene (since ca. 3.8 ^{14}C kyr BP or ~4.2 cal. kyr BP) and the Dadiwan section for the early and middle Holocene (~8.9–3.8 ^{14}C kyr BP or ~10.0–4.2 cal. kyr BP). The stratigraphy and the percentage of trees and shrubs at both sections demonstrate that the early and middle Holocene was wet and the late Holocene was dry. The reconstructed Holocene moisture optimum occurred between ~7.5 and ~5.8 ^{14}C kyr BP (i.e., ~8.3 and ~6.6 cal. kyr BP) when forest-dominated vegetation occupied the landscape. Steppe vegetation was reconstructed for the loess unit underlying the wetland–swamp complex (i.e., before ~8.9 ^{14}C kyr BP) and also for the loess unit overlying the wetland–swamp complex (i.e., after 3.8 ^{14}C kyr BP).

Northeastward to the Inner Mongolian Autonomous Region, the pollen data from Lake Daihai (Fig. 2; site a4 in Fig. 1) show that after relatively dry period (before ~7.9 cal. kyr BP), large-scale covers of mixed coniferous and broadleaved forests marked a warm and humid mid-Holocene (between ~7.9 and ~4.4 cal. kyr BP) (Xiao et al., 2004; Xu et al., 2010). The data exhibit a dramatic drop in tree and shrub pollen percentage at 4.4–4.2 cal. kyr BP. A secondary peak of tree and shrub pollen percentage appeared between 4.2 and 2.8 cal. kyr BP and was followed by very low percentages of tree and shrub pollen. And, this is generally supported by the moisture sequences from nearby Diaojiaohaizi section (site a20 in Fig. 1) (Zhang et al., 1997) and Lake Barhhar Nuur section (site a18 in Fig. 1) in the Ordos Plateau (Guo et al., 2007), although the latter two (i.e., Diaojiaohaizi and Barhhar Nuur) are not included in this in-depth review for their low quality index scores. Further northeastward to Lake Bayanchagan (Fig. 2; site a5 in Fig. 1), after a gradual wetting before 8.4 cal. kyr BP the Holocene optimum of effective moisture (i.e., P/E = ratio of precipitation and potential evaporation) occurred between 8.4 and 5.4 cal. kyr BP (Jiang et al., 2006). The moisture optimum was followed by a drought lasting from 5.4 to 4.2 cal. kyr BP and the drought was in turn followed by a moderately wet period between 4.2 and 2.2 cal. kyr BP. A less wet period sustained for the last ~1800 years after a short interval of drought between 2.2 and 1.8 cal. kyr BP. The last sequence to be reviewed from the semiarid belt is Lake Hulun (Fig. 2; site a6 in Fig. 1) that

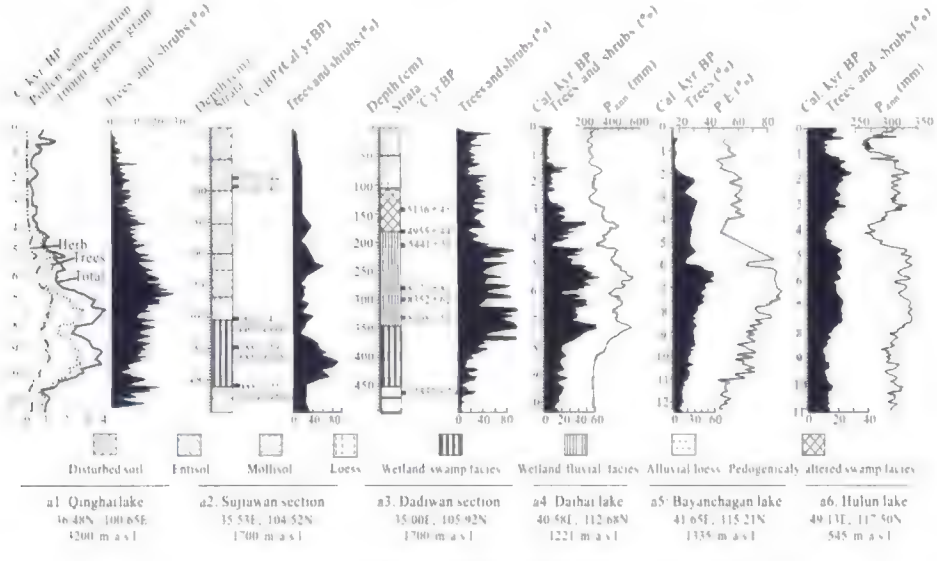

Fig. 2. Holocene variations of moisture proxies from summer monsoon-influenced semiarid belt.

Notes for the sources of references: Lake Qinghai (Liu et al., 2002a,b; Shen et al., 2005); Sujiawan and Dadiwan Sections (Feng et al., 2004, 2006b); Lake Daihai (Xiao et al., 2004; Xu et al., 2010); Lake Bayanchagan (Jiang et al., 2006); Lake Hulun (Wen et al., 2010a,b).

was recently reported by Wen and his colleagues (Wen et al., 2010a, b). Both the percentage of tree and shrub pollen and the reconstructed precipitation exhibit a mid-Holocene moisture optimum occurred between 7.9 and 4.7 cal. kyr BP. The optimum was preceded by a relatively dry period and also followed by a relatively dry period lasting from 4.7 to 3.5 cal. kyr BP, the latter being followed by another wet period lasting from 3.5 to 1.0 cal. kyr BP (Wen et al., 2010a,b).

To sum up, the aforementioned Holocene sequences from the summer monsoon-influenced semiarid belt all demonstrate that a pronounced mid-Holocene moisture optimum occurred approximately between ~8.5 and ~4.5 cal. kyr BP and that both the preceding and the following periods were dry. The second point to be noted is that the well-documented mid–late Holocene transitional drought occurring at 4.5–4.0 cal. kyr BP was followed by moisture recoveries in five of the six in-depth reviewed records with an exception of Lake Qinghai in which the pollen-based moisture level was never recovered. The third point is that the record from Lake Hulun exhibits a pronounced wet late-Holocene lasting from 3.5 to 1.0 cal. kyr BP, which is somewhat corroborated by the record from Lake Bayanchagan.

3.2. Winter monsoon-dominated Southern Siberia

Our review will focus on two areas where the Holocene climate variations were retrieved from many lake cores and peatland sections: (1) Lake Baikal area in the east, and (2) Altai Mountains in the west.

3.2.1. Lake Baikal area

Lake Baikal spans 4° of latitude from 51.5 to 55.5°N. The vegetation in the lake basin is mainly dominated by dark coniferous forests with Scots pine-dominated light coniferous open forests becoming progressively more important southward (Demske et al., 2005). Due to relatively high relief in the middle section of the basin (ranging from 340 to 2850 m a.s.l.), the altitudinal differentiation of the vegetation is well displayed and the vegetation zones from low to high elevations are: light coniferous open forests, dark coniferous open forests, subalpine shrubs, alpine meadows, and montane tundra. Lake cores and peatland sections in the basin have been intensively studied to reconstruct the Holocene bioclimate changes and those recent publications (e.g., Prokopenko et al., 1999; Horiuchi et al., 2000; Karabanov et al., 2000; Bezrukov et al., 2005; Demske et al., 2005; Tarasov et al., 2005, 2007; Prokopenko et al., 2007; Bezrukov et al., 2009; Shichi et al., 2009; Tarasov et al., 2009) well reflect the intensity of research. Overall, nearly all of the published Holocene pollen records from the Lake Baikal basin display approximately similar temporal variations. Generally speaking, birch and spruce mixed forests and shrubs replaced wormwood steppe during the early Holocene and Scots pine open forests became dominant vegetation since ~7 cal. kyr BP (Demske et al., 2005). And, this succession exhibits a time-transgressive trend from the south to the north (Prokopenko et al., 2007).

For this review paper, we examined 12 chronologically comparable pollen and/or diatom sequences (b1–b4 and b10–b17 in Fig. 1 and Table 1) and four of them (Vydrino Shoulder, Posolskoe High, Continental Ridge, Buguldeika; i.e., b1–b4) passed our quality scrutiny (i.e., quality score ≥ 22) and are presented in Fig. 3. These four sequences not only reasonably cover the entire lake basin from the south to the north, but also have the needed semi-quantitative or quantitative reconstructions of moisture and temperature. The semi-quantitative reconstructions (Fig. 3; sites b1–b3 in Fig. 1) were achieved using PFT-based bioclimatic framework. That is, temperature index and moisture index were calculated based on the ratios between groups of pollen taxa that represent different temperature and moisture conditions (Demske et al., 2005). The quantitative reconstruction at Buguldeika (Fig. 3; site b4 in Fig. 1) was achieved using the best modern analog technique (Tarasov et al., 2007). As shown in Fig. 3, the three semi-quantitative reconstructions display approximately the same trends of temperature and moisture indices (Demske et al., 2005). That is, increasing (i.e., warming) trends of the temperature index and decreasing (i.e., drying) trends of the moisture index are undeniable for the early Holocene (before ~6.0 cal. kyr BP). After ~6 cal. kyr BP the moisture index had a slight increasing (i.e., wetting) trend and the temperature index had a relatively steep declining (i.e., cooling) trend. However, the quantitative reconstruction from site b4 (i.e., lower-right panel of Fig. 3) seems to tell a different story (Tarasov et al., 2007). The reconstructed annual precipitation and winter temperature have parallel trends and both exhibit three stages of variations. The first stage was warming and wetting from ~11.0 to 8.3 cal. kyr BP, the second stage cooling and drying from ~8.3 to 5.8 cal. kyr BP, and the third stage again wetting and warming during the past ~5800 years.

The semi-quantitative reconstructions of the three sites (sites b1–b3) and the quantitative reconstruction of one site (site b4) share two commonalities: (1) a sharp turning point of temperature at ~6.0 cal. kyr BP and (2) a slight increasing (i.e., wetting) trend of moisture index after ~6.0 cal. kyr BP. Nevertheless, two differences between the semi-quantitative reconstructions (sites b1–b3) and the quantitative reconstruction (site b4) are striking. Firstly, temperature index had a decreasing trend after ~6.0 cal. kyr BP in the semi-quantitative reconstructions, while both summer and winter temperatures had slight increasing trends after ~6.0 cal. kyr BP in the quantitative reconstruction. Secondly, one-stage (i.e., warming/drying) climatic variation characterized the first half of the Holocene (from ~11.5 to ~6.0 cal. kyr BP) in the semi-quantitative reconstructions, while two-stage (i.e., warming/wetting, and cooling/drying) climatic variations were the characteristics of the first half of the Holocene in the quantitative reconstruction.

3.2.2. Altai Mountains

The modern distribution of vegetation in the Altai Mountains well reflects the north–south gradient of decreasing moisture and the west–east gradient of increasing continentality as the result of mostly Atlantic sources of moisture from the west and the influence of the Mongolian High Pressure System from the east. Although the Altai Mountains are situated at the latitude of the forest-steppe and steppe zones of the plains, the high relief promotes the expansion of mountain forests on the western and northern slopes of the mountain ranges. The northwestern Altai Mountains receive most precipitation from the westerlies and are covered by dark-coniferous forests (mainly *Abies sibirica*, *Picea obovata*, and *Pinus sibirica*). Farther southeast, with decreasing moisture and increasing continentality, light-conifer forest (mainly *P. sibirica* and *Larix sibirica*) are dominant. Low-elevation valleys are occupied by steppe vegetation and high-mountain vegetation includes shrubs, alpine meadows and tundra (Blyakharchuk et al., 2004, 2007).

The Altai Mountains has also been intensively studied during the past several decades and those published data were thoroughly reviewed by Rudaya and her colleagues in 2009 (Rudaya et al., 2009). Their review, primarily based on recent publications (e.g., Dorofeyuk and Tarasov, 1998; Tarasov et al., 2000; Blyakharchuk et al., 2004, 2007, etc.), concluded that in the eastern Altai area within Mongolia the first half of the Holocene (11.0–5.0 cal. kyr BP) was warm and wet and the second half (5.0–0 cal. kyr BP) was cool and dry, being consistent with the East Asian monsoon-dominated climate pattern. In the western Altai area within Kazakhstan the first half of the Holocene was warm and dry and the second half was cool and wet, being consistent with the westerlies-dominated climate pattern. In the northern Altai area within Russia the first half of the Holocene was warm and wet (being similar to the eastern Altai) and the second half was cool and wet (being similar to the western Altai) (Rudaya et al., 2009).

We totally examined 11 Holocene sequences and 5 of them (sites b5–b9 in Fig. 1 and Table 1) passed our quality scrutiny (Fig. 4). The

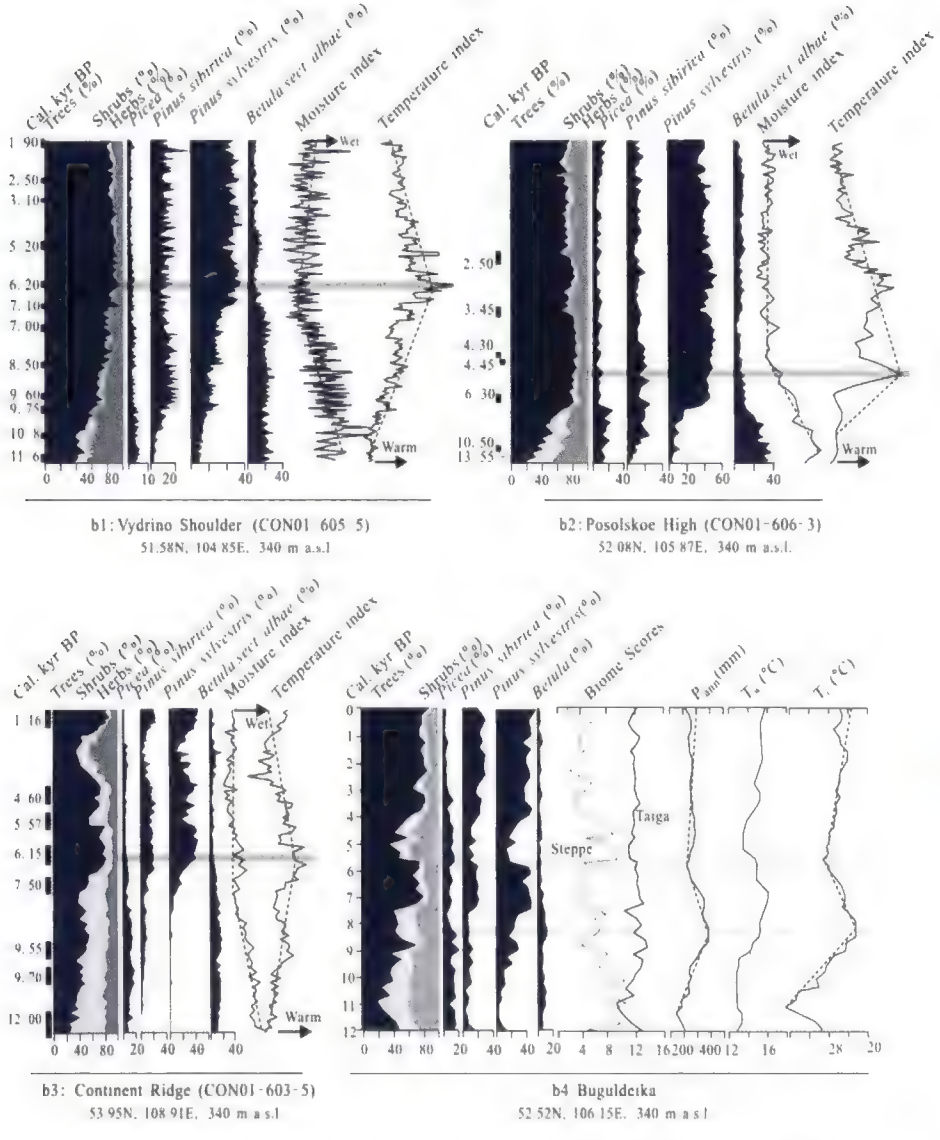

Fig. 3. Holocene variations of moisture proxies from winter monsoon-dominated Lake Baikal area (dashed lines indicate the trends of the proxy variations). Notes for the sources of references: Vydrino Shoulder, Posolskoe High and Continental Ridge (Demske et al., 2005) and Buguldeika (Tarasov et al., 2007).

first site to be reviewed here is the newly recovered sequence from Lake Hoton Nuur (Fig. 4; site b5 in Fig. 1) within the Mongolian Altai area (Rudaya et al., 2009) that significantly improved the sampling resolution over the old sequence reported by Tarasov et al. (2000). Before 10.5 cal. kyr BP cool steppe predominated around Lake Hoton Nuur as suggested by higher herb pollen percentages and associated higher steppe biome score. Biome reconstruction demonstrates a decrease in steppe scores and an associated increase in taiga scores, suggesting the spread of boreal trees and open woodland vegetation between 10.5 and 6.5 cal. kyr BP. After 6.5 cal. kyr BP the high-amplitude variations in the arboreal pollen (AP) and also in non-arboreal pollen (NAP) taxa percentages suggest rather unstable environmental conditions and an increased importance of the non-arboreal vegetation in the region. Relatively high quantities of *Picea*, *Abies*, *P. sibirica* and *Larix* pollen suggest that trees were still well present in the regional vegetation until ~5.0 cal. kyr BP. From ~5.0 cal. kyr BP onward steppe taxa in the pollen spectra increase significantly, indicating a strengthening of steppe communities and a weakening of taiga communities. This interpretation is also supported by low pollen concentrations and the disappearance of conifer stomata (Rudaya et al., 2009). The pollen-based quantitative reconstruction of precipitation using the best modern analog technique suggests that the regional climate was relatively dry prior to 10.5 cal. kyr BP and became substantially wetter during the following interval between 10.5 and 5.0 cal. kyr BP. A drying trend of the past ~5000 years is well expressed by all pollen proxies (Rudaya et al., 2009).

Towards north at Lake Akkol and Lake Grusha within the Russian Altai area, the modern vegetation in the watershed is steppe and the nearest forest (~30 km away) is *P. sibirica* and *L. sibirica* forest. The Holocene pollen spectrum at Akkol and Grusha (Fig. 4; sites b6 and b7 in Fig. 1) is dominated by *P. sibirica* pollen. Since *L. sibirica* is normally under-represented in pollen spectrum (Minckley and Whitlock, 2000;

Andreev et al., 2001; Ma et al., 2008), the *P. sibirica*-dominated pollen spectrum at Akkol and Grusha may well represent the expansion history of a coniferous forest. Because the *P. sibirica* and *L. sibirica* forest is presently representing the humidity-controlled lower limit of montane forests and also the humidity-controlled southeastern limit of zonal forests, the *P. sibirica*-dominated tree percentage can be interpreted as an indicator of moisture. If above reasoning is accepted, the tree percentage-suggested moisture curves at Lake Akkol and Lake Grusha within Russian Altai area resemble the reconstructed precipitation curve at the Lake Hoton Nuur within Mongolian Altai area, thus enhancing the acceptability of the moisture reconstructions. Further northwestward at Uzunkol and Kendegelukol (Fig. 4; sites b8 and b9 in Fig. 1) within Russian Altai area, pollen spectra exhibit different characteristics than those at Hoton Nuur, Lake Akkol and Lake Grusha. Specifically, Siberian pine co-varies with Scots pine and varies inversely with spruce during the entire Holocene. If the interpretation that the rising of spruce percentage is an indicator of the rising of temperature (Tarasov et al., 2000; Demske et al., 2005; Rudaya et al., 2009) is justifiable and acceptable, warm climate during the first half of the Holocene (10.5–5.0 cal. kyr BP) and cool climate during the second half (5.0–0 cal. kyr BP) should be the temperature history for the entire Altai Mountains.

3.3. *Westerlies-affected Northern Xinjiang*

Our focal area is northern Xinjiang where the mean annual precipitation is only ~100 mm and the potential evaporation is as high as >2000 mm, resulting in typical desert and desert steppe landscapes. The arid and hyper-arid northern Xinjiang is surrounded by the Chinese Altai Mountain area in the east and north and by the Tianshan Mountains in the west. The altitudinal differentiation of vegetation is

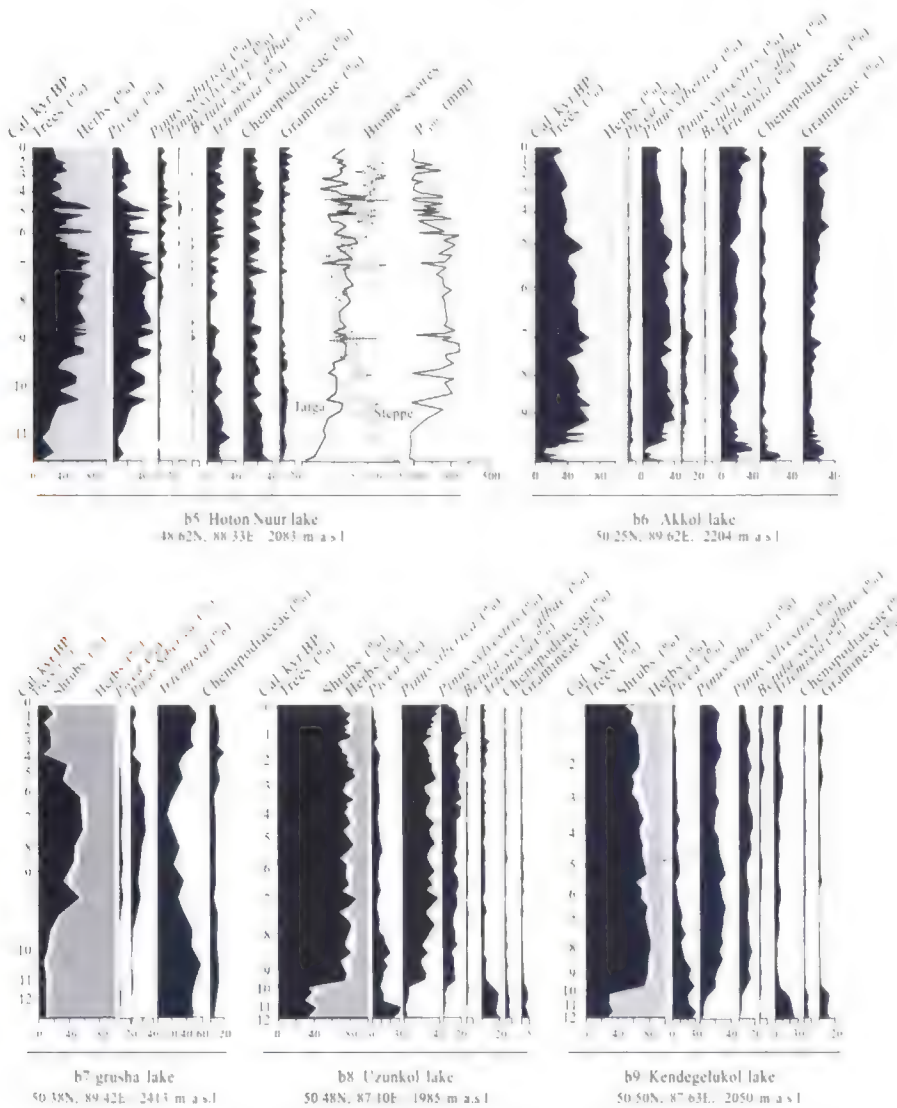

Fig. 4. Holocene variations of moisture proxies from winter monsoon-dominated Altai Mountains (within Russia and Mongolia)
Notes for the sources of references: Lake Hoton Nuur (Rudaya et al., 2009); Lake Akkol and Lake Grusha (Blyakharchuk et al., 2004); and Lake Uzunkol and Lake Kendegelukol Blyakharchuk et al., 2007

well displayed both in the Altai Mountains and the Tianshan Mountains. In the Chinese Altai Mountains the vertical vegetation zones from high to low elevations are: subalpine meadow, coniferous forest, forest steppe, steppe, and desert steppe. In the Tianshan Mountains the vertical zones are: subalpine meadows, forest, forest steppe, steppe, and desert steppe (Wu, 1980; Hu, 2004; Chen, 2010).

The earlier works of Holocene reconstructions were primarily based on the earlier belief that the cold-season precipitation was westerlies-related and the warm-season precipitation was Asian monsoon-related. Westerlies-related climates were characterized by alternating modes between cool/wet and warm/dry (Mangerud et al., 1974; Wendland and Bryson, 1974), whereas the Asian monsoon-related climates were characterized by alternating modes between warm/wet and cold/dry (Shi et al., 1993). Subsequently, the Holocene climate history in northern Xinjiang was heatedly debated in 1990s based on then-available data and two schools of thought were in the central stage of this debate. The first was the Asian monsoon-domination school (Wen and Qiao, 1990; Sun et al., 1994; Lin et al., 1996; Rhodes et al., 1996; Lin and Wei, 1998) and the second was the westerlies-domination school (Han and Yuan, 1990; Li, 1990; Han, 1992). Although the Asian summer monsoon (either from Pacific Ocean or/and from Indian Ocean) was repeatedly reported to be the source of warm-season precipitation at least for the eastern part of northern Xinjiang (Zhou, 1983; Li, 1991; Wei et al., 2003; Chen et al., 2005; Wang et al., 2005), the importance of the Asian summer monsoon was dismissed by recent works based on the observation of modern climates of central Asia (Aizen et al., 2001; Chen, 2010). These works demonstrate that cold-season precipitation in the western Tianshan Mountains areas including northern Xinjiang and the areas to the west (Aizen et al., 2001; Chen, 2010) is basically related to the polar front-forced southward shifting of the westerlies during cold seasons (Aizen et al., 2001). The warm-season precipitation in northern Xinjiang was also resulted from the westerlies, i.e., the northward-shifted westerlies that were forced by northward shifting of Azores High during warm seasons, being similar to the situations in Russian Plains and southern Siberia. The high-latitude cold air excursions are the snow storm-producing processes during cold seasons and are also rainfall-producing processes during warm seasons (Zhang and Shi, 2002; Wei et al., 2003; Hu, 2004; Chen, 2010).

To address the issue regarding the debates between the westerlies-domination school and the Asian monsoon-domination school, our review focuses on four lacustrine sequences including three published lacustrine sequences and one unpublished sequence (Lake Aibi): Lake Wulungu (site c1 in Fig. 1), Lake Aibi (site c2 in Fig. 1), Lake Bosten (site c3 in Fig. 1) and Lake Balikun (site c4 in Fig. 1) (Fig. 5). The Lake Wulungu area in the northern margin of the Zunggar Basin had experienced an arid early Holocene (~10–6.7 cal. kyr BP) under a small and shallow lake or swamp environment (Xiao et al., 2006; Jiang et al., 2007; Liu et al., 2008). However, this dry phase was not explicitly supported by the pollen assemblage. In other words, the pollen record of this zone may not actually reflect regional vegetation and climate for two reasons. Firstly, the pollen assemblage may be blurred by the strong contribution of wetland pollen types including *Sparganium* and small-sized Poaceae of *Phragmites* (Liu et al., 2008). Secondly, if the lake level was indeed very low before 6.7 cal. kyr BP as the reconstruction shows (see Fig. 5), the pollen assemblage before 6.7 cal. kyr BP might be only of local significance because lake size normally dictates the areal extent of pollen source (Prentice, 1985; Sugita, 1994). The lake level, reconstructed on the basis of carbon isotope and grain size with reference to pollen types (e.g., percentage of swamp pollen), had been rising from 6.7 to 4.0 cal. kyr BP and maintaining a high level from 4.0 to 0.5 cal. kyr BP (Jiang et al., 2007; Liu et al., 2008) (Fig. 5; site c1 in Fig. 1). A general wetting trend since 6.7 cal. kyr BP is also suggested by an increasing trend of A/C ratio and a decreasing trend of pollen-based desert biome scores, suggesting that the Holocene moisture optimum occurred between 4.2 and 0.5 cal. kyr BP. The second site is Lake Aibi (Fig. 5; site c2 in Fig. 1) in the western margin of the Zunggar Basin. Our review solely focuses on our unpublished pollen data because the earlier reconstructions at Lake Aibi (sites c7 and c8 in Fig. 1) (Li, 1993; Wu, 1995; Wu et al., 1996) did not have adequately chronologic control. The A/C ratio unequivocally indicates that the moisture in Lake Aibi area has been constantly rising since ~7.0 cal. kyr BP. The third site is Lake Bosten (Fig. 5; site c3 in Fig. 1) in the northeastern margin of the Tarim Basin. The lake water temperature was relatively low from ~5.7 to ~1.5 cal. kyr BP, as suggested by higher percentages of cold-water diatom and lower percentages of warm-water diatom (Yang, 2008). This cold-water period from ~5.7 to ~1.5 cal. kyr BP approximately corresponds with the high A/C-ratio period (Huang, 2006), suggesting that the period from ~5.7 to ~1.0 cal. kyr BP was cool and wet. This wet climate was also evidenced by the A/C ratio-indicated moisture increasing trend at Lake Balikun (Fig. 5; site c4 in Fig. 1) in the eastern margin of the Zunggar Basin (Tao et al., 2010). At the latter site (i.e., Balikun) superimposed on a general increasing trend of A/C ratio are two A/C ratio-indicated peaks of moisture. The first peak occurred from 7.5 to 4.3 cal. kyr BP and the second peak has lasted for past 2200 years. It is noticeable that our review-indicated wetting trend since ~7.5 cal. kyr BP is also supported by a recently published pollen sequence from Lake Tuolekule (site c15 in Fig. 1 and Table 1), a closed lake near Lake Balikun (An et al., 2011).

To sum up, a dry early Holocene and a progressive wetting middle and late Holocene pattern can be established for all of the aforementioned four sites. All four reconstructions (i.e., Lake Wulungu, Lake Aibi, Lake Bosten and Lake Balikun) generally support a contention (Chen et al., 2008) that the early Holocene (from ~11.5–10.0 to 7.5–6.7 cal. kyr BP) was dry and the middle to late Holocene (from 7.5–6.7 to 1.2 cal. kyr BP) was wet.

3.4. Arid areas of the Mongolian Plateau

The modern climate in the Mongolian Plateau becomes moister and warmer from the Gobi in the center towards the south because both the precipitation and the temperature increase southward (Wu, 1980). It becomes wetter and cooler from the Gobi towards the north because the precipitation increases and the temperature decrease northward (Tuvdendorzh and Myagmarzhav, 1985; Hilbig, 1995). The vegetation distributions closely follow the aforementioned precipitation–temperature combinations. From the Gobi to Russian Siberia (i.e., northward) the vegetation zones are: (1) desert (core of Gobi), (2) desert steppe, (3) cold steppe, (4) cold steppe-forest, and (5) coniferous forest (Hilbig, 1995). From the Gobi to the Chinese Loess Plateau (i.e., southward) the vegetation zones are: (1) desert (core of Gobi), (2) desert steppe, (3) temperate steppe, and (4) temperate steppe-forest (Wu, 1980; Hilbig, 1995). Our following review focus on two areas where Holocene climate reconstructions are available: (1) arid and semi-arid belt in the northern Mongolian Plateau within Mongolia, and (2) arid and hyper-arid belt in the southern Mongolian Plateau within the Mongolian Autonomous Region of China.

3.4.1. Northern Mongolian Plateau

We have examined 13 Holocene sequences (lacustrine, eolian and fluvial) from northern Mongolian Plateau (not including those from Mongolian Altai Mountains) and four of them are qualified for in-depth review. The four sections are: 1) Lake Ugii Nuur (site d1 in Fig. 1 and Table 1) in central Mongolia (Wang et al., 2009, 2011), 2) Lake Telmen (site d2 in Fig. 1) in central-west Mongolia (Peck et al., 2002; Fowell et al., 2003), 3) Lake Hovsgol (site d3 in Fig. 1) in northern Mongolia (Prokopenko et al., 2007) and 4) Lake Gun Nuur (site d4 in Fig. 1) in northern Mongolia (Dorofeyuk and Tarasov, 1998).

Our first site is Lake Ugii Nuur (Fig. 6; site d1 in Fig. 1) where our multi-proxy reconstruction shows that a mild climate with moderate

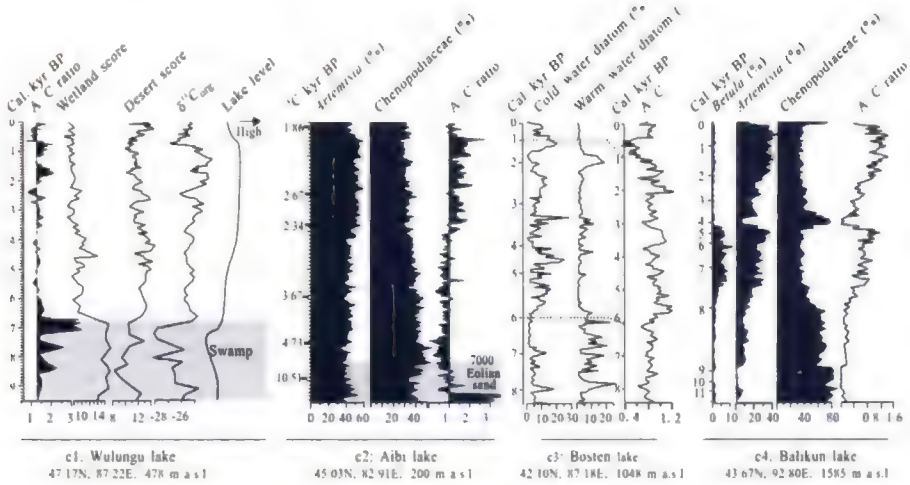

Fig. 5. Holocene variations of moisture proxies from the westerlies-affected northern Xinjiang.
Notes for the sources of references: Lake Wulungu (Xiao et al., 2006; Jiang et al., 2007; Liu et al., 2008); Lake Aibi (our unpublished data); Lake Bosten (Huang, 2006; Yang, 2008; Huang et al., 2009); Lake Balikun (Tao et al., 2010).

moisture conditions supported a desert steppe vegetation during 8.1–5.8 ^{14}C kyr BP (i.e., ~9.1–6.7 cal. kyr BP), as indicated by a moderate percentage of Chenopodiaceae, a generally high planktonic/benthic diatom ratio, and a moderately high pollen-based moisture index. This relatively humid and mild phase was followed by a mid-Holocene dry phase lasting from 5.8 to 3.1 ^{14}C kyr BP (i.e., ~6.7–3.3 cal. kyr BP) that is marked by a high percentage of Chenopodiaceae pollen and an extremely low planktonic/benthic diatom ratio. More importantly, this dry phase was well marked by the pollen-based moisture index. All of the three aforementioned variables exhibit a wet period between ~2.5 and ~1.0 ^{14}C kyr BP (i.e., 2.6–1.0 cal. kyr BP) that was followed by a relatively dry period (i.e., the past ~1000 years) (Wang et al., 2009, 2011). The Holocene climate sequence at Lake Telmen (Fig. 6; site d2 in Fig. 1) spans only past 6090 ^{14}C yr (i.e., 7100 cal. yr). The pollen-based aridity index (i.e., [A + C]/P; A = *Artemisia*, C = Chenopodiaceae, P = Poaceae) exhibits a similar mid-Holocene dry phase lasting from 6.1 to 4.1 ^{14}C kyr BP (i.e., from 7.1 to 4.6 cal. kyr BP), being generally supportive to the mid-Holocene dry phase reconstructed at Lake Ugii Nuur. The following period from 4.1 to 0 ^{14}C kyr BP (i.e., ~4.6–0 cal. kyr BP) has been generally wet with two short dry intervals at ~2.5 and at ~1.5 ^{14}C kyr BP (Peck et al., 2002; Fowell et al., 2003). The pollen-based steppe-forest index (i.e., SFI = (A + C + E + Ca) / T; A = *Artemisia*, C = Chenopodiaceae, E = *Ephedra*, Ca = Caryophllaceae, T = trees) at Lake Hovsgol (Fig. 6; site d3 in Fig. 1) in northern Mongolia unequivocally denotes a mid-Holocene dry phase lasting from ~6.0 to ~3.5 cal. kyr BP. It should be particularly noted that the dry phase (i.e., from ~6.0 to ~3.5 cal. kyr BP) was also characterized by disappearance of cold-water diatom species (e.g., *Cyclotella bodaniza*), implying that the mid-Holocene dry phase was probably also a warm phase. The early Holocene from ~9.5 to ~6.0 cal. kyr BP was a wet period and the late Holocene after 3.5 cal. kyr BP has also been relatively wet (Prokopenko et al., 2007). However, the fourth sequence, Lake Gun Nuur (Fig. 6; site d4 in Fig. 1), does not exhibit a similar trend to those from the other three sequences. Considering the recently reported carbon reservoir effect of 1060 years at Lake Gun Nuur (Zhang et al., 2012), the period from ~9.5 to ~8.0 cal. kyr BP was an interval of arbor pollen increasing and the period from ~8.0 to ~0 cal. kyr BP was an interval of a high percentage of arbor pollen (i.e., AP), suggesting that the moisture level has been generally high during the past 8000 years (Dorofeyuk and Tarasov, 1998). Nevertheless, a recently published non-pollen work on Gun Nuur (site d16 in Fig. 1) (Zhang et al., 2012) tells a story that seems to be supportive to the aforementioned mid-Holocene dry phase. That is, the lake level was generally low approximately from 7.0 to 2.5 cal. kyr BP as suggested by higher salinity and coarser grain size. The conflicting evidence from AP data at Gun Nuur against the mid-Holocene dry-phase contention is resulted from the unsettled bioclimate issue regarding Scots pine pollen, the dominant pollen species at Gun Nuur. For example, the Scots pine pollen was categorized as a dry-indicative species by Demske et al. (2005), but it was grouped into wet-indicative species by Ma et al. (2008). In addition, the mid-Holocene dry phase appears to be corroborated by the stratigraphy- and pollen-indicated climate history at nearby Shaamar eolian–paleosol section (Feng and Khosbayar, 2004; Feng et al., 2007). Specifically, at Shaamar section (Fig. 6; site d15 in Fig. 1), although not passing quality scrutiny because of a lower-than-22 quality index, the pedo- and litho-stratigraphic data (e.g., sand percentage and TOC content) and pollen data (e.g., coniferous percentage) well mark a mid-Holocene dry phase lasting from ~7.0 to 3.0 ^{14}C kyr BP (i.e., from ~7.8 to 3.1 cal. kyr BP). The mollisol-like paleosol developed in ~8.7–7.0 ^{14}C kyr BP (i.e., ~9.7–7.8 cal. kyr BP) represents a relatively wet early Holocene and the drastic increase in coniferous pollen percentage represents a relatively wet late Holocene (i.e., after ~3.0 ^{14}C kyr BP, i.e., 3.1 cal. kyr BP).

To sum up, a mid-Holocene dry phase can be established for the northern Mongolian Plateau and the dry phase was also likely a warm phase. Both the early Holocene and the late Holocene are characterized by relatively wet (and also probably cool) climates. The reviewed reconstructions exhibit the timing differences of the mid-Holocene dry phase and the differences were most likely resulted from one or combination of following factors: chronological uncertainties, different sampling resolution, and regional or local differences of the used proxies in responding to large-scale climatic forcing factors. In addition, we want to add that our proposed mid-Holocene dry phase in northern Mongolian Plateau is consistent with an early proposal by Tarasov et al. (1999) who argued for a mid-Holocene dry phase in central Mongolia. Finally, we want to stress that we are fully aware of recent publications arguing against the mid-Holocene dry-phase contention. For example, a mid-Holocene wet phase (from 8.0 to 4.0 cal. kyr BP) was inferred from mineralogical and geochemical proxy data at Lake Ugii Nuur (Schwanghart et al., 2009) and a mid-Holocene wet phase was also inferred from a palaeosol

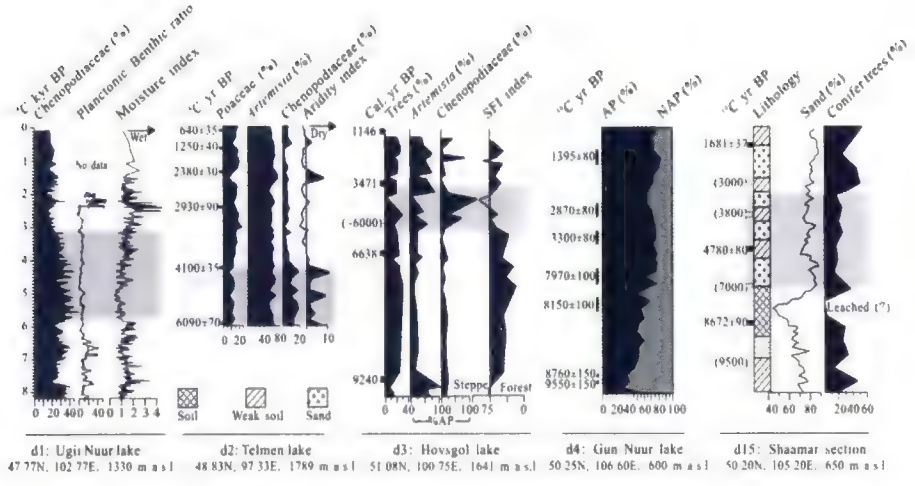

Fig. 6. Holocene variations of moisture proxies from northern Mongolian Plateau.

Notes for the sources of references: Lake Ugii Nuur (Wang et al., 2009, 2011); Lake Telmen (Peck et al., 2002; Fowell et al., 2003); Lake Hovsgol (Prokopenko et al., 2007); Lake Gun Nuur (Dorofeyuk and Tarasov, 1998). Data of Shaamar section (Feng et al., 2005) was also presented for discussion (not participated in our RA-moisture calculation).

dated at 5530 cal. yr BP in Orkhon Valley (Lehmkuhl et al., 2011). But, we think that their arguments (Schwanghart et al., 2009; Lehmkuhl et al., 2011) need to be validated with higher qualities of data (both proxies and chronologies).

3.4.2. Southern Mongolian Plateau

The southern Mongolian Plateau has been extensively investigated to reconstruct the Holocene climatic changes and the investigations have been primarily focusing on Lake Juyanze (e.g., Mischke et al., 2002; Chen et al., 2003b; Herzschuh et al., 2004; Hartmann and Wünemann, 2009), Lake Zhuyeze (Chen et al., 2003b, 2006; Zhao et al., 2008; Li et al., 2009; Long et al., 2010) and Lake Yanhaizi (Chen et al., 2003a). A mid-Holocene dry phase lasting from ~7.0 to ~4.6 ^{14}C kyr BP (i.e., from ~7.8 to ~5.2 cal. kyr BP) was first established based on stratigraphic records from Lake Juyanze and Lake Zhuyeze (Chen et al., 2003b) and gained supports from grain size and TOC data at Lake Yanhaizi (Chen et al., 2003a) and from pollen data at Lake Zhuyeze (Chen et al., 2006). It should be added that the mid-Holocene dry phase at Lake Juyanze spanning from 7.5 to 5.4 cal. kyr BP was unequivocally demarcated by sand deposits (Chen et al., 2003a) and seemly indicated by a slightly lower A/C ratio and a slightly higher desert biome score in comparison with those during the immediately preceding and immediately following periods (Herzschuh et al., 2004) (Fig. 7, site d5 in Fig. 1). In addition, the dry mid-Holocene contention was also supported by the geochemical mineralogical data at Lake Juyanze (Hartmann and Wünemann, 2009), although the data are not qualified to enter our regionally-averaged moisture reconstruction (Fig. 7; site d18 in Fig. 1). The sand-marked mid-Holocene dry phase lasting from 7.1 to 3.8 cal. kyr BP at Lake Zhuyeze was corroborated by high *Nitraria* pollen percentage and also by low pollen concentration, and the dry phase was preceded and followed by relatively wet periods (Fig. 7, site d6 in Fig. 1) (Chen et al., 2006). The mid-Holocene dry phase was also recorded by the extremely high sand percentage and low TOC content at Lake Yanhaizi (Fig. 7, site d7 in Fig. 1) and the dry phase lasted from 8.0 to 4.3 ^{14}C kyr BP (Chen et al., 2003a), being consistent with an early report of mid-Holocene high-salinity phase as indicated by inorganic isotopic data from the same lake (site d25 in Fig. 1 and Table 1) (Qian et al., 2002). With a full consideration of chronological uncertainties, these three sequences (Juyanze, Zhuyeze and Yanhaizi) of the stratigraphy-backed (primarily sand-rich layers) mid-Holocene dry phase might have occurred more or less synchronously.

However, the mid-Holocene dry-phase issue is not settled yet. For example, two pollen sequences (Fig. 7; sites d19 and d20 in Fig. 1) recently retrieved from a deeper part of the Lake Zhuyeze (Zhao et al., 2008; Li et al., 2009) failed to show the mid-Holocene dry phase. In our judgment, the stratigraphy-marked mid-Holocene dry-phase contention (Chen et al., 2003a,b, 2006) is more acceptable than the pollen-indicated "no dry-phase" contention (Zhao et al., 2008; Li et al., 2009). Our judgment is based on three reasons: (1) sand-rich layers in lacustrine sequences are normally associated with shallow water levels (Peng et al., 2005; Wünnemann et al., 2006); (2) the mid-Holocene dry-indicative eolian-sandy layers embedded in the palaeo-laustrine section were extensively reported from the Juyanze and Zhuyeze areas of Alashan Plateau in the western part of the Inner Mongolian Autonomous Region (see Chen et al., 2003b); and (3) the scarcity of pollen grains in eolian or fluvial sandy layers within lacustrine sequences may statistically distort the climatic interpretations of pollen data (Bennett, 1983).

4. Synthesis and discussion

4.1. Summer monsoon-influenced semiarid belt

As stated earlier, we used the region-averaging method to depict a regional pattern of the Holocene moisture variations. The method does smooth out details of individual reconstructions, but it provides a geographically coherent picture of moisture variations if all individual reconstructions exhibit generally similar trends. The proxies for averaging the regional moisture variations in the summer monsoon-influenced semiarid belt are: percentage of tree and shrub pollen at Lake Qinghai, Sujiawan and Dadiwan sections, reconstructed annual precipitation (pollen-based) at Lake Daihai, reconstructed ratio of precipitation over potential evaporation (pollen-based) at Lake Bayanchagan, reconstructed annual precipitation (pollen-based) at Lake Hulun. The regionally-averaged moisture history (diagram A: RA-Moisture Index of Monsoonal Margin in the lower-right panel of Fig. 8) of the six sequences demonstrates that the RA-moisture index curve in the summer monsoon-influenced semiarid area is in broad agreement with the synthesized East Asian Monsoon strength curve (diagram A1 in Fig. 8; Herzschuh, 2006; Zhao et al., 2009). The East Asian Monsoon strength curve in turn closely follows the general trends of the West Tropical Pacific SST (Stott et al., 2004) and precessional

cycle-related summer insolation anomaly of northern Hemisphere (COMHAP Members, 1988; Berger and Loutre, 1991) (diagram A2 in Fig. 8), suggesting that the East Asia monsoon has been influenced or controlled by the change of hydrologic cycle across the whole Pacific basin. That is, the enhancement of solar heating in the northern tropics during the early Holocene might have pulled the ITCZ north off its present summer latitude (Liu et al., 2000) and thus injected more water vapor into the East Asian monsoon system. In addition, the increased thermal contrast between the ocean and the Asian lands in response to the increased summer insolation in the northern hemisphere (COMHAP Members, 1988) might be an equally important factor in enhancing the Asian summer monsoon during the early Holocene. It is quite noticeable that our reconstructed RA-moisture index in Region A (i.e., summer monsoon-influenced semiarid belt) indicates that the monsoon advanced later and retreated earlier than the mean monsoon strength reconstructed by Zhao et al. (2009) and the mean effective moisture reconstructed by Herzschuh (2006), reflecting time-transgressive nature of the summer monsoon during the early Holocene

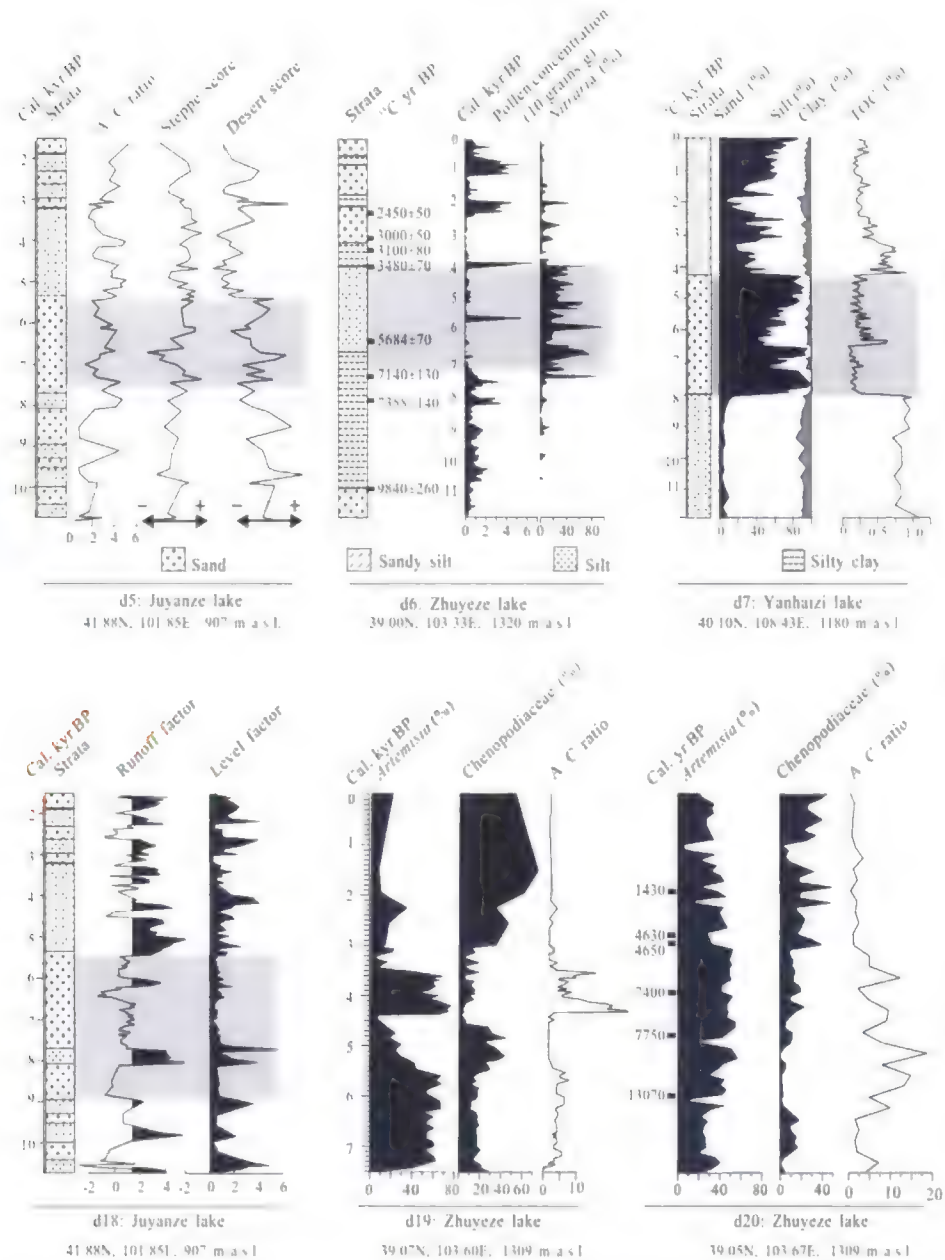

Fig. 7. Holocene variations of moisture proxies from southern Mongolian Plateau.

Notes for the sources of references: Lake Juyanze (Herzschuh et al., 2004); Lake Zhuyeze (Chen et al., 2003b, 2006); Lake Yanhaizi (Chen et al., 2003a). The sequences that did not participate in the RA-moisture reconstruction (e.g., Zhao et al., 2008; Hartmann and Wünemann, 2009; Li et al., 2009) were also presented to demonstrate the contradictions.

and during the late Holocene. It is also notable that there was about 1000 years of time lag of the East Asian Monsoon strength (9.5–7.5 cal. kyr BP) behind the West Tropical Pacific SST (10.5–9.0 cal. kyr BP) and the time lag suggests that the monsoon had a delayed response to the West Tropical Pacific SST during the early Holocene (An et al., 2000).

4.2. Winter monsoon-dominated southern Siberia

The used proxies for averaging the regional moisture variations in the winter monsoon-dominated southern Siberia are: pollen-based moisture index at three sites across Lake Baikal (Vydirino Shoulder, Posolskoe High, and Continental Ridge), reconstructed annual precipitation (pollen-based) at Buguldeika of Lake Baikal, reconstructed annual precipitation (pollen-based) at Lake Hoton Nuur and arboreal pollen percentage at four sites of Russian Altai Mountains (Akkol, Grusha, Uzunkol, and Kendegelukol). The RA-moisture index from Lake Baikal area (diagram B1 in the upper-left panel of Fig. 8) displays a slight rising trend from ~12.0 to 10.0 cal. kyr BP, a constant declining trend from ~10.0 to ~5.6 cal. kyr BP, and relatively stable low values after ~5.6 cal. kyr BP. The RA-moisture index for the Altai Mountains exhibits a drastic rising trend from ~11.0 to 9.6 cal. kyr BP, a constant peak from 9.6 to 6.6 cal. kyr BP and a fluctuating and declining trend after 6.6 cal. kyr BP (diagram B2 in Fig. 8).

We compared our regionally-averaged moisture index curves from Lake Baikal area and from Altai Mountains with the reported warm-season temperature and annual precipitation curve from Russian Plain (diagram B3 in Fig. 8; Velichko et al., 2002), assuming that the Holocene climate in Russian Plain was directly associated with that in southern Siberia (including Lake Baikal and Altai Mountains). This assumption is based on the observed modern climatic association between Russian Plain and southern Siberia via warm-season westerlies (Aizen et al., 2001). Specifically, the westerlies are forced to move northward during warm seasons by two factors: (1) Earth's tilt-driven northward shift of the atmospheric circulation cells (including Ferrel Cell associated with the westerlies), and (2) expansion and northward shift of the Azores High Pressure System (Bridgman and Oliver, 2006). As a result of the northward shift of the westerlies, the Russian Plain and southern Siberia are under the domination of the westerlies during warm season (Aizen et al., 2001). The warm-season temperature and annual precipitation that mainly occurred during warm seasons in Russian Plain (diagram B3 in Fig. 8) were in turn related by Velichko and his colleagues (Velichko et al., 2002) to the temperature (especially warm-season temperature) in Greenland (Stuiver et al., 1995; diagram B2 in Fig. 8). In addition, the well-developed Eastern Asian Low Pressure System during warm seasons that occupies the entire eastern half of China extending into southeastern Siberia "allures" the westerlies to move further eastward, enhancing the warm-season domination of the westerlies over the entire middle Asia stretching from the Caspian Sea to the Hinggan Mountains (Aizen et al., 2001). We thus attribute the declining trends of the Holocene RA-moisture indices in Lake Baikal area and in the Altai Mountains to the Holocene declining trends of the warm-season temperature in the North Atlantic region and in the downwind Russian Plain. Three points need to be made here regarding the reconstructed Holocene moisture trends in Lake Baikal area and in Altai Mountains and their comparison with the climate in Russian Plain. Firstly, the moisture increase in Lake Baikal area responded to the dramatic increases of the warm-season temperature and the annual precipitation in Russian Plain at the beginning of the Holocene more promptly than the moisture increase in Altai Mountains. The difference of responding time was probably resulted from the difference of elevations between the Lake Baikal area (340 m a.s.l.) and the Altai Mountains (~2000 m a.s.l.). Secondly, the increasing deviation of the reconstructed moisture trends in Lake Baikal area and in Altai Mountains from the warm-season temperature and annual precipitation trends in Russian Plain since 6.0 cal. kyr BP probably implies that the influence of North Atlantic Ocean on the precipitation in southern Siberia has been attenuating during the past 6000 years, following the general declining trend of the mean temperature in northern hemisphere. Thirdly, the error bars of the reconstructed RA-moisture index for the past 4000 years in Altai Mountains are undesirably large and the large error is resulted from an abnormally high moisture level as indicated by abnormally high AP percentage at Lake Uzunkol. The abnormally high moisture level may be of partially local significance under a fully-covered forest.

4.3. Westerlies-affected northern Xinjiang

The used proxies for averaging the regional moisture variations in the westerlies-affected northern Xinjiang are: reconstructed lake level (multiproxy-based including pollen) at Lake Wulungu and A/C ratio at three sites: Lake Aibi, Lake Bosten and Lake Balikun. The predominant feature of the RA-moisture index in northern Xinjiang (diagram C in lower-left panel of Fig. 8) is a persistent increasing trend since ~8 cal. kyr BP and the period between ~6.0 and 0.6 cal. kyr BP was the "Holocene Moisture Optimum". This RA-moisture trend is somewhat different from that by Chen et al. (2008) and considerably different from that by Herzschuh (2006) (C1 in Fig. 8). Specifically, both the RA-moisture index reconstructed in this study and the mean effective moisture reconstructed by Chen et al. (2008) exhibit a dry early Holocene (before ~8.0 cal. kyr BP), being opposite to the mean effective moisture reconstructed by Herzschuh (2006). The climbing trend of our reconstructed RA-moisture index for the period between 8.0 and 0.6 cal. kyr BP is different from the declining trends of the mean effective moisture reconstructed both by Chen et al. (2008) and by Herzschuh (2006), especially during the late Holocene. The climbing trend (i.e., wetting) in our reconstruction turned to a declining trend (i.e., drying) that lasted for the past ~600 years. Furthermore, the RA-moisture index of the northern Xinjiang seems to be approximately parallel with the winter insolation of the north hemisphere (Berger and Loutre, 1991) (panel C in Fig. 8) and also with the cold-season temperature of northwestern Europe (Davis et al., 2003) (C2 in Fig. 8). Logic reasoning is that the warming of North Atlantic area resulted from the rising winter insolation and the associated increasing of water vapor input into the westerlies system in cold seasons was responsible for the aforementioned parallel relationships.

4.4. Arid areas of the Mongolian Plateau

The used proxies for averaging the regional moisture variations in the arid areas of the Mongolian Plateau are: pollen-based moisture index at Lake Ugii Nuur, pollen-based aridity index at Lake Telmen, pollen-based SFI (steppe/forest index) at Lake Hovsgol, percentage of tree pollen at Lake Gun Nuur, A/C ratio at Lake Juyanze, *Nitraria* pollen percentage at Lake Zhuyeze and TOC content at Lake Yanhaizi. As shown in Fig. 8 (upper-right panel), the RA-moisture index curve exhibits a mid-Holocene dry phase lasting from ~7.0 to ~3.8 cal. kyr BP in the northern Mongolian Plateau (diagram D1 in Fig. 8) and the dry phase was preceded by a relative wet period (from ~10.0 to 7.0 cal. kyr BP) and followed by a considerably wet period (from ~3.8 cal. kyr BP onward). This mid-Holocene dry phase was approximately synchronous with the pollen-indicated warm interval in Lake Baikal basin lasting from ~6.5 to 2.5 cal. kyr BP (Demske et al., 2005). It should be noted the AP curve at Gun Nuur is not supportive to the mid-Holocene dry-phase contention although it was used in calculating the RA-moisture index simply because we do not have sufficient reason to reject the data. In the Southern Mongolian Plateau, the stratigraphy-backed "mid-Holocene dry-phase" contention first proposed by Chen and his colleagues (Chen et al., 2003b) seems to be more acceptable than "no dry phase" contention. The regionally-averaged moisture index curve (diagram D2 in Fig. 8) from the three stratigraphy-backed sequences in the southern Mongolian Plateau

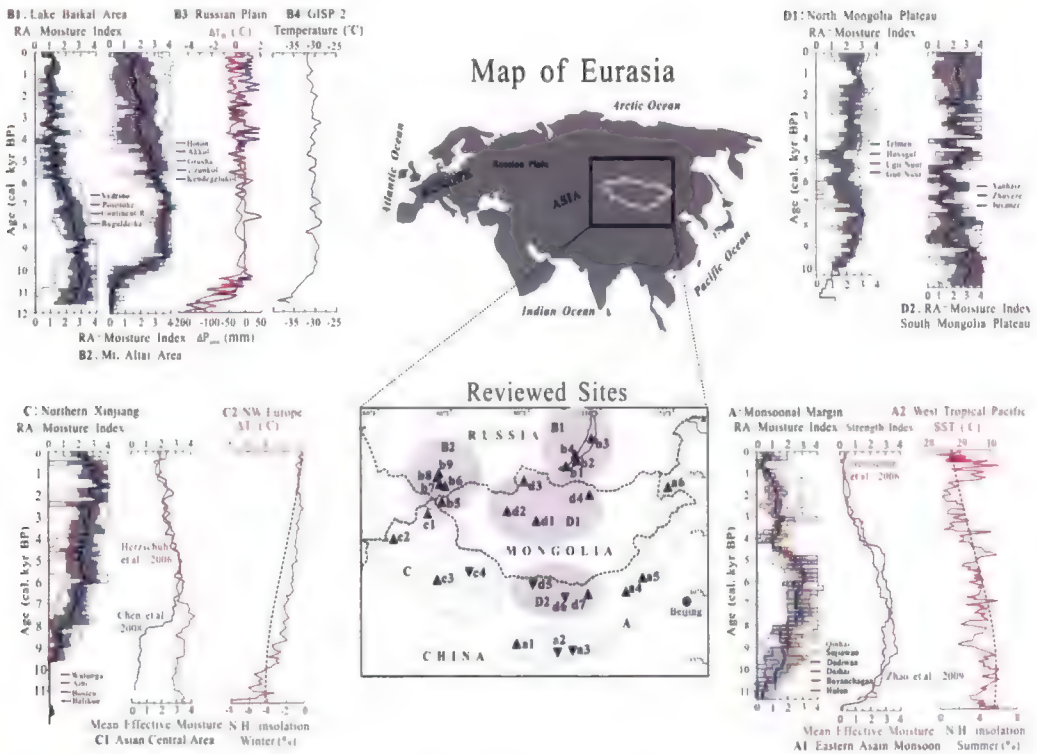

Fig. 8. RA-moisture indices and the comparison with the associated climate systems.

Notes: (1) the index from the summer monsoon influenced semiarid belt is compared with the synthesized East Asian Monsoon (ESM) Strength index (Zhao et al., 2009), Mean Effective Moisture Index of monsoonal China (Herzschuh, 2006), West Tropical Pacific SST (Stott et al., 2004) and the Northern Hemispheric Summer Insolation Anomaly (COHMAP members, 1988; Berger and Loutre, 1991); (2) the index from southern Siberian is compared with warm-season temperature and annual precipitation from Russian Plain (Velichko et al., 2002), the temperature of Greenland (Stuiver et al., 1995); and (3) the index from the northern part of Xinjiang is compared with the average moisture index of Asian Central Area (ACA) by Chen et al. (2008) and Mean Effective Moisture Index by Herzschuh (2006), the cold-season temperature deviation in northern Europe (Davis et al., 2003), and the northern hemispheric winter insolation (Berger and Loutre, 1991).

(i.e., upper panel in Fig. 7) suggests that a mid-Holocene dry phase occurred between ~8.0 and 4.0 cal. kyr BP. The mid-Holocene dry phase was chronologically corresponding with the warm and humid mid-Holocene (mainly warm-season) in the Southern Siberia to the north (Demske et al., 2005) and also with the warm and humid mid-Holocene (mainly warm-season) in monsoonal China to the south (Shi et al., 1993), suggesting that the mid-Holocene dry phase in the arid and semiarid portions of the Mongolian Plateau was most likely the result of high warm-season temperatures during the mid-Holocene (Bush, 2005; Wang et al., 2011). That is, the evaporation increase resulted from rising temperature might have exceeded the precipitation increase (if any) in the arid and semiarid portions of the Mongolian Plateau, resulting in the aridity increase. The relative wet climates in the arid and semiarid portions of the Mongolian Plateau before and after the mid-Holocene dry phase were most likely the results of relatively low warm-season temperatures.

5. Concluding remarks

(1) The Holocene moisture history in the summer monsoon-influenced semiarid belt has been broadly in phase with the synthesized history of the East Asian Monsoon strength, the latter being the delayed response to the Western Tropical Pacific SST that directly followed the trend of N.H. summer insolation.

(2) The Holocene moisture history in southern Siberia seems to be a part of the moisture history of the entire middle strip of Eurasia where the westerlies system contributes to the major portion of the warm-season precipitation.

(3) The reconstructed increasing trend of Holocene moisture in northern Xinjiang may be related to the increasing trend of cold-season temperature in northern Europe that was in turn related to the climbing trend of Holocene winter insolation.

(4) The chronological correspondences between dry phases and warm intervals in the northern Mongolian Plateau within Mongolia and southern Mongolian Plateau within China lend a support to the proposal that the mid-Holocene dry phase was most likely the result of mid-Holocene high warm-season temperatures. The relative wet climates before and after the mid-Holocene dry phase were likely the results of relatively low warm-season temperatures.

Acknowledgment

This paper is a result of research projects supported by three Chinese Nature Science Foundation grants (No. 40930102, No. 40331102 and No. 41162004) and one Inner Mongolia Autonomous Region's Nature Science Foundation grant (No. 2009BS601). Thanks

were also given to the anonymous reviewers for their constructive advices.

References

Aizen, E.M., Aizen, V.B., Melack, J.M., Nakamura, T., Ohta, T., 2001. Precipitation and atmospheric circulation patterns at mid-latitudes of Asia. International Journal of Climatology 21, 535–556.

An, Z., Kukla, G.J., Porter, S.C., Xiao, J., 1991. Magnetic susceptibility evidence of monsoon variation on the Loess Plateau of central China during the last 130,000 years. Quaternary Research 36, 29–36.

An, Z.S., Porter, S.C., Kutzbach, J.E., Wu, X.H., Wang, S.M., Liu, X.D., Li, X.Q., Zhou, W.J., 2000. Asynchronous Holocene optimum of the East Asian monsoon. Quaternary Science Reviews 19 (8), 743–762.

An, C.B., Feng, Z.D., Barton, L., 2006. Dry or humid? Mid-Holocene humidity changes in arid and semi-arid China. Quaternary Science Reviews 25 (3–4), 351–361.

An, C.B., Chen, F., Barton, L., 2008. Holocene environmental changes in Mongolia: a review. Global and Planetary Change 63, 283–289.

An, C.B., Zhao, J.J., Tao, S.C., Lv, Y.B., Dong, W.M., Li, H., Jin, M., Wang, Z.L., 2011. Dust variation recorded by lacustrine sediments from arid Central Asia since 15 cal ka BP and its implication for atmospheric circulation. Quaternary Research 75, 566–573.

An, Z.S., Colman, S.M., Zhou, W.J., Li, X.Q., Brown, E.T., Jull, A.J.T., Cai, Y.J., Huang, Y.S., Lu, X.F., Chang, H., Song, Y.G., Sun, Y.B., Xu, H., Liu, W.G., Jin, Z.D., Liu, X.D., Cheng, P., Liu, Y., Ai, L., Li, X.Z., Liu, X.J., Yan, L.B., Shi, Z.G., Wang, X.L., Wu, F., Qiang, X.K., Dong, J.B., Lu, F.Y., Xu, X.W., 2012. Interplay between the Westerlies and Asian monsoon recorded in Lake Qinghai sediments since 32 ka. Scientific Reports 2, 1–7.

Andreev, A.A., Klimanov, V.A., Sulerzhitsky, L.D., 2001. Vegetation and climate history of the Yana River lowland, Russia, during the last 6400 yr. Quaternary Science Reviews 20, 259–266.

Bennett, K.D., 1983. Devensian Late-glacial and flandrian vegetational history at Hockham mere, Norfolk, England. II. Pollen accumulation rates. New Phytologist 95, 489–504.

Berger, A., Loutre, M.F., 1991. Insolation values for the climate of the last 10 million years. Quaternary Science Reviews 10, 297–317.

Bezrukov, E.V., Abzaeva, A.A., Letunova, P.P., Kulagina, N.V., Vershinin, K.E., Belov, A.V., Orlova, L.A., Danko, L.V., Krapinina, S.M., 2005. Post-glacial history of Siberian spruce (*Picea obovata*) in the Lake Baikal area and the significance of this species as a paleo-environmental indicator. Quaternary International 136, 47–57.

Bezrukov, E.V., Abzaeva, A.A., Letunova, P.P., Kulagina, N.V., Orlova, L.A., 2009. Evidence of environmental instability of the Lake Baikal area after the last glaciation (based on pollen records from peatlands). Archaeology, Ethnology and Anthropology of Eurasia 37 (3), 17–25.

Birks, H.J.B., 1995. In: Maddy, D., Brew, J.S. (Eds.). Quantitative Palaeoenvironmental Reconstructions. Statistical Modeling of Quaternary Science Data. Quaternary Research Association, Cambridge, pp. 161–254.

Blyakharchuk, T.A., Wright, H.E., Borodavko, P.S., van der Knaap, W.O., Ammann, B., 2004. Late Glacial and Holocene vegetational changes on the Ulagan high-mountain plateau, Altai Mountains, southern Siberia. Palaeogeography, Palaeoclimatology, Palaeoecology 209 (1–4), 259–279.

Blyakharchuk, T.A., Wright, H.E., Borodavko, P.S., van der Knaap, W.O., Ammann, B., 2007. Late Glacial and Holocene vegetational history of the Altai Mountains (southwestern Tuva Republic, Siberia). Palaeogeography, Palaeoclimatology, Palaeoecology 245 (3–4), 518–534.

Bridgman, B.H., Oliver, J.E., 2006. The Global Climate System: Patterns, Processes, and Teleconnections. Cambridge University Press, New York (243 pp.).

Bush, A.B.G., 2005. CO_2/H_2O and orbitally driven climate variability over central Asia through the Holocene. Quaternary International 136, 15–23.

Chen, X., 2010. Geography of Chinese Arid Region. Science Press, Beijing (in Chinese).

Chen, F.H., Bloemendal, J., Wang, J.M., Li, J.J., Oldfield, F., 1997. High-resolution multi-proxy climate records from Chinese loess: evidence for rapid climatic changes over the last 75 kyr. Palaeogeography, Palaeoclimatology, Palaeoecology 130, 323–335.

Chen, F.H., Shi, Q., Wang, J.M., 1999. Environmental changes documented by sedimentation of Lake Yiema in arid China since the Late Glaciation. Journal of Paleolimnology 22, 159–169.

Chen, C.T.A., Lan, H.C., Lou, J.Y., Chen, Y.C., 2003a. The dry Holocene Megathermal in Inner Mongolia. Palaeogeography, Palaeoclimatology, Palaeoecology 193, 181–200.

Chen, F.H., Wu, W., Holmes, J.A., Madsen, D.B., Zhu, Y., Jin, M., Oviatt, C.G., 2003b. A mid-Holocene drought interval as evidenced by lake desiccation in the Alashan Plateau, Inner Mongolia, China. Chinese Science Bulletin 48, 1401–1410.

Chen, T.Y., Li, Z.R., Chen, Q., Li, B.Z., 2005. The analysis of climate characteristics of water vapor distribution over northwest China with water vapor field retrieved from GMS5 satellite data. Chinese Journal of Atmospheric Sciences 29, 864–871 (in Chinese with English Abstract).

Chen, F.H., Cheng, B., Zhao, Y., Zhu, Y., Madsen, D.B., 2006. Holocene environmental change inferred from a high-resolution pollen record, Lake Zhuyeze, arid China. The Holocene 16, 675–684.

Chen, F.H., Yu, Z.C., Yang, M.L., Ito, E., Wang, S.M., Madsen, D.B., Huang, X.Z., Zhao, Y., Sato, T., Birks, H.J.B., Boomer, I., Chen, J.H., An, C.B., Wünnemann, B., 2008. Holocene moisture evolution in arid central Asia and its out-of-phase relationship with Asian monsoon history. Quaternary Science Reviews 27 (3–4), 351–364.

Davis, B.A.S., Brewer, S., Stervenson, A.C., Guiot, J., Contributors, D., 2003. The temperature of Europe during the Holocene reconstructed from pollen data. Quaternary Science Reviews 22, 1701–1706.

Demske, D., Heumann, G., Granoszewski, W., Nita, M., Mamokowa, K., Tarasov, P.E., Oberhansli, H., 2005. Late glacial and Holocene vegetation and regional climate variability evidenced in high-resolution pollen records from Lake Baikal. Global and Planetary Change 46, 255–279.

Dorofeyuk, N.I., Tarasov, P.E., 1998. Vegetation and lake levels in Northern Mongolia in the last 12,500 years as indicated by data of pollen and diatom analyses. Stratigraphy and Geological Correlation 6 (1), 70–83.

El-Mosilimany, A.P., 1990. Ecological significance of common non-arboreal pollen: examples from drylands of the Middle East. Review of Palaeobotany and Palynology 64, 343–350.

Fang, X.M., Ono, Y., Fukusawa, H., Pan, B.T., Li, J.J., Guan, D.H., Oi, K., Tsukamoto, S., Torii, M., Mishima, T., 1999. Asian summer monsoon instability during the past 60,000 years: magnetic susceptibility and pedogenic evidence from the western Chinese Loess Plateau. Earth and Planetary Science Letters 168, 219–232.

Fang, X.M., Lv, L.Q., Mason, J.A., Yang, S.L., An, Z.S., Li, J.J., Guo, Z.L., 2003. Pedogenic response to millennial summer monsoon enhancements on the Tibetan Plateau. Quaternary International 106, 79–88.

Feng, Z.D., 2001. Gobi dynamics in the Northern Mongolian Plateau during the past 20,000+ yr: preliminary results. Quaternary International 76, 77–83.

Feng, Z.D., Khosbayar, P., 2004. Paleosubarctic Eolian environments along the southern margin of the North American Icesheet and the southern margin of Siberia during the Last Glacial Maximum. Palaeogeography, Palaeoclimatology, Palaeoecology 212 (3–4), 265–275.

Feng, Q., Liu, W., 2005. Environmental conditions leading to the formation of Holocene soil layers in the Northern Taklimakan Desert, Tarim Basin, Northwest China. Geological Journal 40 (1), 23–34.

Feng, Z.D., An, C.B., Tang, L.Y., Jull, A.J.T., 2004. Stratigraphic evidence of a Megahumid climate between 10,000 and 4000 years B.P. in the western part of the Chinese Loess Plateau. Global and Planetary Change 43 (3–4), 145–155.

Feng, Z.D., Wang, W.G., Guo, L.L., Khosbayar, P., Narantsetseg, T., Jull, A.J.T., An, C.B., Li, X.Q., Zhang, H.C., Ma, Y.Z., 2005. Lacustrine and eolian records of Holocene climate changes in the Mongolian Plateau: preliminary results. Quaternary International 136 (1), 25–32.

Feng, Z.D., An, C.B., Wang, H.B., 2006a. Holocene climatic and environmental changes in the arid and semi-arid areas of China: a review. The Holocene 16 (1), 119–130.

Feng, Z.D., Tang, L.Y., Wang, H.B., Ma, Y.Z., Liu, K.B., 2006b. Holocene vegetation variations and the associated environmental changes in the western part of the Chinese Loess Plateau. Palaeogeography, Palaeoclimatology, Palaeoecology 241, 440–456.

Feng, Z.D., Zhai, X.W., Ma, Y.Z., Huang, C.Q., Wang, W.G., Zhang, H.C., Khosbayar, P., Narantsetseg, T., Liu, K.B., Rutter, N.W., 2007. Eolian environmental changes in the Northern Mongolian Plateau during the past 35,000 yr. Palaeogeography, Palaeoclimatology, Palaeoecology 245 (3–4), 505–517.

Fowell, S.J., Hansen, B., Peck, J.A., Khosbayar, P., Ganbold, E., 2003. Mid to late Holocene climate evolution of the Lake Telmen Basin, North Central Mongolia, based on palynological data. Quaternary Research 59 (3), 353–363.

Fukumoto, Y., Kashima, K., Orkhonselenge, A., Ganzorig, U., 2012. Holocene environmental changes in northern Mongolia inferred from diatom and pollen records of peat sediment. Quaternary International 254, 83–91.

Gao, Y.X., 1962. Some Problems on East Asia Monsoon. Science Press, Beijing 49–63 (in Chinese).

Gong, D.Y., Wang, S.W., Zhu, J.H., 2001. East Asian winter monsoon and Arctic Oscillation. Geophysical Research Letters 28 (10), 2073–2076.

Grunert, J., Lehmkuhl, F., Walther, M., 2000. Paleoclimatic evolution of the Uvs Nuur basin and adjacent areas (Western Mongolia). Quaternary International 65 (66), 171–192.

Guiot, J., 1990. Methodology of the last climatic cycle reconstruction from pollen data. Palaeogeography, Palaeoclimatology, Palaeoecology 80, 49–69.

Gunin, P.D., 1999. Vegetation Dynamics of Mongolia. Kluwer Academic Publisher, Copenhagen (238 pp.).

Guo, L.L., Feng, Z.D., Li, X.Q., Liu, L.Y., Wang, L.X., 2007. Holocene climatic and environmental changes recorded in Baahar Nuur Lake core in the Ordos Plateau, Inner Mongolia of China. Chinese Science Bulletin 52 (7), 959–966.

Han, S.T., 1992. Holocene environmental change sequence of Barkol Lake, northern Xinjiang. Scientia Geologica Sinica 12, 247–260 (in Chinese with English abstract).

Han, S.T., Yuan, Y.J., 1990. The sequence of paleoclimatic variation of Balikun Lake of Xinjiang in the past 35,000 years. Acta Geographica Sinica 45, 350–362 (in Chinese with English abstract).

Harrison, S.P., Yu, G., Tarasov, P.E., 1996. Late Quaternary lake-level record from northern Eurasia. Quaternary Research 45 (2), 138–159.

Hartmann, K., Wünemann, B., 2009. Hydrological changes and Holocene climate variations in NW China, inferred from lake sediments of Juyanze palaeolake by factor analyses. Quaternary International 194, 28–44.

He, Y., Theakstone, W.H., Zhang, Z.L., Zhang, D.A., Yao, T.D., Chen, T., Shen, Y.P., Pang, H.X., 2004. Asynchronous Holocene climatic change across China. Quaternary Research 61 (1), 52–63.

Herzschuh, U., 2006. Palaeo-moisture evolution in monsoonal Central Asia during the last 50,000 years. Quaternary Science Reviews 25 (1–2), 163–178.

Herzschuh, U., Tarasov, P., Wünemann, B., Hartmann, K., 2004. Holocene vegetation and climate of the Alashan Plateau, NW China, reconstructed from pollen data. Palaeogeography, Palaeoclimatology, Palaeoecology 211 (1–2), 1–17.

Hilbig, W., 1995. The Vegetation of Mongolia. SPB Academic Publishing, Amsterdam (258 pp.).

Horiuchi, K., Minoura, K., Hoshino, K., Oda, T., Nakamura, T., Kawai, T., 2000. Palaeoenvironmental history of Lake Baikal during the last 23,000 years. Palaeogeography, Palaeoclimatology, Palaeoecology 157 (1–2), 95–108.

Hu, R.J., 2004. Geography of Tienshan, China. Chinese Environment Science Press, Beijing (443 pp. in Chinese).

Huang, X.Z., 2006. Holocene climate variability of arid central Asia documented by Bosten Lake, Xinjiang, China. Ph.D. Dissertation, Lanzhou University (in Chinese with English Abstract).
Huang, X.Z., Chen, F.H., Fan, Y.X., Yang, M.L., 2009. Dry late-glacial and early Holocene climate in arid central Asia indicated by lithological and palynological evidence from Bosten Lake, China. Quaternary International 194, 19–27.
Jiang, W.Y., Guo, Z.T., Sun, X.J., Wu, H.B., Chu, G.Q., Yuan, B.Y., Hatte, C., Guiot, J., 2006. Reconstruction of climate and vegetation changes of Lake Bayanchagan (Inner Mongolia): Holocene variability of the East Asian monsoon. Quaternary Research 65 (3), 411–420.
Jiang, Q.F., Shen, J., Liu, X.Q., Zhang, E.L., Xiao, X.Y., 2007. A high-resolution climatic change since Holocene inferred from multi-proxy of lake sediment in westerly area of China. Chinese Science Bulletin 52 (14), 1970–1979.
Karabanov, E.B., Prokopenko, A.A., Williams, D.F., Khursevich, G.K., 2000. A new record of Holocene climate change from the bottom sediments of Lake Baikal. Palaeogeography, Palaeoclimatology, Palaeoecology 156 (3–4), 211–224.
Kim, J.-H., Kim, J.-H., Rumbu, N., Lorenz, S.J., Lohmann, G., Nam, S.-Il, Schouten, S., Ruhlemann, C., Schneider, R.R., 2004. North Pacific and North Atlantic sea-surface temperature variability during the Holocene. Quaternary Science Reviews 23, 2141–2154.
Klimanov, V.A., 1984. Paleoclimatic reconstruction based on the information-statistical method. In: Velichko, A.A., Wright, H.E., Barnosky, C.W. (Eds.), Late Quaternary Environments of the Soviet Union. University of Minnesota Press, Minneapolis, pp. 297–303.
Kutzbach, J.E., Liu, Z., 1997. Response of the African monsoon to orbital forcing and ocean feedbacks in the middle Holocene. Science 278, 440–443.
Lehmkuhl, F., Hilgers, A., Fries, S., Hulle, D., Schlutz, F., Shumilovskikh, L., Felauer, T., Protze, J., 2011. Holocene geomorphological processes and soil development as indicator for environmental change around Karakorum, Upper Orkhon Valley (Central Mongolia). Catena 87, 31–44.
Li, J.J., 1990. The patterns of environmental changes since late Pleistocene in northwestern China. Quaternary Sciences 3, 197–204 (in Chinese with English Abstract).
Li, J.F., 1991. Climate of Xinjiang. Meteorological Press, Beijing 1–85 (in Chinese).
Li, G.S., 1993. Records of stable oxygen and carbon isotopes and abrupt climatic changes in Aibi Lake since 20 ka B.P. Marine Geology & Quaternary Geology 13, 75–64 (in Chinese with English Abstract).
Li, X.Q., Zhou, W.J., An, Z.S., Dodson, J., 2003a. The vegetation and monsoon variations at the desert–loess transition belt at Midiwan in northern China for the last 13 ka. The Holocene 13 (5), 779–784.
Li, X.Q., Zhou, W.J., Dodson, J., 2003b. The vegetation characteristics of the Yuan area at Yaoxian on the Loess Plateau in China over the last 12000 years. Review of Palaeobotany and Palynology 124, 1–7.
Li, Y., Wang, N., Cheng, H., Long, H., Zhao, Q., 2009. Holocene environmental change in the marginal area of the Asian monsoon: a record from Zhuye Lake, NW China. Boreas 38, 349–361.
Lin, R.F., Wei, K.Q., 1998. Palaeoclimate implications of oxygen isotope record from lacustrine sediments of Manas Lake, Xinjiang: a comparison with those from Qinhai Lake and Siling Lake. Quaternary Sciences 4, 308–318 (in Chinese with English Abstract).
Lin, R.F., Wei, K.Q., Cheng, Z.-Y., Wang, Z.X., Gasse, F., Fontes, J.-C., Gibert, E., Tucholka, P., 1996. A palaeoclimatic study on lacustrine cores from Manas Lake, Xinjiang, western China. Geochimica 25, 63–72 (in Chinese with English Abstract).
Lister, G.S., Kelts, K., Zao, C.K., Yu, J.-Q., Niessen, F., 1991. Lake Qinghai, China: closed-basin lake levels and the oxygen isotope record for ostracoda since the latest Pleistocene. Palaeogeography, Palaeoclimatology, Palaeoecology 84, 141–162.
Liu, Z., Kutzbach, I., Wu, L., 2000. Modeling climate shift of El Nino variability in the Holocene. Geophysical Research Letters 27, 2265–2268.
Liu, X.Q., Shen, J., Wang, S.M., Yang, X.D., Tong, G.B., Zhang, E.L., 2002a. A 16000-year pollen record of Qinghai Lake and its paleoclimate and paleoenvironment. Chinese Science Bulletin 47, 1931–1936.
Liu, H.Y., Xu, L.H., Cui, H.T., 2002b. Holocene history of desertification along the woodland–steppe border in northern China. Quaternary Research 57, 259–270.
Liu, X.Q., Herzschuh, U., Shen, J., Jiang, Q.F., Xiao, X.Y., 2008. Holocene environmental and climatic changes inferred from Wulungu Lake in northern Xinjiang, China. Quaternary Research 70 (3), 412–425.
Long, H., Lai, Z.P., Wang, N.A., Li, Y., 2010. Holocene climate variations from Zhuyeze terminal lake records in East Asian monsoon margin in arid northern China. Quaternary Research 74 (1), 46–56.
Lydolph, P.E., 1977. Climates of the Soviet Union in World Survey of Climatology, 7. Elsevier Scientific Publishing, New York (115 pp.).
Ma, Y.Z., Zhang, H.C., Pachur, H.J., Wünnemann, B., Li, J.J., Feng, Z.D., 2004. Modern pollen-based interpretations of mid-Holocene palaeoclimate (8500 to 3000 cal. BP) at the southern margin of the Tengger desert, northwestern China. The Holocene 14 (6), 841–850.
Ma, Y.Z., Liu, K.-B., Feng, Z.D., Sang, Y.L., Wang, W., Sun, A.Z., 2008. A survey of modern pollen and vegetation along a south–north transect in Mongolia. Journal of Biogeography 35, 1512–1532.
Mangerud, J., Andersen, S.T., Berglund, B.E., Donner, J.J., 1974. Quaternary stratigraphy of Norden, a proposal for terminology and classification. Boreas 3 (3), 109–126.
Mayewski, P.A., Rohling, E.E., Stager, J.C., Karlén, W., Maasch, K.A., Meeker, L.D., Meyerson, E.A., Gasse, F., van Kreveld, S., Holmgren, K., Lee-Thorp, J., Rosqvist, G., Rack, F., Staubwasser, M., Schneider, R.R., Steig, E.J., 2004. Holocene climate variability. Quaternary Research 62 (3), 243–255.
Meeker, L.D., Mayewski, P.A., 2002. A 1400-year high-resolution record of atmospheric circulation over the North Atlantic and Asia. The Holocene 12 (3), 257–266.
C.O.H.M.A.P. Members, 1988. Climatic changes of the last 18,000 years: observations and model simulations. Science 241, 1043–1052.
Minckley, T., Whitlock, C., 2000. Spatial variation of modern pollen in Oregon and southern Washington, USA. Review of Palaeobotany and Palynology 112, 97–123.
Mischke, S., Fuchs, D., Riedel, F., Schudack, M.E., 2002. Mid to Late Holocene palaeoenvironment of Lake Eastern Juyanze (north-western China) based on ostracods and stable isotopes. Geobios 35, 99–110.
Moore, P.D., Webb, J.A., Collinson, M.E., 1991. Pollen Analysis, 2nd edition. Blackwell Scientific Publication, Oxford (216 pp.).
Morley, D.W., Leng, M.J., Mackay, A.W., Sloane, H.J., 2005. Late glacial and Holocene environmental change in the Lake Baikal region documented by oxygen isotopes from diatom silica. Global and Planetary Change 46, 221–233.
Morrill, C., Overpeck, J.T., Cole, J.E., 2003. A synthesis of abrupt changes in the Asian summer monsoon since the last deglaciation. The Holocene 13 (4), 465–467.
Murakami, T., Katsuta, N., Yamamoto, K., Takamatsu, N., Takano, M., Oda, T., Matsumoto, G.I., Horiuchi, K., Kawai, T., 2010. A 27-kyr record of environmental change in central Asia inferred from the sediment record of Lake Hovsgol, northwest Mongolia. Journal of Paleolimnology 43, 369–383.
Overpeck, J.T., Webb, T., Prentice, I.C., 1985. Quantitative interpretation of fossil pollen spectra: dissimilarity coefficients and the method of modern analogs. Quaternary Research 23, 87–108.
Pachur, H.-J., Wünemann, B., Zhang, H., 1995. Lake evolution in the Tengger Desert, Northwestern China, during the last 40,000 years. Quaternary Research 44, 171–180.
Peck, J.A., Khosbayar, P., Fowell, S.J., Pearce, R.B., Ariunbileg, S., Hansen, B., Soninkhishig, N., 2002. Mid to Late Holocene climate change in north central Mongolia as recorded in the sediments of Lake Telmen. Palaeogeography, Palaeoclimatology, Palaeoecology 183 (1–2), 135–153.
Peng, Y., Xiao, J., Nakamura, T., Liu, B., Inouchi, Y., 2005. Holocene East Asian monsoonal precipitation pattern revealed by grain-size distribution of core sediments of Daihai Lake in Inner Mongolia of north-central China. Earth and Planetary Science Letters 233 (3–4), 467–479.
Prentice, I.C., 1985. Pollen representation, source area, and basin size: toward a unified theory of pollen analysis. Quaternary Research 23, 76–86.
Prentice, I.C., Guiot, J., Huntley, B., Jolly, D., Cheddadi, R., 1996. Reconstructing biomes from palaeoecological data: a general method and its application to European pollen data at 0 and 6 ka. Climate Dynamics 12, 185–194.
Prokopenko, A.A., Williams, D.F., Karabanov, E.B., Khursevich, G.K., 1999. Response of Lake Baikal ecosystem to climate forcing and pCO_2 change over the last glacial/interglacial transition. Earth and Planetary Science Letters 172 (3–4), 239–253.
Prokopenko, A.A., Alexander, A., Khursevich, G.K., Bezrukova, E.V., Kuzmin, M.I., Boes, X., Williams, D.F., Fedenya, S.A., Kulagina, N.V., Letunova, P.P., Abzaeva, A.A., 2007. Paleoenvironmental proxy records from Lake Hovsgol, Mongolia, and a synthesis of Holocene climate change in the Lake Baikal watershed. Quaternary Research 68 (1), 2–17.
Qian, Z.H., Kenneth, J.H., Yuan, Z., 2002. Kataglacial age of Quaternary period and climatic characteristics of Holocene epoch—a record of carbon isotope from Yanhaizi Ya02 borehole in Yi league of Inner Mongolia. Geology of Chemical Minerals 24, 95–100 (in Chinese with English Abstract).
Rhodes, T.E., Gasse, F., Lin, R.F., Fontes, J.-C., Wei, K.Q., Bertrand, P., Gibert, E., Melieres, F., Tucholka, P., Wang, Z.X., Cheng, Z.-Y., 1996. A late Pleistocene–Holocene lacustrine record from Lake Manas, Zunggar (northern Xinjiang, western China). Palaeogeography, Palaeoclimatology, Palaeoecology 120, 105–121.
Ricketts, R.D., Johnson, T.C., Brown, E.T., Rasmussen, K.A., Romanovsky, V.V., 2001. The Holocene paleolimnology of Lake Issyk-Kul, Kyrgyzstan: trace element and stable isotope composition of ostracodes. Palaeogeography, Palaeoclimatology, Palaeoecology 176, 207–227.
Rudaya, N., Tarasov, P., Dorofeyuk, N., Solovieva, N., Kalugin, I., Andreev, A., Daryin, A., Diekmann, B., Riedel, F., Tserendash, N., Wagner, M., 2009. Holocene environments and climate in the Mongolian Altai reconstructed from the Hoton-Nur pollen and diatom records: a step towards better understanding climate dynamics in Central Asia. Quaternary Science Reviews 28 (5–6), 540–554.
Ruddiman, W.F., 2007. Earth's Climate, Past and Future, 2nd ed. Freeman and Company, New York (484 pp.).
Schwanghart, W., Frechen, M., Kuhn, N.J., Schütt, B., 2009. Holocene environmental changes in the Ugii Nuur basin, Mongolia. Palaeogeography, Palaeoclimatology, Palaeoecology 279 (3–4), 160–171.
Shen, J., Liu, X.Q., Wang, S.M., Ryo, M., 2005. Palaeoclimatic changes in the Qinghai Lake area during the last 18,000 years. Quaternary International 136, 131–140.
Shi, Y.F., Kong, Z.C., Wang, S.M., Tang, L.Y., Wang, F.B., Yao, T.D., Zhao, X.T., Zhang, P.Y., Shi, S., 1993. Mid-Holocene climates and environments in China. Global and Planetary Change 7 (1–3), 219–233.
Shi, Q., Chen, F.-H., Zhu, Y., Madsen, D., 2002. Lake evolution of the terminal area of Shiyang River drainage in arid China since the last glaciation. Quaternary International 93 (94), 31–43.
Shichi, K., Takahara, H., Krivonogov, S.K., Bezrukova, E.V., Kashiwaya, K., Takehara, A., Nakamura, T., 2009. Late Pleistocene and Holocene vegetation and climate records from Lake Kotokel, central Baikal region. Quaternary International 205, 98–110.
Sklyarov, E.V., Solotchina, E.P., Vologina, E.G., Ignatova, N.V., Izokh, O.P., Kulagina, N.V., Sklyarova, O.A., Solotchin, P.A., Stolpovskaya, V.N., Ukhova, N.N., Fedorovskii, V.S., Khlystov, O.M., 2010. Detailed Holocene climate record from the carbonate section of saline Lake Tsagan-Tyrm (West Baikal area). Russian Geology and Geophysics 51, 237–258.
Stott, L., Cannariato, K., Thunell, R., Haug, G.H., Koutavas, A., Lund, S., 2004. Decline of surface temperature and salinity in the western tropical Pacific Ocean in the Holocene epoch. Nature 431, 56–59.

Stuiver, M., Grootes, P.M., Braziunas, T.F., 1995. The GISP2 $\delta^{18}O$ record of the past 16,500 years and the role of the sun, ocean and volcanoes. Quaternary Research 4, 341–354.
Sugita, S., 1994. Pollen representation of vegetation in Quaternary sediments: theory and method in patchy vegetation. Journal of Ecology 82 (4), 881–897.
Sun, X.J., Du, N.Q., Weng, C.Y., Lin, R.F., Wei, K.Q., 1994. Paleovegetation and paleoenvironment of Manasi Lake, Xinjiang, N.W. China during the last 14,000 years. Quaternary Sciences 3, 239–248 (in Chinese with English Abstract).
Tao, S.C., An, C.B., Chen, F.H., Tang, L.Y., Wang, Z.L., Lu, Y.B., Li, Z.F., Zheng, T.M., Zhao, J.J., 2010. Pollen-inferred vegetation and environmental changes since 16.7 ka BP at Balikun Lake, Xinjiang. Chinese Science Bulletin 55 (22), 2449–2457.
Tarasov, P.E., Guiot, J., Cheddadi, R., Andreev, A.A., Bezusko, L.G., Blyakharchuk, T.A., Dorofeyuk, N.I., Filimonova, L.V., Volkova, V.S., Zernitskaya, V.P., 1999. Climate in northern Eurasia 6000 years ago reconstructed from pollen data. Earth and Planetary Science Letters 171 (4), 635–645.
Tarasov, P., Dorofeyuk, N., Metl'tseva, E., 2000. Holocene vegetation and climate changes in Hoton-Nur basin, northwest Mongolia. Boreas 29 (2), 117–126.
Tarasov, P., Granoszewski, W., Bezrukova, E., Brewer, S., Nita, M., Abzaeva, A., Oberhansli, H., 2005. Quantitative reconstruction of the last interglacial vegetation and climate based on the pollen record from Lake Baikal, Russia. Climate Dynamics 25, 625–637.
Tarasov, P., Bezrukova, E., Karabanov, E., Nakagawa, T., Wagner, M., Kulagina, N., Letunova, P., Abzaeva, A., Granoszewski, W., Riedel, F., 2007. Vegetation and climate dynamics during the Holocene and Eemian interglacials derived from Lake Baikal pollen records. Palaeogeography, Palaeoclimatology, Palaeoecology 252 (3–4), 440–457.
Tarasov, P., Bezurkova, E., Krivonogov, S., 2009. Late Glacial and Holocene changes in vegetation cover and climate in southern Siberia derived from a 15 kyr long pollen record from Lake Kotokel. Climate of Past Discussion 5, 127–151.
ter Braak, C.J.F., Juggins, S., 1993. Weighted averaging partial least squares regression (WA-PLS): an important method for reconstructing environmental variable from species assemblages. Hydrobiologia 269–270, 485–502.
Tong, G.B., Yang, X.D., Wang, S.M., Chen, Z.Y., Xia, L.H., 1997. Ecotype exploration of polynoflora from Zhalainor since the late Quaternary. Acta Geographica Sinica 52, 72–79 (in Chinese with English abstract).
Tuvdendorzh, D., Myagmarzhav, B., 1985. Atlas of the Climate and Ground Water Resources in the Mongolian People's Republic. GUGMS of Mongolia, Ulan Bator.
Velichko, A.A., Catto, N., Dernova, A.N., Klimanov, V.A., Kremenetski, C., Nechaev, V.P., 2002. Climate changes in East Europe and Siberia at the Late Glacial–Holocene transition. Quaternary International 91, 75–99.
Visbeck, M., 2002. The ocean's role in Atlantic climate variability. Science 297, 2223–2224.
Wang, B.Y., Sun, X.J., 1997. A primary study on the Holocene climate change inffered from Chasuqi peat section, Inner Mongolia. Chinese Science Bulletin 42, 514–518 (in Chinese with English Abstract).
Wang, H., Liu, H., Cui, H., Abrahamsen, N., 2001. Terminal Pleistocene/Holocene palaeoenvironmental changes revealed by mineral-magnetism measurements of lake sediments for Dali Nor area, southeastern Inner Mongolia Plateau, China. Palaeogeography, Palaeoclimatology, Palaeoecology 170, 115–132.
Wang, K., Jiang, H., Zhao, H.Y., 2005. Atmospheric water vapor transport from westerly and monsoon over the Northwest China. Advances in Water Science 16, 432–438 (in Chinese with English Abstract).
Wang, W., Ma, Y.Z., Feng, Z.D., Meng, H.W., Sang, Y.L., Zhai, X.W., 2009. Vegetation and climate changes during the last 8660 cal. a BP in central Mongolia, based on a high-resolution pollen record from Lake Ugii Nuur. Chinese Science Bulletin 54 (9), 1579–1589.
Wang, Y.B., Liu, X.Q., Herzschuh, U., 2010. Asynchronous evolution of the Indian and East Asian Summer Monsoon indicated by Holocene moisture patterns in monsoonal central Asia. Earth-Science Reviews 103, 135–153.
Wang, W., Ma, Y.Z., Feng, Z.D., Narantsetseg, Ts, Liu, K.B., Zhai, X.W., 2011. A prolonged dry mid-Holocene climate revealed by pollen and diatom records from Lake Ugii Nuur in central Mongolia. Quaternary International 229 (1–2), 74–83.
Wanner, H., Beer, J., Bütikofer, J., Crowley, T.J., Cubasch, U., Flückiger, J., Goosse, H., Grosjean, M., Joos, F., Kaplan, J.O., Küttel, M., Müller, S.A., Prentice, I.C., Solomina, O., Stocker, T.F., Tarasov, P., Wagner, M., Widmann, M., 2008. Mid- to Late Holocene climate change: an overview. Quaternary Science Reviews 27 (19–20), 1791–1828.
Wei, W.S., He, Q., Liu, M.Z., Gao, W.D., 2003. Climate change and the desert environment in Junggar basin, Xinjiang, China. Journal of Desert Research 23, 101–105 (in Chinese with English Abstract).
Wen, Q.Z., Qiao, Y.L., 1990. Preliminary probe of climatic sequence in the last 13,000 years in Xinjiang region. Quaternary Sciences 4, 363–371 (in Chinese with English Abstract).
Wen, R.L., Xiao, J.L., Chang, Z.G., Zhai, D.Y., Xu, Q.H., Li, Y.C., Itoh, S., 2010a. Holocene precipitation and temperature variations in the East Asian monsoonal margin from pollen data from Hulun Lake in northeastern Inner Mongolia, China. Boreas 39 (2), 262–272.
Wen, R.L., Xiao, J.L., Chang, Z.G., Zhai, D.Y., Xu, Q.H., Li, Y.C., Itoh, S., Lomtatidze, Z., 2010b. Holocene climate changes in the mid-high-latitude-monsoon margin reflected by the pollen record from Hulun Lake, northeastern Inner Mongolia. Quaternary Research 73 (2), 293–303.
Wendland, W.M., Bryson, R.A., 1974. Dating climatic episodes of the Holocene. Quaternary Research 4 (1), 9–14.
Wu, Z.Y., 1980. Vegetation of China. Science Press, Beijing (1375 pp. in Chinese).
Wu, J.L., 1995. Characters of the evolution of climate and enivronment during the last 10 ka years in Aibi lake basin, Xinjiang. Scientia Geographica Sinica 15, 39–47 (in Chinese with English Abstract).
Wu, J.L., Wang, S.M., Wang, H.D., 1996. Characters of the evolution of climate and environment of Holocene in Aibi lake basin in Xinjiang. Oceanologia et Limnologia Sinica 27, 524–530 (in Chinese with English Abstract).
Wünnemann, B., Chen, F., Riedel, F., Zhang, C., Mischke, S., Chen, G., Demske, D., Ming, J., 2003. Holocene lake deposits of Bosten Lake, southern Xinjiang, China. Chinese Science Bulletin 48, 1429–1432.
Wünnemann, B., Mischke, S., Chen, F., 2006. A Holocene sedimentary record from Bosten lake, China. Palaeogeography, Palaeoclimatology, Palaeoecology 234 (2–4), 223–238.
Xia, D.S., Ma, Y.Z., Chen, F.H., Wang, J.M., 1998. High-resolution record of vegetation and climate variations in Longxi Loess Plateau during Holocene. Journal of Lanzhou University (Natural Sciences) 34, 119–127 (in Chinese with English abstract).
Xiao, J.L., Nakamura, T., Lu, H.Y., Zhang, G.Y., 2002. Holocene climate changes over the desert/loess transition of north-central China. Earth and Planetary Science Letters 197, 11–18.
Xiao, J.L., Xu, Q.H., Nakamura, T., Yang, X.L., Liang, W.D., Inouchi, Y.W., 2004. Holocene vegetation variation in the Daihai Lake region of north-central China: a direct indication of the Asian monsoon climatic history. Quaternary Science Reviews 23 (14–15), 1669–1679.
Xiao, X.Y., Jiang, Q.F., Liu, X.Q., Xiao, H.F., Shen, J., 2006. High resolution sporopollen record and environmental change since Holocene in the Wulungu Lake, Xinjiang. Acta Micropalaeontologica Sinica 23 (1), 77–86 (in Chinese with English Abstract).
Xu, Q.H., Xiao, J.L., Li, Y.C., Tian, F., Nakagawa, T., 2010. Pollen-based quantitative reconstruction of Holocene climate changes in the Daihai Lake Area, Inner Mongolia, China. Journal of Climate 23 (11), 2856–2868.
Xue, J.B., Zhong, W., Zhao, Y.J., Peng, X.Y., 2008. Holocene abrupt climate shifts and mid-Holocene drought intervals recorded in Barkol Lake of northern Xinjiang of China. Chinese Geographical Science 18, 54–61.
Yan, S., Xu, Y.Q., 1992. The Holocene vegetation and environment in Daluoba basin of Altay Mountains, Xinjiang. Xinjiang Geology 10, 279–284 (in Chinese with English abstract).
Yang, M.L., 2008. Holocene climate change pattern recorded mainly by diatom and other proxies from Bosten Lake. Ph.D. Dissertation, Lanzhou University (in Chinese with English Abstract).
Yang, X.D., Wang, S.M., 1994. Pollen assemblage and environmental changes in the last 12000 years in Wulungu Lake. Arid Zone Research 11, 7–10 (in Chinese with English abstrct).
Zhang, J.B., Shi, Y.Z., 2002. Climate Change of Xinjiang and Short-term Prediction. Meteorology Press, Beijing (266 pp. in Chinese).
Zhang, L.S., Fang, X.Q., Ren, G.Y., Suo, X.F., 1997. Environmental changes in the north China farming–grazing transitional zone. Earth Science Frontiers (China University of Geosciences, Beijing) 4 (1–2), 127–136 (in Chinese with English Abstract).
Zhang, C.J., Feng, Z.D., Yang, Q.L., Gou, X.H., Sun, F.F., 2010. Holocene environmental variations recorded by organic-related and carbonate-related proxies of the lacustrine sediments from Bosten Lake, northwestern China. The Holocene 20, 363–373.
Zhang, J.W., Chen, F.H., Holmes, J.B., Li, H., Guo, X.Y., Wang, J.L., Li, S., Lv, Y.B., Zhao, Y., Qiang, M.R., 2011. Holocene monsoon climate documented by oxygen and carbon isotopes from lake sediments and peat bogs in China: a review and synthesis. Quaternary Science Reviews 30, 1973–1987.
Zhang, C.J., Zhang, W.Y., Feng, Z.D., Mischke, S., Gao, X., Gao, D., Sun, F.F., 2012. Holocene hydrological and climatic change on the northern Mongolian Plateau based on multi-proxy records from Lake Gun Nuur. Palaeogeography, Palaeoclimatology, Palaeoecology 323–325, 75–86.
Zhao, Y., Yu, Z., Chen, F., Li, J., 2008. Holocene vegetation and climate change from a lake sediment record in the Tengger sandy desert, northwest China. Journal of Arid Environments 72, 2054–2064.
Zhao, Y., Yu, Z.C., Chen, F.H., Zhang, J.W., Yang, B., 2009. Vegetation response to Holocene climate change in monsoon-influenced region of China. Earth-Science Reviews 97 (1–4), 242–256.
Zhong, W., Xue, J.B., Li, X.D., Xu, H.J., Jiang, O.Y., 2010. A Holocene climatic record denoted by geochemical indicators from Barkol Lake in the northeastern Xinjiang, NW China. Geochemistry International 48, 792–800.
Zhou, Q.N., 1983. A Study on Vapor Source of Xinjiang. Beijing university Press, Beijing 179–181 (in Chinese).
Zhou, W.J., Donahue, D.J., Porter, S.C., Jull, T.A., Li, X.Q., Stuiver, M., An, Z.S., Matsumoto, E., Dong, G.R., 1996. Variability of monsoon climate in East Asia at the end of the last glaciation. Quaternary Research 46, 219–229.

[General Information]
□□=[□□□□□□□□□□□□□□□□□□□□□□□□□□□□]=Vegetation changes and associated climate variations in the Mongolian Plateau during the past 40 000 years
□□=[□□□□□□□□□□□□□□□□]
□□=359
SS□=13845122
DX□=
□□□□=2015.06
□□□=[□□□□□□□□□□□□]

Feng, Z.-D. And Khosbayar, P., 2004. Paleosubarctic Eolian environments along the southern margin of the North American Icesheet and the southern margin of Siberia during the Last Glacial Maximum. Paleogeography Paleoclimatology Paleoecology, 212: 265-275

Feng, Z.-D., Ma, Y. Z., Zhang, H. C., Narantsetsega, Ts. and Zhang, X. S., 2013. Holocene climate variations retrieved from Gun Nuur lake-sediment core in the nortern Mongolian Plateau. The Holocene, 23(12): 1721-1730

Feng, Z.-D., Wang, L. X., Ji, Y. H., Guo, L. L., Lee, X, Q. and Dworkin, S. I., 2008. Climatic dependency of soil organic carbon isotopic composition along the S-N Transect from 34° N to 52° N in central-east Asia. Paleogeography Paleoclimatology Paleoecology, 257: 33

Feng, Z.-D., Zhai, X. W., Ma, Y. Z., Huang, C. Q., Wang, W. G., Zhang, H. C., Khosbayar, P., Narantsetsega, Ts., Liu, K.-B. and Rutter, N. W., 2007. Eolian environmental changes in the Northern Mongolian Plateau during the past 35,000 yr. Paleogeography Paleoclimatology Pal

Feng, Z.-D., Wu, H. N., Zhang, C. J., Ran, M., and Sun, A. Z., 2013. Bioclimatic change of the past 2500 years within the Balkhash Basin,

eastern Kazakhstan, Central Asia. Quaternary International, 311: 63-70

Ma, Y. Z., Liu, K.-B., Feng, Z.-D., Meng, H. W., Sang, Y. L., Wang, W. and Zhang, H. C., 2013. Vegetation changes and associated climate variations during the past 38,000 years reconstructed from the Shaamar eolian-paleosol section, northern Mongolia. Quaternary Inter

Ma, Y. Z., Liu, K.-B., Feng, Z.-D., Sang, Y. L., Wang, W. and Sun, A. Z., 2008. A survey of modern pollen and vegetation along a south-north transect in Mongolia. Journal of Biogeography, 35: 1512-1532

Ran, M., Zhang, C. J. and Feng, Z.-D., 2014. Climatic and hydrological variations during the past 8000 years in northern Xinjiang of China and the associated mechanisms. Quaternary International, Quaternary International, 358: 21-34

Sun, A. Z. and Feng, Z.-D., 2013. Holocene climatic reconstructions from the fossil pollen record at Qigai Nuur in the southern Mongolian Plateau. The Holocene, 23(10): 1391-1402

Sun, A. Z., Feng, Z.-D., Ran, M. and Zhang, C. J., 2013. Pollen-recorded bioclimatic variations of the last 22,600 years retrieved from Achit Nuur core in the western Mongolian Plateau. Quaternary International, 311: 36-43

Wang, W., Ma Y. Z., Feng Z.-D., Ts Narantsetseg., Liu K.-B. and Zhai X. W., 2011. A prolonged dry mid-Holocene climate revealed by pollen and diatom records from Lake Ugii Nuur in central Mongolia. Quaternary International, 229: 74-83

Wang, W. and Feng, Z.-D., 2013. Holocene moisture evolution across the Mongolian Plateau and its surrounding areas: A synthesis of climatic records. Earth-Science Reviews, 122: 38-57